Pegmatites of the Cape Cross-Uis pegmatite belt, Namibia: structural, mineralogical, geochemical and mineral chemical characterisation with implications for petrogenesis and mineralisation

Warrick C. Fuchsloch

374933

A dissertation submitted to the Faculty of Science, University of the Witwatersrand, Johannesburg, in fulfilment of the requirements for the degree of Doctor of Philosophy.
Johannesburg, 2018

Declaration

I declare that this thesis is my own, unaided work. It is being submitted for the degree of Doctor of Philosophy at the University of the Witwatersrand, Johannesburg. It has not been submitted before for any degree or examination in any other university.



_____

Warrick C. Fuchsloch

15th of February, 2018

Abstract

The Neoproterozoic Pan-African Damara Orogen in Namibia is host to a variety of mineral resources, most occurring within the metasedimentary and igneous lithologies of the inland branch of the orogen, known as the Damara Belt. Examples of economic deposits include base metals, semi-precious stones and rare-metal pegmatites hosting minerals such as cassiterite, columbite-group minerals, petalite, spodumene, lepidolite and U-bearing phases.

The Cape Cross-Uis pegmatite belt is one of several pegmatite belts within the Damara Belt, located in the Northern tectonostratigraphic Zone. The LCT-type pegmatites of the belt were divided into three different types based on characteristics, mineralogy and whole-rock geochemistry. The types from most abundant to least are: 1) metasediment-hosted, Nb-Ta-Sn-bearing, unzoned pegmatites, 2) granite-hosted, garnet-tourmaline-bearing, crudely zoned pegmatites and 3) metasediment-hosted, Li-bearing, complexly zoned pegmatites. To the southeast of Uis, the Nainais pegmatites occur within the Nainais-Kahero pegmatite belt and were studied for comparison to the Cape Cross-Uis pegmatites. They are similar in almost all aspects to the Nb-Ta-Sn-bearing type pegmatites and were grouped together accordingly.

Field characteristics and structural analyses of the pegmatites indicate an overall northeast trend of pegmatites in line with the belt-wide northeast regional lineation. Furthermore, the pegmatites intrude various Damaran structures, however, they are not co-genetic with these structures and cross-cutting relationships and a lack of micro- or macroscopic deformational features within pegmatites indicate an exclusively post-orogenic emplacement age. Regional mapping of the pegmatite types also indicates that there is no apparent mineralogical or whole-rock geochemical spatial relationship of pegmatites with resident granites.

Whole-rock geochemistry of fine-grained border zones within pegmatites reveals that fractionation was the dominant process by which incompatible elements within the pegmatitic melt were enriched. Assimilation was discounted as a potential process in which elements such as Sn were incorporated into the pegmatitic magma as assimilation indicators such as MgO+FeO-CaO do not correlate with any trace elements. In addition, there is a mass balance problem since biotite schist country rocks on average show 70 ppm Sn and pegmatites may reach up to 1 wt% Sn in late-stage

alteration zones such as greisens. Furthermore, the dominant morphologies of greisens indicate that late-stage, Cl-complexed, Sn- and possibly Ta-Nb-enriched fluids were trapped by larger feldspar crystals and therefore could not have remobilised Sn from country rocks in a leaching, circulating, hydrothermal system.

Whole-rock geochemistry also shows that pegmatites and granites either follow completely different fractionation trends or overlap in fractionation trends, suggesting a decoupling of elements and preclusion from being coeval. Rare-earth elements confirm that a granite-pegmatite cogenetic relationship is unlikely since REE values of pegmatites (0.1-5 chondrite normalised) are two orders of magnitude lower than granites (10-100 chondrite normalised) where one would expect concentrations of incompatible elements in pegmatites to be far greater than in granites if a granite-parent, pegmatite-daughter type relationship is implied. In addition, a lack of pegmatite spatial association with granites supports this hypothesis.

Fractionation trends and minor element substitution trends in CGM suggest that mineral competition for elements within the melt produced Fe-rich CGM phases over a wide range of T/(Ta+Nb) values (fractionation indicator in CGM; 0.03-0.96) which supports an LCT, Petalite-subtype pegmatite signature. Furthermore, the CGM mineral chemical data and textures of zonation patterns in CGM may indicate that Ta, Nb and Sn were complexed and subsequently enriched in a late-stage exsolved pegmatitic aqueous fluid, which led to economic mineralisation of cassiterite, CGM and tapiolite in greisenised zones within pegmatites. Additional evidence is shown by the elevated values of Ta, Nb and Sn in host rock metasomatic contact zones which are abundant in tourmaline. Tourmaline mineral chemistry reveals that assimilation played a negligible role in the element diversity of the pegmatites, supporting whole-rock geochemical data. Tourmaline compositions indicate that the pegmatite magmas went through a phase of mafic depletion and Fe-enrichment in the early stages of crystallisation. During an intermediate stage of magma evolution, early CGM stabilised and competed with tourmaline for Fe in the magma, subsequently decreasing Fe contents in tourmaline and increasing Al, Li and Mn (elbaitic compositions). Highly mafic tourmaline compositions from pegmatites are rare and most likely indicate a crustal anatexis petrogenetic model for the pegmatites of the Cape Cross-Uis pegmatite belt, confirming whole-rock geochemical and field observations.

Co-authorship statement

The following thesis consists of eight chapters, three of which are in manuscript format. Chapter four has been published in Lithos and Chapters five and six have been submitted to Mineralogical Magazine. Following the first submission of this thesis, Chapter five underwent two separate reviews processes and is now accepted into Mineralogical Magazine, therefore Chapter five has been updated to the accepted version of the manuscript. The chapters are all referenced as journal articles in text and are found in the reference list. I.e. there is no citation to the specific chapters in text; instead the text references the publication itself. Furthermore, this thesis provides one complete reference list. The following in text citations are used:

Fuchsloch et al. (2018*a*) – Chapter 4

Fuchsloch et al. (2018*b*) – Chapter 5

Fuchsloch et al. (2018*c*) – Chapter 6

The manuscripts display the publications and submitted versions word for word, however, the formatting and writing style of the script is identical to the thesis. Furthermore, the manuscripts are ordered according to the thesis in terms of the table of contents. Due to the nature of manuscripts within a thesis, some sections in chapters four, five and six may be repetitive, however, the results and discussions display the core findings of the research project.

This project was funded by Professors Judith Kinnaird and Paul Nex. One sample of cassiterite and tapiolite was analysed by John Spratt at the London Natural History Museum. Riana Rossouw analysed whole-rock samples for chapter four using ICP-MS. All other sample preparation and data collection was performed by myself under the guidance of relevant lab staff (see acknowledgements). The intellectual development of this project and its ideas are my own with the guidance and input provided by my supervisors, Judith Kinnaird and Paul Nex and collaborators, Deon Van Niekerk.

Acknowledgements

First and foremost, I am indebted to my supervisors, Prof. Paul A.M. Nex and Prof. Judith A. Kinnaird. They provided such a unique, exciting and interesting project to work on, something I had been geologically unfamiliar with at first: pegmatites. It was their guidance that helped me find my geological passion in pegmatology and with their guidance, endless discussion and wisdom, helped me achieve my academic goals.

I am grateful to CIMERA (project code: MERA 015) whose funding significantly helped to bring this project into completion. Any student that can find the support of such a funding body is indeed lucky.

I would like to thank Gabi Schneider and the Geological Survey of Namibia who supported this project from its beginning and provided much discussion and made the process of accessing the field area easy. With that, I would like to say a thank you to all the friends I met along the road in the desert and particularly to Sheldon Pretorius who was an epic field assistant and desert companion.

As with any analytical project many laboratories are involved, and I would like to thank the technical teams at the Earth Sciences and School of Geosciences laboratories, University of the Witwatersrand. In particular to Caiphas Majola for the production of thin sections and many hours spent helping me create the perfect ore blocks for the microprobe. To Joe Aphane for sharing his expertise in mineral separation techniques and allowing me to make use of the instruments in the Earth Sciences lab. Thank you to Riana Rossouw for conducting the whole-rock geochemistry using ICP-MS at the University of Stellenbosch. A big thank you to Deon Van Niekerk, who spent hours with me in the microprobe lab at Rhodes University. In addition, Deon provided many discussions regarding one of the publications to come out of this thesis.

I would to thank Tim Marais together with Bushveld Minerals and Afritin Mining for providing extra field time in the Cape Cross-Uis pegmatite belt. With projects like this, the ability to go back into the field is immensely valuable and appreciated.

This journey was made easy by the following geologists at the University of the Witwatersrand. It was a pleasure spending time and sharing insights with the geological friend group now known as Room 120. Natalie Brand, Gruffudd Gigler, Kevin Dalton, Ben Hayes, Tremain Woods and Katie Hill, you guys truly made the days spent in and out the office fun. My geological journey began with Stephan Fuchsloch who inspired my initial love for the subject. You are more than a cousin and I look forward to all our future geological endeavours.

To my friends outside university, you guys helped take the edge off and spending a day or two on the golf course with the Wake and Rakers really helped me to clear my mind and tackle the project anew the next day. To name a few, special thanks go to Graham Axten, Scott McIntosh, Nick Loake, Craig Rowan, Joel Jackson and Devon Hagedorn-Hansen for the lifetime friendship starting in grade one.

To my family, uncles, aunts and cousins, a lifetime spent with you guys has been magnificent, and the rarity of such a close family is something I will be eternally grateful for. You have all supported me over the years, encouraged me to follow my dreams and helped out where ever you could. To my girlfriend Kirsten Macaulay; you were closest to me throughout this journey and your towering support was indescribable. Through the difficult times and celebrations (when the first paper was accepted), you were there, always, and I will forever be grateful.

Lastly to my mother and father, Cherryl and Patrick Fuchsloch. To say you both are amazing parents is an understatement and you have believed in me from the get go. Thank you for the lifetime of support and I dedicate this one to you.

Table of contents

Declaration i

Abstract ii

Co-authorship statement iv

Acknowledgements v

Table of contents vii

List of figures xiii

List of tables xxii

Chapter 1: An overview of the Damara Belt 1

1.1 Introduction 1

1.2 The regional geology of the Damara Belt 2

1.2.1. Tectonic and depositional history 5

1.2.2 Structural setting 8

1.2.3 Metamorphism 9

1.2.4 Magmatism 11

1.3 Pegmatites of the Damara Belt 13

1.3.1 Sn-Ta-Nb-bearing pegmatites 16

1.3.2 Li-Be-bearing pegmatites 16

1.3.3 Tourmaline- and gem-bearing pegmatites 16

1.3.4 Pegmatitic sheeted leucogranites 17

1.4 Project Aims 17

Chapter 2: Geology of the Cape Cross-Uis pegmatite belt 19

2.1 Introduction: 19

2.2 Research background 20

2.2.1 Regional setting of the CUPB 20
2.2.2 Pegmatites of the Cape Cross-Uis pegmatite belt 24
2.2.3 Pegmatite mineralisation 26
2.3 The pegmatite groups of the Cape Cross-Uis pegmatite belt 27
2.3.1 The CGM-cassiterite pegmatites (Nb-Ta-Sn type) 28
2.3.1.1 The 2faced pegmatite 28
2.3.1.2 The P2.2 pegmatite 32
2.3.1.3 The Strathmore pegmatites 34
2.3.1.4 The MT-pit pegmatite 36
2.3.1.6 The B-12 pegmatite 39
2.3.1.7 The C1 pegmatite 41
2.3.1.8 The Uis pegmatites 43
2.3.2 The Garnet-Tourmaline pegmatites (Gnt-Tml type) 45
2.3.2.1 The Rose Quartz pegmatites 45
2.3.2.2 Villet Tourmaline 48
2.3.3 The Li-bearing pegmatites 49
2.3.3.1 The Petalite pegmatite (Li-Nb-Ta-Sn-Be type) 50
2.3.3.2 The Karlowa North pegmatite (Li-Nb-Ta-Sn type) 53
2.3.4 The Nainais pegmatites (Nb-Ta-Sn type) 56

Chapter 3: A background to pegmatites 60
3.1. Introduction 60
3.2 The general geological setting of pegmatites 61
3.3 The classification of pegmatites 63
3.3.1 LCT-type pegmatites 65

3.3.2 NYF-type pegmatites 65
3.4 The formation and petrogenesis of pegmatitic melts 66
3.4.1 Derivation from a granite 66
3.4.2 Derivation from anatexis 69

Chapter 4: Classification, mineralogical and geochemical variations in pegmatites of the Cape Cross-Uis pegmatite belt, Namibia 70
4.1 Abstract 70
4.2 Introduction 71
4.3 Background 74
4.3.1 Regional geology 74
4.4 Description of pegmatites and country rocks 75
4.4.1 Field relationships 75
4.4.2 Pegmatite types 77
4.4.2.1 CGM-cassiterite pegmatites (Nb-Ta-Sn) 77
4.4.2.2 Tourmaline-garnet, crudely zoned, intragranitic pegmatites (Gnt-Tml) 79
4.4.2.3 Lithium-bearing pegmatites (Li-Nb-Ta-Sn-Be and Li-Nb-Ta-Sn; Table 4.1) 79
4.4.2.3.1 The Li-Nb-Ta-Sn-Be pegmatites 79
4.4.2.3.2 The Li-Nb-Ta-Sn pegmatites 81
4.4.2.4 The Nainais pegmatites 82
4.4.3 Structural characteristics 82
4.5 Methodology 84
4.6 Geochemistry 85
4.6.1 Metasedimentary rocks 85
4.6.2 Granites 85
4.6.3 Pegmatites 86

4.7. Discussion 98
4.7.1 Structural emplacement and timing 98
4.7.2 Origin of the Cape Cross-Uis pegmatites 99
4.7.2.1 Assimilation 100
4.7.2.2 Fractionation of a pegmatite from a granite 100
4.7.2.3 Source control on variability of pegmatite compositions 102
4.8 Conclusion 103
4.9 Acknowledgements 104

Chapter 5: The geochemical evolution of Nb-Ta-Sn oxides from pegmatites of the Cape Cross–Uis pegmatite belt, Namibia 105
5.1 Abstract 105
5.2 Introduction 106
5.3 Geological setting 107
5.3.1 Regional overview 107
5.3.2 The Cape Cross – Uis pegmatite belt 108
5.4 Sampling and analytical techniques 111
5.5 Results 113
5.5.1 Columbite-group minerals and tapiolite 116
5.5.1.1 Occurrence and internal structure 116
5.5.1.2 Mineral chemistry 118
5.1.1.3 Intra-crystal tapiolite chemistry 121
5.5.1.4 Columbite-group minerals and tapiolite mineral chemistry 122
5.5.2 Cassiterite 128
5.5.2.1 Occurrence and internal structure 128
5.5.2.2 Cassiterite mineral chemistry 128

5.6 Discussion 131
5.6.1 Minor element evolution 131
5.6.2 Fractional crystallisation evolution of pegmatitic melts 132
5.6.3 Magmatic vs exsolved aqueous fluid crystallisation 134
5.6.4 Regional aspects 138
5.7 Conclusions 141
5.8 Acknowledgements 142

Chapter 6: The mineral chemistry of tourmaline from pegmatites of the Cape Cross-Uis pegmatite belt, Namibia: implications for source, contamination and pegmatite fractionation. 143
6.1 Abstract 143
6.2 Introduction 144
6.3 Geological background 145
6.3.1 The Damara Orogen 145
6.3.2 Local geology and background research 146
6.4 Tourmaline occurrence and characteristics 148
6.5 Experimental methods 152
6.6 Results 153
6.6.1 Y-site Al content covariations 158
6.6.2 Tourmaline species classification and comparison to suggested trends. 161
6.7 Discussion 162
6.7.1 Substitution mechanisms and fractionation implications 162
6.7.1.1 Trend one of the 2-fold trend 163
6.7.1.2 Trend two of the 2-fold trend 165
6.7.2 Pegmatite source 166
6.8 Conclusions 169

6.9 Acknowledgements 169

Chapter 7: The Cape Cross-Uis pegmatite belt: overview and discussion 170

7.1 Introduction 170

7.2 Pegmatitic melt production 170

7.2.1 Granite related 170

7.2.2 Anatexis 172

7.3 Structural timing and emplacement 174

7.4 Crystallisation to mineralisation 176

7.5 Regional setting and pegmatite classification 179

Chapter 8: Summary and Conclusions 182

8.1 Introduction 182

8.2 Summary and conclusions 182

8.3 Future potential research 183

References 184

Appendices 211

Appendix A: sample inventory 212

Appendix B: whole-rock data 220

Appendix C: mineral chemistry data 227

Appendix D: Glossary of important terms 284

List of figures

Figure 1.1: Cratonic and mobile belt map of Gondwana during the Neoproterozoic. Ages of rifting and collision are indicated in purple and blue respectively (modified by Ashworth, 2013 from Gaucher et al., 2009 and Frimmel et al., 2011). *3*

Figure 1.2: The tectonostratigraphic zones of the Damara Belt (modified after Miller, 1979, 1983, 2008). The image also shows the Kaoko Belt, Southern Kaoko Zone (part of the Kaoko Belt) and major structural features. *4*

Figure 1.3: Map showing peak metamorphic zones in the Damara Orogen (modified by Ashworth, 2013 from Goscombe et al., 2004). *10*

Figure 1.4: Several pegmatite belts within the Damaran tectonostratigraphic zones. This image is a modified version of Figure 1.2 that has the pegmatite belts of the Damara Belt superimposed over the tectonostratigraphic zones (From Fuchsloch et al., 2018*a*). *14*

Figure 2.1: Simplified geological map of the Cape Cross-Uis pegmatite belt, Namibia. The map shows the three pegmatite swarms within the pegmatite belt as well as the metasediments and igneous rocks of the Damara Orogen and post-Damaran magmatism (modified after "Geological map of Namibia, Sheet 2114 - Omaruru"). *20*

Figure 2.2: Simplified geological map of the Strathmore swarm showing each pegmatite location and pegmatite type studied in the swarm (Table 2.1). *22*

Figure 2.3: Simplified geological map of the Karlowa swarm showing each pegmatite location and pegmatite type studied in the swarm (Table 2.1). *23*

Figure 2.4: Simplified geological map of the Uis swarm showing each pegmatite location and pegmatite type studied in the swarm (Table 2.1). *23*

Figure 2.5: Geological map of the 2faced pegmatite showing the location of pegmatite intruded tension gashes and the quartz core of the pegmatite. The two quartz core locations are in the two excavations that run perpendicular to the pegmatite strike. *30*

Figure 2.6: Field outcrop photographs of features in the pegmatite and host rock biotite schist at the 2faced pegmatite locality. A) Secondary precipitate, rectangular black minerals in the intermediate zone of the 2faced pegmatite. These zones have scintillometre readings of approximately 526 counts per second. B) Cm-scale tension gashes in biotite schist country rock that have been intruded by small sigmoidal shaped pegmatites. C) Pegmatite layering in the intermediate zone of the 2faced pegmatite. D) Graphic intergrowths of quartz and feldspars in the intermediate zone of the pegmatite. *31*

Figure 2.7: Geological maps of the following localities (see text for descriptions). A) The P2.2 pegmatite – section 2.3.1.2. B) The Strathmore pegmatites – section 2.3.1.3. C) The MT-pit pegmatite – section 2.3.1.4. D) The Small-GG pegmatite – section 2.3.1.5. *33*

Figure 2.8: Various outcrop photographs from the Strathmore pegmatite locality. A) Large metasedimentary xenoliths within the main pegmatite body. B) Bifurcating medium sized pegmatites with associated thinner pegmatite veins. C) 40 cm thick pegmatite vein intruding bedding parallel to biotite schist host rocks. D) Anhedral columbite group minerals in a greisenised zone of the Strathmore pegmatite. *34*

Figure 2.9: Sample D-4 showing fine-grained pegmatite rock near the contact of pegmatites with the biotite schist host rock. *37*

Figure 2.10: Outcrop photographs of pegmatites and host rocks at the Small-GG pegmatite locality. A) Thin boudinaged pegmatite vein approximately bedding-parallel to the host rock. B) Extremely metasomatised host rock contact with pegmatite. *38*

Figure 2.11: A geological map of the B-12 pegmatite showing greisenised zones, faults and lithologies. *40*

Figure 2.12: A geological map of the extensive C1 pegmatite. Field work suggests that outcrop in the SW and NE join up to make a single pegmatite body. *42*

Figure 2.13: A thin bifurcated extension of the C1 pegmatite that shows a quartz core and muscovite-rich border zone. *43*

Figure 2.14: Photographs of pegmatites in the Uis area. A) Overview image of a large pegmatite in the Uis area showing a NW dip direction. B) Highly greisenised area with a pegmatite showing abundant, large, anhedral cassiterite grains. *45*

Figure 2.15: Geological map of the Rose Quartz area showing variously orientated, intragranitic Gnt-Tml type pegmatites. *46*

Figure 2.16: Various outcrop photographs of the pegmatites in the Rose Quartz area. A) Thin pegmatite veins showing a dextral sense of shear. B) A contact between fine-grained and coarse-grained Salem-type granites. C) Unidirectional solidification texture tourmaline in the border zone of a Rose Quartz pegmatite. D) Crudely zoned pegmatite showing a quartz core and perthite intermediate zone. *47*

Figure 2.17: Photograph of the Granite Dome locality in Figure 2.3. Hundreds of pegmatite veins form a stockwork-like appearance on the surface of the granite dome. *49*

Figure 2.18: Geological map of the Petalite pegmatite showing the mineralogical zonation the pegmatite displays. *52*

Figure 2.19: Photographs of the Petalite pegmatite. A) A dolerite dyke cross-cutting both pegmatite and host rock biotite schist. B) Highly metasomatised biotite schist contact with the Petalite pegmatite. The metasomatic contact shows microliths rich in tourmaline adjacent to bleached sedimentary layers in the rock where biotite is absent. *53*

Figure 2.20: A geological map of the Karlowa North pegmatite showing a single moderately sized greisen zone (4 by 2 m). *55*

Figure 2.21: Geological map of the historical Nainais mine showing four of the mined-out pegmatites. *57*

Figure 2.22: Photographs of pegmatites in the Nainais historical mine. A) Almost completely mined out pegmatite dyke with only the wall zone of the pegmatite remaining. B) Anastamosing thin pegmatite vein that displays an identical mineralogical composition to the larger pegmatite bodies. *58*

Figure 2.23: Large black tourmaline grains rimmed by green tourmaline in feldspar crystals in the Nainais area. *59*

Figure 3.1: Illustration of the spatial association shared by granites and pegmatites in a pegmatite swarm (modified after Černý, 1989). *62*

Figure 3.2: The currently accepted pegmatite classification scheme of Černý and Ercit (2005). The writing in red shows how the classification scheme correlates with the two pegmatite families, NYF and LCT (Niobium-Yttrium-Fluorine and Lithium-Cesium-Tantalum respectively). *64*

Figure 3.3: Illustration showing progressive separation of pegmatites from a parent granite undergoing fractionation. The image shows each subsequent pegmatite separated at varying percentages of granite crystallisation, dissolved H_2O and enriched elements (The Jahns and Burnham, 1969, model, modified after Simmons and Webber, 2008). *68*

Figure 4.1: The tectono-stratigraphic zones of the Damara Orogen showing the approximate location of six of the main pegmatite belts (modified after Keller et al., 1999; Miller, 1983 and Richards, 1986). *72*

Figure 4.2: A) Simplified geological map of the Cape Cross-Uis pegmatite belt, showing metasediments and igneous rocks of the Damara Orogen and post-Damaran magmatism (modified after "Geological map of Namibia, Sheet 2114 - Omaruru"). B) Simplified geological map of the Strathmore pegmatite swarm showing the locations of several different pegmatite types (see Table 4.1 for pegmatite types). *73*

Figure 4.3: Field outcrop photographs of pegmatites in the Strathmore area. A and B are from the Rose Quartz pegmatite at co-ordinates 33K 414644 m E 7591110 m S and C and D are from the Petalite pegmatite at co-ordinates 33K 41827 m E 7599061 m S (Fig. 4.2B). A) Unidirectional crystal growth of tourmaline from an intragranitic pegmatite. B) A crudely zoned pegmatite within the area showing a quartz core and a feldspar perthite intermediate zone. C) Highly metasomatised biotite schist at the Petalite pegmatite. Note tourmaline within metasediment. D) A crudely zoned Nb-Ta-Sn pegmatite intruding Swakop Group biotite schist showing a quartz core and a feldspar perthite intermediate zone. *81*

Figure 4.4: Rose Diagrams depicting the average trend of the pegmatites (Left) and the poles of planes of the Swakop Group metasediments (Right) in the Cape Cross-Uis pegmatite belt. The red arrow indicates the mean vector. *83*

Figure 4.5: Photographs of macroscopic structural features from the Rose Quartz area located at co-ordinates 33K 414644 m E 7591110 m S. (Left) Intragranitic pegmatite veins showing dextral shearing. (Right) Pegmatites intruding tension gashes within Swakop Group banded biotite schist metasediments. *84*

Figure 4.6: Granitic classification plots. A) The Shand index granitic classification plot depicting the aluminosity of granitic rocks (Maniar and Piccoli, 1989). B) The tectonic discrimination diagram of Pearce et al. (1984). C) FeO_t and MgO plot against SiO_2 depicting the boundary between ferroan and magnesian intrusions (Frost et al., 2001). D) The $Na_2O + K_2O - CaO$ vs. SiO_2 from Frost and Frost (2008) showing the calcic or

alkalic nature of the intrusions. The triangles indicate different pegmatite types (Table 4.3) and the circles indicate granite in the belt. *91*

Figure 4.7: Ternary diagrams showing the relationship of granites and pegmatites in terms of Sr-Rb-Ba (A), Zr-Ce-Y (B) and Nb-Sn-Ta (C). A) The Rb-Ba-Sr ternary diagram from El Bouseily and El Sokkary (1975): 1) diorites, 2) granodiorites and quartz diorites, 3) anomalous granites, 4) normal granites and 5) strongly differentiated granites. *93*

Figure 4.8: Various element, element ratio, distance and A/CNK plots showing granites and pegmatites or just pegmatites. A) The K_2O/Rb vs. Ba plot showing that granites have significantly higher Ba values compared to pegmatites. B) Sn vs. the McKeough et al. (2013) hybridisation factor, showing no relationship. C) The HFSEs and Cs compared to the aluminosity of pegmatites and granites. D) The Ta and Cs element concentration relative to the distance from the outcropped granitic plutons. E, F) weak positive trends in plots of Ce-Y and Ta-Nb for pegmatites. *95*

Figure 4.9: Fractionation trends in pegmatites using various element ratios and element concentrations. Plot B is divided into two fields: the barren granite field (>100 K_2O/Rb) and the mineralised granite field (<100 K_2O/Rb; Stavrov et al., 1969). *96*

Figure 4.10: Rare earth element plots of Gnt-Tml pegmatites and Salem-type granites (top) and Nb-Ta-Sn pegmatites, greisens and albitised rocks. Chondrite normalised using values from McDonough and Sun (1995). *97*

Figure 5.1: A simplified geological map of the Cape Cross-Uis pegmatite belt, Namibia (modified after Fuchsloch et al., 2018*a*). The black squares show the approximate locations of the twenty pegmatite areas that were sampled. A total of 25 individual samples were collected from these pegmatites. Pegmatites in the southwest are part of the Strathmore swarm, those in the Karlowa area are part of the Karlowa swarm and those in the northeast are part of the Uis swarm. *108*

Figure 5.2: The Damara Belt showing the different stratigraphic zones defined by Miller, 2008 (modified after Miller, 1983 and Fuchsloch et al. 2018*a*). *110*

Figure 5.3: The atomic proportions of Ta and Nb of the columbite-group minerals from the Cape Cross-Uis pegmatite belt. Points that plot below the boundary are considered to be of the wodginite and ixiolite family. Points within the boundary are considered to be of ideal columbite-group mineral compositions where Ta and Nb are in the correct proportions to constitute the columbite-group minerals (Neiva, 1996; Tindle and Breaks, 2000). *113*

Figure 5.4: Back-scattered electron images of various columbite-group minerals and cassiterite crystals. A) Oscillatory-zoned columbite-group mineral enclosing a euhedral cassiterite grain showing a resorption texture along the margins of the cassiterite crystal. B) progressively-zoned columbite-group mineral with later-stage patchy zonation along the rim and centre zone. C) Platy progressively-zoned columbite-group mineral. D) Oscillatory-zoned columbite-group mineral with resorptions textures in the large centre zones. E) Multiple zonation of a columbite-group mineral showing later resorption of the rim and renewed oscillatory-zonation. F) Complexly-zoned columbite-group mineral showing patchy zonation. *119*

Figure 5.5: Back-scattered electron images of individual tapiolite grains from sample 3.1-2 coupled with their corresponding mineral chemical analyses of elements Ta, Fe, Nb, Mn, Ti, Sn at different points in the grains. Note that the numbers in the corresponding graphs (x-axis) are ordered from darkest zones to lightest zones and not in ascending order. A) Oscillatory-zoned tapiolite crystal. B) Twinned complexly zoned tapiolite crystal. C-D) complexly zoned tapiolite crystals. *123*

Figure 5.6: Compositional variation plots of columbite-group minerals and tapiolite (data are in a.p.f.u.; TAP = tapiolite; CGM = columbite-group minerals). (A) Sn and Ti values in tapiolite plotted against Ta# (Ta/(Ta+Nb)). (B) Sn and Ti values in columbite-group minerals plotted against Ta#. (C) W in both tapiolite and columbite-group minerals plotted against Ta#. (D) Ca and Mg in both tapiolite and columbite-group minerals plotted against

Ta#. Each plot (A-D) groups elements of the same charge whereas tapiolite and columbite group minerals are separated by a dashed line in plots c and d. (E) Columbite-group minerals and tapiolite in a section of the (Sn+Ti) – (Mn+Fe) – (Ta+Nb) triangle. The diagonal line connecting to (Mn, Fe)(Ta, Nb)2 indicates ideal substitution whereby the ratio of (Mn, Fe) to (Ta, Nb), or A-site to B-site, is 1:2. Points falling below this line indicate B-site deficiency in the crystal structure of columbite-group minerals, tapiolite or cassiterite. *125*

Figure 5.7: Columbite-group minerals and tapiolite compositions for individual samples in the columbite quadrilateral (Table 5.1). The samples are roughly grouped according to the trend they display which is shown by the red arrows in each plot. A-C) Typical trends subparallel to the Ta/(Ta+Nb) axis, defined by increasing Ta# with little variation in the Mn#. (D) Apparent bimodal fractionation trends in samples J-5, 4-4 and 4-11. Samples 12-1 shows a concomitant trend of equal increases in the Ta# and Mn# whereas sample G-4 clusters in the ferrocolumbite field with no discernible trend. (E,F) Columbite-group minerals and tapiolite that display scattered or uncharacteristic data. Sample 4-9 potentially shows a bimodal trend with missing data in the ferrocolumbite field (indicated by red arrows). Sample W-3 potentially shows a trend of decreasing Mn# with slight increases in the Ta# (indicated by the red arrow in f). Other data is scattered. The tapiolite immiscibility gap is shown in the figures as dashed lines in the ferrotantalite field (top left). *126*

Figure 5.8: The combined compositional data of columbite-group minerals and tapiolite from all samples in the Cape Cross-Uis pegmatite belt. Samples are plotted on the basis of pegmatite group to which they belong (Table 5.1) and whether a sample is an altered greisenised zone (Blue crosses). *127*

Figure 5.9: Chemical characteristics and trends in cassiterite from the Cape Cross-Uis pegmatite belt. A) (Sn,Ti)-(Ta,Nb)-(Fe,Mn) triangular plot showing the ideal substitution for Ta, Nb, Mn and Fe in cassiterite. The line marked $(Fe,Mn)(Ta,Nb)_2$ represents the ideal substitution. This graph is a zoomed in image of the bottom left portion of the triangular

diagram where (Sn,Ti) = 100 % and (Ta,Nb) and (Mn,Fe) up to 10 %. B) Cassiterite compositions plotted in the columbite quadrilateral. *130*

Figure 5.10: Country rock whole-rock data showing the Ta plotted against Sn and Nb in the right and left graphs respectively. The rock types include general host rocks which show no alteration and occur at variable distances to pegmatites and metasomatised, tourmalinised host rock contacts with pegmatites. Plots are given in logarithmic scales due to orders of magnitude differences between the data. *138*

Figure 5.11: Geological maps of the three swarms of the Cape-Cross Uis pegmatite belt showing the average Ta# (Ta/Ta+Nb) of the pegmatites which contained columbite-group minerals. Top: Strathmore Swarm; bottom: Karlowa Swarm. Below (Figure 5.11 cont.): Uis swarm. *139*

Figure 6.1: Geological map of the Cape Cross – Uis pegmatite belt, Namibia based on the localities bearing tourmaline (modified after Fuchsloch et al., 2018*a*). Pegmatite localities are shown by the black squares. Pegmatites in the NE quadrant, from Villet Tourmaline to T-Mag are situated in the Uis swarm. Karlowa-S and Small-GG occur in the Karlowa swarm and all the pegmatite localities in the SW quadrant are situated in the Strathmore Swarm. Nain-1, -2 and Nainais are located SE of the Autseib Fault in the Central Tin Belt. *147*

Figure 6.2: Photographs showing tourmaline morphologies in the CUPB. A) A zoned tourmaline crystal from the Nainais pegmatite with large black core and green to transparent rim. B) An interstitial aggregate of blue tourmaline in massive feldspar from the SmallGG pegmatite. C) Rosettes of green euhedral tourmaline (right) and blue anhedral tourmaline aggregates (left). D) Thin euhedral, black tourmaline crystals associated with massive quartz from the Petalite pegmatite. *150*

Figure 6.3: Tourmaline chemical classification diagrams. A) Provenance rock diagram from Henry and Guidotti (1985): 1 Li-rich granitoids; 2, Li-poor granitoids; 3, metasediments

with Al-saturating phase; 4, metasediments without Al-saturating phase; 5, low-Ca meta-ultramafic rocks and Cr, V rich metasediments; 6, metacarbonates and metapyroxenites. B) Classification of tourmaline based on the X-site occupation from Henry et al. (2011). Values are in a.p.f.u. *158*

Figure 6.4: Y-site Al covariation with Ca, Na, Mg, Fe, Ti and Mn in a.p.f.u respectively shown in graphs A-F. Suggested substitution mechanisms are shown in each plot along with the dominant fractionation trends. The underlined substitution mechanisms represent the dominant mechanism shown by the plot, whereas other substitution mechanisms are implied or suggested to be occurring simultaneously. Implied mechanisms do not necessarily contribute major abundance changes and may represent minor solid solutions exchanging elements during co-occurring dominant substitution mechanisms. *160*

Figure 6.5: Various compound/ratio element plots of tourmaline compositions. A) Classification of tourmaline based on the Mg# and Ca# of tourmaline from Novák et al. (2009). B) Classification of tourmaline based on the Al# and Na# from Tindle et al. (2002). C) Tindle et al. (2002) suggested contamination diagram based on tourmaline compositions. Compositions plotting in the lower field are suggested to be uncontaminated whereas raised values of Mg+Ti+Ca indicate contamination. D) Tourmaline evolution diagram minus the foitite component from London (2008). *162*

List of tables

Table 1.1: Summarised stratigraphy of the Damara Supergroup (modified after Miller, 1983, 2008; Geological map of Namibia, sheet 2114 – Omaruru, 1997; Ashworth, 2013). *6*

Table 1.2: Summarised ages of the Salem-type granites, Red and Grey granites and pegmatites within the Damara Belt. *15*

Table 2.1: Table summarising the pegmatites of the Cape Cross-Uis pegmatite belt studied. The table shows their geographic location, pegmatite type, host rock and common mineralogy. Qtz. = quartz; musc. = muscovite; alb. = albite; tml. = tourmaline; apt. = apatite; CGM. = columbite group minerals; cass. = cassiterite; gnt. = garnet.

29

Table 4.1: Pegmatite type table showing the pegmatite types in the Cape Cross-Uis pegmatite belt, their common mineralogy, host rocks and distinguishing features. Pegmatites are arranged from most common to least common. CGM. = Columbite-group minerals.

78

Table 4.2: Selected representative whole-rock major- and trace-element data for country rock metasediment and granite host rocks of the Cape Cross-Uis pegmatite belt. Selected samples were chosen to best represent the variations the dataset shows. S-Gran. = Salem-type granite; RG-Gran. = Red/Grey granite; Knot. = Knotenschiefer; BioSch. = biotite schist; Qtzite. = quartzite; TourBS. = tourmalinised biotite schist; n.a. = not analysed.

88

Table 4.2 continued: Selected representative whole-rock major- and trace-element data for pegmatites of the Cape Cross-Uis pegmatite belt. Grs. = Greisen.; d.l. = below detection limit. *89*

Table 4.3: Compositional comparison between host granite and pegmatites. Oxides are in wt% and trace elements in ppm. *90*

Table 5.1: Ta-Nb- and Sn-oxides and characteristics of pegmatites studied in the Cape Cross-Uis pegmatite belt. Gnt-Tml indicates the garnet-tourmaline pegmatite type, Ta-Nb-Sn indicates the unzoned Ta-Nb-Sn mineralised pegmatites and the Li-pegmatites indicate the unzoned and zoned Li-mineralised pegmatites. FeC, ferrocolumbite; FeT, ferrotantalite; MnC, manganocolumbite; MnT, manganotantalite; Cas, cassiterite; Tap, tapiolite; Wdg, wodginite; Ix, ixiolite. *115*

Table 5.2: Representative electron microprobe analyses of columbite-group minerals and tapiolite from the Cape Cross-Uis pegmatite belt. FeC, ferrocolumbite; FeT, ferrotantalite; MnC, manganocolumbite; MnT, manganotantalite; Cas, cassiterite; Tap, tapiolite. *120*

Table 5.3: Representative electron microprobe analyses of cassiterite from the Cape Cross-Uis pegmatite belt. *129*

Table 6.1: Tourmaline occurrences from pegmatites of the CUPB and Central Tin Belt. The different tourmaline species, occurrence and other accessory phases in the pegmatites are shown. The first character in the sample number indicates a specific pegmatite body. Ta Nb-Sn indicates the unzoned Ta-Nb-Sn mineralised type pegmatites, Gnt-Tml indicates the Garnet-tourmaline type pegmatite and Li-bearing indicates the unzoned to zoned Li-pegmatites. The last 3 rows represent the pegmatites of the Nainais area, Central Tin Belt. CGM, Columbite-group minerals; cas, cassiterite. *151*

Table 6.2: Representative chemical compositions of tourmaline from pegmatites of the Cape Cross-Uis pegmatite belt and Central Tin Belt. Each sample in Table 6.1 is depicted in this table together with its dominant occurring tourmaline species. Pegmatite types and sample number descriptions are given in Table 6.1 and the text. *155*

Chapter 1: An overview of the Damara Belt

1.1 Introduction

The Pan-African Damara Orogen, Namibia, is host to a variety of mineral deposits that are contained in packages that represent the depositional and orogenic stages of the orogen (Miller, 1983, 2008). To list a few, mineral deposits include: uranium-associated sheeted leucogranites (Rössing), vein-hosted tin and tungsten and pegmatite hosted lithium, tin, niobium-tantalum, uranium, and semi-precious stones (Richards, 1986; Miller, 1992; Schneider and Seeger, 1992; Diehl, 1992*a*,*b*,*c*, 1993; Nex, 2003; Singh, 2007; Ashworth, 2013). Mineralisation spans the entire lifecycle of the orogeny, however, most mineralisation within metasedimentary units and magmatic intrusive bodies is associated with the syn- to post-tectonic phases.

This dissertation is based on three published/submitted articles which are found in chapters 4, 5 and 6. The thesis investigates the pegmatites of the Cape Cross-Uis pegmatite belt, focusing on aspects such as the characterisation of the pegmatites, mineralisation and element diversity, pegmatite classification and assessing the source of the pegmatites (Appendix A,D). It summarises previous, but sparse, research on the belt, the structural characteristics of the pegmatites and classifies the pegmatites based on their whole-rock geochemical signature and mineralogical makeup. Additionally, whole-rock geochemistry (Appendix B) was used to evaluate fractionation trends within pegmatite bodies and how they relate to Ta-Nb-Sn- and Li-mineralisation and pegmatite petrogenesis. Furthermore, this dissertation summarises the CGM, cassiterite, tourmaline and apatite mineral chemistry data and how the data relates to the origin of the pegmatitic melts, element behaviour during crystallisation and what late-stage processes were active during alteration (Appendix D; glossary) of the pegmatites. However, the apatite mineral chemistry data was found to be unacceptable to constitute a publication or a chapter within this thesis due to the following factors (described in Appendix C): limited quantity of data covering few pegmatites, below detection limit values for 50 % of the dataset and no observable correlation between any data.

1.2 The regional geology of the Damara Belt

The Damara Orogen is a Neoproterozoic Pan-African orogenic belt that trends northeast through central Namibia into Botswana and north into Angola and the Democratic Republic of Congo (Martin and Porada, 1977; Miller, 2008). The orogen represents a triple junction located near Swakopmund, Namibia, where the Congo (north), Kalahari (south) and Rio de la Plata (west) cratons amalgamated during the assembly of Gondwana (Prave, 1996; Trompette, 1997; Miller, 1983, 2008). The Damara Orogen consists of three belts/arms: (1) the northwest-trending Kaoko Belt, (2) the north-trending Gariep Belt and (3) the northeast-trending Damara Belt (Fig. 1.1). The Damara Belt represents a collisional suture between the Congo and Kalahari cratons. The belt is approximately 400 km in width, 1000 km in length and was active from approximately 900 to 440 Ma (Martin and Porada, 1977; Stanistreet et al., 1991; Gray et al., 2006; Miller, 1983, 2008; Miller and Frimmel, 2009; Frimmel et al., 2011).

The Damara Belt formed during a typical Wilson Cycle, starting with the rifting and spreading of Rodina (break up) to the final subduction and continental collision to form Gondwana. Miller (1979, 1983, 2008) separated the Damara Belt into tectonostratigraphic zones based on variations in structure, stratigraphy, igneous activity and metamorphic history (Fig. 1.2). The tectonostratigraphic zones are as follows from north to south: The Northern Platform (NP), Northern Margin Zone (NMZ), Northern Zone (NZ), Central Zone (CZ), Southern Zone (SZ), Southern Margin Zone (SMZ) and Southern Platform (SP) (Fig. 1.2).

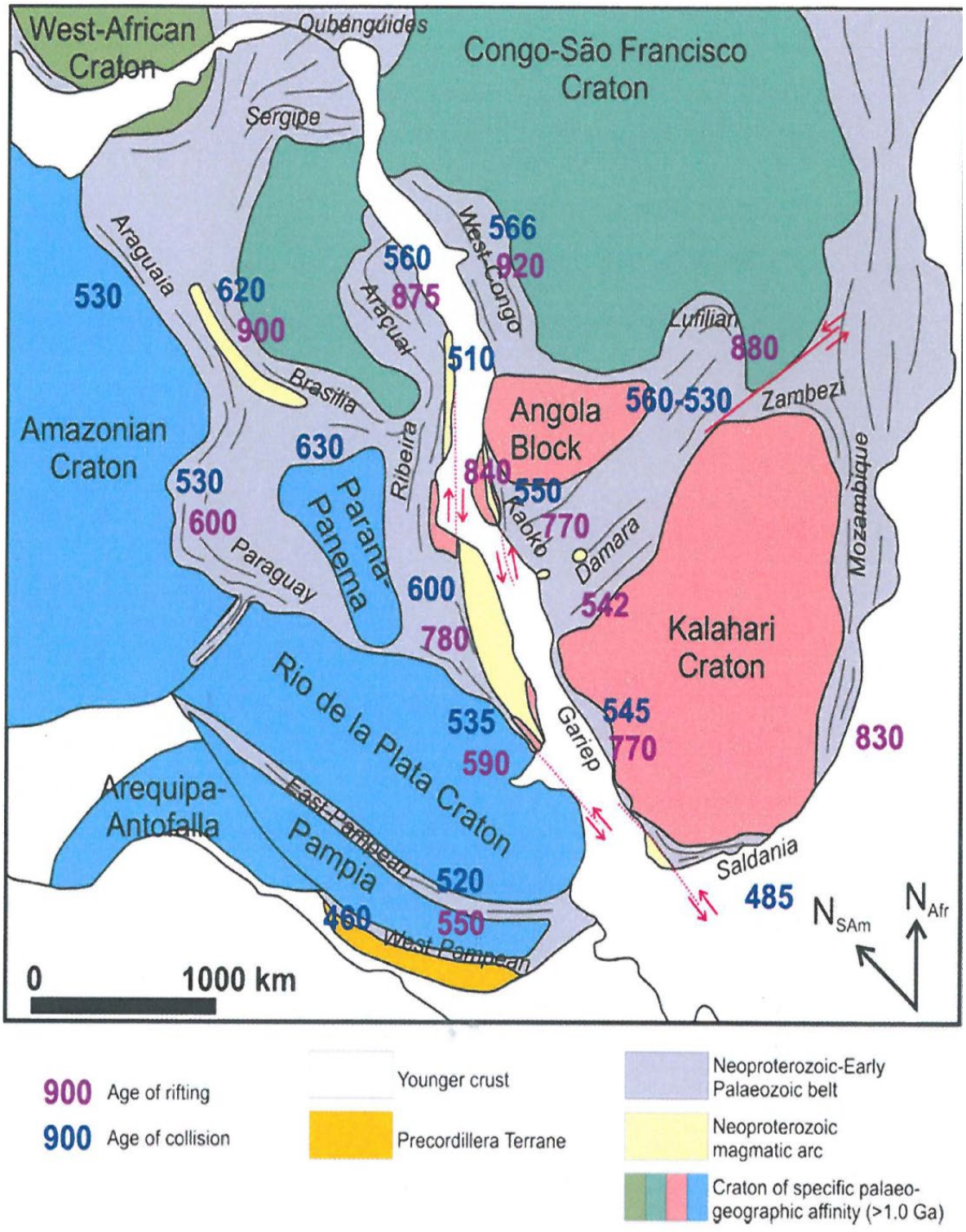


Figure 1.1: Cratonic and mobile belt reconstruction map of Gondwana during the Neoproterozoic. Ages of rifting and collision are indicated in purple and blue respectively (modified by Ashworth, 2013 from Gaucher et al., 2009 and Frimmel et al., 2011).

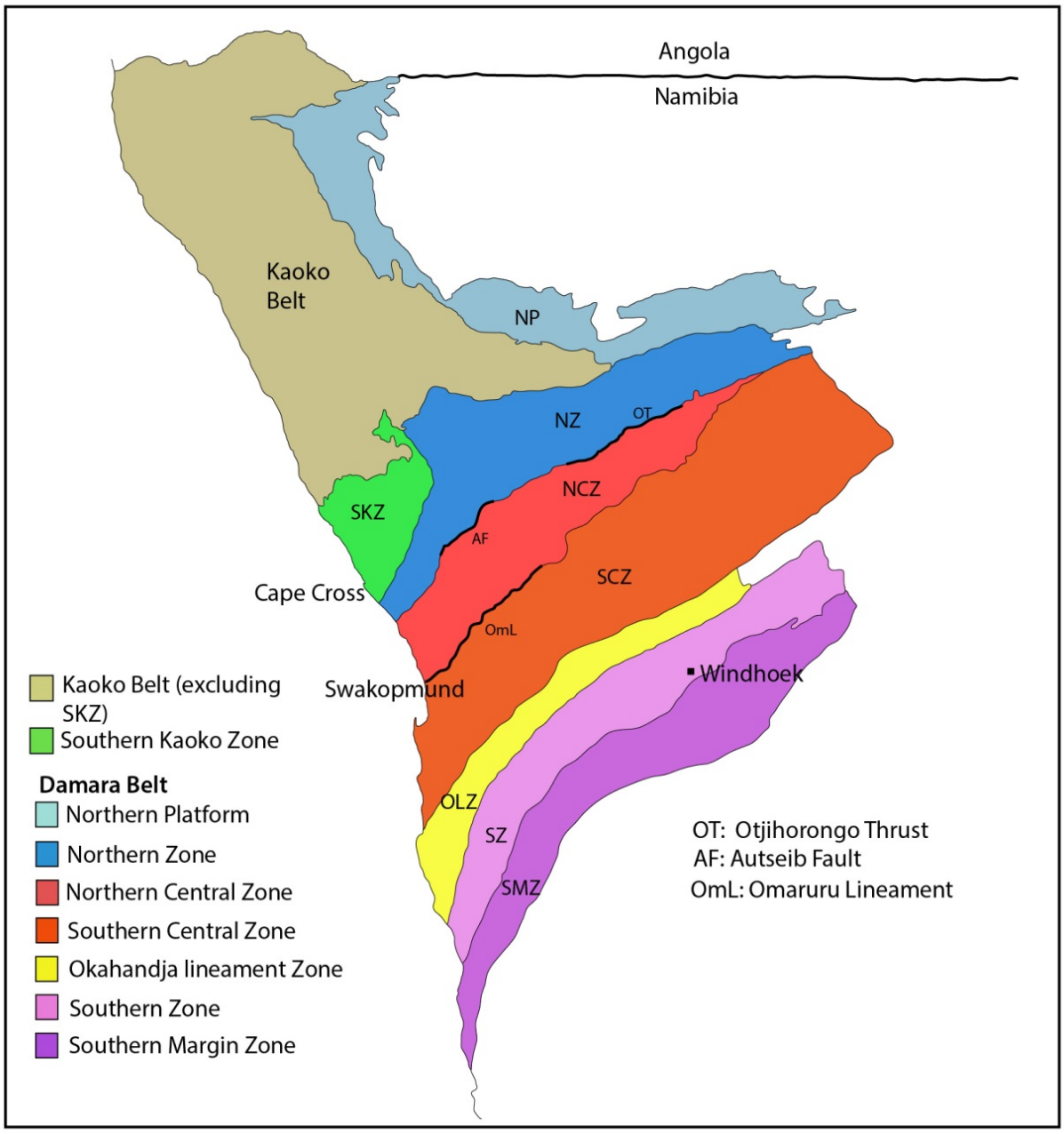


Figure 1.2: The tectonostratigraphic zones of the Damara Belt (modified after Miller, 1979, 1983, 2008). The image also shows the Kaoko Belt, Southern Kaoko Zone (part of the Kaoko Belt) and major structural features.

1.2.1. Tectonic and depositional history

The Damara Belt is represented by metasedimentary lithologies belonging to the Damara Supergroup which were deposited unconformably on the pre-Damara Palaeoproterozoic gneisses of the Abbabis Complex during the cycles of rifting, spreading and convergence between the Congo and Kalahari cratons (Miller, 2008). The lithologies are dominantly continental rift and shelf sediments which were subsequently metamorphosed during the deformational stages of the tectonic history. Miller (2008) provides a good summary of the stratigraphy and details of these lithological units. Table 1.1 places them in the context of the tectonostratigraphic zones seen in Figure 1.2.

The Nosib Group (Table 1.1) was the first stratigraphic unit to be deposited during the rifting stages of the Damara Orogen, when the breakup of Rodina was initiated. Rift sedimentation was initiated between approximately 900 and 800 Ma during the opening of the Adamaster Ocean (Hoffman et al., 1996; Prave, 1996; Gray et al., 2006; Miller, 2008). During the rifting phases two parallel grabens with a northeast trend developed, which later formed the Outjo and Khomas Seas of the Damara Ocean, in which sediment was subsequently deposited (Stanistreet et al., 1991; Miller, 2008). Metasediments include; quartzite, arkose, conglomerate, phyllite, calc-silicate and subordinate limestone and evaporitic rocks (Miller, 1992). Intrusive alkaline and peralkaline rocks such as gabbro, syenite, foyaite and carbonatite are associated with the Nosib group and constrain the ages of the group (Miller, 1992). Zircon and titanite dating of such rocks indicate an age of 750 Ma (Jung et al., 2007). The thickness of the Nosib group is highly variable due to deposition of sediment in grabens, however, and although outcrop is sparse due to the thickness of Swakop Group cover, some areas can show thicknesses of thousands of metres whereas in other areas, rift edges and palaeohighs, show only several metre thicknesses (Miller, 1983, 2008; e.g. Etusis Formation).

Table 1.1: Summarised stratigraphy of the Damara Supergroup (modified after Miller, 1983, 2008; Geological map of Namibia, sheet 2114 – Omaruru, 1997; Ashworth, 2013).

Damara Belt										
Age	Northern Platform		Southern Kaoko Zone/Northern Zone		Central Zone		Southern Zone	Southern Margin Zone		Southern Foreland
600-550 Ma	Mulden Group						Khomas Complex			Nama Group
650-600 Ma	Otavi Group	Tsumeb Sub-Gp	Zerrissene Group	Amis River Fm Gemsbok River Fm Brak River Fm Brandberg West Fm Zebraputs Fm	Swakop Group	Navachab Sub-Gp		Hakos Group	Vadgras Sub-Gp	Zerrissene Group
750-650 Ma		Abehab Sup-Gp				Usakos Sub-Gp			Kudks Sub-Gp	
		Ombombo Sub-Gp				Ugab Sub-Gp				
850-750 Ma	Nosib Group							Nosib Group		

At around the time rifting transitioned to spreading, the first of two snowball earth glaciations occurred and produced intercalated banded ironstones, glacio-marine sediments and quartzites of the Chuos Formation, which is the Sturtian equivalent dated at 730 Ma (Killick, 1986; Stanistreet et al, 1991; Bühn et al., 1992; Miller, 1992; Frimmel, 2009). During this depositional episode the laterally equivalent Otavi (northern carbonate platform), Witvlei (southern platform), Swakop (central basin) and Zerrissene (deep water turbidites) Groups were deposited (Table 1.1; Miller, 1992). The Chuos Formation only appears in the first three groups as evidence of the first snowball earth episode, however, the Marinoan-equivalent Ghaub Formation produced by the second glaciation episode appears in all four and was dated at 635 Ma by Hoffman et al. (2004). Lithologically the Ghaub Formation has a highly calcareous matrix, granite and carbonate clasts and is pyritic but lacks primary iron oxides (Miller, 2008). Following deposition of the Ghaub Formation, large scale subsidence occurred as the rift deepened during spreading. This is in part because of deposition of large siliciclastic successions and tholeiitic magmatic activity (Miller, 1983, 1992, 2008; Stanistreet, 1991; Ashworth, 2013). Subsidence scaled from the NZ to the SZ and caused the deposition of the Kuiseb Formation, in both the Khomas and Outjo Seas, which is

a 10 km thick succession of greywacke. The greywacke succession marks the end of the spreading phase of the Damara Belt (Miller, 1992, 2008; Frimmel et al., 2002, 2011).

Although the crust beneath the Outjo Sea (northern graben) did not rupture, Besshi-type volcanic-associated sulphide deposits occur in the Matchless Amphibolite Member in the southern graben that represents the Khomas Sea. This member provides evidence of continental rupture in the Khomas Sea (Miller, 1992; Killick, 2000). The Matchless Member forms a linear outcrop which can be traced over 350 km from the Namib Desert to the Steinhausen area and consists of interlayered amphibolites and metagabbros (Kukla, 1992). The Matchless Member has a MORB or plume-type geochemical signature, deformed pillow lavas, cupreous pyrite deposits and Cu-Fe sulphide deposits which are indicative of an active mid-oceanic ridge (Barnes and Sawyer, 1980; Miller, 1992; Kukla, 1992, Killick, 2000). On either side of the rift, turbiditic successions occur in a passive margin type setting which swamped the mid-oceanic ridge, depositing yet another 10 km sequence of greywackes (Barnes and Sawyer, 1980; Miller, 1992, 2008, 2009; Kukla, 1992; Killick, 2000).

The next tectonic event to occur was the reversal of plate motion and the subduction of the Kalahari Craton under the Congo Craton (Miller, 2008; Frimmel et al., 2011). At present, the exact timing of this event is unclear, however, dating of the Hartelust rhyolite by Nagel (1999) and the oldest syn-tectonic garnets formed during the first stages of transpressive continental collision dated by Goscombe et al. (2005) constrains the ages of plate reversal and subduction. The ages show an approximate time period from between 609 and 595 Ma from the Hartelust rhyolite to the oldest syn-tectonic garnets respectively. With the onset of subduction, the Adamaster and Damara Oceans began to close and large-scale uplift and erosion took place in an Alpine-type mountain belt setting (Miller, 1992; 2008). This created two new groups of sedimentary successions, being deposited in the closing Khomas Sea, in the now karst Otavi Group with sediment derived from the approaching Gariep and Damara Belts. Uplift and erosion produced a northern molasse which is known as the Mulden group (Table 1.1) consisting of highly carbonaceous shales, greywackes, sandstones and carbonates deposited in a karst Otavi Group. Within a foreland basin, formed by subduction, a ramp succession of sandstones, shales and carbonates were deposited and represent

the Nama Group (Table 1.1; Stanistreet, 1991; Miller, 1983, 1992, 2008, 2009; Frimmel et al., 2011).

1.2.2 Structural setting

Closure of the Damara Ocean and final continent-continent collision is confined to an age between 560 and 545 Ma and is represented by the Damara Orogen (Stanistreet, 1991; Jacob et al., 2000; Frimmel et al., 2011). Structurally this event produced polyphase deformation within all the lithologies of the Damara Belt. The Kalahari craton and ocean floor (Matchless Amphibolite) subducted beneath the Congo craton during their northeasterly transpressive collision deforming the Southern Zone and Southern Marginal Zone, which show the highest level of deformation in the orogen (Miller, 2008; Will et al., 2009; Frimmel et al., 2011).

The currently accepted view is that three deformational events occurred (D_1, D_2, and D_3) within the Damara Orogen, however, some previous authors, for example, Barns and Sawyer (1980), have ascribed five or more deformation events. However, D_1 is not seen as a major deformational event since it has only been shown to affect groups occurring before the Mulden and Nama Groups which show no evidence of D_1 structures. D_1 structures, although locally and weakly developed, include huge regional scale nappes and folds, isoclinal folds and associated minor thrusts dated to have occurred between 588 and 564 Ma (Coward, 1983; Miller, 2008).

The second stage and the first major deformational event, D_2, is ascribed to the initial continent-continent collision between the Kalahari and Congo Cratons (Miller, 2008). D_2 resulted in more open folds with a gentle north dip compared to the isoclinal D_1 folds along with associated S-verging thrusts, shear zones, boudinaged layers and the formation of a penetrative fabric. Although in some places D_2 cannot be dated (e.g. Central Zone) the consensus for an age constraint is between 555 and 550 Ma (Coward, 1983; Kinnaird and Nex, 2007; Will et al., 2009; Frimmel et al., 2011).

The final major deformational event, D_3, marks continental closure and is well constrained by dating of zircons from syn-D_3 granites at 542 Ma (Marlow, 1983; Miller, 2008). This event was accountable for the re-folding and tightening of pre-D_3 structures and creation of upright

northeasterly-trending folds. The reworking of previous structures by D_3, focused at the basement/cover interface, created the dome structures shown today in the Southern Central Zone (Kinnaird and Nex, 2007). Domes are elongate, usually about 5 km in length and may extend up to tens of kilometres along strike with most dome cores being composed of the Abbabis Complex basement rocks (Smith, 1965; Kinnaird and Nex, 2007; Miller, 2008; Will et al., 2009; Frimmel et al., 2011). D_2 and D_3 are pertinent to this project because they are responsible for post-orogenic magmatism and mineralisation (crustal thickening and anatexis), giving rise to the granitoids and pegmatites of the Damara Orogen (Wagener 1989; Diehl, 1993; Kinnaird and Nex, 2007; Miller 2008; Longridge, 2012; Ashworth, 2013).

1.2.3 Metamorphism

In a regional sense, the Damara and Kaoko Belt can be seen as paired metamorphic belts (Miller, 2008). Both have high pressure, low temperature and low pressure, high temperature paired metamorphism, where both pre-Damaran and Damaran rocks have been affected (Miller, 2008). Metamorphism increases from the edges of the belt (NP and SF) to the centre and from inland in the east to the coast line in the west with the highest metamorphic grade rocks centred around Swakopmund and Walvis Bay (Kinnaird and Nex, 2007; Miller 2008; Will et al., 2009; Fig. 1.3). Metamorphic mineral assemblages of high pressure, low temperature (~ 588 °C and ~1002 MPa; Kasch, 1983) include kyanite-staurolite whereas low pressure, high temperature zones (~750 °C and ~450 MPa; Kasch, 1983) include cordierite-sillimanite.

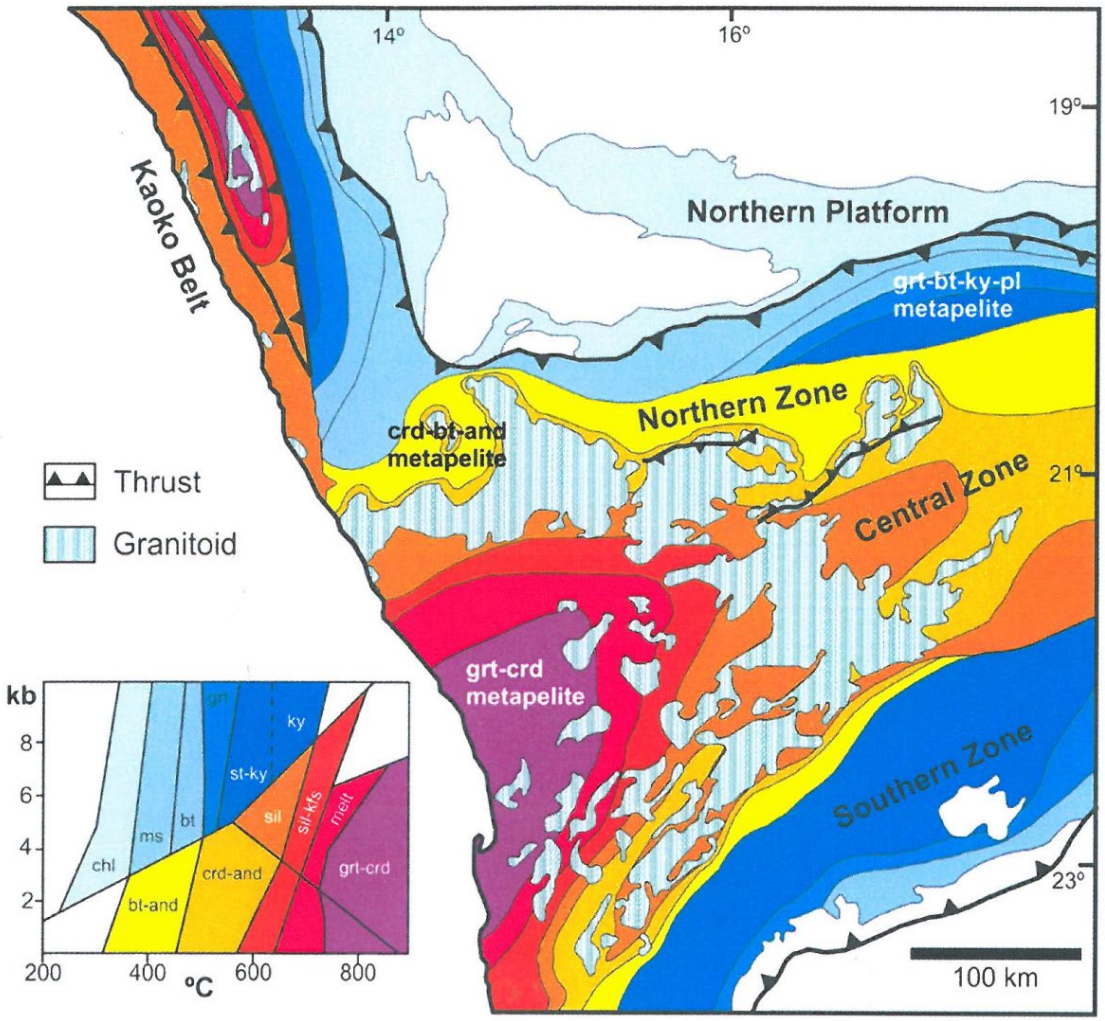


Figure 1.3: Map showing peak metamorphic zones in the Damara Orogen (modified by Ashworth, 2013 from Goscombe et al., 2004).

Jung and Mezger (2003) suggested that peak metamorphism occurred between 530 and 523 Ma based on garnet and monazite dating, representing the M_2 event. The number of metamorphic events is debated in the Damara Orogen. Some authors such as Barnes and Saywer (1980), Kasch (1983), Jung and Mezger (2003), Goscombe et al. (2004), Miller (2008) and Gray et al. (2008) suggest two metamorphic events and others such a Longridge (2012) give evidence leaning towards one event. Longridge presents a single P-T path which peaked at a temperature of 800 °C at 4.5-5.0 kbar pressure between 510 and 505 Ma. However, due to lack of petrographic evidence of M_1, Longridge (2012) cannot discount unequivocally there being two metamorphic events, thus the consensus still accepts a two-stage metamorphic episode for the Damara Orogen.

The first metamorphic event, M_1 occurred when the Kalahari craton was thrust against the Congo craton during continental collision. This created a high pressure, low temperature event. The second stage of metamorphism, M_2, occurred later and was due to large amounts of magmatism in the Damara Orogen. M_2 metamorphism (700 °C; 4 kbar) over-printed the D_3 deformational event and created higher temperature granulite facies rocks. Magmatism is mostly granitic in composition and occurred syn- to post-tectonically (Goscombe et al., 2004; Miller, 2008).

1.2.4 Magmatism

The Damara Plutonic Suite is almost exclusively granitic in composition with a diorite to tonalite/granodiorite to granite ratio of 2:2:96 (Miller, 1983). The plutonic suite consists of over 200 plutons, plugs and stocks of syn- to post-tectonic granitic rocks and thousands of granite and pegmatite dykes, covering an area of approximately 74000 km^2 (Miller, 2008; Miller and Frimmel, 2009). The plutonic suite primarily occurs in the CZ which formed the active margin of the Congo Craton above the Damara subduction zone with emplacement spanning the entire tectonic history of the Damara Belt (Wagener, 1989; Kisters et al., 2004; Kisters, 2005; Miller, 2008). Other plutonic rocks such as granites also occur further north and south in the NZ and SZ respectively (e.g. the Donkerhuk Granite, northern edge of the SZ; Miller, 2008). Metagabbros occur as disrupted fragments, xenoliths and mega xenoliths in the oldest diorites but only form about 1% of the plutonic suite. Other alkali granites and plugs of hornblendite also occur in the suite (Miller, 2008; Miller and Frimmel, 2009).

Characteristics and descriptive features of the plutonic suite are based on the stratigraphic level of occurrence, the sequence of intrusive events and the shape of the intrusion (i.e. early lopolithic shape or later balloon-like shape). Frimmel and Miller (2009) summarise the plutonic suite well, using sources such as Miller, (1983), Tack et al. (2002), Jacob et al. (2000), Johnson et al. (2006) and Miller (2008) for detailed sequenced magmatic events and dates. The oldest plutonic rocks within the Damara Belt formed during the transpressional stages (post D_1 to pre- or syn-D_2) at an age between 573 and 558 Ma (Jacob et al., 2000; Milani et al., 2015). These igneous rocks comprise mainly of diorites and minor metagabbros of the Goas Intrusive Suite (GIS) and occur in the area south of Karibib as a number of plutons (Miller, 2008). De Kock (1991) suggested, based on geochemical evidence, that the metagabbros represent volcanic arc magmatism that was

incorporated into the dioritic plutons formed during active margin calc-alkaline magmatism. Schist xenoliths from the Kuiseb Formation occur within the mafic components and contain an axial planar foliation interpreted as S_1, thus De Kock (1991) concluded that foliation in the diorites is D_2 in age.

The next group of plutonic rocks that formed was the famous Salem-type Granites which comprise the largest portion volumetrically of the plutonic suite (Miller, 2008; Frimmel and Miller, 2009). A large amount of work has been done on these granites and the age constraints in which they form is debated but a generally accepted time constraint is between 565 and 514 Ma (Hawkesworth et al., 1983; Johnson et al., 2006; Miller, 2008; Longridge, 2012; Ashworth, 2013). Longridge (2012) suggested that the formation of the suite was due to slab break-off followed by asthenospheric upwelling which provided the heat for magmatism and thus, extensive melting of the lower crust occurred between 539 and 511 Ma. The suite is not only composed of granites but monzogranites and granodiorites as well and the suite is subdivided into non-porphyritic gneissic granite, porphyritic biotite granite and leucogranite (Miller, 2008). Due to the large number of granitic bodies included in the Salem-type Granite suite, many authors currently debate which granites belong to the suite (Nex and Kinnaird, per. Comm., 2015).

The Red Granites which are younger than Salem-type Granites, were initially thought to be the oldest of the plutonic suite. However, field relationships confirmed by Nex et al. (2003) and dating of Red Granites at 534 Ma by Briqueu et al. (1980) confirm that the Red Granites are both younger than Salem-type Granites and older than subsequent Grey Granites. Granite types within the Red Granites include gneissic red granites, buff leucocratic granites and homogeneous red granites, occurring dominantly within the Central Zone, although the gneissic Red Granites occur at lower stratigraphic levels in the southwestern parts of the Damara Belt (Brandt, 1987; Miller, 2008).

The Grey Granites (also known as homogeneous syn-tectonic granites) are monzogranitic in composition and were emplaced syn-D_2 and show both D_2 and D_3 structural characteristics. Grey Granites, occurring mostly in the CZ, have been dated by both Briqueu (1980) and Longridge (2012) with ages obtained of 517 Ma and between 519 and 520 Ma respectively indicating younger ages than the Red Granites.

The last set of granite intrusions within the Damara Plutonic Suite are the post-tectonic leucogranites. They occur as plugs and dykes as well as two plutons (The Donkerhuk and Bloedkoppie pluton) in the Central Zone (Miller, 2008). These sheeted leucogranites are post-M_2 and occur at an age of 509 Ma (Briqueu, 1980; Frimmel and Miller, 2009). By field characteristics, geochemical analyses and assessing the structural setting, in some areas, these granites can be separated into six different groups and are shown to have correlation per group with high abundances of radioactive elements as some are uranium enriched (Nex et al., 2003).

1.3 Pegmatites of the Damara Belt

A variety of syn- and post-tectonic granitic pegmatites occur throughout the Damara Belt including in the Northern Zone, Central Zone and Southern Zone (Miller, 2008). The variety includes both NYF (niobium-, yttrium- and fluorine-bearing; Černý, 1991*a,b*; Černý and Ercit, 2005) and LCT (lithium- cesium- and tantalum-bearing; Černý, 1991*a,b*; Černý and Ercit, 2005) pegmatite types, however, none have been identified as mixed LCT-NYF pegmatites. The pegmatites range from either clearly mineralogically zoned to completely homogenous (Keller, 1999). Some authors such as Richards (1986) argue that the pegmatites of the Damara Belt span the entire syn- to post-tectonic history, whereas others suggest that they are exclusively post-tectonic in age (Kinnaird and Nex, 2007; Ashworth, 2013; Fuchsloch et al., 2018*a*). It is, however, generally accepted that they represent the youngest magmatism in the orogen, being the last phase of granitic magmatism to crystallise, regardless of earlier dated syn-tectonic pegmatites (Richards, 1986; Longridge, 2012; Ashworth, 2013; Fuchsloch et al., 2018*a*). Various authors have dated the pegmatites to occur from approximately 509-429 Ma (Briqueu et al., 1980; Diehl, 1993; Longridge, 2012; Melcher et al., 2013). Table 1.2 summarises the various ages obtained for Salem-type granites, Red and Grey granites and pegmatites in the Damara belt.

Pegmatites in the Damara Belt are divided into several major pegmatite belts that occur throughout the tectonostratigraphic zones (Fig 1.4). The boundaries of the pegmatite belts are not clearly defined, and several different authors show maps indicating the position of the belts with slightly different boundary locations and extensions (e.g. Richards, 1989; Keller, 1999; Ashworth, 2013; Fuchsloch et al., 2018*a*). The names of the belts differ depending on which map is considered and some author's group two pegmatite belts into one. For example, Keller (1999) groups the

Otjimbojo pegmatite belt together with the Helicon-Rubicon pegmatite belt to form the Karibib pegmatite belt, also shown in Ashworth (2013) (Fig.1.4; belts E and F). Most authors also agree that the pegmatite belts are bound by and restricted to specific tectonostratigraphic zones, however, when comparing all the available graphical information, these boundaries are vague and overlap into different tectonostratigraphic zones. To add to the confusion, Fuchsloch et al. (2018*a*) also shows no significant geochemical, characteristic or mineralisation style differences between pegmatites of the Cape Cross-Uis pegmatite belt and some pegmatites of the Nainais-Kahero pegmatite belt. What defines the boundaries of the pegmatite belts is currently unclear and many pegmatites within the different belts share many similarities.

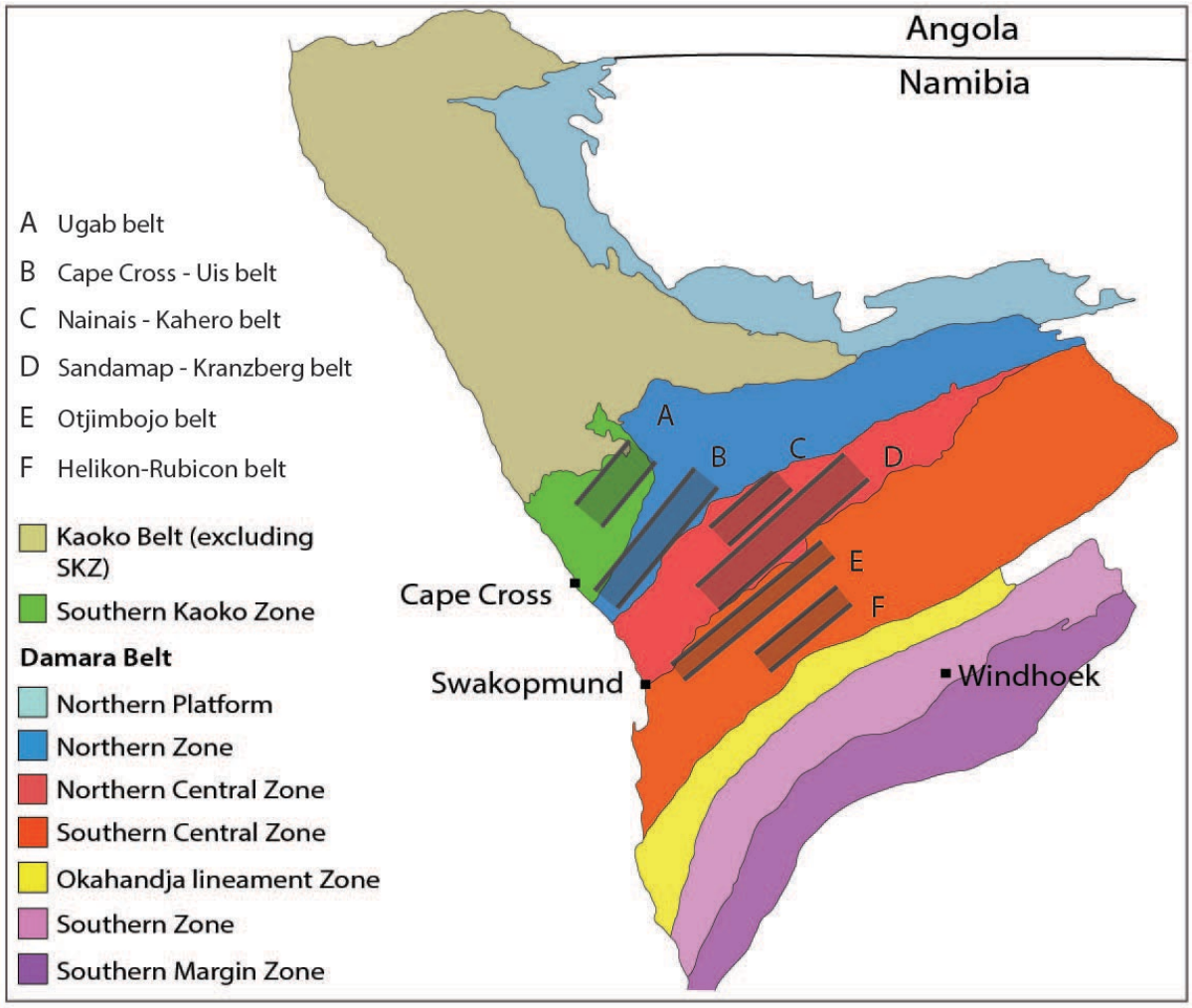


Figure 1.4: Pegmatite belts within the Damaran tectonostratigraphic zones. This image is a modified version of Figure 1.2 that has the pegmatite belts of the Damara Belt superimposed over the tectonostratigraphic zones (From Fuchsloch et al., 2018*a*).

The pegmatite belts of the Damara Orogen in geographical summary remain poorly defined, however, this is mainly due to the high frequency of new pegmatites being discovered, large and small, either by on the ground inspection or by satellite imagery. Similarly, most studies tend to focus on the larger and well mineralised pegmatites of each belt instead of understanding the extent and boundaries of belts (e.g. Ashworth, 2013; Grassi, 2014). Overall different pegmatite types, mineralisation styles and element enrichments are not restricted to specific belts and may occur in one or more of the pegmatite belts.

Table 2.2: Summarised ages of the Salem-type granites, Red and Grey granites and pegmatites within the Damara Belt.

Rock	Method	Age (Ma)	Reference
Salem granites			
Salem-type granite	Rb-Sr whole-rock	601 ± 79	Marlow (1983)
Salem-type granite	Rb-Sr whole-rock	563 ± 63	Hawkesworth et al. (1983)
Salem-type granite	Rb-Sr whole-rock	554 ± 17	Kröner (1982)
Sorris Sorris granite	U-Pb discordia	542 ± 19	Milani et al. (2015)
Omangambo granite	U-Pb zircon	527 ± 7	Milani et al. (2015)
Red and Grey granites			
Red granite	U-Pb zircon	539 ± 17	Longridge (2012)
Red granite	Concordant monazite	536 ± 7,2	Longridge (2012)
Goanikontes Red granite	U-Pb discordia	534 ± 7	Briqueu et al. (1980)
Ida Dome grey granite	U-Pb single zircon	542 ± 6	Tack et al. (2002)
Bauwkwab leucogranite	Pb-Pb zircon evaportation	525 ± 1	Jung et al. (1998)
Oetmoed granite	U-Pb monazite, titanite	526 ± 16	Jung et al. (2003)
Grey granite	U-Pb zircon	520 ± 4,2	Longridge (2012)
Garnet-bearing leucogranite	U-Pb zircon	520 ± 4,6	Longridge (2012)
Pegmatites			
Uraniferous leucogranite	Discordant monazite	514 ± 22	Longridge (2012)
Goanikontes uraniferous alaskite	Concordant monazite	508 ± 2	Briqueu et al. (1980)
Rubicon pegmatite	U-Pb columbite	505 ± 2	Melcher et al. (2013)
Rubicon pegmatite	Rb-Sr mineral age	496 ± 30	Haack and Gohn (1988)
Uis pegmatite, K5 mine pit	Rb-Sr whole-rock	496 ± 30	Haack and Gohn (1988)
Uis pegmatite	Rb-Sr muscovite	486 ± 8	Diehl (1993)
Sandamap Noord pegmatite	Rb-Sr whole-rock	473 ± 23	Steven et al. (1993)
Sandamap tin pegmatite	Rb-Sr whole-rock	468 ± 14	Steven et al. (1993)

1.3.1 Sn-Ta-Nb-bearing pegmatites

The Cape Cross-Uis, Nainais-Kahero and Sandamap-Kranzberg pegmatite belts are also known as the Northern, Central and Southern Tin belts respectively (Fig. 1.4; Richards, 1986). This is mainly due to the majority of pegmatites occurring in these belts having a high abundance of tin with minor tantalum, niobium and occasionally lithium mineralisation. These pegmatites are large, unzoned, lensoidal to dyke-shaped bodies that intrude the dominant north-northeast structural fabric of the belts (Richards, 1986; Wagener, 1989; Diehl, 1992*a*, 1993). The pegmatites are of the LCT family and rare-element enriched class. Dominant mineralogy is granitic and minor phases include apatite, tourmaline, lepidolite, petalite, spodumene, columbite group minerals, cassiterite, and beryl depending on the complexity of the pegmatite. Historically these pegmatites have been mined at a scale varying from major production (e.g. Uis mine; Chapter 2) to artisanal workings.

1.3.2 Li-Be-bearing pegmatites

The Rubicon and Helicon pegmatites of the Rubicon-Helicon pegmatite belt (Fig 1.4; Richards, 1986), or Karibib pegmatite belt (Keller, 1999), are the classic examples of the Li-Be-bearing pegmatites in the Damara Belt. However, other examples also occur in other pegmatite belts, for example, the Petalite pegmatite in the Cape Cross-Uis pegmatite belt (Fig. 1.4; Chapter 2). These pegmatites are large, symmetrically to asymmetrically complexly zoned and lensoidal in shape. They display the classic granitic mineralogy common to pegmatites (London, 2008) with a variety of accessory minerals common to the LCT family pegmatites (Černý and Ercit, 2005). These minerals include petalite, lepidolite, beryl, amblygonite, pollucite, bismuth and bismuth oxides, apatite, and tourmaline. The Li-Be-bearing pegmatites are the most extensively studied pegmatites in the Damara Belt (e.g. Roering, 1963, 1964, 1966; Diehl and Schneider, 1990) focusing on mapping and mineral chemistry. The Helicon and Rubicon pegmatites have been mined since the 1950s for Li, Cs, Be and Ta, however, more recently they have been reworked for industrial minerals such as quartz (Diehl, 1992*b*).

1.3.3 Tourmaline- and gem-bearing pegmatites

Tourmaline is generally a ubiquitous mineral to the pegmatites of the Damara Belt; however, most tourmaline occurs at an economically minable scale in the Otjimbojo and Helicon-Rubicon

pegmatite belts (Fig. 1.4). The Usakos, Omapyu and Beckers pegmatites are examples of tourmaline producing pegmatites in Namibia with peak annual production reaching 2580 kg of tourmaline in 1986 in Namibia (Schneider and Seeger, 1992). Gem quality tourmaline occurs as a variety of colours including blue, pink, green, red and watermelon. In addition, the tourmaline- and gem-bearing pegmatites of the Damara Belt host gem quality specimens of beryl and quartz. These LCT family pegmatites are generally large and zoned with most gem-quality minerals occurring in miarolitic cavities (Ashworth, 2013).

1.3.4 Pegmatitic sheeted leucogranites

Also known as uraniferous NYF pegmatites, the sheeted pegmatitic leucogranites occur in the SCZ of the Damara Belt within the Rössing pegmatite belt (southwest portion of the Otjimbojo pegmatite belt; Nex et al., 2001; Kinnaird and Nex, 2007). These pegmatites have an NYF family geochemical signature along with a variety of pegmatitic textures and uranium mineralisation. The Rössing uranium deposit, discovered by exploration in the Rössing area following the first discovery in the 1920s, accounts for approximately 7.5 % of the world's uranium production (Freemantle, 2012; Ashworth, 2013). Currently these pegmatites are the only producers of primary uranium-bearing ore from granitic rocks (Abrahams, 2009). These pegmatites are unique to the Damara Belt as they are the dominant NYF family pegmatite types in the belt, others mostly being of the LCT family.

1.4 Project Aims

The pegmatites of the Cape Cross-Uis belt exhibit unique qualities with varied mineralisation, pegmatite classification, dimensions and characteristics. They occur in a discrete, well-defined area, and up until now, have been subject to little, recent detailed investigations (e.g. Diehl, 1993). Although characteristic variation in the pegmatites is large, the pegmatites have been shown to be co-genetic (Richards, 1986; Wagener, 1989; Diehl, 1993) and provide an excellent opportunity for detailed comparison and studies.

The aim of this project was to characterise the pegmatites of the Cape Cross-Uis pegmatite belt by detailed field geological investigation. In addition, whole-rock geochemical data (major- and trace-element) were obtained for pegmatites and host rocks to further characterise pegmatites and

understand where they potentially fit in the current pegmatite classification scheme. This data was used to evaluate the controls on mineralisation and in particular how country rock association, structure and metamorphic grade affect mineralisation, if at all. Furthermore, in conjunction with this, mineral chemistry data on Ta-Nb and Sn-oxides and tourmaline were used to further understand pegmatite mineralisation and as a tracer of pegmatite petrogenesis.

A pegmatite petrogenetic model was then evaluated using the accumulation of data gathered. The spatial distribution of different mineralisation styles, coupled with above mentioned analyses were used to identify if the pegmatites were derived from a granite parent undergoing fractionation or an individual fluidised partial melt. A potential source for the pegmatites was then investigated and included in the petrogenetic model. Pegmatites of the Cape Cross-Uis pegmatite belt were then evaluated on a regional pegmatite belt scale and compared to the other pegmatite belts of the Damara Orogen.

Chapter 2: Geology of the Cape Cross-Uis pegmatite belt

2.1 Introduction:

The Cape Cross-Uis pegmatite belt (CUPB) is a roughly 120 km in length and 40 km in width, Pan-African age, pegmatite belt that occurs in the Damara Belt, Namibia. The CUPB starts approximately 40 km northeast of Henties Bay and trends east-northeasterly inland as far as the town of Uis (Fig 1.4, 2.1). Twenty-five years have passed since any detailed research has been done on the CUPB which presents a discrete, well defined area for pegmatite research (Richards, 1986; Wagener, 1989; Diehl, 1993). The CUPB is also known as the Northern Tin Belt, representing varied Sn, Ta, Nb and minor Li mineralisation which has been mined sporadically since 1911. Pegmatites in the CUPB intrude various structures within the supracrustal rocks of the Damara Supergroup (Richards, 1986; Keller et al., 1999) as well as Damaran-aged Salem-type or Red and Grey Granites. Pegmatites are granitic in mineralogical composition and, as expected, show considerable variation across the significantly sized pegmatite belt in terms of dimensions, mineralisation, and geochemistry.

To the southeast of the CUPB, approximately 32 km from the town of Uis, the parallel Nainais-Kahero pegmatite belt occurs (NKPB; Fig. 1.4) which is also known as the Central Tin Belt. For comparative purposes, several selected pegmatites from this belt were also studied. The Ta-, Nb- and Sn-bearing pegmatites of the NKPB, which share many characteristics with pegmatites of CUPB, have been subject to even less research (e.g. Richards, 1986). They are also granitic in mineralogical composition (Fuchsloch et al., 2018*a*).

The regional area of the Cape Cross-Uis pegmatite belt at surface is simple. Little to no landforms occur from the coast near Cape Cross up until the start of the Uis swarm. This area is completely flat and mostly consists of sand, gravel, scree and calcrete in an extremely arid setting. Inland, nearing the Uis swarm, occasional elongated ridges begin to occur and become more abundant near the town of Uis which consists of multiple sub-parallel ridges composed of the metasedimentary lithologies of the Amis River Formation. Another geomorphological feature within the regional area are the sporadically occurring granite domes which are more common in the NE portion of the pegmatite belt.

A total of thirty-four pegmatite locations were investigated for the purpose of this study (Fig. 2.2-2.4; Table 2.1; Appendix A). Each location may contain one or more pegmatite bodies which cover a total of 147 samples of host rocks and pegmatites. This chapter outlines the background to CUPB and details the field investigations of this thesis.

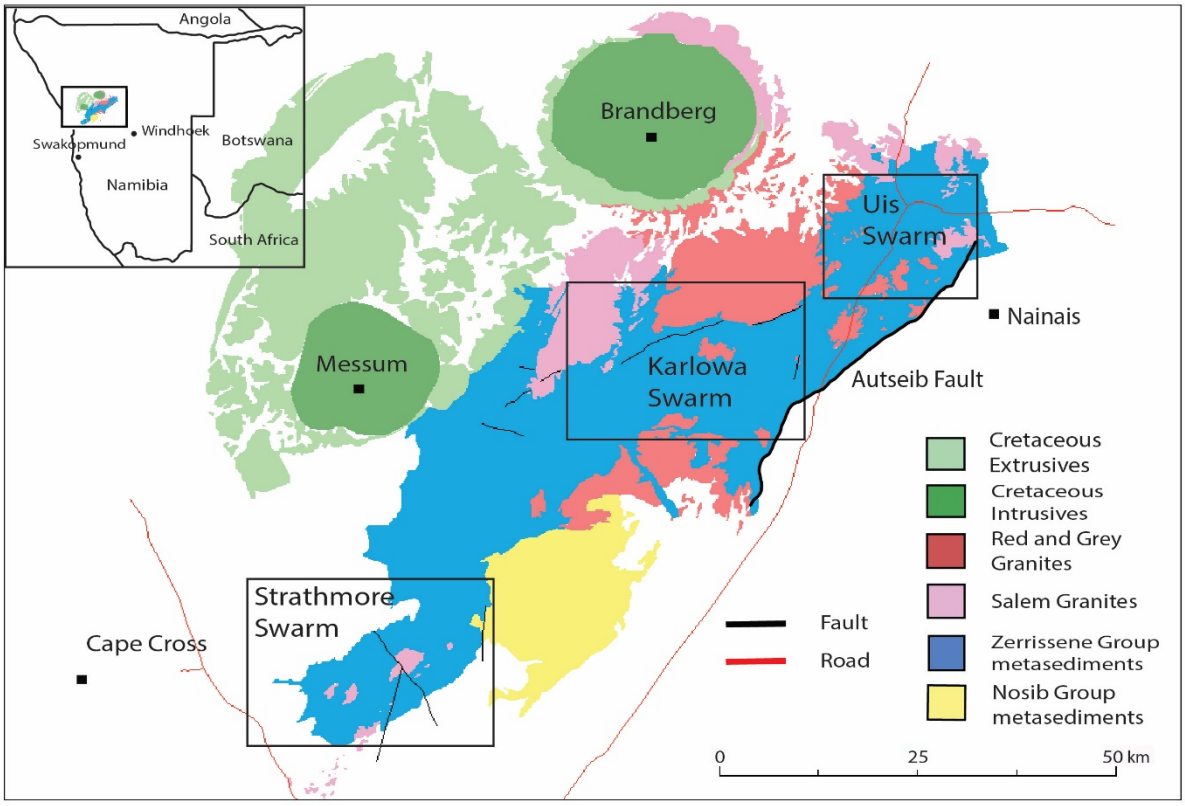


Figure 2.1: Simplified geological map of the Cape Cross-Uis pegmatite belt, Namibia. The map shows the three pegmatite swarms within the pegmatite belt as well as the metasediments and igneous rocks of the Damara Orogen and post-Damaran magmatism (modified after "Geological map of Namibia, Sheet 2114 - Omaruru").

2.2 Research background

2.2.1 Regional setting of the CUPB

The CUPB is located within the Northern Zone of the tectonostratigraphic zones defined by Miller (2008); however, the boundaries of the southwestern portion of the belt are suggested to be located in the Southern Kaoko Zone (Fig. 1.4; Ashworth, 2013). In previous tectonostratigraphic maps (e.g. Miller, 2008) this area of the Damara Orogen is poorly defined as little outcrop exists and defining the boundaries of the tectonostratigraphic zones is difficult. However, more recently, Fuchsloch et al. (2018*a*) suggested that the CUPB is located solely within the Northern Zone since the metasedimentary units that host the pegmatites, uniformly show the same northeast structural

fabric throughout the entire belt whereas metasediments from the Southern Kaoko Zone show a northerly to northwesterly structural orientation. Similarly, the metasediments in the southwestern portion of the CUPB are classified within the same stratigraphic units as the east-northeastern extension on geological maps (Geological map of Namibia, Sheet 2114 – Omaruru). The CUPB represents a half graben which is well-defined in the northeastern extension of the belt (Richards, 1986; Wagener, 1989; Diehl, 1993). The half graben is bounded by the Autseib Fault (Fig. 2.1) which represents the boundary of the CUPB to the southeast and may have been active since Proterozoic times. To the southeast of the Autseib Fault, the NKPB occurs and is located within the Northern Central Zone of the tectonostratigraphic zones defined by Miller (2008) (Fig. 1.4).

The stratigraphy of the CUPB is simple; the entire succession being covered by the Amis River Formation of the Zerrissene Group (Table 1.1; Fig. 2.1; Swart, 1992). The Formation is dominated by biotite schist which may be porphyroblastic and minor metagreywacke and quartzite lithologies. The Amis River Formation has been downthrown by the Autseib Fault against Swakop Group metasediments of the Northern Central Zone (Miller, 1983; Diehl, 1993). The Swakop Group metasediments of the Kuiseb Formation, hosts the NKPB and include porphyroblastic biotite schists similar to the biotite schists of the Amis River Formation and minor calcsilicate, marble and quartzite lithologies (Table 1.1; Miller, 1993; 2008). The Amis River Formation was deposited in a distal basinal sedimentary setting and is classified as a fan fringe deposit or a classical distal outer-fan lobe (Swart, 1992). The sediments were initially regionally metamorphosed to greenschist facies, but later intrusion of Salem-type Granites thermally metamorphosed the Amis River Formation to amphibolite facies giving rise to the porphyroblastic biotite schist known locally as Knotenschiefer. The porphyroblastic 'knots' in Knotenschiefer are pseudomorphs cordierite which have undergone metamorphic retrogression to greenschist facies assemblages of chlorite and Fe-oxides (Richards, 1986; Diehl, 1993). Knotenschiefer lithologies occur sporadically throughout the CUPB and NKPB, some pegmatites being hosted only by biotite schists with no porphyroblasts.

The CUPB also includes the Salem-type and Red and Grey Granites. Salem-type Granites are granodioritic in composition and may be fine- to coarse-grained and porphyritic (Diehl, 1993; Longridge, 2012). They occur throughout the CUPB with large outcrops in the northeastern

extensions. The Red and Grey Granites are monzogranitic in composition and are restricted to the central and northeastern sections of the CUPB (Fig. 2.1). The Nosib Group is also present in the south-central area of the belt and consists of gneiss, quartzite, conglomerate, biotite schist and metarhyolite of the Tsaun and Khan Formations (Diehl, 1993; Miller, 2008; Fig. 1.2). However, no pegmatites as of yet have been known to occur within the Nosib Group.

Pegmatites of the CUPB dominantly intrude the metasedimentary lithologies whereas some of the pegmatites intrude both the Salem-type and Red and Grey Granites. The CUPB has been subdivided into three pegmatite swarms known, from west to east, as the Strathmore, Karlowa and Uis swarms (Richards, 1986; Diehl, 1992*a*, 1993; Fig. 2.2-2.4 respectively). These swarms are localised areas in which a large number of pegmatites outcrop even though individual pegmatite bodies may occur throughout the CUPB. The Strathmore and Uis swarms include 10s to 100s of individual pegmatite bodies whereas the Karlowa swarm is less abundant. The pegmatites in the different swarms are generally similar in characteristics but certain features are unique to specific swarms (Chapter 4; Fuchsloch et al., 2018*a*).

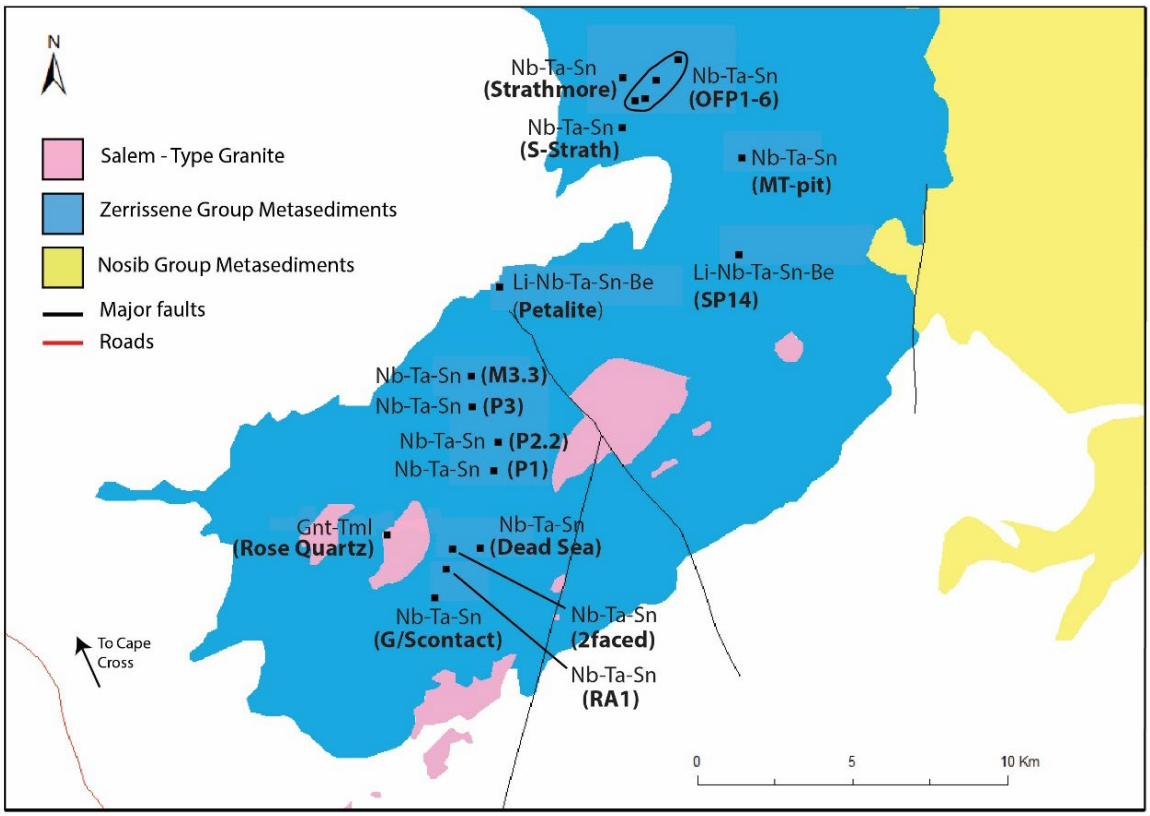


Figure 2.2: Simplified geological map of the Strathmore swarm showing each pegmatite location and pegmatite type studied in the swarm (Table 2.1).

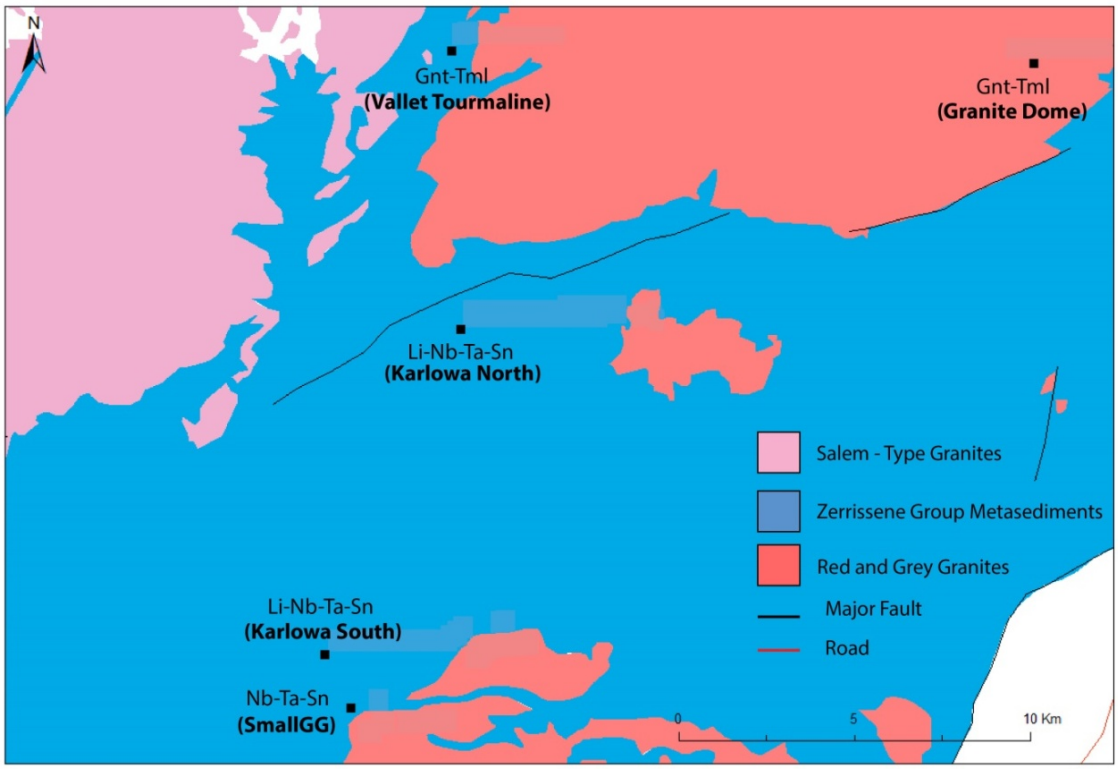


Figure 2.3: Simplified geological map of the Karlowa swarm showing each pegmatite location and pegmatite type studied in the swarm (Table 2.1).

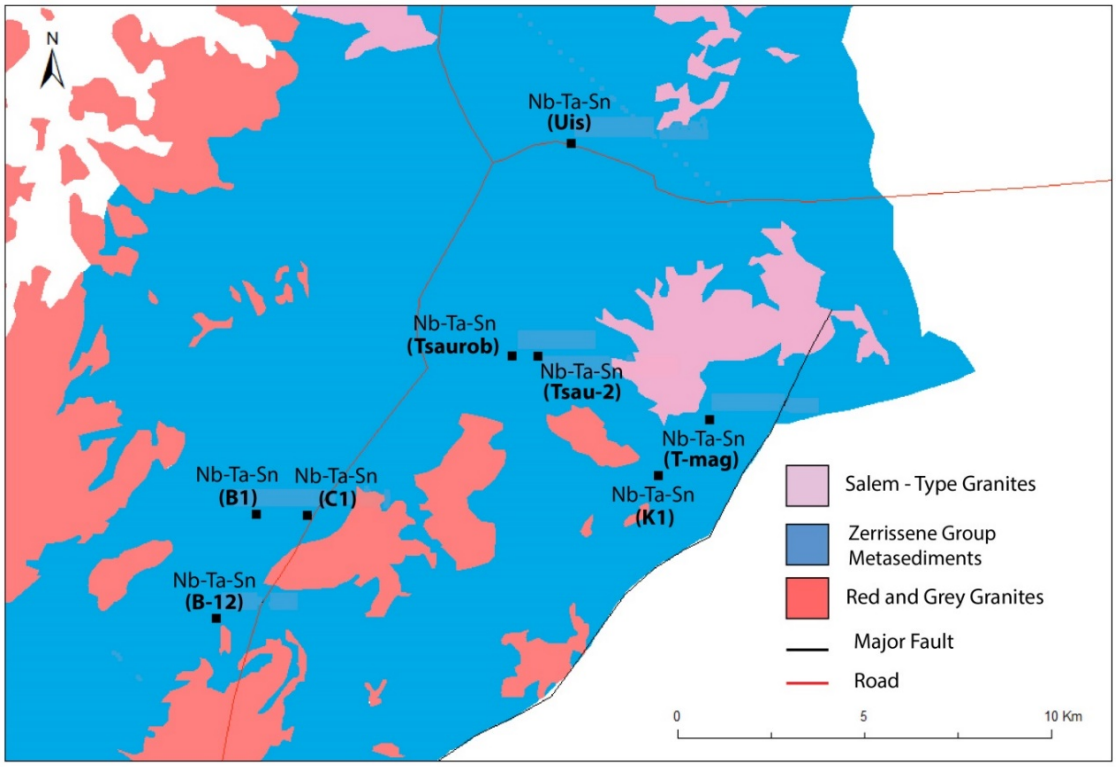


Figure 2.4: Simplified geological map of the Uis swarm showing each pegmatite location and pegmatite type studied in the swarm (Table 2.1).

2.2.2 Pegmatites of the Cape Cross-Uis pegmatite belt

Richards (1986) first proposed that the pegmatites of the CUPB are genetically related to the Salem-type Granites in the classical Jahns and Burnham (1969; Chapter 3) model which was supported by other earlier authors such as Wagener (1989) and Diehl (1993). Later work by Ashworth (2013) began to question the relationship of the Damara Orogen pegmatites to the I- and S-type granitic intrusions, suggesting that pegmatites possibly originated by anatexis instead of sharing a petrogenetic link with granites. More recent work by Fuchsloch et al. (2018*a*) also favours a partial melting origin of pegmatites and develops a clearer understanding of the petrogenesis of pegmatites from the CUPB (Chapter 4). The Uis pegmatites (Fig. 2.4) of the CUPB were first dated by Haack and Gohn (1988) who found an age of 496 ± 30 Ma based on Rb-Sr data. Diehl (1993) similarly dated the Uis pegmatites at 486 ± 8 Ma using Rb-Sr data in muscovite. More recently Melcher et al. (2015) reported an emplacement age of 0.5 Ga for the Uis pegmatites, however, no reference was made to how this age was obtained or sourced.

Pegmatites in the CUPB are granitic in composition, their primary mineralogy consisting of quartz, albite, microcline perthite, microcline and muscovite. Accessory mineralogy includes columbite group minerals (CGM), cassiterite, Fe-oxides, monazite, zircon, garnet, apatite, beryl, tourmaline, petalite, spodumene and lepidolite. Secondary phases are present in the form of hectorite ($Na_{0.3}(Mg,Li)_3Si_4O_{10}(OH)_2$), cleavelandite, eucryptite and new or recrystallised albite, muscovite and quartz (Richards, 1986; Wagener, 1989; Diehl, 1993; Ashworth, 2013; Melcher et al., 2015; Fuchsloch et al., 2018*a*). The pegmatites have a dominant northeast to north-northeast structural orientation which is parallel to sub-parallel with the regional CUPB metasedimentary host rock fabric. They intrude many structural features within the belt such as D_3 moderately- to steeply-inclined folds which have been attributed to the shorting and convergent phases of the Damara Orogen (Diehl, 1993; Goscombe et al., 2004; Gray et al., 2006; Macey and Harris, 2006). In structural summary, the pegmatites of the CUPB take advantage of the many structural weaknesses in the Northern Zone, intruding predominantly aligned to northeast-oriented structural fabric of the belt.

The pegmatites in the CUPB have been classified as LCT-type, rare-element enriched according to the currently accepted classification scheme (Černý and Ercit, 2005; Diehl, 1993), however,

pitfalls in this classification scheme have led authors such as Fuchsloch et al. (2018*a*) to re-examine their classification (Chapter 4). The pegmatites generally exhibit no mineralogical zonation and are mineralogically homogeneous intrusions. However, some larger, Li-mineralised pegmatites show complex, asymmetrical mineralogical zonation (Petalite; Fig. 2.2; Diehl, 1993). Other pegmatites also show a crude mineralogical zonation where a clear quartz core zone and border zone are present (e.g. C1, Rose Quartz; Fig. 2.2, 2.4 respectively), however, they lack the hallmark requirements to fully classify them as mineralogically zoned pegmatites (Chapter 3; London, 2008; Fuchsloch et al., 2018*a*).

The morphologies of the pegmatites in the CUPB are generally consistent, being lensoidal in shape, between 2 and 40 m in thickness and showing impressive lengths, with some pegmatites reaching up to several hundred metres long (Richards, 1986; Diehl, 1993, Ashworth, 2013). However, pegmatites occur on all scales and thin, 1-2 cm pegmatite veins occur but are normally offset intrusions of a main pegmatite body. These smaller pegmatites are more undulating in shape but display the common mineralogy associated with the larger bodies. Less common morphologies include host rock bedding parallel dykes (e.g. Nainais; Fig. 2.1), and pods and sigmoids (e.g. Karlowa North; Fig. 2.3; Ashworth, 2013). Pegmatite emplacement may be simple with an individual pegmatite body being continuous and adhering to a specific morphology, however, some intrusions are complexly arranged, showing bifurcating bodies that pinch out or converge in different areas. These complexly intruded bodies are generally a hallmark for the larger pegmatites, where the extensions of the body show large changes in thickness and bifurcate with depth or length and possibly also include large metasediment xenoliths within the pegmatite body.

Alteration in the pegmatites is ubiquitous in the CUPB and occurs on the macro- and micro-scale. Pegmatites show significant greisenisation or albitised zones that are generally associated with Ta-Nb- and Sn-mineralisation (Appendix D). Greisens may be extensive zones within the mineralogically zoned pegmatite bodies and consist solely of new or recrystallised quartz and muscovite (e.g. Petalite; Fig. 2.2; Diehl, 1993; Fuchsloch et al., 2018*a,b*). Some greisens are lensoidal in shape whereas others occur as parallel-sided layers that extend for several metres along the strike of a pegmatite (Fuchsloch et al., 2018*a*). Greisens may also show partial alteration and occur sporadically, but abundantly, throughout a pegmatite body. Albitised zones are less common

and generally consist of fine-grained, equigranular albite giving the rock a saccharoidal texture. They occur in similar morphologies to greisens and show partial to complete alteration depending on the pegmatite. Subsolidus alteration by external fluids is rare, being limited to the weathering zones within pegmatites. Due to the dry arid nature of the area, generally fresh outcrop is available near-surface. Therefore, the term alteration within this thesis describes internal alteration by late stage fluids which are derived from the pegmatite.

2.2.3 Pegmatite mineralisation

Recorded mining in the CUPB first occurred just after the Uis pegmatites discovery in 1911. Mining has been sporadic throughout the CUPB, with the largest operations conducted in the Uis swarm due to the size and quantity of pegmatites in the area. Large-scale operations peaked in Uis in the 1950s when production rates reached 14 000 kg of tin concentrate a month (Diehl, 1992*a*,*b*). In the 1990s production ceased due to the low tin price at the time. Subsequently, artisanal mining of the pegmatites has occurred for cassiterite and columbite-group minerals.

Most of the previous research surrounding the CUPB focused on aspects of mineralisation up until this study (Richards, 1986; Wagener, 1989; Diehl, 1993; Singh 2007, 2008). The pegmatites in the CUPB generally show Sn, Ta and Nb mineralisation, however, many pegmatites may also be completely barren or, more rarely, contain Li-mineralisation. Sn mineralisation is contained solely in cassiterite whereas Ta and Nb mineralisation is dominantly present in the columbite-group minerals and tapiolite (Fuchsloch et al., 2018*b*). Sn- and Ta-Nb-bearing phases mostly occur in highly altered areas within pegmatites such as greisens and albitised zones, however, lower abundances of these phases have also been observed in magmatic zones with little to no alteration and an equigranular magmatic texture (Diehl, 1993; Fuchsloch et al., 2018*a*). Lithium mineralisation dominantly occurs as both petalite and spodumene, however, minor lepidolite has been observed in some pegmatites and eucryptite occurs as a secondary Li-bearing phase (Diehl, 1993; Fuchsloch et al., 2018*a*). Li-mineralisation does not co-exist with any of the Sn- and Ta-Nb-bearing phases and is mostly found in discrete zones near the quartz core of mineralogically zoned pegmatites (Fuchsloch et al., 2018*a*). Ashworth (2013) suggested that constitutional zone refining and undercooling during fractional crystallisation (Chapter 3) was responsible for Li-mineralisation in these zones which is consistent with research by London (2008).

Early researchers such as Richards (1986) and Wagener (1989) first suggested that Sn mineralisation in pegmatites has an association with the metasedimentary host rocks that the pegmatites intruded into. They theorised, which was later supported by Diehl (1993) and Singh (2007, 2008), that high grade Sn pegmatites were exclusively associated with the Knotenschiefer host rock. The hypothesis is that the pegmatites either melted and assimilated Sn-rich host rock, thereby increasing Sn concentrations in the pegmatite melt, or that late-stage pegmatitic fluids, responsible for alteration and greisenisation, selectively remobilised Sn from host rocks and subsequently crystallised cassiterite in the alteration zones observed in pegmatites (Diehl, 1993). Therefore Sn-rich country rocks are a prerequisite to abundant Sn mineralisation in pegmatites. Diehl (1993) went further to add that mineralisation also has a geographic control whereby Sn mineralisation and metamorphic grade both increase westward towards the Atlantic Ocean. Richards (1986) also noted that the abundance of tourmaline within the host rock is an indicator of a well Sn mineralised pegmatite.

These authors did not consider that mineralisation may be spatially associated with granites, if pegmatites are petrogenetic by-products of granites in the Jahns and Burnham (1969) and subsequent modified models (e.g. London, 2008; Simmons, 2008). This model would imply that mineralisation abundances are controlled by the distance the pegmatites are found from granites (Chapter 3). Furthermore, no assimilation indicator tests were conducted, such as the Fe and Mg concentrations in both the host rocks and pegmatites.

2.3 The pegmatite groups of the Cape Cross-Uis pegmatite belt

In a recent study, Fuchsloch et al. (2018*a*) characterised the pegmatites of the CUPB based on detailed field work and whole-rock geochemistry. Due to the pitfalls associated with currently accepted pegmatite classification schemes, they divided the pegmatites of the CUPB into three unique groups based on mineralogy, pegmatite zonation, and host rock type (Section 2.3.1-2.2.3 respectively). The three groups are as follows: 1. The Sn-, Ta- and Nb-mineralised, unzoned to crudely zoned pegmatites, 2. The Garnet-Tourmaline, crudely zoned pegmatites and 3. The Li-mineralised, complexly to crudely zoned pegmatites. The third group was then further subdivided based on the Li-bearing bearing phase present into the Li-Nb-Ta-Sn spodumene-bearing, crudely

zoned pegmatites and the Li-Nb-Ta-Sn-Be petalite-bearing, complexly zoned pegmatites. The Nainais pegmatites, studied for comparison, were also characterised and due to little differences in their whole-rock geochemistry, mineralogy and morphology, Fuchsloch et al. (2018*a*) grouped them together with the Nb-Ta-Sn pegmatites. The following section describes the field geology of twelve of the large, interesting pegmatites in the CUPB studied in this thesis. A total of thirty-four pegmatite locations were studied (Fig. 2.2-2.4) and sampled. Table 2.1 shows all the different pegmatites and their classification, important features and geographic location.

2.3.1 The CGM-cassiterite pegmatites (Nb-Ta-Sn type)

The Nb-Ta-Sn type pegmatites are the most common pegmatite type in the CUPB, constituting 28 out of the 34 pegmatite locations studied. They typically occur in abundance in the Strathmore and Uis swarms – the Uis swarm having only Nb-Ta-Sn type pegmatites. They generally intrude strike-parallel to host rocks; sometimes showing metasomatic contacts, have a bifurcating emplacement style and are not mineralogically zoned (Fuchsloch et al., 2018*a*). The dominant mineralogy is granitic, consisting of quartz, albite, perthite, microcline and muscovite. Associated mineralogy includes tourmaline, garnet and apatite that have no affinity to specific zones within the pegmatites. Greisens and albitised zones are common features in these pegmatites with associated Sn- and Nb-Ta-bearing phases (Fuchsloch et al., 2018*a*) and minor ilmenite and other Fe-Mn-bearing phases. They are simple in thin section, mostly displaying myrmekitic textures, sericitic alteration of feldspars and little to no deformational features. Greisens and albitised zones within these pegmatites show highly altered characteristics, completely changing the mineralogy of the sample (E.g. fine-grained equigranular albite with a 95 % modal abundance).

2.3.1.1 The 2faced pegmatite

The 2faced pegmatite is a crudely zoned Nb-Ta-Sn type pegmatite in the southwest of the Strathmore swarm (Fig. 2.2, 2.5). The pegmatite locality consists of two medium sized excavations that are perpendicular to the northwest strike of the pegmatite. The excavations are approximately 30 m in length and depict an almost vertical pegmatite dip to the southwest.

Table 2.1: Table summarising the pegmatites of the Cape Cross-Uis pegmatite belt studied. The table shows their geographic location, pegmatite type, host rock and common mineralogy. Qtz. = quartz; musc. = muscovite; alb. = albite; tml. = tourmaline; apt. = apatite; CGM. = columbite group minerals; cass. = cassiterite; gnt. = garnet.

Location	GPS coordinates	Pegmatite type	Host rock	Common mineralogy
Rose Quartz	33K 414455E 7591134S	Gnt-Tml	Salem-type Granite	Qtz+musc+perthite+alb++tml+gnt
Villet tourmaline	33K 454218E 7642985S	Gnt-Tml	Salem-type Granite	Qtz+musc+perthite+tml+gnt+biotite
Granite dome	33K 470754E 7642534S	Gnt-Tml	Red/Grey granite	Qtz+musc+alb+microcline+tml+gnt
Karlowa South	33K 450412E 7625801S	Li-Nb-Ta-Sn	biotite phyllite	Qtz+musc+alb+tml+apt+CGM+cass
Karlowa North	33K 454523E 7635094S	Li-Nb-Ta-Sn	biotite phyllite	Qtz+musc+alb+apt+CGM+cass
Petalite	33K 418205E 7598978S	Li-Nb-Ta-Sn-Be	Knotenschiefer and biotite schist	Qtz+musc+perthite+microcline+alb+tml+apt+CGM+ cass+beryl+eucryptite+petalite+hectorite
Strathmore	33K 417320E 7595887S	Nb-Ta-Sn	Knotenschiefer and quartzite	Qtz+musc+perthite+alb+microcline+apt+CGM
Off pit 1	33K 422891E 7604774S	Nb-Ta-Sn	Biotite schist	Qtz+musc+alb+apt+CGM+cass
Off pit 2	33K 423620E 7605575S	Nb-Ta-Sn	Biotite schist and Knotenschiefer	Qtz+musc+alb+apt
Off pit 3	33K 423868E 7606051S	Nb-Ta-Sn	Biotite schist	Qtz+musc+perthite+alb+apt
Off pit 4	33K 423183E 7605622S	Nb-Ta-Sn	Biotite schist	Qtz+musc+alb+apt
Off pit 5	33K 423260E 7605318S	Nb-Ta-Sn	Biotite schist	Qtz+musc+alb+apt+CGM+cass
Off pit 6	33K 422577E 7604687S	Nb-Ta-Sn	Biotite schist	Qtz+musc+perthite+alb+apt
P1	33k 417930E 7593110S	Nb-Ta-Sn	Biotite schist	Qtz+musc+perthite+alb+tml+apt+CGM
P3	33K 417275E 7595082S	Nb-Ta-Sn	Biotite+musc schist	Qtz+musc+alb+tml+apt+CGM+cass
P2.2	33K 418120E 7594059S	Nb-Ta-Sn	Knotenschiefer	Qtz+musc+alb+tml+gnt+apt+CGM+cass
Uis Tin mine	33K 487318E 7653536S	Nb-Ta-Sn	biotite schist and Knotenschiefer	Qtz+musc+alb+perthite+microcline+tml+apt+cass
Dead Sea	33K 417597E 7590792S	Nb-Ta-Sn	Knotenschiefer	Qtz+musc+alb+tml+CGM
2faced pegmatite	33K 416711E 7590664S	Nb-Ta-Sn	biotite schist	Qtz+musc+perthite+alb+tml+apt+CGM
RA1	33K 416618E 7590162S	Nb-Ta-Sn	Knotenschiefer	Qtz+musc+alb+microcline+tml
G/S contact	33K 416126E 7589229S	Nb-Ta-Sn	Biotite schist	Qtz+musc+perthite+alb+microcline+CGM
MT-pit	33K 426019E 7602831S	Nb-Ta-Sn	Biotite schist	Qtz+musc+perthite+alb+tml+apt+CGM
S-Strath	33K 422125E 7603925S	Nb-Ta-Sn	Knotenschiefer	Qtz+musc+perthite+alb
M3.3	33K 417320E 7595887S	Nb-Ta-Sn	Biotite schist and quartzite	Qtz+musc+perthite
SmallGG	33K 451833E 7623573S	Nb-Ta-Sn	biotite phyllite	Qtz+musc+microcline+alb+tml
B-12	33K 477708E 7640808S	Nb-Ta-Sn	biotite phyllite and quartzite	Qtz+musc+alb+tml+apt+CGM+cass
C1 pegmatite	33K 479892E 7643173S	Nb-Ta-Sn	Biotite phyllite	Qtz+musc+alb+apt+CGM
B1 pegmatite	33K 478771E 7643555S	Nb-Ta-Sn	Biotite schist	Qtz+musc+alb+apt+CGM+cass
Tsaurob	33K 485594E 7647607S	Nb-Ta-Sn	Biotite phyllite	Qtz+musc+perthite+alb+tml+apt+CGM+cas+ lepidolite
Tsau -2	33K 486304E 7647766S	Nb-Ta-Sn	Knotenschiefer	Qtz+musc+perthite+microcline+alb+tml+apt+CGM+cass
K1-pegmatite	33K 0489021E 7644325S	Nb-Ta-Sn	Biotite schist	Qtz+musc+alb
T-mag	33K 490832E 7646084S	Nb-Ta-Sn	Biotite schist	Qtz+musc+alb+microcline+tml
Nainais	33K 506883E 7628269S	Nb-Ta-Sn	Knotenschiefer and biotite schist	Qtz+musc+perthite+alb+tml+apt+CGM+cass
Aubinhonis (Nainais)	33K 513392E 7632584S	Nb-Ta-Sn	Biotite schist	Qtz+musc+microcline+alb+tml+lepidolite

The 2faced pegmatite is roughly pod-like in shape with a 35 m thickness at its centre. Due to lack of outcrop outside the excavations the full extensions of the pegmatite body are currently unknown. However, the pegmatite does appear to bifurcate in the eastern section, enclosing biotite schist host rock. Small, cm-scale pegmatite veins are associated with the large pegmatite body mostly near host rock contacts. Sigmoidal pegmatites, 2-3 cm in size, intrude tension gashes that are located in the north section of the host rock, indicating a σ_1 and σ_3 orientation of 6° and 186° respectively (Fig. 2.6A). Biotite schist host rocks are medium- to coarse-grained and are often layered as shown in Figure 2.6A. The lighter felsic layers have less biotite, are mostly composed of quartz and show cm-scale folds with similar σ_1 and σ_3 orientations as tension gashes, indicating a tectonic origin.

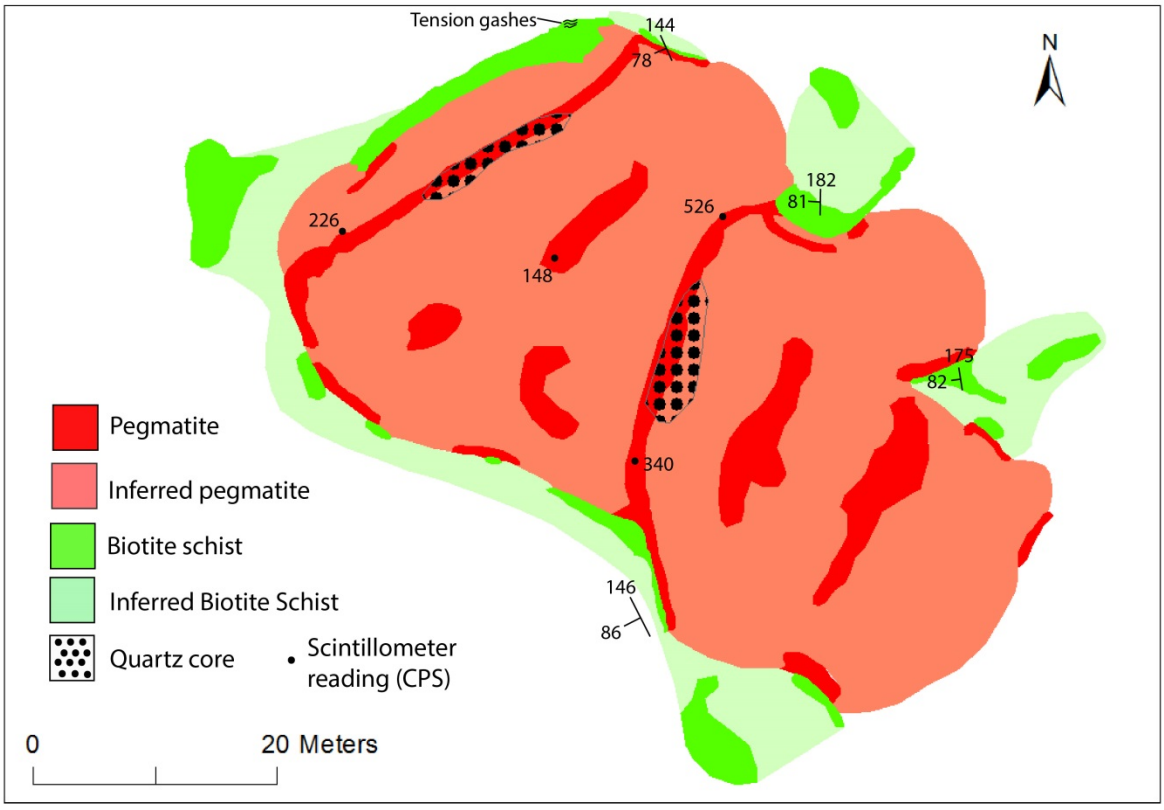


Figure 2.5: Geological map of the 2faced pegmatite showing the location of pegmatite-intruded tension gashes and the quartz core of the pegmatite. The two quartz core locations are in the two excavations that run perpendicular to the pegmatite strike.

The 2faced pegmatite is crudely zoned, exhibiting a prominent quartz core in both perpendicular excavations. The quartz core is traceable across excavations with a similar strike to that of the pegmatite body. Near the quartz core, rectangular shaped black minerals that appear to have a secondary precipitate origin occur (minerals occur at the weathered surface of the outcrop). These grains give scintillometre readings of up to 526 counts per second (Fig. 2.5, 2.6B). The pegmatite

displays a micaceous and tourmaline-rich border zone on contact with host rocks where muscovite and tourmaline have a unidirectional solidification texture (UST). The intermediate zone is a homogeneous mass of coarse- or fine-grained quartz, feldspar and muscovite. Finer-grained areas show thin layers of pegmatite banding of alternating layers rich in muscovite (Fig. 2.6C). The thin muscovite-rich layers contain fine-grained columbite group minerals (CGM) and apatite and show significant sericitic alteration in thin section as opposed to the muscovite-poor, aplitic albite dominated layers. The muscovite-rich layers represent greisenisation in thin, banded layers in the intermediate zone. Macroscopic graphic intergrowths of quartz and feldspar are also a common texture of the minerals in the coarser-grained areas in the intermediate zone (Fig. 2.6D).

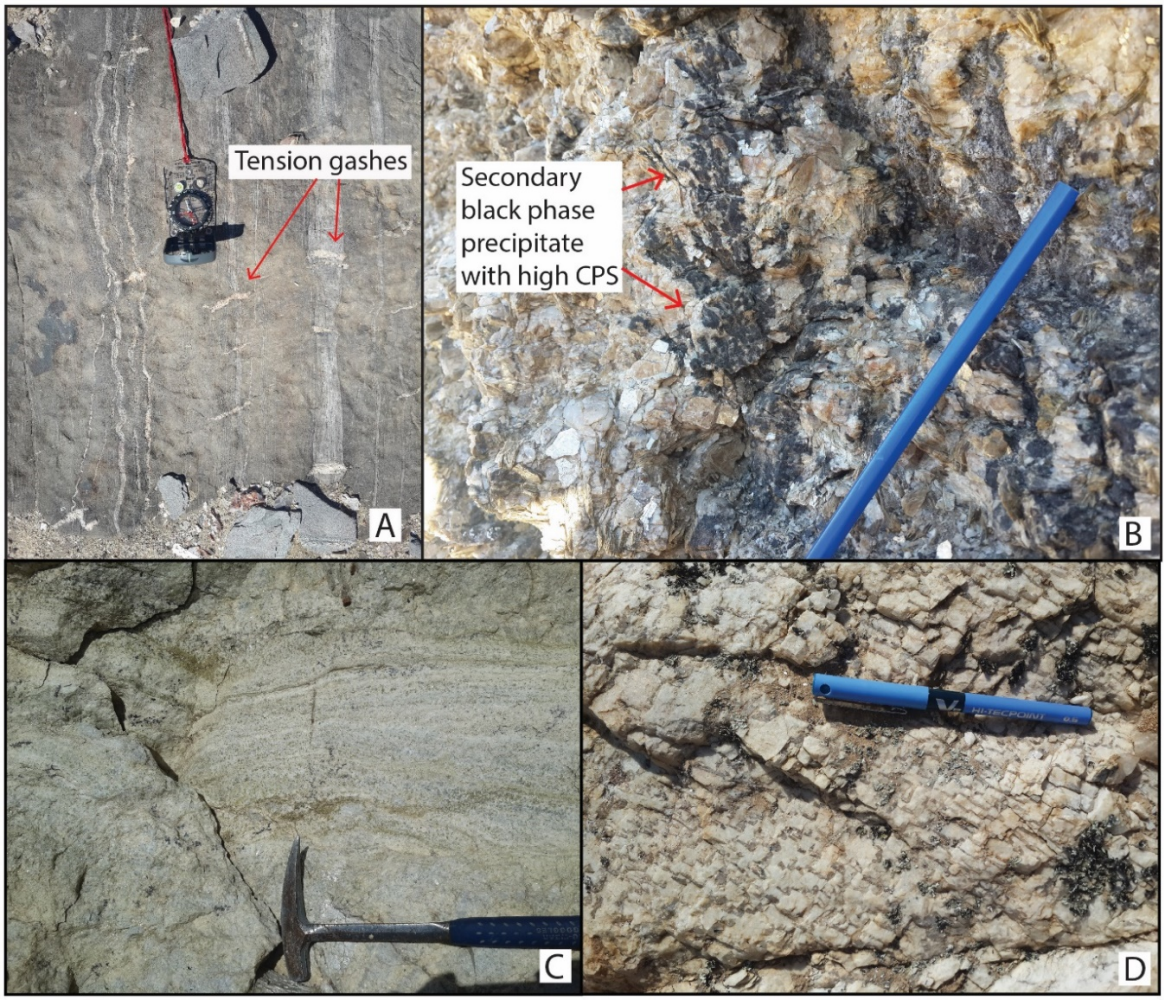


Figure 2.6: Field outcrop photographs of features in the pegmatite and host rock biotite schist at the 2faced pegmatite locality. A) Cm-scale tension gashes in biotite schist country rock that have been intruded by small sigmoidal shaped pegmatites. B) Secondary precipitate, rectangular black minerals in the intermediate zone of the 2faced pegmatite. These zones have scintillometre readings of approximately 526 counts per second. C) Pegmatite layering in the intermediate zone of the 2faced pegmatite. D) Graphic intergrowths of quartz and feldspars in the intermediate zone of the pegmatite.

2.3.1.2 The P2.2 pegmatite

The geological maps of P2.2, Strathmore, MT-pit and SmallGG are shown in Figure 2.7A-D respectively. The P2.2 pegmatite locality occurs approximately in the central part of the Strathmore swarm and has a dominant north-northeast structural orientation (Fig. 2.2). The location consists of two historical mining pits in the northeast and southwest of the locality. The northwest steeply dipping pegmatite outcrop may be linked across both excavations and possibly indicates a large pegmatite, 350 m in length (Fig. 2.7A). The pegmatite in both pits has an approximate 10 m thickness and a simple intrusion style. It is roughly continuous and has a sigmoidal shape when linking the pegmatite outcrop over the two excavations.

The P2.2 pegmatite intrudes Knotenschiefer which has a strong northeast oriented schistosity. The Knotenschiefer is composed of quartz, biotite and minor muscovite and includes 1 cm in size retrogressed cordierite porphyroblasts ("knots"). Host rock contacts are highly metasomatised and tourmalinised, being composed of large poikilitic tourmaline grains, recrystallised quartz and minor muscovite. Biotite is almost absent from these metasomatised host rocks. Tourmaline and blebby quartz in some cases appears to have a graphic texture in the thin sections of these samples, like that of the classical quartz and feldspar intergrowths within pegmatites. The sample also contains opaque grains which are probably cassiterite as these rocks have significantly higher Sn quantities compared to the unaltered host rocks (Fuchsloch et al., 2018*a*).

The P2.2 pegmatite is an unzoned homogeneous body composed dominantly of albite and quartz, however, the contact of the pegmatite shows higher abundances of muscovite and tourmaline. Alteration within the pegmatite is sporadic and is located in areas richer in muscovite and quartz in the internal sections of the body (Fig. 2.7A). These partially greisenised zones contain minor subhedral cassiterite and euhedral CGM grains (highly reflective rectangular grains). Apatite is also a common mineral to the alteration zones and is normally associated with the CGM and cassiterite mineral assemblages whereas tourmaline rarely co-exists with Sn-Nb-Ta mineralisation. Larger quartz and feldspar grains are rimmed by finer-grained crystalline quartz, muscovite and specular hematite. Some larger albite grains are kink-folded, where finer grained quartz and muscovite occur in the fold hinge of the larger albite grain. The folds in the grains are sharp (kink to chevron folds) and not curved as in magmatically folded albite grains.

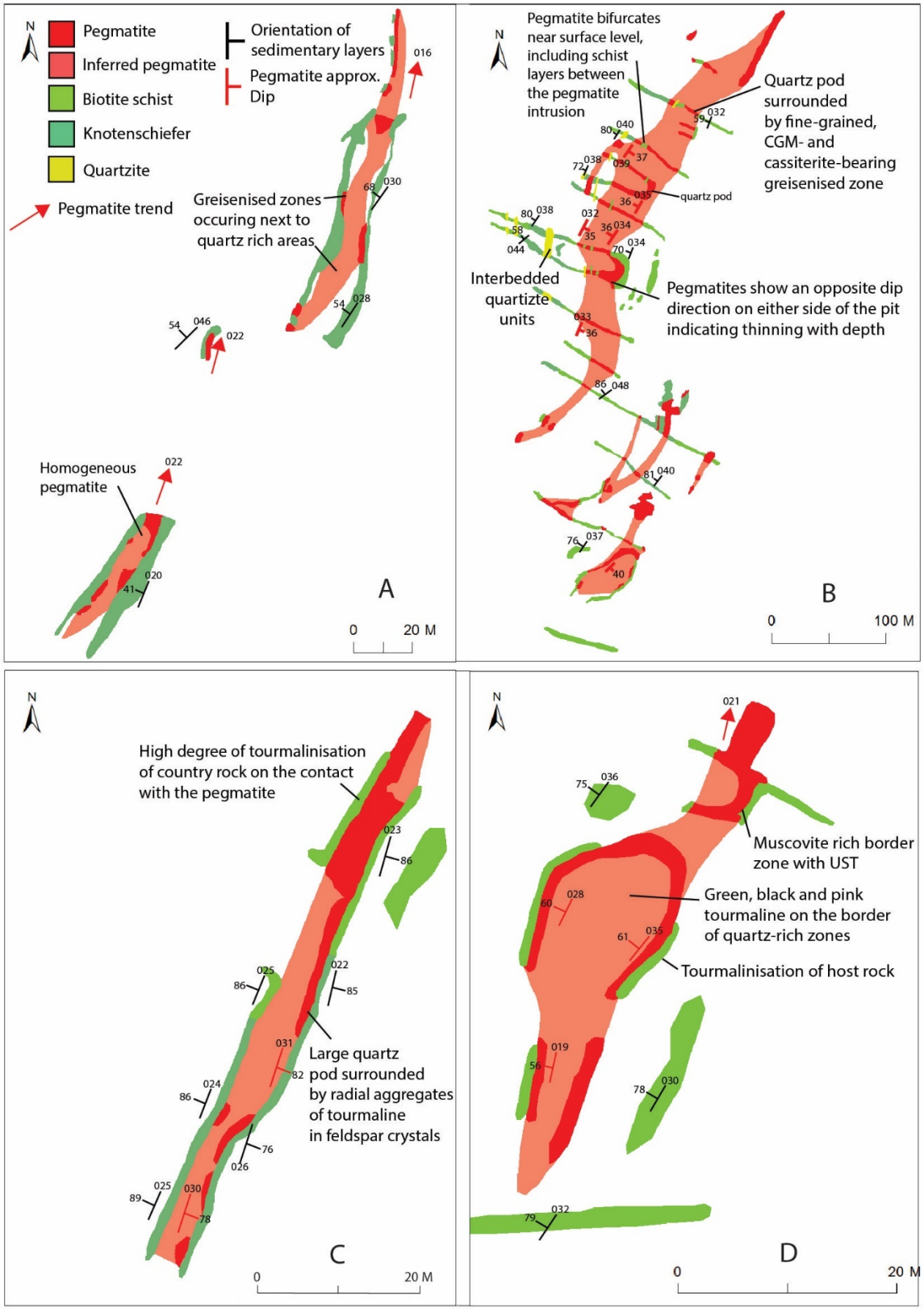


Figure 2.7: Geological maps of the following localities (see text for descriptions). A) the P2.2 pegmatite – section 2.3.1.2. B) The Strathmore pegmatites – section 2.3.1.3. C) The MT-pit pegmatite – section 2.3.1.4. D) The SmallGG pegmatite – section 2.3.1.5.

2.3.1.3 The Strathmore pegmatites

The Strathmore pegmatite locality occurs in the northern portion of the Strathmore swarm where large concentrations of pegmatites are found within several hundred metres of each other (e.g. OFP1-6; Fig. 2.2). Figure 2.7B shows the large, approximately northeast trending Strathmore pegmatite with accompanying smaller bodies in the south of the area. The main pegmatite body is roughly 500 m in length with a maximum thickness of 60 m. The area has been historically, extensively mined with many excavations, perpendicular to pegmatite strike.

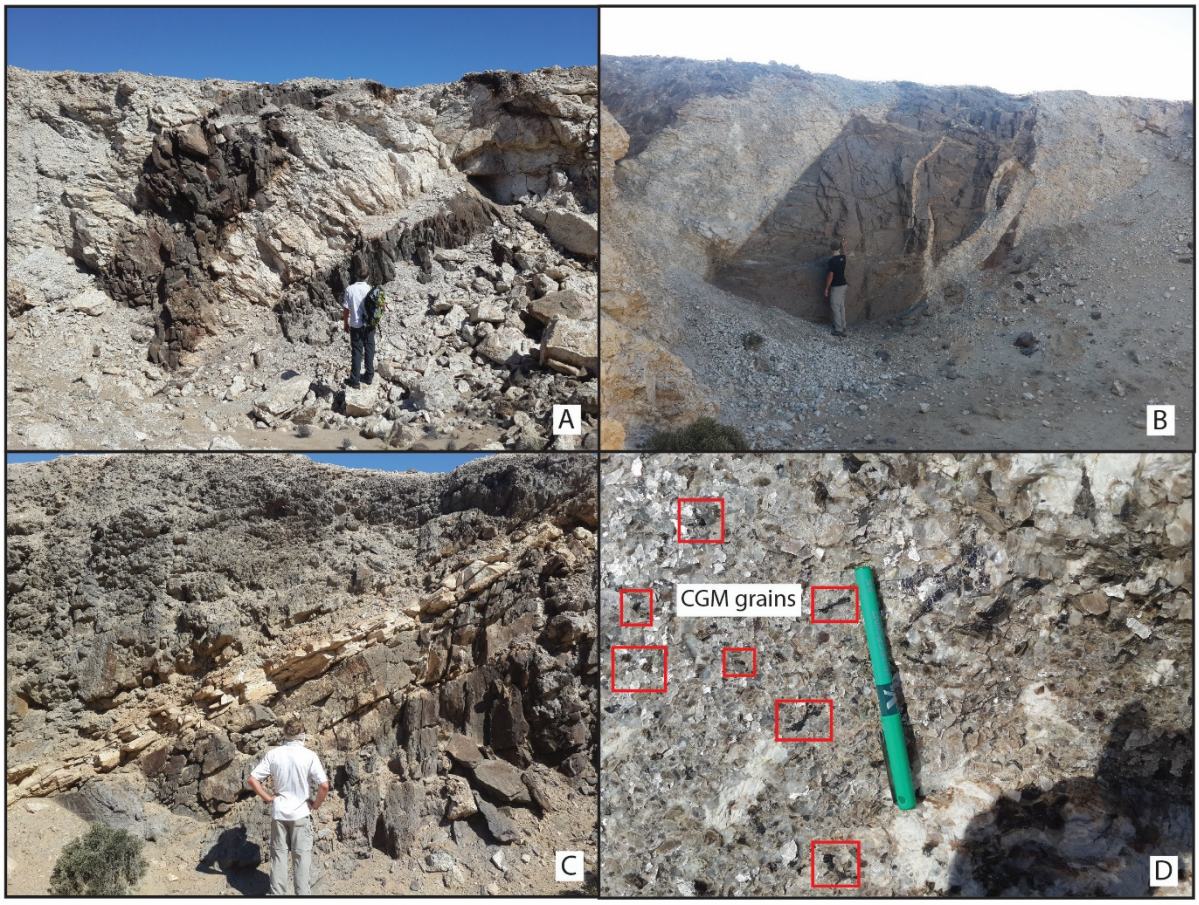


Figure 2.8: Various outcrop photographs from the Strathmore pegmatite locality. A) Large metasedimentary xenoliths within the main pegmatite body. B) Bifurcating medium sized pegmatites with associated thinner pegmatite veins. C) 40 cm thick pegmatite vein intruding bedding parallel to biotite schist host rocks. D) Anhedral columbite group minerals in a greisenised zone of the Strathmore pegmatite.

The intrusion style is complex at this locality, best depicted in the southern pegmatites. Larger xenoliths of biotite schist or Knotenschiefer are included within the main pegmatite body (Fig. 2.8A) and often a bifurcating emplacement style is a hallmark of the pegmatites in this area (Fig. 2.8B) including pegmatites such as OFP1-6 and S-Strath (Fig. 2.2). Thin pegmatite veins,

associated with the larger pegmatite bodies, are also a common feature and intrude mostly bedding-parallel to schist host rock (Fig. 2.8C).

The large Strathmore pegmatite is roughly sigmoidal in shape when extrapolating pegmatite outcrop throughout the historically mined pits. The pegmatites in the southern portion of the locality are difficult to extrapolate due to the complex nature of intrusion and lack of outcrop between excavations. The main pegmatite body shows opposite dip directions on either side of the strike-perpendicular excavations indicating the pegmatite thins out with depth (Fig. 2.7B). The pegmatites in this locality intrude various country rocks, including Knotenschiefer, biotite schist and 1 m thick lithologies of grey quartzites (yellow in Figure 2.7B). The Knotenschiefer host rock shows a strong northeast schistosity with individual biotite grains curving around the large 'knots' in thin section. Like many other pegmatites (e.g. Petalite; P2.2; Fig. 2.2) the Strathmore pegmatites show host rock contact metasomatism in the form of tourmalinisation. These rocks show high concentrations of Sn (Fuchsloch et al., 2018*a*) and lack notable quantities of biotite, being mostly recrystallised quartz and poikilitic tourmaline grains. Tourmaline oikocrysts include blebby quartz, muscovite and highly reflective opaque grains.

The Strathmore pegmatites are homogeneous unzoned bodies with common mineralogy that includes quartz, muscovite, albite, microcline and microcline perthite; however, similar to the P2.2 pegmatite the contact zones are muscovite-rich. Large 1-2 m sized quartz pods occur sporadically in the thicker internal sections of the pegmatites (Fig. 2.7B) and have associated alteration surrounding the pods. Greisenisation and albitisation are the common types of macroscopic alteration near the quartz pods and contain significant abundances of CGM (Fig. 2.8D). Aplitic zones have a saccharoidal texture and contain abundant equigranular albite whereas greisens consist of new or recrystallised quartz and muscovite. CGM minerals are anhedral, 1-4 cm in size and have a blebby elongate texture. Notably, out of the 14 samples collected from this area, none contained cassiterite (Fuchsloch et al., 2018*b*), however, CGM was abundant in many pegmatite samples, not just in the greisen or albitised samples. CGM occurs in the magmatic zones of the pegmatite, showing little alteration and an equigranular magmatic texture, however, CGM abundances are very low in these samples. Apatite is likewise a common mineral associated with samples that yielded CGM grains (Appendix A, C). Sericitic alteration is a common feature in thin

sections, fine-grained muscovite occurring in abundance on the grain boundaries of larger feldspar grains. Quartz and feldspar have a slight undulating extinction; however, no other microscopic deformational features were observed in comparison to the P2.2 pegmatite which has folded albite grains.

2.3.1.4 The MT-pit pegmatite

The MT-pit is located approximately 6 km southeast of the Strathmore locality (Fig. 2.2, 2.7C). The pegmatite is medium in size with length and width dimensions of approximately 80 m and 7 m respectively. The pegmatite is simple in intrusion style with no offsets of bifurcating structures. The lensoidal shaped body has an approximate vertical dip and north-northeast orientation (Fig. 2.7C). Interestingly, while mapping the historical workings which are strike-parallel to the pegmatite, either side of the excavation shows opposite dip directions of the biotite schist host rock (Fig. 2.7C). The orientation of the host rocks show that the pegmatite intruded into a small D_3 fold axis similar to the ones described in Richards (1986). The fold is likely to have created a zone of dilation which permitted fluid/magma flow, allowing pegmatite emplacement (Fuchsloch et al., 2018*a*).

The host rocks include both biotite schist and Knotenschiefer which shows that the metasediments are not mineralogically continuous along strike (Fig. 2.7C). Both biotite schist and Knotenschiefer show a strong northeast schistosity typical of the metasediments of the Amis River Formation: the dominant biotite and quartz mineralogy are completely aligned even on the microscopic scale. Fine-grained tourmaline is common within the host rocks, increasing in abundance and mineral size toward the pegmatite contact where on the contact the metasediments have been highly tourmalinised. Euhedral grains of tourmaline in the metasediments may reach up to 2 cm in length.

The pegmatite is mostly homogeneous with no clearly defined mineralogical zones; however, specific areas within the internal pegmatite body show unique features: near a quartz pod, approximately in the central part of the pegmatite, many radial aggregates of black tourmaline occur in large albite crystals (Fig. 2.7C). The dominant mineralogy consists of quartz, perthite and albite with minor finer-grained muscovite. The MT-pit pegmatite showcases an important feature to the CUPB pegmatites: near the pegmatite contact, finer-grained zones occur which display the

coarse-grained mineralogy of the entire pegmatite in a single sample (Fig. 2.9). These finer-grained samples are important for this study since they present reliable whole-rock geochemistry estimates when analysed (Fuchsloch et al., 2018*a*). They also record the initial composition of the pegmatite after emplacement since they are near the border zone and fine grained, implying they are representatives of quickly cooled magma. Comparing their data with analysis of late-stage alteration zones, such as greisens, records changes in the overall chemistry from initial to the final stages of pegmatite crystallisation (Fuchsloch et al., 2018*a*). Alteration zones in the MT-pit pegmatite are also a common feature, sporadic in occurrence and have m-scale sizes. Similar to the Strathmore pegmatite, accessory phases in greisens include CGM but no cassiterite. Apatite, whilst occurring in the greisenised zones, may also be found in other unaltered areas within the pegmatite.

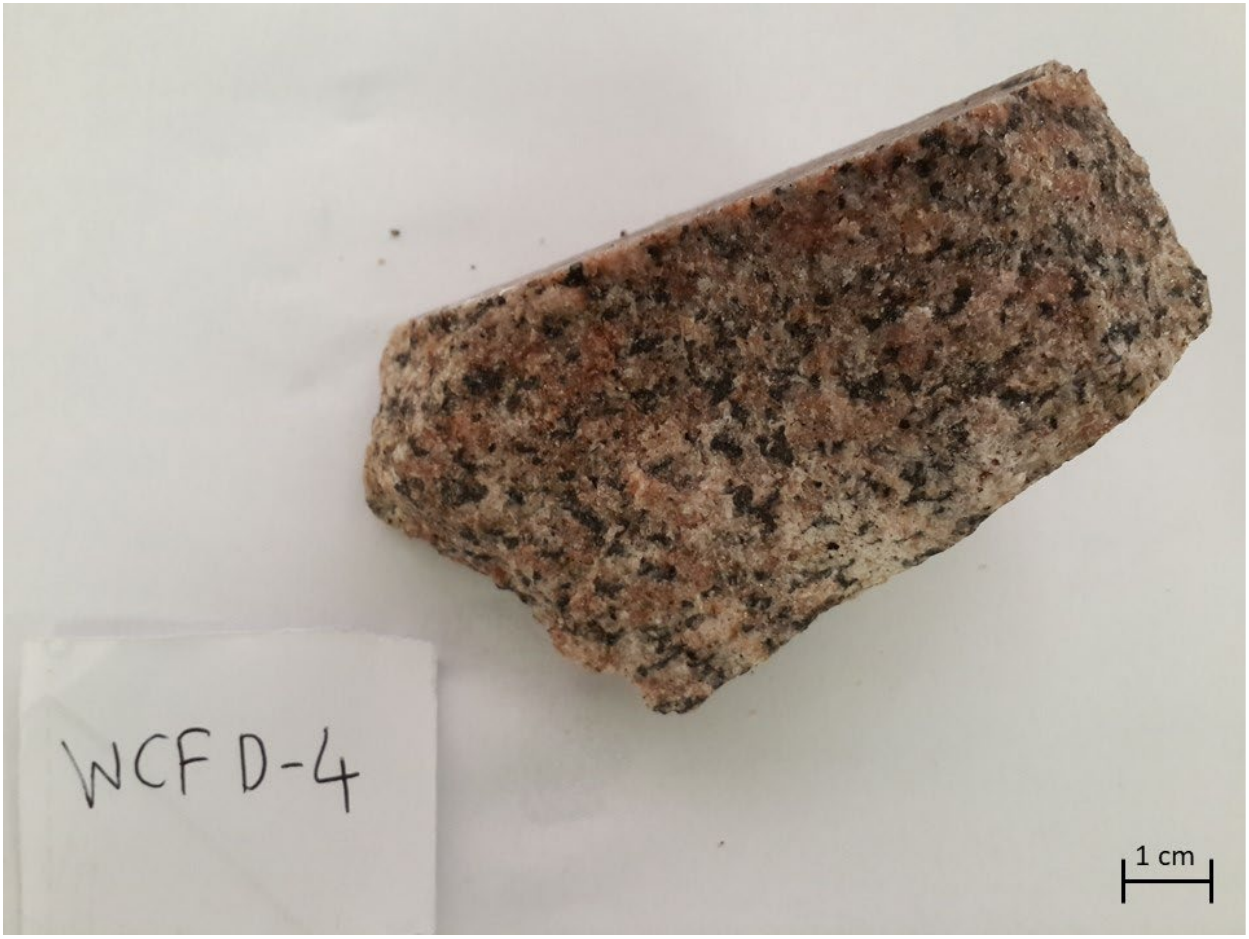


Figure 2.9: Sample D-4 showing fine-grained pegmatite rock near the contact of pegmatites with the biotite schist host rock.

2.3.1.5 The SmallGG pegmatite

The SmallGG pegmatite is located in the southern portion of the Karlowa swarm (Fig. 2.3). The pegmatite is small to medium in size with an approximate length of 50 m. Due to limited outcrop the pegmatite cannot be traced to its maximum length (Fig. 2.7D); however, it becomes significantly thicker in the centre of the body with a width of 12 m. The pegmatite intrudes approximately strike-parallel to host rock biotite schist with a strike of 028° and dip of approximately 60° to the northwest. The intrusion is roughly sigmoidal in shape, thickens in the centre and thins out in its extensions. The SmallGG pegmatite is associated with 0.5m thick, host rock bedding-parallel, pegmatite veins that display pinch and swell structures (Fig. 2.10A). The structure indicates similar σ_1 and σ_3 orientations seen in the tensions gashes in the 2faced pegmatite (approximately 10° and 190° respectively).

The host rock to the SmallGG pegmatite is fine- to medium-grained biotite schist that is composed almost solely of biotite and quartz which shows a strong north-northeast schistosity both microscopically and macroscopically. The host rock contacts at this locality show extreme metasomatism and tourmalinisation (Fig. 2.10B). Multiple thin stock-work-like veins intrude fractures on the contact, essentially bleaching the host rock and crystallising tourmaline. In thin section, these contact host rocks are extremely difficult to characterise because of the intense alteration, only quartz remaining optically intact.

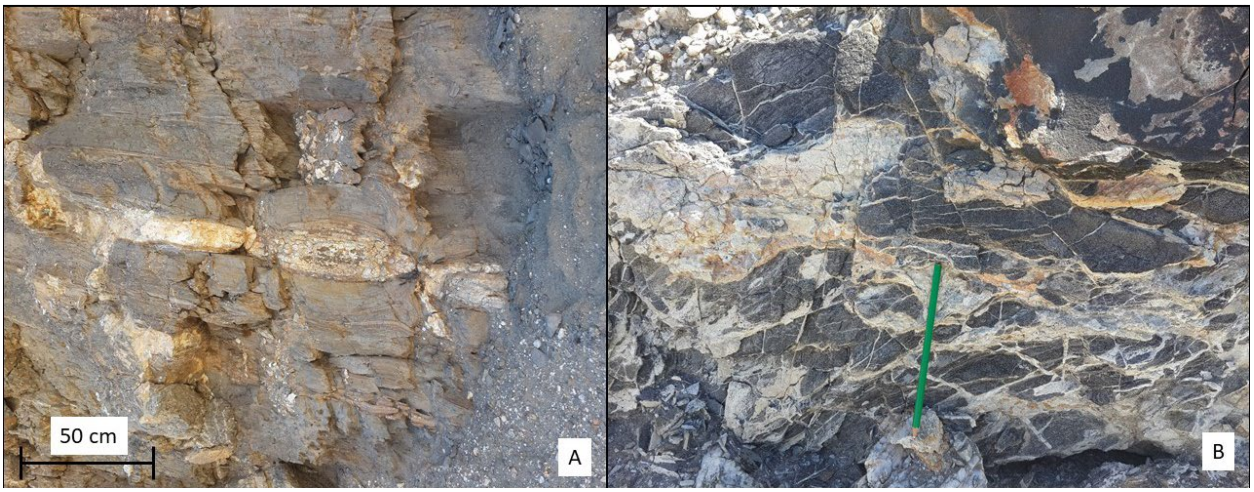


Figure 2.10: Outcrop photographs of pegmatites and host rocks at the SmallGG pegmatite locality. A) Thin boudinaged pegmatite vein approximately bedding-parallel to the host rock. B) Extremely metasomatised host rock contact with pegmatite.

The SmallGG pegmatite is not mineralogically zoned but contains areas richer in quartz and has a muscovite-rich border zone. Near the quartz pods there is abundant blue, green and pink tourmaline which is rare for Nb-Ta-Sn type pegmatites, with most tourmaline at other localities being brown or black. The dominant mineralogy consists of quartz, muscovite, albite and microcline with heterogeneous grain sizes. Large euhedral microcline crystals (up to several cm) are surrounded in a matrix-like fashion by albite, muscovite and quartz. Some larger muscovite grains show slight chevron folding in their cleavages whereas finer-grained muscovite is undeformed. Interestingly, no Ta-Nb- or Sn-bearing phases were recovered from the SmallGG pegmatite and little greisenisation or albitisation was observed in the field. This is contrary to Richards (1986) observation that tin-bearing pegmatites are associated with tourmalinised contact host rocks.

2.3.1.6 The B-12 pegmatite

The B-12 pegmatite occurs in the southwestern portion of the Uis swarm, approximately 15 km from the town of Uis (Fig. 2.4). The pegmatite has an east-northeast orientation and dips at approximately 64° to the northwest, following similar orientations to the host rock biotite schists. The pegmatite is roughly sigmoidal in shape, has a maximum width of 10 m and can be traced along strike for 100 m; however, further extensions are not calculable since outcrop is limited in the northeast section of the locality (Fig. 2.11). Two large faults occur in central portion of the pegmatite which have north-northwest orientations and an almost vertical dip. The pegmatite is displaced by approximately 7 m by the central western fault and by 6 m by the central eastern fault (Fig. 2.11). The B-12 pegmatite has a simple intrusion style, showing little bifurcating structures and few associated smaller pegmatite veins.

The B-12 pegmatite is hosted by fine- to medium-grained biotite schist, although small thin layers, 0.5 m thick, of quartzite are present in the area. The host rock is characteristic of the CUPB biotite schists, showing a strong schistosity and being composed primarily of quartz and biotite. The host rocks contacts show moderate metasomatism and tourmaline abundances.

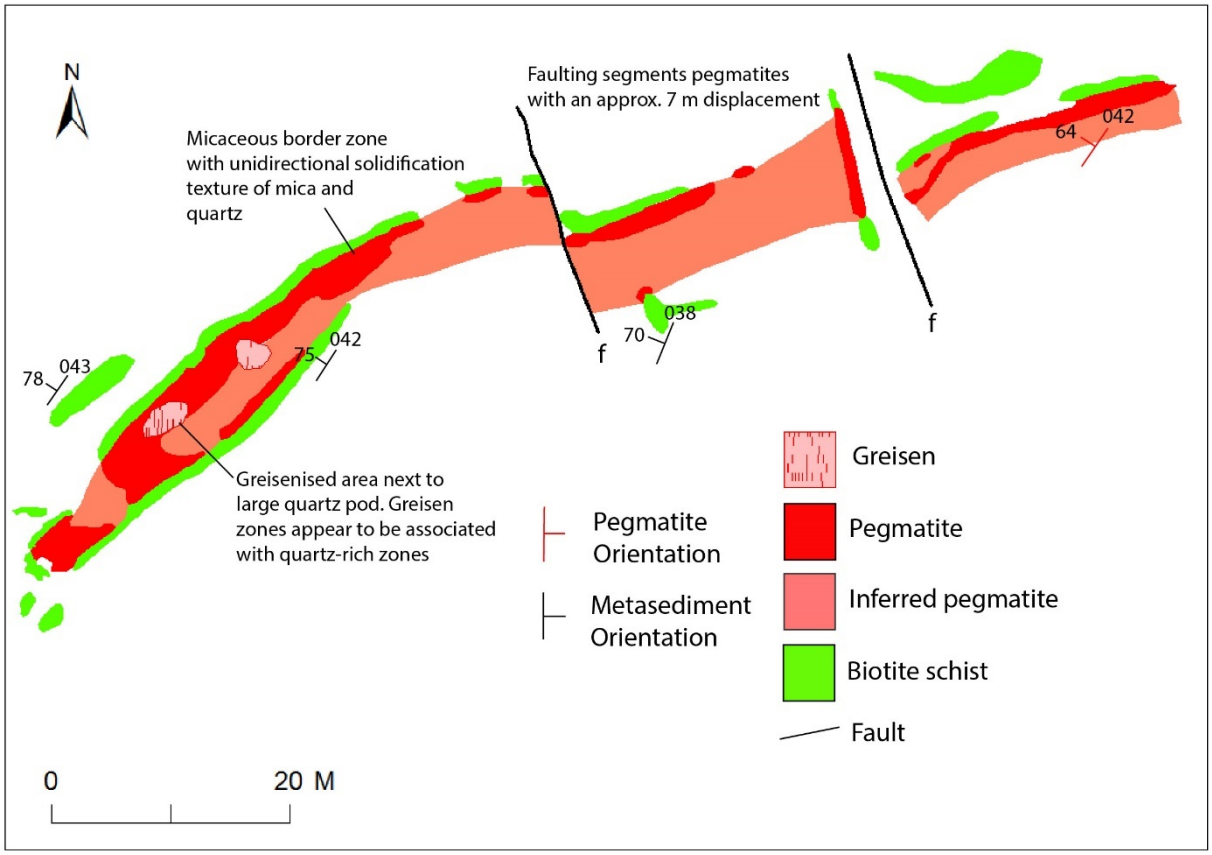


Figure 2.11: A geological map of the B-12 pegmatite showing greisenised zones, faults and lithologies.

The B-12 pegmatite is very representative of the general Nb-Ta-Sn type pegmatites in the CUPB. The pegmatite has a dominant quartz, muscovite and albite mineralogy, shows no mineralogical zonation and has significant alteration zones in the form of greisens and albitised rock. Greisens in this pegmatite are somewhat unique because of their 2-3 m size in which the rock has been completely altered to new or recrystallised quartz and muscovite. This differs from most other Nb-Ta-Sn type pegmatites that show sporadic, partial alteration zones that are generally small (10-20 cm) but abundant. The B-12 pegmatite has significant quantities of subhedral to anhedral cassiterite and CGM respectively that are associated with the two large greisenised zones in the pegmatite (Fig. 2.11). Little of the characteristics displayed, aside from faults and large greisenisation zones, are of specific interest compared to the other pegmatite localities described in this section and therefore the B-12 pegmatite represents the stock-standard Nb-Ta-Sn type pegmatite in the CUPB.

2.3.1.7 The C1 pegmatite

The C1 pegmatite is located approximately 10 km southwest of the town of Uis (Fig. 2.4) and is one of two historically noted Ta-bearing pegmatites within the Uis swarm. It was estimated that the C1 and B1 pegmatites (Fig. 2.4) combined, contain a resource of approximately 2 million tons at 240 g/t Ta_2O_5 (Diehl, 1992*a*). The C1 pegmatite may be significantly extensive within a northeast orientation; however, lack of outcrop across a dry river bed prevents tracing the intrusion along strike (Fig. 2.12). The northeastern extension is roughly sigmoidal in shape but due to a bifurcating emplacement style, determining precise orientational data is difficult. If the southwest and northeast outcrop were linked as one intrusion the C1 pegmatite would have a 1 km length with a moderate 20-30 m thickness.

Although the C1 pegmatite shows no true mineralogical zonation, bifurcated extensions show a clear quartz core and muscovite-rich border zone (Fig. 2.13). The C1 pegmatite intrudes into a fine- to medium-grained biotite schist which shows slight tourmalinisation at the contact between the pegmatite and schist. Mineralogically the C1 pegmatite is simple with a dominant quartz, muscovite and albite composition. Associated accessory mineralogy includes CGM, apatite and minor Fe-oxides. CGM and apatite show a close association with one another, however, they are not restricted to greisenised and albitised zones within the pegmatite as there are many occurrences where they were observed in magmatic zones with little to no alteration. Zircons were also found in this section within the C1 pegmatite samples; however, they are metamict or occur as micron-sized inclusions.

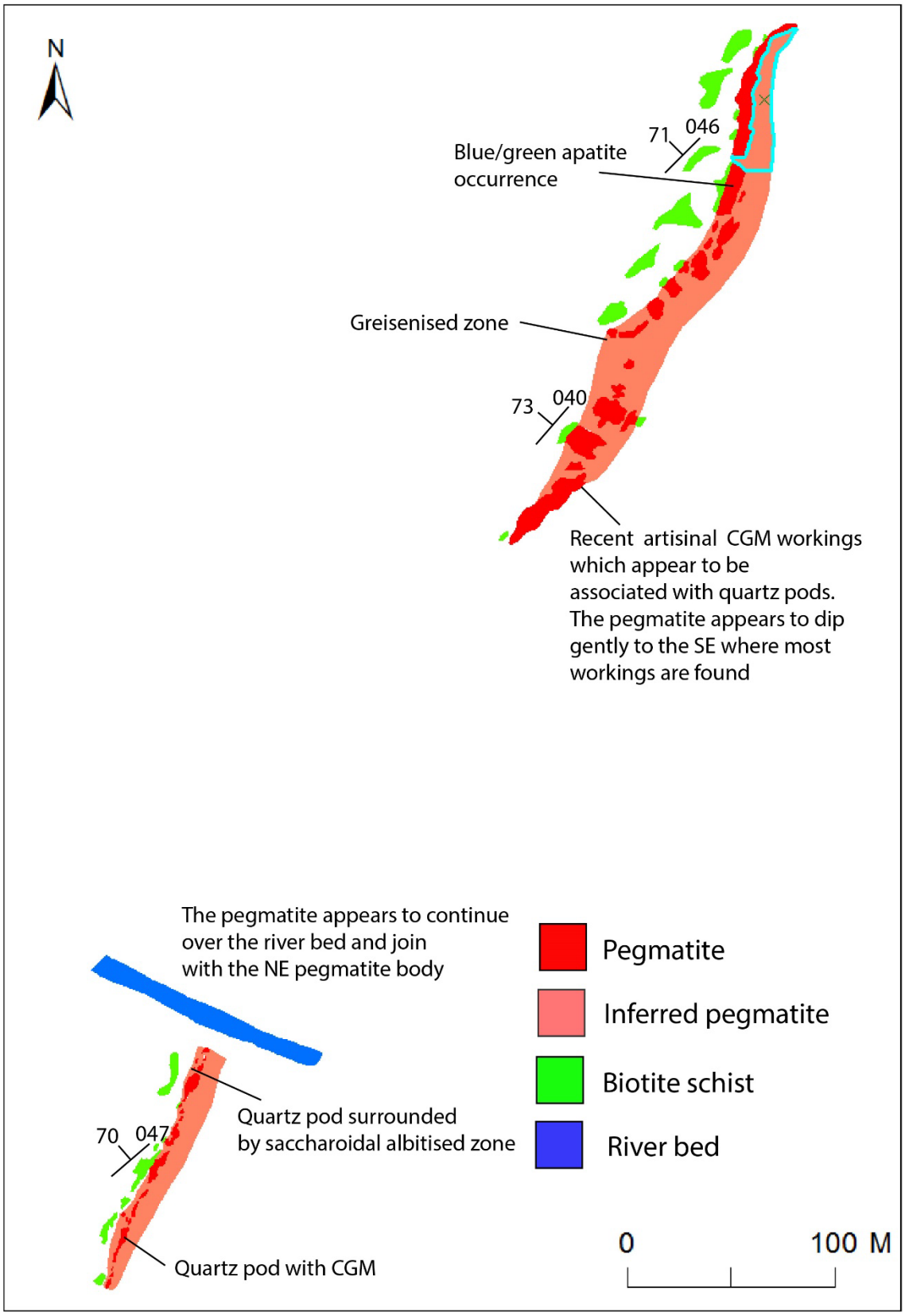


Figure 2.12: A geological map of the extensive C1 pegmatite. Field work suggests that outcrop in the southwest and northeast join up to make a single pegmatite body.

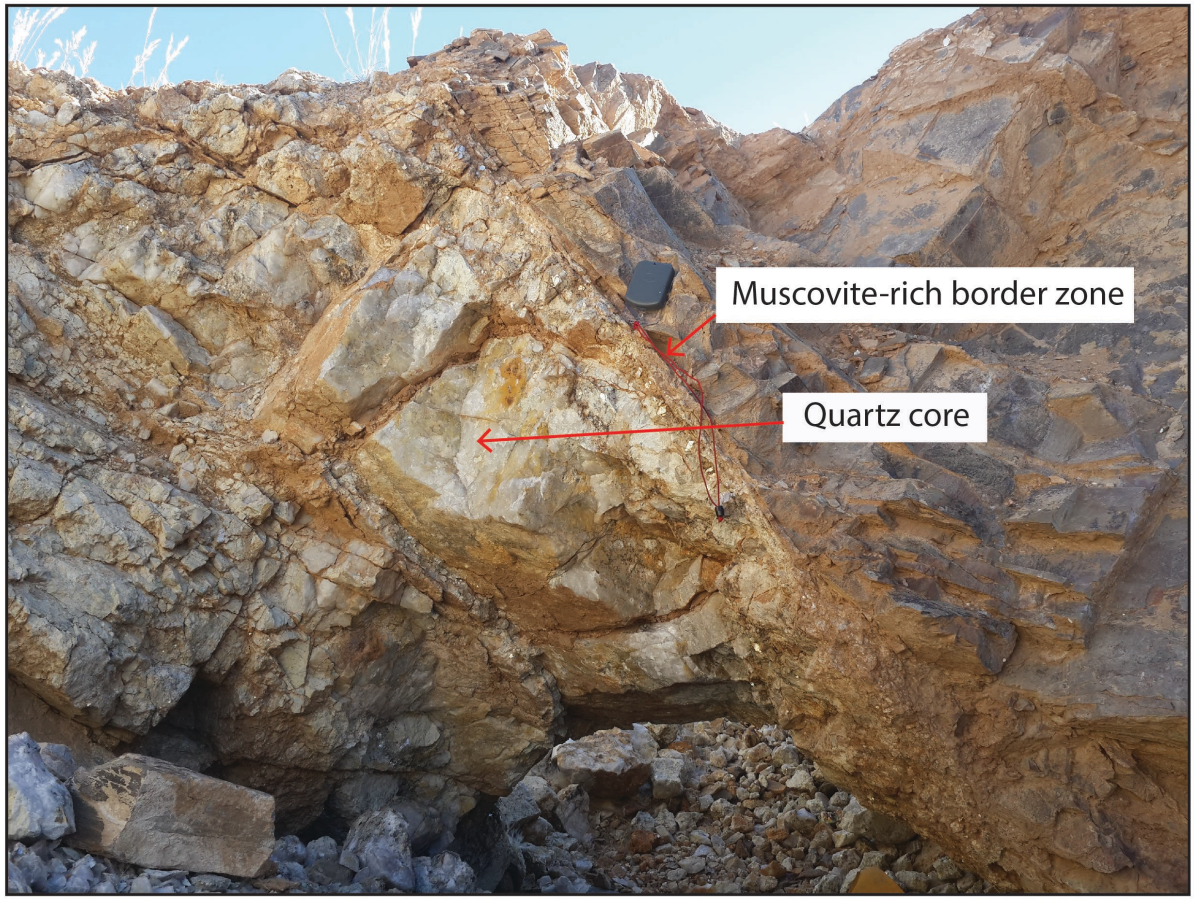


Figure 2.13: A thin bifurcated extension of the C1 pegmatite that shows a quartz core and muscovite-rich border zone.

Aside from being specifically targeted for CGM by the artisanal miners in the surrounding area, the C1 pegmatite is generally simple and extensive. The C1, B1 and B-12 pegmatites appear to be the typical CGM-bearing pegmatites in the Uis swarm with minor to no cassiterite present (Fig. 2.4). This is quite contrasting to the Uis pegmatites in the north of the swarm where CGM are almost absent occurring as individual rare grains with cassiterite the dominant ore mineral present.

2.3.1.8 The Uis pegmatites

The Uis pegmatites of the Uis swarm (Fig. 2.4) are the most historically noted in the CUPB and the Uis mine was once the largest open pit, low grade Sn mine in the world (Diehl, 1993; Section 2.2.3). The Uis mining area roughly starts just north of the town of Uis (Fig. 2.4) and continues south up to and including the Tsaurob pegmatites. The area contains tens of individual pegmatites that are closely spaced with several larger intrusions having been mined in the past for cassiterite. They are all roughly sigmoidal in shape and on a regional scale, an en echelon array of the

pegmatites is observed. The pegmatites reach impressive thicknesses up to 60 m in the central part of larger pegmatite bodies (Fig. 2.14A). Their extensions have been traced to several hundred metres; however, defining the larger bodies is difficult due to extremely complex emplacement styles: bifurcating with depth and/or strike, many intersections between individual bodies and significant quantities of smaller associated pegmatite veins.

The Uis area alone may constitute its own thesis, however, due to the regional nature of this study, only a general outline is available here. Country rocks include Knotenschiefer, biotite schist and finer-grained biotite phyllite. Contact metasomatism is abundant as is tourmalinisation of the host rocks. Abundant structural features are observed in host rocks and include both faults and folds (regional to metre-scale). Most notably in this Uis area, pegmatites intrude bedding perpendicular to host rocks whereas the typical nature of pegmatites in the CUPB is a host rock bedding-parallel style of intrusion. Host rocks likewise show many microscopic structural features and a strong northeast orientated schistosity.

Mineralogically the pegmatites are composed of quartz, albite, muscovite and microcline. No mineralogical zonation is apparent in any of the pegmatites in the Uis area; they are homogenous masses even when compared to other crudely zoned pegmatites in the CUPB. Greisenisation is particularly abundant in the Uis area and generally occurs sporadically within the pegmatites and at various levels of alteration from complete to partial. Greisens are not particularly large (cm- to m-scale), however, some of the pegmatites within the Uis area show continuous greisen lenses or layers. For example, a single, smaller pegmatite near the town of Uis shows a continuous, pegmatite-parallel, 40 cm thick greisen layer near the hanging wall of the pegmatite that may be traced along the entire length of the pegmatite body.

Cassiterite is significantly abundant in the greisenised zones with both euhedral to anhedral crystals present (Fig. 2.14B). Some greisens may even reach grades of 1 wt% Sn in samples acquired by Fuchsloch et al. (2018*a*). Accessory phases are sparse in the Uis pegmatites; however, Li-bearing phases have been observed recently (Fuchsloch et al., 2018*a*) along with tourmaline, Fe-oxides and secondary Mn-bearing phases which are particularly associated with greisenised areas. Li phases include petalite and lepidolite, as lepidolite was observed in the Tsaurob pegmatite

(Fig. 2.4). CGM are rare and mainly occur as inclusions within cassiterite grains but they are not the result of exsolution from cassiterite (Fuchsloch et al., 2018*b*).

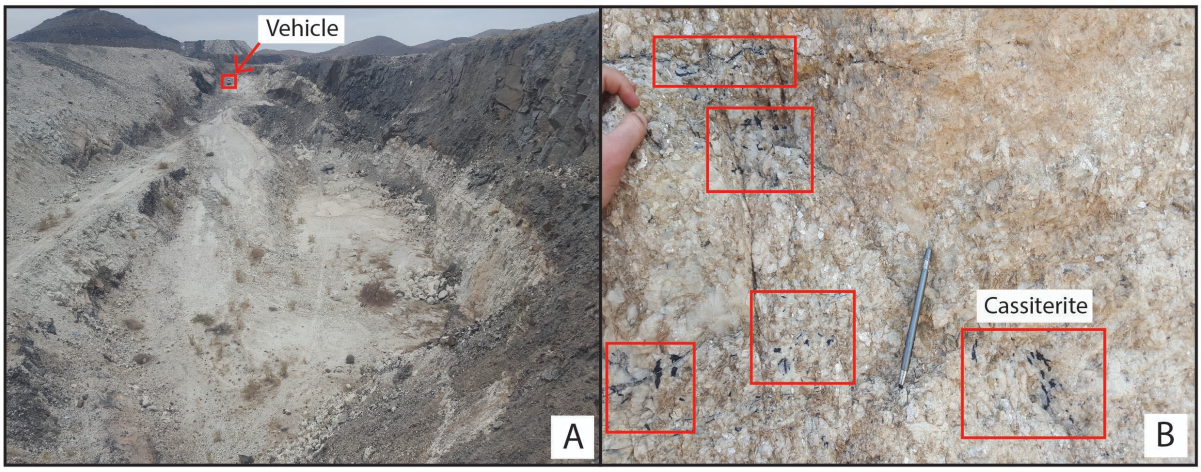


Figure 2.14: Photographs of pegmatites in the Uis area. A) Overview image of a large pegmatite in the Uis area showing a northwest dip direction. B) Highly greisenised area with a pegmatite showing abundant, large, anhedral cassiterite grains.

2.3.2 The Garnet-Tourmaline pegmatites (Gnt-Tml type)

The Gnt-Tml type pegmatites are intragranitic – they are hosted by either the Salem-Type or Red and Grey Granites. They intrude with the typical northeast orientation common to the CUPB despite being intragranitic and they exhibit a crude mineralogical zonation. They are similarly granitic in mineralogical composition and showcase abundant tourmaline and garnet that may be gem quality in some areas. They generally contain no Ta-Nb- and Sn-bearing phases; however, Fuchsloch et al. (2018*a*) did find small quantities of CGM in one Gnt-Tml pegmatite. In thin section, common features include annealing of quartz grains, graphic textures, sericitic alteration and poikilitic tourmaline growth around sericitised feldspars (Fuchsloch et al., 2018*a*).

2.3.2.1 The Rose Quartz pegmatites

The Rose Quartz pegmatites occur in the south westernmost extension of the CUPB (Fig. 2.2). The area includes several pegmatite bodies which are moderate in size compared to their metasediment-hosted counter parts. Typical sizes are several hundred metres length with average widths of approximately 5 to 10 metres (Fig. 2.15). The pegmatites have a lens shape, thinning and terminating at both ends. The area includes many smaller associated pegmatite veins, some of which show a dextral sense of shear in the shear zone running approximately north-south in the

area (Fig. 2.15, 2.16A). The pegmatites are dominantly orientated northeast; however, some pegmatites in the area have a seemingly random orientation (Fig. 2.15).

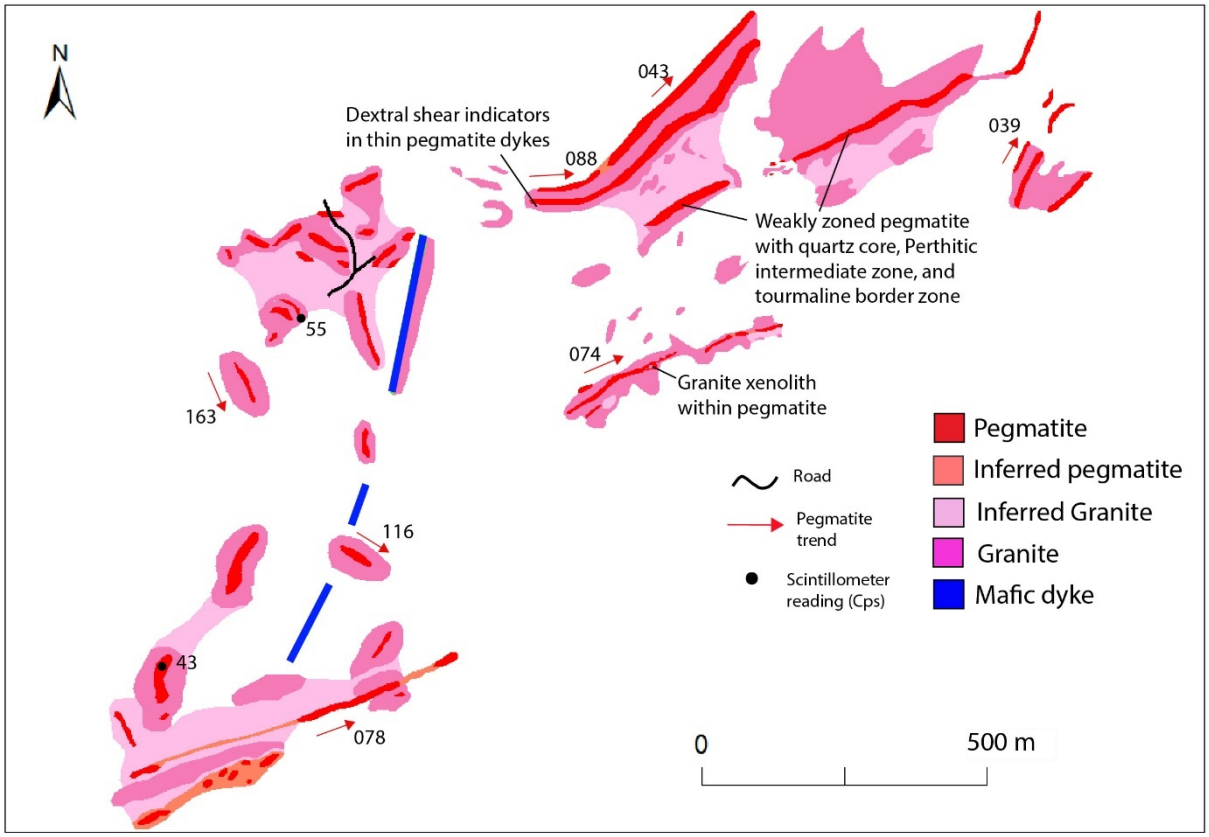


Figure 2.15: Geological map of the Rose Quartz area showing variously orientated, intragranitic Garnet-Tourmaline type pegmatites.

The Rose Quartz pegmatites intrude Salem-type Granites which may be coarse- or fine-grained and porphyritic (Fig. 2.16B). Generally, the pegmatites have no preference for coarser- or finer-grained granites and cross cut the contacts between them. The pegmatites have a sharp contact with the Salem-type Granites and no notable metasomatism was observed in the granites compared to the high degree of contact metasomatism that the metasediment-hosted pegmatites show.

The pegmatites in the Rose Quartz area show a crude mineralogical zonation with a border, intermediate zone and quartz core. The border zone has UST comb-structured black tourmaline and is muscovite-rich (Fig. 2.16C). The intermediate zone dominantly consists of perthitic microcline and often displays a graphic intergrowth and quartz and feldspar (Fig. 2.16D). Near the

contact of the quartz core and intermediate zone there is abundant book mica and transparent, gem quality green and blue tourmaline which has a poikilitic texture with included smaller quartz grains. The core zone is a mass of clear to rose quartz and may occur locally as pods i.e. the core zone is not always extensive along the strike of the pegmatites.

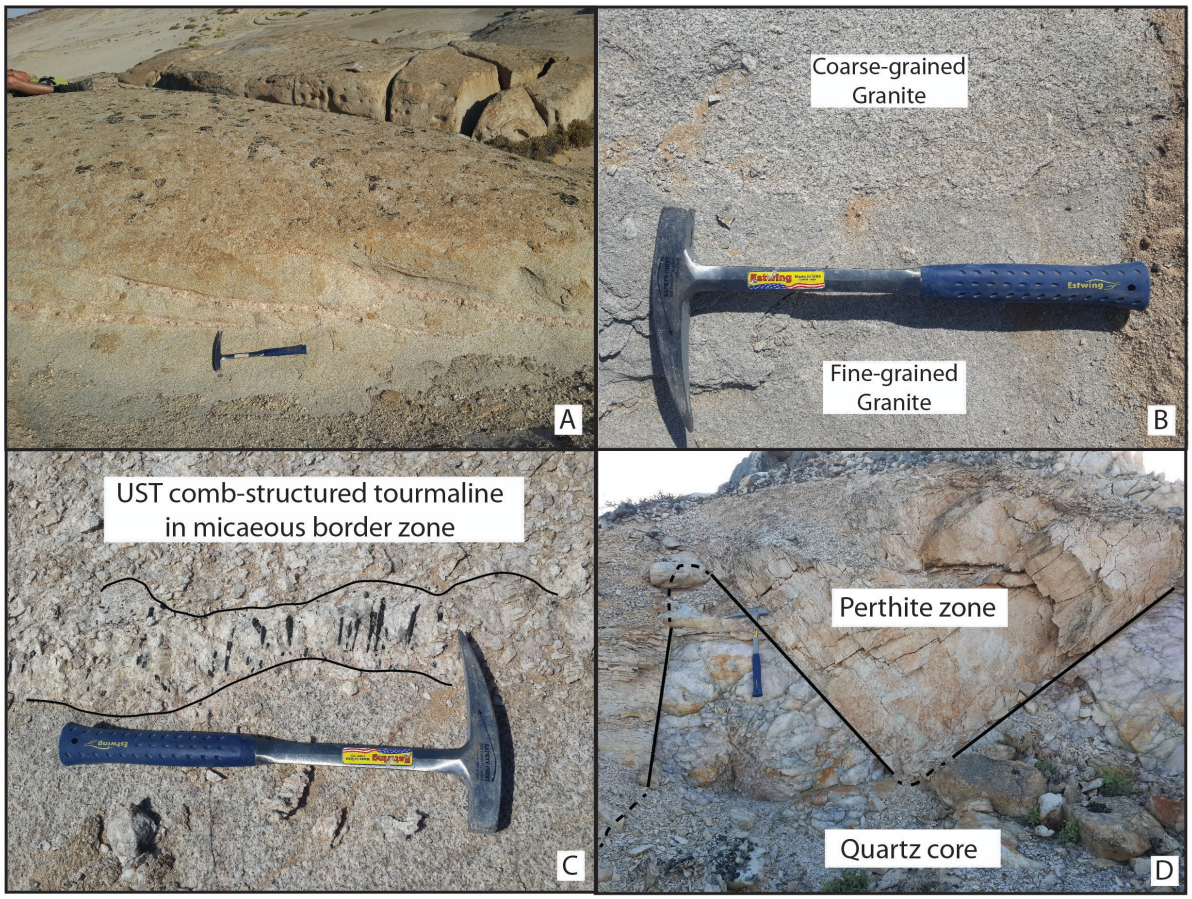


Figure 2.16: Various outcrop photographs of the pegmatites in the Rose Quartz area. A) Thin pegmatite veins showing a dextral sense of shear. B) A contact between fine-grained and coarse-grained Salem-type Granites. C) Unidirectional solidification texture tourmaline in the border zone of a Rose Quartz pegmatite. D) Crudely zoned pegmatite showing a quartz core and perthite intermediate zone.

Alteration in Gnt-Tml pegmatites at the Rose Quartz area is sparse, mainly observable in thin section as sericitic alteration of feldspar grains. These pegmatites show no extensive greisenisation and subsequently have no associated cassiterite and CGM minerals. Garnet occurs sporadically in amorphous pods and appears to have no restriction to any of the mineralogical zones. Interestingly, within the rose quartz area, a large biotite schist xenolith is present and in contact with both the granites and pegmatites. The xenolith is extremely metasomatised and has been almost completely

tourmalinised. Modal abundances of tourmaline within the xenolith suggest that the rock is now a tourmalinite similar to rocks observed by Keller (1999) in the Southern Zone of the Damara Belt.

2.3.2.2 Villet Tourmaline

Villet tourmaline pegmatite is an old artisanally worked tourmaline mine in the Orawab river, Karlowa Swarm and is approximately 8.8 km south of the Brandberg and 34 km west-southwest of Uis along the C34 (Fig. 2.3). The pit and nearby alluvial deposits have been worked artisanally for gem tourmaline. The pegmatite is intragranitic to a small portion of the Red and Grey type monzogranites – to the south-southeast of the main workings a small abandoned house marks the contact of granite with biotite schist. Due to limited outcrop, determining structural data in this area is difficult; however, contacts of granite and pegmatite indicate an approximate northeast orientation similar to the other pegmatites in the CUPB. At the contact of granite schist, the granite is still rich in tourmaline and garnet and minor thin (10-20 cm) pegmatites occur within and across the contact. These thin pegmatites have an orientation of approximately 19° but anastomose along strike. These pegmatites are identical to the main Villet pegmatite but are much smaller in size.

The outcrop in the pit is not large and is around 30 m in length. The pegmatite is mostly mineralogically homogeneous and unzoned with large amounts of quartz, albite, microcline and black tourmaline occurring in the pegmatite. Garnet occurs in amorphous pods within the pegmatite and seems to be concentrated in finer-grained areas. Biotite mica of about 15 cm in length occurs within a saccharoidal area in the pegmatite but is not very abundant, making this a two-mica pegmatite which is rare in the CUPB. Greisenisation and other accessory phases such as cassiterite, CGM and apatite are not present compared to the metasediment-hosted pegmatites in the belt.

To the southwest of the road (Fig. 2.3) there is a small granite dome with a notable network/stockwork-like array of pegmatite veins within the granite (Fig. 2.17). Typical vein widths, although highly variable, range between 30 cm and 2 m. These pegmatites cross-cut and fault each other showing a multiphase generation of pegmatites. Mineralogically they are identical to the Villet tourmaline pegmatite, showing garnet in fine-grained areas and they are homogeneously abundant in black tourmaline. This locality is one of the only places in the belt

where Gnt-Tml type pegmatites outcrop clearly in Red and Grey Granite and beside the abundance of tourmaline and emplacement style observed in Figure 2.17, few differences exist between pegmatites that intrude either type of granite.



Figure 2.17: Photograph of the Granite Dome locality in Figure 2.3. Hundreds of pegmatite veins form a reticulated stockwork-like appearance on the surface of the granite dome.

2.3.3 The Li-bearing pegmatites

The Li-bearing pegmatites have similar intrusion styles and orientations to the Nb-Ta-Sn type pegmatites and are the least common in the CUPB. The mineralogy is likewise granitic, and the pegmatites are complexly and asymmetrically zoned (Diehl, 1993; Fuchsloch et al., 2018*a*). This group was subdivided into two groups by Fuchsloch et al. (2018*a*) based on the dominantly occurring Li-bearing phase: 1. The Li-Nb-Ta-Sn-Be petalite-bearing, complexly zoned type pegmatites and the 2. Li-Nb-Ta-Sn spodumene-bearing, crudely zoned type pegmatites. Their mineralogical variation is extensive with many species occurring in specific zones. The Karlowa

North and Karlowa South pegmatites are typical of the Li-Nb-Ta-Sn pegmatites whereas the Petalite and SP14 (SP14 described in Diehl, 1993) are the only Li-Nb-Ta-Sn-Be pegmatites in the CUPB. Since only four pegmatites showcase these pegmatite types, their features are described below.

2.3.3.1 The Petalite pegmatite (Li-Nb-Ta-Sn-Be type)

The Petalite pegmatite is a Li-bearing type pegmatite and is the larger of two unique pegmatites in the CUPB. The SP-14 pegmatite is a smaller, simpler version of the Petalite pegmatite and displays similar mineralogical zonation, variety of mineral species and characteristics (Diehl, 1993); however, it was not investigated in this project. The Petalite pegmatite occurs in the central region of the Strathmore swarm, approximately 10 km north of the Rose Quartz pegmatites. The pegmatite is large in size with a length extending several hundred metres and an impressive width of 60 m. The pegmatite has a north-northeast orientation and dips steeply to the northwest at an angle of 65°. Although the northeast extensions of the pegmatite are not traceable due to limited outcrop outside of the historical mine excavation, the pegmatite has a lens-like shape which is observed in the southwest section where the pegmatite thins and then ends along strike (Fig. 2.18). Historically the pegmatite was mined for lithium, beryllium, tin and industrial mica; however, recently it has only been the subject of exploration projects.

Aside from the SP-14 pegmatite, the petalite pegmatite is the most complex within the CUPB, displaying a wide variety of mineral species and is the only pegmatite to show true mineralogical zonation which is asymmetrically shaped (Fig. 2.18). The pegmatite intrudes biotite schist and Knotenschiefer and is cross cut by a 1 m thick dolerite dyke, demonstrating clearly post pegmatite emplacement as seen by the cross-cutting relationships in Figure 2.19A. The host rock metasediments have been significantly metasomatised and tourmalinised at the contacts of the pegmatite which is typical of metasediment-hosted pegmatites in the CUPB (Fig. 2.19B).

There are four dominant zones within the Petalite pegmatite: the wall zone, the intermediate zone, the greisen zone and the quartz core. The wall zone consists of UST book mica, fine-grained quartz and apatite and surrounds the entire pegmatite body, being slightly thicker along the northwest contact (1-2 m). The intermediate zone (approximately 60% of the pegmatite volumetrically) is

thicker in the northwest zone and displays a host of mineral species which are not evenly distributed between the northwest and southeast zones (Fig. 2.18). The mineral species include perthitic and non-perthitic microcline, quartz, beryl, petalite, apatite, hectorite, cleavelandite and eucryptite. The Li-bearing phases are most notably associated with an equigranular magmatic texture with little associated alteration. The greisen zone in the Petalite pegmatite is also unique. Although at surface it is difficult to trace due to excavation collapse and targeted mining of the zone, it is likely that it extends for 70 m parallel to the pegmatite strike between the intermediate and core zone (Fig. 2.18).

The greisen zone is the largest, continual, greisen within the CUPB and is found only in the northwest zones of the Petalite pegmatite. Alteration levels within the zone are extremely high with no original minerals being present and contacts with other zones are diffuse. It consists of new or recrystallised quartz and muscovite and has abundant associated CGM, cassiterite and apatite. Tapiolite was also observed microscopically in the greisen zone by Fuchsloch et al. (2018*b*). Grain sizes of cassiterite and CGM are macroscopic, being at a cm-scale and dominantly occur as anhedral crystals. Inclusions of CGM in cassiterite are absent; however, the two mineral species are closely associated and are often rimmed by or adjacent to one another. Cassiterite grains are unzoned and homogenous whereas CGM grains show an abundance of compositional zonations described in Fuchsloch et al. (2018*b*).

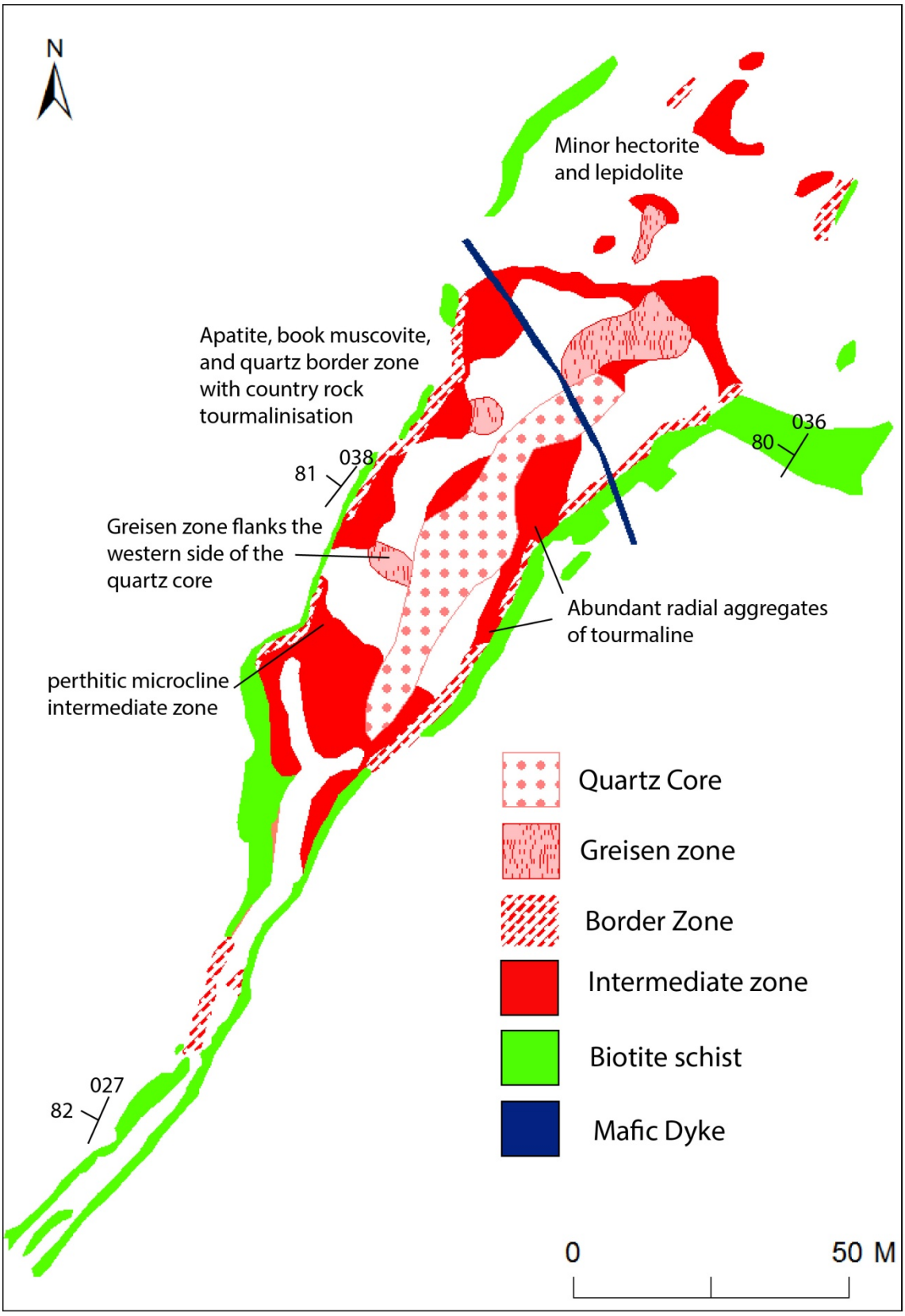


Figure 2.18: Geological map of the Petalite pegmatite showing the mineralogical zonation the pegmatite displays.

The core zone is similar in size to the greisen zone with a length of approximately 70 m and a width of 20 m at surface in the central portions of the pegmatite. The interface between the core zone, intermediate zone and greisen zone shows many secondary phases and textures. For example, petalite is replaced by eucryptite and hectorite whereas primary feldspar is replaced by the radial feldspar variety, cleavelandite. Black tourmaline is also a common species within the pegmatite and does not appear to be restricted to a specific zone. Tourmaline generally occurs as radial aggregates where associated with cleavelandite and is in abundance in the wall zone. Beryl is somewhat rare in this pegmatite but appears to occur mostly in the contact between the intermediate and wall zone. Of all the pegmatites in the CUPB, the Petalite pegmatite displays the hallmarks of a complex petalite-bearing LCT pegmatite similar to other Li-bearing pegmatites in the Damara Belt (Chapter 7).

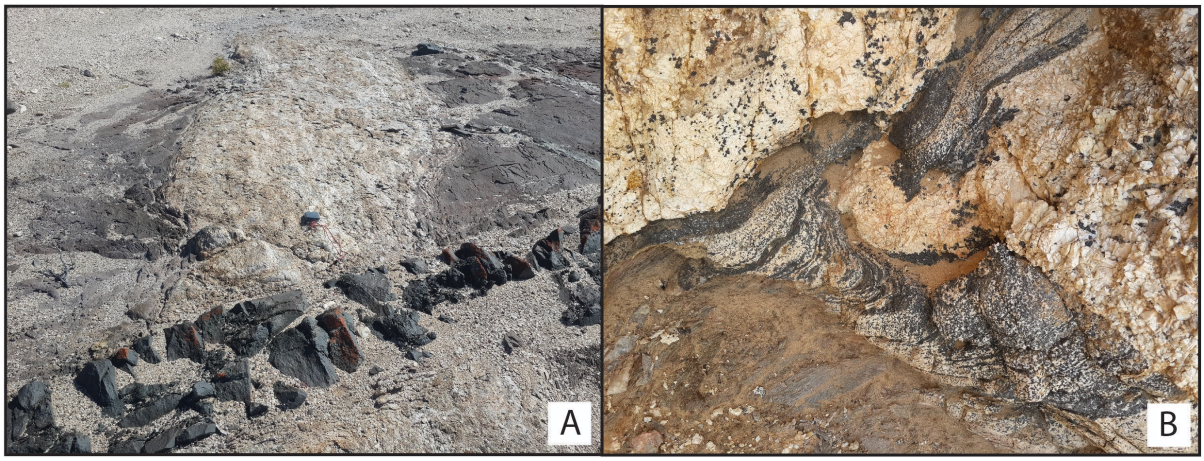


Figure 2.19: Photographs of the Petalite pegmatite. A) A dolerite dyke cross-cutting both pegmatite and host rock biotite schist. B) Highly metasomatised biotite schist contact with the Petalite pegmatite. The metasomatic contact shows microliths rich in tourmaline adjacent to bleached sedimentary layers in the rock where biotite is absent.

2.3.3.2 The Karlowa North pegmatite (Li-Nb-Ta-Sn type)

The Karlowa North pegmatite is located in the central section of the Karlowa swarm (Fig. 2.3) and is one of two Li-Nb-Ta-Sn type pegmatites, the other being Karlowa South. The pegmatite is small to moderate in size with a length of approximately 60 m and width of 20 m. The lensoidal-shaped pegmatite is orientated north-northwest and dips steeply at 70° to the east (Fig. 2.20). The intrusion style is simple with no notable bifurcations even though the pegmatite is roughly perpendicular to host rock bedding which dips to the west. Compared to the other Li-bearing type pegmatites, they

are significantly smaller, less complex in terms of mineralogy, show only a crude mineralogical zonation and have spodumene as the dominantly occurring Li-phase instead of petalite.

The Karlowa North pegmatite intrudes fine- to medium-grained biotite schist where porphyroblasts (knots) are notably smaller in this area compared to other Knotenschiefer in the CUPB. However, like other metasediments in the CUPB, there is a strong northeast schistosity in the rock in which the dominant biotite mineralogy is aligned. Metasomatic contacts are sparse in the Karlowa pegmatite, possibly due to a finer-grained host rock in which fluid migration was hindered.

The pegmatite shows a crude mineralogical zonation – a fine-grained muscovite-rich border zone, a perthitic and quartz intermediate zone, largely occupying most of the pegmatite volumetrically and several disjointed quartz pods/quartz-rich zones. The pegmatite contains a single, but significantly large greisenised zone compared to other pegmatites which only show partially altered greisenised patches (Fig. 2.20). The greisen is approximately 4 by 2 m in size and contains abundant 0.5-1 cm CGM and cassiterite. The main greisen zone and other greisenised areas within the pegmatite are associated with low temperature radial cleavelandite and other saccharoidal replacement zones. Other accessory mineralogy in the pegmatite includes apatite, which may or may not be associated with CGM and cassiterite, and garnet. Garnet is an interesting mineral for the Karlowa North pegmatite since garnet mostly occurs in the Gnt-Tml type pegmatites, however, and unfortunately, no mineral chemistry of garnets has been analysed as of yet. Spodumene occurs mainly in the magmatic zones within the pegmatite which show an equigranular texture and little alteration. Grain sizes are between 0.2 and 1 cm for the subhedral to euhedral spodumene crystals. Notably hectorite and eucryptite are absent from the secondary mineral assemblages of the Karlowa North pegmatite.

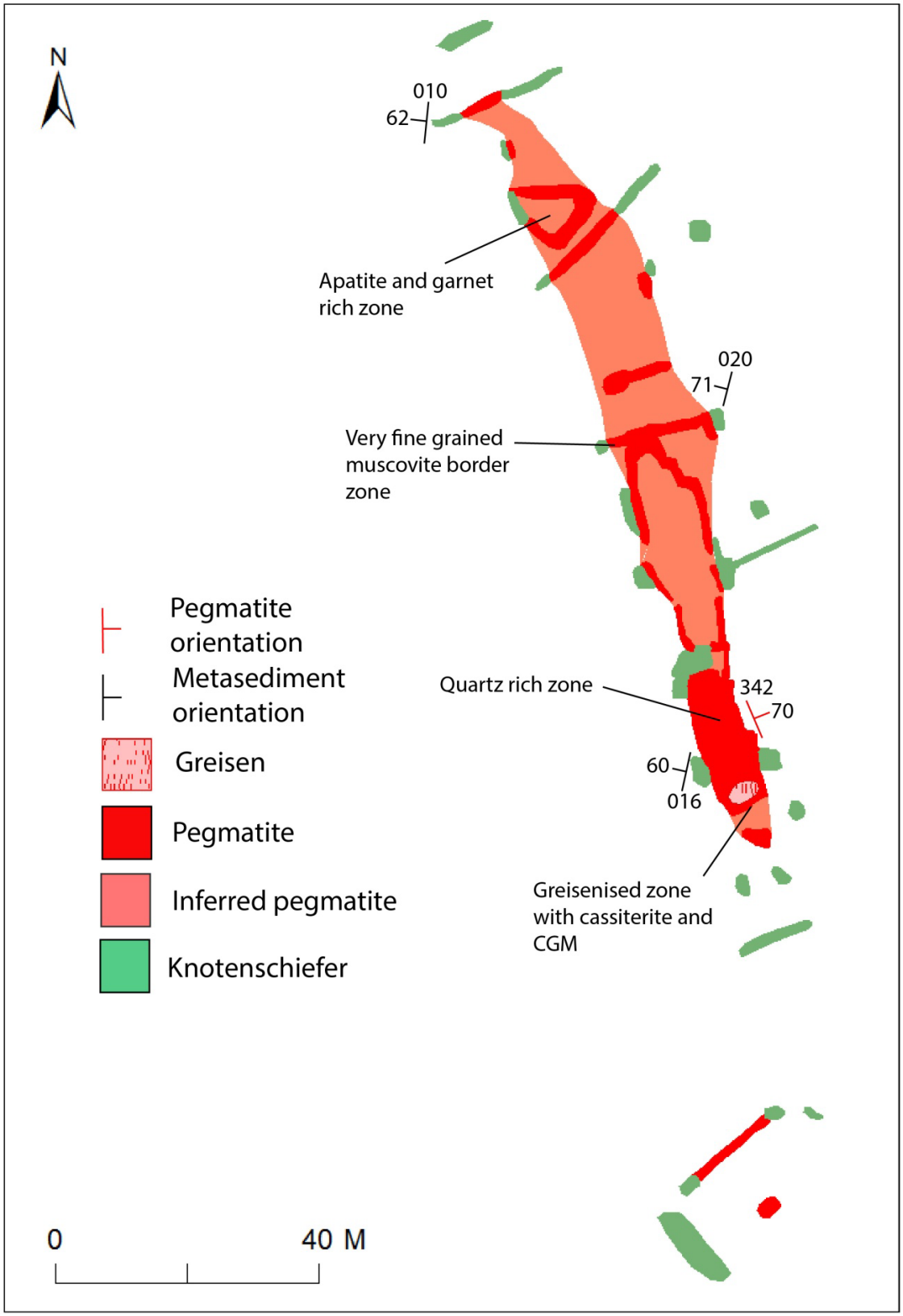


Figure 2.20: A geological map of the Karlowa North pegmatite showing a single moderately sized greisen zone (4 by 2 m).

2.3.4 The Nainais pegmatites (Nb-Ta-Sn type)

Nainais lies approximately 32 km southeast of Uis and is an old tin mine that is within the central tin belt. Although sporadic workings and excavations are present in many pegmatite bodies surrounding the Nainais area, the historical mines based on five main pegmatites are almost completely mined out (Fig. 2.21, 2.22A). The dyke-shaped pegmatites intrude bedding-parallel to Knotenschiefer host rock with a general strike, dip direction and dip angle of 035°, northwest and 69° respectively. Similar dyke-shaped pegmatites can be traced throughout the surrounding ridges in the area. However, one pegmatite was mapped to cross-cut the other pegmatites in the mine with a more north-northeast orientation compared to the northeast orientation of the others.

The pegmatites may extend several hundred metres in length, and most are found at the apex of surrounding ridges. Thicknesses of the pegmatites vary little and reach a maximum width of approximately 25 m in those pegmatites that were mapped (Fig. 2.21). Many smaller pegmatitic veins are associated with the larger pegmatite bodies and generally have a similar mineralogical composition and an anastomosing, worm-like shape (Fig. 2.22B). The host rock Knotenschiefer is medium- to coarse-grained and shares many characteristics with Knotenschiefer from the Strathmore swarm – similar grain size (Uis and Karlowa are fine- to medium-grained), mineralogy, strong northeast schistosity and metamorphic retrogression of the cordierite porphyroblasts. This is an interesting observation since the two similar rocks are located in different stratigraphic horizons and tectonostratigraphic zones (Table 1.1).

The pegmatites are mineralogically unzoned intrusions although the borders of the pegmatites are micaceous, similar to those in the CUPB. They display a similar mineralogy to the CUPB Nb-Ta-Sn type pegmatites, consisting of quartz, muscovite, albite and microcline perthite, however, muscovite in the Nainais area has a yellow colour compared to the white transparent muscovite in the CUPB. The abundance of quartz is also less in the Nainais pegmatites compared to the CUPB pegmatites and as a whole the pegmatites are finer-grained. Associated accessory mineralogy includes apatite, abundant tourmaline, cassiterite, CGM, Fe-oxides and minor petalite in some cases. Alteration within the Nainais pegmatite is more difficult to distinguish compared to the CUPB pegmatites due to the fine-grained nature and consistent yellow muscovite, however, as

with the CUPB, there are areas in the pegmatites that have a higher abundance of mica and show abundant Nb-Ta- and Sn-bearing phases.

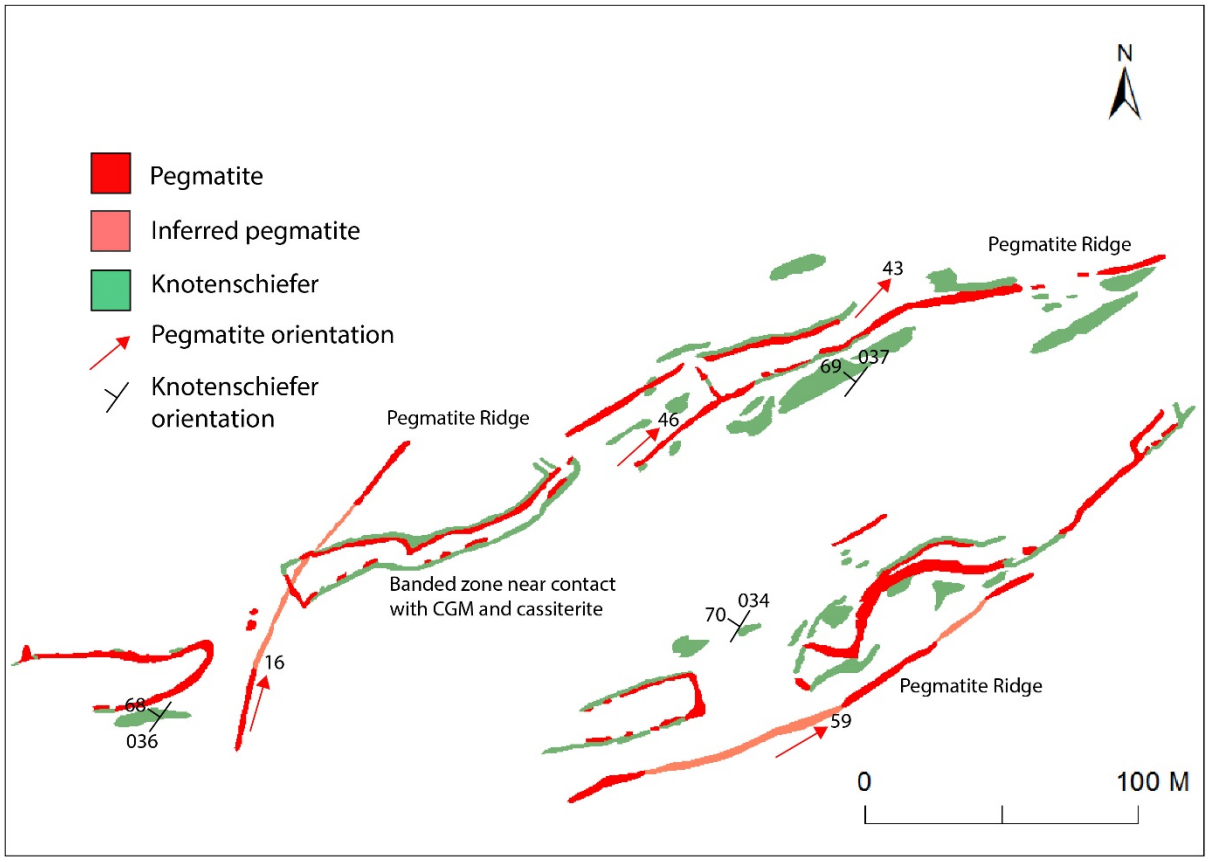


Figure 2.21: Geological map of the historical Nainais mine showing four of the mined-out pegmatites.

Tourmaline is specifically abundant in the Nainais pegmatites and displays many varieties. Blue, green, pink and black tourmalines have all been documented in the pegmatites of the Nainais areas (Fig. 2.23). Blue and pink tourmalines interestingly are found only in areas that also contain minor quantities of lepidolite. Fuchsloch et al. (2018*c*) found the specific species present to be elbaite, schorl, foitite, and dravite.

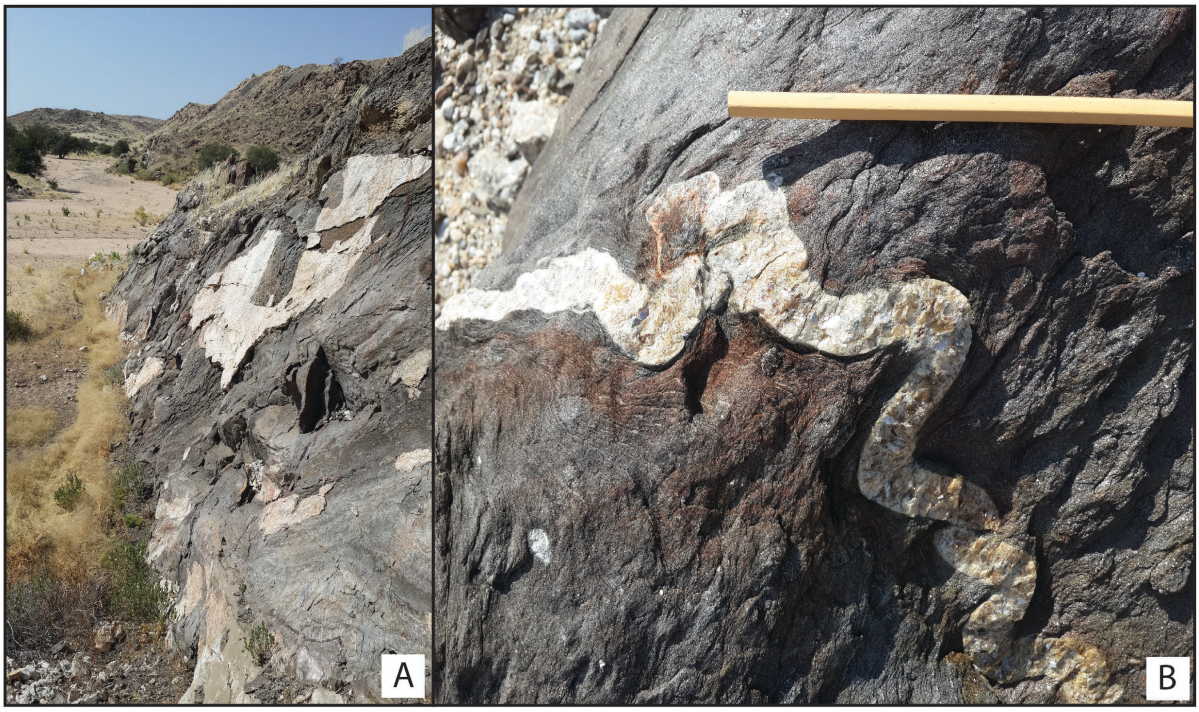


Figure 2.22: Photographs of pegmatites in the Nainais historical mine. A) Almost completely mined out pegmatite dyke with only the wall zone of the pegmatite remaining. B) Anastamosing thin pegmatite vein that displays an identical mineralogical composition to the larger pegmatite bodies.

On the basis of geochemistry and pegmatite geological characteristics, Fuchsloch et al. (2018*a*) groups the Nainais pegmatites together with the Nb-Ta-Sn type pegmatites of the CUPB since little to no differences were found between them. Fuchsloch et al. (2018*b*) then confirmed earlier observations that no differences were found in the mineral chemistry of Ta-Nb- and Sn-bearing phases between the Nainais pegmatites and the CUPB Nb-Ta-Sn type pegmatites. They are therefore categorised in this thesis as Nb-Ta-Sn type pegmatites, although they do not share a similar stratigraphic or tectonostratigraphic zone. All the following hypothesis and deductions pertaining to the Nb-Ta-Sn type pegmatites include the Nainais pegmatite.



Figure 2.23: Large black tourmaline grains rimmed by green tourmaline in feldspar crystals in the Nainais area.

Chapter 3: A background to pegmatites

3.1. Introduction

The word pegmatite is often a descriptive term used for igneous rocks that contain extremely coarse-grained minerals (London, 2008); however, for an intrusion to qualify as a pegmatite, other characteristics are required. Aside from being coarse-grained, a pegmatite should have a skeletal or granophyric texture, mineralogical layering, a coarsening of the crystal size towards the interior of the intrusion and a unidirectional solidification growth structure of minerals (London and Kontak, 2012). For example, the inward growth of tourmaline from the contact of the pegmatite with its host rock is known as a tourmaline comb-structure (Fig. 2.16; Keller, 1999; Simmons, 2007; London, 2008). Although most pegmatites are granitic in composition, being composed primarily of quartz, muscovite and feldspar, mafic, carbonatitic and alkaline varieties also occur (London and Kontak, 2012). In general, pegmatites display simple granitic compositions, large grain sizes and unique textures, however, some pegmatites are literally warehouses of rare and uncommon accessory mineralogy, and in some instances, and one would even consider the rare or uncommon minerals to be rock-forming instead of accessory. Aside from countless uncommon to rare minerals that are exclusively found in pegmatites, they are resources of industrial minerals, strategic metals and what most people adore pegmatites for are their large unique coloured gemstones (Glover et al., 2012; Linnen et al., 2012; Simmons et al., 2012). The exotic mineral species found in pegmatites is reflected by them being enriched in various rare elements such as REE, Sn, Nb, Ta, Li, Cs, Y, Be, Rb, Sc, Ga, U, Th, Zn, Zr and Hf (London, 2008).

In addition to the study of fabrics, extremely large crystals and swelling number of known mineral species, extensive research has gone into the investigation of pegmatitic intrusions such as their petrogenesis, geochemical and mineral chemical signatures, classification and internal anatomy (Černý et al., 2012; London and Morgan, 2012). As it is with most geological factions, the pegmatology arena is filled with academic debate which drives further research into the field. The following chapter outlines the pertinent information regarding pegmatites that is important to this study (reviews in London, 2008). For example, since the pegmatites in the CUPB are mostly mineralogically unzoned (Appendix D), this thesis does not go into detail regarding the possible internal anatomies of pegmatites.

3.2 The general geological setting of pegmatites

Pegmatites do not generally occur as isolated intrusions with one or perhaps two being present in a given geological setting. They generally occur as a cluster or group of many pegmatites, known as a pegmatite swarm, which may occupy an area on the metre- to kilometre-scale (e.g. the Strathmore Swarm). All the pegmatites in the swarm have a similar genetic relationship and structural setting whereby they intrude the various dominant structural fabrics in the area such as major fault zones or lineaments (Černý, 1989; Černý, 1991*a*, London, 2008). By extension the pegmatites in a given swarm therefore share similar ages and are related to a single tectono-magmatic event (e.g. Ashworth, 2013).

Pegmatite swarms may be grouped together into a pegmatite belt whereby each swarm shares the same dominant geological structural setting of the belt (Černý, 1991*b*). However, unlike an individual swarm, the swarms in the belt may be produced by different tectono-magmatic events and various pegmatite classes may be present within a given belt (e.g. the Cape Cross-Uis pegmatite belt; Černý, 1991*a,b*).

When many pegmatite belts are present within an orogenic belt, such as the Damara Belt, they are grouped together to form a pegmatite province. Pegmatites in the province only share the crustal evolution of the mobile belt and may include various pegmatite types, tectono-magmatic events and structural settings (Černý, 1991*a*; London, 2008). For example, different classes of pegmatites within the belt are attributed to the different stages of crustal evolution such as subduction or orogenesis (Section 3.3).

Pegmatites in a given swarm are often, but not always, associated spatially with granitic intrusions within the pegmatite swarm (Černý, 1989; Simmons, 2007; London, 2008). In such cases, pegmatites of the swarm are systematically distributed around a granitic body from the interior where pegmatites are potentially granite-hosted and less fractionated, to the highly evolved complex pegmatites in the outer regions of the swarm (Černý, 1991*a,b*; Fig. 3.1), such that with increasing distance from the granitic body, the associated pegmatites become more fractionated and become more mineralogically and structurally complex. As the complexity of the pegmatites

increases, the abundance of pegmatitic intrusions decreases, as less pegmatites are generally observed further away from the granitic bodies (Černý, 1991*a,b*; Fig. 3.1). The reason the more complex pegmatites may travel further from the granite body is due to the distal pegmatites containing more abundant volatile components which enabled them to remain in a fluid phase at lower temperatures and thus travel greater distances into the surrounding country rock due to buoyancy and a low viscosity (Černý, 1989; Černý, 1991*a*; London and Morgan, 2012). This concept relies upon the petrogenetic model of pegmatites sharing a genetic link to granites and therefore if a spatial association of pegmatites with granites is present, they are connected in a parent-daughter type relationship (Section 3.4.1).

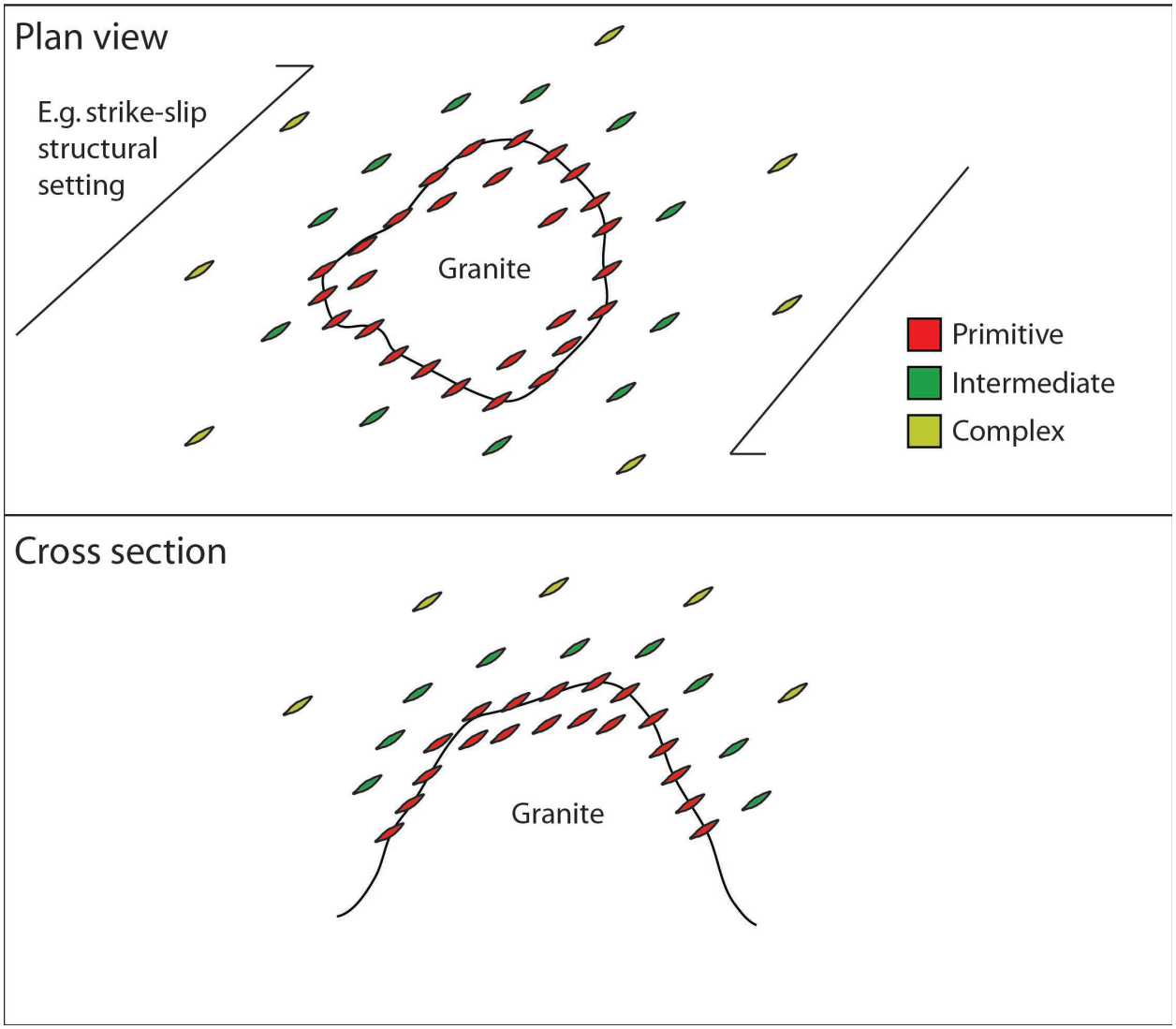


Figure 3.1: Illustration of the spatial association shared by granites and pegmatites in a pegmatite swarm (modified after Černý, 1989).

3.3 The classification of pegmatites

The classification of pegmatites is a highly debated aspect of their study, still being one of the most highly debated concepts in current times. Pegmatites have been classified throughout history based on nearly every aspect of their being. The list includes their emplacement depth and what metamorphic terrane they are emplaced in (similar to the depth zone classification of granites after Buddington, 1959), mineralogical and textural characteristics, the temperature and pressure conditions during petrogenesis, trace element signatures and mineral chemical data (Černý and Ercit, 2005; Ercit, 2005, London, 2008).

The currently accepted pegmatite classification scheme originated from Ginsburg (1979) and was later modified by Černý (1990), Černý (1991a) and Černý and Ercit (2005). The classification scheme is complex; however, it may be broken down into a simple nomenclature (Fig. 3.2) which involves a series of different groupings. Initially pegmatites are subdivided into four major classes: the abyssal, muscovite, rare-element and miarolitic classes (Fig. 3.2). Each class may then have varying subclasses, types and sub-types associated with one of the four major classes (Fig. 3.2). Aside from the nomenclature, each distinction of pegmatite is also given a pegmatite family of which there are two pegmatite families, the Niobium-Yttrium-Fluorine (NYF) and Lithium-Cesium-Tantalum (LCT) families (Fig. 3.2; Černý and Ercit, 2005). One of the major pegmatite classes may have both LCT and NYF family subclasses, however, the two pegmatite families may not occur in a single subclass of pegmatites. It is also hypothesised that the two pegmatite families are derived in different tectonic settings and thus have a different petrogenesis (Martin and De Vito, 2005). As with most geological aspects, intermediates between the two family endmembers occur, termed the mixed LCT-NYF pegmatite family.

The mixed family is theorised to derive from NYF pegmatites that are crustally contaminated by host rocks to give the pegmatite a strong LCT signature (Martin and De Vito, 2005; Martin et al., 2009). In the NYF pegmatites late-stage hydrothermal fluids remobilise Li and B from the metasedimentary host rocks and overprint an LCT signature on the NYF pegmatite (Černý et al., 2012).

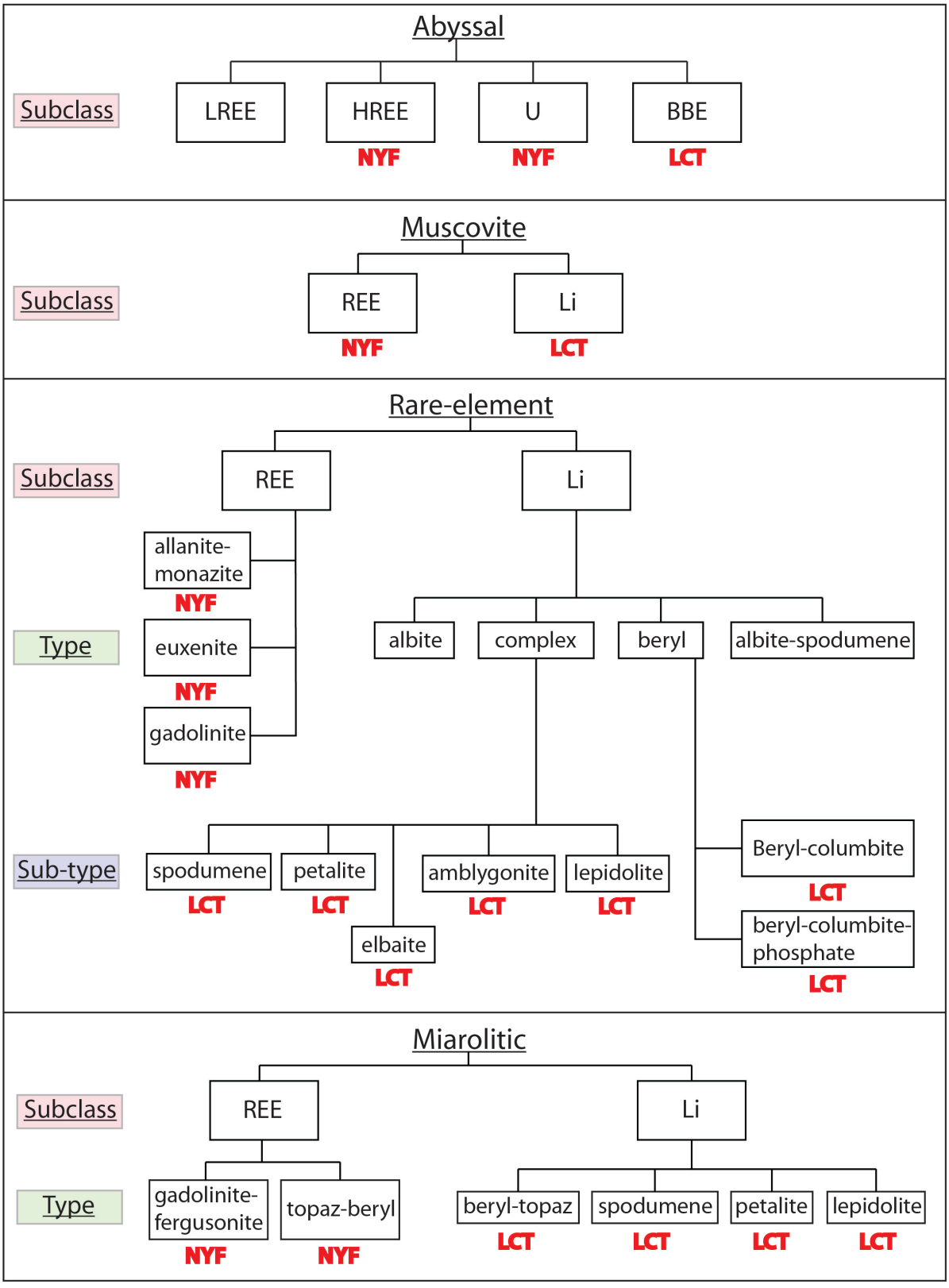


Figure 3.2: The currently accepted pegmatite classification scheme of Černý and Ercit (2005). The text in red shows how the classification scheme correlates with the two pegmatite families, NYF and LCT (Niobium-Yttrium-Fluorine and Lithium-Caesium-Tantalum respectively).

3.3.1 LCT-type pegmatites

The whole-rock geochemistry of a typical LCT pegmatite should share a compositional affinity with S-type granites, being derived from a S-type source rock such as enriched supracrustal lithologies (Chappell and White, 1974; London, 2008; Chappell et al., 2012; London and Kontak, 2012). However, some Archean examples occur that show LCT characteristics with a relationship to I-type granites. LCT pegmatites are generally sub- to per-aluminous, contain abundant muscovite, tourmaline and/or garnet. LCT pegmatites originate from hydrous magmas enriched in the incompatible elements Nb, Ta, Sn, B, F, P, Li, Be, Cs, Rb, Ga, Hf and Mn which are progressively enriched in the residual magma during quartz and feldspar crystallisation (Černý, 1991*b*; Martin and De Vito, 2005; Simmons and Webber, 2008).

Li is generally present within LCT pegmatites as spodumene, petalite, or more rarely, lepidolite. Tantalum and niobium occur as columbite-group minerals and minor phases of tapiolite, ixiolite and wodginite. Cesium, when present, generally occurs in the mineral pollucite, cesian beryl and trioctahedral mica. The source of these elements is somewhat poorly understood but suggestions summarised by London (2008) include melting of a muscovite-biotite-, potentially, ilmenite-bearing source. During partial melting of the source, muscovite incongruently melts and gives rise to an orthoclase restate which is a Ba sink, giving LCT pegmatites a Ba-poor chemical signature.

3.3.2 NYF-type pegmatites

NYF pegmatites are essentially the inverse of the LCT pegmatites, crystallising from dry, H_2O-poor magmas with an A-type geochemical signature (anorogenic). They are meta- to sub-aluminous and generally enriched in REE, U, Th, Zr, Ti, Nb, and Y (London, 2008; Simmons and Webber, 2008; Černý et al., 2012). Although they are H_2O undersaturated, Skjerlie and Johnson (1992) suggested that F is accumulated in the magma via pyroxene growth from mica and amphiboles. Common mineralogy includes sodic pyroxenes, amazonitic K-feldspar, amphiboles, topaz and monazite. Source rocks are suggested to be depleted lower-crustal granitoids or granulites and in some cases their constituents contain a mantle geochemical signature (Lenharo et al., 2003; Černý and Ercit, 2005). The origin of trace element signatures of NYF pegmatites is poorly understood compared to their LCT pegmatite counterparts (Martin and De Vito, 2005; Martin et al., 2009; London, 2008).

3.4 The formation and petrogenesis of pegmatitic melts

Since the early 1900s the generation and consolidation of pegmatite melts have been studied and hypothesised (e.g. Cameron et al., 1949). There are basically two fields of thought when it comes to the production of a pegmatitic magma that is rich in all the necessary volatiles and rare-elements required to crystallise a pegmatite, either at the site of melt generation or some distance away. Further and numerous hypotheses then surround how the pegmatitic melts are consolidated into the intrusions we see today (Cameron et al., 1949; Jahns and Burnham, 1969; London, 2008; Simmons and Webber, 2008; London and Morgan, 2012).

Historically the first field of thought was that pegmatites have a genetic relationship to granites. Various hypothesis then stem from that relationship on how exactly a pegmatitic melt is derived from a parent granitic melt. There are numerous examples of where this model is plausible and the pegmatites in question share a spatial association (Section 3.2) and similar geochemical signature to the granites (Jahns and Burnham, 1969; London, 2008; Simmons and Webber, 2008; London and Kontak, 2012). The second, and more recently accepted, field of thought is that pegmatitic melts may be generated by direct crustal anatexis of a source rock at the correct partial melt percentage and composition of the source rock (Simmons and Webber, 2008). This hypothesis takes on a more direct approach with arguments only focused around what geological process might cause such an event. The ideas have also led to many controversies in the classification of pegmatites and other aspects of their characteristics.

3.4.1 Derivation from a granite

The following model was proposed by Jahns and Burnham (1969) and is still widely accepted today, following various modifications to the original hypothesis, for different pegmatite provinces. In summary, the model involves the separation of an aqueous fluid phase from a granitic melt that is undergoing fractional crystallisation. Potassium and other incompatible elements (Na retained in the granitic melt) then partition into the separated fluid phase and either migrate or crystallise in situ to form a pegmatite (Fig. 3.3). This model is progressive: as the granitic melt continues to crystallise, more pegmatitic melts are generated and, due to fractionation, become increasingly enriched in incompatible elements and dissolved H_2O (Fig. 3.3). The pegmatitic melts

may then migrate to higher crustal levels along structural weaknesses in the crust (Section 3.2; Fig. 3.1), the later pegmatites being more complex and geochemically evolved.

The granitic melt in this model essentially acts as a reservoir for the pegmatitic melts and thus a genetic relationship is formed between granite parent and pegmatite daughter. For this model to be plausible, the pegmatites and genetically related granites should therefore share certain characteristics such as the spatial association seen in Section 3.2 (Černý, 1989; Simmons and Webber, 2008; London, 2008). Other shared features include a geochemical similarity and a similar age. Geochemical logic should also be apparent between the parent granite and daughter pegmatite such as the pegmatite should have higher concentrations of incompatible elements, such as REE, compared to the granite (e.g. Simmons et al., 1986). Another aspect which is not widely studied is that the resulting pegmatites should also lack highly mafic signatures since early granitic crystallisation should have depleted mafic components in the melt before the onset of pegmatite melt generation (London, 2008).

Aside from the generational aspects of the model, various processes and geological hypotheses are derived for the model. For example, a chemical quench scenario or an undercooled pegmatitic magma (see reviews in London, 2008 and Simmons and Webber, 2008). A more recent model for the genesis of pegmatites, that draws on aspects from other previous models, has become widely accepted and is known as constitutional zone refining (London, 2008; Simmons and Webber, 2008; London and Morgan, 2012). In essence the model suggests that a silicate liquid boundary layer, rich in fluxes, forms at the crystal-melt interface. With continued crystallisation, the boundary layer becomes significantly enriched in fluxes compared to the bulk pegmatitic melt. The fluxes then act as complexes for incompatible elements and subsequent crystallised phases are able to reach extremely large sizes with few impurities. The constitutional zone refining model points out the importance of fluxes and volatiles in the pegmatitic magma, their presence being paramount in the creation of textures, crystal sizes and mineralogical zonation observed in pegmatites (see reviews in Simmons, 2007; London, 2008; Simmons and Webber, 2008; Nabelek et al., 2010; Thomas et al., 2012).

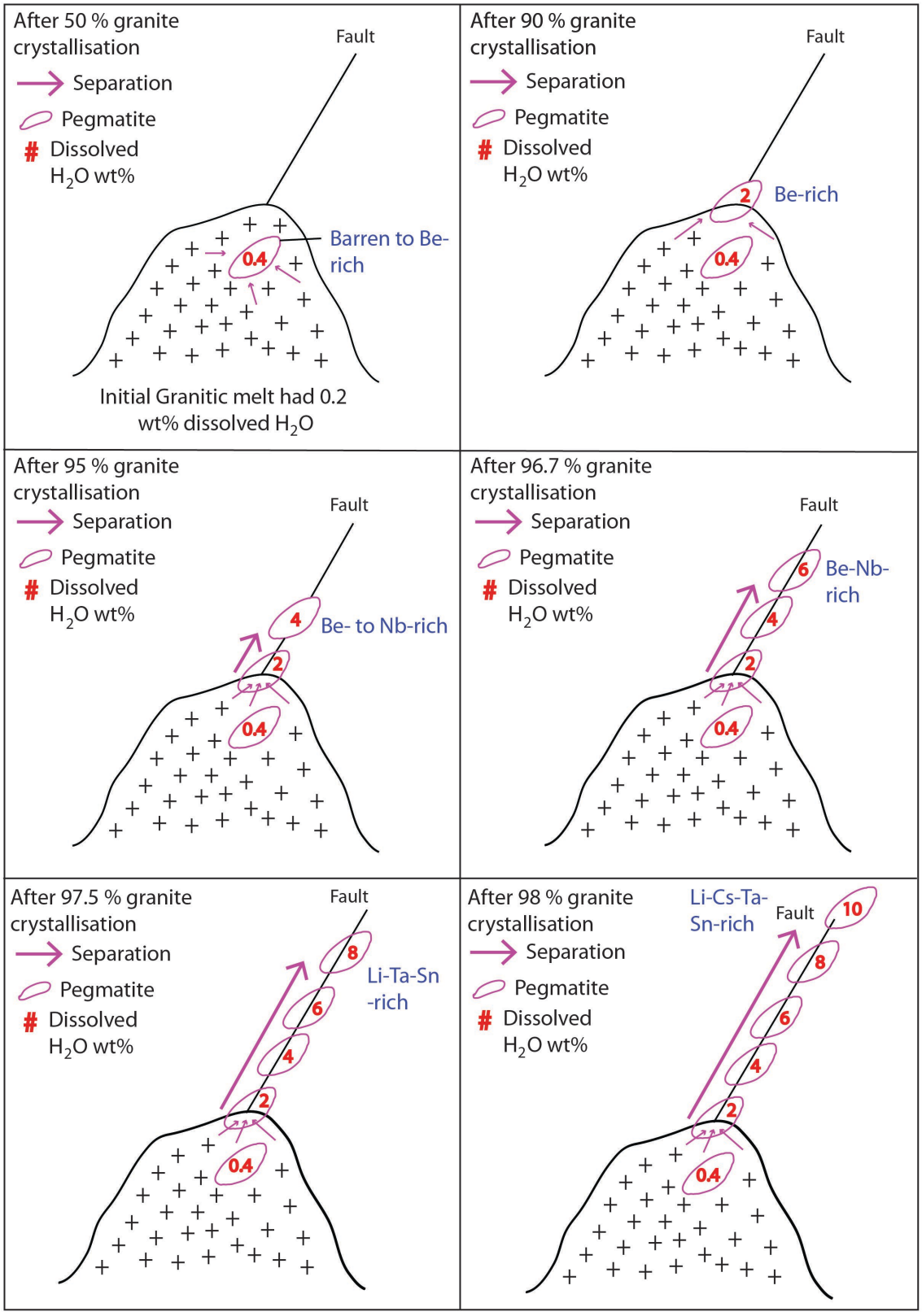


Figure 3.3: Illustration showing progressive separation of pegmatites from a parent granite undergoing fractionation. The image shows each subsequent pegmatite separated at varying percentages of granite crystallisation, dissolved H_2O and enriched elements (the Jahns and Burnham, 1969, model, modified after Simmons and Webber, 2008).

3.4.2 Derivation from anatexis

This theory only pertains to the actual creation of a pegmatitic melt. For example, pegmatite melt migration, crystallisation rates and consolidation theories, such as constitutional zone refining, remain the same for this model. It was the geological outliers to the Jahns and Burnham (1969) model that first led authors such as Simmons et al. (1995 and 1996) to suggest that a pegmatitic melt may be generated via direct partially melting of a source rock with an appropriate composition. These pegmatites, such as the ones in Western Maine, do not show the genetic connections that should be apparent in a granite parent, pegmatite daughter type relationship (Section 3.4.1.1). Various other examples also exist where authors have suggested that an anatexis model for pegmatite melt generation is more plausible (e.g. Nabelek et al., 1992; Roda et al., 1999; Falster et al., 2005). The model suggests that during orogenesis, a source rock rich in fluxes and the necessary elements required to form a pegmatite may be directly partially melted and produce a pegmatitic melt that may migrate, or crystallise in situ.

The hypothesis that pegmatitic melts may be produced by anatexis is a contributing factor to the current controversies surrounding the classification of pegmatites. Martin and De Vito (2005) suggested a revised pegmatitic classification scheme separating pegmatites into two types, pegmatites formed by anatexis and others derived from progressive separation and fractional crystallisation of a parent granite body. Furthermore, pegmatites may be categorised by the tectonic environment in which they form: LCT = orogenic and NYF = anorogenic. However, in some instances, coeval NYF and LCT type pegmatites occur; the Damara Belt being an example of such as case (Ashworth, 2013). This adds to the complexity of classification models of various authors.

The Cape Cross-Uis pegmatite belt provides an excellent example of an understudied pegmatite belt which may contribute to our understanding of pegmatite petrogenesis, from melt creation phases to consolidation and mineralisation. The pegmatites of the CUPB display varying characteristics and element diversity in a discrete, well-defined area, ideal for the testing of currently accepted views and different hypotheses.

Chapter 4: Classification, mineralogical and geochemical variations in pegmatites of the Cape Cross-Uis pegmatite belt, Namibia

Warrick C. Fuchsloch, Paul A.M. Nex, Judith A. Kinnaird

Lithos **296-299**, 79-95

Keywords: Granitic pegmatite, Pegmatite classification, Namibia, Damara Orogen, Pegmatite geochemistry, Anatexis

4.1 Abstract

The Pan African aged Damara Orogen in Namibia is host to the Cape Cross-Uis pegmatite belt, one of several NE trending pegmatite belts which host Li, Nb, Ta and Sn mineralisation. Field mapping and structural analysis of thirty-seven pegmatite bodies has shown that the pegmatites intrude along crustal weaknesses such as fold axes and bedding planes, predominantly following the approximate NE orientated regional structural fabric. The lack of deformation together with cross-cutting relationships mapped, suggest that pegmatites were emplaced during post-tectonic extension that resulted from end-orogeny crustal relaxation. Based on mineralogy, geochemistry and ore mineralogy, three groups of pegmatites are distinguished within the Cape Cross-Uis belt. (1) The most common are the unzoned Nb-Ta-Sn type with mineralised alteration areas in the form of greisenised and albitised zones that occur sporadically in the pegmatites in various morphologies. (2) The garnet-tourmaline, crudely zoned pegmatites are slightly less common. They are granite-hosted and differ from other pegmatite types in terms of their low Rb, Sr, Nb, Ta, Sn, Cs (30 ppm) but higher REE, U, Th, and Y values. (3) The zoned lithium-bearing pegmatites are rare but the most complex. They are subdivided into two groups: The Li-Nb-Ta-Sn spodumene-bearing pegmatites of the Karlowa swarm and the Li-Nb-Ta-Sn-Be petalite-bearing pegmatites of the Strathmore swarm. They are highly fractionated with typical values of Nb (206 ppm), Ta (185 ppm) and Sn (10,016 ppm). There is no spatial distribution or regional zonation of the pegmatites type relative to granite outcrops within the belt. Contrasting geochemical fractionation patterns and the lower concentrations of REE in pegmatites than in granites suggests that pegmatites resulted from varying degrees of partial melting of a muscovite-ilmenite-bearing source. The Sn, Nb and Ta in pegmatites is likely to have originated from this source rather than from assimilation of metasedimentary host rocks as clear fractionation trends from fine-grained pegmatite margins

to alteration zones show that fractionation was the dominant process in which Nb, Ta, Cs and Sn were enriched.

4.2 Introduction

There are several pegmatite belts within western Namibia (Fig. 4.1) including the Cape Cross-Uis belt, also known as the northern tin belt (Richards, 1986; Wagener, 1989) and until now has not been investigated for the last twenty-five years. This Pan-African age pegmatite belt is hosted in the Damara Orogen (Fig. 4.2A) and contains multiple rare element pegmatites and is approximately 120 km in length and 40 km in width with a NE orientation (Diehl, 1992*a*, 1993; Richards, 1986; Wagener, 1989). For comparative purpose, Sn-, Nb- and Ta-bearing pegmatites were also studied from the parallel Nainais-Kahero tin-bearing pegmatite belt (Fig. 4.1, 4.2A). The Nainais historical tin workings, 32 km southeast of Uis, include four bedding parallel pegmatites over an area of approximately 0.25 km^2.

Economically mineralised pegmatites appear to be exclusively post tectonic with emplacement ages of between 510 and 500 Ma (Ashworth, 2013; Diehl, 1993; Kinnaird and Nex, 2007; Longridge, 2012; Melcher et al., 2015; Miller, 2008; Wagener, 1989). Previous research on the Cape Cross-Uis pegmatite belt is sparse and is largely focused on the controls of the mineralisation. Richards (1986) suggested that the pegmatites of the Damara Orogen were associated with S-type or I-type granitic and granodioritic intrusions; however, the relationship between the granites and pegmatites is debatable and pegmatites might represent individual partial melts of a metasedimentary source (Ashworth, 2013). On a regional scale, Diehl (1993) suggested that the increase in metamorphic grade to the west coincided with an increased grade of mineralisation. Richards (1986), Singh (2007, 2008) and Wagener (1989) suggested that assimilation of country rocks and concomitant remobilisation of Sn by late-stage pegmatitic fluids, were responsible for the mineralisation with the abundance of tourmaline at the margins of the pegmatite being a marker for mineralisation.

The Cape Cross-Uis pegmatite belt has been divided into three separate pegmatite swarms: Strathmore (Fig. 4.2A,B), Karlowa and Uis (Fig. 4.2A) and based on the classification of Černý and Ercit (2005), the pegmatites are of the LCT family, rare-element class and beryl complex type.

This paper introduces the first whole-rock geochemical study of the pegmatites, granites and metasediments of the Cape Cross-Uis pegmatite belt, combined with petrography, structural and geological mapping. This paper questions whether these pegmatites fit into the typical classification scheme and assesses the timing of their structural emplacement. The data are used to evaluate whether mineralisation resulted from assimilation of country rock, fractionation of a granite parent or internal pegmatite processes such as fractionation. By assessing these trends, this paper adds to the debate of whether these pegmatites are products of partial melting or share a parent-daughter relationship with surrounding granites.

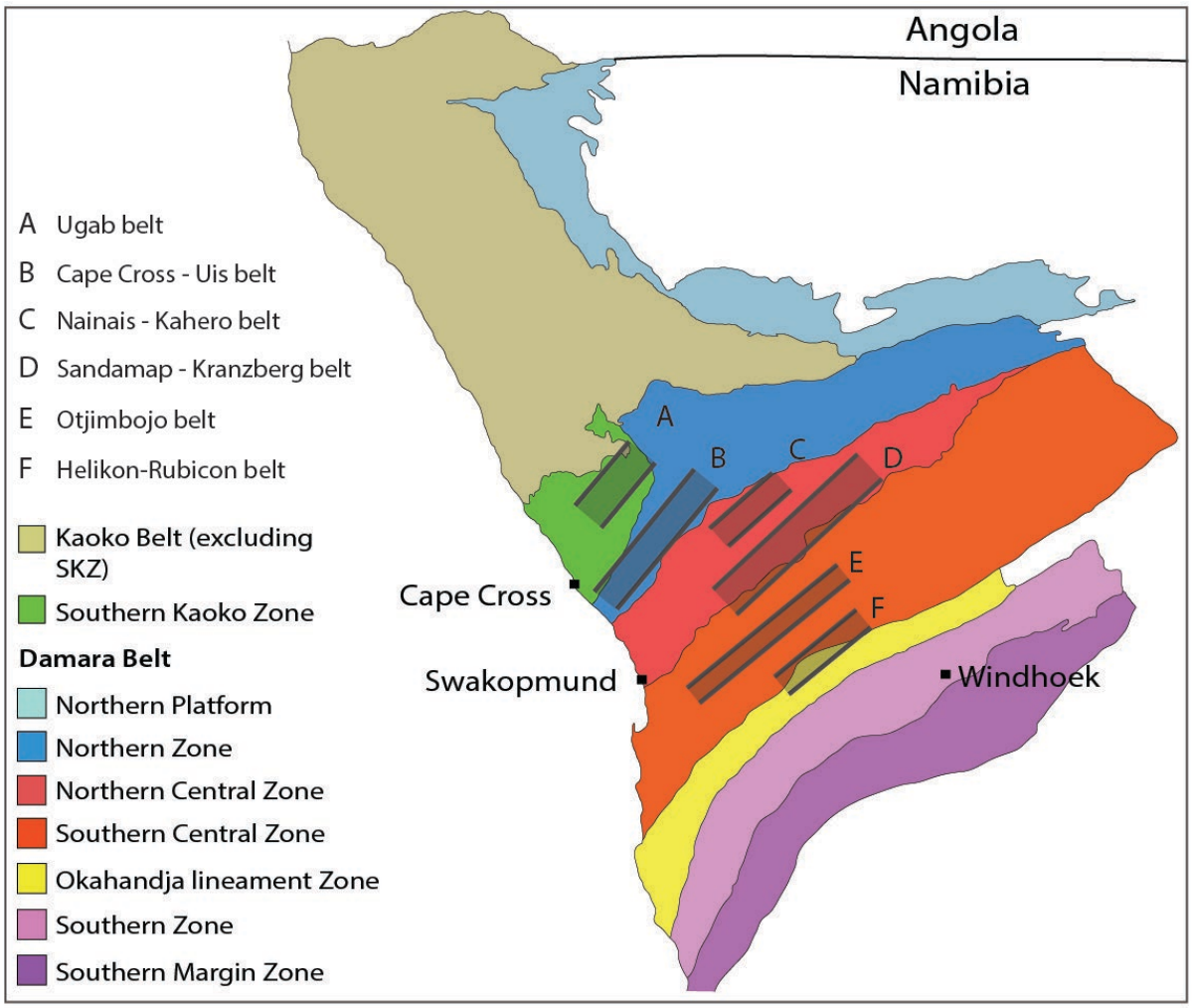


Figure 4.1: The tectono-stratigraphic zones of the Damara Orogen showing the approximate location of six of the main pegmatite belts (modified after Keller et al., 1999; Miller, 1983 and Richards, 1986).

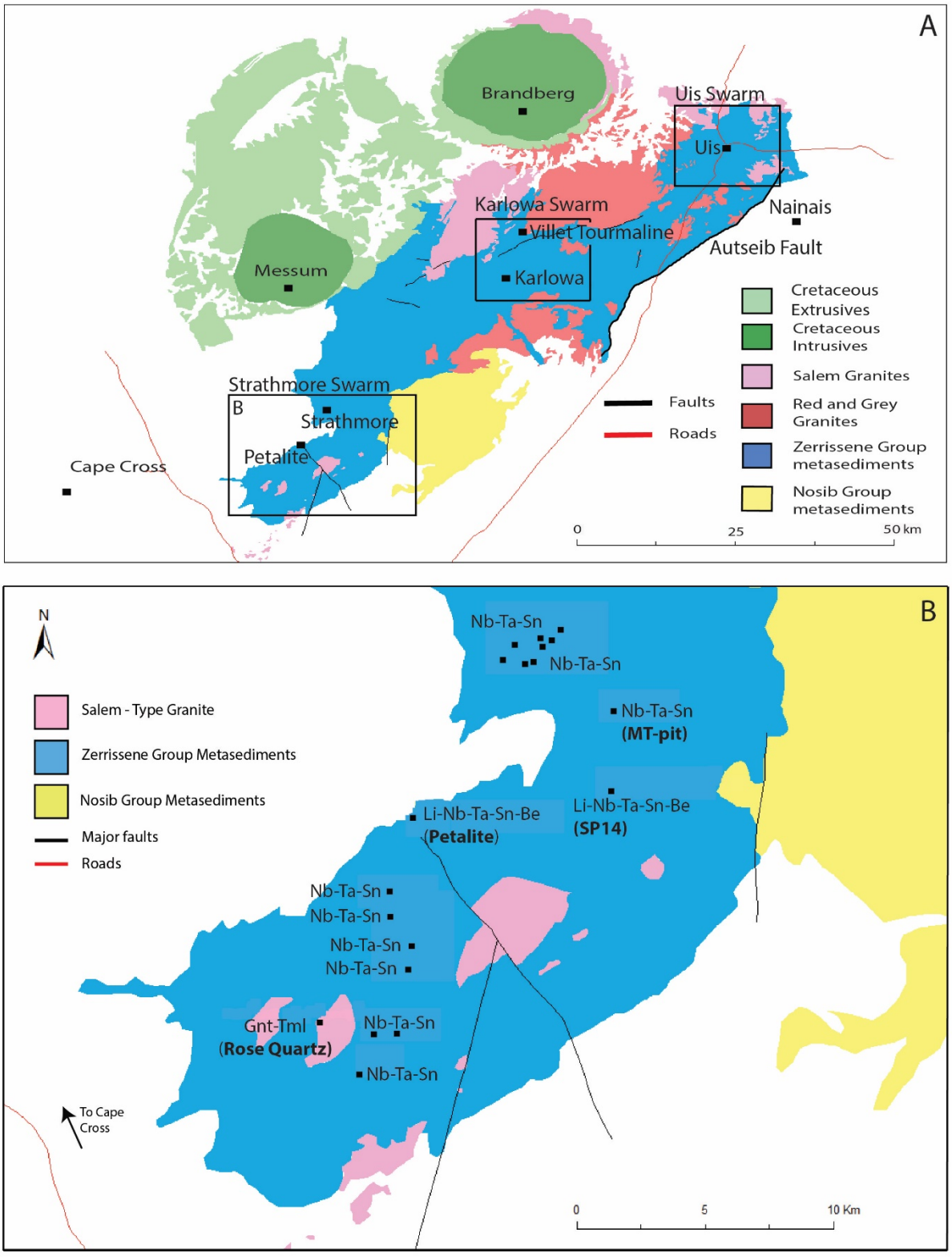


Figure 4.2: A) Simplified geological map of the Cape Cross-Uis pegmatite belt, showing metasediments and igneous rocks of the Damara Orogen and post-Damaran magmatism (modified after "Geological map of Namibia, Sheet 2114 - Omaruru"). B) Simplified geological map of the Strathmore pegmatite swarm showing the locations of several different pegmatite types (see Table 4.1 for pegmatite types).

4.3 Background

4.3.1 Regional geology

The NE-trending Damara Orogen formed during the Pan-African tectono-thermal event. Age-dating of volcanic units within the Nosib Group indicates a span of activity between 750 Ma and 440 Ma (De Kock et al., 2000; Hoffman et al., 1996). The orogen represents a triple point between the Congo, Kalahari and Rio de la Plata cratons that amalgamated during the assembly of Gondwana (Gray et al., 2006; Martin and Porada, 1977; Miller, 1983, 2008; Miller and Frimmel, 2009). The Damara Orogen (Fig. 4.1) represents a Wilson cycle with extension during the break up of Rodina, spreading, sedimentary deposition, subduction and orogenesis during which metasediments and igneous rocks, including a large number of pegmatites, of the orogen formed (Prave, 1996; Trompette, 1997). Miller (1979, 1983, 2008) divided the Damara Orogen into a number of tectono-stratigraphic zones based on variations in structure, stratigraphy, igneous activity and metamorphic history (Fig. 4.1). The various pegmatite belts roughly occur in different zones and therefore at different stratigraphic levels within the Damara Orogen. The Cape Cross-Uis pegmatite belt described in this paper lies in the Northern Zone (Richards, 1986).

Onset of subduction-related magmatism in the Damara Orogen is marked by the intrusive Goas suite and spans an age from 580 to 545 Ma (Milani et al., 2015). Later orogenesis-related magmatism is associated with the D3 deformation event (~542 Ma; Tack et al., 2002) which is depicted in the Northern Zone as tight north-south-striking, moderately- to steeply-inclined folds attributed to the convergent and shortening phases (Goscombe et al., 2004; Gray et al., 2006; Macey and Harris, 2006; Miller, 2008). The D3 deformation event is responsible for magma production and therefore mineralisation in syn- and post orogenic pegmatites and other associated intrusive bodies (Kinnaird and Nex, 2007; Kisters, 2005; Kisters et al., 2004). Pegmatite emplacement ages within the Damara Orogen range from 509 to 429 Ma (Briqueu et al., 1980; Longridge, 2012; Miller, 2008). For the Uis pegmatite swarm an age of 496 ± 30 Ma was suggested by Haack and Gohn (1988; based on Rb-Sr data) whilst Diehl (1993) suggested emplacement at 486 ± 8 Ma using Rb-Sr data in muscovite. Melcher et al. (2015) also reported an age of 0.5 Ga for age of emplacement of the Uis pegmatite but with no details of the methodology used to obtain this age.

Regional mineralisation trends have been inferred by authors such as Diehl (1993) and Richards (1986). Diehl (1993) suggested that the increased metamorphic grade to the west of the belt coincides with an increase in mineralisation. Another suggestion by a variety of authors (e.g. Černý, 1989) is that the type and grade of mineralisation in a pegmatite is spatially distributed around parent granitic bodies. If this were the case, then the pegmatite type and mineralisation abundance should be zoned around the parent granite body with the barren pegmatites closest to the granite and more complexly mineralised bodies furthest from the granite.

4.4 Description of pegmatites and country rocks

Mapping was completed at a local pegmatite scale and at a regional pegmatite swarm scale with a focus on the structural aspects of pegmatite dimensions and host rock folding, faulting and shearing. Mineralogical and petrographical observations were recorded and pegmatite zoning, although sparse, was studied. Accessory phases from pegmatites were investigated and identified using a FEI Quanta 200 SEM using Energy Dispersive Spectroscopy (EDS) at the University of the Witwatersrand at the MMU facility. The operating conditions for the SEM were 15 kV and 100 s for the spectra collection time.

4.4.1 Field relationships

The Cape Cross-Uis pegmatite belt is largely covered by desert sands with outcrop more common further inland. Metasediment-hosted pegmatites can be found in historically and artisanally mined areas and excavations are often filled in and/or the pegmatites are mostly mined out. Although metasediment-hosted pegmatites are more abundant, granite-hosted pegmatites show more prominent outcrop due to the resistant granite domes present in the belt. The Strathmore and Uis swarms are the most abundant in terms of pegmatite outcrop, with over fifty individual large pegmatite bodies exposed. The Karlowa swarm is less abundant at surface but it is possible that many more pegmatite bodies occur at depth. Pegmatites range in size from several hundred metres in length with maximum widths of approximately 60m, to thin anastomosing veins no more than a few centimetres in width. Pegmatites generally occur as lenticular bodies although veins, en echelon arrays, pods, dykes (Nainais) and sigmoids (Uis) also occur.

Stratigraphically, the Cape Cross-Uis pegmatite belt is situated within the Zerrissene Group (stratigraphically equivalent to the Swakop Group) of the Damara Supergroup (Fig. 4.2). The Group includes metagreywacke, biotite schist and quartzite of the Amis River Formation which has been downthrown by the Autseib fault against marble, calcsilicate, quartzite and schist from the Rössing, Oberwasser, Karibib and Kuiseb Formations of the Swakop Group (Diehl, 1993; Miller, 1983, 2008). The Nainais pegmatites intrude the Kuiseb Formation porphyroblastic schists of the Swakop Group which are similar to the porphyroblastic schists of the Amis River Formation. The Amis River Formation is classified as a fan fringe deposit or a classical distal outer fan lobe, deposited in a distal basin plain environment. It covers the entire succession within the Cape Cross-Uis pegmatite belt (Swart, 1992). These metasediments are regionally metamorphosed to greenschist facies and later thermally metamorphosed to amphibolite facies by the intrusion of Salem-type granites resulting in a cordierite biotite schist known as Knotenschiefer (Goscombe et al., 2004; Macey, 2003; Wagener, 1989). The cordierite porphyroblastic 'knots' underwent metamorphic retrogression to greenschist facies assemblages but retained their morphologies (pseudomorphs).

Pegmatites predominantly intrude the metasedimentary units whereas other pegmatites are hosted by fine- to coarse-grained, porphyritic Salem granodiorites and Red and Grey monzogranites. The pegmatites are orientated NE and contacts with the host rocks are sharp. The pegmatites are characterised by quartz, plagioclase, microcline perthite and muscovite with minor microcline sometimes common in larger pegmatites such as the Petalite pegmatite. Accessory minerals are typically apatite, magnetite, cleavelandite, beryl, monazite, zircon, garnet and tourmaline (black, green and pink varieties). Cleavelandite is a low temperature variety of albite that forms radial aggregates within or near alteration zones. Common ore-forming minerals include petalite, lepidolite, spodumene, amblygonite, cassiterite, columbite-group minerals (CGM) and tapiolite. Since no mineral chemistry data are available, the specific mineral species belonging to the mineral groups mentioned above are not used.

Greisenisation is common and appears to be restricted to metasediment-hosted pegmatite-types. Some greisens are extensive and composed solely of muscovite and quartz, whereas often the greisenisation is patchy, shows partial alteration and occurs sporadically abundantly throughout a

pegmatite body. Greisens also occur either as elongate discontinuous lenses or occasionally as parallel-sided layers extending for several metres along the strike of a pegmatite. Greisens are well mineralised with CGM and cassiterite (Nb, Ta and Sn) as are saccharoidal albite-rich fluid-altered zones. It is important to note that when mentioning albitised and greisenised zones, this does not imply that the pegmatite itself is classically zoned since most pegmatites in the Cape Cross-Uis pegmatite belt are unzoned. This references the observation that there are areas within the pegmatites where greisens and albitic units occur, sometimes sporadically throughout a pegmatites body or in a discrete layer or lens. Petalite, lepidolite and spodumene Li-mineralisation, although rare, is hosted in the magmatic zones within classically zoned pegmatites, displaying an equigranular magmatic texture and little muscovite and albite alteration.

4.4.2 Pegmatite types

Pegmatites are divided into three main groups based on their host rock, their mineralogy, whether they were zoned, and the nature of oxide ore minerals. The lithium-bearing pegmatites are further subdivided into two groups, depending on whether the dominant lithium mineral is spodumene or petalite (Table 4.1).

4.4.2.1 CGM-cassiterite pegmatites (Nb-Ta-Sn)

The type localities of Nb-Ta-Sn pegmatites are the Strathmore and Uis areas. They are the most abundant type of pegmatite in the belt and occur in a variety of morphologies, from thin veins to larger intrusions of 50 × 5 m in size. They intrude strike-parallel to Knotenschiefer, quartzite and biotite schist country rocks and have a bifurcating emplacement style often joining at depth (Fig. 4.3D). The Nb-Ta-Sn pegmatites show similar metasomatic contacts with country rocks as the Li-bearing pegmatites. The pegmatites are not zoned although the wall rock is generally fine-grained and muscovite-rich. The pegmatites are dominated by quartz, albite, microcline perthite and muscovite with minor non-perthitic microcline. CGM, cassiterite and minor ilmenite occur within greisenised or albitised zones that occur on a centimetre to metre-scale. Garnet, tourmaline and apatite are sporadically distributed throughout the pegmatites but are not ubiquitous to all pegmatites of this type. Magnetite and Fe- and Mn-rich phases are more abundant in these pegmatites than other types and are often associated with ore zones/pods of greisen material. In

thin section these pegmatites often display a graphic and myrmekitic texture and sericitic alteration of most feldspar.

Table 4.1: Pegmatite type table showing the pegmatite types in the Cape Cross-Uis pegmatite belt, their common mineralogy, host rocks and distinguishing features. Pegmatites are arranged from most common to least common. CGM. = Columbite-group minerals

Pegmatite Type	Swarms	Common Mineralogy	Host rocks	Distinguishing features
Columbite-tantalite, cassiterite, unzoned pegmatites (Nb-Ta-Sn)	all swarms Nainais	CGM, cassiterite, tourmaline, apatite, quartz, albite, muscovite	metasediments	Unzoned but sometimes exhibit a quartz rich core. They vary in size from a metre to tens of metres in scale. Greisen zones contain CGM and cassiterite. The most common pegmatite in the belt
Tourmaline-garnet, crudely zoned, intragranitic pegmatites (Gnt-Tml)	Strathmore Karlowa	garnet, tourmaline, quartz, perthite, muscovite ± biotite	intragranitic	Often crudely zoned with a quartz core, a perthite intermediate zone and a muscovite rich, unidirectional crystal tourmaline growth border zone. They vary in size but are usually laterally extensive and 2-3 m in width
Lithium, niobium, tantalum and tin ± beryllium, zoned/unzoned pegmatites (Li-Nb-Ta-Sn-Be)	Strathmore	beryl, tourmaline, apatite, cassiterite, CGM, hectorite, petalite, eucryptite, muscovite, quartz, perthite, albite	metasediments	Zoned with several distinguishable zones; complex mineralogy and geochemistry. They are rare in the belt and large, reaching 40m in width and extending a few hundred metres in length.
Lithium (spodumene), niobium, tantalum and tin, unzoned pegmatites (Li-Nb-Ta-Sn)	Karlowa	tourmaline, apatite, quartz, columbite-tantalite, perthite, albite, spodumene	metasediments	Unzoned but with a quartz-rich core, characterised by spodumene and abundant green apatite

Compared to the Uis pegmatites, the Strathmore pegmatites generally show more abundant, large CGM crystals, up to 4 cm in size, that are compositionally zoned, with adjacent or included minor cassiterite. The Uis pegmatites have larger (several centimetres) cassiterite crystals with minor (0.1mm) zoned CGM inclusions. The historically mined Uis pegmatites are almost devoid of individual CGM grains, rather these minerals only occur as inclusions in cassiterite, whereas Strathmore pegmatites host both cassiterite and CGM as individual grains.

4.4.2.2 Tourmaline-garnet, crudely zoned, intragranitic pegmatites (Gnt-Tml)

The intragranitic pegmatites hosted by Salem-type granodiorites and Red/Grey granite are generally smaller bodies than those hosted by metasediment within the belt. These pegmatites are less than a few metres in width, may extend a few hundred metres in length and consist of muscovite, quartz and perthite. They are crudely zoned, exhibit a border zone with micaceous quartz and tourmaline that shows a unidirectional solidification texture (UST; Fig. 4.3A), an intermediate perthite-muscovite-tourmaline zone in which gem tourmaline occurs and a quartz core (Fig. 4.3B). Black and transparent green tourmaline occur at the contact with the quartz core whilst garnet occurs in amorphous pods sporadically across different zones. Common features in thin section include a graphic texture, sericitic alteration of most feldspar, annealing of quartz and a poikilitic tourmaline growth around sericitised feldspars. Salem-type host granodiorites are fine- to coarse-grained and porphyritic with sericitic alteration throughout. Tourmaline and garnet have not been found within the Salem-type granodiorites whereas the Red/Grey granites are both tourmaline and garnet bearing. Occasionally xenoliths of biotite schist occur within the granite and pegmatite outcrop. Xenoliths are highly metasomatised and severely tourmalinised when a xenolith is in contact with a pegmatite (Fig. 4.3C).

4.4.2.3 Lithium-bearing pegmatites (Li-Nb-Ta-Sn-Be and Li-Nb-Ta-Sn; Table 4.1)

Lithium-bearing pegmatites are the least common within the Cape Cross-Uis pegmatite belt although petalite and lepidolite do occur sparsely in other pegmatites near Uis. The Li-Nb-Ta-Sn-Be pegmatites are generally large, asymmetrically zoned, lens-shaped bodies that are the most complexly zoned and most highly evolved. They have been subdivided into the two following groups.

4.4.2.3.1 The Li-Nb-Ta-Sn-Be pegmatites

Two Li-Nb-Ta-Sn-Be zoned pegmatites occur in the Strathmore swarm, the Petalite pegmatite and the smaller SP-14 pegmatite (Fig. 4.2B; Diehl, 1993), both of which are similarly zoned. Each has a muscovite-quartz-alkali feldspar wall zone, a quartz-microcline-albite-muscovite intermediate zone and a quartz core (Diehl, 1993). Extensive greisens surround the quartz core and host centimetre sized CGM and cassiterite (Diehl, 1993). Beryl sporadically occurs at the contact of the intermediate zone with the border zone.

The Petalite pegmatite is the most complex pegmatite within the belt that has been mined sporadically for lithium, industrial mica, beryllium and tin. The NNE trending pegmatite is ~60 m wide, over a 100 m in length and has a steep 65° dip to the NW. The pegmatite is complexly and asymmetrically zoned and intrudes Amis River Formation Knotenschiefer and biotite schist. The schist at the contact has been highly metasomatised resulting in centimetre scale layers of tourmaline (Fig. 4.3C). The wall zone of the pegmatite ranges from 1 to 2 m in width and consists of UST book mica and finer-grained quartz and apatite. The intermediate zone is the largest volumetrically (approximately 60%) and consists of quartz, albite, microcline perthite and minor non perthitic microcline. The original feldspar has been completely altered in the extensive greisen zone which occurs in the NW intermediate zone. The greisen is ~35 m in length and several metres in width and is host to centimetre sized cassiterite and CGM. The contacts between the greisen and unaltered pegmatite are diffuse. The core zone is primarily massive quartz and volumetrically occupies approximately 20% of the pegmatite. Petalite occurs at the interface between the intermediate and core zone on the SE side of the asymmetrically zoned pegmatite. In albitised replacement zones, secondary hectorite (smectite-group mineral; $Na_{0.3}(Mg,Li)_3Si_4O_{10}(OH)_2$ and eucryptite ($LiAlSiO_4$) replace petalite in areas which host abundant cleavelandite. Radial aggregates of tourmaline are also commonly associated with Li minerals and occur near the quartz core zone.

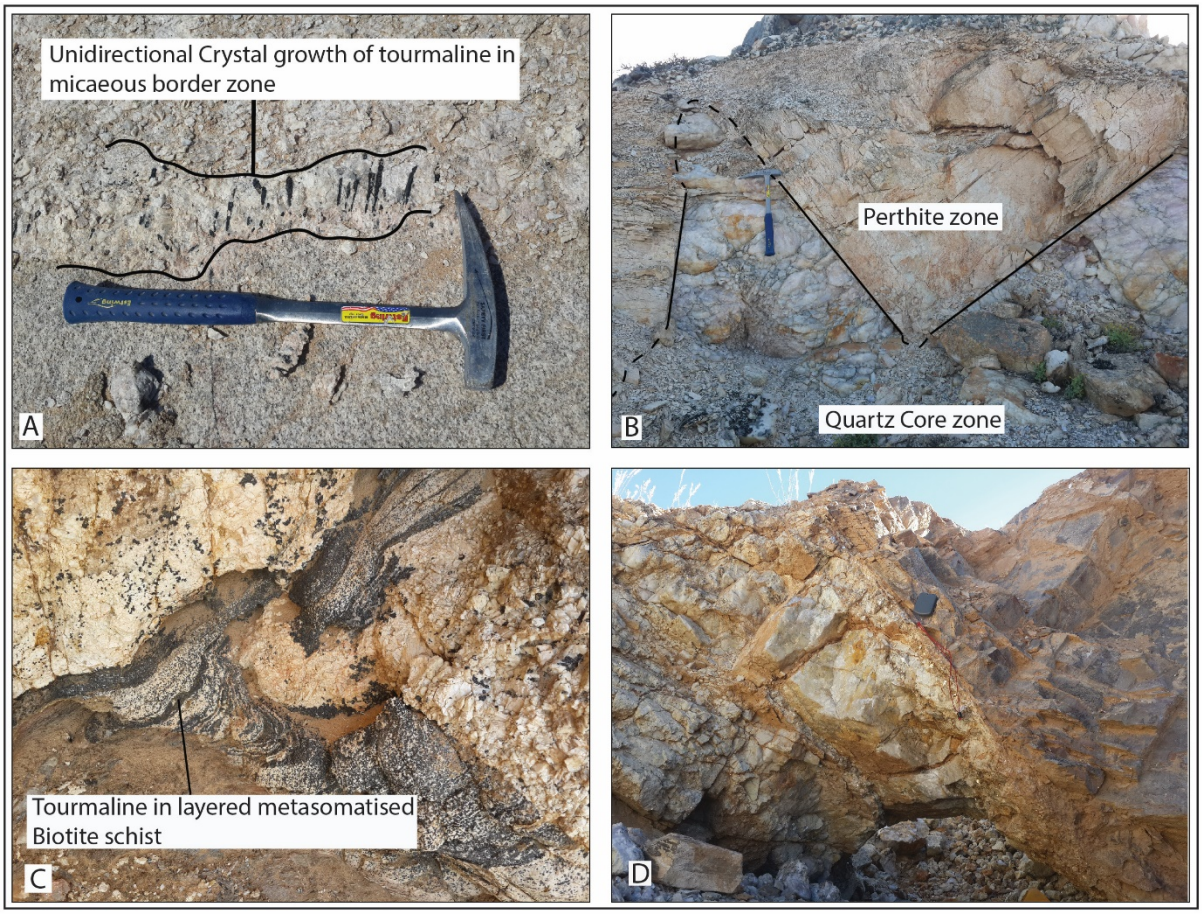


Figure 4.3: Field outcrop photographs of pegmatites in the Strathmore area. A and B are from the Rose Quartz pegmatite at co-ordinates 33K 414644 m E 7591110 m S and C and D are from the Petalite pegmatite at co-ordinates 33K 41827 m E 7599061 m S (Fig. 4.2B). A) Unidirectional crystal growth of tourmaline from an intragranitic pegmatite. B) A crudely zoned pegmatite within the area showing a quartz core and a feldspar perthite intermediate zone. C) Highly metasomatised biotite schist at the Petalite pegmatite. Note tourmaline within metasediment. D) A crudely zoned Nb-Ta-Sn pegmatite intruding Swakop Group biotite schist showing a quartz core and a feldspar perthite intermediate zone.

4.4.2.3.2 The Li-Nb-Ta-Sn pegmatites

The Li-Nb-Ta-Sn pegmatites are much simpler and smaller than the Li-Nb-Ta-Sn-Be pegmatites and they intrude finer-grained biotite schists. They are approximately 100–200 m in length, several metres in width with a NNE trend. They are crudely zoned with a thin micaceous border zone that is several centimetres wide, a feldspar-dominated intermediate zone and a quartz core. The intermediate zone occupies most of the pegmatite volumetrically with small metre-scale, disjointed quartz pods forming the core. Lithium minerals occur as spodumene (Diehl, 1993) and hectorite in the intermediate zone. Apatite is abundant throughout the intermediate zone, with some crystals up to 5 cm in size. The Karlowa pegmatites (Fig. 4.1) show centimetre-scale patchy greisenisation

which hosts 0.5–1 cm CGM crystals. Greisens are often associated with low temperature minerals such as radial cleavelandite and other albitised replacement zones.

4.4.2.4 The Nainais pegmatites

The four pegmatites in the Nainais area are strike parallel (NE) with the host Knotenschiefer and dip steeply towards the NW, although one of the four pegmatites cross-cuts other strike- parallel pegmatites. Pegmatites are up to 15 m in width and extend several tens of metres in length locally becoming more lenticular in shape. The pegmatites are fine-grained, have low quartz abundance, and are massive and unzoned with the dominant mineralogy consisting of feldspars and muscovite. Greisenisation is patchy and occasionally occurs as metre scale pods, hosting centimetre-scale CGM and cassiterite crystals. There are two main differences between the Cape Cross-Uis and Nainais pegmatites: (1) muscovite in the Nainais pegmatites has a yellow colour and is finer-grained than muscovite in the Cape Cross-Uis pegmatite belt. (2) The Nainais pegmatites have less abundant quartz.

4.4.3 Structural characteristics

The regional structural NE-orientated schistosity extends throughout the pegmatite belt and is observed in most metasediments of the Amis River Formation. On a microscale, the schistosity is a prominent feature. The muscovite schistosity in Knotenschiefer is displaced around the porphyroblasts (knots), showing that contact metamorphism took place after the regional metamorphism.

Many pegmatites have an anastomosing habit although the larger more prominent pegmatites show a more consistent NE trend with an approximate mean vector of 33˚(Fig. 4.4) and NW steep dip. The dominant pegmatite orientation follows the regional structural trend of the Cape Cross-Uis pegmatite belt; however, some pegmatites cross-cut the regional structural fabric. This feature is due to pegmatites taking advantage of structural weaknesses within the belt. For example, pegmatites intrude along shear zones and within fold axes; the MT-pit (SE of Strathmore; Fig. 4.2B) intrudes into a D_3 fold axis. No Damaran-aged structural deformation of pegmatites has been observed.

Pegmatites at the Rose Quartz locality (Fig. 4.2B) show that a post-Damaran shearing event has affected their orientation (Fig. 4.5) which is most likely due to the Cretaceous intrusives/extrusives, as this shear zone is not consistent with any Damaran structures. En-echelon intragranitic pegmatite veins of ~20 cm width show a dextral sense of shear on this shear zone running approximately north. The most abundant structural features within the belt are small scale, post-D_3, pegmatites that intrude tension gashes (Fig. 4.5), and pegmatites that have been boudinaged. Tension gashes and boudinage show approximately the same interpreted σ_3 and σ_1 orientations of 186˚and 106˚respectively. Although pegmatites take on a general NE trend, some are emplaced into large scale en-echelon sigmoidal tension gashes (e.g. at Uis).

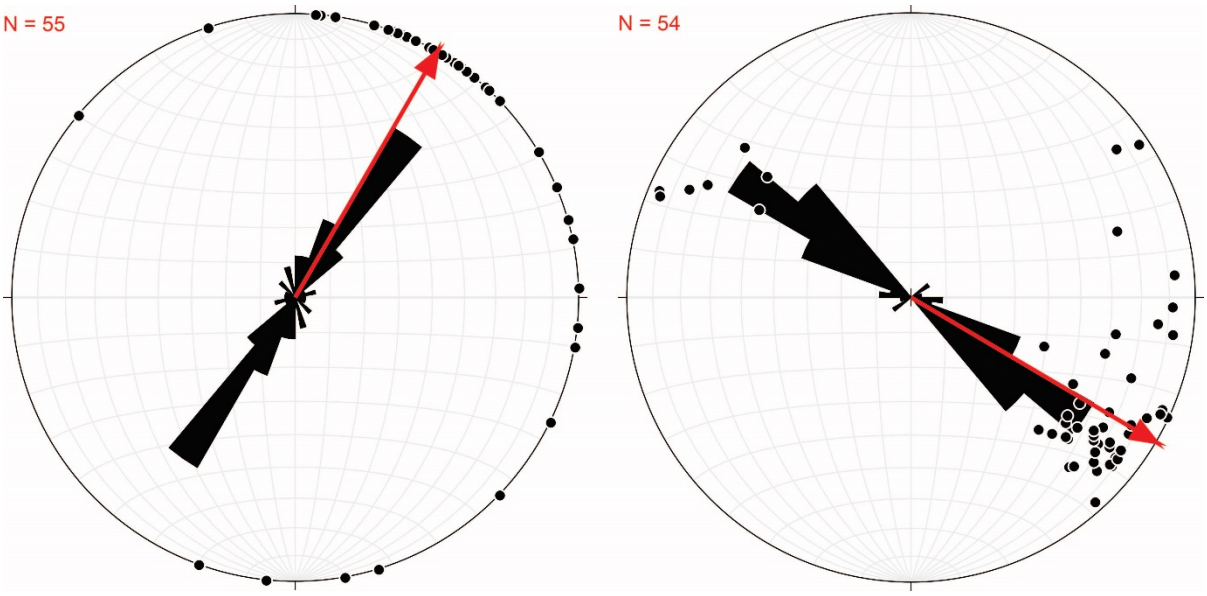


Figure 4.4: Rose Diagrams depicting the average trend of the pegmatites (Left) and the poles of planes of the Swakop Group metasediments (Right) in the Cape Cross-Uis pegmatite belt. The red arrow indicates the mean vector.

In thin sections, four of the thirty seven pegmatite bodies investigated exhibit folding and faulting of muscovite and feldspars, indicative of higher compressional deformation after intrusion. These features are only apparent in the primary mineralogy. Late-stage greisens show none of these deformational features on the microscale anywhere in the pegmatite belt indicating that alteration muscovite was not deformed. Field and structural relationships within the Cape Cross-Uis pegmatite belt show no evidence for in situ anataxis of country rock being responsible for pegmatite partial melt generation.

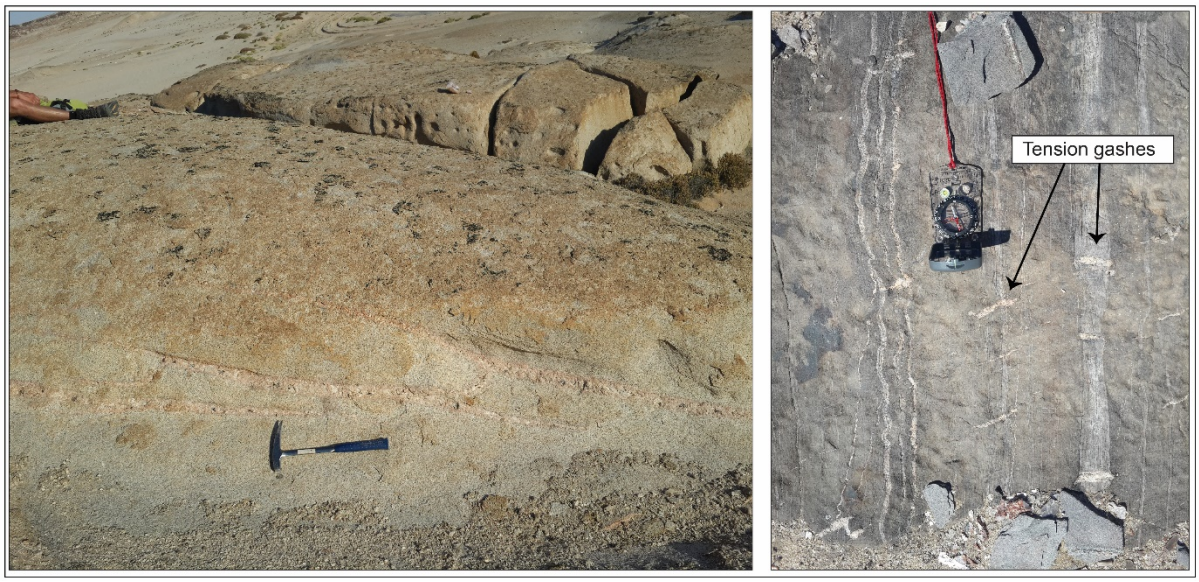


Figure 4.5: Photographs of macroscopic structural features from the Rose Quartz area located at co-ordinates 33K 414644 m E 7591110 m S. (Left) Intragranitic pegmatite veins showing dextral shearing. (Right) Pegmatites intruding tension gashes within Swakop Group banded biotite schist metasediments.

4.5 Methodology

Pegmatite, granite and country rock samples were collected in April/June 2014. Samples were selected from fine-grained and border zones of individual pegmatites to provide the best possibility of obtaining material representative of the geochemistry of the whole pegmatite. A total of 37 whole-rock pegmatite, 34 metasediment, and 5 granite samples were geochemically investigated from 37 individual pegmatite bodies throughout the Cape Cross-Uis pegmatite belt and in the Nainais area (Fig. 4.1).

Whole-rock pegmatite samples, metasediment and granite samples were crushed using a carbon-steel jaw crusher and milled by a carbon-steel swing mill in the School of Geosciences, University of the Witwatersrand. Major element data were collected at the University of the Witwatersrand earth lab using XRF with procedures described in Wilson (2012). Trace elements were analysed using an Agilent 7500ce ICP-MS at the University of Stellenbosch. Sample preparation was done using fusion disks prepared by an automatic Claisse M4 Gas Fusion instrument and ultrapure lithium borate Claisse Flux at a ratio of 1:10 (sample: flux). Trace elements are quantified using NIST 612 for calibration and the SiO_2 content from XRF analyses as an internal standard. Two replicate measurements were made on each sample and the calibration standard was run every 12 samples. The calibration standards used were BCR-2 or BHVO 2G. Data were processed using

Glitter software, distributed by Access Macquarie Ltd., Macquarie University, NSW 2109. Selected representative whole-rock major- and trace-element geochemistry of metasediments, granites and pegmatites are shown in Table 4.2.

Supplementary data were acquired for Salem-type granites from McDermott (1986) for comparison and addition to the dataset in this study. This dataset, however, includes elements that were not analysed for in McDermott (1986) and thus the following figures only show data from McDermott (1986) where possible.

4.6 Geochemistry

4.6.1 Metasedimentary rocks

Host rock types include metasomatised, tourmalinised schists, fine- to coarse-grained biotite schist, quartzite and fine- to coarse-grained Knotenschiefer resulting in a wide compositional range. SiO_2 and Al_2O_3 compositions range from 56.2-84.7 wt % and 7.2-21.4 wt % respectively, the former high SiO_2 and later low Al_2O_3 values representing the quartzite rock type. Fe_2O_3 contents are generally ~4.5 wt % and MgO values reach up to 4 wt % but generally are below 3 wt %. TiO_2 content does not exceed 1 wt %. Trace elements also show variable concentrations: Rb contents range from 24-1858 ppm, Sr from 35-1280 ppm and Ba from 29- 2737 ppm. V and Cr values reach up to ~200 ppm and Zn and Zr as much as ~550 ppm. Sn, Nb and Ta values are highly variable in metasediments and rock type seems to control these values such that tourmalinised metasediments at the pegmatite contact show much higher values with <1084 Sn, 251 Ta, and 162 Nb ppm. Cs often corresponds with these high values and reaches up to 867 ppm. In schist host rocks further from the pegmatites contact that show no interaction with pegmatite fluids, the average values of Sn are 72, Nb 20 and Ta 2 ppm. Trace elements such as REE, Th, U, Hf, Pb, Ni, Co, Y and Mo do not exceed ~20 ppm.

4.6.2 Granites

Salem-type and Red and Grey Granites show little variation in SiO_2 and Al_2O_3 content with a range of 73.3-76.5 and 13.42-15.53 wt % respectively. Salem-type granites have consistent CaO ~1.5, K_2O 3.5 and Na_2O 4.5 wt % values, whereas Red/Grey granites show a wider range of compositions with Na_2O varying from 3.2-5.8 wt % and K_2O from2.1-5.1 wt % (Table 4.3). All

the granites have an ASI (alumina Saturation Index; A/CNK; Fig. 4.6A) of between 1.05-1.20. Trace element values are fairly consistent in all granite types with Rb and Sr values of ~200 ppm, Ba values ~400 ppm, Zn and Zr between 50-100 ppm with some Zr values reaching 200 ppm. Total REE values range from 50-150 ppm. Trace element values of Ta, Nb, Sc, V, Cr, Co, Ni, Cu, Y, Mo, Cs, Hf, Pb, U and Th do not exceed 50 ppm.

4.6.3 Pegmatites

It is pertinent to note at this point that no apparent differences in geochemistry are observed between the Nainais and Cape Cross-Uis pegmatites and are thus grouped together with the Nb-Ta-Sn pegmatites since they show the same geochemical characteristics. Garnet-tourmaline and Li-Nb-Ta-Sn pegmatites average ~73 wt % SiO_2 and ~14 wt % Al_2O_3. Nb-Ta-Sn pegmatites show wider ranges of SiO_2 and Al_2O_3 with 65-76 wt % SiO_2 and 13-19 wt % Al_2O_3. Greisen and albitised zones are the most variable such that SiO_2 can be as low as 42 wt % and Al_2Ocan be as high as 35 wt % reflecting their dominant mineralogy. All pegmatite types show an average of ~ 6 wt % Na_2O and 2 wt % K_2O. Albitised samples show ~9 wt % Na_2O and greisens show ~9 wt % K_2O due to the abundance of muscovite. The CaO abundances range between 0.2 and 1 wt % reflecting the occurrence of apatite but P_2O_5 values which reach up to 5.78 wt % (Table 4.3) are also due to the presence of monazite and other phosphate minerals. Pegmatite ASI ranges from 1.05-1.69 (Fig. 4.6A) while greisen and albitised zones reaches 2.86 ASI.

Although trace elements contents of pegmatites are variable in the dataset (Table 4.2, 4.3), the Nb-Ta-Sn and Li-pegmatites have similar trace element values with ranges between 32 and 1521 ppm Rb, 20 and 1482 ppm Sr and 20 and 3325 ppm Zn and Zr. In comparison garnet-tourmaline pegmatites show low values of these elements with ranges between 140 and 640 ppm Rb, 20 and 230 ppm Sr and less than 1000 and 100 ppm Zn and Zr respectively (Table 4.3). Zones that have been altered differ considerably from the pegmatite chemistry as a whole with zones of albitisation depleted in Rb, Sr, Zn and Zr whereas greisenised zones are depleted in Sr (5-159 ppm) but are the most enriched in Rb, Zn and Zr up to 8889, 4141 and 650 ppm respectively. Nb-Ta-Sn and Li-pegmatites show intermediate values of 30-5357 ppm whereas garnet-tourmaline pegmatites do not exceed 200 ppm for the elements Rb, Sr, Zn and Zr (Table 4.3). Greisenised and albitised zones show the highest concentrations of Sn with up to ~1 wt % Sn (Table 4.3). Nb and Ta values vary

but are highest (300 and 200 ppm respectively) in the Nb-Ta-Sn and Li-pegmatites. Garnet-tourmaline pegmatites show maximum values of82 and 15 ppm Nb and Ta respectively whereas altered zones reach up to 310 ppm Nb and 650 ppm Ta. Pegmatites are also enriched in Cs, with garnet-tourmaline pegmatites having as low as 65 ppm Cs, Nb-Ta-Sn and Li-pegmatites up to 200 ppm Cs, whereas greisen and albitised zones may have up to 1479 ppm Cs. Rb/Sr values range from 0.6-23.36 in pegmatites, 14-992 in greisen rocks and 1.96-7.46 in albitised rocks.

Although the Cape Cross-Uis pegmatites and granites are dominantly peraluminous, there is a distinction between granites and pegmatites (Fig. 4.6A). Some granites are metaluminous and have considerably higher A/NK values. Greisens are extremely peraluminous (A/CNK > 1.6) and are not shown in Figure 4.6A. Pegmatites scatter around the WPG, syn- and post- collisional fields whereas the granites dominantly plot well within the post-collisional field (Fig. 4.6B). Pegmatites are dominantly ferroan, containing magnetite and little ilmenite, whereas granites are dominantly magnesian (Fig. 4.6C). Pegmatites and granites both show a large scatter in terms of their alkalic-calcic character. Generally, CaO values are low in both groups and granites tend to be in the transition between alkalic and alkali-calcic whereas pegmatites plot mainly in the alkalic field (Fig. 4.6D).

Table 4.2: Selected representative whole-rock major- and trace-element data for country rock metasediment and granite host rocks of the Cape Cross-Uis pegmatite belt. Selected samples were chosen to best represent the variations the dataset shows. S-Gran. = Salem-type granite; RG-Gran. = Red/Grey granite; Knot. = Knotenschiefer; BioSch. = biotite schist; Qtzite. = quartzite; TourBS. = tourmalinised biotite schist; n.a. = not analysed.

Sample	WCF 8-1	WCF 8-2	WCF 8-3	WCF 8-6	WCF X-1	WCF 2-1	WCF 4-6	WCF D-2	WCF J-3	WCF XX-2	WCF 6-3	WCF 3.3-1	WCF 3-2
rock type	*S-Gran*	*S-Gran*	*S-Gran*	*RG-Gran*	*RG-Gran*	*Knot*	*Knot*	*Knot*	*Knot*	*BioSch*	*BioSch*	*Qtzite*	*TourBS*
SiO_2	73,5	72,6	73,3	74,8	74,2	61,9	61,4	60,1	69,9	62,79	57,5	84,7	57,00
Al_2O_3	14,6	14,7	14,7	14,8	14,6	17,3	18,0	17,5	14,8	16,56	18,1	7,2	18,96
Fe_2O_3	1,18	1,19	1,14	0,57	1,37	5,06	5,23	5,39	2,88	5,01	5,98	1,52	5,07
MnO	0,03	0,03	0,07	0,11	0,05	0,11	0,11	0,16	0,05	0,11	0,13	0,04	0,06
MgO	0,46	0,47	0,42	0,14	0,36	3,69	3,20	3,63	2,15	3,45	4,20	0,86	2,68
CaO	1,27	1,83	1,39	0,84	1,32	0,94	0,53	1,20	0,52	0,77	3,47	1,78	1,29
Na_2O	3,37	3,5	3,67	3,32	5,57	1,69	0,70	2,62	0,53	1,45	2,21	1,32	0,73
K_2O	4,79	4,5	4,28	5,14	1,8	4,21	4,51	4,20	4,35	4,25	3,53	0,69	3,66
TiO_2	0,254	0,268	0,242	0,070	0,218	0,791	0,846	0,876	0,681	0,8168	0,796	0,524	0,891
P_2O_5	0,09	0,07	0,08	0,04	0,16	0,15	0,21	0,17	0,13	0,13	0,19	0,11	1,05
Cr_2O_3	0,004	0,006	0,004	0,005	0,005	0,017	0,016	0,008	0,011	0,0109	0,019	0,002	0,02
NiO	0,001	0,001	0,000	0,003	0,002	0,003	0,005	0,006	0,003	0,0039	0,008	0,001	0,00
LOI	0,84	1,14	0,74	0,95	0,51	2,54	3,72	2,04	2,82	3,82	2,01	0,84	4,21
Total	100,34	100,28	100,03	100,86	100,16	98,48	98,45	97,87	98,86	99,18	98,21	99,65	95,64
Rb	202,90	203,92	226,77	270,72	200,85	176,28	187,27	432,73	389,98	1069,49	189,98	36,43	574,01
Sr	218,85	238,70	228,51	43,60	140,53	139,30	55,79	151,38	59,46	37,13	155,13	189,21	1280,50
Ba	572,53	697,73	680,27	67,29	434,07	567,25	720,11	566,43	672,26	718,80	867,47	207,25	445,17
Sc	15,08	14,71	14,99	14,54	15,70	23,66	23,25	22,32	20,96	22,00	22,94	14,50	21,92
V	30,82	31,66	32,08	20,48	30,72	143,23	184,26	153,15	122,93	151,82	160,18	59,55	187,19
Cr	15,39	17,15	14,28	13,76	16,87	108,01	111,46	102,78	92,52	163,62	110,93	38,54	132,65
Co	5,30	8,57	5,10	3,37	6,38	25,15	20,20	17,26	6,06	8,21	21,84	4,96	6,27
Ni	11,44	10,54	13,64	9,65	25,21	54,83	50,19	43,14	43,11	87,35	61,46	15,83	28,72
Cu	31,35	61,33	31,32	56,04	62,72	65,76	45,76	35,15	37,58	35,27	25,12	26,83	32,29
Zn	66,85	60,36	68,29	15,43	132,04	150,83	175,32	170,20	95,13	161,45	184,40	45,76	366,14
Y	14,30	10,67	13,29	18,78	21,23	36,61	41,96	36,66	24,63	38,00	41,57	18,12	35,83
Zr	194,09	145,65	136,54	67,82	165,00	155,51	183,85	199,04	153,71	246,02	156,44	298,70	225,45
Nb	17,91	18,96	20,84	27,83	47,53	15,59	15,14	17,19	12,64	16,15	15,38	9,43	79,12
Mo	2,14	1,26	1,21	3,14	1,17	0,71	2,42	1,01	0,72	1,14	1,77	1,64	4,38
Sn	n.a.	n.a.	n.a.	n.a.	n.a.	4,94	16,35	80,73	10,79	231,65	7,72	0,68	833,17
Cs	14,88	13,93	15,68	11,72	18,70	24,15	32,43	210,16	116,39	344,74	78,71	17,80	80,75
Hf	5,30	4,18	4,31	2,94	4,72	4,62	5,41	5,92	4,92	7,03	4,77	8,36	6,75
Ta	1,73	1,89	2,41	5,73	7,29	1,17	1,20	1,24	1,13	1,22	1,21	0,85	19,66
Pb	38,32	37,95	40,70	38,69	20,47	16,14	15,58	15,49	14,54	16,36	17,41	11,40	17,58
Th	20,17	16,03	15,55	6,11	15,93	16,14	15,58	15,49	14,54	16,36	17,41	11,40	17,58
U	7,62	3,33	3,79	6,61	6,35	4,08	3,68	3,84	3,11	5,45	3,57	4,37	10,78
La	40,88	32,49	33,29	7,89	40,19	47,54	46,79	44,95	41,14	44,73	44,29	27,29	46,02
Ce	85,48	68,00	70,75	17,91	79,70	97,35	96,15	90,82	76,90	87,37	92,77	62,56	92,18
Pr	8,38	7,01	6,74	1,89	7,62	10,95	11,77	11,02	8,49	10,42	10,77	6,70	10,29
Nd	28,50	23,24	22,38	6,50	25,56	42,04	46,62	43,77	31,17	39,68	42,98	26,38	38,61
Sm	5,46	4,42	4,24	2,02	4,53	8,75	9,93	8,67	6,15	7,43	9,69	4,83	8,07
Eu	0,78	0,73	0,70	0,22	0,82	1,65	1,56	1,68	1,18	1,09	1,58	0,96	1,54
Gd	3,88	3,49	3,23	2,16	4,21	7,84	8,69	7,41	5,30	6,69	8,39	4,75	7,25
Tb	0,53	0,44	0,45	0,44	0,62	1,14	1,23	1,19	0,76	1,06	1,28	0,67	1,07
Dy	2,93	2,13	2,41	3,04	3,79	6,76	7,98	6,96	4,52	6,84	7,58	3,87	6,56
Ho	0,53	0,44	0,46	0,59	0,78	1,40	1,58	1,46	0,95	1,36	1,62	0,77	1,37
Er	1,41	1,04	1,27	1,78	2,07	3,99	4,81	4,17	2,93	4,12	4,26	2,05	4,08
Tm	0,21	0,16	0,17	0,32	0,31	0,58	0,65	0,56	0,41	0,57	0,59	0,31	0,53
Yb	1,32	1,00	1,34	2,23	2,40	3,81	4,42	3,66	2,89	4,32	4,36	2,01	3,94
Lu	0,20	0,16	0,20	0,34	0,34	0,56	0,61	0,52	0,42	0,66	0,66	0,35	0,62

Table 4.2 continued: Selected representative whole-rock major- and trace-element data for pegmatites of the Cape Cross-Uis pegmatite belt. Grs. = Greisen.; d.l. = below detection limit.

Sample	WCF 5.1-4	WCF X-2	WCF 7-6	WCF T-5	WCF J-5	WCF C-1	WCF 4-4	WCF 3.1-1	WCF W-5	WCF K-3	WCF 5.1-1	WCF G-4	WCF M-2
Peg-type	*Li-Nb-Ta-Sn*	*Gnt-Tml*	*Gnt-Tml*	*Nb-Ta-Sn*	*Nb-Ta-Sn*	*Nb-Ta-Sn*	*Nb-Ta-Sn*	*Nb-Ta-Sn*	*Nb-Ta-Sn*	*Nb-Ta-Sn*	*Grs*	*Grs*	*Grs*
SiO_2	52,6	73,2	73,9	67,7	68,3	73,2	70,7	70,7	69,1	72,3	52,6	51,1	51,0
Al_2O_3	31,7	14,4	14,0	17,1	17,4	15,4	17,4	15,9	17,7	15,9	31,7	32,0	32,2
Fe_2O_3	0,59	0,50	0,65	0,16	0,21	0,22	0,40	0,42	0,10	0,98	0,59	0,35	0,38
MnO	0,02	0,12	0,07	0,02	0,02	0,01	0,10	0,16	0,02	0,44	0,02	0,01	0,03
MgO	0,13	0,11	0,18	0,07	0,04	0,05	0,08	0,09	0,05	0,10	0,13	0,10	0,40
CaO	0,18	0,68	0,61	0,60	0,65	0,37	0,25	1,30	0,94	0,49	0,18	0,14	0,31
Na_2O	2,01	3,04	5,16	7,50	7,45	7,27	9,93	6,93	9,85	4,02	2,01	3,69	1,81
K_2O	7,95	6,08	3,88	0,62	0,94	1,37	0,40	1,06	0,19	2,56	7,95	7,32	8,20
TiO_2	0,018	0,039	0,047	0,015	0,011	0,013	0,007	0,010	0,008	0,015	0,018	0,070	0,136
P_2O_5	0,10	0,34	0,36	3,00	2,18	0,39	0,28	1,37	0,88	0,43	0,10	0,20	0,23
Cr_2O_3	d.l.	0,001	d.l.	d.l.	d.l.	d.l.	d.l.	0,001	d.l.	d.l.	d.l.	d.l.	d.l.
NiO	d.l.	0,000	d.l.	d.l.	d.l.	d.l.	d.l.	0,001	d.l.	d.l.	d.l.	d.l.	d.l.
LOI	0,83	2,54	2,12	1,49	1,23	2,04	4,22	3,82	1,49	1,4	0,95	1,66	0,85
TOTAL	99,38	101,08	100,96	98,32	98,41	100,32	103,71	101,68	100,32	98,61	96,32	96,63	95,57
Rb	1757	574	644	484	1521	495	89	379	27	889	8890	4981	6598
Sr	113,39	68,51	27,59	188,82	1388,02	39,43	45,35	1482,76	676,09	75,35	159,03	5,02	21,88
Ba	34,93	230,64	92,55	10,66	49,41	13,04	43,83	100,54	25,24	61,57	26,48	2,31	100,56
Sc	5,80	7,14	6,40	6,57	6,02	6,38	5,75	5,45	5,91	6,92	4,47	5,63	5,52
V	12,67	11,31	17,35	9,67	9,63	10,62	18,55	16,91	9,79	31,48	15,35	12,82	19,64
Cr	8,67	8,82	10,65	10,26	7,70	8,09	7,89	6,94	7,28	7,06	8,38	6,61	6,73
Co	1,64	9,37	2,78	1,56	11,31	1,29	1,00	2,56	0,86	19,61	30,99	36,20	2,10
Ni	12,61	10,57	17,17	10,37	9,40	10,65	8,76	12,65	10,16	20,65	10,99	10,46	12,24
Cu	178,84	220,93	402,89	60,08	219,59	114,20	21,60	94,12	43,90	721,93	623,56	535,16	51,96
Zn	97,61	965,16	184,82	80,00	1306,90	34,15	85,23	103,59	38,26	1591,35	4141,52	3563,67	293,02
Y	0,89	7,05	1,52	0,19	0,67	0,46	0,08	0,11	0,05	0,41	0,17	3,95	0,13
Zr	14,86	29,73	5,75	7,10	17,02	10,33	17,80	2,49	12,08	9,22	2,43	650,95	13,26
Nb	215,81	69,13	61,41	303,57	191,39	190,17	311,83	29,90	242,35	139,08	60,73	209,25	106,37
Mo	0,74	0,65	0,71	0,64	0,71	0,52	1,27	1,85	0,58	4,03	0,62	0,53	0,50
Sn	1187	240	47	5358	1388	3643	31	559	1288	245	751	10016	852
Cs	210,12	18,73	60,54	33,38	107,67	40,39	15,79	31,36	4,03	175,35	1317,41	180,94	1479,13
Hf	1,40	1,62	0,33	0,86	2,33	1,12	2,40	0,24	2,49	1,45	0,47	57,67	3,19
Ta	329,94	15,50	12,09	81,72	153,22	99,98	255,63	15,65	463,48	168,19	102,27	185,61	650,94
Pb	24,48	56,14	50,82	14,44	8,39	40,04	17,67	27,01	16,90	13,89	26,74	23,07	15,99
Th	0,38	2,78	0,34	0,45	0,57	0,85	0,27	0,16	2,02	1,41	6,82	7,63	1,03
U	6,59	12,35	5,70	8,93	6,36	2,68	2,01	6,67	3,25	5,43	7,00	10,45	4,61
La	0,18	6,04	0,94	0,25	0,21	0,66	0,07	0,11	0,07	0,42	0,05	0,05	0,09
Ce	0,26	11,47	1,58	0,38	0,33	0,90	0,13	0,14	0,11	0,49	0,10	0,10	0,13
Pr	0,04	1,26	0,19	0,04	0,03	0,08	0,02	d.l.	d.l.	0,05	d.l.	d.l.	d.l.
Nd	0,20	4,15	0,60	0,13	d.l.	0,22	d.l.	d.l.	d.l.	0,18	d.l.	d.l.	d.l.
Sm	0,06	0,90	0,17	0,05	0,05	0,06	d.l.	d.l.	d.l.	0,06	d.l.	d.l.	d.l.
Eu	0,05	0,23	0,07	d.l.	d.l.	d.l.	d.l.	d.l.	d.l.	d.l.	d.l.	d.l.	d.l.
Gd	0,14	0,88	0,23	d.l.	d.l.	d.l.	d.l.	d.l.	d.l.	d.l.	d.l.	d.l.	d.l.
Tb	0,02	0,19	0,05	d.l.	0,03	d.l.	d.l.	d.l.	d.l.	d.l.	d.l.	0,03	d.l.
Dy	0,11	1,14	0,25	d.l.	0,13	0,09	d.l.	d.l.	d.l.	0,05	d.l.	0,33	d.l.
Ho	0,03	0,24	0,06	d.l.	d.l.	d.l.	d.l.	d.l.	d.l.	d.l.	d.l.	0,11	d.l.
Er	0,06	0,63	0,13	d.l.	d.l.	0,05	d.l.	d.l.	d.l.	d.l.	d.l.	0,50	d.l.
Tm	d.l.	0,12	0,02	d.l.	d.l.	d.l.	d.l.	d.l.	d.l.	d.l.	d.l.	0,13	d.l.
Yb	0,06	0,95	0,17	d.l.	d.l.	0,05	d.l.	d.l.	d.l.	d.l.	d.l.	1,30	d.l.
Lu	d.l.	0,16	0,03	d.l.	d.l.	d.l.	d.l.	d.l.	d.l.	d.l.	d.l.	0,26	d.l.

Table 4.3: Compositional comparison between host granite and pegmatites. Oxides are in wt% and trace elements in ppm.

Geochemical parametre	Granites		Pegmatites			
	Salem-Type	Red/Grey	Gnt-Tour	Nb-Ta-Sn	Li-pegmatites	Greisens
SiO_2	76.5-73.3		73	65-76	73	42-78
Al_2O_2	15.53-13.42		14	13-19	14	13-36
P_2O_5	< 0.15 wt %		< 0.5	0.22-3.41		0.2-5.78
A/CNK	1.05-1.20		1.10-1.50	1.05-1.69		1.91-3.12
Rb	200		140-640	32-1521		930-8889
Sr	< 200		20-230	20-1482		5-159
Ba	400		50-270	< 100		4-100
Zr	70-200		< 100	3-60		1-650
Zn	60-130		< 1000	20-3325		31-4141
Sn	< 50		< 200	30-5357		750-10000
Nb	< 50		15-82	30-300		60-310
Ta	< 10		2-15	10-325		55-650
Cs	< 30		< 100	20-175		180-1500
Ce	< 100		10-20	< 1		< 1
Y	100		10	< 1		< 1
TREE	55-147		5-25	< 1		< 1

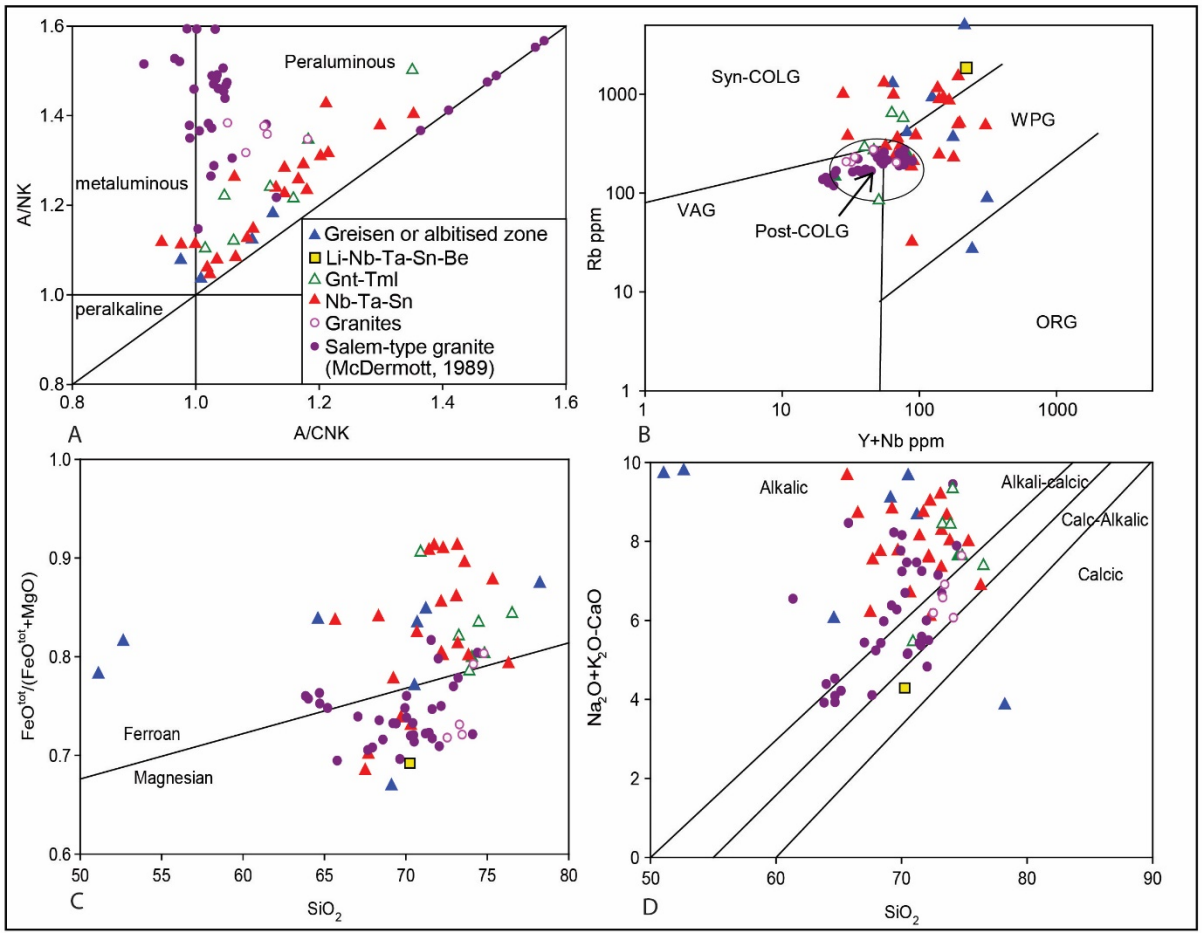


Figure 4.6: Granitic classification plots. A) The Shand index granitic classification plot depicting the aluminosity of granitic rocks (Maniar and Piccoli, 1989). B) The tectonic discrimination diagram of Pearce et al. (1984). C) FeO_t and MgO plot against SiO_2 depicting the boundary between ferroan and magnesian intrusions (Frost et al., 2001). D) The $Na_2O + K_2O$ – CaO vs. SiO_2 from Frost and Frost (2008) showing the calcic or alkalic nature of the intrusions. The triangles indicate different pegmatite types (Table 4.3) and the circles indicate granite in the belt.

In terms of large ion lithophile elements in a Sr-Rb-Ba ternary diagram there is a distinct difference between granites and pegmatites (Fig. 4.7A). Nb-Ta-Sn-, Li-pegmatites and altered zones show similar character, having a broad range of Sr and Rb and are Ba depleted, being on the margin of the ternary diagram whereas garnet-tourmaline pegmatites are slightly Ba enriched and Sr depleted. Granites contain above 50% Ba relative to near equal proportions of between 10-30% Rb and Sr. Pegmatites that show high Rb and low Sr values plot within the strongly differentiated granite field of the diagram whereas others do not plot in any of the defined fields given in El Bouseily and El Sokkary (1975). The granites dominantly plot within the anomalous granite field. In Figure 4.7B different pegmatite types show no clear differences and most are above 90 % Zr relative to Ce and Y with the exception of garnet-tourmaline pegmatites which show slightly more

enriched Ce and Y values. A single garnet-tourmaline pegmatite shows an outlier value of Y above 50 % relative to Zr and Ce. Granites are slightly less rich and more variable showing relative values of between 30 and 80 %Zr. Granites show the highest relative Ce values and are similar to garnet-tourmaline pegmatites in terms of Y values. Although pegmatites are Sn rich relative to Nb and Ta, no discernible trend is observed in the relative abundances of Nb, Ta and Sn (Fig. 4.7C).

With respect to pegmatites, no relationship is apparent between the ratio of K_2O/Rb and Ba (Fig. 4.8A): Granites appear to lie on a somewhat linear trend whereas pegmatites show a scatter in the data. McKeough et al. (2013) use the $CaO+MgO+FeO_{tot}$ to determine the hybridisation of pegmatites: The higher the value the greater the degree of country rock assimilation. Although pegmatites in the Cape Cross-Uis pegmatite belt do show signs of host rock interaction (tourmalinised layers, metasomatic features), there is no clear relationship between the abundance of Sn in pegmatites and their $CaO+MgO+FeO_{tot}$ value (Fig. 4.8B). The dominant HFSEs in pegmatites of the Cape Cross-Uis pegmatite belt are Nb, Ta, and Zr. Other HFSEs do not exceed 10 ppm. The incompatible elements Cs and HFSE combined show an increasing trend with greater peraluminosity from lowest to highest: Garnet-tourmaline-, Nb-Ta-Sn-, Li-pegmatites and Greisenised zones (Fig. 4.8C). This increase is accounted for by the increased values of Nb, Ta, Cs and Zr not the total rare earth elements (TREE; sum of REE) and Y contents.

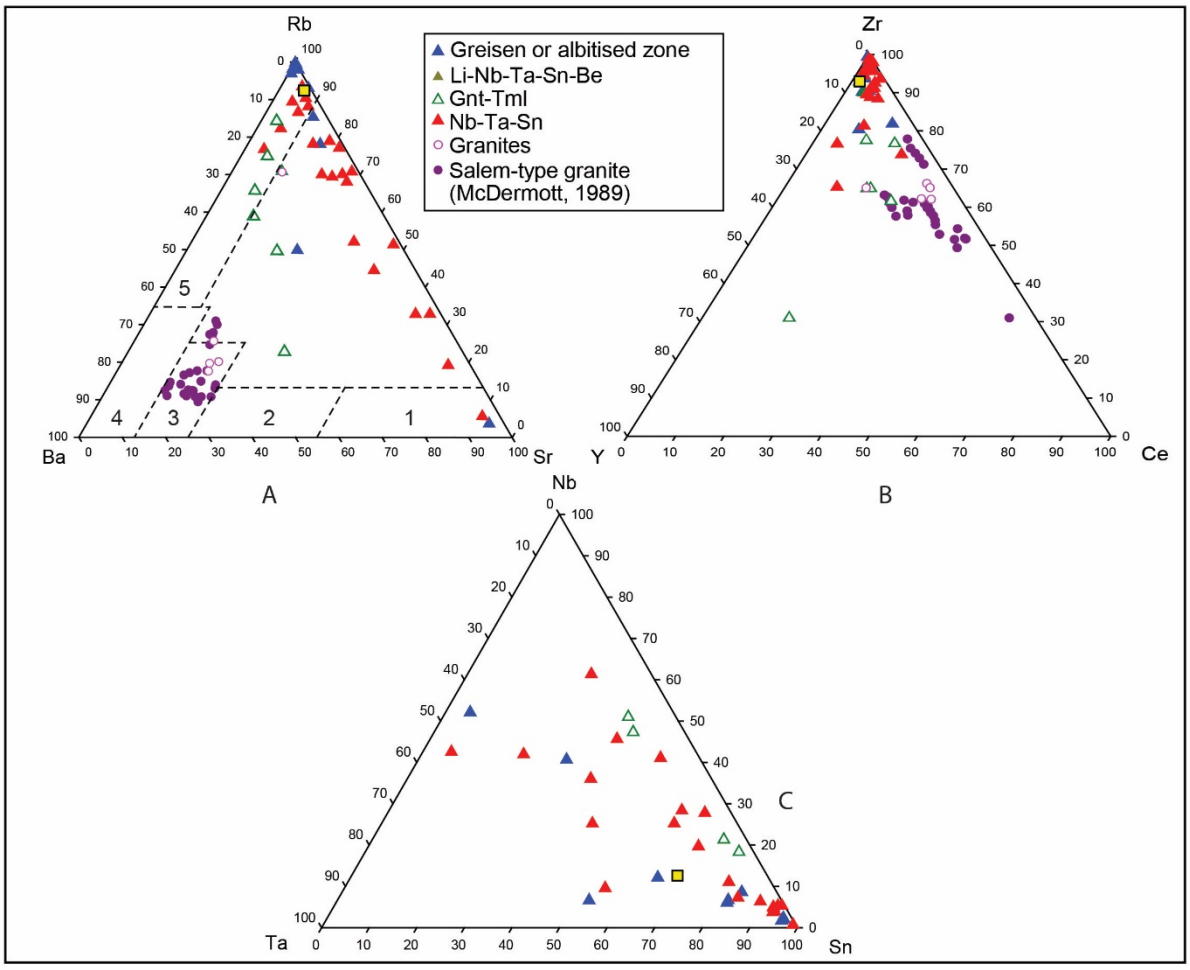


Figure 4.7: Ternary diagrams showing the relationship of granites and pegmatites in terms of Sr-Rb-Ba (A), Zr-Ce-Y (B) and Nb-Sn-Ta (C). A) The Rb-Ba-Sr ternary diagram from El Bouseily and El Sokkary (1975): 1) diorites, 2) granodiorites and quartz diorites, 3) anomalous granites, 4) normal granites and 5) strongly differentiated granites.

Concentrations of Ta and Cs show no correlation relative to the distance from a granite outcrop at which the pegmatite occurs (Fig. 4.8D). Slight exponential trends are observed between Ce-Y and Nb-Ta (Fig. 4.8E,F respectively). These incompatible elements are expected to increase during pegmatite fractionation and this is observed for the Nb-Ta plot: garnet-tourmaline pegmatites plot near the origin, Nb-Ta-Sn pegmatites plot intermediately and Li-pegmatites show the highest values of the unaltered samples. Greisenised samples have the overall highest Nb-Ta values in the dataset whereas granites often show below detection limit values and are therefore not featured in Figure 4.8F. There is an unexpected relationship in the Ce-Y plot since overall fractionation should increase the Ce and Y contents (Fig. 4.8E): granites show the highest values with garnet-tourmaline pegmatites plotting just below or over overlapping granites. Li-pegmatites, Nb-Ta-Sn pegmatites and altered units show almost negligible values and plot far below that of granites and

garnet-tourmaline pegmatites. Aside from the elements Ce and Y, Garnet-tourmaline pegmatites are relatively primitive, Nb-Ta-Sn pegmatites show intermediate character and Li-pegmatites show the most evolved nature. Altered zones and granites are typically showing the most evolved and least evolved values respectively. Interestingly, garnet-tourmaline pegmatites have significantly higher values of Nb relative to Ta (Fig. 4.8F, 4.9A) and have very low Li and Cs values (Table 4.2) which perhaps reflect a slightly more NYF-family affinity compared to the other pegmatite types that show a distinct LCT-family character.

The element ratios Ta/Nb, K_2O/Rb, Cs and Zr/Hf are good tracers of fractionation and can be used to compare trends between a granite fractionation trend, those of a pegmatite and different pegmatite zones (Fig. 4.9; Clarke, 1992; Shearer et al., 1987). Pegmatites and granites lie on a similar fractionation trend: garnet-tourmaline pegmatites are the most primitive and plot near to granites (Fig. 9A,C,D), Nb-Ta-Sn pegmatites are intermediate and Li-type pegmatites show a highly evolved character in terms of fractionation. It is important to note that although a similar fractionation trend is viewed, distinct overlaps between granites and pegmatites occur suggesting a decoupling of elements. In some cases, garnet-tourmaline pegmatites show even more primitive values than that of granites (Fig. 4.9C). Albitised rocks show an intermediate to evolved nature, whereas greisens show the most fractionated values. Figure 4.9B shows pegmatites and granites that follow a separate fractionation trend in terms of the K_2O/Rb vs Rb relationship. Similarly, granites plot in the barren granite field whereas pegmatites mostly plot in the mineralised granite field of Stavrov et al. (1969). Some of the greisens occasionally show a distinct gap between themselves and other samples along the fractionation trend (Fig. 4.9B). In terms of the chosen incompatible elements ratios pegmatites generally show higher fractionation levels than granites.

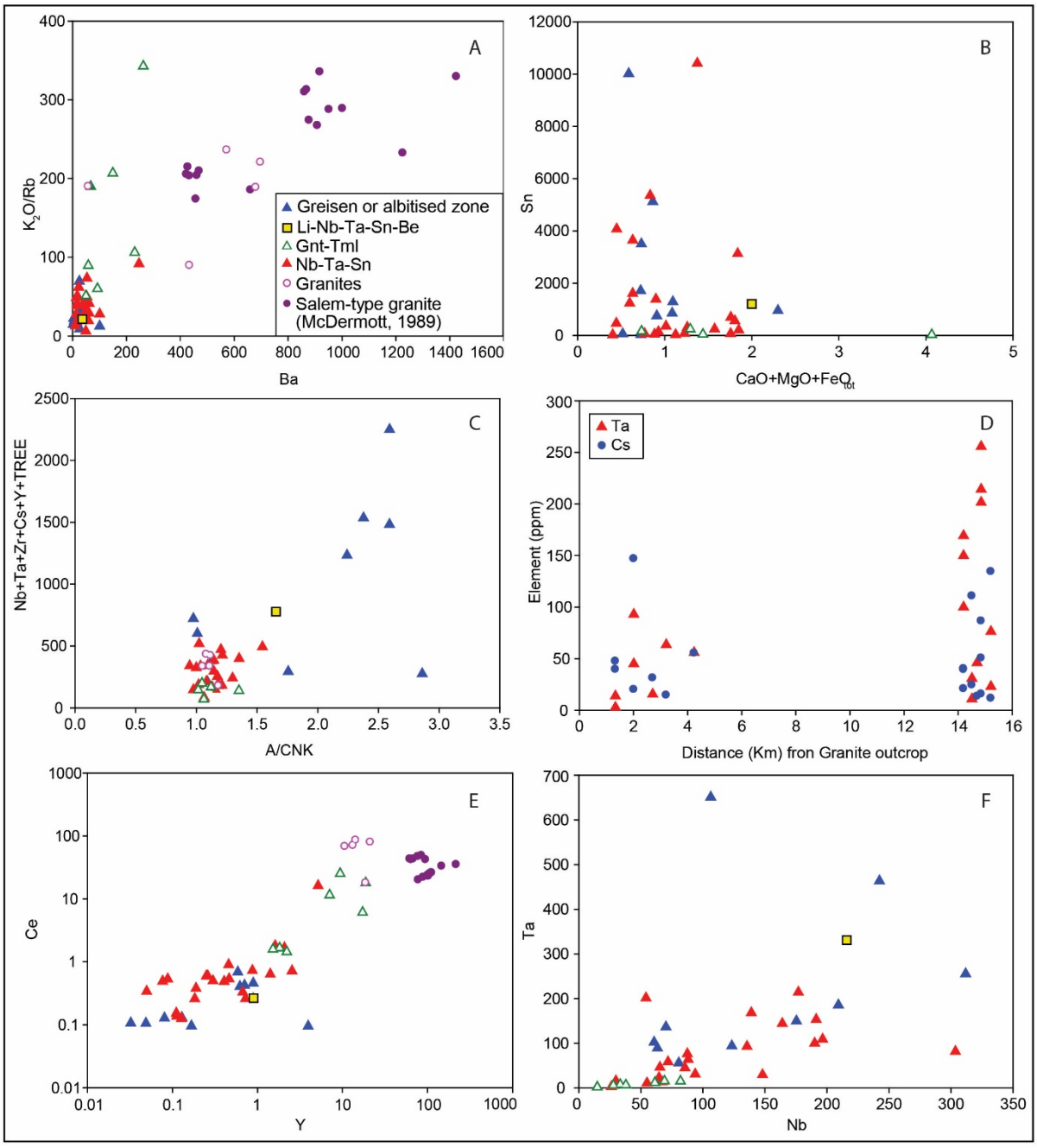


Figure 4.8: Various element, element ratio, distance and A/CNK plots showing granites and pegmatites or just pegmatites. A) The K_2O/Rb vs. Ba plot showing that granites have significantly higher Ba values compared to pegmatites. B) Sn vs. the McKeough et al. (2013) hybridisation factor, showing no relationship. C) The HFSEs and Cs compared to the aluminosity of pegmatites and granites. D) The Ta and Cs element concentration relative to the distance from the outcropped granitic plutons. E, F) weak positive trends in plots of Ce-Y and Ta-Nb for pegmatites.

Granites have consistent REE patterns with La-Gd (LREE) enrichment and moderate negative Eu anomalies (Eu/Eu* between 0.32 and 0.96; Fig. 4.10). Pegmatites show lower total REE contents compared to granites and either negative or positive Eu anomalies. For most pegmatites Eu/Eu* is

greater than 1.5 and only 4 pegmatites show values less than 1. For most pegmatites, REEs are below the detection limit which makes ascertaining their REE nature difficult since data may be unreliable. However, this indicates significant qualitative observations such as pegmatites, and especially replacement zones, plot far below that of granites. As a group, pegmatites appear to have no LREE or Tb-Lu + Y (HREE) preference; most trends have an average, flat horizontal shape. The garnet-tourmaline pegmatites are the only group to show slight overlaps with granites, mostly in the HREE section of the REE plot (Fig. 4.10). Greisens and albitised samples show the lowest REE values; however, one albitised sample shows HREE enrichment to a value of approximately 10.

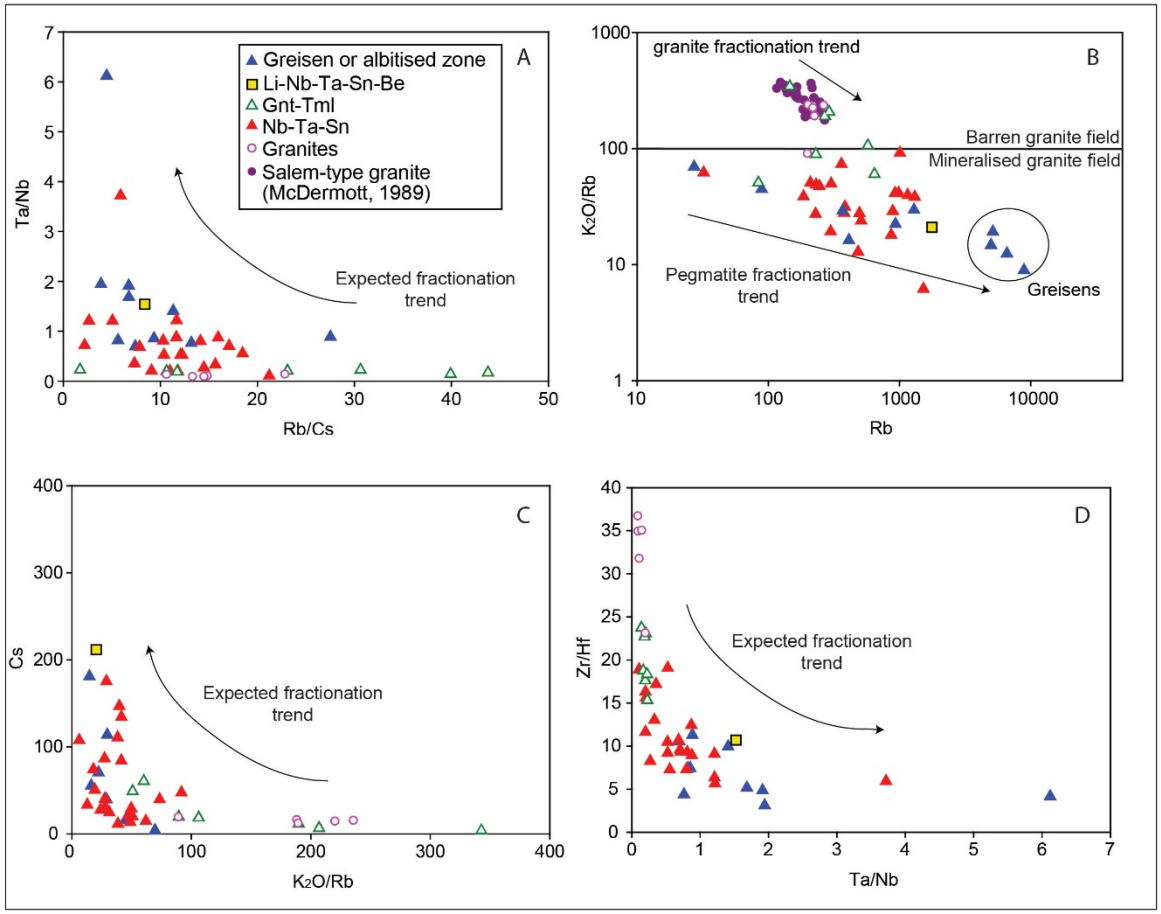


Figure 4.9: Fractionation trends in pegmatites using various element ratios and element concentrations. Plot B is divided into two fields: the barren granite field (>100 K_2O/Rb) and the mineralised granite field (<100 K_2O/Rb; Stavrov et al., 1969).

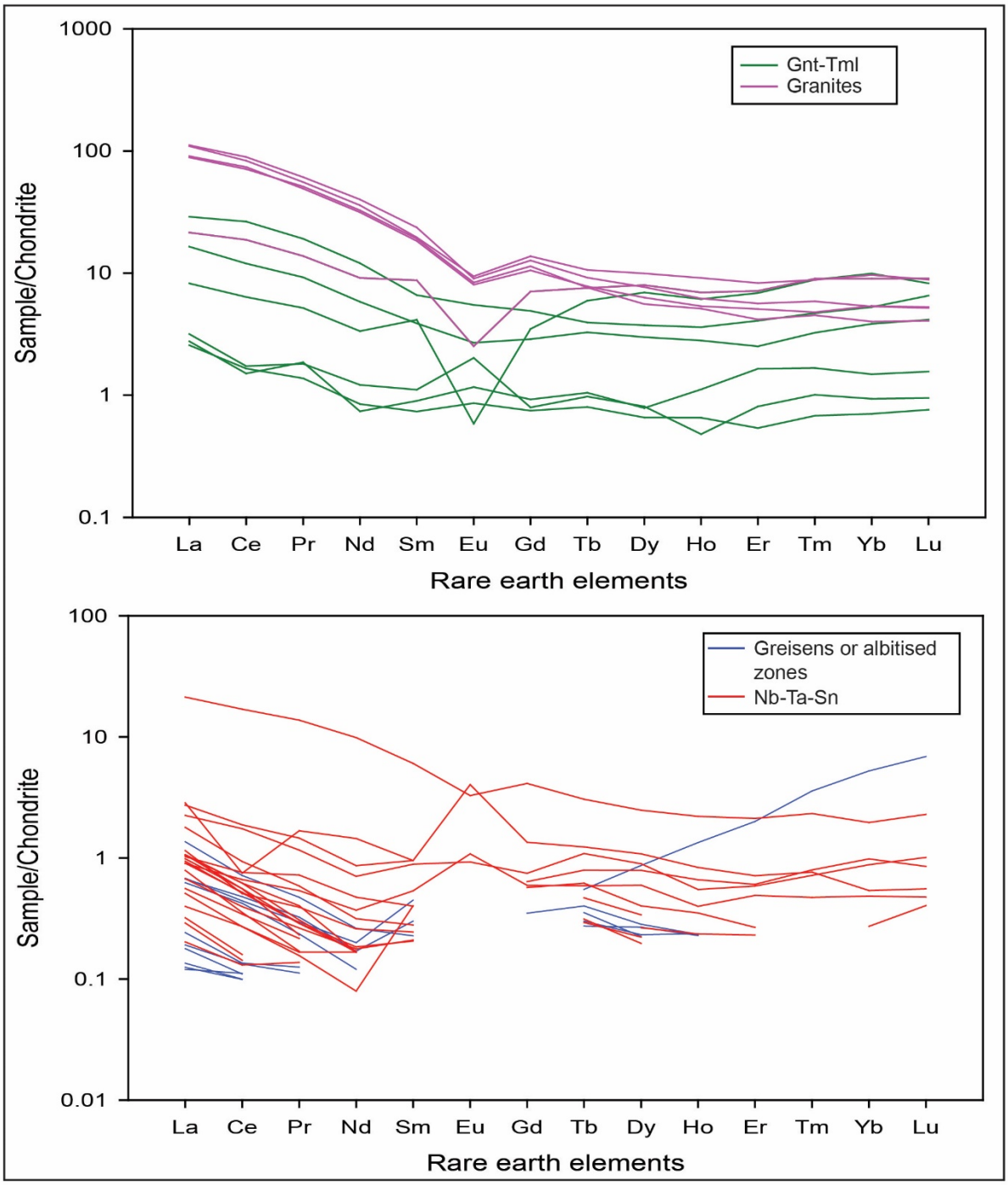


Figure 4.10: Rare earth element plots of Gnt-Tml pegmatites and Salem-type granites (top) and Nb-Ta-Sn pegmatites, greisens and albitised rocks. Chondrite normalised using values from McDonough and Sun (1995).

4.7. Discussion

The classification of pegmatites is a topic of significant debate. The currently accepted classification scheme, modified after Ginsburg et al. (1979), is by Černý (1990, 1991) and later Černý and Ercit (2005), although other classification schemes also exist (e.g. Martin and De Vito, 2005; Martin et al., 2009; Wise, 1999). Within the Cape Cross-Uis pegmatite belt, pegmatites are difficult to classify. The Sn-Ta-Nb and Li-pegmatites show LCT characteristics in that they are highly peraluminous, have low values of REE, U and Y, with significant Li, Cs and Nb-Ta values. Garnet-tourmaline pegmatites show intermediate characteristics between NYF and LCT. They have significantly higher values of Nb relative to Ta, have low Cs and Li components (Fig. 4.8F, 4.9A; Table 4.2) and whilst they are not necessarily enriched in REE, U and Y compared to other NYF pegmatites worldwide (London, 2008), they do show significant enrichment when compared to the other pegmatite types in the Cape Cross-Uis pegmatite belt. It may not be possible to classify them as true NYF pegmatites in accordance with the current classification schemes; however, their intermediate signature is interesting since they co-occur with definite LCT-type pegmatites.

4.7.1 Structural emplacement and timing

Authors such as Richards (1986) suggest that pegmatite and granite petrogenesis lasted from early syn-tectonic to post-tectonic, intruding into all types of D_1-D_3 structures. Goscombe et al. (2004), Macey (2003) and Macey and Harris (2006) suggest that the Salem-type granites added largely to the thermal metamorphism of the belt. Longridge (2012), however, shows that peak metamorphism at 520 Ma in the Damara Orogen, caused by crustal relaxation and orogenic collapse, was responsible for providing the heat that produced the Salem-type granites and pegmatites. Pegmatites show no evidence of contact aureoles and must have been a product of thermal metamorphism and not its cause. Furthermore, pegmatites cross-cut Damaran age structures and show no evidence of being subjected to Damaran age deformation. This would imply that pegmatites are post collisional and represent the final magmatism in the Cape Cross-Uis pegmatite belt. Considering the low crystallisation temperatures obtained by Ashworth (2014), 450 °C for LCT pegmatites in the Damara Orogen, it is possible that Salem-type granites provided enough heat to generate small-scale low degrees of fluidised partial melting to produce pegmatites post-tectonically during a late-stage phase of continued thermal relaxation.

Due to the lack of field evidence for in situ partial melting, pegmatites must have migrated from their source position (Ashworth, 2013; Freemantle, 2012; Longridge, 2012; Owen, 2011). Pegmatites would have migrated rapidly from the site of crustal anatexis due to the high abundance of H_2O, P, B and F which significantly reduces their viscosity and the temperature of crystallisation (Jung et al., 1998; Manning, 1981; Nabelek et al., 2010; Pichavant, 1987). This would imply that pegmatites reached their crustal emplacement depths relatively quickly. Pegmatite wall zone samples therefore confidently represent the whole-rock geochemistry of the initial pegmatitic melt once migration and emplacement have occurred.

Although early syn-tectonic structures host pegmatites, this does not mean their emplacement age was congruent. Pegmatites have utilised structural weaknesses of all Damaran ages. Late thermal relaxation of the Damara Orogen resulted in an extensional environment, shown by boudinaged pegmatite veins, which would promote passageways for melt migration. Structural features, such as localised shearing, are most likely related to Cretaceous magmatism as the northern orientation of these structures do not coincide with any Damaran age structures within the Cape Cross-Uis pegmatite belt.

4.7.2 Origin of the Cape Cross-Uis pegmatites

The relationship of granites and pegmatites is largely debated. Jahns and Burnham (1969) suggested that pegmatites progressively separated from parent granites undergoing fractionation and this model has been suggested for pegmatites in the Damara Orogen (Miller and Mittlefehldt, 1982, Mittlefehldt and Miller, 1983 and Phillips et al., 1981). In contrast, Walker et al. (1989) state that compositional variability of the pegmatites cannot be produced by simple fractionation from granites and that other processes must be involved such as varying degrees of partial melting of a heterogeneous crustal source (Ashworth, 2013; Černý, 1991*a*; Jung et al., 1998, 2003; McDermott, 1996). Assimilation of country rock has also been suggested as a mechanism to generate the compositional diversity (McKeough et al. 2013). Diehl (1993), Richards (1986), Singh (2007, 2008), and Wagener (1989) suggested that Sn was sourced from country rocks and therefore either assimilation or late-stage remobilisation of Sn was the controlling factor in Sn enrichment whereas fractionation of a pegmatitic magma is implied in the enrichment of Nb, Ta and Li (London, 2008). The geochemical data are useful to determine whether the pegmatites progressively separated from

parent granites undergoing fractionation or if pegmatites were generated via a partial melting method. Whether there has been significant assimilation of country rock by late-stage remobilisation of Sn or by melting and incorporation of host rock may also be evaluated.

Although it can be argued that the coarse-grained nature and zonation of pegmatites would preclude obtaining an overall composition, sampling of the wall zone rocks within pegmatites has been shown to be useful (e.g. Ashworth, 2013; Grassi, 2014; Jolliff et al., 1992; McKeough et al., 2013; Simmons et al., 1986). The fine-grained wall zone is the first major zone to crystallise (Jahns and Burnham, 1969), having crystallised at the magmatic stage rather than from a later fluid-dominated phase. Sampling the wall rock provides geochemical information on the early stages of crystallisation and this can be compared with late-stage greisens and albitised zones to provide a geochemical gradient between initial and final crystallisation stages to evaluate processes such as fractionation and which elements are incompatible until the end stages of crystallisation.

4.7.2.1 Assimilation

If the tin was sourced from the country rock by assimilation then the tin-rich metasomatised and tourmalinised contact zones would have required 5-15% or more of assimilation of biotite schist to achieve these wallrock Sn grades, as the biotite schist country rock has an average concentration of 72 ppm Sn and the pegmatites contact zones have 400-1000 ppm. McKeough et al. (2013) suggested that for the Wollaston Domain in Canada, such element enrichment should correlate with greater CaO, MgO and FeO values during assimilation but Figure 4.8B shows that Sn has no correlation to this hybridisation factor. Ashworth (2013) found crystallisation temperatures for two Uis and two Karlowa pegmatites to be 428-467 °C and 491-538 °C respectively using Ti in quartz geothermometry typical of hydrous pegmatites (Nabelek et al., 2010). Considering the amount of assimilation required, lack of correlation to other elements typically enriched during assimilation, and the low temperatures of crystallisation, together with the field evidence, it seems unlikely that Sn was enriched by melting and assimilation of country rock in the early stages of pegmatite crystallisation.

4.7.2.2 Fractionation of a pegmatite from a granite

The fractionation-separation model was developed by Jahns and Burnham (1969) and later modified by numerous authors (see reviews in London, 2008). This model implies that (1)

pegmatites at greater distances from parent granite plutons should be more evolved and fractionated (Baker, 1998) and (2) there should be a distinct geochemical fractionation trend from granite through primitive pegmatite and intermediate pegmatite, to evolved pegmatite. It is important to note that overlapping between granites and pegmatites and different pegmatite types in a fractionation sequence indicates geochemical decoupling which precludes origin from a single starting composition such as a parent granite magma (Jolliff et al., 1992).

Figures 9A, C and D show that pegmatites and granites lie on a similar fractionation trend whereas, on the K_2O/Rb vs. Rb plot, pegmatites and granites follow a completely different trend. Although a similar fractionation trend is observed in some plots, the garnet-tourmaline pegmatites, considered here to be the primitive end member in the belt, show an overlap with granites in the geochemical data which suggests element decoupling and therefore does not support the theory that pegmatites progressively separate from a granite parent undergoing fractionation. In addition, some of the greisens occasionally show a distinct compositional gap between themselves and other samples along the fractionation trend (Fig. 4.9A,B) and whilst fractionation should increase total REE abundances, the pegmatites of the Cape Cross-Uis belt show extremely low to undetectable REE values (Fig. 4.10) such that their REE patterns are primitive and well below those of Salem-type granites (Fig. 4.10). Whilst it is common for LCT pegmatites to have low REE values due to their peraluminosity (Cullers and DeGraf, 1982), the Salem-type granites are also peraluminous, yet they differ from the pegmatite REE content by two orders of magnitude (Fig. 4.10). Simmons et al. (1986) observed similar results when sampling wall rocks and suggested the reason for low REE abundances is that REEs partitioned into residual fluids and are therefore trapped in altered zones. However, this study analysed altered zones which show the lowest REE values in the dataset. We also considered that REE might partition into a vapour stage and exit the pegmatite, however, Flynn and Barnham (1978) show that the partition coefficients of REEs into a Cl vapour stage is not greater than 1. The key parametre here is that whilst pegmatites appear to follow a similar fractionation trend in some plots as granites, other compositional patterns and overlapping data cannot be explained by the Jahns and Burnham (1969) model.

On a regional scale, at surface level, different pegmatite types and degree of mineralisation are randomly distributed relative to granite outcrop in the Cape Cross-Uis pegmatite belt, (Fig. 4.2)

providing further evidence that the pegmatites were not directly derived from late-stage granite evolution (Fig. 4.8D). It is concluded therefore, that the proximity of a pegmatite to a granite outcrop does not control mineralisation.

4.7.2.3 Source control on variability of pegmatite compositions

The Damaran pegmatites have also been considered to have been derived by low degrees of fluidised partial melting of a homogeneous or heterogeneous source to account for the compositional variations (Ashworth, 2013; Černý, 1991*a*; Jung et al., 1998, 2003; McDermott, 1996). Different degrees of partial melting of a homogeneous source or the same degree of partial melting of a heterogeneous source could occur (Stewart, 1978). These models imply that if pegmatites resulted from different degrees of partial melting a gradational trend of primitive to evolved pegmatites would show no spatial trend. Given the peraluminosity of the pegmatites, it is likely that the source was metapelitic for the pegmatites of the Cape Cross-Uis pegmatite belt (Ashworth, 2013; Barbarin, 1998; Chappell and White, 1974; Chappell et al., 2012; Freemantle, 2012; Jung et al., 2003). If biotite was the primary reservoir of rare alkali and alkaline earth metals (Li-Rb-Cs-Be-Sr-Ba) in the source and biotite remained in a partially melted residue at low degrees of partial melt as suggested by Thompson (1982) and Walker et al. (1989), the melt would not be enriched in these elements. The low values of CaO, MgO FeO and Ba in the Cape Cross-Uis pegmatite belt indicate that biotite remained in the residue. London (2008), however, suggests that muscovite is also a major source of rare alkali and alkaline earth metals and that the breakdown of muscovite forms orthoclase which is a major Ba sink. This could account for the low values of Ba and high values of rare alkali and alkaline earth metals in pegmatites from the Cape Cross-Uis pegmatite belt (Table 4.3). In support of this, Harris and Inger (1992) suggest that muscovite melts incongruently during partial melting. Granites show higher Ba compositions (Table 4.3) which might be due to a higher degree of partial melting where biotite is not retained in the source. Clemens (2014) also stressed that protolith texture, foliation and location of accessories also plays a large role in the partial melt that is produced.

Considering fractionation of a pegmatitic melt, Sn, B, Nb and Ta have an affinity to complex into hydroxyl-Cl saline fluids (Alfonso and Melgarejo, 2008; Kovalenko et al., 1986). During the greisenisation process, late-stage pegmatitic fluids could have complexed these various elements as suggested by London (2008). From the data in Figures 4.8 and 4.9 it seems clear that after

pegmatite emplacement, fractionation increased Nb, Ta and Sn in the late-stage melt or hydrothermal fluids such that these elements were concentrated into Nb-Ta oxides and cassiterite in late-stage internal altered zones of the pegmatites. When Li minerals occur, they are generally located in discrete zones in the pegmatites near the quartz core. London (2008) suggests constitutional zone refining and undercooling during fractional crystallisation was responsible for producing large pure crystals in discrete zones. This method is most likely the cause of the formation of Li minerals in pegmatites such as Petalite.

Well mineralised patchy greisens with up to 1 wt% Sn show sharp contacts with enclosing large unaltered feldspar crystals. This suggests that where greisenisation was generally incomplete, fluid migration was restricted because the amount of trapped fluid was small. Where locally the fluid volume was greater, the alteration process completely replaced all feldspar in the large greisen pods/zones and layered greisens. The larger fluid volume not only migrated through the pegmatite but also out into the country rocks such that the degree of tourmalinisation in the country rock is directly proportional to the size of the greisen pods/zones or layered greisens. This also indicates that the Sn was deposited in situ from a late-stage, fluid-rich phase rather than having been remobilised from country rocks as mentioned above by other authors.

The regional patterns of mineralisation are slightly more difficult to account for in the pegmatite belt. There is no evidence to suggest that the abundance of Sn, Nb and Ta increases towards the west of the belt as stated by Diehl (1993). However, there are differences between pegmatite swarms: the Strathmore and Karlowa swarm show more abundant Nb, Ta and Li whereas the Uis swarm is far more Sn rich. The dominant Li mineral in Karlowa is spodumene whereas in Strathmore it is petalite suggesting higher pressures of crystallisation in the former.

4.8 Conclusion

Mineralisation is largely controlled by internal pegmatite fractionation which concentrated Nb, Ta, Sn, Cs. Late-stage fluids then complexed these elements and caused large-scale alteration to produce highly mineralised greisens. Assimilation was not a cause of mineralisation although significant host rock interaction occurred as late-stage pegmatitic fluids rich in B and Sn migrated outwards into country rock, tourmalinising and metasomatising the host rock. The abundance of

tourmaline in contact zones therefore indicates that internal late-stage pegmatitic fluids had the ability to migrate throughout the pegmatite but does not indicate mineralisation since patchy confined greisens occur and show that remobilisation of Sn, Nb, Ta and Cs from host rocks was not the process in which element enrichment occurred.

Pegmatites are likely to have resulted from localised anatexis of a heterogeneous metasedimentary, muscovite- and ilmenite-bearing source. Decoupling of element ratios, a large scatter in pegmatite trace element trends and low total REE values compared to granites provides the evidence that a progressive fractionation-separation method of deriving pegmatites is null and cannot account for many features of the Cape Cross – Uis pegmatite belt such as the complexly distributed pegmatite types and mineralisation.

The lack of deformation features within the pegmatites, their overall NE structural emplacement and cross-cutting relationships with Damaran structures would suggest that the pegmatites were emplaced in an extensional environment during post-tectonic crustal relaxation. The irregular spatial distribution of the pegmatites, the post-tectonic timing of emplacement and the lack of evidence for evolution by granite fractionation suggests that a partial melting model is likely for the Cape Cross-Uis pegmatites. Further isotopic and geochronological data will be investigated to confirm that these pegmatites have a partial melting origin.

4.9 Acknowledgements

Thanks to Riana Rossouw at the University of Stellenbosch for conducting whole-rock geochemistry ICP-MS. We are grateful for the standards for Sn and Ta for XRF analysis - AMIS 0343, 0019 and 034 provided by Mike McWha at African Mineral Standards. We are indebted to the Geological Survey of Namibia, in particular Gabi Schneider, for providing insight and discussion on the field area and for their support of this project. This project was funding by the CIMERA research centre and we are grateful for the invaluable financial support. Timothy Marais together with Bushveld Minerals helped with an extra field season in which to study the pegmatites and we are indebted to them accordingly.

Chapter 5: The geochemical evolution of Nb-Ta-Sn oxides from pegmatites of the Cape Cross–Uis pegmatite belt, Namibia

Warrick C. Fuchsloch, Paul A.M. Nex, Judith A. Kinnaird

Accepted by *Mineral Magazine* (06 August 2018)

Keywords: CGM, tapiolite, cassiterite, granitic pegmatite, Damara Orogen, Namibia

5.1 Abstract

The Cape Cross-Uis pegmatite belt, Damara Orogen, north-central Namibia hosts multiple Ta-Nb- and Sn-oxide-bearing pegmatites. Columbite-group minerals, tapiolite, cassiterite and minor ixiolite and wodginite occur in abundance within pegmatites and display various compositional and internal structural mineralogical variations. Ta-Nb oxides display various zonation patterns indicative of multiple crystallisation phases, whereas cassiterite is dominantly homogeneous with minor euhedral columbite-group mineral inclusions. Ta-Nb-oxides are mostly Fe-rich, with fractionation patterns in the columbite quadrilateral being sub parallel to the Ta/(Ta+Nb) axis; increasing Ta/(Ta+Nb) with little change in Mn/(Mn+Fe), which is consistent with classical trends in beryl to spodumene type rare-element pegmatites. In addition, these trends suggest that co-crystallising minerals compete with Ta-Nb-oxides for elements such as Mn, preventing Ta-Nb-oxides from attaining Mn-rich compositions during the fractionation process. Cassiterite shows similar fractionation patterns with Fe>Mn and notable increases in the Ta content. Minor element substitution in Ta-Nb-oxides shows sharp decreases with increasing fractionation supporting the hypothesis that newly stabilised co-occurring minerals compete with columbite-group minerals for certain elements. Tapiolite shows the same minor element trend, however, only for the elements Sn and Ti suggesting cassiterite was a dominant competing mineral phase. Although crystallisation of Ta-Nb-oxides from an aqueous fluid at the late-stages of pegmatite petrogenesis is highly debated, significantly elevated values of Ta in metasomatised country rock, compared to unaltered country rock, may give new insight into the debate, suggesting that Ta may indeed partition into and be transported by an exsolved aqueous fluid. However, further studies of the country rock metasomatic contacts are required as currently the dataset is limited. The degree of fractionation as depicted by Ta-Nb- and Sn-oxides within pegmatites, indicate that a zonation from primitive to evolved pegmatites surrounding granites is not present and that pegmatites are not likely to have

been related to granites in the typical parent-daughter type relationship, confirming similar observations in Fuchsloch et al. (2018*a*).

5.2 Introduction

The internal evolution processes of a pegmatite forming magma, such as fractionation (Černý and Ercit, 1985; Mulja et al, 1996; Novák and Černý, 1998; Martins et al., 2009) and crystallisation conditions (Ercit et al., 1995; Van Lichtervelde et al., 2007) can be traced using the composition of Ta-Nb-Sn oxides. While many studies have focused on the pegmatite or crystal scale (Lahti, 1987; Splide and Shearer, 1992; Hanson et al., 1998), new data have begun to emerge in which columbite-group minerals [$(Fe,Mn)(Ta,Nb)_2O_6$] compositional databases are based on a group, a district and may even cover the continental scale (Alfonso et al., 1995; Tindle and Breaks, 2000; Beurlen, 2008; Melcher et al., 2013, 2015, 2017). In addition, columbite-group minerals have been the subject of many experimental studies (e.g. Černý et al., 1992b; Linnen et al., 1996; Linnen and Keppler, 1997; Linnen, 1998), and they have been used in conjunction with whole-rock pegmatite geochemistry (Raimbault, 1998) and even used as a datable mineral (Romer and Lehmann, 1995; Smith et al., 2004; Baumgartner et al., 2006; Van Lichtervelde et al., 2017).

In the Cape Cross-Uis pegmatite belt (CUPB) of Namibia, numerous granitic pegmatite bodies intrude the metasedimentary and granitic rocks of the Zerrissene Group and Salem-type granites. These pegmatites have been mined sporadically in the past for Li, Sn, Ta and Nb. Fuchsloch et al. (2018*a*) have reported in detail on the field characteristics, mineralogy and whole-rock geochemistry of pegmatites from the CUPB. These pegmatites show a wide variety of characteristics in terms of intrusion dimensions, complexity, mineralogy, mineralisation and whole-rock geochemistry, throughout the 120 km long by 40 km wide CUPB (Richards, 1986 Diehl, 1993; Fuchsloch et al., 2018*a*).

Despite the emergence of district and continent scale columbite-group minerals compositional databases (Wise et al., 2012; Melcher, et al., 2013, 2015), many pegmatite groups, such as those of the CUPB have not yet been studied in detail. The aim of this paper is to present the first detailed compositional study of columbite-group minerals, tapiolite and cassiterite from the Cape Cross – Uis pegmatite belt. High definition back-scattered electron images (BSE) combined with mineral

geochemical data are used to evaluate the fractionation trends within the pegmatites at all scales from an individual crystal through the pegmatite body, to a regional pegmatite belt scale. An evaluation of the degree of fractionation gives insight into the granite-pegmatite relationship, which Fuchsloch et al. (2018*a*) found questionable, suggesting an anatectic model for pegmatite petrogenesis rather than fractionation from a parent granite body. Crystallisation conditions and paragenetic sequences of crystallisation of columbite-group minerals and cassiterite are also assessed by evaluating the homovalent and heterovalent substitutions in these minerals.

5.3 Geological setting

5.3.1 Regional overview

Several rare-element pegmatite belts in Namibia occur within the Damara Belt which is the northeast-trending intracontinental branch of the Neoproterozoic Pan-African Damara Orogen (See Richards, 1986 and Keller et al., 1999; Fig. 5.1). The Damara Belt extends from the Atlantic coast near Swakopmund inland towards Botswana and represents a typical 'Wilson Cycle' between 750 Ma to 440 Ma, which culminated in the collision of the Kalahari and Congo cratons (Martin and Porada, 1977; Hoffman et al., 1996; Prave, 1996; De Kock et al., 2000; Gray et al, 2006; Miller, 2009). On the basis of structure, stratigraphy, igneous activity and metamorphic grade, Miller (1983, 2008, and 2009) divided the Damara Belt into a number of tectonostratigraphic zones bound by major lineaments and faults (Fig. 5.1). The CUPB is located in the Northern Zone of the Damara Belt, which is bounded by the Autseib fault and the Otjihorongo thrust (Fig. 5.1, 5.2).

During the stages of extension, spreading, subduction and final continental closure, various sedimentary, volcanic and intrusive rocks were formed that represent the magmatism in the polydeformed and polymetamorphic Damara Belt (Prave, 1996; Trompette, 1997). Initial Damaran intrusive magmatism was triggered by subduction which occurred between 580 Ma and 545 Ma and is represented by the Goas Suite (Milani et al., 2015). The final deformation event, D3, has been dated at between 542 and 519 Ma and is largely responsible for the voluminous granodioritic and granitic magmatism during the orogenesis stages of the Damara Belt (Tack et al., 2002; Kisters, 2005; Longridge, 2012). Pegmatites form part of this magmatic episode and are ubiquitous within the Damara Belt. They were emplaced within the time period 509–429 Ma

(Briqueu et al., 1980; Longridge, 2012), however, economic mineralisation appears to be exclusively post-tectonic (Wagener, 1989; Diehl, 1993; Kinnaird and Nex, 2007; Miller, 2008; Longridge, 2012; Ashworth, 2013).

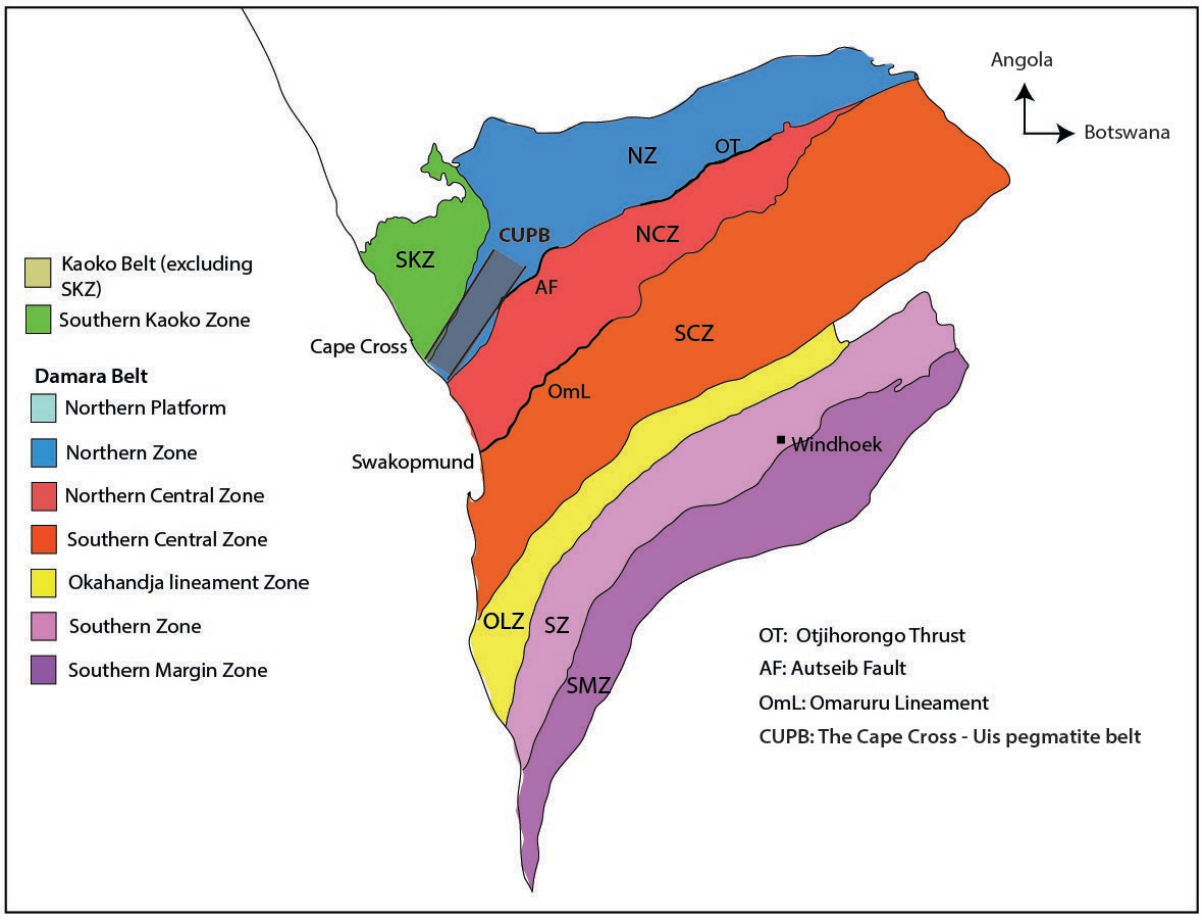


Figure 5.1: The Damara Belt showing the different stratigraphic zones defined by Miller, 2008 (Modified after Miller, 1983 and Fuchsloch et al. 2018*a*).

5.3.2 The Cape Cross – Uis pegmatite belt

Pegmatites of the CUPB intrude metasediments and granites of the Northern Zone which is dominated by the Amis River Formation of the Zerrissene Group (Fuchsloch et al., 2018*a*). Granites are fine- to coarse-grained, porphyritic granodiorites of the Salem-type and monzogranites of the Red and Grey granites. Metasedimentary rocks represent a fan fringe deposit and consist typically of biotite schist ± cordierite porphyroblasts and minor metagreywacke and quartzite units (Swart, 1992). Metasedimentary rocks show both earlier regional metamorphism to greenschist facies and later thermal metamorphism induced by the intrusion of Salem-type granites (Goscombe et al., 2004). Structural features of the area are characterised by moderately- to steeply-

inclined, north-south-striking folds (Macey and Harris, 2006). However, Fuchsloch et al. (2018*a*) show that pegmatites are exclusively post-tectonic and were emplaced into pre-existing north-northeast structural weaknesses in the crust.

The pegmatite belt is divided into three pegmatite swarms known as the Strathmore, Karlowa and Uis swarms (Fig. 5.2). Diehl (1993) suggested that increased Sn mineralisation in pegmatites coincides with an increase in the metamorphic grade to the west. Fuchsloch et al. (2018*a*) found no evidence for the westward increase of the mineralisation grade but instead describes different features in the swarms. The authors found that the Uis pegmatites show the highest cassiterite abundances whereas the Karlowa pegmatites are Li-Nb-Ta-rich with spodumene occurring as the dominant Li-mineral. Furthermore, the Strathmore pegmatites show enrichment in Li-Ta-Nb-Sn-Be with petalite occurring as the dominant Li-mineral. Strathmore is the only swarm in which complex mineralogically zoned pegmatites occur, for example, the Petalite pegmatite (Fig. 5.2).

Pegmatites in the CUPB are classified as LCT-type based on the classification of Černý and Ercit (2005). Some pegmatites show the hallmarks of LCT-type pegmatites whereas others, such as the intragranitic garnet-tourmaline pegmatites, show intermediate characteristics between NYF and LCT pegmatite types. Short-comings in the current classification schemes have led authors such as Fuchsloch et al. (2018*a*) to subdivide the pegmatites of the CUPB into three separate groups based on geochemical and mineralogical characteristics: 1) the barren to Nb-Ta-Sn mineralised, unzoned pegmatites; 2) garnet-tourmaline, intragranitic, crudely zoned pegmatites; 3) zoned and unzoned Li-mineralised pegmatites. The petrology and characteristics of the pegmatite groups are well documented (Richards, 1986; Wagener, 1989; Diehl, 1993; Ashworth, 2013; Fuchsloch et al., 2018*a*). Table 5.1 assigns the pegmatites studied to these different groups. The bulk mineralogical composition of the pegmatites is granitic, with quartz, muscovite, albite and microcline as essential minerals. Primary accessory mineralogy varies between the pegmatite groups and includes columbite-group minerals, cassiterite, tapiolite, magnetite, ilmenite, tourmaline, apatite, beryl, petalite, lepidolite, spodumene, zircon and monazite. Secondary mineralogy includes cleavelandite, hectorite, eucryptite and alteration zones of muscovite, quartz and albite.

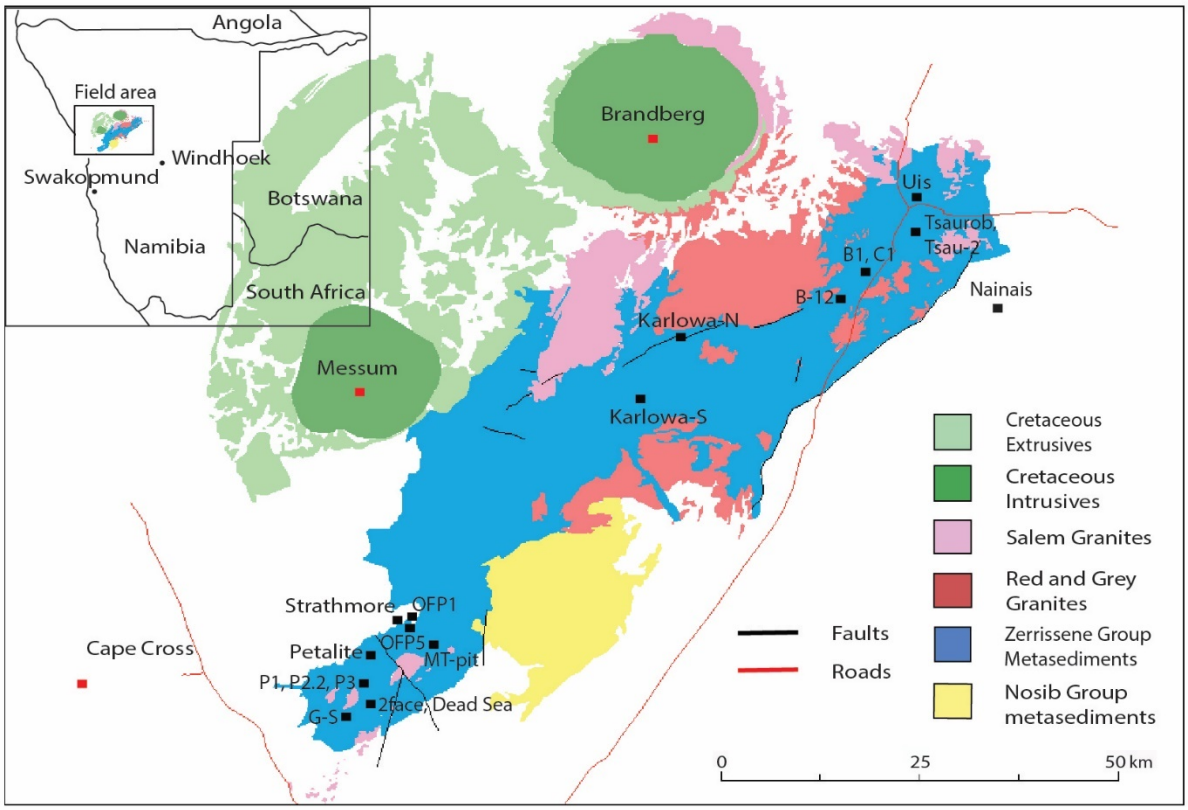


Figure 5.2: A simplified geological map of the Cape Cross-Uis pegmatite belt, Namibia (modified after Fuchsloch et al., 2018*a*). The black squares show the approximate locations of the twenty pegmatite areas that were sampled. A total of 25 individual samples were collected from these pegmatites. Pegmatites in the southwest are part of the Strathmore swarm, those in the Karlowa area are part of the Karlowa swarm and those in the northeast are part of the Uis swarm.

Various authors such as Richards (1986) suggest that pegmatites of the Damara Belt are associated with I- and S-type granitic and granodioritic intrusions. However, Fuchsloch et al. (2018*a*) questioned this relationship and showed, using the spatial distribution of pegmatites of the CUPB together with whole-rock geochemistry, that a parent-daughter type relationship between granites and pegmatite is unlikely. Fuchsloch et al. (2018*a*) favours an anatexis model for pegmatite petrogenesis. The Uis pegmatites have been dated at 496 ± 30 Ma and 486 ± 8 Ma by Haack and Gohn (1988) and Diehl (1993) respectively using Rb-Sr dating. Richards (1986), Wagener (1989), Diehl (1993) and Singh (2007, 2008) agreed that mineralisation of elements such as Sn was controlled by assimilation of country rock. However, Fuchsloch et al. (2018*a*) shows, using field evidence and whole-rock geochemistry, that assimilation was not likely to have been the cause of mineralisation and that internal pegmatite fractionation was the dominant process in which element enrichment of Nb, Ta, Cs and Sn occurred.

Ta-Nb and Sn-oxides occur in abundance in late-stage greisenised and albitised zones but also occur in magmatic zones with an equigranular magmatic texture (Table 5.1; Fuchsloch et al., 2018*a*). The alteration zones have been shown to have the highest levels of fractionation in terms of whole-rock geochemistry, occur sporadically or in discrete zones within pegmatites and are not restricted to a pegmatite type. Columbite-group minerals occur in all the different pegmatite types in the CUPB but to a lesser extent in the garnet-tourmaline type pegmatites since only one such pegmatite was found to have columbite-group minerals (Fuchsloch et al., 2018*a*). Cassiterite occurs sporadically in different pegmatites, is completely absent from the garnet-tourmaline type and is abundant in the Uis Swarm. Previous studies (Melcher et al., 2013, 2015) and this study have reported the occurrence of other Ta-Nb oxides such as tapiolite, ixiolite and wodginite based on compositions obtained by microprobe. Melcher et al. (2013, 2015) suggests that the Uis pegmatites and the C1 pegmatite (Fig. 5.2) show concomitant Fe-Mn and Nb-Ta fractionation trends (increasing Ta/(Ta+Nb) and Mn/(Mn+Fe) in a 1 to 1 ratio) in columbite-group minerals, which is typical of the complex spodumene pegmatite type. However, that study is on a continental scale and lacks the detailed investigation of this report.

5.4 Sampling and analytical techniques

Twenty-five different pegmatite bodies were sampled in twenty different pegmatite locations in the CUPB (Fig. 5.2). Although the pegmatites are predominantly unzoned (Fuchsloch et al., 2018*a*), samples were selected from greisenised zones, albitised zones and magmatic zones with a magmatic equigranular texture. Samples ranged in size from 1 to 3 kg of bulk material and were selected to best represent the alteration or magmatic zone. Each sample was crushed, milled and sieved to below 500 µm grain size and then processed on a Wilfley table. Samples were further processed on a Franz magnetic separator. These processes extracted the heavy and magnetic mineral populations that were then mounted into resin blocks ready for microprobe analysis. All samples yielded columbite-group minerals ± tapiolite whereas cassiterite was only recovered in fifteen samples (Table 5.1).

A total of 535 quantitative mineral chemical analyses were obtained using a JEOL JXA-8230 electron micro-analyser with four wavelength dispersive spectrometres at Rhodes University for columbite-group minerals, tapiolite and cassiterite. The beam was generated by a tungsten cathode

at 30 nA current with a 1 μm beam size. Counts for Mg, Fe, Ca, Mn, Ti, and Sc were measured on K-alpha peaks, Sn, W and Nb on L-alpha peaks and U and Ta on M-alpha peaks. Counting times were 10 seconds on the peak and 10 seconds total on the background, for all elements. Minerals were standardised for Sn on metallic-Sn, Ta on metallic-Ta, U on metallic-U, Ca/W on scheelite, Mg/Fe on chromite, Mn on rhodonite, Nb on metallic-Nb, Ti on rutile and Sc on metallic-Sc. Calibration acquisitions were peaked on the standards whilst unknown acquisitions were peaked on the samples before each point analysis. The data were collected with JEOL software. An automated ZAF matrix algorithm was applied to correct for differential matrix affects.

Individual, complexly zoned, tapiolite crystals and cassiterite crystals were analysed using a Cameca SX100 electron microprobe at the London Natural History Museum. A total of 87 points on 15 tapiolite crystals and 24 points on 5 cassiterite crystals for samples 3.1-2 and 6-1 respectively (Table 5.1) were analysed. A current of 20 nA was used with an accelerating potential of 20 keV, a beam size of 1 μm and various counting times ranging from 10–60 seconds. Counts for Na, Mg, Al, Si, Ca, Ti, Mn, Fe, Sc were measured on K-alpha peaks, Nb, Sn, Zr, Ta, Hf and W on L-alpha peaks and U and Th on M-alpha peaks. Minerals were standardised for Na on jadeite, Mg on forsterite, Al on corundum, Si/Ca on wollastonite, Nb on niobium metal, Sn on cassiterite, Ti on rutile, Mn on manganese titanium oxide, Fe on hematite, Zr on zircon, Ta on tantalum metal, Hf on hafnium metal, Th on monazite, U on uranium oxide, W on pure tungsten and Sc on scandium metal. The data were collected on Cameca software and a default JOEL ZAF matrix algorithm (Heinrich/Duncumb-Reed correction with FFAST NIST-2005 mass absorption coefficients) was used to correct for differential matrix affects. Oxygen was calculated using stoichiometry and the atoms per formula unit (a.p.f.u.) were calculated based on 3 cations and 6 oxygens per formula unit for all data collected.

The data collected were screened to ensure that only columbite-group minerals, tapiolite and cassiterite were evaluated since wodginite and ixiolite are very minor constituents or completely absent from most pegmatites and therefore detailed studies of these species is beyond the scope of this study. In addition, no Ca-bearing Ta-Nb-oxides were recovered such as pyrochlore or microlite.

The data were plotted on a Nb vs Ta diagram (Fig. 5.3) where ideal columbite-group minerals and tapiolite compositions should plot within a boundary between Nb + Ta = 2.0 (a.p.f.u.) and Nb + Ta = 1.8 (a.p.f.u.). Ideal compositions refer to the correct stoichiometric proportions of Nb to Ta in a given crystal that constitutes the specific crystal being of the columbite-group minerals (Neiva, 1996). Ten data points plotted below this boundary and are considered to belong to the wodginite and ixiolite family as defined by Neiva (1996). Table 5.1 shows the Ta-Nb- and Sn-oxide mineralogy of each pegmatite.

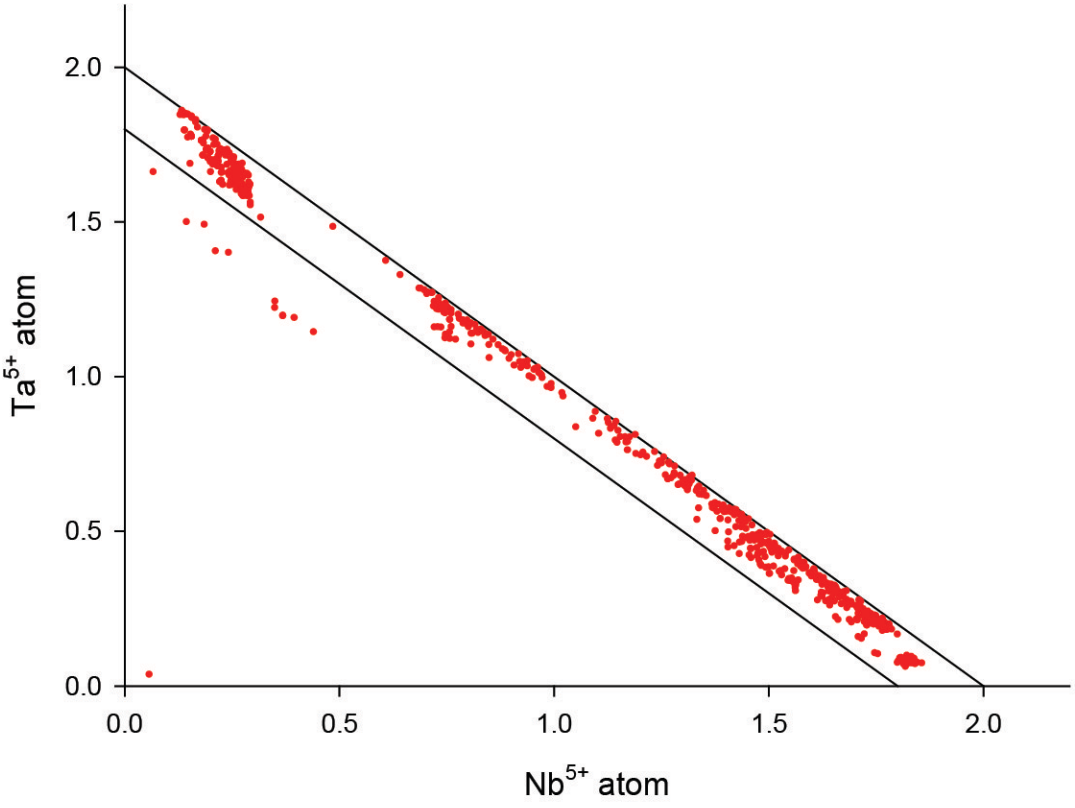


Figure 5.3: The atomic proportions of Ta and Nb of the columbite-group minerals and tapiolite from the Cape Cross-Uis pegmatite belt. Points that plot below the boundary are considered to be of the wodginite and ixiolite family. Points within the boundary are considered to be of ideal columbite-group mineral compositions where Ta and Nb are in the correct proportions to constitute the columbite-group minerals (Neiva, 1996; Tindle and Breaks, 2000).

5.5 Results

Columbite-group minerals and cassiterite are the dominant Ta-Nb-Sn-bearing phases in the CUPB. Subordinate tapiolite, wodginite and ixiolite occur but have not been observed macroscopically and have restricted distributions occurring only in highly altered zones of the pegmatites. Wodginite and ixiolite were only identified from their composition as analysed by microprobe, whereas tapiolite has been observed microscopically but as a secondary phase in all samples except

in sample 3.1-2 (Table 5.1). Although many samples include Ta-Nb-Sn-bearing phases in magmatic zones with a distinct equigranular texture, they are more abundant in greisenised or albitised zones within the pegmatites. These altered zones do not indicate that the pegmatite itself is zoned; only the Petalite pegmatite shows a true mineralogical zonation (Fig. 5.2; Table 5.1). The greisens essentially consist of new or recrystallised quartz and muscovite, with accessory columbite-group minerals, tapiolite, and cassiterite. They were formed by late-stage pegmatitic fluids and show varying degrees of alteration. They occur as patchy networks, layered units or in the case of the Petalite pegmatite as a large metre-scale zones surrounding the quartz core of the pegmatite. Their sizes range from several centimetre patches, sporadically occurring in pegmatites, to metre-scale lensoidal or layered units. Albitised zones share similar features to greisens but consist of a homogeneous mass of saccharoidal albite. Ta-Nb-Sn-bearing phases show varying grain sizes in greisens but are mostly macroscopic whereas albitised zones rarely display distinguishable grains.

Most Ta-Nb- and Sn-oxide studies (e.g. Černý et al., 2004) are related to complexly zoned pegmatites, each zone having uniquely occurring Ta-Nb-Sn-bearing phases with distinct compositions. Although only one pegmatite shows true pegmatite zonation in this study, in other examples, a comparison between magmatic and altered zones yields a similar distinction in characteristics and mineralogy of Ta-Nb-Sn oxides. The whole-rock geochemical and mineralogical differences in these zones have already been characterised by Fuchsloch et al., (2018*a*).

Table 5.1: Ta-Nb- and Sn-oxides and characteristics of pegmatites studied in the Cape Cross-Uis pegmatite belt (shown in Figure 5.1). Gnt-Tml indicates the garnet-tourmaline pegmatite type, Ta-Nb-Sn indicates the unzoned Ta-Nb-Sn mineralised pegmatites and the Li-pegmatites indicate the unzoned and zoned Li-mineralised pegmatites. FeC, ferrocolumbite; FeT, ferrotantalite; MnC, manganocolumbite; MnT, manganotantalite; Cas, cassiterite; Tap, tapiolite; Wdg, wodginite; Ix, ixiolite.

Pegmatite	Sample #	Pegmatite type	Ta-Nb-Sn-oxides	Oxide occurrence	CGM zonation
G-S	12-1	Gnt-Tml	FeC, MnC, Cas	Magmatic zone	Oscillatory
Dead Sea	2-4	Nb-Ta-Sn	FeC	Magmatic zone	Progressive
Nainais	Na-5	Nb-Ta-Sn	FeC, FeT, Cas	Magmatic zone	Oscillatory, patchy
	Na-6	Nb-Ta-Sn	FeC, FeT, Cas	Magmatic zone	Progressive
Petalite	G-4	Li-pegmatite	FeC, Cas	Greisen zone	progressive
Strathmore	4-3	Nb-Ta-Sn	FeC, FeT	Magmatic zone	Progressive
	4-4	Nb-Ta-Sn	FeC	Albitised zone	Progressive
	4-9	Nb-Ta-Sn	FeC, FeT, MnC	Magmatic zone	Oscillatory
	4-11	Nb-Ta-Sn	FeC, MnC, Tap	Magmatic zone	Oscillatory
	4-12	Nb-Ta-Sn	FeC	Magmatic zone	Progressive
2face	10-4	Nb-Ta-Sn	FeC, FeT	Magmatic zone	Progressive
Tsau-2	J-5	Nb-Ta-Sn	FeC, FeT, MnC, Cas	Magmatic zone	Oscillatory, patchy
OFP5	B-2	Nb-Ta-Sn	FeC, FeT, MnC, Cas, Wdg/Ix	Greisen zone	Oscillatory, patchy
C1	W-3	Nb-Ta-Sn	MnC, MnT, Tap	Greisen zone	Oscillatory, patchy
OFP1	A-2	Nb-Ta-Sn	FeC, FeT, Cas	Magmatic zone	Oscillatory
B1	X-1	Nb-Ta-Sn	FeC, FeT, MnC, MnT, Tap, Cas	Greisen zone	Complexly zoned
B-12	M-2	Nb-Ta-Sn	FeT, FeC, Tap, Wdg/Ix, Cas	Greisen zone	Complexly zoned
Tsaurob	T-4	Nb-Ta-Sn	FeC, FeT, Cas	Magmatic zone	Oscillatory
P2.2	3-3	Nb-Ta-Sn	FeC, FeT, Cas	Magmatic zone	Progressive
P3	3.2-1	Nb-Ta-Sn	FeC, Cas	Magmatic zone	Progressive
Karlowa-S	5-3	Li-pegmatite	FeC, FeT, Tap, Cas	Magmatic zone	Oscillatory, patchy
Karlowa-N	5.1-1	Li-pegmatite	Tap, Cas	Greisen zone	Progressive
Uis	6-1	Nb-Ta-Sn	Cas, (CGM inclusions)	Magmatic zone	Oscillatory
MT-pit	D-4	Nb-Ta-Sn	FeC, FeT	Magmatic zone	Oscillatory
P1	3.1-2	Nb-Ta-Sn	Tap	Greisen zone	Complexly zoned

Columbite-group minerals have the general formula of AB_2O_6 where the A-site is occupied mostly by Fe and Mn and the B-site mostly by Ta and Nb. The columbite-group minerals comprise four end members all with an orthorhombic crystal structure: ferrocolumbite ($FeNb_2O_6$), ferrotantalite ($(Fe>Mn)(Ta>Nb)_2O_6$), manganocolumbite ($MnNb_2O_6$) and manganotantalite ($MnTa_2O_6$). Ferrotantalite only requires Fe > Mn and Ta > Nb and occurs as an orthorhombic crystal whereas tapiolite belongs to the tetragonal crystal system and occurs as the end member compositions, $FeTa_2O_6$, within the ferrotantalite field. A compositional gap separates tapiolite and ferrotantalite within the ferrotantalite field (Černý et al., 1992b). The overall proportions of Ta to Nb and Fe to Mn [Ta/(Ta+Nb), Ta#; Mn/(Mn+Fe), Mn#] in the columbite quadrilateral are used to show fractionation trends within pegmatite bodies where various different trends have been observed

and linked to certain petrochemical processes and abundances (e.g. Černý and Ercit, 1985; Tindle and Breaks, 2000). In addition, the quadrilateral is also used to determine the species of columbite-group minerals, distinguishing between ferrotantalite and tapiolite which have the same chemical formula. An increase in Ta# in columbite-group minerals, and in tapiolite and cassiterite is widely accepted as an indication of higher levels of fractionation whereas changes in the Mn# are debated (see discussion in Van Lichtervelde et al., 2007). Columbite-group minerals, tapiolite and cassiterite compositional data were used to evaluate fractionation trends within pegmatites of the CUPB. Element substitution by Ti, Ca, W, Mg, and Sn was also assessed. The data were then used to compare compositions from different pegmatite groups and swarms in the CUPB. The shape of certain fractionation trends in the columbite quadrilateral for columbite-group minerals have also been used as a classification tool (Černý and Ercit, 1989).

5.5.1 Columbite-group minerals and tapiolite

5.5.1.1 Occurrence and internal structure

Columbite-group minerals in the CUPB occur in various morphologies depending on their location within a given pegmatite and are the most abundant Ta- and Nb-bearing phases. The most common occurrence of columbite-group minerals is in the form of platy striated black crystals with a metallic lustre which can either occur as amalgamated laths, several centimetres in length or as single plates with smaller grain sizes between 100 and 500 µm. The largest amalgamated crystals occur in the unaltered magmatic zones of the pegmatite whereas the equigranular plates mostly occur in the alteration zones. Large tabular crystals are rare. Columbite-group minerals occur uniformly throughout the CUPB and no swarm in particular favours higher abundances. The most common end-member in the CUPB is ferrocolumbite followed by ferrotantalite. Manganese end members are rare but are present in several samples, particularly in greisens (Table 5.1). Tapiolite exclusively forms anhedral crystals up to 0.5 mm in size and similar to manganese end members occur rarely. Only one sample was found to contain abundant tapiolite (Sample 3.1-2; Table 5.1).

The internal structure of columbite-group minerals and tapiolite shows multiple, singular and/or complex zonation patterns (Fig. 5.4). Columbite-group minerals are sometimes associated with cassiterite either enclosing cassiterite grains or co-occurring with cassiterite (Fig. 5.4A). The complexity of zonation in a single crystal corresponds to the degree of alteration in the pegmatite

zone in which the crystal occurs. Zonation patterns in columbite-group minerals and tapiolite have been compared to typical feldspar zoning of which there are three dominant types (Lahti, 1987). The following classifies the zonation patterns in columbite-group minerals in accordance with Lahti (1987) classification scheme.

(1) The most common type of zonation seen in the CUPB is a progressive zonation whereby crystals, from core to rim, have a mono-directional compositional variation that can either be in a single direction (Fig. 5.4B) or concentrically arranged (Fig. 5.4C). Each subsequent zone that crystallised may show either a progressive increase in Ta or Nb, from core to rim. Subsequently crystallised zones may not show alternating increases and decreases of Ta or Nb, which would be considered oscillatory zonation. Within each individual zone (e.g. Fig. 5.4B has four individual zones), slight changes in the BSE brightness show that progressive zonation may occur within individual zones as well. Elevated levels of brightness in the BSE are indicative of higher Ta and lower Nb proportions in the crystal structure. In comparison to oscillatory zonation, crystals such as in Figure 5.4B and c are still considered to be progressively zoned since there is an overall increase in the Ta proportions from core to rim, even though their individual zones also show changes in brightness and therefore composition.

(2) Oscillatory zonation is a common feature of columbite-group minerals and tapiolite and is generally the most abundant zonation type in Ta-Nb-bearing pegmatites (e.g. Zhang et al., 2004). However, oscillatory zonation, which is not as widespread in the CUPB as progressive zonation, occurs equally in columbite-group minerals in both magmatic and altered zones. Oscillatory zonation occurs as repeating, alternating zones of different Ta and Nb compositions (Fig. 5.4D). As with progressively-zoned crystals, each specific zone may also show individual progressive zonation (Fig. 5.4E). The width of the zones in the oscillatory-zoned crystals may vary widely. In the case of Figure 5.4D, zones at the core have an average width of several microns and then a larger 40 μm zone occurs, followed by extremely thin banded zones. Tapiolite shows the most prominent oscillatory zonation (Fig. 5.5). Thin, less than a micron in thickness, zones occur as banded layers that can either be concentric (Fig. 5.5A,B,D) or unidirectional (Fig. 5.5C) across the specific crystal face. Individual oscillatory zones similarly show varying widths with either slight changes in BSE brightness or more notable changes.

(3) Abundant patchy zonation is typical of samples from altered zones. Patchy zonation may occur as resorption textures that have replaced primary grains/zones with later secondary undulating or irregularly shaped grains/rims (Fig. 5.4A,D,E,F). Patchy zonation has no particular affinity for grain cores or rims and is superimposed on either oscillatory or progressive zonation or both, giving the crystals complex zonation patterns (Fig. 5.4B,E,F). Patchy zonation generally shows the highest BSE brightness in all crystals, having the highest Ta contents, but may also occur as darker zones which appear to intrude a previously crystallised zone (Fig. 5.4D,E). Tapiolite exclusively occurs as patchy zones except in sample 3.1-2 (Fig. 5.5; all crystals are tapiolite in this figure).

5.5.1.2 Mineral chemistry

Representative compositions of columbite-group minerals and tapiolite are given in Table 5.2. Columbite-group minerals displays an extremely wide range of Ta_2O_5 and Nb_2O_5 compositions from 1.8–82.3 and 1.8–72.9 wt.% respectively. FeO and MnO values show similar broad ranges, 0.9–16.4 and 0.5–16.1 wt.% respectively, however, most compositions are Fe-rich compared to Mn and show an average of 12.4 wt.% FeO and 5.1 wt.% MnO. SnO_2 and TiO_2 compositions in general average ~0.9 wt.% but may exceed 4 wt.% in rare cases. Sc, U, Ca and W show low to non-detectable values that do not generally exceed 0.5 wt.%, however, it is notable that columbite-group minerals in the garnet-tourmaline type pegmatites have WO_3 contents up to 4.0 wt.%. Furthermore, Ca values are consistently low to non-detectable which is unusual for granitic pegmatites as minerals such as pyrochlore or microlite are generally present. Anomalous elevated minor element substitutions in columbite-group minerals are not unique to specific pegmatite groups, with the exception of W in garnet-tourmaline type pegmatites. However, the ferrocolumbite end-member, where present, shows the highest abundance of minor elements compared to the other end members. The total a.p.f.u. for columbite-group minerals and tapiolite cluster at 3 units for unaltered samples, however, greisenised samples show slightly elevated values of 3.1 a.p.f.u. Tapiolite shows less variation with respect to Ta_2O_5 and Nb_2O_5, having average values of 77.2 and 6.7 wt.% respectively. FeO values cluster around 13.0 wt.% whereas MnO values are much lower at an average of 1.0 wt.%. SnO_2 and TiO_2 values are elevated compared to columbite-group minerals, more often reaching 4.4 and 2.5 wt.% respectively. Mg, Ca, U, Sc and W were not detectable in tapiolite.

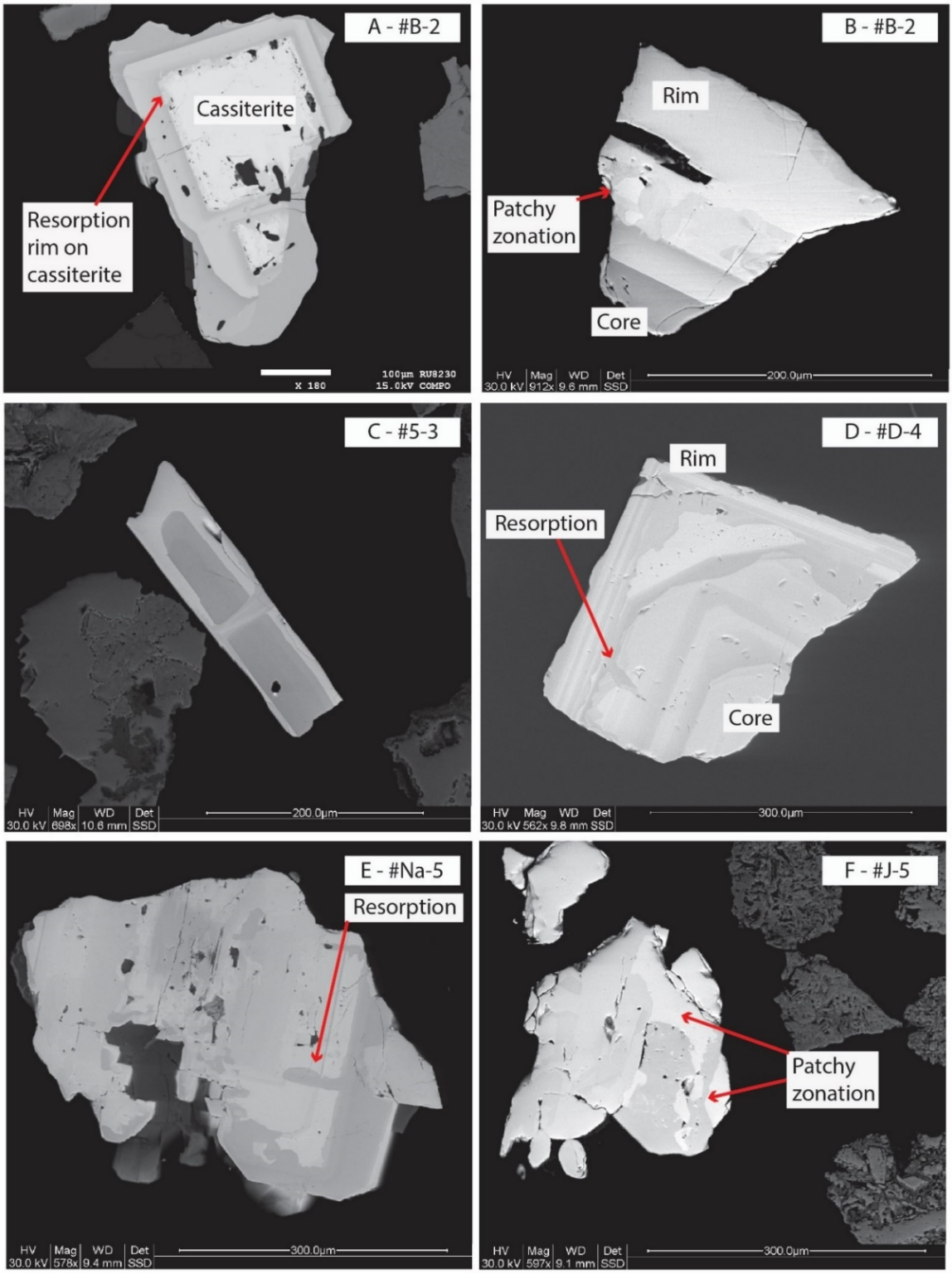


Figure 5.4: Back-scattered electron images of various columbite-group minerals and cassiterite crystals. (A) Oscillatory-zoned columbite-group mineral enclosing a euhedral cassiterite grain showing a resorption texture along the margins of the cassiterite crystal. (B) Progressively-zoned columbite-group mineral with later-stage patchy zonation along the rim and centre zone. (C) Platy progressively-zoned columbite-group mineral. (D) Oscillatory-zoned columbite-group mineral with resorption textures in the large centre zones. (E) Multiple zonation of a columbite-group mineral showing later resorption of the rim and renewed oscillatory-zonation. (F) Complexly-zoned columbite-group mineral showing patchy zonation.

Table 5.2: Representative electron microprobe analyses of columbite-group minerals and tapiolite from the Cape Cross-Uis pegmatite belt. FeC, ferrocolumbite; FeT, ferrotantalite; MnC, manganocolumbite; MnT, manganotantalite; Cas, cassiterite; Tap, tapiolite.

Sample #	12-1	5-3	A-2	2-4	Na-5	Na-6	4-3	4-9	4-11	4-12	10-4	J-5
Peg-type	*Gnt-Tml*	*Li-peg*	*Ta-Nb-Sn*	*Ta-Nb-Sn*	*Ta-Nb-Sn*	*Ta-Nb-Sn*	*Ta-Nb-Sn*	*Ta-Nb-Sn*	*Ta-Nb-Sn*	*Ta-Nb-Sn*	*Ta-Nb-Sn*	*Ta-Nb-Sn*
Mineral	*FeC*	*FeT*	*FeC*	*FeC*	*FeC*	*FeC*	*FeT*	*FeC*	*FeC*	*FeC*	*FeC*	*FeC*
SnO_2 wt.%	n.d.	0,09	0,19	0,03	0,14	0,74	0,24	0,15	0,17	0,17	0,75	0,22
MgO	0,40	0,08	n.d.	0,09	n.d.	n.d.	n.d.	n.d.	n.d.	n.d.	0,36	n.d.
Ta_2O_5	6,44	59,36	25,76	30,76	28,38	36,68	52,67	37,53	14,52	31,62	25,00	25,31
FeO	15,65	11,03	13,18	13,61	13,75	12,44	9,81	10,66	12,47	11,37	14,10	11,09
MnO	4,32	5,52	6,27	5,13	5,30	5,47	6,10	6,65	7,70	7,04	4,28	8,07
Nb_2O_5	67,85	22,67	54,98	50,23	52,70	43,99	27,90	44,15	64,72	49,26	52,20	55,13
TiO_2	2,16	0,34	0,60	0,70	0,39	0,88	0,85	0,19	0,56	0,33	2,32	0,44
Sc_2O_3	0,07	0,02	0,03	0,02	0,01	0,03	n.d.	0,03	n.d.	0,01	0,03	0,03
U_2O	n.d.	n.d.	n.d.	n.d.	n.d.	n.d.	n.d.	n.d.	n.d.	n.d.	n.d.	n.d.
CaO	n.d.	0,01	n.d.	n.d.	0,01	0,01	n.d.	n.d.	n.d.	0,02	n.d.	0,02
WO_3	3,93	n.d.	0,34	n.d.	n.d.	0,66	1,28	0,06	0,82	n.d.	1,46	0,77
Total	100,81	99,12	101,34	100,59	100,68	100,91	98,86	99,43	100,97	99,82	100,49	101,09
Sn a.p.f.u	n.d.	0,003	0,005	0,001	0,004	0,019	0,007	0,004	0,004	0,004	0,019	0,005
Mg	0,034	0,009	n.d.	0,009	n.d.	n.d.	n.d.	n.d.	n.d.	n.d.	0,033	n.d.
Ta	0,100	1,201	0,432	0,530	0,485	0,649	1,033	0,677	0,233	0,553	0,420	0,425
Fe	0,750	0,687	0,679	0,722	0,722	0,677	0,592	0,591	0,616	0,611	0,728	0,573
Mn	0,209	0,348	0,328	0,276	0,282	0,302	0,372	0,374	0,385	0,384	0,224	0,422
Nb	1,756	0,763	1,532	1,439	1,496	1,295	0,910	1,324	1,728	1,432	1,457	1,540
Ti	0,093	0,019	0,028	0,033	0,018	0,043	0,046	0,010	0,025	0,016	0,108	0,021
Sc	0,004	0,001	0,002	0,001	n.d.	0,002	n.d.	0,002	n.d.	0,001	0,001	0,002
U	n.d.	n.d.	n.d.	n.d.	n.d.	n.d.	n.d.	n.d.	n.d.	n.d.	n.d.	n.d.
Ca	n.d.	0,001	n.d.	n.d.	0,001	0,001	n.d.	n.d.	n.d.	0,001	n.d.	0,001
W	0,058	n.d.	0,005	n.d.	n.d.	0,011	0,024	0,001	0,013	n.d.	0,023	0,012
Total	3,004	3,031	3,010	3,011	3,007	2,999	2,985	2,982	3,004	3,002	3,012	3,002
Mn/(Mn+Fe)	0,054	0,612	0,220	0,269	0,245	0,334	0,532	0,338	0,119	0,279	0,224	0,216
Ta/(Ta+Nb)	0,218	0,336	0,325	0,276	0,281	0,308	0,386	0,387	0,385	0,386	0,235	0,424

Table 5.2 cont.

Sample #	D-4	T-4	3-3	3.2-1	5.1-1	3.1-2	G-4	B-2	W-3	x-1	M-2	4-4
Peg-type	*Ta-Nb-Sn*	*Ta-Nb-Sn*	*Ta-Nb-Sn*	*Ta-Nb-Sn*	*Greisen*	*Greisen*	*Greisen*	*Greisen*	*Greisen*	*Greisen*	*Greisen*	*albitised*
Mineral	*FeC*	*FeC*	*FeC*	*FeC*	*Tap*	*Tap*	*FeC*	*FeC*	*MnT*	*FeT*	*FeT*	*FeC*
SnO_2 wt.%	0,23	0,20	0,20	0,39	3,29	4,35	0,22	0,23	0,06	n.d.	0,95	0,39
MgO	0,02	n.d.	0,01	0,26	0,02	n.d.	0,03	0,07	n.d.	n.d.	0,07	0,03
Ta_2O_5	17,57	33,03	31,97	27,71	73,12	75,53	24,82	25,54	63,08	52,73	57,55	26,38
FeO	13,69	11,25	12,25	13,38	14,77	13,03	14,98	12,73	4,77	9,37	11,87	12,29
MnO	5,63	7,44	6,08	5,16	0,69	0,75	6,21	6,40	11,48	7,34	4,31	7,58
Nb_2O_5	59,40	47,13	48,70	51,81	6,14	5,56	51,83	55,51	21,46	28,94	23,51	53,28
TiO_2	1,19	0,27	0,54	1,24	0,62	1,11	0,82	0,70	0,15	0,18	1,91	0,56
Sc_2O_3	0,02	0,04	n.d.	0,02	0,02	n.d.	n.d.	0,01	0,03	n.d.	0,09	n.d.
U_2O	n.d.	n.d.	n.d.	n.d.	n.d.	n.d.	n.d.	n.d.	n.d.	n.d.	n.d.	n.d.
CaO	n.d.	n.d.	0,02	n.d.	n.d.	n.d.	n.d.	n.d.	0,02	0,03	n.d.	n.d.
WO_3	2,43	0,34	0,24	0,62	n.d.	n.d.	0,11	0,18	n.d.	0,77	1,01	0,03
Total	100,17	99,69	100,00	100,59	98,66	100,89	99,02	101,36	101,05	99,36	101,26	100,55
Sn a.p.f.u	0,006	0,005	0,005	0,010	0,108	0,140	0,006	0,006	0,002	n.d.	0,027	0,010
Mg	0,002	n.d.	0,001	0,024	0,002	n.d.	0,003	0,006	n.d.	n.d.	0,008	0,003
Ta	0,289	0,584	0,559	0,471	1,630	1,658	0,427	0,427	1,268	1,030	1,119	0,448
Fe	0,692	0,611	0,659	0,699	1,012	0,880	0,793	0,654	0,295	0,563	0,710	0,642
Mn	0,288	0,409	0,331	0,273	0,048	0,051	0,333	0,333	0,719	0,447	0,261	0,401
Nb	1,624	1,385	1,415	1,464	0,228	0,203	1,483	1,542	0,717	0,940	0,760	1,504
Ti	0,054	0,013	0,026	0,058	0,038	0,068	0,039	0,032	0,009	0,010	0,102	0,026
Sc	0,001	0,002	n.d.	0,001	0,001	n.d.	n.d.	n.d.	0,002	n.d.	0,006	n.d.
U	n.d.	n.d.	n.d.	n.d.	n.d.	n.d.	n.d.	n.d.	n.d.	n.d.	n.d.	n.d.
Ca	n.d.	n.d.	0,001	n.d.	n.d.	n.d.	n.d.	n.d.	0,002	0,002	n.d.	n.d.
W	0,038	0,006	0,004	0,010	n.d.	n.d.	0,002	0,003	n.d.	0,014	0,019	n.d.
Total	2,994	3,016	3,000	3,010	3,067	3,000	3,086	3,003	3,012	3,006	3,012	3,035
Mn/(Mn+Fe)	0,151	0,297	0,283	0,243	0,878	0,891	0,224	0,217	0,639	0,523	0,596	0,229
Ta/(Ta+Nb)	0,294	0,401	0,334	0,281	0,045	0,055	0,296	0,337	0,709	0,442	0,269	0,384

5.1.1.3 Intra-crystal tapiolite chemistry

Sample 3.1-2 is the only sample in the CUPB where primary magmatic textures, such as concentric oscillatory-zoning in subhedral grains, were observed in individual tapiolite crystals (Fig. 5.5). However, multiple patchy zonation and resorption textures overprint oscillatory-zonation. Individual crystals show the typical overall increase in Ta with respect to Nb, from the core outwards, despite alternating changes in Nb and Ta in oscillatory zonation (Fig. 5.5). Little change is observed in the Fe and Mn content through individual crystals (Fig. 5.5). The highest abundance

of Ta (greatest BSE brightness) occurs in patchy zonation regardless of whether the patch is at the core or on the rim. Sn and Ti show that, at single crystal-scale, as Ta is enriched, minor element substitution decreases (Fig. 5.5A,B,C). There is also an apparent 'jump' in the decrease in Ti and Sn from the oscillatory zones to the patchy zones (Fig. 5.5B,C). These discrete tapiolite grains show that, on an individual crystal scale and between the magmatic and late-stage patchy zonation, minor element trends are similar to those of the samples seen in Figure 5.6A-D. In addition, Figure 5.5A-C show that there is a decrease in the Nb values from oscillatory to patchy zonation indicating an increase in the Ta/(Ta+Nb) value from different textural zones. Calculations of the Ta# in both oscillatory and patchy zonation show that patchy zonation has a Ta# 0.05 to 0.1 greater than oscillatory zonation.

5.5.1.4 Columbite-group minerals and tapiolite mineral chemistry

When the minor elements, Ti, Sn, Ca, Mg and W are plotted against Ta# for the entire dataset, weak hyperbolic trends are seen (Fig. 5.6A-D). Figure 5.6A showcases this trend the best where early-crystallised (lower ranges of Ta#) tapiolite has high concentrations of Sn and Ti and later growth gradually became depleted in Sn and Ti with increasing Ta#. For the entire dataset these trends are less defined in Figure 5.6B-D, however, by plotting each sample separately this trend is clear and ubiquitous to all samples. Essentially there is an overall decrease in minor element heterovalent substitution in columbite-group minerals and tapiolite with increasing Ta#. Tapiolite compositions are different compared to columbite-group minerals in that they have elevated Sn and Ti concentrations, which is why individual plots for tapiolite and columbite-group minerals were used in Figure 5.6A and B. Furthermore, tapiolite data shows low contents of W, Mg and Ca compared to columbite group minerals at lower Ta# values. This is an interesting observation since zonation patterns and Ta# show columbite-group minerals as an early-stage Ta-Nb-oxide whereas tapiolite is mostly observed with patchy zonation, appearing to be a late-stage Ta-Nb-oxide. If we consider a transition from crystallising only columbite-group minerals to columbite-group minerals and tapiolite, there is a marked increase in the Ti and Sn contents in newly crystallised tapiolite, followed by a repeat of the trend of decreasing minor element heterovalent substitution with increasing Ta#. This 'jump' is absent for other minor elements, such as W, Ca and Mg, which remain at low concentration in tapiolite (Fig. 5.6C,D).

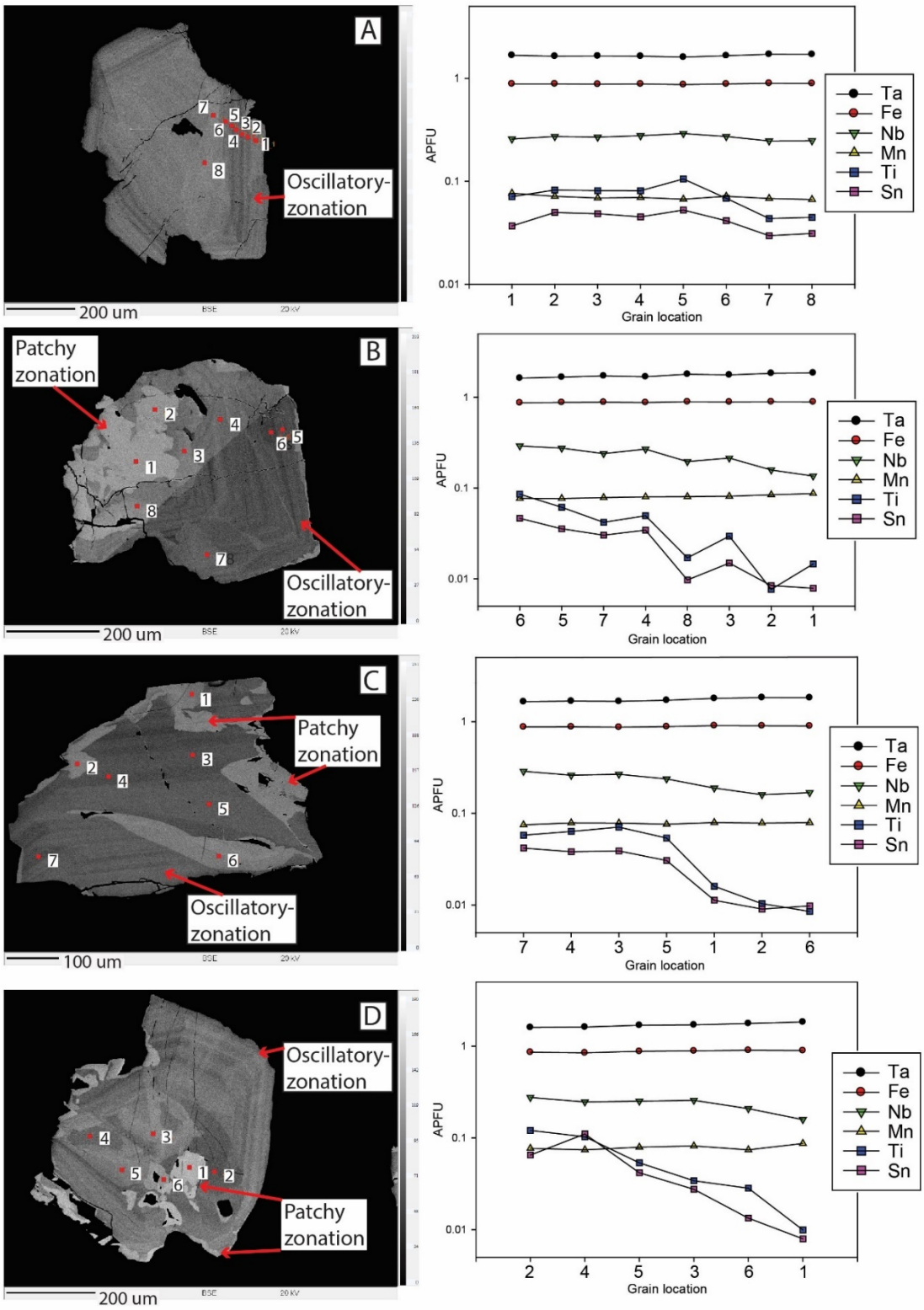


Figure 5.5: Back-scattered electron images of individual tapiolite grains from sample 3.1-2 with their corresponding analyses of elements Ta, Fe, Nb, Mn, Ti, Sn at different points in the grains. Note that the numbers in the corresponding graphs (x-axis) are ordered from darkest zones to lightest zones and not in ascending order. (A) Oscillatory-zone tapiolite crystal. (B) twinned complexly zoned tapiolite crystal. (C-D) complexly zoned tapiolite crystals.

Columbite-group minerals and tapiolite generally conform to an ideal Fe-Mn and Ta-Nb substitution with a 1:2 ratio of the A-site to the B-site (Fig. 5.6E). Ideal substitution is shown by the (Mn, Fe) = 2(Ta, Nb) tie line in Figure 5.6E. Deviations from the ideal substitution are dominantly found in columbite-group minerals and tapiolite from greisen samples where there is a notable deficiency in the B-site cations, Ta and Nb, as these samples plot below the ideal substitution line (Fig. 5.6E). Columbite-group minerals in Li-pegmatites show a similar distinct depletion in the B-site cations, Ta and Nb, being Fe-Mn-enriched relative to Ta and Nb.

Compositionally, columbite-group minerals in most samples plot in a linear fashion from the ferrocolumbite field into the ferrotantalite field with increasing Ta# and little or no change in the Mn# in the columbite quadrilateral (Fig. 5.7A-C). Compositions then terminate against the tapiolite gap described in Černý et al. (1992b). The tapiolite gap is a compositional gap between the tetragonal tapiolite field and orthorhombic columbite-group minerals field (Fig. 5.7) where it is not uncommon for some data to plot on or near the boundary of the field. Some samples show that co-occurring tapiolite is present to give a complete trend: ferrocolumbite □ ferrotantalite □ ferrotantalite + tapiolite (Fig. 5.7C). As Ta# is an indication of fractionation, these samples that have co-occurring tapiolite are the most fractionated. Data points that plot in the tapiolite field are notably Fe-rich and co-occurring ferrotantalite and tapiolite show moderate gradient (1:1) lines linking the two Ta-Nb phases. Figure 5.7D shows that some samples have columbite-group minerals which appear to have a bimodal fractionation trend, with initial compositions clustering in the ferrocolumbite field and then proceeding both towards the ferrotantalite field with increasing Ta# and towards the manganocolumbite field with equal increases in Ta# and Mn#. Sample 4-9 (Table 5.1), Figure 5.7E, also possibly shows this bimodal trend. It is also notable in Figure 5.7D, Sample 12-1, that the columbite-group minerals of the garnet-tourmaline type pegmatite have the lowest Ta# in the dataset and show a distinct concomitant trend, starting in the ferrocolumbite field with equal increases in Ta# and Mn# into the manganocolumbite field. Other samples (Fig. 5.7E,F) show a scattering of data where no discernible trends are observed, with the exception of sample W-3 (Fig. 5.7F) that possibly evolves from the manganotantalite field toward the ferrotantalite field. It appears that data with the lowest Ta# in sample W-3 have the highest Mn#, subsequent data being more scattered at higher Ta# and lower Mn#.

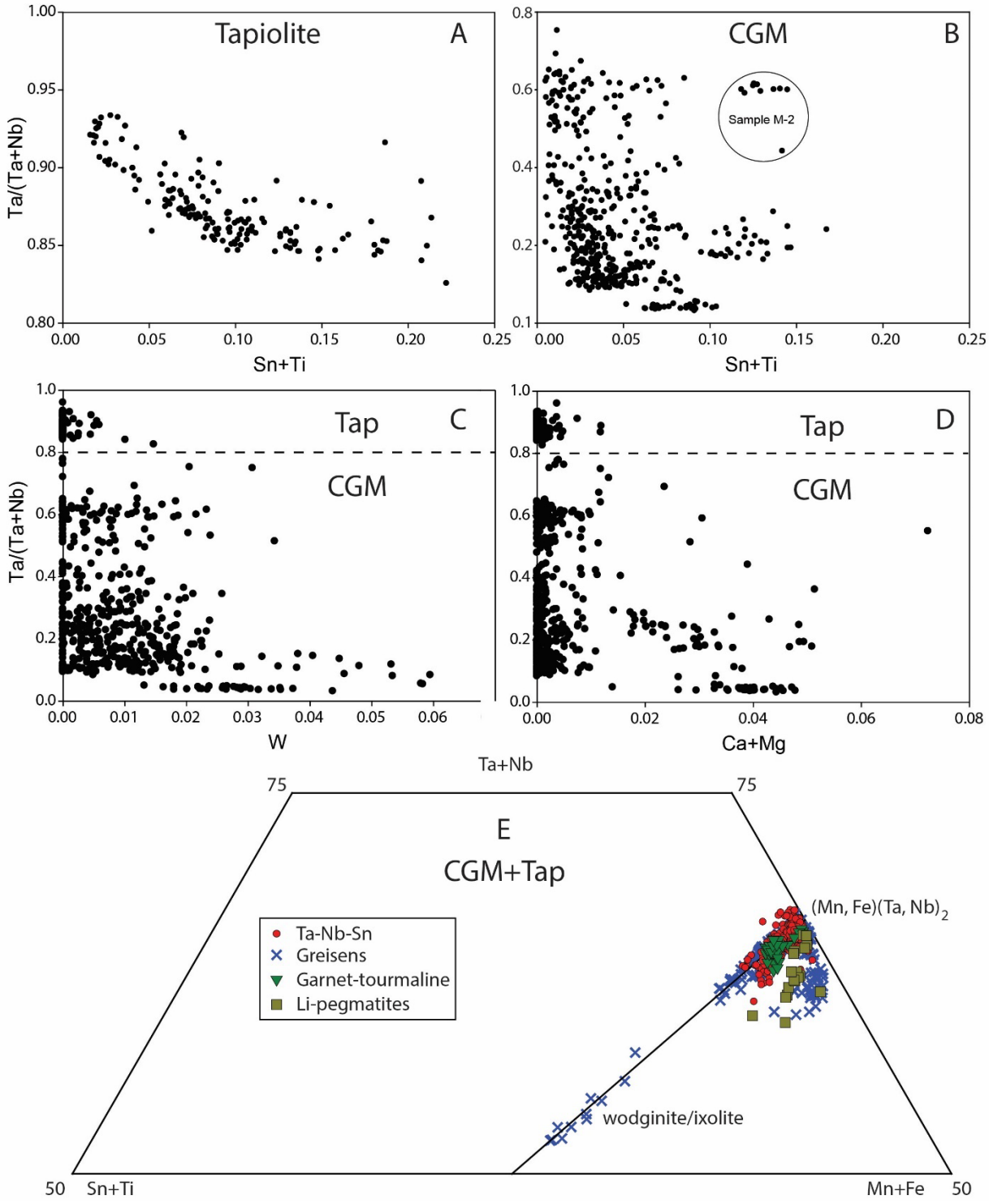


Figure 5.6: Compositional variation plots of columbite-group minerals and tapiolite (data are in a.p.f.u.; TAP = tapiolite; CGM = columbite-group minerals). (A) Sn and Ti values in tapiolite plotted against Ta# (Ta/(Ta+Nb)). (B) Sn and Ti values in columbite-group minerals plotted against Ta#. (C) W in both tapiolite and columbite-group minerals plotted against Ta#. (D) Ca and Mg in both tapiolite and columbite-group minerals plotted against Ta#. Each plot (A-D) groups elements of the same charge whereas tapiolite and columbite group minerals are separated by a dashed line in plots c and d. (E) Columbite-group minerals and tapiolite in a section of the (Sn+Ti) – (Mn+Fe) – (Ta+Nb) triangle. The diagonal line connecting to (Mn, Fe)(Ta, Nb)2 indicates ideal substitution whereby the ratio of (Mn, Fe) to (Ta, Nb), or A-site to B-site, is 1:2. Points falling below this line indicate B-site deficiency in the crystal structure of columbite-group minerals, tapiolite or cassiterite.

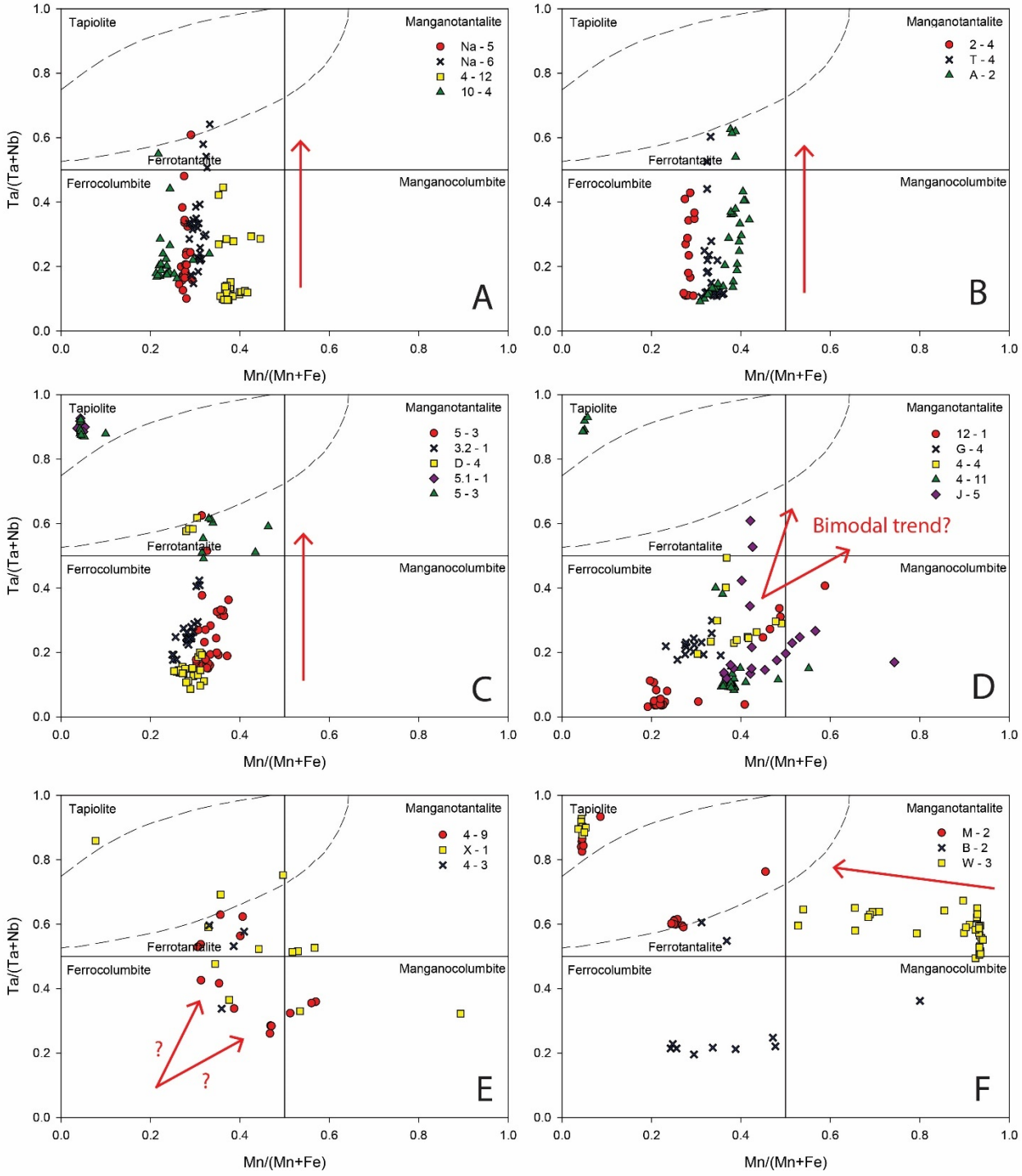


Figure 5.7: Columbite-group minerals and tapiolite compositions for individual samples in the columbite quadrilateral (Table 5.1). The samples are roughly grouped according to the trend they display which is shown by the red arrows in each plot. A-C) Typical trends subparallel to the Ta/(Ta+Nb) axis, defined by increasing Ta# with little variation in the Mn#. (D) Apparent bimodal fractionation trends in samples J-5, 4-4 and 4-11. Samples 12-1 shows a concomitant trend of equal increases in the Ta# and Mn# whereas sample G-4 clusters in the ferrocolumbite field with no discernible trend. (E,F) Columbite-group minerals and tapiolite that display scattered or uncharacteristic data. Sample 4-9 potentially shows a bimodal trend with missing data in the ferrocolumbite field (indicated by red arrows). Sample W-3 potentially shows a trend of decreasing Mn# with slight increases in the Ta# (indicated by the red arrow in f). Other data is scattered. The tapiolite immiscibility gap is shown in the figures as dashed lines in the ferrotantalite field (top left).

On a regional pegmatite belt scale when comparing data from all samples, columbite-group minerals show an overall trend in the columbite-group minerals quadrilateral subparallel to the Ta/(Ta+Nb) axis due to increasing Ta# with little change in the Mn# (Fig. 5.8). Columbite-group minerals and tapiolite from greisen samples display the highest Ta# in the dataset with most tapiolite occurring in greisenised samples (Fig. 5.8). Likewise, only greisens show compositions that plot in the manganotantalite field. Li-pegmatites also show high Ta# plotting well within the ferrotantalite and tapiolite field with only one datum plotting in the ferrocolumbite field. Nb-Ta-Sn type pegmatites show a wide variety of compositions, having intermediate Ta# and Mn# values compared to the other pegmatite types and altered zones.

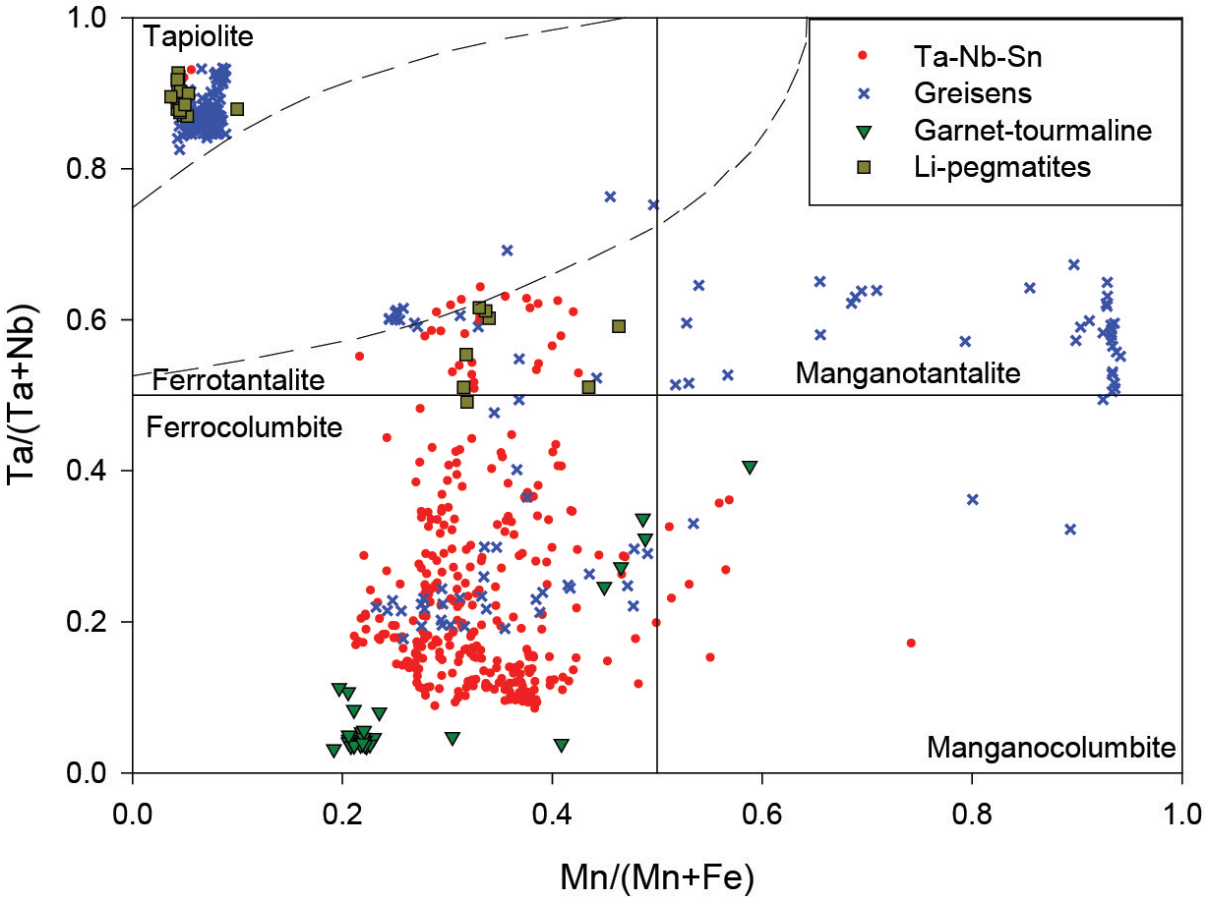


Figure 5.8: Combined compositional data of columbite-group minerals and tapiolite from all samples in the Cape Cross-Uis pegmatite belt. Samples are plotted on the basis of pegmatite group to which they belong (Table 5.1) and whether a sample is an altered greisenised zone (Blue crosses).

5.5.2 Cassiterite

5.5.2.1 Occurrence and internal structure

In the CUPB cassiterite has been observed in fewer pegmatites than columbite-group minerals, although it has a greater overall abundance in terms of tonnage when present. The Uis swarm hosts most of the cassiterite in the area, possibly reflecting the larger dimensions of the pegmatites in the swarm and the increased degree of greisenisation compared to other swarms (Fuchsloch et al., 2018*a*). Cassiterite generally occurs as black anhedral to subhedral grains ranging from rectangular 5x1 cm crystals to fine-grained 0.5–1mm grains in albitised zones. Rare euhedral, bipyramidal and sub-transparent crystals up to a size of 1.3 cm along the a-axis also occur. Local artisanal miners have also identified 'red tin' which has a red hue and rusty texture and occurs mostly as 1–2 mm equidimensional grains.

Microscopically cassiterite is generally homogeneous and rarely shows any zonation on BSE imagery (Fig. 5.4A). Cassiterite occasionally co-occurs in association with columbite-group minerals in unaltered magmatic assemblages either adjacent to or as individual crystals. In altered zones, columbite-group minerals are observed as epitaxial overgrowths around cassiterite crystals where the rims of the cassiterite show resorption textures (Fig. 5.4A). A feature in the Uis swarm is the occurrence of oscillatory-zoned, columbite-group mineral inclusions within cassiterite. Some inclusions show resorption textures but there is no indication of the columbite-group minerals having been derived from exsolution in cassiterite.

5.5.2.2 Cassiterite mineral chemistry

Cassiterite shows little to moderate variation in its composition, with most analyses showing almost pure SnO_2 (Table 5.3). Some homogenous grains with no associated columbite-group mineral inclusions exhibit elevated Ta_2O_5 contents of ~5 wt.% (Table 5.3; Sample Na-5 and J-5). Generally, it is the cassiterite from greisens that show slightly higher Ta_2O_5 contents between 1 and 3 wt.%. No distinguishable differences were observed between cassiterite from different pegmatite groups except for the absence of Ta_2O_5 in cassiterite from the Li-pegmatites. Although cassiterite typically contains 0.16–1.83 wt.% FeO, there is no specific variation between pegmatite groups. Nb_2O_5 values are generally < 0.5 wt.%, however, some samples show cassiterite with a Nb_2O_5 content > 2 wt.%. Mn is present in low concentrations along with Sc, U, W, Ca and Ti.

Table 5.3: Representative electron microprobe analyses of cassiterite from the Cape Cross-Uis pegmatite belt.

Sample #	5-3	Na-5	J-5	A-2	T-4	3-3	3.2-1	B-2	X-1	M-2	G-4	3.1-2
Peg-type	*Li-peg*	*Ta-Nb-Sn*	*Ta-Nb-Sn*	*Ta-Nb-Sn*	*Ta-Nb-Sn*	*Ta-Nb-Sn*	*Ta-Nb-Sn*	*Greisen*	*Greisen*	*Greisen*	*Greisen*	*Greisen*
SnO_2 wt.%	98,21	94,57	93,25	100,69	98,91	99,51	97,93	99,27	94,08	97,89	95,26	94,24
MgO	0,07	0,11	0,08	0,12	0,08	0,11	0,09	0,09	0,09	0,10	0,08	n.d.
Ta_2O_5	n.d.	4,18	5,75	0,34	0,18	0,85	1,74	0,26	2,66	1,15	n.d.	3,07
FeO	1,05	0,91	0,90	0,11	0,12	0,16	0,43	0,17	0,82	0,19	1,83	0,88
MnO	0,04	n.d.	0,08	0,02	0,01	0,02	0,01	n.d.	0,05	0,01	0,04	n.d.
Nb_2O_5	0,28	1,20	0,25	0,04	0,63	0,22	0,59	0,70	2,00	0,10	2,40	1,76
TiO_2	0,01	0,08	n.d.	0,13	0,03	0,07	0,26	0,16	0,09	0,25	0,30	0,07
Sc_2O_3	n.d.	n.d.	n.d.	n.d.	n.d.	n.d.	n.d.	n.d.	n.d.	n.d.	n.d.	n.d.
U_2O	n.d.	n.d.	n.d.	n.d.	n.d.	n.d.	n.d.	n.d.	n.d.	n.d.	n.d.	n.d.
CaO	n.d.	0,50	0,51	0,52	0,51	0,54	0,49	0,53	0,50	0,52	n.d.	n.d.
WO_3	n.d.	0,37	n.d.	n.d.	n.d.	n.d.	n.d.	n.d.	0,02	n.d.	n.d.	n.d.
Total	99,66	101,91	100,82	101,97	100,47	101,48	101,54	101,18	100,31	100,20	99,90	100,02
Sn a.p.f.u	2,949	2,777	2,787	2,952	2,938	2,933	2,880	2,924	2,791	2,920	2,820	2,816
Mg	0,008	0,012	0,009	0,013	0,009	0,013	0,010	0,010	0,011	0,011	0,009	n.d.
Ta	n.d.	0,084	0,117	0,007	0,004	0,017	0,035	0,005	0,054	0,023	n.d.	0,063
Fe	0,066	0,056	0,056	0,007	0,007	0,010	0,027	0,010	0,051	0,012	0,114	0,055
Mn	0,003	n.d.	0,005	0,001	0,001	0,001	0,001	n.d.	0,003	0,001	0,003	n.d.
Nb	0,010	0,040	0,008	0,001	0,021	0,007	0,020	0,024	0,067	0,003	0,081	0,060
Ti	0,001	0,004	n.d.	0,007	0,002	0,004	0,014	0,009	0,005	0,014	0,017	0,004
Sc	n.d.	n.d.	n.d.	n.d.	n.d.	n.d.	n.d.	n.d.	n.d.	n.d.	n.d.	n.d.
U	n.d.	n.d.	n.d.	n.d.	n.d.	n.d.	n.d.	n.d.	n.d.	n.d.	n.d.	n.d.
Ca	n.d.	0,039	0,041	0,041	0,041	0,043	0,039	0,042	0,040	0,042	n.d.	n.d.
W	n.d.	0,007	n.d.	n.d.	n.d.	n.d.	n.d.	n.d.	n.d.	n.d.	n.d.	n.d.
Total	3,036	3,019	3,024	3,029	3,023	3,027	3,024	3,024	3,022	3,026	3,042	2,997
Mn/(Mn+Fe)	0,037		0,086	0,130	0,077	0,099	0,019		0,055	0,041	0,022	
Ta/(Ta+Nb)		0,677	0,934	0,840	0,149	0,700	0,640	0,181	0,445	0,880		0,512

In a (Ta,Nb) – (Sn,Ti) – (Mn,Fe) plot, cassiterite compositions mostly show ideal compositional variations along a line defined by the substitution reaction $(Fe, Mn)^{2+} + 2(Ta, Nb)^{5+} = 3(Sn,Ti)^{4+}$ (Fig. 5.9A). This line indicates that the proportions of Fe-Mn and Ta-Nb conform to the ideal ratio of 1:2. However, cassiterite from Li-pegmatites plot below the ideal substitution line indicating $(Ta, Nb)^{5+}$ depletion with respect to $(Fe, Mn)^{2+}$ and show the lowest Ta#. Some cassiterite from greisen samples also plot below the ideal substitution line whereas none of the compositions plot significantly above it. Ta# of cassiterite in the dataset shows a wide variety of values whereas the Mn# is mostly below 0.2 (Fig. 5.9B). No specific trend is observed in a plot of Ta# vs. the Mn#, however, data with Ta# > 0.6 appear to show slightly higher Mn# values.

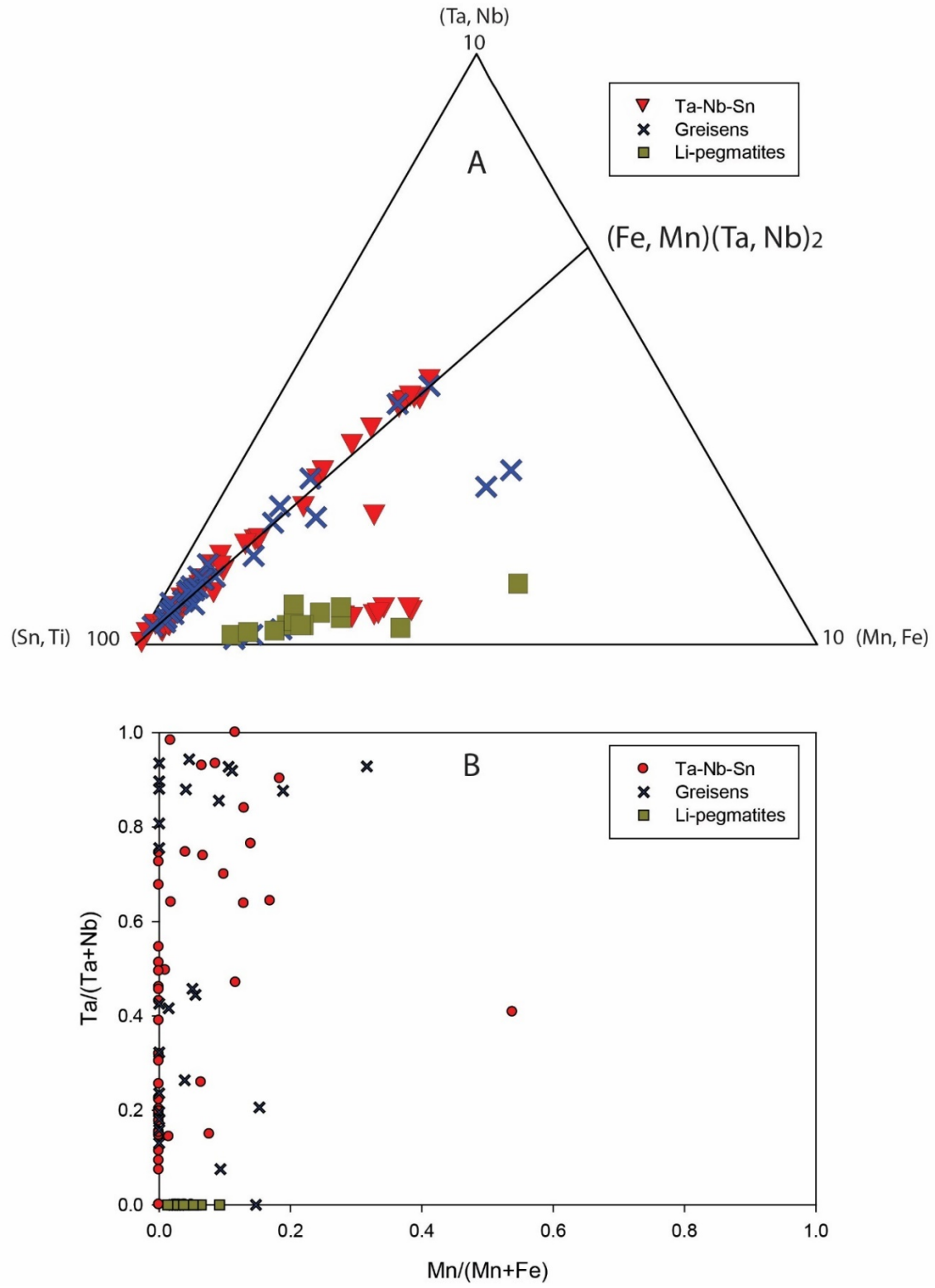


Figure 5.9: Chemical characteristics and trends in cassiterite from the Cape Cross-Uis pegmatite belt. (A) (Sn,Ti)-(Ta,Nb)-(Fe,Mn) triangular plot showing the solid solution with columbite-group minerals (ideally with rutile structured tapiolite). The line marked (Fe,Mn)(Ta,Nb)2 represents the ideal substitution. This graph is a zoomed in image of the bottom left portion of the triangular diagram where (Sn,Ti) = 100 % and (Ta,Nb) and (Mn,Fe) up to 10 %. (B) Cassiterite compositions plotted in the columbite quadrilateral.

5.6 Discussion

The approach we take in this study is to characterise three main factors that occur during the paragenesis of the pegmatites and subsequent Ta-Nb and Sn-oxides: (1) the minor element evolution in Ta-Nb-oxides, (2) the fractional crystallisation evolution and (3) the potential of a phase transition from a magmatic to an exsolved pegmatitic aqueous fluid.

5.6.1 Minor element evolution

The fractionation of Ta from Nb is well established in experimental work (Linnen and Keppler, 1997; Linnen, 1998) which found that in silicate melts, Ta-bearing phases are more soluble than their Nb-bearing counterparts (Ta# increases during fractionation). Minor element heterovalent substitution in Ta-Nb-oxides is greatest in the early stages of pegmatite crystallisation and decreases with fractionation into the late stages of crystallisation (Fig. 5.6A-D). Although similar trends have been recorded in the Varuträsk pegmatite, Sweden (Černý et al., 2004), an explanation of the phenomenon is not clear. Ercit et al. (1995) questioned whether this evolutionary compositional trend is crystal-chemical or geochemical in origin by comparing the minor element trend to the state of order in the crystal structure of columbite-group minerals. I.e. do the mechanisms of heterovalent substitution induce cation disorder, or do columbite-group minerals with high contents of minor elements form early in the crystallisation history of the pegmatite when disordered states are more stable, allowing higher levels of minor element substitution? A possible explanation, favouring the crystal-chemical origin, is that as other phases in the magma chamber began to stabilise, the minor elements favoured these newly stabilised minerals and therefore their abundances in columbite-group minerals and tapiolite decreased during fractionation. This hypothesis is important for Fe-Mn fractionation trends in columbite-group minerals as some authors suggest (e.g. Van Lichtervelde et al., 2007) that co-existing phases competing for Mn, also control the fractionation of Fe from Mn.

Tapiolite is considered to form at late stages in pegmatites (Černý et al., 1992b). This is supported by abundant tapiolite being primarily found in greisenised zones of the pegmatites of the CUPB (Fig. 5.8). Furthermore, and with the exception of some grains in sample 3.1-2, tapiolite exclusively has patchy zonation within pegmatites (Fig. 5.5). Co-occurring tapiolite and columbite group minerals generally represents a composition that plots within the tapiolite gap giving rise to

the pair of mineral phases, however, tapiolite shows much higher values of Sn and Ti at a low Ta# (Fig. 5.6A; Černý et al., 1992b). If the crystallisation sequence is considered to transfer from columbite-group minerals to columbite-group minerals and tapiolite, then there is an observed jump in the Sn and Ti contents in tapiolite compared to columbite-group minerals. Tapiolite has a tetragonal crystal structure and therefore a greater affinity for Sn and Ti which can account for the increase in concentration of these minor elements in tapiolite (e.g. Neiva, 1996). Tapiolite then repeats the same trend for Sn and Ti as seen in columbite-group minerals of decreasing minor element substitution with increasing Ta# and fractionation. The abundance of cassiterite within the greisenised zones suggests that cassiterite competed for Sn and Ti, which favoured cassiterite as the solubility of cassiterite decreased and cassiterite stabilised.

Tapiolite shows no change in concentration compared to columbite-group minerals when other minor elements, Ca, Mg and W are compared to Sn and Ti. This is difficult to account for, considering the limited research of partition coefficients of specific elements into the tapiolite crystal structure. In essence, tapiolite might have no affinity for these minor elements or perhaps they had already been depleted in the crystallising liquid at the late-stages of crystallisation. In addition, these elements may have had a low activity during this phase of crystallisation if tapiolite is considered to crystallise from an exsolved aqueous fluid phase that did not preferentially partition Ca, Mg and W. Aside from the Ca, Mg and W concentrations in tapiolite, we suggest that minor element trends in columbite-group minerals and tapiolite are governed by competing mineral phases.

5.6.2 Fractional crystallisation evolution of pegmatitic melts

Many authors have debated the controlling factors that lead to the fractionation of Fe from Mn or the lack of fractionation of Fe from Mn in Ta-Nb and Sn-oxides. For example, Mulja et al. (1996), Raimbault (1998), Van Lichtervelde et al. (2007) and Beurlen et al. (2008) suggest that co-existing phases competing with columbite-group minerals for Fe in the pegmatites deplete Fe in columbite-group minerals during fractionation leading to Mn-rich end members. Van Lichtervelde et al. (2007) elaborate on this and show late-stage Ta-Nb-oxides become progressively Fe-rich during fractionation and suggest that the natural fractionation progression of Ta-Nb-oxides is one of Fe-enrichment when competing mineral phases are absent. The depletion of Fe in columbite-group

minerals is typical of the lepidolite-type pegmatites and often precedes fractionation of Ta from Nb. Other authors (Černý, 1992b; Tindle and Breaks, 2000; Černý et al., 2004; Wise et al., 2012) suggest that an increased alkali-fluoride activity promotes the extreme Fe-Mn fractionation before the onset of Ta enrichment, instead of a competing mineral phase control.

It is difficult to add to this debate based on the current study since the dominant pegmatite fractionation trend in Ta-Nb- and Sn-oxides is controlled by increasing Ta# (Fig. 5.7, 5.8 and 5.9) where Ta is enriched relative to Nb and there is little fractionation between Fe and Mn, similar to pegmatites observed in Mulja et al. (1996), Tindle and Breaks (2000) and Beurlen et al. (2008). Essentially the pegmatites in the CUPB show both a lack of F-bearing phases and minerals that may compete for Mn, both of which may cause the observed fractionation trend. Evaluating the outliers that do not conform to the typical trend may provide some insight (Fig. 5.7D-F). It may be possible that sample W-3 (late-stage greisenised sample; Fig. 5.7F) follows a similar fractionation trend to the ones observed by Van Lichtervelde et al. (2007) in that Fe enrichment is the natural progression of fractionation in columbite-group minerals. The garnet-tourmaline type pegmatite also shows a concomitant fractionation trend in the CUPB (Fig. 5.7D) similar to that noted in the pegmatites of the Preissac-Lacorne batholith, Canada, by Mulja et al. (1996), where garnet occurrence in pegmatites is a controlling factor in Fe-Mn fractionation. This favours a co-existing mineral phase argument instead of the amount of alkali-fluoride activity. However, this trend might also be attributed to the garnet-tourmaline pegmatites having a slight NYF affinity (Fuchsloch et al., 2018*a*) and, although not measured, might potentially have higher abundances of F (Wise et al., 2012). Other bimodal trends and scattered data are more difficult to account for (Fig. 5.7D-F). Scattered data have been attributed to disequilibrium crystallisation in Ta-Nb- and Sn-oxides from other pegmatites (Splide and Shearer, 1992; London, 2008) and the changes in thickness of oscillatory-zones observed in columbite-group minerals and tapiolite (Fig. 5.4D, 5.5B,C) support disequilibrium crystallisation (Lahti, 1987). Bimodal fractionation trends may likewise be a consequence of disequilibrium or in situ crystallisation, however, to our knowledge, no other similar bimodal trends have been observed in previous literature. Local saturation in a boundary layer may be discredited as the cause of bimodal trends since the samples and pegmatites are homogenous and not mineralogically zoned (e.g. Gonzàlez et al., 2017). Perhaps these samples

reflect a period in the crystallisation history of the pegmatites where Mn-competing phases stabilised in the melt thus changing the trend of newly crystallised columbite-group minerals.

Minor element substitution trends in columbite-group minerals and tapiolite favours a co-existing mineral phase argument, if one agrees that minor element substitution in Ta-Nb-oxides induces mineral structural disorder, however, Ercit et al. (1995) stresses that a broader range of Ta-Nb-bearing rock types requires investigation. Whatever the ultimate explanation as to the controlling factors of Fe-Mn fractionation, the pegmatites of the CUPB have a beryl to spodumene Ta-Nb-oxide pegmatite-type signature (Černý, 1992b) and a typical Ta# increase during fractionation with little change in the Mn#.

5.6.3 Magmatic vs exsolved aqueous fluid crystallisation

There is a general consensus amongst authors that patchy zonation in columbite-group minerals and tapiolite (Fig. 5.4, 5.5) is the result of re-equilibration of columbite-group minerals and tapiolite with later fluids, whether they were magmatic (Tindle and Breaks, 2000; Van Lichtervelde et al., 2007, 2008), metamorphic (Černý et al., 1992a) or exsolved aqueous fluid (Novák and Černý, 1998; Zhang et al., 2004; Alfonso and Melgarejo, 2008; Ashworth, 2013; Ballourad et al., 2016). Similarly, oscillatory- and progressive-zoning are indicative of a magmatic regime (see discussions in Lahti, 1987 and Van Lichtervelde et al., 2007).

The underlying principle surrounding the debate is not if a pegmatitic magma will exsolve an aqueous fluid but instead is directed at the partition coefficients of Ta and Nb into the aqueous fluid. Many authors have shown that the presence of an aqueous fluid being exsolved from the pegmatitic magma in the late-stages of petrogenesis is likely (London, 2008). For example, the muscovite chemistry of greisens in the Tanco pegmatite, Canada, show characteristics of crystallisation from an aqueous fluid (Van Lichtervelde et al., 2008). In essence, are Ta-Nb-bearing phases crystallised from a highly fractioned magma (Van Lichtervelde et al., 2008) with or without a co-existing aqueous fluid or are they crystallised directly from the aqueous fluid itself? In the case of aqueous fluid crystallisation, Ta and Nb preferentially partition into the aqueous fluid, causing saturation of Ta and Nb and subsequently crystallising Ta-Nb-bearing phases (Alfonso and Melgarejo, 2008). In either case, the authors on both sides of the debate present evidence for

and against crystallisation from a magmatic phase. For example, Van Lichtervelde et al. (2008) suggests, based on the experimental evidence of Chevychelov et al. (2005), that a late, rare-metal and flux-enriched magma may produce metasomatic features such as patchy zonation whereas other authors (Zhang et al., 2004; Alfonso and Melgarejo, 2008) use patchy zonation as evidence of crystallisation from an aqueous fluid since Ta-Nb-oxides are synchronous with greisenisation and other late-stage fluid alteration products.

Chevychelov et al. (2005) showed that the partition coefficients of Ta and Nb into a co-existing aqueous fluid were very low (0.002–0.080 and 0.005–0.080 respectively). Van Lichtervelde et al. (2007, 2008) argue based on this study that an aqueous fluid could not transport significant quantities of Ta and Nb and subsequently crystallise Ta-Nb-bearing phases during alteration of K-feldspars to muscovite in greisens. However, the experimental study of Chevychelov et al. (2005) was based on fluoride aqueous fluids only and at temperatures exceeding 900 °C. More likely pegmatitic crystallisation temperatures for the CUPB, shown by Ashworth (2013), are between 450 °C and 550 °C with hypersaline and aqueo-carbonic fluid compositions. In addition, the experimental study shows that decreasing temperatures cause significant increases in the partition coefficient of Ta in an aqueous fluid whereas the Nb partition coefficient shows negligible changes with decreasing temperatures. Perhaps at pegmatitic conditions, the Ta partition coefficients for an aqueous fluid may be higher than the Nb partition coefficient.

A suitable example from this research is the Ta# variation between patchy zonation and oscillatory zonation. Figure 5.5 shows that patchy zonation has lower Nb contents than Ta compared to oscillatory zonation indicating patchy zonation has a higher Ta#. If the partition coefficient of Ta into an aqueous fluid increases with decreasing temperature and the Nb partition coefficient remains relatively unchanged, it can therefore be inferred that patchy zonation, at pegmatitic temperatures, has a higher Ta# if crystallised from an aqueous fluid. However, Chevychelov et al. (2005) only extrapolate their data for Ta to lower temperatures of 600°C and do not extrapolate data for Nb. Since this is only an extrapolation and in light of the limited experimental research, only hypothetical situations may be discussed. For example, Van Lichtervelde et al. (2007) found that Ta# in both patchy and co-existing oscillatory/progressive zonation is roughly constant for

both types of zonation, therefore, since Nb and Ta have different partition coefficients (Chevychelov et al., 2005) for an aqueous fluid phase, crystallised from a magmatic phase.

Some of the data for columbite-group minerals, tapiolite and cassiterite show non-stoichiometric values (Fig. 5.6E, 5.9A) in terms of the ratio of A-site and B-site cations. It is notable that these minerals occur ubiquitously, expect for sample 5-3, in greisens and are depleted in Ta and Nb (B-site) relative to Fe and Mn (A-site). As Ercit et al. (1995) points out, this may be geochemically or crystal-chemically controlled. The stoichiometry may be controlled by the state of order of the crystals, being different in the early- and late-stages of Ta-Nb-Sn oxide crystallisation. Another hypothesis is that the Ta and Nb in magmatically crystallised minerals are remobilised preferentially over Fe and Mn during the greisenisation process by either a highly differentiated magma in the late-stages of crystallisation or an exsolved pegmatitic hydrothermal fluid. This would account for Ta-Nb-Sn oxides in greisens having a B-site deficiency. However, which fluid that may cause remobilisation is still debatable and comes down to the understudied partition coefficients of these elements at pegmatitic conditions.

The characteristics of zonation and associated minerals is important when considering their co-crystallising nature. Minor elements show that cassiterite competes with Ta-Nb-bearing phases for Sn and Ti (Fig. 5.6A). Cassiterite is known to preferentially crystallise from an aqueous phase with partition coefficients of Sn into an aqueous fluid being high, examples being cassiterite-bearing quartz veins (e.g. Kovalenko et al., 1986). Cassiterite, tapiolite and columbite-group minerals show an intimate mineralogical relationship, specifically in synchronous alteration zones such as greisens (Fig. 5.4A). It would therefore be plausible that the crystallising medium of cassiterite is concomitant to the fluid or magma crystallising Ta-Nb-bearing phases. Since abundant cassiterite is suggested to crystallise from an aqueous fluid specifically in greisen zones (Fuchsloch et al., 2018*a*), it would be incongruent for the Ta-Nb-bearing phases to be synchronously crystallising from another phase such as a highly fractionated magma simultaneously.

Other evidence that would suggest that Ta and Nb preferentially partition into an aqueous fluid phase is the presence of high concentrations of Ta and Nb in metasomatic, tourmalinised host rock schist contact zones in pegmatites. Fuchsloch (2018*a*) and Fuchsloch et al. (2018*a*) report data of

host rock schists in contact with pegmatites, that show a high degree of tourmalinisation and metasomatism, which have significantly elevated values of Sn, Ta, and Nb (Fig. 5.10). Out of six metasomatic contact schists, five are above that of general host rock schists that show no metasomatic features and occur some distance away from pegmatites. Furthermore, the increases in the Ta concentrations of the metasomatic contacts show a correlation with increases in Sn and Nb indicating these elements are co-genetic with Ta (Fig. 5.10). Only one metasomatic schist showed lower Sn concentrations coupled with high Ta concentrations. In one case, the Ta content of the metasomatic schist is two orders or magnitude higher than schists which do not show metasomatic features (250 ppm Ta compared to 1-2 ppm respectively). This metasomatic schist sample is so enriched in Ta it is comparable to economically mineralised pegmatites.

If the physical mobility of the crystallising fluid, magmatic or aqueous, is considered, it would be more reasonable for an aqueous fluid to transport these elements and enrich country rock contacts. This is particularly evident in zoned pegmatite bodies which crystallise inwards, essentially trapping the highly fractionated magma in the late-stages of petrogenesis within itself. An aqueous fluid is likely to percolate through to country rocks which London (2008) suggests is the cause of massive tourmalinisation of country rocks since these fluids also carry B.

In summary, until repeatable results can be obtained on the partition coefficients of Ta and Nb in various aqueous fluids at pegmatitic conditions, no factual hypothesis may be derived with respect to crystallisation of Ta-Nb-bearing phases in the late-stages of pegmatitic petrogenesis. Although some studies have begun to tackle this problem (e.g. Smirnov et al., 2012), these studies did not measure the Ta contents of the aqueous fluid and the Ta-bearing experiments did not reach equilibrium. Moreover, country rock contacts were not a detailed focus of Fuchsloch (2018*a*) and therefore the dataset is limited to few samples which have not been studied in detail, for example, which minerals contain the Ta, Nb and Sn in metasomatised country rocks. A detailed investigation should be carried out on these country rocks in future which should involve a systematic sampling programme, whole-rock geochemistry, mineral chemistry and petrography. From an initial perspective, the Ta, Nb and Sn contents of country rock contacts and the intimate relationship between cassiterite, columbite-group minerals and tapiolite in greisen zones in pegmatites of the CUPB is more consistent with crystallisation from an aqueous fluid during greisenisation.

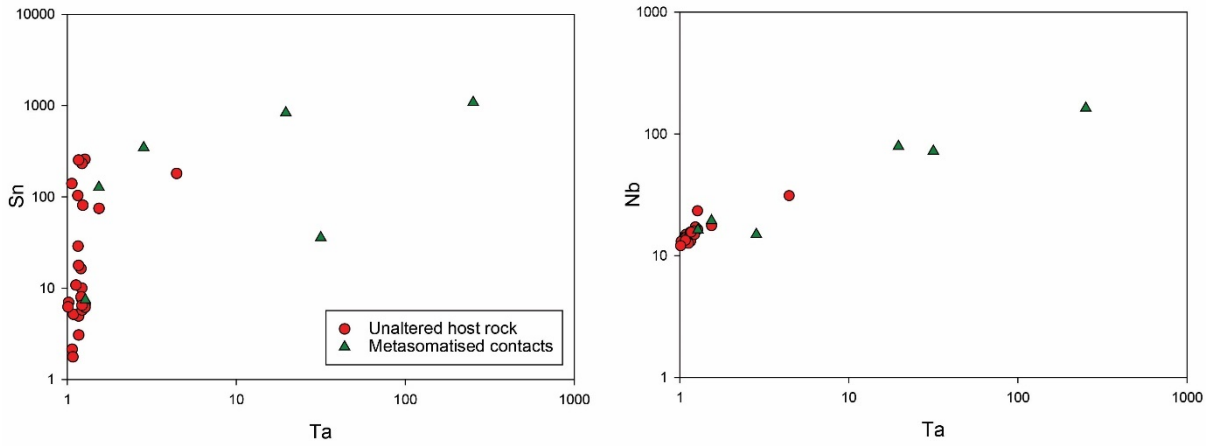


Figure 5.10: Country rock whole-rock data showing the Ta plotted against Sn and Nb in the right and left graphs respectively. The rock types include general host rocks which show no alteration and occur at variable distances to pegmatites and metasomatised, tourmalinised host rock contacts with pegmatites. Plots are given in logarithmic scales due to orders of magnitude differences between the data.

5.6.4 Regional aspects

Fuchsloch et al. (2018*a*) showed that the different pegmatite types in the CUPB are not only different in terms of mineralogy and host-rock but also have different fractionation signatures and degrees of fractionation. The garnet-tourmaline pegmatites show primitive fractionation signatures whereas the Nb-Ta-Sn type show intermediate fractionation signatures while the Li-pegmatites show evolved fractionation signatures. The authors showed that the spatial distribution of the different pegmatite types is random rather than displaying the regional zonation patterns observed in other belts by Černý (1989). Fuchsloch et al. (2018*a*) attributed this random distribution as evidence that the pegmatites are not related to the granites in the classical parent-daughter type relationship. When comparing the location of the pegmatites studied relative to the granites (Fig. 5.2) and their individual Ta-Nb and Sn-oxide fractionation patterns (Fig. 5.7) there is a similar random distribution of pegmatites with varying degrees of fractionation. Figure 5.11 displays this character numerically in terms of the average Ta# in each pegmatite, where columbite-group minerals were analyses, which corresponds to the level of fractionation. Although some bias is expected for pegmatites where only greisen samples contained columbite-group minerals, the overall homogeneity of the pegmatites is well represented by the average Ta#. In all cases, no spatial relationship to fractionation level in terms of Ta# is observed, especially with regards to distance from granite bodies (Figure 5.11). This supports that argument that the pegmatites in the CUPB are not related to the granites in the typical parent-daughter scenario.

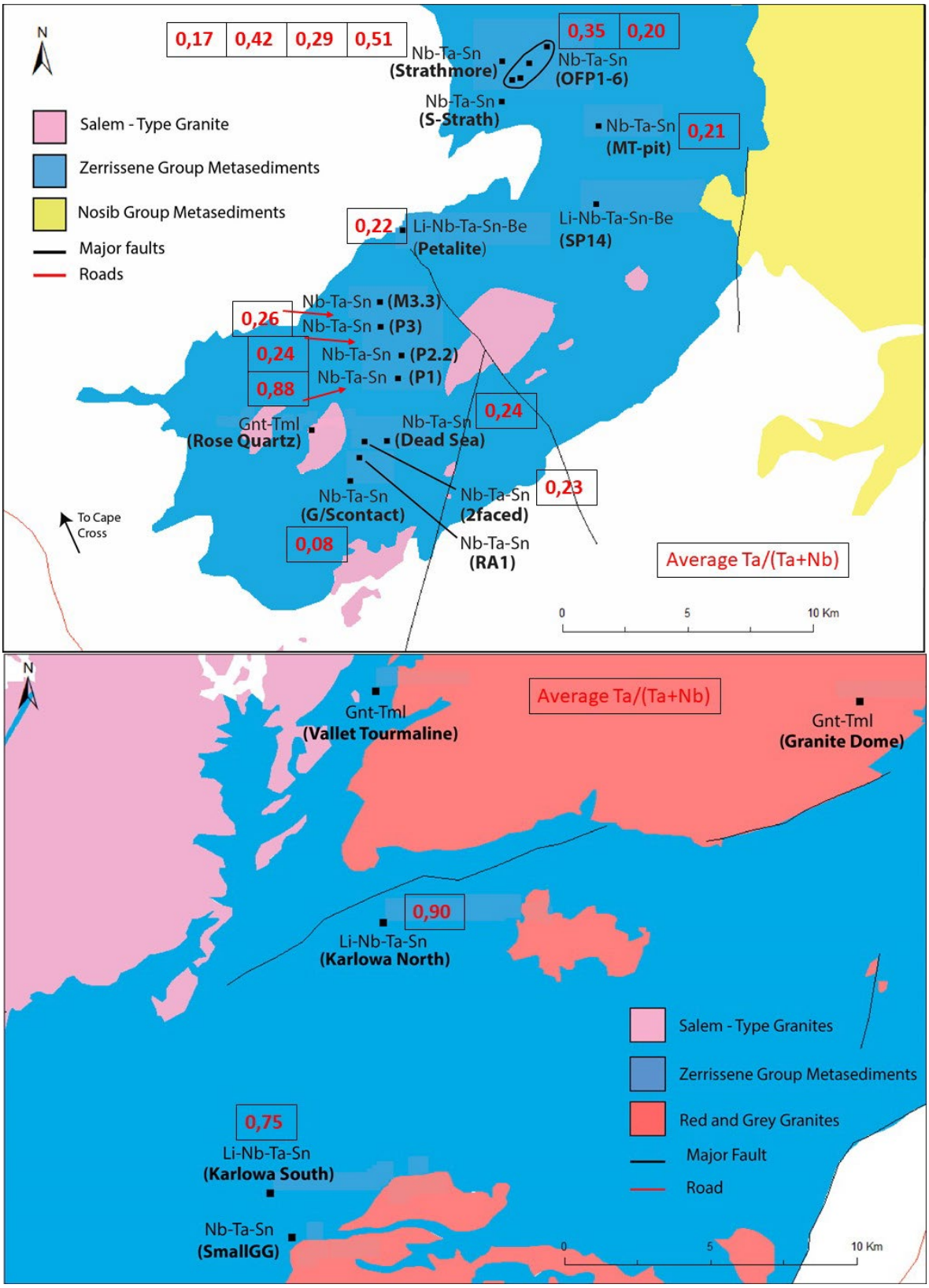


Figure 5.11: Geological maps of the three swarms of the Cape-Cross Uis pegmatite belt showing the average Ta# (Ta/Ta+Nb) of the pegmatites which contained columbite-group minerals. Top: Strathmore Swarm; bottom: Karlowa Swarm. Below (Figure 5.11 cont.): Uis swarm.

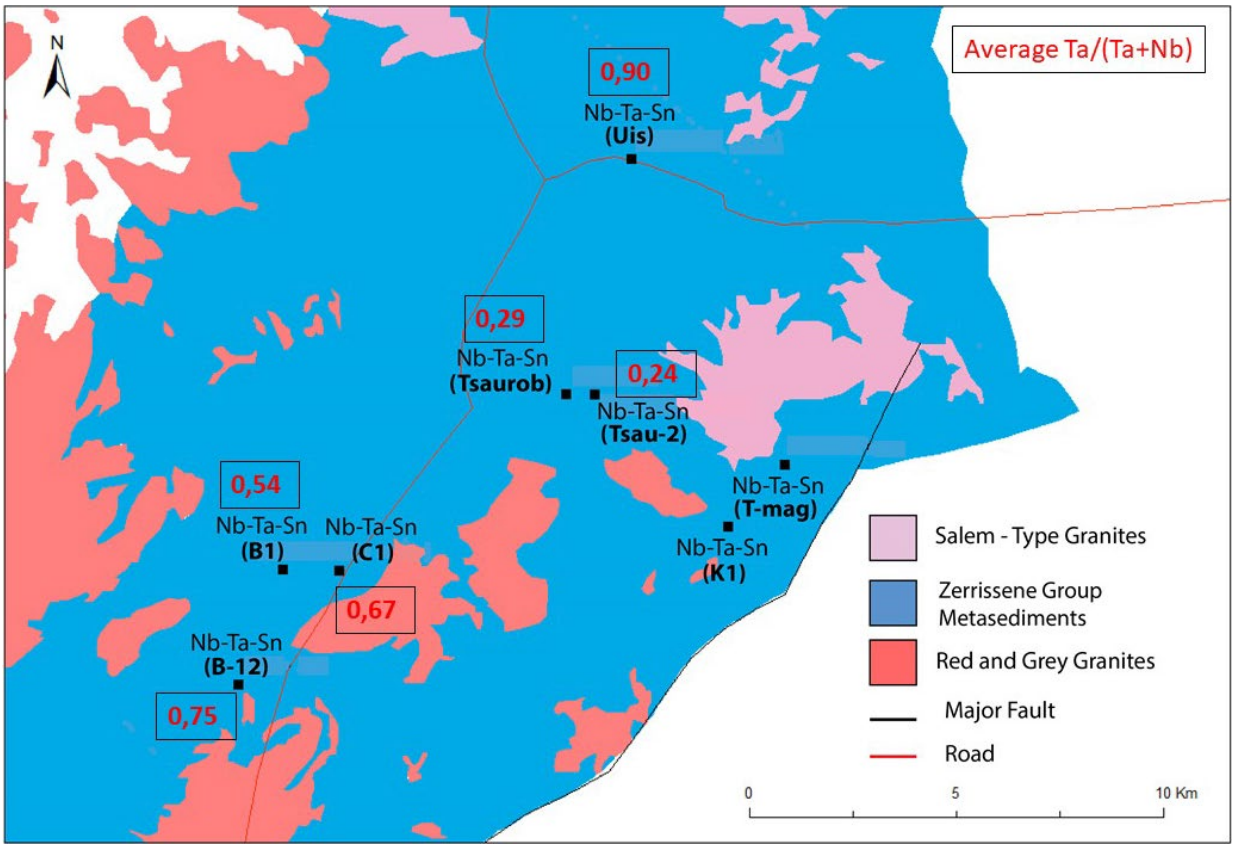


Figure 5.11: Cont. Uis Swarm.

Melcher et al. (2015) suggested that columbite-group minerals in the Uis pegmatites show concomitant fractionation trends in the columbite quadrilateral based on two of the pegmatites studied in the CUPB. Contrary to this finding, we suggest that the dominant fractionation trend in the belt is subparallel to the Ta/(Ta+Nb) axis: increasing Ta# with little change in the Mn# (Fig. 5.8). This trend is typical of beryl-type pegmatites and similar to the Karibib pegmatites studied in Melcher et al. (2015). The other pegmatite belts of the Damara Belt are not studied in detail in terms of Ta-Nb oxides, however, Melcher et al. (2015), while building an African scale database, showed that most Ta-Nb oxides are Mn-rich and have typical lepidolite pegmatite-type fractionation patterns (e.g. Rubicon, Helicon, Mon Repos, Klein Rössing). The variation in Ta-Nb-oxide composition in the Damara Belt may be due to the abundance of fluorine in other pegmatite belts, leading to Mn-enrichment (Wise et al. 2012). An interesting case is that of the columbite-group minerals fractionation trend in garnet-tourmaline pegmatites, being the only pegmatite type that shows concomitant fractionation, where significant increases in the Mn# occur. Fuchsloch et al. (2018*a*) found that garnet-tourmaline type pegmatites have significantly higher

abundances of REE compared to other pegmatite types within the CUPB. The authors suggested, that the garnet-tourmaline type pegmatites may have a slight NYF pegmatite family affinity and perhaps, although not measured, contain a higher abundance of F compared to other pegmatite types and therefore it may be the cause of Mn-enrichment in columbite-group minerals from these pegmatites. Although Melcher et al. (2015) disagree and suggest that there is little difference between the fractionation trends of NYF- and LCT-type pegmatites in Ta-Nb-oxides, future detailed studies of coexisting NYF and LCT pegmatites in the same orogenic belt, such as the Damara Belt, might provide some insight into the matter.

5.7 Conclusions

Columbite-group minerals and tapiolite fractionation trends, consistent with beryl to spodumene type rare-element pegmatites, are dominantly controlled by increasing Ta# with little change in the Mn# resulting in a crystallisation sequence of ferrocolumbite - ferrotantalite - tapiolite. Tapiolite is generally a secondary mineral phase as indicated by its patchy zonation texture. The decrease in minor element substitution with increasing Ta# in columbite-group minerals and tapiolite, suggests that as new phases began to crystallise in the magma chamber, they competed with columbite-group minerals and tapiolite for these minor elements, and thus their abundances decreased during crystallisation. Unusual bimodal columbite-group mineral fractionation trends and scattered columbite-group minerals data for specific samples were likely due to disequilibrium crystallisation which is supported by textural evidence such as changes in the thickness of oscillatory zones in oscillatory-zoned crystals.

Aqueous fluid vs. highly fractionated magmatic crystallisation of Ta-Nb-Sn oxides has been the subject of appreciable debate. Some authors would argue, based on experimental evidence, that Ta and Nb do not partition into an exsolved pegmatitic aqueous fluid during the late-stages of pegmatitic evolution. However, experimental studies are limited and mostly not at pegmatitic conditions (low temperatures of crystallisation) with varying fluid compositions. Based on significantly elevated Ta contents in metasomatised country rocks in contact with pegmatites, compared to low values in unaltered host rocks, we suggest that Ta may have partitioned into an aqueous fluid phase and had a significant effect on Ta-Nb-mineralisation along with Sn-mineralisation. Ultimately without more experimental evidence, only proxy evidence may be used,

and we suggest that future studies on the partition coefficients of Ta into various aqueous fluids at pegmatitic compositions be conducted. Moreover, a more detailed investigation should be carried out on the Cape Cross-Uis host rocks as the current data is limited.

Fractionation levels in columbite-group minerals, tapiolite and cassiterite from specific pegmatites show an irregular spatial distribution relative to granites in the CUPB. This supports the hypothesis of Fuchsloch et al. (2018*a*) that pegmatites were most likely to have been produced from anatexis. If a parent-daughter relationship existed between pegmatites and granites, a distinct zonation pattern surrounding the granitic bodies should be present, with the pegmatites furthest from granites showing the most evolved columbite-group mineral compositions.

5.8 Acknowledgements

We thank Deon Van Niekerk for the use and assistance on the Electron Microprobe at Rhodes University (Partially funded by NRF national Equipment Program grant UID 74464). John Spratt was instrumental in this study, confirming early cassiterite results and analysing individual tapiolite crystals at the London Natural History Museum. We are grateful to the technical team at the University of the Witwatersrand who provided many tireless hours aiding and advising in the separation of accessory minerals. The funding provided by the CIMERA research centre was instrumental to this study, without whom, the project would not have been possible.

Chapter 6: The mineral chemistry of tourmaline from pegmatites of the Cape Cross-Uis pegmatite belt, Namibia: implications for source, contamination and pegmatite fractionation.

Warrick C. Fuchsloch, Judith A. Kinnaird, Paul A.M. Nex, Deon Van Niekerk

Submitted to *Mineral Magazine* (May 2018)

Keywords: Tourmaline mineral chemistry, pegmatites, Damara Orogen, Namibia, Pegmatite source, Pegmatite contamination

6.1 Abstract

Tourmaline is generally an abundant phase in the pegmatites of the Damara Orogen, Namibia; however, studies of its chemical compositions are sparse. This study presents the first mineral chemistry data on tourmaline from the Cape Cross-Uis pegmatite belt and Central Tin Belt. The pegmatites can be separated into four types: i) metasediment-hosted Ta-Nb-Sn mineralised, unzoned pegmatites; ii) Li-bearing, zoned or unzoned complex pegmatites; iii) intragranitic garnet- and tourmaline-bearing pegmatites; iv) Ta-Nb-Sn mineralised Nainais pegmatites of the Central Tin Belt. Tourmaline occurs in three morphologies; the occurrence of these are not correlated with pegmatite-type and they show no significant compositional variation. Mineral zoning is rare, but when present records an increase in fractionation from core to rim with a concurrent change in colour from black to green. Comparison of the compositional variations in tourmaline from different pegmatite types within the study area show two dominant trends: i) Mg-rich [dravite-schorl-foitite], and ii) Li, Mn, Al-bearing [elbaite]. The first trend reflects the evolution of an unusually Mg-rich (Mg# > 0.7) composition [dravite] towards a progressively Mg-depleted composition [schorl then foitite]. The second trend reflects the subsequent evolution of the first trend towards increasingly Li-, Mn- and Al-rich elbaitic compositions. The dominant substitution vectors for this evolution are: $FeMg_{-1}$, $Al\square(NaMg)_{-1}$, and Fe_3Ti_{-2} and then $LiAlMnFe_{-3}$, $AlO(FeOH)_{-1}$, and $NaF(\square OH)_{-1}$. Because tourmaline from intragranitic and metasediment-hosted pegmatites are compositionally indistinct from each other, we suggest that fractionation, as opposed to contamination from wall rocks, was the dominant process that drove the crystal-chemical substitution. The Mg-enriched end-members of tourmaline represent a comparatively primitive magma, unusual for pegmatitic tourmaline, that was derived via low volume partial

melting. If pegmatites were the daughter magmas of granites, initial ferromagnesian components would have already been consumed by initial granitic fractionation, and thus pegmatites resulting from granites would be depleted in ferromagnesian elements and reflected in the tourmaline compositions of subsequent pegmatites.

6.2 Introduction

Tourmaline is common species in pegmatites, is an excellent recorder of the chemical and physical conditions from which it crystallised and has the nature of preserving this information over significant time spans in geological terms (Henry and Dutrow, 1996; London et al., 1996; Slack, 1996). Likewise, tourmaline shows negligible intracrystalline diffusion and the use of its chemical composition allows for the fingerprinting of various igneous magmas (London, 2008; Novák and Škoda, 2011; Marks et al., 2013; Büttner et al., 2016). Tourmaline has been used widely as a fractionation indicator in pegmatites and has been shown to be sensitive to contamination processes, changes in fO_2 and the activity of certain elements in the melt (Jolliff et al., 1986; Federico *et* al., 1998; Keller, 1999; Tindle et al., 2002; Trumbull et al., 2008). Tourmaline has also been shown to indicate the activity of boron in the melt which has an indirect, but important, effect on the mineralisation of Ta, Nb and Sn from late-stage pegmatitic fluids (e.g. Manning, 1981; London, 1995; London et al., 1996).

Numerous rare-element pegmatites are hosted by the Damara Orogen, Namibia, and provide an excellent ground for new research since many of them are poorly understood and few previous studies have been done (e.g. Ashworth, 2013). Pegmatites of the Cape Cross-Uis pegmatite belt (CUPB), also known as the Northern Tin Belt, are poorly studied and only recently are new detailed studies beginning to emerge (e.g. Fuchsloch et al., 2018*a,b*). The CUPB is located in western portion of central Namibia and extends from Cape Cross to Uis with an impressive length of 120 km (Fig. 6.1). To the southeast of Uis, several pegmatites occur in the Nainais area, part of the Central Tin Belt, and were studied for comparison to the CUPB. Fuchsloch et al. (2018*a*) have detailed the characteristics and whole-rock geochemistry of these pegmatites while Fuchsloch et al. (2018*b*) have reported on the mineral chemistry of the Ta-Nb-Sn oxides. The pegmatites widely vary in their characteristics: they occur from thin veins to impressive 50 m in width lensoidal

bodies, are dominantly unzoned, barren to rare-element (Ta-Nb-Sn-Li-Be) mineralised and show an abundance of tourmaline varieties.

Despite tourmaline being a well understood and vastly studied mineral in pegmatites, there is no compositional data for tourmaline from pegmatites in the CUPB and central tin belt. This paper presents the first study of tourmaline from the pegmatites of the CUPB and aims to characterise the different species and substitution mechanisms involved that equate to the variety of compositions observed. Processes such as fractionation and contamination are then assessed using the tourmaline data on a belt wide scale with comparison to the Nainais pegmatites. Little acknowledgement has been paid to the ferromagnesian components of tourmaline and what they might represent in terms of a pegmatite source, and therefore we evaluate tourmaline in terms of a potential source indicator for pegmatites as a whole.

6.3 Geological background

6.3.1 The Damara Orogen

The NE trending inland branch of the Damara Orogen, Namibia, extends from Swakopmund near the Atlantic coast towards Botswana and is host to several rare-element pegmatite belts (Richards, 1986; Keller, 1999). This Pan-African age orogenic belt showcases a typical 'Wilson Cycle' which was active from approximately 750 to 500 Ma (Martin and Porada, 1977; Hoffman et al., 1996; Prave, 1996; Grey et al., 2006; Milani et al., 2015). The depositional (Stanistreet et al., 1991; Miller, 1992), metamorphic (Trompette, 1997; Will et al., 2009), structural (Coward, 1983; Frimmel et al., 2011) and igneous (McDermott, 1986; Tack et al., 2002; Longridge, 2012) history of the Damara Orogen is summarised well in Miller (2008). During the syn- to post- tectonic phases of the Damara Orogen, voluminous granodioritic, granitic and pegmatitic magma was produced, which gave rise to the igneous rocks we see in the orogen today (Kinnaird and Nex, 2007; Longridge, 2012; Ashworth, 2013). The Damara Orogen is divided into tectonostratigraphic zones (Miller, 2008) which are bound by major faults and lineaments. The CUPB is situated within the Northern Zone and is bound and separated by the Autseib Fault from the Northern Central Zone (See Fuchsloch et al., 2018*a*,*b*). The Nainais pegmatites of the Central Tin Belt occur in the Northern Central Zone, southeast of the Autseib Fault.

6.3.2 Local geology and background research

The pegmatites of the CUPB are either metasediment-hosted, intruding biotite schists ± retrogressed cordierite porphyroblasts of the Amis River Formation (Fig. 6.1; Zerrissene Group) or intragranitic, intruding Salem-type and Red and Grey Granites (Fig. 6.1; Swart 1992). Occurrences of the Nainais pegmatites are restricted to metasedimentary units of similar composition and being biotite schists with retrogressed porphyroblasts of cordierite known as Knotenschiefer. Although these metasediments are characterised by multiple phases of deformation and metamorphism (Goscombe et al., 2004), the pegmatites of both the CUPB and Central Tin Belt show negligible deformational features and Fuchsloch et al. (2018*a*) shows that they are dominantly post-orogenic and take advantage of the structural weaknesses in the crust upon intrusion.

The CUPB is separated into Strathmore, Karlowa and Uis pegmatite swarms whereas the Nainais pegmatites are from a discreet area within the Central Tin Belt (Fig. 6.1; see caption). Pegmatites have a granitic composition being composed dominantly of quartz, feldspars, and muscovite with an assortment of minor phases such as tourmaline, apatite, Ta-Nb-Sn oxides, magnetite, ilmenite, petalite, spodumene, zircon and monazite (Fuchsloch et al., 2018*a*,*b*). Fuchsloch et al. (2018*a*) tentatively used the classification scheme of Černý and Ercit (2005) to show that the pegmatites are of LCT-type, however, they further sub-divided the pegmatites into 3 separate groups unique to the CUPB: (1; Ta-Nb-Sn) The most commonly occurring, metasediment-hosted, pegmatite type in the belt known as the barren to Ta-Nb-Sn mineralised, unzoned pegmatites, (2; Li-bearing) the rare, metasediment-hosted, zoned to unzoned Li-mineralised, spodumene or petalite pegmatites and (3; Gnt-Tml) the intragranitic, ubiquitously tourmaline- and garnet-bearing, occasionally crudely zoned pegmatites. The pegmatite types are distinguished by whole-rock geochemical data and geological characteristics and Fuchsloch et al. (2018*a*) found no significant differences between the Ta-Nb-Sn type and the Nainais pegmatites, however, data presented here are the first to show differences by comparison with regards to tourmaline compositions. Table 6.1 summarises each sample and assigns each to a pegmatite type.

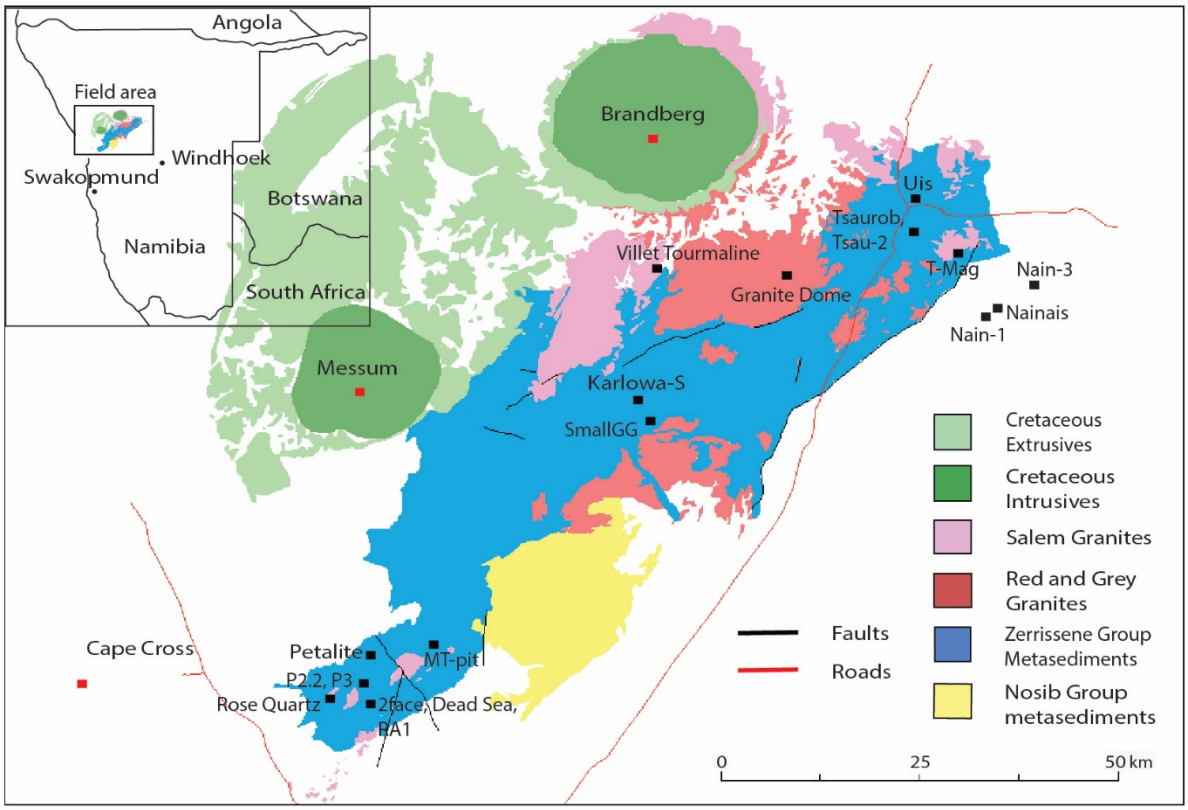


Figure 6.1: Geological map of the Cape Cross – Uis pegmatite belt, Namibia based on the localities bearing tourmaline (modified after Fuchsloch et al., 2018*a*). Pegmatite localities are shown by the black squares. Pegmatites in the NE quadrant, from Villet Tourmaline to T-Mag are situated in the Uis swarm. Karlowa-S and Small-GG occur in the Karlowa swarm and all the pegmatite localities in the SW quadrant are situated in the Strathmore Swarm. Nain-1, -2 and Nainais are located SE of the Autseib Fault in the Central Tin Belt.

The Ta, Nb and specifically Sn mineralisation has been studied in the CUPB (Richards, 1989; Wagener, 1989; Diehl; 1993; Singh; 2007; Fuchsloch et al., 2018*a,b*) and earlier authors suggested that tin was sourced from country rocks, being remobilised by late-stage pegmatitic fluids or incorporated into pegmatitic melt by the direct assimilation of host-rock. Fuchsloch et al. (2018*a*), however, disagree, and show using whole-rock geochemical data and evidence from the variety of greisen morphologies that mineralisation was likely in situ and that fractionation was the key process in which elements such as Ta, Nb, Sn, and Cs were concentrated within the magma. Fuchsloch et al. (2018*b*) studied the mineral chemistry of Ta-Nb-Sn oxides which shows significant fractionation trends in an F-poor environment and further confirm fractionation as a dominant process. Furthermore, Ta-Nb-Sn oxides compositions are Fe-rich and show that abundant Ta-Nb-Sn mineralisation is potentially associated with a late-stage exsolved pegmatitic

aqueous fluid that may have complexed elements such as Sn, Cs, B, Ta and Nb. However, whether or not Ta and Nb can be transported by such a fluid is still highly debated (Fuchsloch et al., 2018*b*).

On a global level, the source of pegmatites is often debated and the CUPB and Central Tin Belt pegmatites are likewise under scrutiny. Authors globally, generally argue toward two end member models summarised in both London (2008) and Simmons and Webber (2008): (1) Pegmatites are the product of fractionation from a granitic magma or (2) pegmatites represent direct individual, low degree, fluidised partial melts. In early studies, only tentative suggestions were made specifically for the CUPB and Central Tin Belt (Richards, 1986) that the pegmatites are associated genetically with the S-type Salem and Red and Grey Granites, however, on the scale of the Damara Orogen, most authors tend to follow the same view, that pegmatites are related to the granites in a parent-daughter type relationship (e.g. Miller, 2008). The recent studies of Ashworth (2013) and Fuchsloch et al. (2018*a,b*) begin to specifically look at the source control on the pegmatites of the Damara Orogen, CUPB and Central Tin Belt. Fuchsloch et al. (2018*a*) suggests that a direct low-volume partial melting model is more likely since there is no whole-rock geochemical relationship between the granites and pegmatites and the spatial distribution of pegmatites surrounding granitic bodies is lacking the classical zonation pattern seen in other studies (e.g. Černý, 1989). These authors understood that a variety of constraints is further required to confirm a partial melting model and suggest that precise age-dating and isotopic evidence specific to the CUPB and Central Tin Belt is required. Age dates of 496 ± 8 Ma (Rb-Sr data; Haack and Gohn, 1988) for the Uis pegmatites are limited and more precise techniques are required. Tourmaline data may provide further insight into the subject which is explored in this study.

6.4 Tourmaline occurrence and characteristics

Table 6.1 summarises the occurrence of tourmaline and tourmaline species for each sample studied in the CUPB and notes other accessory minerals within each pegmatite. Further information on the pegmatite bodies, types and characteristics found in Fuchsloch et al. (2018*a, b*). Tourmaline is common to most of the pegmatites in the CUPB and occurs typically as a minor phase, however, extremely tourmaline-rich assemblages are notable in some of the pegmatites for example, the Villet tourmaline pegmatite (Table 6.1; Fig. 6.1). Tourmaline is a ubiquitous phase in the intragranitic, Gnt-Tml type pegmatites whereas metasediment hosted, Li-bearing, Ta-Nb-Sn and

Nainais type pegmatites may lack notable tourmaline. It is important to note that there is no observed relationship between morphological occurrence and pegmatite type. Exocontact tourmaline is also abundant in the metasedimentary host-rock of the Ta-Nb-Sn, Li-bearing and Nainais type pegmatites but is not a ubiquitous feature to all metasediment-hosted pegmatites. I.e. not every pegmatite within the CUPB contains exocontact tourmaline, regardless of pegmatite type.

In the CUPB tourmaline generally has simple and common morphological occurrences compared to the wide variety seen in the Southern Tin belt by Keller (1999). Four dominant morphological occurrences of tourmaline have been identified. (1) fine- to coarse-grained euhedral black, brown and uncommonly green tourmaline that rarely exhibits intracrystalline zonation. This morphological type is dominant in the belt with 90% of the tourmaline expressed in this manner. Sizes range from a few mm to 15 cm large individual crystals. It is mainly associated with massive feldspar or quartz and intracrystalline zonation, where apparent, generally shows a black tourmaline core with a thin green tourmaline rim (Fig. 6.2A,D). (2) medium-grained anhedral blue tourmaline aggregates up to 1 cm in size. These interstitial aggregates are very rare, always occur as blue tourmaline and are associated with the interior feldspars of the pegmatites, with notable abundances of fine-grained muscovite (Fig. 6.2B). (3) Rosettes of tourmaline are uncommon but occur both as green and black fans of tourmaline that terminate and thin inwards (Fig. 6.2C). Typically, on the outer portions of the rosettes, quartz or feldspar begin to fill the spaces between individual tourmaline crystals. Rosettes may also be associated with cleavelandite as in the Petalite pegmatite (Table 6.1, Fig. 6.1) and dominantly occur in the interior of the pegmatite bodies. (4) comb-structured medium- to coarse-grained tourmaline associated with the borders of pegmatite bodies. Tourmaline crystals display a unidirectional solidification texture comprised of aligned tourmaline grains which grow perpendicular to pegmatite contacts and increase in size away from the contact. These tourmaline crystals reach appreciable sizes, up to 2 cm in width and several centimetres long.

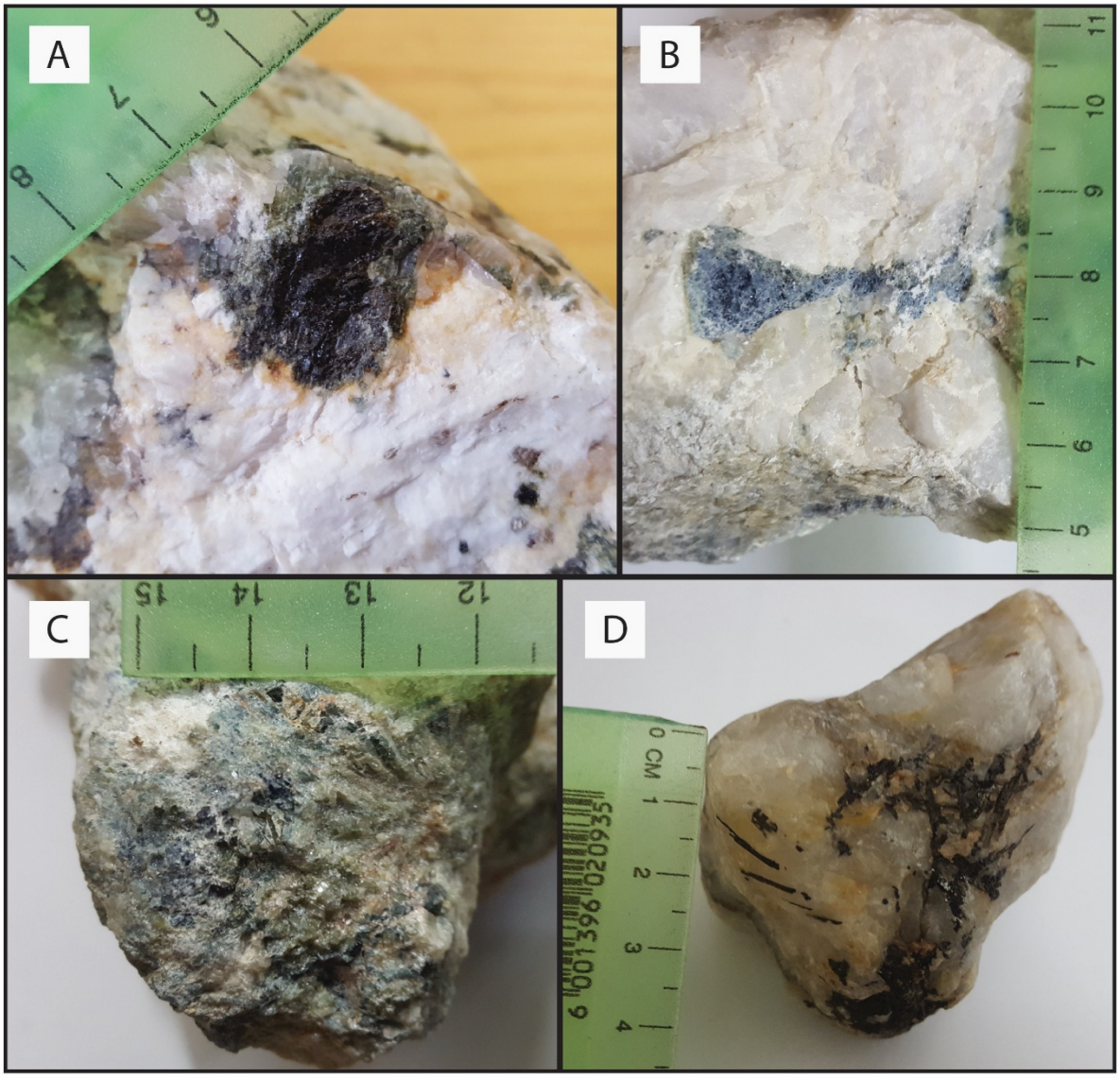


Figure 6.2: Photographs showing tourmaline morphologies in the CUPB. A) A zoned tourmaline crystal from the Nainais pegmatite with large black core and green to transparent rim. B) An interstitial aggregate of blue tourmaline in massive feldspar from the SmallGG pegmatite. C) Rosettes of green euhedral tourmaline (right) and blue anhedral tourmaline aggregates (left). D) Thin euhedral, black tourmaline crystals associated with massive quartz from the Petalite pegmatite.

Microscopically tourmaline is even simpler, mostly occurring as euhedral singular crystals with almost no significantly notable pleochroic zonation. Only 21 grains in the dataset were found to have be microscopically zoned. Mineral associations with quartz and feldspar grains have a primary euhedral texture and they appear to co-crystallise with tourmaline. Occasionally tourmaline may display a graphic intergrowth texture with quartz which is also visible on a macroscopic level in some samples. The blue tourmaline has the most observed differences and mineral associations. The individual grains have an interstitial texture with feldspar and muscovite

becomes more common in the areas where blue tourmaline occurs. Considerable sericitic alteration is commonly associated with the blue tourmaline.

Table 6.1: Tourmaline occurrences from pegmatites of the CUPB and Central Tin Belt. The different tourmaline species, occurrence and other accessory phases in the pegmatites are shown. The first character in the sample number indicates a specific pegmatite body. Ta-Nb-Sn indicates the unzoned Ta-Nb-Sn mineralised type pegmatites, Gnt-Tml indicates the Garnet-tourmaline type pegmatite and Li-bearing indicates the unzoned to zoned Li-pegmatites. The last 3 rows represent the pegmatites of the Nainais area, Central Tin Belt. CGM, Columbite-group minerals; cas, cassiterite.

Pegmatite	Sample #	Peg-type	Tml Species	Occurrence	Accessory phases
MT-pit	D-3	Ta-Nb-Sn	Schorl, foitite	Individual fine-grained brown tourmaline	CGM, apatite
T-mag	O-2	Ta-Nb-Sn	Schorl	Medium-grained, 0.5 cm, euhedral brown tourmaline grains	None
P3	3.2-1	Ta-Nb-Sn	Schorl, dravite	Fine-grained aggregates of brown to green tourmaline	CGM, cas, apatite
Uis	6-2	Ta-Nb-Sn	Schorl	Medium-grained comb-structured brown tourmaline on pegmatite border	CGM, cas
2face	10-1	Ta-Nb-Sn	Schorl	Comb-structured brown tourmaline	CGM, apatite
Tsaurob	T-3	Ta-Nb-Sn	Schorl, foitite	Rosettes of thin brown, euhedral tourmaline, up to 1 mm in width	CGM, cas, minor lepidolite
RA1	11-1	Ta-Nb-Sn	Schorl, foitite	Coarse-grained, 5-10 cm, brown tourmaline	None
P2.2	3-6	Ta-Nb-Sn	Schorl, elbaite	Brown to green subhedral medium-grained tourmaline	CGM, cas, apatite
Dead Sea	2-2	Ta-Nb-Sn	Schorl, dravite	fine-grained euhedral brown and minor green tourmaline	CGM
SmallGG	K-4	Ta-Nb-Sn	Schorl, foitite, elbaite	Brown to green rosettes of tourmaline. Blue tourmaline occurs as anhedral interstitial aggregates	None
Tsau-2	J-1	Ta-Nb-Sn	Schorl, elbaite	Medium-grained, up to 1 cm, subhedral brown tourmaline	CGM, cas, apatite
Granite-dome	X-1	Gnt-Tml	Schorl, dravite	Fine-grained aggregates of brown tourmaline	Garnet
Rose Quartz	1-1	Gnt-Tml	Elbaite	Clear green, euhedral tourmaline up to 1 cm in length	Garnet
Rose Quartz	1-2	Gnt-Tml	Schorl, foitite	Border zone comb-structured brown tourmaline	Garnet
Villet Tourmaline	7-1	Gnt-Tml	Schorl	Large, up to 8 cm in length, aggregates of brown tourmaline	CGM, garnet
Villet Tourmaline	7-2	Gnt-Tml	Schorl	Large, up to 8 cm in length, aggregates of brown tourmaline	CGM, garnet
Petalite	PET-2	Li-bearing	Schorl, dravite	Rosettes of brown, euhedral tourmaline up to 5 cm in length occuring in the intermediate zone	Petalite, CGM, cas, apatite, beryl, Eucryptite
Karlowa-S	5-2	Li-bearing	Schorl, dravite	Comb-structured brown tourmaline	Spodumene, CGM, cas, apatite
Nain-1	en-1	Ta-Nb-Sn	Elbaite	Medium-grained, 1-5 cm, tourmaline grains with green rims and brown cores	CGM
Nain-3	eh-1	Ta-Nb-Sn	Schorl, elbaite	Various sizes of brown and green tourmaline. Large grains are zoned with green edges and brown centres	None
Nainais	Na-2	Ta-Nb-Sn	Schorl, foitite	Black 1-3 mm sized, subhedral, brown tourmaline	CGM, cas, apatite

6.5 Experimental methods

Tourmaline from 22 samples acquired from 19 pegmatite bodies was investigated using a JEOL JXA-8230 electron micro-analyser at Rhodes University, Grahamstown, South Africa. Tourmaline separates were acquired from each sample using density and magnetic mineral separation techniques and then mounted into ore blocks and analysed. Although tourmaline zonation is infrequent, where apparent the different zones were analysed. 431 quantitative mineral chemical analyses were obtained using 4 wavelength dispersive spectrometres. The beam conditions, generated by a tungsten cathode, were 15 kV accelerating potential, 10nA current and a 10 µm beam size. Counts for Ca, Mg, Fe, K, Si, Na, F, Al, Mn and Ti were measured on K-alpha peaks. Counting times were 10 seconds on the peak and 10 seconds on the total background. Commercial "SPI" standards were used. Tourmaline was standardised for Si/Al/Ca/Ti/Fe/Mg on kaersutite, Na on plagioclase, K on orthoclase, Mn on willemite and F on MgF_2. Calibration acquisitions were peaked on standards, while unknown acquisitions were peaked on the samples before each point analysis. Data was collected with JEOL software and an automated default JOEL ZAF matrix algorithm (Heinrich/Duncumb-Reed correction with FFAST NIST-2005 mass absorption coefficients) was applied to correct for differential matrix effects. Oxygen was calculated by stoichiometry.

Since the elements Li, H, and B were not measured, initial data was processed using a similar method to that of Tindle et al. (2002) where the structural formula was calculated on the basis of 31 anions and stoichiometric amounts of F and OH corresponding to four atoms/molecules per formula unit. Although boron has been found to occasionally occupy the tetrahedral site in tourmaline (Ertl et al., 2006), this calculation assumes boron saturation with no boron on the tetrahedral site. Fe and Mn are assumed to be bivalent due to charge balance calculations while Li is assumed to occupy the Y site up to a total of 3 atoms per formula unit. Calculations were done using the Excel spreadsheet available from http://www.open.ac.uk/earth-research/tindle/AGT/AGT_Home_2010/Microprobe-2.html. Although stoichiometric calculations of tourmaline such as this may contain bias and would not be suitable for detailed intracrystalline studies, they have been shown to be useful for studies on scales such as this (e.g. Keller et al., 1999; Tindle et al., 2002; Büttner et al., 2016; Zheng et al., 2016).

6.6 Results

Representative chemical compositions of tourmaline from each sample in Table 6.1 are shown in Table 6.2. Due to the iterative stoichiometric calculations of tourmaline, elements such as Li, H, and O were used only where necessary to reduce overall bias from calculations. Species that pertain to the H and O end members were therefore not included in the classification of tourmaline, for example the oxy-schorl and oxy-dravite end members (Henry et al., 2011). Although these elements and subsequent substitution mechanisms involving them cannot be directly depicted, other bivariate relationships can imply the behaviour of these elements and therefore are shown in subsequent figures as implied relationships and substitution mechanisms. Such mechanisms are evaluated only in the discussion.

The dataset shows a wide variety of tourmaline chemical compositions, specifically in the quantity of Al_2O_3, MgO, FeO, TiO_2 and to a lesser extent, Na_2O. Compositions of CaO and MnO likewise show a large variation but pertain only to specific samples or pegmatites types. The Ta-Nb-Sn type pegmatites best display these variations probably due to the large abundance of this pegmatite type in the belt. Al_2O_3, MgO, FeO and TiO_2 compositions range from 30.62-35.90, 0-7.02, 5.28-15.06 and 0-1.07 wt % respectively. Na_2O compositions vary slightly less with a range of 1.25-2.64 wt %. Only sample 2-2 of the Ta-Nb-Sn pegmatites (Table 6.1, Fig. 6.1) show increased CaO values up to 1.49 wt %. Tourmaline from the Nainais pegmatites show negligible MgO and CaO contents, however, the Al_2O_3 and MnO contents obtain the highest values in the dataset of 39.15 and 1.61 wt % respectively and FeO the lowest value in the dataset of 3.09 wt%. Four data points in the Nainais pegmatites show intermediate TiO_2 up to 0.66 wt % but all other compositions are negligible. Na_2O shows a similar range to the Ta-Nb-Sn pegmatites. In most regards the composition of tourmaline from the Gnt-Tml and Li-bearing type pegmatites are similar: they show an Al_2O_3 variation of 30.22-32.73 wt % but do not reach the significantly higher Al_2O_3 quantities of the Ta-Nb-Sn and Nainais pegmatites. They are similarly MgO and TiO_2 rich with values ranging between 0.76-6.68 and 0.06-1.05 wt % respectively. FeO contents are likewise similar ranging between 5.89-14.51 wt %, however, the Li-bearing pegmatites are on the low end of the spectrum. Na_2O contents are similar to the other pegmatite types; however, the Gnt-Tml and Li-bearing pegmatites show negligible MnO. CaO contents only reach high quantities in the one Gnt-Tml sample, sample 1-1 from the Rose Quartz pegmatite (Table 6.1, Fig. 6.1), with values

reaching up to 0.83 wt%. Sample 1-2 from the Rose Quartz pegmatite is the predictable exception, being gem-like green tourmaline. Values are similar to the end member compositions of the Nainais pegmatites spectrum with considerable MnO and Al_2O_3, low FeO and negligible MgO, CaO and TiO_2 values.

No significant differences in composition were observed from tourmaline occurring in the different morphologies which is similar to the observations of Novák et al. (2011). If anything, the comb-structured brown tourmaline is only slightly more Mg-rich on average, however, intermediately occurring rosettes of black tourmaline may have even higher Mg values from one pegmatite to another. Only interstitial blue tourmaline shows significantly higher Al values (>39 wt %) with negligible Mg, Ca and Ti, however, these occurrences are extremely sparse. Likewise, very little intracrystalline compositional variation occurs in the sparsely populated database of zoned tourmaline crystals from the CUPB. It is, however, important to note that where significant intracrystalline compositional variation does occur, such as the black cores and green rims of the Nain-3 pegmatite (Table 6.1; Fig. 6.1, 6.2A), most core zones are significantly Mg-rich and Al-poor whereas the green rims are Mg-poor and Al-rich. Eleven out the 21 zoned crystals studied display this compositional zonation from core to rim, 5 crystals show negligible variations and 5 show the reverse trend from core to rim. Such compositional variation from core to rim of the zoned crystals mostly follows the trend of decreasing Mg and increasing Al and Fe, similar to the overall compositional trend viewed in the entire belt seen below. These features are important to this overall study, such that intracrystalline variations and variations between different morphological occurrences (e.g. Marks et al., 2013) do not hinder the belt wide scale of the study. Furthermore, since most of the pegmatites in this study are not zoned, internal zonation, that has been shown to significantly affect tourmaline compositions (Selway, 1999), plays little role in this study.

Table 6.2: Representative chemical compositions of tourmaline from pegmatites of the Cape Cross-Uis pegmatite belt and Central Tin Belt. Each sample in Table 6.1 is depicted in this table together with its dominant occurring tourmaline species. Pegmatite types and sample number descriptions are given in Table 6.1 and the text.

Sample #	**D-3**	**O-2**	**3.2-1**	**6-2**	**10-1**	**T-3**	**11-1**	**3-6**	**2-2**	**K-4**	**J-1**
	Ta-Nb-Sn	*Ta-Nb-Sn*	*Ta-Nb-Sn*	*Ta-Nb-Sn*	*Ta-Nb-Sn*	*Ta-Nb-Sn*	*Ta-Nb-Sn*	*Ta-Nb-Sn*	*Ta-Nb-Sn*	*Ta-Nb-Sn*	*Ta-Nb-Sn*
Peg-type											
Mineral	*Schorl*	*Schorl*	*Dravite*	*Schorl*	*Schorl*	*Foitite*	*Schorl*	*Schorl*	*Dravite*	*Elbaite*	*Elbaite*
SiO_2 wt%	35,54	35,30	36,43	35,54	36,49	35,70	36,06	36,65	37,06	37,11	36,53
TiO_2	0,22	0,81	0,57	0,81	0,21	0,23	0,15	0,07	0,54	0,00	0,01
Al_2O_3	33,88	31,64	31,44	32,66	32,52	32,03	32,57	34,13	31,15	35,06	34,59
FeO	12,38	13,09	8,36	9,48	9,63	15,06	12,80	11,34	8,80	7,03	9,63
MgO	0,88	2,52	5,29	3,85	3,84	0,75	1,65	0,74	5,34	0,21	0,00
CaO	0,03	0,15	0,11	0,38	0,04	0,05	0,02	0,02	0,13	0,11	0,02
MnO	0,15	0,12	0,10	0,08	0,13	0,13	0,08	0,16	0,09	0,65	0,39
Na_2O	1,65	2,21	2,12	1,78	1,99	1,46	1,58	1,79	2,22	2,62	2,01
K_2O	0,05	0,05	0,05	0,07	0,05	0,06	0,04	0,03	0,04	0,03	0,02
F	0,38	0,63	0,48	0,12	0,41	0,14	0,06	0,45	0,26	1,04	0,74
H_2O*	3,38	3,26	3,38	3,54	3,42	3,47	3,54	3,41	3,52	3,15	3,25
B_2O_3*	10,33	10,31	10,45	10,41	10,47	10,24	10,33	10,49	10,55	10,57	10,43
Li_2O*	0,43	0,25	0,42	0,35	0,46	0,32	0,44	0,83	0,53	1,65	1,20
O=F	0,16	0,27	0,20	0,05	0,17	0,06	0,02	0,19	0,11	0,44	0,31
Total	99,32	100,06	98,99	99,02	99,49	99,58	99,28	99,91	100,12	98,79	98,51
Cations based on 31 anions (O, OH, F)											
T:Si											
a.p.f.u	5,98	5,95	6,06	5,94	6,06	6,06	6,07	6,07	6,10	6,10	6,09
Al	0,02	0,05	0,00	0,06	0,00	0,00	0,00	0,00	0,00	0,00	0,00
Z:Al	6,00	6,00	6,00	6,00	6,00	6,00	6,00	6,00	6,00	6,00	6,00
Mg	0,00	0,00	0,00	0,00	0,00	0,00	0,00	0,00	0,00	0,00	0,00
Y:Al	0,70	0,23	0,16	0,37	0,36	0,41	0,46	0,66	0,05	0,80	0,79
Ti	0,03	0,10	0,07	0,10	0,03	0,03	0,02	0,01	0,07	0,00	0,00
Mg	0,22	0,63	1,31	0,96	0,95	0,19	0,41	0,18	1,31	0,05	0,00
Mn	0,02	0,02	0,01	0,01	0,02	0,02	0,01	0,02	0,01	0,09	0,06
Fe^{2+}	1,74	1,84	1,16	1,32	1,34	2,14	1,80	1,57	1,21	0,97	1,34
Li*	0,29	0,17	0,28	0,24	0,31	0,22	0,30	0,55	0,35	1,09	0,81
X:Ca	0,01	0,03	0,02	0,07	0,01	0,01	0,00	0,00	0,02	0,02	0,00
Na	0,54	0,72	0,68	0,58	0,64	0,48	0,52	0,58	0,71	0,83	0,65
K	0,01	0,01	0,01	0,02	0,01	0,01	0,01	0,01	0,01	0,01	0,00
X-Vacancy	0,45	0,24	0,29	0,34	0,34	0,50	0,47	0,41	0,26	0,14	0,34
OH	3,80	3,66	3,75	3,94	3,79	3,93	3,97	3,77	3,86	3,46	3,61
F	0,20	0,34	0,25	0,06	0,21	0,07	0,03	0,23	0,14	0,54	0,39

Table 6.2 cont.

Sample #	**en-1**	**eh-1**	**Na-2**	**PET-2**	**5-2**	**X-1**	**1-1**	**1-2**	**7-1**	**7-2**
Peg-type	*Ta-Nb-Sn*	*Ta-Nb-Sn*	*Ta-Nb-Sn*	*Li-peg*	*Li-peg*	*Gnt-tour*	*Gnt-tour*	*Gnt-tour*	*Gnt-tour*	*Gnt-tour*
Mineral	*Elbaite*	*Elbaite*	*Schorl*	*Schorl*	*Dravite*	*Dravite*	*Elbaite*	*Schorl*	*Schorl*	*Schorl*
SiO_2 wt%	36,61	35,96	35,11	36,16	37,25	36,18	37,21	35,25	36,06	35,90
TiO_2	0,00	0,55	0,05	0,51	0,15	0,42	0,04	0,92	0,36	0,27
Al_2O_3	39,15	32,86	34,21	31,61	31,50	31,32	35,43	31,09	31,39	30,52
FeO	3,34	8,39	12,12	10,08	7,99	11,04	4,78	14,32	10,80	12,44
MgO	0,05	4,23	0,17	4,10	4,99	4,01	0,18	1,83	3,56	3,08
CaO	0,08	0,09	0,01	0,08	0,08	0,07	0,16	0,19	0,13	0,06
MnO	1,61	0,17	0,06	0,12	0,07	0,18	1,29	0,23	0,20	0,14
Na_2O	2,02	1,65	1,72	1,99	1,66	2,12	2,63	2,10	1,94	2,08
K_2O	0,01	0,04	0,04	0,06	0,58	0,02	0,04	0,08	0,08	0,06
F	0,44	0,19	0,53	0,21	0,41	0,52	1,27	0,54	0,26	0,36
H_2O*	3,50	3,50	3,27	3,48	3,43	3,34	3,05	3,28	3,44	3,36
B_2O_3*	10,76	10,40	10,22	10,39	10,51	10,39	10,57	10,25	10,33	10,23
Li_2O*	1,46	0,31	0,57	0,38	0,75	0,30	1,89	0,25	0,42	0,42
O=F	0,18	0,08	0,22	0,09	0,17	0,22	0,53	0,23	0,11	0,15
Total	98,86	98,26	97,86	99,07	99,19	99,68	98,01	100,10	98,87	98,76
Cations based on 31 anions (O, OH, F)										
T:Si a.p.f.u	5,91	6,01	5,97	6,05	6,16	6,05	6,12	5,97	6,07	6,10
Al	0,09	0,00	0,03	0,00	0,00	0,00	0,00	0,03	0,00	0,00
Z:Al	6,00	6,00	6,00	6,00	6,00	6,00	6,00	6,00	6,00	6,00
Mg	0,00	0,00	0,00	0,00	0,00	0,00	0,00	0,00	0,00	0,00
Y:Al	1,37	0,47	0,83	0,23	0,14	0,18	0,86	0,19	0,22	0,11
Ti	0,00	0,07	0,01	0,06	0,02	0,05	0,01	0,12	0,05	0,03
Mg	0,01	1,05	0,04	1,02	1,23	1,00	0,04	0,46	0,89	0,78
Mn	0,22	0,02	0,01	0,02	0,01	0,03	0,18	0,03	0,03	0,02
Fe^{2+}	0,45	1,17	1,72	1,41	1,10	1,54	0,66	2,03	1,52	1,77
Li*	0,95	0,21	0,39	0,25	0,50	0,20	1,25	0,17	0,29	0,29
X:Ca	0,01	0,02	0,00	0,01	0,01	0,01	0,03	0,03	0,02	0,01
Na	0,63	0,53	0,57	0,65	0,53	0,69	0,84	0,69	0,63	0,69
K	0,00	0,01	0,01	0,01	0,12	0,00	0,01	0,02	0,02	0,01
X-Vacancy	0,35	0,44	0,42	0,33	0,33	0,30	0,12	0,26	0,33	0,29
OH	3,78	3,90	3,71	3,89	3,79	3,72	3,34	3,71	3,86	3,80
F	0,22	0,10	0,29	0,11	0,21	0,28	0,66	0,29	0,14	0,20

Tourmaline compositional data is most useful when evaluating it in terms of atoms per formula unit (a.p.f.u) and assessing the number of cations in each structural site with the general formula $XY_3Z_6(T_6O_{18})(BO_3)V_3W$. Hence-forth, all numerical data is given in a.p.f.u. The classification of tourmaline is first considered in terms of the dominant element that occupies the X-site (Fig. 6.3A; Hawthorne and Henry, 1999; Henry et al., 2011). Most tourmaline compositions plot along the base of the ternary diagram with negligible Ca contents and thus dominantly belong to the Alkali group (Fig. 6.3A). Samples 2-2 and 1-2 have anomalous high Ca contents with regards to the CUPB but do not fall into or come significantly close to the calcic group. Na contents are variable and X-site vacancies become significant in a few compositions from all pegmatite types: some compositions plot on the boundary and into Vacancy group (Fig. 6.3A).

In terms of the Al-Fe-Mg ternary diagram (Henry and Guidotti, 1985), tourmaline data display unique compositions for tourmaline with a pegmatitic origin, some data plotting in field of the metasediments with Al-saturating phase (Fig. 6.3B, Field 3). Previous literature sparsely records such Mg-rich pegmatitic tourmaline; however, Novák et al. (2004) shows similar values from the granitic pegmatites of the Moldanubium Zone, Czech Republic. Tindle et al. (2002) and Novák et al. (2011) likewise show similar Mg and Fe contents but data from Novák et al. (2011) have significantly lower Al contents (< 6.0 a.p.f.u.). Figure 6.3B is the first discrimination diagram to show the two-fold compositional trend in tourmaline data from the CUPB and Central Tin Belt. Initial compositions plot in Field 3 and are considerably Mg-rich. The first trend follows Mg depletion towards increasing Fe in the Li-poor granitoid field over a small range of Al contents for all pegmatite types. The second upward trend follows Fe depletion with increasing Al contents into the Li-rich granitoid field. Surprisingly few tourmaline compositions from Li-bearing pegmatite types occur in the Li-poor granitoid field whereas the Central Tin Belt, Nainais pegmatites plot predominantly in the field of Li-rich granitoids, with the exception of the black core zone in tourmaline crystals which plot on the boundary between Li-poor granitoids and Field 3 (Fig 6.2A, 6.3B). Ta-Nb-Sn pegmatites span the entire two-fold trend whilst Gnt-Tml pegmatites mostly plot from Field 3 towards and well into the Li-poor granitoid field, again with one exception: the gem-like green tourmaline from sample 1-1 (Table 6.1, 6.2) which shows extremely high Al contents plotting in the Li-rich granitoid field. Other tourmaline data from Namibian pegmatites in the Damara Orogen (Keller, 1999; Trumbull, 2008; Grassi 2014), show similar

compositions, plotting well within the Li-poor and Li-rich granitoid fields and display the second upward trend of increasing Al contents, however, they lack the highly Mg-rich compositions seen in the CUPB.

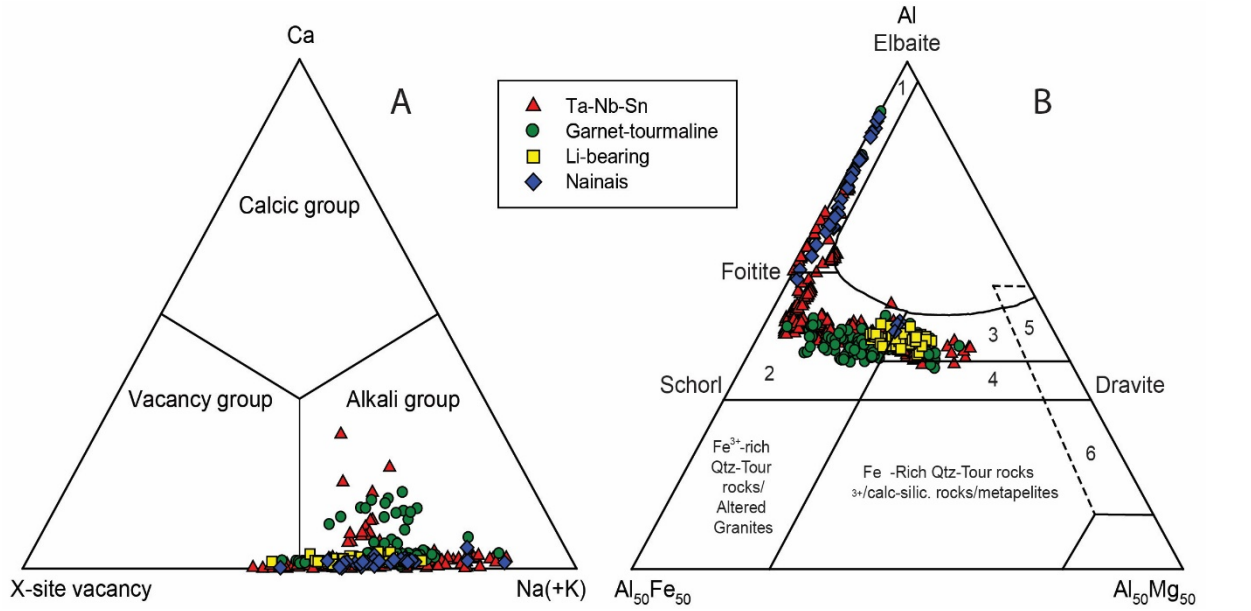


Figure 6.3: Tourmaline chemical classification diagrams. A) Provenance rock diagram from Henry and Guidotti (1985): 1 Li-rich granitoids; 2, Li-poor granitoids; 3, metasediments with Al-saturating phase; 4, metasediments without Al-saturating phase; 5, low-Ca meta-ultramafic rocks and Cr, V rich metasediments; 6, metacarbonates and metapyroxenites. B) Classification of tourmaline based on the X-site occupation from Henry et al. (2011). Values are in a.p.f.u.

6.6.1 Y-site Al content covariations

The Al content at the Y-site in tourmaline has been shown as a useful tool in tracing magmatic processes in pegmatites such as fractionation and determining the activity of certain elements at different stages (Linnen and William-jones, 1993; Tindle et al., 2002; London, 2008). During progressive crystallisation of a pegmatitic magma, tourmaline should generally show a consistent increase in the Al content as the melt becomes more peraluminous (London, 2008).

Figure 6.4A,C and E depict the first of the 2-fold trends seen in Figure 6.3B, where there is a sharp decrease in the contents of Ca, Mg and Ti towards slightly higher Al contents, from approximately 0.0-0.4 a.p.f.u., and therefore higher fractionation levels. During this trend, we observe that there is a similar, but lesser, decrease in Na content with increasing X-site vacancies and Al content (Fig. 6.4B). Fe behaves differently, and its content increases during this process (Fig. 6.4B) whereas the Mn content is largely unchanged (Fig. 6.4F). The first trend can be summarised by

means of tourmaline species starting with a significant dravite component which evolves towards a schorl dominated species. During the second stage of the 2-fold trend, at approximately 0.4 Al a.p.f.u., Mg, Ca and Ti contents are largely unchanged: Mg and Ca show almost negligible values whereas Ti continues to decrease over a broader range of increasing Al contents. The Na and Fe trends are reversed and increase and decrease respectively. The Mn contents show a sharp increase; however, this only occurs at 0.8 Al a.p.f.u compared to 0.4 Al a.p.f.u for the other elements in the second stage of the 2-fold trend. In summary, the schorl dominated species evolves toward the foitite end member and in the case of increased Li-contents towards the elbaite end member at the highest levels of fractionation (Fig. 6.4). The compositional trend: schorl-dravite towards foitite, towards elbaite is a common feature in tourmaline compositional variations (London, 2008) and has been shown in similar Li-poor pegmatites (Henry and Guidotti, 1985; Roda et al., 1995; Gaweda et al., 2002) including the Damara Orogen (Keller, 1999; Grassi, 2014); however, extreme Mg contents have rarely been found in tourmaline of pegmatitic origin (Tindle et al. 2002; Novák et al. 2004; Novák et al. 2011).

The Gnt-Tml and Li-bearing pegmatites only display tourmaline compositions in the first stage of the 2-fold trend with the exception of the green gem-like tourmaline from sample 1-1 (Table 6.1) which plot well within the late stages of the second trend. Gnt-tourmaline pegmatites, however, show a more evolved pattern becoming more depleted in Mg, Ca and Ti and Fe-rich compared to Li-bearing pegmatites. Ta-Nb-Sn pegmatites span the entire 2-fold trend but do not reach the extremes shown by the Nainais and sample 1-1 pegmatites. The Nainais pegmatites are also significantly Al-rich, reaching the highest Al contents in the dataset and are separated from the other pegmatite types shown in Figure 6.4B, D and F. Tourmaline from the Nainais pegmatites are notably Li-rich and are shown to contain the highest elbaite component (Fig. 6.4D)

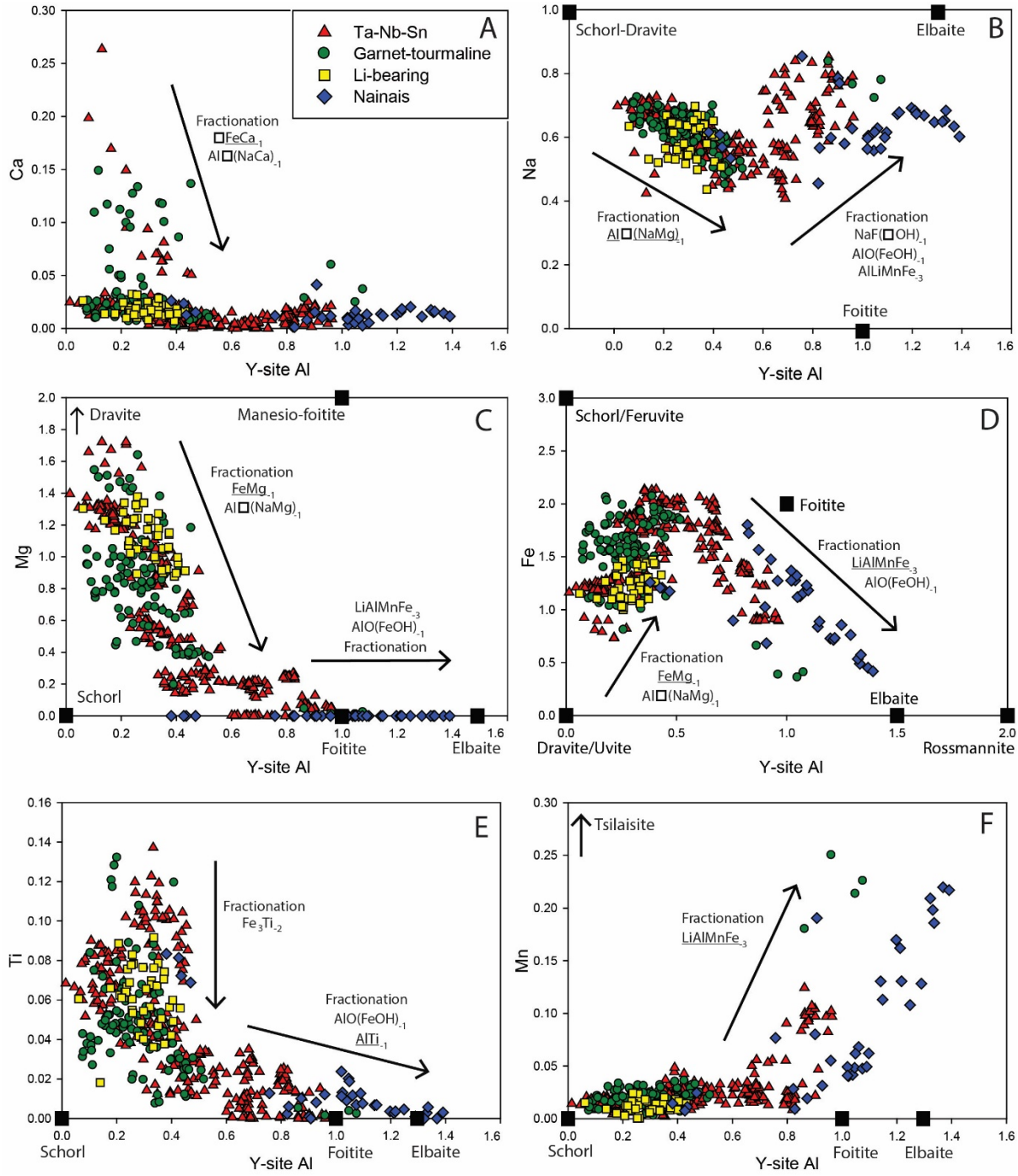


Figure 6.4: Y-site Al covariation with Ca, Na, Mg, Fe, Ti and Mn in a.p.f.u respectively shown in graphs A-F. Suggested substitution mechanisms are shown in each plot along with the dominant fractionation trends. The underlined substitution mechanisms represent the dominant mechanism shown by the plot, whereas other substitution mechanisms are implied or suggested to be occurring simultaneously. Implied mechanisms do not necessarily contribute major abundance changes and may represent minor solid solutions exchanging elements during co-occurring dominant substitution mechanisms.

6.6.2 Tourmaline species classification and comparison to suggested trends.

Often tourmaline is classified in terms of the end member components it contains (Novák et al., 2009; Henry et al., 2011). For example, Figure 6.5A shows that primitive tourmaline has essentially equal proportions of dravite and schorl which progressively evolve toward an increasing schorl component, with little change in the Ca/(Ca+Na) with the exceptions, Sample 2-2 and 1-2, as mentioned above. Li-bearing and Gnt-Tml type pegmatites show the most primitive, largest dravitic component (Fig. 6.5A). This diagram, however, does not include other important tourmaline end members since only Ca, Na, Mg and Fe are considered. Figure 6.5B likewise excludes the dravite component (Mg) and includes Al and the X-site vacancies. This plot shows compositions starting with a large schorl component that first evolve toward an increasing foitite component, followed by an evolution toward the elbaite end member. The Nainais pegmatites and Sample 1-1 notably obtain the highest elbaite component with some points starting to evolve toward an increasing rossmanite component (Fig. 6.5B).

Tindle et al. (2002) proposed the diagram in Figure 6.5C as a means to infer pegmatite host rock interaction. To surmise, the authors suggest that increasing Mg, Ti and Ca contents, at relatively constant and low Li+Mn values, indicates significant contamination by a mafic/metapelitic host rock. Almost 70% of the dataset lie in the field of contamination/complex origin and interestingly the Gnt-Tml type pegmatites, which are intragranitic, solely occupy this field. Likewise, Li-bearing pegmatites are exclusively in the suggested highly contaminated field, whereas Nainais pegmatites, which are similar in character and host rock, do not fall in this field. London (2008) proposed Figure 6.5D which removes the foitite component to further classify tourmaline compositional trends with a focus on the Mn content. The diagram likewise can infer the Li content of the tourmaline since Li is a calculated composition. The figure shows that although Mn contents become important in later stage pegmatite evolution (Fig. 6.4F), in terms of the Mn end member 'Tsilaisite', compositions plot below the evolution line, seen in Figure 6.5D. This diagram notes that Nainais pegmatites become largely elbaite and infers an increasing Li content. Ta-Nb-Sn type pegmatites are likewise evolved but do not contain the higher elbaite component that the Nainais and Sample 1-1 pegmatites do.

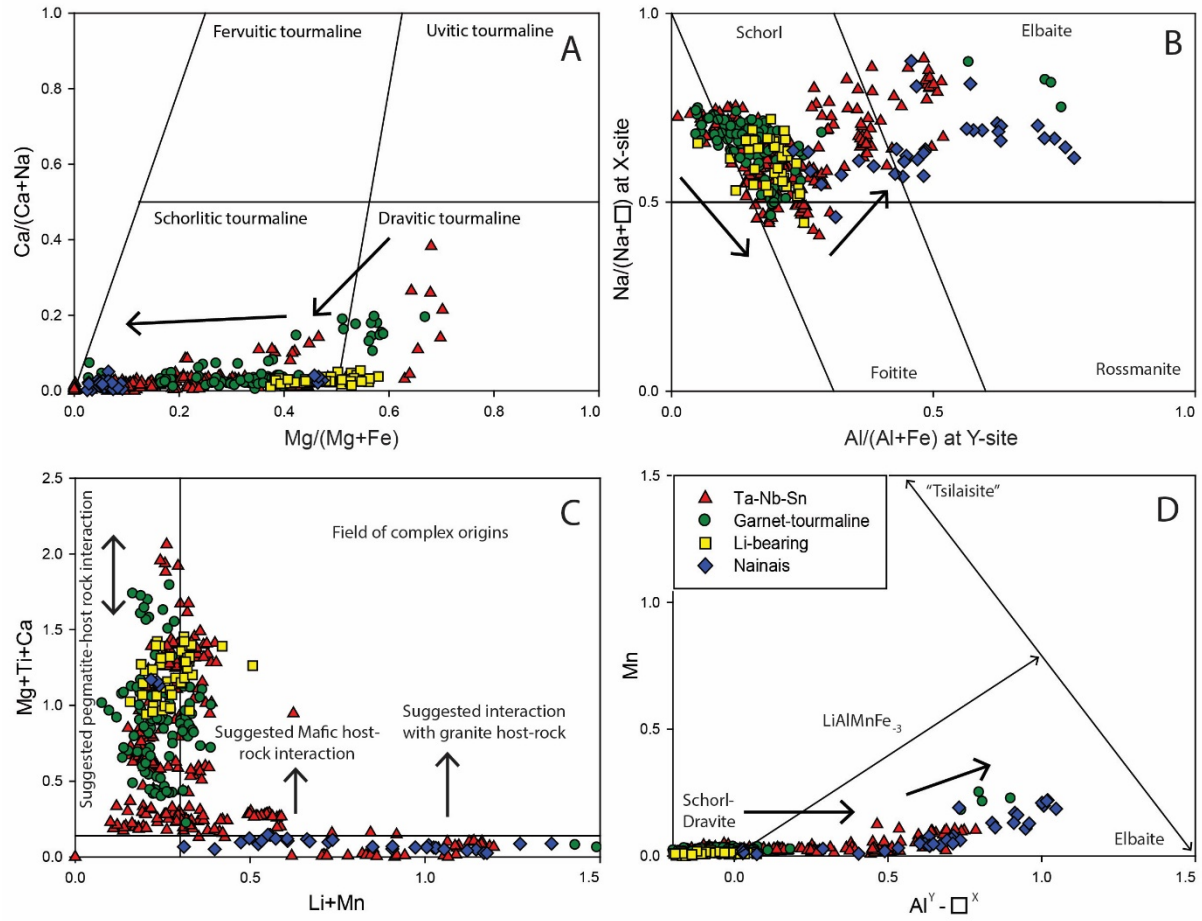


Figure 6.5: Various compound/ratio element plots of tourmaline compositions. A) Classification of tourmaline based on the Mg# and Ca# of tourmaline from Novák et al. (2009). B) Classification of tourmaline based on the Al# and Na# from Tindle et al. (2002). C) Tindle et al. (2002) suggested contamination diagram based on tourmaline compositions. Compositions plotting in the lower field are suggested to be uncontaminated whereas raised values of Mg+Ti+Ca indicate contamination. D) Tourmaline evolution diagram minus the foitite component from London (2008).

6.7 Discussion

6.7.1 Substitution mechanisms and fractionation implications

In Figures 6.4 and 6.5D the general substitution mechanisms that may be operating in tourmaline during pegmatite evolution are shown. The mechanisms involved are either singular element exchange vectors or coupled substitution reactions involving 3 or more elements. Tourmaline may contain extremely complex chemical variations and therefore such simple substitution mechanisms are unlikely to be the sole mechanisms which occur at any given stage of pegmatite evolution. It is more likely that a combination of such mechanisms are acting simultaneously some being dominant and others being minor. This section aims to suggest the dominantly acting substitution

mechanisms that occur throughout the 2-fold trend and also attempts to imply the behaviour of the light elements, H, Li and O, which are not measured by EPMA methods.

6.7.1.1 Trend one of the 2-fold trend

Initially, tourmaline compositions are highly Mg-, Ti- and some Ca-rich. Na is slightly elevated but not to the contents seen in later evolved tourmaline whereas Al, Fe and Mn contents are low. During the first phase of the 2-fold trend, we see extreme depletion in the Mg, Ti and Ca contents with significant Fe increases and moderate Al- and Na-depletion (Fig. 6.4). The Mg depletion can be largely accounted for via the exchange vector:

$$MgFe_{-1} \quad (1)$$

However, Linnen and William-Jones (1993) point out that this mechanism cannot solely be operating, and other mechanisms must be operating simultaneously but perhaps to a lesser extent. The data confirms this since the Fe content increase and Mg content decrease are not of equal proportions (Fig. 6.4C,D). These figures also show that the Al content increases slightly from just above 0 to approximately 0.4 a.p.f.u., which can be accounted for by the substitution mechanism, similar to Henry and Dutrow (2012):

$$Al\square(NaMg)_{-1} \quad (2)$$

This exchange vector is also displayed in Figure 6.4B where the Na contents of tourmaline show moderate decreases over the same range of Al contents. Notably during this exchange vector, tourmaline accepts a vacancy at the X-site. Ca and Ti contents are likewise involved during the first fractionation sequence, however, only the sample 1-2 and 2-2 display the Ca decrease and contents of these elements are not significantly high and therefore the following substitution mechanisms that involve their depletion are only minor (Fig. 6.4A,E):

$$FeCa_{-1} \quad (3)$$

$$Al\square(NaCa)_{-1} \quad (4)$$

$$Fe_3Ti_{-2} \quad (5)$$

Mechanism (4) is even more minor since only the Ta-Nb-Sn pegmatites confidently show slight Al increases with decreasing Ca values. Likewise, the Ti content does not show confident correlation with the Al content and the data are scattered (Fig. 6.4E) implying Al has little effect on the relationship in the first stage of fractionation and therefore the sharp decrease in Ti contents must be accounted for by increases in Fe or Na since these are the only elements that increase their

abundances during the first fractionation trend. Novák et al. (2011) also shows that trivalent Fe might be involved in mechanism (5).

Fractionation is recorded in the first phase of tourmaline crystallisation whereby tourmaline removes the ferromagnesian components of melt in its initial stage of crystallisation (London, 2008). As ferromagnesian components are consumed, tourmaline records the decreases in the Mg, Ti, Ca and, to a lesser extent, the Na concentrations reflecting substitution mechanisms (1) to (5). Elevated Ca values in Samples 1-2 and 2-2 possibly reflect the absence of major plagioclase in these pegmatites which should consume initial Ca (Tindle et al., 2002). Gnt-Tml and Li-bearing type pegmatites do not continue into the second phase. This is expected for the Gnt-Tml pegmatites since Fuchsloch et al. (2018*a,b*) show them to be the most primitive pegmatites in the belt based on whole-rock geochemical data and Ta-Nb-Sn oxide geochemistry. The exception of Sample 1-1 is apparent for the Gnt-Tml pegmatites, obtaining highly fractionated levels (Fig. 6.4, 6.5) and is possibly due to extremely late-stage crystallisation in these pegmatites where trace Li quantities are available. The Li-bearing type pegmatites should reflect highly fractionated tourmaline compositions since Fuchsloch et al. (2018*a,b*) show them to be the most fractionated and complex spodumene and petalite subtype LCT pegmatites in the belt. Tourmaline compositions, however, show a primitive signature which is actually expected since Sample 5-3 has a border zone comb-structure morphology, being the first tourmaline to crystallise in the pegmatite and the Petalite pegmatite is complexly mineralogically zoned (Table 6.1; Section 2.3.3.1). The pegmatite zonation of these types hinders the overall belt-wide study since it is well documented that different zones within a pegmatite body frequently show different tourmaline compositions (Selway et al., 1999) and therefore the tourmaline from the Li-bearing type pegmatites is biased since many phases of tourmaline may be present in these pegmatite bodies. However, no other tourmaline phases were observed in the largely mined out Li-bearing pegmatites but Fuchsloch et al. (2018*b*) points out the importance of co-crystallising phases that may compete for elements such as Mn and Fe in the pegmatites. Perhaps since Li becomes a dominant mineral phase in the Li-bearing pegmatites, Li is consumed by petalite and spodumene instead of later-stage tourmaline and therefore the species elbaite is not able to crystallise. Whether species such as elbaite have already been mined out or were never present is unknown.

6.7.1.2 Trend two of the 2-fold trend

During the second stage of the 2-fold trend, Fe contents decrease rapidly (Fig. 6.4D), to lower contents than initial tourmaline and Ti contents gradually continue to decrease. Na, Al and Mn contents increase; however, the Mn contents have a delayed response, only increasing in value at around 0.8 a.p.f.u. Al (Fig. 6.4B,F). The Na content increase at late-stages of tourmaline crystallisation is common and London (2008) proposed the mechanism:

$$NaF(\square OH)_{-1} \qquad (6)$$

Although the light elements, O, H and Li are not measured, their behaviour is implied in this exchange vector. Similarly, other mechanisms that imply the behaviour of light elements can account for the Mn and Al increases and Fe decreases (Federico et al., 1998; Novák *et* al., 2004; London 2008; Henry and Dutrow, 2012):

$$AlO(FeOH)_{-1} \qquad (7)$$

$$LiAlMnFe_{-3} \qquad (8)$$

Substitution mechanisms (7) and (8) largely involve the depletion of Fe, however, to what extent each mechanism is operating is unknown since the concentrations of the light elements are assumed. Likewise, but to a far lesser extent since concentrations are already very low (Fig. 6.4E), the gentle decrease in Ti can be accounted for by the minor substitution mechanism:

$$AlTi_{-1} \qquad (9)$$

Roughly 30% of the dataset continue to the second stage of the 2-fold fractionation trend and only the Ta-Nb-Sn and Nainais type pegmatites show these compositions (Fig. 6.4, 6.5). The Nainais pegmatites show the most evolved nature and contain the largest elbaite component together with exception of Sample 1-1 (Fig. 6.5B). These fractionation patterns and substitution mechanisms (6) to (9) are common for late-stage tourmaline in Li-poor pegmatites (Henry and Guidotti, 1985; Roda et al., 1995; Gaweda et al., 2002) and have been recorded in many other examples (Jolliff et al., 1986; Jiang et al., 1997; Tindle et al., 2002; London, 2008; Zheng et al., 2016). In terms of whole-rock geochemistry and compositional trends in Ta-Nb-Sn oxides (Fuchsloch et al., 2018*a,b*) the Nainais pegmatites of the Central Tin Belt show no differences from the Ta-Nb-Sn type pegmatites in the CUPB, however, tourmaline data is the first to show major difference, reaching the most Li-rich evolved character. Li was not recorded in the whole-rock from Fuchsloch et al. (2018*a*) and perhaps this signature might have been recorded if Li was analysed, however, it is

also notable that the Nainais pegmatites are quartz-poor, contain lepidolite and when compared to the CUPB, perhaps indicates higher levels of Li in specific. Muscovite mineral chemistry is, however, yet to be studied and more insight into this feature is required since a variety of muscovite colours occur such as yellow and green.

6.7.2 Pegmatite source

In a recent publication, Novák et al. (2011) pose the question: "what factors control the specific composition of tourmaline". Aside from the B content, peraluminous nature, fO_2 conditions and internal pegmatite processes (Foit and Rosenberg, 1979; London, 1996; Slack, 1996; Wolf and London, 1997; Fuchs et al., 1998; Keller, 1999; London, 1999) we examine a possible source control on tourmaline and attempt to contribute to the debate on pegmatite magma genesis from an empirical stand point.

Jahns and Burnham (1969), reviewed and summarised in London (2008) and Simmons and Webber (2008), proposed that pegmatites formed from residual late-stage granitic fluids, after the granitic parent has undergone significant fractionation in order to concentrate the rare-elements observed in pegmatites. These late-stage magmas (pegmatitic magmas) progressively separate from the granitic parent; the later in the genesis of the granite, the more fractionated and rare-element enriched the magmas become and intrude to higher levels within the host-rock (e.g. Simmons and Webber, 2008). However, this model, although favoured by many researchers, does not satisfactorily explain the diverse features of pegmatites in totality. Some authors believe that some pegmatites and pegmatite provinces are generated by low degrees of fluidised partial melting directly from a source rock instead of having a granitic interim or parent (Walker et al., 1989; Nabelek et al., 1992; Simmons and Webber, 2008).

In a recent publication on the CUPB, Fuchsloch et al. (2018*a*) provide evidence that the pegmatites are most likely formed by direct partial melting and are not genetically related to the granites in the CUPB. Evidence for this is based on the distinct whole-rock geochemical differences between granites and pegmatites and the lack of the classical pegmatite zonation pattern (see Černý, 1989) surrounding granitic bodies in the CUPB. With regards to the composition of tourmaline we must consider what chemical signature the source would have on the tourmaline composition. Does a

granitic source as in the Jahns and Burnham (1969) model have a different signature to that of a direct partial melt to produce a pegmatitic magma? Does potential contamination overprint this signature?

The ferromagnesian component in pegmatites is mostly represented by tourmaline and B in the initial pegmatite magma should consume all the ferromagnesian components first via tourmaline crystallisation (London, 2008). Once the ferromagnesian components are depleted in the magma, more fractionated and evolved tourmaline compositions begin to reflect the overall progress of fractional crystallisation. If we ignore potential contamination for now (see below), one would expect pegmatitic magma, generated via separation from a granite undergoing fractionation, to be almost completely depleted in ferromagnesian elements since initial granitic crystallisation would likewise deplete the granitic magma of its ferromagnesian components. McDermott (1986) shows this to be true for the Salem-type and Red and Grey granites of the Damara Orogen where the Mg content decreases with increasing Si contents. Tourmaline from pegmatites in CUPB, however, show extremely high Mg, Ti, and Ca values (Table 6.2; Fig. 6.4, 6.5) which is rarely seen in tourmaline that has a pegmatitic origin (e.g. Novák et al., 2011). Initially, this provides further evidence that the pegmatites are not related to the granites of the CUPB since the ferromagnesian component should have been consumed by initial granitic crystallisation and the resulting pegmatites depleted in ferromagnesian elements which is not the case. We suggest that by generating a pegmatitic magma via low volume partial melting, it obtains its own ferromagnesian component that must be consumed at the onset of crystallisation and therefore the ferromagnesian tourmaline compositions observed in the CUPB reflect this initial ferromagnesian component and suggest a low volume partial melting model for the pegmatites of the CUPB. Furthermore, this also suggests that pegmatites with a partial melting origin may achieve economic Li concentrations and complex mineralogical zonation patterns (e.g. the Petalite pegmatite; Fig. 6.1).

Other authors would argue that these highly ferromagnesian signatures in pegmatitic tourmaline represent the extremities of contamination whereby elements such as Mg, Ti and Ca are sourced from a metasedimentary host-rock rich in these elements and tourmaline is the dominant mineral to utilize these elements in crystallisation (Fig. 6.5C; Tindle et al., 2002). The composition and rock type of the contaminant would therefore be particularly important (Federico et al., 1998), and

Tindle et al. (2002) specifically show different contamination signatures by granitic host-rocks compared to mafic host-rocks. One might expect such contamination signatures from the Ta-Nb-Sn, Li-bearing and Nainais type pegmatites since they intrude biotite schists, however, specifically, the Gnt-Tml type pegmatites likewise show significant Mg, Ti and Ca enrichment (Fig. 6.4A,C,E, 6.5C), similar to the other pegmatites types which precludes contamination as the main factor in element enrichment for this pegmatite type. In summary, contamination cannot account for the significant ferromagnesian component of the Gnt-Tml type pegmatites. Likewise, Fuchsloch et al. (2018*a*) show that contamination played very little role in element diversity for all the pegmatites of the CUPB with regards to Sn, Ta and Nb. Some pegmatites in the CUPB do show exocontact tourmaline similar to most pegmatite provinces rich in B (London, 2008), however, this is not a ubiquitous feature and tourmaline from pegmatites without exocontact tourmaline likewise show extremely high ferromagnesian signatures. Exocontact tourmaline likely represents the ability for late-stage fluids to migrate into the country rock, enriching them in B, Sn, Ta, Nb and Cs (Fuchsloch et al. 2018*a,b*).

Intracrystalline tourmaline zonation commonly occurs with a reverse trend where outer zones are more primitive to core zones and London (2008) suggests that this represents a late-stage where the pegmatite system becomes open and elements such as Mg, Ti, Ca and Fe from the country rock leach into the pegmatite magma. Consequently, tourmaline rims become more ferromagnesian and primitive, however, the compositional zonation pattern of the few tourmaline grains in this study do not show this feature and more gains become more evolved toward the rim of the grain (Fig. 6.2A). This supports the argument of Fuchsloch et al. (2018*a*) that the net flow of late-stage pegmatitic fluid was outward and Sn was not sourced from the country rocks. The mineralisation controls suggested by Diehl (1993) and Richards (1986) are therefore unlikely, that Sn was remobilised from country rocks by late-stage fluids. Most evidence points to contamination playing little role in tourmaline compositional variations and signatures and therefore more likely indicates that the pegmatites form from direct partial melting of a metapelitic source (see Fuchsloch et al. 2018*a*) and acquire their own ferromagnesian component which is reflected in the tourmaline compositions from the CUPB.

6.8 Conclusions

Initial tourmaline compositions from the CUPB show a significant ferromagnesian (Mg-rich) component, which is uncommon in pegmatitic derived tourmaline and undocumented previously in tourmaline from pegmatites in the Damara Orogen. The ferromagnesian components are significantly depleted in the first trend of the 2-fold trend observed during fractionation, which coincides with increases in the Fe and Al content. During the second stage of the 2-fold trend, Fe is now depleted and Na, Mn and Li enriched similar to evolved tourmaline compositional fractionation trends. These compositional trends are summarised by the substitution mechanisms (1) to (9).

Nainais type pegmatites from the Central Tin Belt show distinguishable highly evolved tourmaline compositions whereas, and unexpectedly, the Li-bearing pegmatites show significantly primitive tourmaline composition. Specifically, for the Li-bearing pegmatites, the lack of evolved compositions are either the result of competing mineral phases such as petalite or the present day absence of evolved tourmaline from the zoned Li-bearing pegmatites, pointing out the importance and hindrance of pegmatite zonation in belt wide studies of tourmaline. The lack of evolved tourmaline compositions from the Gnt-Tml pegmatites confirms that these pegmatites represent the most primitive pegmatites in the belt.

We suggest that the highly ferromagnesian compositions of initial tourmaline reflect a mafic component in the initial pegmatite magma that was derived from a direct partial melt of a metapelitic source. This is relatively new idea to our knowledge since previously highly ferromagnesian components in pegmatitic tourmaline were attributed to contamination which is unlikely for the CUPB pegmatites. If a granite parent was the source of the pegmatites, the granitic magma would have already consumed the ferromagnesian elements and resulting pegmatites would lack this highly ferromagnesian signature in tourmaline.

6.9 Acknowledgements

We thank Rhodes University for access to the Electron Microprobe which is partially funded by NRF National Equipment Program grant UID 74464. The CIMERA research centre provided significant researching funding for this project and we are indebting to them accordingly.

Chapter 7: The Cape Cross-Uis pegmatite belt: overview and discussion

7.1 Introduction

This chapter is designed to highlight and summarise the most important findings of the three articles on which this thesis is based: Fuchsloch et al. (2018*a,b,c*). It will lack the finer details of the original publications; however, it will tie the work of all three articles together and compare them in a regional sense to the other pegmatites of the Damara Belt.

The chapter is designed to display a geological history of the pegmatites from the Cape Cross-Uis pegmatite belt (CUPB), from pegmatitic melt generation and magma migration to structural emplacement, consolidation and final mineralisation of the pegmatites.

7.2 Pegmatitic melt production

This section hinges on Section 3.4.1 and assesses whether the pegmatitic melts that gave rise the pegmatites of the CUPB were produced via anatexis or are related to the surrounding Salem-type Granites in a parent-daughter type relationship. Assessing these two end member models of pegmatite melt generation is a difficult task and more often than not relies on a lack of supporting evidence rather than direct evidence.

7.2.1 Granite related

Originally, several authors proposed that the pegmatites of the Damara Belt were related to the Salem-type Granites in the classical Jahns and Burnham (1969) model (Miller and Mittlefehldt, 1982; Mittlefehldt and Miller, 1983; Phillips, 1981). In adherence to the model, the authors suggested that the pegmatites of the Damara Belt are progressive magmatic separates from a parent Salem-type Granite undergoing fractional crystallisation. However, these studies were based on regional scales, concurrent with assessment of other geological aspects of the Damara Belt and no detailed specific attention was paid to the pegmatite intrusions. Furthermore, the pegmatites of the CUPB and Damara Belt have not been scrutinised in the sense of their origin until recently (Owen, 2011; Freemantle, 2012; Longridge, 2012; Ashworth, 2013; Fuchsloch et al., 2018*a,c*).

Fuchsloch et al. (2018*a*) discounted a granite-pegmatite relationship for the pegmatites of the CUPB, stating a lack of evidence based on detailed field studies and whole-rock geochemistry of

the pegmatites: Fuchsloch et al. (2018*a*) first observed that there was likely to have been a significant time gap between the syn-tectonic Salem-type Granites and pegmatite intrusions within the CUPB, based on structural and deformational characteristics, although dating of both has not yet been evaluated. Furthermore, the pegmatites of CUPB should show a spatial association with potential parent granites if the Jahns and Burnham (1969) model is applied in this case (e.g. Baker, 1998). However, Fuchsloch et al. (2018*a*) found no spatial correlation between granite bodies and pegmatites of increasing element complexity with further distance away from granites (Section 3.2). Fuchsloch et al. (2018*b*) then supported this showing that fractionation levels within CGM and cassiterite from pegmatites have no spatial correlation to the granites of the CUPB (Fig 5.11).

Aside from a timing aspect and spatial association, since underlying granites may be present and in unique shapes, the bulk evidence of Fuchsloch et al. (2018*a*) is based on whole-rock geochemistry which is shown to be reliable data due to the finer-grained border zones of the pegmatites (Fig. 2.9). Apatite data supports the fact that the whole-rock analysis of Fuchsloch et al. (2018*a*) is reliable due to REE content in apatite being undetectable by microprobe analysis (see Appendix C discussion on apatite data).

If pegmatites are related to granites as in the classical Jahns and Burnham (1969) model, there should be geochemical similarities between them. For example, using fractionation indicators from whole-rock data, pegmatites and granites should lay on a similar fractionation trend where pegmatites have higher levels of fractionation (i.e. from granite to pegmatite). However, the data points of pegmatites and granites should not overlap within the trend (Jolliff et al., 1992). Fuchsloch et al. (2018*a*), using fractionation indicators such as K_2O/Rb vs. Rb, showed that pegmatites and granites in the CUPB in some cases lie on completely different fractionation trends. Furthermore, when a similar trend was observed (Ta/Nb vs. Rb/Cs) the granite and pegmatite data significantly overlapped suggesting a decoupling of elements which precludes an origin from a single starting composition (Jolliff et al., 1992; Fuchsloch et al., 2018*a*).

The geochemical logic of the Jahns and Burnham model implies that incompatible elements should favour the pegmatitic melt when created within the granitic body and therefore should subsequently be enriched compared to the parent granitic melts. Although the peraluminous nature

of LCT pegmatites suggests low REE concentrations within subsequent pegmatitic melts (Cullers and DeGraf, 1992), Fuchsloch et al. (2018*a*) found that pegmatites in the CUPB have a two order of magnitude difference in the REE contents compared to the Salem-type and Red and Grey Granites (Appendix B). It is notable that the granites are also peraluminous and that peraluminosity alone could not account for such a difference. In most cases, REE values in pegmatite were undetectable by ICP-MS. This observation is not unique to the CUPB, however, authors in the past would explain the phenomena by suggesting that the REEs partitioned into late-stage vapour of fluid phases which subsequently caused large amounts of alteration of the pegmatite (Simmons et al., 1986). This requires that the REEs are trapped within the alteration zones and therefore whole-rock analysis of fine-grained border zones do not pick up high REE contents. However, Fuchsloch et al. (2018*a*) analysed the replacement alteration zones (Appendix D) of the pegmatites and found that they are even more depleted in REE contents than border zones and therefore suggested that the pegmatites are not related to the granites within the CUPB.

In summary, there is a lack of direct evidence that pegmatites in the CUPB are related to the Salem-type Granites as the granites and pegmatites share no spatial association and geochemical characteristics. whilst, more direct evidence should be acquired, structural and deformational characteristics suggest a significant time difference between granite and pegmatite emplacement, in the future precise age dating of both should be evaluated.

7.2.2 Anatexis

It is difficult to give direct evidence that a pegmatitic melt was generated via hydrous partial melting of a source rock since more often than not, the pegmatitic melt will migrate and be emplaced at higher crustal levels. However, there are some cases where in situ partial melting and subsequent crystallisation has occurred without migration of the magma which provides direct evidence that a pegmatite was the result of anatexis (e.g. Snook, 2014). Field evidence such as contact aureoles should be apparent when there is a case of in situ partial melting and further consolidation of magma. However, pegmatites of the CUPB display no field evidence of in situ crystallisation and therefore must have migrated to some distance away to final emplacement depths (Ashworth, 2013; Fuchsloch et al., 2018*a*). The lack of contact aureoles also implies that the pegmatites were the result of metamorphism and not its cause. Other geochemical linear trends

should also be observed between pegmatites and country rocks in the case that in situ melting and subsequent crystallisation occurred which were not observed by Ashworth (2013) (Jung et al., 1998).

A growing number of authors now favour a partial melting model for generation of pegmatitic melts, specifically for the LCT type pegmatites (Černý, 1991*a*; Martin and De Vito, 2005; Ashworth, 2013; Snook, 2013). In essence, authors that favour an anatexis model for pegmatites argue that the Jahns and Burnham (1969) model cannot produce pegmatitic melts with the compositional diversity we see at present (e.g. Walker et al., 1989) and therefore the hydrous partial melting of a heterogeneous source must occur to generate the compositional diversity in pegmatites. As an analogy, the Jahns and Burnham model may be compared to a water filter. The granitic melt acts as the filter (internal magmatic processes), and various compositions (initial granitic composition) of water are sieved through the filter. The water that comes out is essentially depleted in certain elements and has a higher concentration of water and in the case of pegmatites, incompatible elements. This process restricts the possible compositional diversities the end product may have (i.e. a buffer) since all pegmatites share a similar granitic process (the filter). For example, the granitic melt should deplete itself of its mafic/ferromagnesian components first due to fractionation within the magma chamber and the Fe and Mg content of subsequent pegmatites should be negligible. This feature is observed in some cases and London (2008) notes that Fe-Mg-bearing phases are a rarity in pegmatites, Fe mostly being consumed during early crystallisation by schorl and the Mg end member, dravite, completely absent in pegmatite-derived tourmaline.

Tourmaline data acquired by Fuchsloch et al. (2018*c*) shows highly ferromagnesian compositions which plot well within the field of 'Tourmaline Derived from Metasedimentary Lithologies' as defined by Henry and Guidotti (1985) (Appendix C). This was an interesting observation by Fuchsloch et al. (2018*c*) since even the complex Li-type pegmatites showed such ferromagnesian compositions of tourmaline which should not occur rather evolved tourmaline phases such as elbaite and rossmanite should be a hallmark of such complex pegmatites. Fuchsloch et al. (2018*c*) attributed the ferromagnesian compositions to be a reflection of the source of the pegmatites and evidence that the pegmatites were derived from anatexis of said source. They based this theory on

the fact that if the pegmatites were derived from granitic magmas, the ferromagnesian components should have been preferentially fractioned out of the system before the late-stage onset of pegmatite melt production within the granitic magma chamber. Furthermore, the authors suggested that the ferromagnesian compositions were direct evidence that pegmatitic melts derived from anatexis would obtain their own, however small, ferromagnesian component during melting and be reflected in the subsequent tourmaline compositions (no granitic filtering of mafic components). Some authors might argue that crustal contamination introduced the ferromagnesian components (Tindle et al., 2002), however, this was discounted by the fractionation trends in individual tourmaline grains and the whole-rock geochemistry of Fuchsloch et al. (2018*a*).

Identifying a possible source rock undergoing anatexis to produce a pegmatite is difficult since the mineral reservoirs of certain elements are poorly understood (London, 2008). For example, London (2008) suggested that melting an ilmenite-bearing source rock would yield sufficient Ta and Nb to produce Ta-Nb-Sn mineralised pegmatites. Likewise, if biotite is retained in the source and muscovite is melted preferentially, an orthoclase restite is formed which acts as a Ba sink (London, 2008). Fuchsloch et al. (2018*a*) used that hypothesis to account for the low concentrations of Ba in the pegmatites compared to the high concentrations in the granites of the CUPB. Muscovite is also known to be a reservoir for Li, Cs, Rb and Be in a source rock (London, 2008). In summary, due to peraluminosity of the pegmatites, their significant concentrations of Ta, Nb and Sn and poor Ba values, Fuchsloch et al. (2018*a*) suggested an ilmenite-muscovite metapelitic source for the pegmatites of the CUPB and that pegmatitic melts were generated via anatexis of that source, confirming observations by previous authors (Jung et al., 2003; Freemantle, 2012; Ashworth, 2013; Fuchsloch et al., 2018*b,c*).

7.3 Structural timing and emplacement

The pegmatites of the CUPB intrude various structural features (Section 2.3; Fuchsloch et al., 2018*a*) including folds, faults and tension gashes. The deformational history of the Damara Belt is well documented (Section 1.2.2) which led authors such as Richards (1986) and Wagener (1989) to suggest that pegmatites were syn-genetic with the structures they intruded, implying a magmatic episode that lasted from early syn-tectonic to post-collisional times. Longridge (2012) then re-evaluated the deformational and magmatic history of the Damara Belt and concluded that the

voluminous granitoids of the Damara Belt were produced during peak thermal metamorphic conditions, at approximately 850 °C and 520 Ma, caused by crustal relaxation and orogenic collapse. Longridge (2012) then proposed that the pegmatites of the Central Zone were emplaced shortly after peak metamorphic conditions between 510 and 505 Ma. However, Haack and Gohn (1988) and Diehl (1993) reported ages for the Uis pegmatites of 496 and 486 Ma respectively, based on Rb-Sr data. Despite these ages being potentially unreliable due to dated technologies and now inappropriate isotope systems, they indicate ages that are significantly younger than peak metamorphic conditions, considering pegmatites may crystallise in as short a time as a few decades and pegmatitic magma accent would have been rapid (London, 2008).

After the pegmatitic melt was created at source, the magmas would have migrated to the current emplacement depths observed today since no field evidence of anatexis and in situ consolidation is observed (Ashworth, 2013). The abundance of H_2O, P, B, and F in the pegmatitic melt would have reduced its viscosity and crystallisation temperatures, essentially delaying crystallisation to facilitate further transportation (Jung et al., 1998; Nabelek et al., 2010). Pegmatites would have therefore migrated from their source rapidly, ascending through the crust to their final emplacement depths. This implies that the whole-rock geochemistry of Fuchsloch et al. (2018*a*) closely represents the bulk magmatic composition of the pegmatites, shortly after emplacement sites were achieved, aside from some elemental loss to the surrounding country rocks (e.g. Morgan and London, 1987)

Pegmatites of the CUPB generally have a structural framework similar to the dominant, belt wide, northeast lineation, however, Fuchsloch et al. (2018*a*) found some cases where the pegmatites completely cross-cut Damaran-aged structures. Furthermore, the authors found no observable deformational features within the pegmatites themselves on the macro- and microscopic-level. Only a few cases were present where quartz or muscovite showed deformational features such as folding and an undulatory extension (Fuchsloch et al., 2018*a*). The only macroscopic observation was where thin pegmatite veins were boudinaged. These details led Fuchsloch et al. (2018*a*) to suggest that pegmatites are exclusively post-tectonic in age, confirming a significant time gap between granites and pegmatites. Furthermore, pegmatite magmas would have utilised the

structural weaknesses in the crust, intruding, for example, D_3-folds, however, the presence of the pegmatites in these structures does not imply a consanguineous age.

The pegmatites of the CUPB are likely to have originated post-tectonically during further crustal relaxation. The thin boudinaged pegmatite veins support a continued, less intense, extensional environment, being the only Damaran orientated structures to macroscopically deform the pegmatites. A high heat flow provided by the voluminous granitic magmas and the continued decrease in pressures due to orogenic collapse would have facilitated the production of fluidised, very low degree partial melts, perhaps at higher crustal levels compared to granite source rocks, since granitic source rocks would already be in the restite state and further melting is unlikely.

7.4 Crystallisation to mineralisation

Mineral chemistry is a useful tool for tracking the chemical changes in a pegmatitic magma during crystallisation, especially when the mineral in question has the potential for accommodating an abundance of different elements. Fuchsloch et al. (2018*c*) used the mineral chemistry of tourmaline whereas Fuchsloch et al. (2018*b*) used CGM and cassiterite to track the chemical evolution of CUPB pegmatites for the early and late stages of crystallisation, respectively. Tourmaline and Ta-Nb-Sn-oxides only co-occur in one sample and therefore track the chemical evolution of the pegmatites at different stages of crystallisation (Appendix A): Tourmaline tracks the initial stages, it is found in border zones, and areas of little alteration; Ta-Nb-Sn-oxides track the late stages, limited in magmatic zones with an equigranular texture, abundant in greisenised and albitised zones. Notably, tourmaline often co-occurs with the minor Li-phases within the pegmatites indicating similar crystallisation times (Fuchsloch et al., 2018*a,c*).

Fuchsloch et al. (2018*c*) found tourmaline compositions to have a 2-fold fractionation trend. Early tourmaline compositions are Mg-, Ti-, Na- ± Ca-rich (Dravite) and with continued crystallisation and fractionation the compositions become depleted in Mg, Ti, Na and Ca with increasing amounts of Fe and minor Al. After the full depletion of Mg and Ca in tourmaline to negligible values, tourmaline compositions are then essentially Fe-Al-phases (Foitite). Following continued crystallisation in the second stage of the 2-fold trend, Fe values in tourmaline rapidly drop to be replaced by further Al and Mn, Li and minor increases in the Na content. It is at the transition from

stage one to two in tourmaline when the Ta-Nb-Sn-oxides potentially play a large role (Fuchsloch et al. 2018*b*) such that late-stage tourmaline crystallisation overlapped with early stage CGM, as shown in one sample where both phases are found (Appendix A). In the overlap, the rapid drop of Fe contents in tourmaline can be accounted for by highly Fe-rich CGM phases beginning to crystallise within the pegmatitic magma (tourmaline competes for Fe but Fe favours CGM). CGM minerals continue to have highly Fe-rich contents throughout fractional crystallisation with little change in the Mn content, as shown by the Ta/Ta+Nb number in CGM (Ferrocolumbite → Ferrotantalite; Fuchsloch et al. 2018*b*). CGM compositions then show little change with regard to their major-element contents, conforming to Fe-rich phases during crystallisation and Fuchsloch et al. (2018*b*) attributed this to other phases competing for Mn in the magma.

Minerals in competition with one another for specific elements in a pegmatitic melt is not a universally accepted model for Ta-Nb-Sn oxides (e.g. Wise et al., 2012), however, using the minor element trends in CGM, Fuchsloch et al. (2018*b*) discounted a low F activity as the sole cause for no apparent change in the Mn content in CGM. Furthermore, the authors favour the hypothesis of Van Lichtervelde et al. (2007) that Fe-enrichment is the natural state of CGM evolution. The transition of tourmaline to CGM crystallisation supports this argument where Fe favours CGM once stabilised, coinciding with a decrease in the Fe content in tourmaline with ongoing fractionation (Fuchsloch et al. 2018*b,c*).

Cassiterite, and to a lesser extent, CGM mineralisation within the pegmatites of the CUPB was a focus of many previous authors (Richards, 1969; Diehl, 1993; Singh, 2007) with most suggesting that assimilation of country rocks was the cause of Sn-enrichment in pegmatites, Sn being sourced from Knotenschiefer host rocks (Section 2.2.3). Fuchsloch et al. (2018*a*) evaluated this hypothesis in detail using both field observations and whole-rock geochemistry. Initially the authors investigated the style of mineralisation in the alteration zones of the pegmatites and found that the morphologies of most greisens suggest that alteration fluids were trapped (e.g. by larger feldspars crystals), implying no 3D fluid interconnected network that might have remobilised Sn from country rocks in a circulating hydrothermal system suggested by Diehl (1993). Therefore, in such cases, Sn crystallised in situ in a closed system and was able to reach wt % concentrations (Fuchsloch et al. 2018*a*).

Fuchsloch et al. (2018*a*) then evaluated the geochemistry of the pegmatites, tourmalinised host rock contacts and host rocks far from contacts. They found minimal concentrations of Sn (Approx. 70 ppm) in host rocks at some distance from pegmatites and concluded that such large amounts of melting and assimilation of country rock would be required to enrich pegmatites to wt% levels. Furthermore, considering the low temperatures of pegmatite crystallisation, found by Ashworth (2013; approx. 450 °C), the amount of heat required for such great amounts of assimilation would be far higher.

Fuchsloch et al. (2018*a,c*) then noted that assimilation or late-stage remobilisation of Sn should be indicated by whole-rock geochemistry and tourmaline compositions and mineral zoning. Fuchsloch et al. (2018*a*) then used McKeough et al. (2013) pegmatite hybridization factor to test if accompanying elements such as Mg, Ca and Fe increased within pegmatites with a correlation to Sn and found no such case, suggesting Sn was not sourced from country rocks. Fuchsloch et al. (2018*c*) then confirmed this hypothesis by showing that tourmaline crystals which are concentrically and regularly compositionally zoned imply that there were no outer elemental influences acting on the pegmatitic magma during the later stages of petrogenesis. In cases of assimilation, tourmaline rims should revert back to primitive schorlitic compositions (green core and black rim; e.g. Tindle et al., 2002; London, 2008; Novák and Škoda, 2011).

By comparing Sn, Ta and Nb to whole-rock fractionation indicators, Fuchsloch et al. (2018*a*) showed that these elements increase greatly within the pegmatite magma during fractional crystallisation and that they are likely to have originated from the pegmatites source, since no evidence was found that Sn, Ta and Nb were sourced from country rocks. This was confirmed later by Fuchsloch et al. (2018*b*) who showed, using minor element trends and fractionation indicators in CGM that internal magmatic fractionation was the dominant cause of Sn, Ta and Nb enrichment. Furthermore, the authors showed that during late-stage pegmatite petrogenesis, elements such as Sn would have likely to have been partitioned into an exsolved pegmatitic aqueous fluid phase by complexing with Cl and subsequently developing highly Sn-mineralised greisens and albitised zones (Nabelek, 2010). Fluid inclusion work by Ashworth (2013) confirmed the presence of Cl in

fluid compositions in the late-stage hydrothermal fluids and also suggested the complexing of Ta, Nb and Sn with Cl.

Some authors discount the mobility of Ta and Nb in exsolved aqueous fluids, suggesting, based on limited experimental evidence, that Ta and Nb do not partition into these fluids (Van Lichtervelde et al., 2007; Discussion in Chapter 5). Although this is a highly debated subject, Fuchsloch et al. (2018*c*) suggested that Ta and Nb do partition into the exsolved aqueous fluid which subsequently causing alteration and mineralisation. The authors based this hypothesis on the evidence of the intimate relationship between CGM minerals and cassiterite, the higher abundances of Ta-Nb-Sn-oxides in greisenised zones and the elevated Ta, Nb and Sn concentrations in metasomatic host rocks. Furthermore, they pointed out that the existing experimental evidence is limited (Chevychelov et al., 2004) to F-bearing fluids at far higher temperatures that those at which to pegmatites crystallised. No additional experimental evidence exists at pegmatitic conditions with a range of fluid chemistries and therefore it cannot be discounted that Ta and Nb may partition into late-stage exsolved pegmatitic aqueous fluids.

7.5 Regional setting and pegmatite classification

On the regional pegmatite belt scale, discerning regional trends is difficult, mainly because no pegmatite spatial association with granitic bodies is apparent (Section 3.2). However, Fuchsloch et al. (2018*a*) did confirm certain differences between the pegmatite swarms and later Fuchsloch et al. (2018*c*) showed that tourmaline compositions in the Nainais pegmatite belt were slightly different to those in the CUPB.

Firstly, the authors showed that the pegmatites surrounding the Uis area (Fig. 2.4) are cassiterite-rich with minor CGM minerals only occurring as inclusions in cassiterite and rarely as individual grains. The Strathmore swarm is host to the only known complexly mineralogically zoned pegmatites (Petalite and SP14; Fig. 2.2) that have significant Li mineralisation in the form of petalite and secondary Li-phases. The Karlowa swarm is unique in the fact that Li-phases occur as spodumene, suggesting crystallisation at higher pressures (London, 2008) in the swarm. The Nainais pegmatites were shown to be indistinct compared to the Nb-Ta-Sn type pegmatites of the CUPB, even though they belong to a Nainais-Kahero belt (Fuchsloch et al. 2018*a*). However, later

work by Fuchsloch et al. (2018*c*) shows that tourmaline compositions in the Nainais pegmatites show significantly more evolved compositions (elbaite) compared to tourmaline from the CUPB. In addition, tourmaline from the Nainais pegmatites shows regular crystal zonation from core to rim.

Many aspects of the CUPB pegmatites are comparable to other pegmatites worldwide and Fuchsloch et al. (2018*a,b,c*) document these comparisons in three papers presented in chapters 4, 5 and 6. For example, the low whole-rock REE values of any of the CUPB pegmatites is in strong contrast to the pegmatites in Colorado described by Simmons et al. (1986). Significantly ferromagnesian tourmaline compositions presented by Fuchsloch et al. (2018*c*) are documented rarely, for example, the primitive pegmatites of Moldanubium Zone, Czech Republic described by Novák et al. (2004). When comparing pegmatites in a regional sense it is more appropriate to compare their classification since different classes occurring in similar areas might provide insight into the shortfalls of the currently used classification schemes.

The pegmatites of the CUPB are classified as LCT type, with further designations into Rare Element class, Li subclass, Complex type (Fig. 3.2) with a variety of sub-types, in accordance with Černý and Ercit (2005). The fractionation patterns in CGM minerals have also been used as a classification tool (Černý and Ercit, 1989) and Fuchsloch et al. (2018*b*) confirms a Complex type for the pegmatites of the CUPB. However, The Gnt-Tml type pegmatites (Section 2.3.2) of the CUPB may show a slight NYF affinity: higher Nb values relative to Ta values, negligible whole-rock Li and Cs contents, atypical Ta-Nb fractionation patterns in CGM and significantly higher REE contents than other pegmatite types in the CUPB (values still lower than those of granites; Fuchsloch et al. 2018*a,b*). Although an apparent NYF affinity may be present in the Gnt-Tml type pegmatites, they cannot be classified as mixed LCT-NYF type pegmatites since crustal contamination has been shown previously to be negligible (Section 3.3.2). This observation points out the shortfalls in the Martin and De Vito (2005) classification scheme whereby NYF and LCT pegmatites should occur in different tectonic settings and thus not be closely associated with one another as described here for the CUPB (Section 3.4.1.2).

Ashworth (2013) made a similar observation in the regional study of the pegmatites of the Damara Belt: with coeval NYF and LCT pegmatites occurring at the same time within the same orogenic belt. In addition, other observations were also made in the Kibaran pegmatites of South Africa and the Pan-African pegmatites of Mozambique whereby NYF and LCT type pegmatites both occur within the same tectonic setting (Hugo, 1969 and Von Knorring and Condliffe, 1987, respectively).

Chapter 8: Summary and Conclusions

8.1 Introduction

The main purpose of this study was to build a petrogenetic model and create a geological foundation for the pegmatites of the Cape Cross-Uis pegmatite belt since previous academic work is limited and sparse for such an important mineralised pegmatite belt. This chapter outlines and summarises the conclusions of this thesis and it is derived from publications found in Chapter 4 to 6.

8.2 Summary and conclusions

The pegmatitic melts that gave rise to the pegmatites of the CUPB were likely to have been created by direct crustal anatexis of an ilmenite-muscovite metapelitic source rock. Lack of evidence to support a Jahns and Burnham (1969) type model and the presence of an initial ferromagnesian component in tourmaline support this hypothesis. Deformational features, or lack thereof, of the pegmatites indicate a post-tectonic timing of pegmatitic melt generation, which is likely to have resulted from further crustal relaxation during orogenic collapse.

Pegmatite melt migrated from the site of crustal anatexis as no field evidence indicates in situ melting and crystallisation. Migration was likely to have been rapid, due to the high flux contents of the melts, and pegmatites were subsequently emplaced in various Damara-aged structures, capitalising on the weaknesses in the crust. The pegmatites mostly have taken advantage of the northeast regional lineation within the Cape Cross-Uis pegmatite belt.

Pegmatite crystallisation underwent several stages of element activity which is tracked by the compositional variations on both tourmaline and CGM. Early crystallisation involved ferromagnesian depletion as tourmaline preferentially consumed Mg, Ti and Na within the pegmatite-forming magmas increasing the Fe and Al content of the residual melt. The magma then entered a stage where Fe was largely consumed by both tourmaline and early magmatic CGM. Fe favoured the CGM as their Fe contents are continually high compared to their Mn contents over a broad range of Ta/(Ta+Nb) values. Subsequently, the Fe contents in tourmaline decreased, being replaced by Li, Mn and Na producing evolved elbaitic compositions. CGM remained Fe-rich over

the course of its history into the late-stages of greisenisation where economic quantities are present along with cassiterite. Compositional trends in CGM and tourmaline indicate that competing mineral phases within the pegmatitic magma controlled the overall element movement into specific phases. Minor element trends in CGM confirm the presence of a late-stage hydrothermal fluid phase which subsequently caused large amounts of alteration in the form of greisenised and albitised zones. Fractionation within the magma is shown to be the dominant process in which incompatible elements concentrated into the late-stages of pegmatite petrogenesis. Elements such as Ta, Nb, B and Sn then complexed with Cl-rich fluids and entered the hydrothermal phase. The morphologies of greisens, geochemistry of host-rocks and pegmatites and a lack of contamination indicators in tourmaline and whole-rock geochemistry indicate that the Sn, Ta and Nb abundances in pegmatites are derived from its source rock and that crustal assimilation or late-stage remobilisation of elements from country rocks did not occur as previously thought.

8.3 Future potential research

This research has provided evidence to argue in favour of certain models and sets a standard for future research in a well-defined pegmatite belt showing a variety of characteristics, mineralisation and compositional diversity. The immediate primary focus of future research should be precise dating of the granites and pegmatites within the area to constrain their ages and confirm the suggested, significant, time gap between them. This task will be difficult since zircons within the pegmatites are metamict and monazite is a rarely seen phase. Furthermore, although dating of CGM minerals is more common in current times, the necessary standards are rarer, and the procedure is still uncommon to most analytical facilities. Perhaps apatite may be easier to date in future, however, given the undetectable values of U and Pb in the apatite data by microprobe (Appendix C), sufficient quantities which relate to accurate ages may be lacking.

As with many igneous rocks, isotopic studies should prove very useful in the pegmatites. They may confirm a different identity to the granites confirming no such parent-daughter type relationship exists. Other potential research is Ti in quartz thermometry and other mineral chemistry studies such as muscovite or feldspars to develop a greater understanding of the chemical evolution of the pegmatites.

References

Abraham, I. M. (2009). Geology and spatial distribution of uranium mineralisation in the SK anomaly area, Rössing area, Namibia. Unpublished M.Sc. thesis, University of the Witwatersrand, pp 184.

Alfonso, P.A., Corbella, M.C. and Melgarejo, J.C.D. (1995). Nb-Ta-Minerals from the Cap de Creus pegmatite field, eastern Pyrenees: Distribution and geochemical trends. *Mineralogy and Petrology* **55**, 53-69.

Alfonso, P. and Melgarejo, J.C. (2008). Fluid evolution in the zoned rare-element pegmatite field at Cap de Creus, Catalonia, Spain. *The Canadian Mineralogist* **46**, 597-617.

Ashworth, L. (2013). Mineralised pegmatites of the Damara Belt, Namibia. Fluid inclusion and geochemical Characteristics with implications of post tectonic mineralisation. Unpublished Ph.D. thesis, University of the Witwatersrand, Johannesburg.

Baker, D.R. (1998). The escape of pegmatite dikes from granitic plutons: constraints from new models of viscosity and dike propagation. *The Canadian Mineralogist* **36**, 255-263.

Ballourad, C., Poujol, M., Boulvais, P., Branquet, Y., Tartèse, R. and Vigneresse, J.-L. (2016). Nb-Ta fractionation in peraluminous granites: a marker of the magmatic-hydrothermal transition. *Geology* **44**, 231-234.

Barbarin, B. (1999). A review of the relationships between granitoid types, their origins, and their geodynamic environments. *Lithos* **46**, 605-626.

Barnes, S.J. and Sawyer, E.W. (1980). An alternative model for the Damara Mobile Belt. Ocean crust subduction and continental convergence. *Precambrian Research* **13**, 297-336.

Baumgartner, R., Romer, R.L. and Moritz, R. (2006). Columbite-tantalite-bearing granitic pegmatites from the Seridó belt, northeastern Brazil: genetic constraints from U-Pb dating and Pb isotopes. *The Canadian Mineralogist* **44,** 69-86.

Belousa, E.A., Walters, S., Griffin, W.L. and O'Reilly, S.Y. (2001). Trace-element signatures of apatites in granitoids from the Mt Isa Inlier, northwestern Queensland. *Australian Journal of Earth Sciences* **48:4***,* 603-619, DOI: 10.1046/j.1440-0952.2001.00879.x

Belousa, E.A., Griffin, W.L., O'Reilly, S.Y. and Fisher, N.I. (2002). Apatite as an indicator mineral for mineral exploration: trace element compositions and their relationship to host rock type. *Journal of Geochemical Exploration* **76**, 45-69.

Beurlen, H., Da Silva, M.R.R., Thomas, R., Soares, D.R. and Olivier, P. (2008). Nb-Ta-(Ti-Sn) oxide mineral chemistry as tracer of rare-element granitic pegmatite fractionation in the Borborema Province, Northeastern Brazil. *Mineralium Deposita* **43,** 207-228.

Beurlen, H., Ihlen, P.M., Martin, R., Muller, A., Simmons, W., Thomas, R. and Wise, M. (2013). Elaboration of a new classification of (granitic) pegmatites. *Pegmatite classification group,* draft version 20.12.2013.

Briqueu, L., Lancelot, J.P., Valois, J.P. and Walgenwitz, F. (1980). Géochronologie U-Pb d'un type de mineralisation uranifère: les alaskites de Goanikontes (Namibie) 231 et leur encaissant. *Bulletin du Centre de Récherches-Production, Elf-Aquitaine* **4**, 759-811.

Buddington, A.F. (1959). Granite emplacement with special reference to North America. *Geological Society of America Bulletin* **70**, 671-747.

Bühn, B., Stanistreet, I.G. and Okrusch, M. (1992). Late Proterozoic outer shelf manganese and iron deposits at Otjosondu (Namibia) related to Damara oceanic opening. *Economic Geology* **87**, 1393-1411.

Büttner, S.H., Reid, W., Glodny, J., Wiedenbeck, M., Chuwa, G., Moloto, T. and Gucsik, A. (2016).Fluid sources in the Twangiza-Namoya Gold Belt (Democratic Republic of Congo): Evidence from tourmaline and fluid compositions, and from boron and Rb-Sr isotope systematics. *Precambrian Research* **280**, 161-178.

Černý, P. (1989). Exploration strategy and methods for pegmatite deposits of tantalum. In: Möller, P., Černý, P. and Saupé, F. (eds.), Lanthanides, Tantalum and Niobium. *Springer-Verlag,* Heidelberg, pp.274-310.

Černý, P. (1990). Distribution, affiliation and derivation of rare-element granitic pegmatites in the Canadian Shield, *Geologische Rundschau* **79**, 183-226.

Černý, P. (1991*a*). Rare-element granitic pegmatites. Part I: Anatomy and internal evolution of pegmatite deposits: *Geoscience Canada* **18,** 29-46.

Černý, P. (1991*b*). Rare-element granitic pegmatites. Part II: Regional to global environments and petrogenesis. *Geoscience Canada* **18,** 49-62.

Černý, P. and Ercit, T.S. (1985). Some recent advances in the mineralogy and geochemistry of Nb and Ta in rare-element granitic pegmatites. *Bulletin de Minéralogie* **108,** 499-532.

Černý, P. and Ercit, T.S. (1989). Mineralogy of niobium and tantalum: crystal chemical relationships, paragenetic aspects and their economic implications. In: Möller, P., Černý, P. and Saupé, F. (eds.), Lanthanides, Tantalum and Niobium. *Springer-Verlag, Heidelberg*, pp. 27-79.

Černý, P. and Ercit, T.S. (2005). The classification of granitic pegmatites revisited. *Canadian Mineralogist* **43**, 2005-2026.

Černý, P., Chapman, R., Chackowsky, L.E. and Ercit, T.S. (1992*a*). A ferrotantalite-ferrotapiolite Intergrowth from Spittalad Drau, Carinthia, Austria. *Mineral Petrology* **41**, 53-63.

Černý, P., Ercit, T.S. and Wise, M.A. (1992*b*). The tantalite-tapiolite gap: natural assemblages versus experimental data. *The Canadian Mineralogist* **30,** 587-596.

Černý, P., Chapman. R., Ferreira, K. and Smeds, S.-A. (2004). Geochemistry of oxide minerals of Nb, Ta, Sn and Sb in the Varuträsk granitic pegmatite, Swede: The case of an "anomalous" columbite tantalite trend. *American Mineralogist* **89**, 505-518.

Černý, P., London, D. and Novák, M. (2012). Granitic Pegmatites as Reflections of their Sources. *Elements: An International Magazine of Mineralogy, Geochemistry, and Petrology* **8(4)**, 289-294.

Chappell, B.W. and White, A.J.R. (1974). Two contrasting granite types. *Pacific Geology* **8**, 173-174.

Chappell, B.W., Bryant, C.J. and Wyborn, D. (2012). Peraluminous I-type granites. *Lithos* **153**, 142-153.

Chevychelov, V., Zaraisky, C., Borisovsky, S. and Borkov, D. (2004). Partitioning of Ta and Nb between magmatic melt and aqueous (K,Na,H)F-containing fluid: effects of temperature and chemical composition of the melt: Experimental Mineralogy, Petrology and Geochemistry Symposium, 10th, Abstracts, *Lithos Supplement* **73**, pp.17.

Clarke, D.B. (1992). Granitoid Rocks. Chapman and Hall, London, pp. 283.

Clemens, J.D. (2014). Element concentrations in granitic magmas: Ghosts of textures past? *Journal of the Geological Society, London* **171**, 13-19.

Coward, M.P. (1983). The tectonic history of the Damaran Belt. *Special Publication of the Geological Society of South Africa* **11**, 409-421.

Cullers, R.L. and DeGraf, J.L. (1982). Rare earth elements in igneous rocks of the continental crust: intermediate and silicic rocks – ore petrogenesis. In: Henderson, P. (Eds.), Rare Earth Element Geochemistry. *Elsevier,* Amsterdam, The Netherlands, Pp. 275-316

De Kock, G.S. (1991). The mafic Audawib Suite in the Central Damara orogeny of Namibia: geochemical evidence for volcanic arc volcanism. *Journal of African Earth Science* **12**, 593- 599.

De Kock, G.S. Eglington, B., Armstrong, R.A., Harmer, R.E. and Walraven, F. (2000). U-Pb and Pb-Pb ages of the Naauwpoort rhyolite, Kawakeup leptite and Okongava Diorite: implications for the onset of rifting and orogenesis in the Damara Belt, Namibia. *Communications of the Geological Survey of Namibia, Henno Martin Volume* **12**, 81-88.

Diehl, B.T.M. (1992a). Tin. In: Miller, R.McG. Mineral resources of Namibia*, Ministry of Mines and Energy, Geological Survey of Namibia*, Windhoek, **2.8**, pp. 1-30.

Diehl, B.T.M. (1992b). Lithium, beryllium and caesium. In: Miller, R.McG (Ed.). Mineral resources of Namibia*, Ministry of Mines and Energy, Geological Survey of Namibia*, Windhoek, **6.15**, pp. 1-18.

Diehl, B.T.M. (1992c). Niobium and tantalum. In: Miller, R.McG. Mineral resources of Namibia*, Ministry of Mines and Energy, Geological Survey of Namibia*, Windhoek, **3.5**, pp. 1-20.

Diehl, B.T.M. (1993). Rare metal pegmatites of the Cape Cross – Uis pegmatite belt, Namibia: geology, mineralisation, rubidium-strontium characteristics and petrogenesis. *Journal of African Earth Sciences* **17**, 167-181.

Diehl, B.T.M. and Schneider, G.I.C. (1990). Geology and mineralisation of the Rubicon Pegmatite, Namibia. Geological Survey of Namibia Open File Report, 20 pp.

El Bouseily, A.M. and El Sokkary, A.A. (1975). The relationship between Rb-Ba and Sr in granitic rocks. *Chemical Geology* **16**, 207-219.

Ercit, T.S., Wise, M.A. and Černý, P. (1995). Compositional and structural systematics of the columbite group. *American Mineralogist* **80,** 613-619.

Ercit, T.S. (2005). REE-enriched granitic pegmatites. In: Linnen, R.L. and Samson, I.M. (Eds.). Rare-element Geochemistry and Mineral Deposits. *Geological Association of Canada Short Course Notes* **17**, 175-199.

Ertl, A., Hughes, J.M., Prowatke, S., Ludwig, T., Prasad, P.S.R., Brandstätter, F., Körner, W., Schuster, R., Pertlik, F. and Marschall, H.R. (2006). Tetrahedrally coordinated boron in tourmalines from the liddicoatite-elbaite series from Madagascar: structure, chemistry, and infrared spectroscopic studies. *American Mineralogist* **91**, 1847-1856.

Falster, A.U., Simmons, Wm.B. and Webber, K.L. (2005). Origin of pegmatites in the Hoskin Lake pegmatite field, Florence, Co., Wisconsin. Crystallisation processes in granitic pegmatites, initial meeting, Elba Island, Italy. MSA website: http://www.minsocam.org/MSA/Special/Pig/PIG_articles/Elba%20abstracts%207%20Flaster.pdf.

Federico, M., Andreozzi, G.B., Lucchesi, S. and Graziani, G. (1998). Compositional variation of tourmaline in the granitic pegmatite dykes of the Cruzeiro mine, Minas Gerais, Brazil. *The Canadian Mineralogist* **36**, 415-431.

Foit, F.F.Jr. and Rosenberg, P.E. (1979). The structure of vanadium-bearing tourmaline and its implications regarding tourmaline solid solutions. *American Mineralogist* **64**, 788-798.

Freemantle, G. (2012). Granite-hosted Uranium Deposits of the Central Damara Orogen, Namibia. Unpublished M.Sc. thesis, University of the Witwatersrand, Johannesburg.

Frost, R.B. and Frost, C.D. (2008). A geochemical classification for feldspathic igneous rocks. *Journal of Petrology* **49**, 1955-1969.

Frost, R.B., Barnes, C.G., Collins, W.J., Arculus, R.J., Ellis, D.J. and Frost, C.D. (2001). A geochemical classification for granitic rocks. *Journal of Petrology* **42(11)**, 2033-2048.

Flynn, R.T. and Burnham, C.W. (1978). An experimental determination of rare earth partition coefficients between a chloride containing vapour phase and silicate melts. *Geochimica et Cosmochimica Acta* **42,** 685-701.

Frimmel, H.E. (2009). Configuration of Pan-African orogenic belts in Southwestern Africa. In: Gaucher, C., Sial, A.N., Halverson, G.P., Frimmel, H.E. (Eds.). Neoproterozoic-Cambrian tectonics, global change and evolution: a focus on southwestern Gondwana. *Developments in Precambrian Geology* **16**, pp. 45-151.

Frimmel, H.E. and Miller, R.McG. (2009). Continental rifting. Neoproterozoic to Early Palaeozoic evolution of Southwestern Africa. In: Gaucher, C., Sial, A.N., Halverson, G.P. and Frimmel, H.E. (Eds.), Neoproterozoic-Cambrian tectonics, global change and evolution: a focus on southwestern Gondwana. *Developments in Precambrian Geology* **16**, pp. 153-159.

Frimmel, H.E., Fölling, P.G. and Eriksson, P. (2002). Neoproterozoic tectonic and climatic evolution recorded in the Gariep Belt, Namibia and South Africa. *Basin Research* **14**, 55-67.

Frimmel, H.E., Basei, M.S. and Gaucher, C. (2011). Neoproterozoic geodynamic evolution of SW-Gondwana: a southern African perspective. *International Journal of Earth Sciences* **100**, 323-354.

Fuchs, Y., Lagache, M. and Linares, J. (1998). Fe-tourmaline synthesis under different T and fO_2 conditions. *American Mineralogist* **83**, 525-534.

Fuchsloch, W.C., Nex, P.A.M. and Kinnaird, J.A. (2018a). Classification, mineralogical and geochemical variations in pegmatites of the Cape Cross-Uis pegmatite belt, Namibia. *Lithos* **296-299**, 79-95.

Fuchsloch, W.C., Nex, P.A.M. and Kinnaird, J.A. (2018b). The geochemical evolution of the Nb-Ta-Sn oxides from pegmatites of the Cape Cross-Uis pegmatite belt, Namibia. *Mineralogical Magazine,* DOI: 10.1180/mgm.2018.151.

Fuchsloch, W.C., Nex, P.A.M., Kinnaird, J.A. and Van Niekerk, D. (2018c). The mineral chemistry of tourmaline from pegmatites of the Cape Cross-Uis pegmatite belt, Namibia: implications for source, contamination and pegmatite fractionation. *Submitted, Mineralogical Magazine.*

Gaucher, C., Frimmel, H.E. and Germs, G.J.B. (2009). Tectonic events and palaeogeographic evolution of southwestern Gondwana in the Neoproterozoic and Cambrian. In: Gaucher, C., Sial, A.N. Halverson, G.P. and Frimmel, H.E. (Eds.). Neoproterozoic-Cambrian tectonics, global change and evolution: a focus on southwestern Gondwana. *Developments in Precambrian Geology* **16**, pp. 295-316.

Gaweda, A., Pieczka, A. and Kraczka, J. (2002). Tourmalines from the Western Tatra Mountains (W-Carpathians, S-Poland): their characteristics and petrogenetic importance. *European Journal of Mineralogy* **14**, 943-955.

Ginsburg, A.I., Timofeyev, I.N. and Feldman, L.G. (1979). Principles of geology of the granitic pegmatites. Nedra Moscow, pp. 296 [in Russian].

Glover, A.S., Rogers, W.Z. and Barton, J.E. (2012). Granitic Pegmatites: Storehouses of Industrial Minerals. *Elements: An International Magazine of Mineralogy, Geochemistry, and Petrology* **8(4)**, 269-273.

González, T.L., Polonio, F.G., Moro, F.J.L., Fernández, A.F., Contreras, J.L.S. and Benito, M.C.M. (2017). Tin-tantalum-niobium mineralisation in the Penouta deposit (NW Spain): Textural features and mineral chemistry to unravel the genesis and evolution of cassiterite and columbite group minerals in a peraluminous system. *Ore Geology Reviews* **81**, 79-95.

Goscombe, B., Gray, D. and Hand, M. (2004). Variation in metamorphic style along the northern margin of the Damara Orogen. *Journal of Petrology* **45(6)**, 1261-1295.

Goscombe, B., Gray, D.R., Armstrong, R., Foster, D.A. and Vogl, J. (2005). Event geochronology of the Pan-African Kaoko Belt, Namibia. *Precambrian Research* **140**, 1-41.

Grassi, L.R. (2014). A Geochemical Investigation of the Usakos Gem Tourmaline Pegmatite, Namibia. *University of New Orleans Theses and Dissertations*. Paper 1803.

Gray, D.R., Foster, D.A., Goscombe, B., Passchier, C.W. and Trouw, R.A.J. (2006). $^{40}Ar/^{39}Ar$ thermochronology of the Pan-African Damara Orogen, Namibia, with implications for tectonothermal and geodynamic evolution. *Precambrian Research* **150**, 49-72.

Gray, D.R., Foster, D.A., Meert, J.G., Goscombe, B.D., Armstrong, R.A., Trouw, R.A.J. and Passchier, C.W. (2008). A Damara Orogen perspective on the assembly of southwestern Gondwana. *Geological Society of London Special Publication* **294**, 257-278.

Haack, U. and Gohn, E. (1988). Rb-Sr data on some pegmatites in the Damara Orogen, Namibia. *Communications of the Geological Survey of South West Africa/Namibia* **4**, 13-17.

Hanson, S.L., Simmons, W.B. and Falster, A.U. (1998). Nb-Ta-Ti oxides in granitic pegmatites from the Topsham pegmatite district, Southern Maine. *The Canadian Mineralogist* **36,** 601-608.

Harris, N.B.W. and Inger, S. (1992). Trace element modelling of pelite-derived granites. *Contributions to Mineralogy and Petrology* **110,** 46-56.

Hawkesworth, C.J. and Marlow, A.G. (1983). Isotope evolution of the Damara orogenic belt. *Special Publication of the Geological Society of South Africa* **11**, 397-407.

Hawkesworth, C.J., Gledhill, A.R., Roddick, J.C., Miller, R. McG. and Kröner, A. (1983). Rb-Sr and $^{40}Ar/^{39}Ar$ studies bearing on models for the thermal evolution of the Damara Belt, Namibia. *In* Miller, R. McG. (Ed.) *Evolution of the Damara Orogen.* Special publication of the Geological Society of South Africa **11**, 323-338.

Henry, D.J. and Dutrow, B.L. (1996). Metamorphic tourmaline and its petrologic applications. In: Grew, E.S. and Anovitz, L.M. (Eds.), Boron: mineralogy, petrology and geochemistry. *Reviews in Mineralogy* **11**, pp. 503-557.

Henry, D.J. and Dutrow, B.L. (2012). Tourmaline at diagenetic to low-grade metamorphic conditions: its petrological applicability. *Lithos* **154**, 16-32.

Henry, D.J. and Guidotti, Ch.V. (1985). Tourmaline as petrogenetic indicator mineral: an example from staurolite-grade metapelites of NW Maine. *American Mineralogist* **70**, 1-15.

Henry, D.J., Novák, M., Hawthorne, F.C., Ertl, A., Dutrow, B.L., Uher, P. and Pezzotta, F. (2011). Nomenclature of the tourmaline-supergroup minerals. *American Mineralogist* **96**, 895-913.

Hoffman, P.F., Hawkins, D.P., Isachsen, C.E. and Bowring, S.A. (1996). Precise U-Pb zircon ages for early Damaran magmatism in the Summas Mountains and Welwitschia Inlier, northern Damara Belt, Namibia. *Communications of the Geological Survey of Namibia* **11**, 47-52.

Hoffmann, K.-H., Condon, D.J., Bowring, S.A. and Crowley, J.L. (2004). U-Pb zircon date from the Neoproterozoic Ghaub Formation, Namibia: Constraints on Marinoan glaciation. *Geology* **32**, 817-820.

Hugo, P.J. (1969). The pegmatites of the Kenhardt and Gordonia Districts, Cape Province. *Memoir of the Geological Survey of South Africa* **58**, pp 94.

Jacob, R.E., Moore, K.M. and Armstrong, R.A. (2000). Zircon and titanite age determination from igneous rocks in the Karibib District, Namibia: implications for Navachab vein-style gold mineralisation. *Communications of the Geological Survey of Namibia* **12**, 157-166.

Jahns, R.H. and Burnham, C.W. (1969). Experimental studies of pegmatite petrogenesis: I. A model for the derivation and crystallization of granitic pegmatites. *Economic Geology* **64**, 843-863.

Jiang, S.Y., Palmer, M.R. and Slack, J.F. (1997). Alkali-deficient tourmaline from the Sullivan Pb-Zn-Ag deposit, British Columbia. *Mineral Magazine* **61**, 853-860.

Johnson, S.D., Poujol, M. and Kisters, A.F.M. (2006). Constraining the timing and migration of collisional tectonics in the Damara Belt, Namibia: U-Pb zircon ages for the syntectonic Salem- type Stinkbank granite. *South African Journal of Geology* **109**, 611-624.

Jolliff, B.L., Papike, J.J. and Shearer, C.K. (1986). Tourmaline as a recorder of pegmatite evolution: Bob Ingersoll pegmatite, Black Hills, South Dakota. *American Mineralogist* **71**, 472-500.

Jolliff, B.L., Papike, J.J., Shearer, C.K. and Shimizu, N. (1989). Inter- and Intra-crystal REE variations in apatite from the Bob Ingersoll pegmatite, Black Hills, South Dakota. *Geochimica et Cosmochimica Acta* **53**, 421-441.

Jolliff, B.L., Papike, J.J. and Shearer, C.K. (1992). Petrogenetic relationships between pegmatites and granite based on geochemistry of muscovite in pegmatite wall zones, Black Hills, South Dakota, USA. *Geochimica et Cosmochimica Acta* **56,** 1915-1939.

Jung, S. and Mezger, K. (2003). U-Pb garnet chronometry in high-grade rocks; case studies from the central Damara Orogen (Namibia) and implications for the interpretation of Sm-Nd garnet ages and the role of high U-Th inclusions. *Contributions to Mineralogy and Petrology* **146**, 382-396.

Jung, S., Mezger, K. and Hoernes, S. (1998). Petrology and geochemistry of syn- to post-collisional metaluminous A-type granites – a major and trace element and Nd-Sr-Pb-O isotope study from the Proterozoic Damara Belt, Namibia. *Lithos* **45**, 147-175.

Jung, S., Mezger, K. and Hoernes, S. (2003). Petrology of basement-dominated terranes II. Contrasting isotopic (Sr, Nd, Pb and O) signatures of basement derived granites and constraints on the source region of granite (Damara orogen, Namibia). *Chemical Geology* **199**, 1-28.

Jung, S., Hoffer, E., and Hoernes, S. (2007). Neoproterozoic rift-related syenites (Northern Damara Belt, Namibia): geochemical and Nd-Sr-Pb-O isotope constraints for mantle sources and petrogenesis. *Lithos* **96**, 415-435.

Kasch, K.W. (1983). Regional P-T variations in the Damara Orogen with particular reference to early high-pressure metamorphism along the southern margin. In: Miller, R.McG. (Eds.), Evolution of the Damara Orogen of South West Africa/ Namibia. *Geological Society of South Africa Special Publication* **11**, pp. 243-253.

Keller, P. (1991). The occurrence of Li-Fe-Mn phosphate minerals in granitic pegmatites of Namibia. *Communications of the Geological Survey of Namibia* **7**, 21-35.

Keller, P., Robles, E.R., Pérez, A.P. and Fontan, F. (1999). Chemistry, paragenesis and significance of tourmaline in pegmatites of the southern Tin Belt, Central Namibia. *Chemical Geology* **158**, 203-225.

Killick, A.M. (1986). A review of the economic geology of northern South West Africa/Namibia. In: Anhaeusser, C.R. and Maske, S. (Eds.), *Mineral Deposits of Southern Africa* **2**, Geological Society of South Africa, Johannesburg, pp. 1709-1717.

Killick, A.M. (2000). The Matchless Belt and associated sulphide mineral deposits, Damara Orogen, Namibia. *Communications of the Geological Survey of Namibia* **12**, 73-80.

Kinnaird, J.A. and Nex, P.A.M. (2007). A review of geological controls on uranium mineralisation in sheeted leucogranites within the Damara Orogen, Namibia. Trans I.M.M. *Applied Earth Sciences* **116(2)**, 68-85.

Kisters, A.F.M. (2005). Controls of gold-quartz vein formation during regional folding in amphibolite-facies, marble-dominated metasediments of the Navachab Gold Mine in the Pan-African Damara Belt, Namibia. *South African Journal of Geology* **108**, 365-380.

Kisters, A.F.M., Jordaan, L.S. and Neumaier, K. (2004). Thrust-related dome structures in the Karibib district and the origin of orthogonal fabric domains in the south Central Zone of the Pan-African Damara Belt, Namibia. *Precambrian Research* **133**, 283-303.

Kovalenko, N.I., Ryzhenko, B.N., Barsukov, V.L., Klintsova, A.P., Velyukhanova, T.K., Volynets, M.P. and Kytayeva, L.P. (1986). The solubility of cassiterite in HCl + NaCl(KCl) solutions at 550 ºC and 1000 atm under fixed redox conditions. *Geochemistry International* **23**, 1-16.

Kröner, A. (1982). Rb-Sr geochronology and tectonic evolution of the Pan-African Damara Belt of Namibia, south-western Africa. *American Journal of Science* **282**, 1471-1507.

Kukla, P.A. (1992). Tectonic and sedimentation of a late Proterozoic Damaran convergent continental margin, Khomas Hochland, central Namibia. *Memoirs of the Geological Survey of Namibia* **12**, 62-68.

Lahti, S.I. (1987). Zoning in columbite-tantalite crystals from the granitic pegmatites of the Eräjärvi area, southern Finland. *Geochimica et Cosmochimica Acta* **51**, 509-517.

Lenharo, S.L.R., Pollard, P.J. and Born, H. (2003). Petrology and textural evolution of granites associated with tin and rare metals mineralisation at the Pitinga mine, Amazonas, Brazil. *Lithos* **66**, 37-61.

Linnen, R.L. (1998). The solubility of Nb-Ta-Zr-Hf-W in granitic melts with Li and Li + F: constraints for mineralisation in rare metal granites and pegmatites. *Economic Geology* **93**, 1013-1025.

Linnen, R.L. and Keppler, H. (1997). Columbite solubility in granitic melts: consequences for the enrichment and fractionation of Nb and Ta in the Earth's crust. *Contributions to Mineralogy and Petrology* **128**, 213-227.

Linnen, R.L. and Williams-Jones, A.E. (1993). Mineralogical constraints on magmatic and hydrothermal Sn-W-Ta-Nb mineralisation at the Nong Sua aplite-pegmatite, Thailand. *European Journal of Mineralogy* **5**, 721-736.

Linnen, R.L., Pichavant, M. and Holtz, F. (1996). The combined effects of fO_2 and melt composition on SnO_2 solubility and tin diffusivity in haplogranitic melts. *Geochimica et Cosmochimica Acta* **60,** 4965-4976.

Linnen, R.L., v. Lichtervelde, M. and Černý, P. (2012). Granitic Pegmatites as Sources of Strategic Metals. *Elements: An International Magazine of Mineralogy, Geochemistry, and Petrology* **8(4)**, 275-280.

London, D. (1995). Geochemical features of peraluminous granites, pegmatites, and rhyolites as sources of lithophile metal deposits. In: Thompson, J.F.H. (Eds.), Magmas, fluids, and ore deposits. *M.A.C. short course series* **23**, Victoria, British Columbia.

London, D. (1999). Stability of tourmaline in peraluminous granite systems: the boron cycle from anatexis to hydrothermal aureoles. *European Journal of Mineralogy* **11**, 253-262.

London, D. (2008). Pegmatites. *Canadian Mineralogist Special publication* **10**, pp. 347.

London, D. and Manning, D.A.C. (1995). Chemical variation and significance of tourmaline from Southwest England. *Economic Geology* **90**, 495-519.

London, D. and Kontak, D.J. (2012). Granitic Pegmatites: Scientific Wonders and Economic Bonanzas. *Elements: An International Magazine of Mineralogy, Geochemistry, and Petrology* **8(4)**, 257 - 261.

London, D. and Morgan VI, G.B. (2012). The Pegmatite Puzzle. *Elements: An International Magazine of Mineralogy, Geochemistry, and Petrology* **8(4)**, 263-268.

London, D., Morgan, G.B.VI. and Wolf, M.B. (1996): Boron in granitic rocks and their contact aureoles. In: Grew, E.S. and Anovitz, L.M. (Eds.), Boron: Mineralogy, petrology and geochemistry. *Reviews in Mineralogy* **11**, pp. 299-330.

Longridge, L. (2012). Tectonothermal Evolution of the southwestern Central Zone, Damara Belt, Namibia. Unpublished Ph.D. thesis, University of the Witwatersrand, Johannesburg, pp. 524.

Louis, R. (1998). Composition of complex lepidolite-type granitic pegmatites and of constituent columbite-tantalite, Chèdeville, Massif Central, France. *The Canadian Mineralogist* **36**, 563-583.

Macey, P.H. (2003). The characteristics of regional-scale fluids, fluid flow and hydrothermal mineralization in meta-sedimentary terranes: a stable isotope and fluid inclusion study of the Zerrissene Group metaturbidites and Sn–W deposits, Brandberg West area,

Neoproterozoic Damara Orogen, central western Namibia. Unpublished Ph.D. thesis, University of Cape Town, Cape Town, pp. 332.

Macey, P. and Harris, C. (2006). Stable isotope and fluid inclusion evidence for the origin of the Brandberg West area Sn-W vein deposits, NW Namibia. *Mineralium Deposita* **41**, 671-690.

Maniar, P.D. and Piccoli, P.M. (1989). Tectonic discrimination of granitoids. *Geological Society of American Bulletin* **101,** 635-643.

Manning, D.A.C. (1981). The effect of fluorine on liquidus phase relationships in the system Oz-Ab-Or with excess water at 1 kb. *Contributions to Mineralogy and Petrology* **76**, 205-215.

Marks, M.A.W., Marschall, H.R., Schühle, P., Guth, A., Wenzel, T., Jacob, D.E., Barth, M. and Markl, G. (2013). Trace element systematics of tourmaline in pegmatitic and hydrothermal systems from the Variscan Schwarzwald (Germany): The importance of major element composition, sector zoning, and fluid or melt composition. *Chemical Geology* **344**, 73-90.

Marlow, A. (1983). Geology and Rb-Sr geochronology of mineralised and radioactive granites and alaskites, Namibia. In: Miller, R.McG. (Eds.), Evolution of the Damara Orogen of South West Africa/Namibia. *Special Publication of the Geological Society of South Africa* **11**, pp. 515.

Martin, H. and Porada, H. (1977). The intracratonic branch of the Damara Orogen in South West Africa. I. Discussion of geodynamic models. II. Discussion of relationships with the Pan-African Mobile Belt system. *Precambrian Research* **5**, 311 - 338 and 339-357.

Martin, R.F. and De Vito, C. (2005). The patterns of enrichment in felsic pegmatites ultimately depend on tectonic setting. *Canadian Mineralogist* **43**, 2027-2048.

Martin, R.F., De Vito, C. and Sokolov, M. (2009). Pegmatites and pegmatites, just like granites and granites: apples and oranges are just not the same! *Estudos Geológicos* **19(2)**, 11-14.

Martins, T., Lima, A. and Noronha, F. (2009). Evolution trends in columbite-tantalite minerals from pegmatites from the Barroso-Alvão pegmatite field-Northern Portugal. *Estudos Geológicos* **19**, 212-216.

McDermott, F. (1986). Granite petrogenesis and crustal evolution studies in the Damara Pan-African orogenic belt, Namibia. Unpublished Ph.D. Thesis, The Open University.

McDonough, W.F. and Sun, S.-S. (1995). The composition of the earth. *Chemical Geology* **120**, 223-253.

McKeough, M.A., Lentz, D.R., McFarlane, C.R.M. and Brown, J. (2013). Geology and evolution of the pegmatite-hosted U-Th ± REE-Y-Nb mineralisation, Kulyk, Eagle, and Karin Lakes region, Wollaston Domain, northern Saskatchewan, Canada: examples of the dual role of extreme fractionation and hybridization processes. *Journal of Geosciences* **58**, 321-346.

Melcher, F., Graupner, T., Gäbler, H.-E.Sitnikova, M., Henjes-Kunst, F., Oberthür, T., Gerdes, A. and Dewaele, S. (2013). Tantalum-(niobium-tin) mineralisation in African pegmatites and rare metal granites: Constraints from Ta-Nb oxide mineralogy, geochemistry and U-Pb geochronology. *Ore Geology Reviews*, (2013), 10.1016/j.oregeorev.2013.09.003.

Melcher, F., Graupner, T., Gäbler, H., Sitnikova, M., Henjes-Kunst, F., Oberthur, T., Gerdes, A. and Dewaele, S. (2015). Tantalum-(niobium-tin) mineralisation in African pegmatites and rare metal granites: Constraints from Ta-Nb oxide mineralogy, geochemistry and U-Pb geochronology. *Ore Geology Reviews* **64**, 667-719.

Milani, L., Kinnaird, J.A., Lehmann, J., Naydenov, K.V., Saalmann, K., Frei, D. and Gerdes, A. (2015). Role of crustal contribution in the early stage of the Damara Orogen, Namibia:

New constraints from combined U-Pb and Lu-Hf isotopes from the Goas Magmatic Complex. *Gondwana Research* **28**, 961-986.

Miller, R.McG. (1979). The Okahandja lineament, a fundamental tectonic boundary in the Damara Orogen of South West Africa/Namibia. *Transactions of the Geological Society of South Africa* **82**, 349-361.

Miller, R.McG. (1983). The Pan-African Damara Orogen of South West Africa/Namibia. In: R.McG Miller (Eds.), The Evolution of the Damara Orogen of South West Africa/Namibia. *Geological Society of South Africa Special Publication* **11**, pp. 431-515.

Miller, R.McG. (1992). Mineral exploration targets in Namibia. In: Miller, R.McG. (Eds.), Mineral Resources of Namibia. *Ministry of Mines and Energy*, Geological Survey of Namibia, Windhoek **1.1**, pp. 1-8.

Miller, R.McG. (2008). Neoproterozoic and early Palaeozoic rocks of the Damara Orogen. In: Miller, R.McG. (Eds.), The Geology of Namibia **2**. *Ministry of Mines and Energy*, Geological Survey of Namibia, Windhoek, 13-1 - 13-410.

Miller, C.F. and Mittlefehldt, D.W. (1982). Depletion of light rare earth elements in felsic magmas. *Geology* **10,** 129-133.

Miller, R.McG. and Frimmel, H.E. (2009). Syn- to post-orogenic magmatism. Neoproterozoic evolution of southwestern Africa. In: Gaucher, C., Sial, A.N., Halverson, G.P. and Frimmel, H.E. (Eds.), Neoproterozoic-Cambrian tectonics, global change and evolution: a focus on southwestern Gondwana. *Developments in Precambrian Geology* **16**, pp. 219-226.

Miller, R.McG., Frimmel, H.E. and Will, T.M. (2009). Geodynamic synthesis of the Damara Orogen *sensulato*. Neoproterozoic to Early Palaeozoic evolution of Southwestern Africa. In: Gaucher, C., Sial, A.N., Halverson, G.P., Frimmel, H.E. (Eds.), Neoproterozoic-

Cambrian tectonics, global change and evolution: a focus on southwestern Gondwana. *Developments in Precambrian Geology* **16**, pp. 231-235.

Mittlefehldt, D.W. and Miller, C.F. (1983). Geochemistry of the Seawater Grenville Province of Seawater Wash pluton, California: implications for 'anomalous' trace element behaviour during differentiation of felsic magmas. *Geochimica et Cosmochimica Acta* **47,** 109-124.

Morgan, G.B. and London, D. Alteration of amphibolitic wallrocks around the Tanco rare-element pegmatite, Bernic Lake, Manitoba. *American Mineralogist* **72(11-12)**, 1097-1121.

Mulja, T., Williams-Jones, A.E., Martin, R.F. and Wood, S.A. (1996) Compositional variation and structural state of columbite-tantalite in rare-element granitic pegmatites of the Preissac-Lacorne batholith, Quebec, Canada. *American Mineralogist* **81**, 146-157.

Nabelek, P.I., Russ-Nabelek, C. and Denison, J.R. (1992). The generation and crystallization conditions of the Proterozoic Harney Peak Leucogranite, Black Hills, South Dekota, USA: petrologic and geochemical constraints. *Contributions to Mineralogy and Petrology* **110**, 173-191.

Nabelek, P.I., Whittington, A.G. and Sirbescu, M.-L.C. (2010). The role of H_2O in rapid emplacement and crystallisation of granite pegmatites: resolving the paradox of large crystals in highly undercooled melts. *Contributions to Mineralogy and Petrology* **160**, 313-325.

Nagel, R. (1999). *Eine Milliarde Jahre geologischer Entwicklung am NW-Rand des Kalahari Kratons*. Unpublished Ph.D. thesis, University of Göttingen, pp. 171.

Neiva, A.M.R. (1996). Geochemistry of cassiterite and its inclusions and exsolution products from tin and tungsten deposits in Portugal. *The Canadian Mineralogist* **34**, 745-768.

Nex, P.A.M., Oliver, G.J.H. and Kinnaird, J.A. (2001). Spinel-bearing assemblages and the P-T-t evolution of the Central Zone of the Damara Orogen, Namibia. *Journal of African Earth Sciences* **32(3)**, 471-489.

Nex, P.A.M., Kinnaird, J.A. and Herd, D.A. (2003). The occurrence, mineralogy and chemistry of betafite and pyrochlore from sheeted leucogranites of the Rössing area, Namibia: implications for the composition of ceramics for radioactive waste disposal. *Economic Geological Research Institute Information Circular,* No. 374.

Novák, M. and Černý, P. (1998). Niobium-tantalum oxide minerals from complex granitic pegmatites in the Moldanubicum, Czech Republic: primary versus secondary compositional trends. *The Canadian Mineralogist* **36**, 659-672.

Novák, M. and Škoda, R. (2011). Compositional trends in tourmaline from intragranitic NYF pegmatites of the Třebíč pluton, Czech Republic: an electron Microprobe, Mössbauer and LA-ICP-MS study. *The Canadian Mineralogist* **49**, 359-380.

Novák, M., Povondra, P. and Selway, J.B. (2004). Schorl-*oxy-schorl* to dravite-*oxy-dravite* tourmaline from granitic pegmatites; examples from the Moldanubicum, Czech Republic. *European Journal of Mineralogy* **16**, 323-333.

Novák, M., Henry, D.J., Hawthorne, F.C., Ertl, A., Uher, P., Dutrow, B. and Pezzotta, F. (2009). Nomenclature of the tourmaline-group minerals. Report of the Subcommittee on Tourmaline Nomenclature to the International Mineralogical Association's Commission on New Minerals, Nomenclature and Classification.

Owen, G.J. (2011). Geology of the Kranzberg Syncline and emplacement controls of the Usakos Pegmatite Field, Damara Belt, Namibia. Unpublished M.Sc. Thesis, University of Stellenbosch, pp. 168.

Pearce, J.A., Harris, N.B. and Tindle, A.G. (1984). Trace element discrimination diagrams for the tectonic interpretation of granitic rocks. *Journal of Petrology* **25,** 956-983.

Phillips, G.N., Wall, V.J. and Clemens, J.D. (1981). Petrology of the Strathbogie batholiths-a cordierite bearing granite. *Canadian Mineralogist* **19,** 47-63.

Pichavant, M. (1987). Effects of B and H_2O on liquidus phase relations in the haplogranite system at 1 kbar. *American Mineralogist* **72**, 1056-1070.

Prave, A.R. (1996). Tale of three cratons: tectonostratigraphic anatomy of the Damara Orogen in north-western Namibia and the assembly of Gondwana. *Geology* **24**, 1115-1118.

Pyle, J.M., Spear, F.S. and Wark, D.A. (2002). Electron microprobe analysis of REE in apatite, monazite and xenotime: protocols and pitfalls. *Reviews in Mineralogy and Geochemistry*, **42(1)**, 337-362.

Raimbault, L. (1998). Compositions of complex lepidolite-type pegmatites and of constituent columbite-tantalite, Chédeville, Massif central, France. *Canadian Mineralogist* **36**, 563-583.

Richards, T.E. (1986). Geological characteristics of rare-metal pegmatites of the Uis type in the Damara orogen, South West Africa/Namibia. In: Anhaeusser, C.R. and Maske, S. (Eds.), Mineral Deposits of Southern Africa **2**. *Geological Society of South Africa*, Johannesburg, pp.1845-1862.

Roda, E., Pesquera, A. and Velasco, F. (1995). Tourmaline in granitic pegmatites and their country rocks, Fregenda area, Salamanca, Spain. *Canadian Mineralogist* **33**, 835-848.

Roda, E., Pesquera, A., Velasco, F. and Fontan, F. (1999). The granitic pegmatites of the Fregeneda area (Salamanca, Spain): characteristics and petrogenesis. *Mineral Magazine* **66**, 535-556.

Roering, C. (1963). Pegmatite investigations in the Karibib district, South West Africa. Unpublished Ph.D. thesis, University of the Witwatersrand, Johannesburg.

Roering, C. and Gevers, T.W. (1964). Lithium- and beryllium-bearing pegmatites in the Karibib District, South West Africa. In: Haughton, S.H. (Eds.), The Geology of Some Ore Deposits in Southern Africa. *Geological Society of South Africa* **2**, pp. 462-495.

Roering, C. (1966). Aspects of the generation and crystallization sequence of the Karibib pegmatites, South West Africa. *Economic Geology* **61**, pp. 1064-1089.

Romer, R.L. and Lehmann, B. (1995). U-Pb columbite age of Neoproterozoic Ta-Nb mineralization in Burundi. *Economic Geology* **90**, 2303-2309.

Schneider, G.I.C. and Seeger, K.G. (1992). Semi-precious stones. In: Miller, R.McG. (Ed.), Mineral Resources of Namibia. *Ministry of Mines and Energy*, Geological Survey of Namibia, Windhoek **5.2**, pp. 1-16.

Selway, J.B., Novák, M., Černý, P. and Hawthorne, F.C. (1999). Compositional evolution of tourmaline in lepidolite-subtype pegmatites. *European Journal of Mineralogy* **11**, 569-584.

Sha, L.-K. and Chappell, B.W. (1999). Apatite chemical composition, determined by electron microprobe and laser-ablation inductively coupled plasma mass spectrometry, as a probe into granite petrogenesis. *Geochimica et Cosmochimica Acta* **63**, 3861-3881.

Shearer, C.K., Papike, J.J. and Laul, J.C. (1987). Mineralogical and chemical evolution of a rare-element granite-pegmatite system: Harney Peak Granite, Black Hills, South Dakota. *Geochimica et Cosmochimica Acta* **51**, 473-486.

Simmons, W.B. (2007). Chapter 8: Gem-bearing pegmatites. In: Groat, L.A. (Ed.), Geology of Gem Deposits. *Mineralogical Association of Canada,* Short Course Series **37**, Québec, pp. 169-206.

Simmons, Wm.B. and Webber, K.L. (2008). Pegmatite genesis: state of the art. *European Journal of Mineralogy* **20**, 421-438.

Simmons, W.B., Lee, M.T. and Brewster, R.H. (1986). Geochemistry and evolution of the South Platte granite-pegmatite system, Jefferson Country, Colorado. *Geochimica et Cosmochimica Acta* **51**, 455-471.

Singh, P.K. (2007). Tantalite exploration in "Block A" of Uis region, Namibia. *Trabajosde Geologia* **27**, 41-69.

Singh, P.K. (2008). Revelation of tin and niobium occurrences in southern Uis region of Namibia through a geological reconnaissance study. *Trabajos de Geologia* **28**, 33-39.

Skjerlie, K.P. and Johnston, A.D. (1992). Vapor-absent melting at 10kbar of a biotite and amphibole-bearing tonalitic gneiss: Implications for the generation of A-type granites. *Geology* **20**, 263-266.

Slack, J.F. (1996). Tourmaline associations with hydrothermal ore deposits. In: Grew, E.S. and Anovitz, L.M. (Eds.), Boron: mineralogy, petrology and geochemistry. *Reviews in Mineralogy* **11**, pp. 559-643

Smith, D.A.M. (1965). The geology of the area around the Khan and Swakop Rivers in Namibia. *Memoir of the Geological Survey of South Africa* **3**, pp. 113.

Smith, S.R., Foster, L.G., Romer, R.L., Tindle, A.G., Kelley, S.P., Noble, S.R., Horstwood, M. and Breaks, F.W. (2004). U-Pb columbite-tantalite chronology of rare-element pegmatites using TIMS and Laser Ablation-Multi Collector-ICP-MS. *Contributions to Mineralogy and Petrology* **147**, 549-564.

Snook, B.R. (2014). Towards exploration tools for high purity quartz: an example from the South Norwegian Evje-Iveland pegmatite belt. Unpublished Ph.D. thesis, University of Exeter, United Kingdom

Splide, M.N. and Shearer, C.K. (1992). A comparison of tantalum-niobium oxide assemblages in two mineralogically distinct rare-element granitic pegmatites, Black Hills, South Dakota. *The Canadian Mineralogist* **30**, 719-737.

Stanistreet, I.G., Kukla, P.A. and Henry, G. (1991). Sedimentary basinal responses to a late Precambrian Wilson Cycle: the Damara Orogen and Nama Foreland, Namibia. *Journal of African Earth Science* **13**, 141-156.

Stavrov, O.D., Stolyarov, I.S and Iocheva, E.I. (1969). Geochemistry and origin of the VerkhIset granitoid massif in central Ural. *Geochemistry International* **6**, 1138-1146.

Steven, N.M., Armstrong, R.A. and Moore, J.M. (1993) New Rb-Sr data from the Central Zone of the Damara Orogen, Namibia. *Communications of the Geological Survey of Namibia* **8**, 5-14.

Stewart, D.B. (1978). Petrogenesis of lithium-rich pegmatites. *American Mineralogist* **63**, 970-980.

Swart, R. (1992). The sedimentology of the Zerrissene turbidite system, Damara Orogen, Namibia. *Memoirs of the Geological Society of Namibia* **13**, pp. 54.

Tack, L., Williams, I., and Bowden, P. (2002). SHRIMP constraints on early post collisional granitoids of the Ida Dome, central Damara (Pan-African) Belt, western Namibia. IAGOD Quadrennial Symposium and Geocongress, Windhoek, Namibia, 11th, abstracts, *Geological Survey of Namibia.*

Simmons, W.B., Pezzotta, F., Shigley, J.E. and Beurlen, H. (2012). Granitic pegmatites as sources of coloured gemstones. *Elements: An International Magazine of Mineralogy, Geochemistry, and Petrology* **8(4)**, 281-287.

Thomas, R., Davidson, P. and Beurlen, H. (2012). The competing models for the origin and internal evolution of granitic pegmatites in the light of melt and fluid inclusion research. *Mineralogy and Petrology* **106**, 55-73.

Thompson, A.B. (1982). Dehydration melting of pelitic rocks and the generation of H_2O-undersaturated granitic liquids. *American Journal of Science* **282,** 1567-1595.

Tindle, A.G. and Breaks, F.W. (2000). Columbite-tantalite mineral chemistry from rare-element granitic pegmatites: Separation Lake area, N.W. Ontario, Canada. *Mineralogy and Petrology* **70**, 165-198.

Tindle, A.G., Breaks, F.W. and Selway, J.B. (2002). Tourmaline in petalite-subtype granitic pegmatites: Evidence of fractionation and contamination from the Pakeagama Lake and Separation Lake areas of northwestern Ontario, Canada. *The Canadian Mineralogist* **40**, 753-788.

Trompette, R. (1997). Neoproterozoic (1600 Ma) aggregation of western Gondwana: a tentative scenario. *Precambrian Research* **82**, 101-112.

Trumbull, R.B., Krienitz, M.-S., Gottesmann, B. and Wiedenbeck, M. (2008). Chemical and boron- isotope variations in tourmalines from an S-type granite and its source rocks: the Erongo granite and tourmalinites in the Damara Belt, Namibia. *Contributions to Mineralogy and Petrology* **155**, 1-18.

Van Lichtervelde, M.V., Beziat, S.S.D. and Linnen, R.L. (2007). Textural features and chemical evolution in tantalum oxides: magmatic versus hydrothermal origins for Ta mineralization in the Tanco Lower Pegmatite, Manitoba, Canada. *Economic Geology* **102**, 257-276.

Von Knorring, O. and Condliffe, E. (1987). Mineralised pegmatites in Africa. *Geological Journal* **22 (thematic issue)**, 253-270.

Wagener, G.F. (1989). Systematic variation in the tin content of pegmatites in western central Namibia. *Journal of Geochemical Exploration* **34**, 1-19.

Walker, R.J., Hanson, G.N. and Papike, J.J. (1989). Trace element constraints on pegmatite genesis: Tin Mountain pegmatite, Black Hills, South Dakota. *Contributions to Mineralogy and Petrology* **101,** 290-300.

Will, T.M., Miller, R.McG., and Frimmel, H.E. (2009). Orogenic tectono-thermal evolution. Neoproterozoic to Early Palaeozoic evolution of Southwestern Africa. In: Gaucher, C., Sial, A.N., Halverson, G.P. and Frimmel, H.E. (Eds.), Neoproterozoic-Cambrian tectonics, global change and evolution: a focus on southwestern Gondwana. *Developments in Precambrian Geology* **16**, pp. 205-218.

Wilson, A.H. (2012). A chill sequence to the bushveld complex: insight into the first stage of emplacement and implications for the parental magmas. *Journal of Petrology* **53,** 1123-1168.

Wise, M.A. (1999). Characterization and classification of NYF-type pegmatites: *Canadian Mineralogist* **37**, 802-803.

Wise, M.A., Francis, C.A. and Černý, P. (2012). Compositional and structural variations in columbite-group minerals from granitic pegmatites of the Brunswick and Oxford fields, Maine: Differential trends in F-poor and F-rich environments. *The Canadian Mineralogist* **50**, 1515-1530.

Wolf, M.B. and London, D. (1997). Boron in granitic magmas: stability of tourmaline in equilibrium with biotite and cordierite. *Contributions to Mineralogy and Petrology* **130**, 12-30.

Zhang, A.C., Wang, R.C., Hu, H., Zhang, H., Zhu, J.C. and Chen, X.M. (2004). Chemical evolution of the Nb-Ta oxides and zircon from the Koktokay No. 3 granitic pegmatite, Altai, northwestern China. *Mineralogical Magazine* **68**, 739-756.

Zheng, Z., Deng, X.-H., Chen, H.-J., Yue, S.-W., Dong, L.-H., Qu, X. and Chen, Y.-J. (2016). Fluid sources and metallogenesis in the Baiganhu W-Sn deposit, East Kunlun, NW China: Insights from chemical and boron isotopic compositions of tourmaline. *Ore Geology Reviews* **72**, 1129-1142.

Appendices

Appendix A: sample inventory

Sample No.	GPS coordinates	Rock Type	Description	Thin section	W-R geochemistry	Cassiterite data	CGM data	Tourmaline data	Apatite data
Rose Quartz									
WCF 1-1	33K 414455E 7591134S	Pegmatite	Tml+qtz+alb						
WCF 1-2	33K 414455E 7591134S	Pegmatite	Tml+alb						
WCF 1-3	33K 414495E 7591134S	Quartz material	Qtz						
WCF 8-1	33K 414638E 7591117S	Granite (600m Distance)	Granodioritic						
WCF 8-2	33K 414680E 7591016S	Granite (15m Distance)	Granodioritic						
WCF 8-3	33K 414518E 7591109S	Granite contact	Granodioritic						
WCF 8-4	33K 414339E 7591108S	Pegmatite	Tml+gnt+musc+quartz+alb						
WCF 8-5	33K 414450E 7591135S	Quartz material	Qtz						
WCF 8-6	33K 414787E 7591111S	Granite dike	Monzogranite						
WCF 8-7	33K 415601E 7591143S	Schist xenolith	Tourmalinised host-rock						
Dead Sea									
WCF 2-1	33K 417597E 7590792S	Schist host-rock	Knotenschiefer						
WCF 2-2	33K 417589E 7590706S	Pegmatite	Qtz+alb+musc+tml						
WCF 2-3	33K 417589E 7590706S	Quartz material	Qtz						
WCF 2-4	33K 417589E 7590706S	Pegmatite	Qtz+alb+musc						
P2.2									
WCF 3 -1	33K 418120E 7594059S	Schist host-rock	Knotenschiefer						
WCF 3-2	33K 418120E 7594060S	Metasomatised contact	Tourmalinised Knotenschiefer						
WCF 3-3	33K 418047E 7593966S	Pegmatite	(No Suggestions)						
WCF 3-4	33K 418045E 7593966S	Banded pegmatite	Qtz+alb+musc						
WCF 3-5	33K 418045E 7593965S	Pegmatite	Qtz+alb						
WCF 3-6	33K 418113E 7594041S	Pegmatite	Tml+qtz+alb+musc						
WCF 3-7	33K 418079E 7594039S	Quartz material	Qtz						
WCF3-8	33K 418045E 7593954S	Schist host-rock	Knotenschiefer						
WCF3-9	33K 418028E 7593944S	Pegmatite	Musc+qtz+apt						
P1									
WCF 3.1-1	33k 417930E 7593110S	Pegmatite	Perthite+qtz+musc+alb						

Sample No.	GPS coordinates	Rock Type	Description	Thin section	W-R geochemistry	Cassiterite data	CGM data	Tourmaline data	Apatite data
WCF 3.1-2	33k 417930E 7593110S	Greisen	CGM+musc+qtz						
WCF 3.1-3	33K 417316E 7595089S	Quartz material	Qtz						
WCF 3.1-4	33K 417316E 7595089S	Aplite/albitised	Alb						
WCF3.1-5	33K 417316E 7595089S	Pegmatite	Tml+qtz+musc+alb						
WCF3.1-6	33K 417296E 7595151S	Host-rock	Biotite schist						
WCF 3.1-7	33k 417930E 7593110S	Pegmatite	Apt+qtz+alb+musc						
P3									
WCF 3.2-1	33K 417275E 7595082S	Pegmatite	Tml+apt+CGM+cas+qtz+alb+musc						
WCF 3.2-2	33K 417275E 7595082S	Host-rock	Biotite+musc schist						
M3.3									
WCF3.3-1	33K 417320E 7595887S	Host-rock	Quartzite						
WCF3.3-2	33K 417363E 7595922S	Pegmatite	Perthite+qtz+musc						
WCF3.3-3	33K 417300E 7595987S	Quartz material	Qtz						
Strathmore									
WCF 4-1	33K 417320E 7595887S	Pegmatite	Qtz+musc+alb+apt						
WCF 4-2	33K 417320E 7595887S	Host-rock	Tourmalinised schist						
WCF4-3	33K 422170E 7605373S	Pegmatite	Musc+qtz+CGM						
WCF 4-4	33K 422180E 7605356S	Albitised pegmatite	Alb+CGM						
WCF 4-5	33K 422132E 7605389S	Host-rock	Knotenschiefer						
WCF4-6	33K 422105E 7605392S	Host-rock	Knotenschiefer						
WCF 4-7	33K 422249E 7605424S	Aplite	Alb+qtz						
WCF 4-8	33K 422223E 7605442S	Host-rock	Quartzite						
WCF 4-9	33K 422255E 7605419S	Pegmatite	Perthite+qtz+musc						
WCF 4-10	33K 422255E 7605419S	Quartz material	Qtz						
WCF 4-11	33K 422263E 7605499S	Pegmatite	Qtz+musc+alb						
WCF 4-12	33K 422263E 7605499S	Pegmatite	Qtz+musc+alb+apt						
WCF 4-13	33K 422263E 7605499S	Pegmatite	Microcline+qtz+musc						
WCF 4-14	33K 422355E 7605347S	Saprolite	Lithified top soil						

Sample No.	GPS coordinates	Rock Type	Description	Thin section	W-R geochemistry	Cassiterite data	CGM data	Tourmaline data	Apatite data
Off pit 1									
WCF A -1	33K 422891E 7604774S	Pegmatite	Qtz+alb+musc						
WCF A-2	33K 422890E 7604747S	Pegmatite	Qtz+alb+musc+CGM+cas						
Off Pit 2 no samples	33K 423620E 7605575S								
Off pit 3									
WCF B-1	33K 423868E 7606051S	Pegmatite	Qtz+alb+musc+apt						
Off pit 4 no samples	33K 423183E 7605622S								
Off pit 5									
WCF B-2	33K 423260E 7605318S	Greisen	Musc+qtz+CGM+cas+apt						
Off pit 6									
WCF C-1	33K 422577E 7604687S	Pegmatite	Qtz+perthite+musc						
WCF C-2	33K 422556E 7604671S	Pegmatite	Qtz+alb+musc+apt						
WCF C-3	33K 422550E 7604686S	Pegmatite	Qtz+alb+perthite						
WCF C-4	33K 422599E 7604734S	Host-rock	Biotite schist						
Karlowa South									
WCF 5-1	33K 450412E 7625801S	Pegmatite	Qtz+alb+musc						
WCF 5-2	33K 450569E 7625819S	Pegmatite	Qtz+alb+tml						
WCF 5-3	33K 450942E 7625779S	Pegmatite	Qtz+musc+alb+CGM+cas+apt						
Karlowa North									
WCF 5-4	33K 454523E 7635094S	Pegmatite	Apt+qtz+alb+musc						
WCF 5.1-1	33K 454523E 7635094S	Greisen	Qtz+musc+CGM+cas+apt						
WCF 5.1-2	33K 454510E 7635101S	Host-rock	biotite phyllite						
WCF 5.1-3	33K 454526E 7635079S	Quartz material	Qtz						
WCF 5.1-4	33K 454331E 7635006S	Pegmatite	Qtz+musc+alb						
Granite dome									
WCF x-1	33K 470754E 7642534S	Host-rock	Granite						
WCF x-2	33K 470754E 7642534S	Pegmatite	Qtz+musc+alb+microcline+tml+gnt						
WCF x-3	33K 470540E 7642790S	Host-rock	Carbonate						

Sample No.	GPS coordinates	Rock Type	Description	Thin section	W-R geochemistry	Cassiterite data	CGM data	Tourmaline data	Apatite data
Uis Tin mine									
WCF 6-1	33K 487318E 7653536S	Pegmatite	Alb+microcline+cas						
WCF 6-2	33K 487298E 7653494S	Pegmatite	Qtz+alb+perthite+tml						
WCF 6-3	33K 487269E 7653500S	Host-rock	Biotite schist						
WCF 6-4	33K 487241E 7653521S	Host-rock	Biotite schist						
Villet tourmaline									
WCF 7-1	33K 454218E 7642985S	Pegmatite	Perthite+tml						
WCF 7-2	33K 454218E 7642985S	Pegmatite	Perthite+musc+tml+gnt						
WCF 7-3	33K 454195E 7643009S	Host-rock	Granite						
WCF 7-4	33K 454138E 7642898S	Host-rock	Granite						
WCF 7-5	33K 454218E 7642985S	Quartz material	Qtz						
WCF 7-6	33K 454264E 7643002S	Pegmatite	Qtz+alb+biotite						
WCF 7-7	33K 453749E 7642860S	Pegmatite	Qtz+perthite						
WCF 7-8	33K 454281E 7642742S	Host-rock	Biotite schist						
2faced pegmatite									
WCF 10-1	33K 416711E 7590664S	Pegmatite	Qtz+musc+alb+tml+apt						
WCF 10-2	33K 416712E 7590630S	Host-rock	Biotite schist						
WCF 10-3	33K 416711E 7590639S	Quartz material	Qtz						
WCF 10-4	33K 416711E 7590639S	Pegmatite	Qtz+alb+CGM+apt						
RA1									
WCF 11-1	33K 416618E 7590162S	Pegmatite	Alb+microcline+tml						
G/S contact									
WCF 12-1	33K 416126E 7589229S	Pegmatite	Qtz+alb+perthite+microcline+CGM						
WCF 12-2	33K 416126E 7589229S	Host-rock	Biotite schist						
WCF 12-3	33K 416069E 7589212S	Host-rock	Granite						
WCF 12-4	33K 416126E 7589229S	Pegmatite	Qtz+perthite+alb						
WCF 12-5	33K 416126E 7589229S	Quartz material	Qtz						
MT-pit									

Sample No.	GPS coordinates	Rock Type	Description	Thin section	W-R geochemistry	Cassiterite data	CGM data	Tourmaline data	Apatite data
WCF D-1	33K 426019E 7602831S	Quartz material	Qtz						
WCF D-2	33K 425990E 7602853S	Host-rock	Biotite schist						
WCF D-3	33K 426026E 7602839S	Pegmatite	Qtz+perthite+alb+tml						
WCF D-4	33K 426014E 7602819S	Pegmatite	Qtz+perthite+alb+musc+CGM+apt						
S-Strath									
WCF F-1	33K 422125E 7603925S	Pegmatite	Alb+perthite						
WCF F-2	33K 422156E 7603936S	Host-rock	Knotenschiefer						
Molopo Petalite									
WCF G-1 and PET-2	33K 418205E 7598978S	Pegmatite	Perthite+musc+qtz+tml+apt						
WCF G-2	33K 418296E 7599021S	Host-rock	Biotite schist						
WCF G-3	33K 418206E 7598991S	Quartz material	Qtz						
WCF G-4	33K 418208E 7599015S	Greisen	Qtz+musc+CGM+cas						
Small-GG									
WCF K-1	33K 451833E 7623573S	Quartz material	Qtz						
WCF K-2	33K 451815E 7623583S	Host-rock	Biotite phyllite						
WCF K-3	33K 451836E 7623592S	Pegmatite	Microcline+musc						
WCF K-4	33K 451831E 7623541S	Pegmatite	Qtz+alb+tml						
B-12									
WCF M-1	33K 477708E 7640808S	Host-rock	Tourmalinised biotite schist						
WCF M-2	33K 477650E 7640795S	Greisen	Qtz+musc+CGM+cas+apt						
WCF M-3	33K 477632E 7640797S	Host-rock	Quartzite						
WCF M-4	33K 477650E 7640795S	Quartz material	Qtz						
C1 pegmatite									
WCF W-1	33K 479892E 7643173S	Pegmatite	Qtz+alb						
WCF W-2	33K 480013E 7643375S	Host-rock	Biotite phyllite						
WCF W-3	33K 480131E 7643569S	Greisen	Qtz+musc+CGM+apt						
WCF W-4	33K 480120E 7643570S	Quartz material	Qtz						
WCF W-5	33K 480151E 7643611S	Pegmatite	Qtz+alb						

Sample No.	GPS coordinates	Rock Type	Description	Thin section	W-R geochemistry	Cassiterite data	CGM data	Tourmaline data	Apatite data
B1 pegmatite									
WCF Ẍ-1	33K 478771E 7643555S	Greisen	Qtz+musc+CGM+cas+apt						
WCF Ẍ-2	33K 478771E 7643555S	Host-rock	Biotite schist						
WCF Ẍ-3	33K 478771E 7643555S	Quartz material	Qtz						
Tsaurob									
WCF T-1	33K 485594E 7647607S	Host-rock	Biotite phyllite						
WCF T-2	33K 485671E 7647826S	Quartz material	Qtz						
WCF T-3	33K 485623E 7647711S	Pegmatite	Qtz+alb+tml						
WCF T-4	33K 485616E 7647726S	Pegmatite	Qtz+alb+musc+lepidolite+CGM+cas						
WCF T-5	33K 485585E 7647690S	Pegmatite	Qtz+perthite+musc+alb						
Tsau -2									
WCF J-1	33K 486304E 7647766S	Pegmatite	Perthite+musc+tml+apt						
WCF J-2	33K 486498E 7647939S	Pegmatite	Qtz+perthite						
WCF J-3	33K 486356E 7647795S	Host-rock	Knotenschiefer						
WCF J-4	33K 486433E 7647853S	Quartz material	Qtz						
WCF J-5	33K 486563E 7647992S	Pegmatite	Qtz+musc+perthite+microcline						
K1-pegmatite									
WCF L-1	33K 0489021E 7644325S	Quartz material	Qtz						
WCF L-2	33K 0489019E 7644320S	Host-rock	Biotite schist						
T-mag									
WCF O-1	33K 490832E 7646084S	Quartz material	Qtz						
WCF O-2	33K 490832E 7646084S	Pegmatite	Qtz+alb+microcline						
WCF O-3	33K 490839E 7646080S	Host-rock	Biotite schist						
Nainais									
WCF Na-1	33K 506883E 7628269S	Quartz material	Qtz						
WCF Na -2	33K 506986E 7628378S	Host-rock	Knotenschiefer						
WCF Na-3	33K 506917E 7628381S	Pegmatite	Perthite+musc+tml						
WCF Na-4	33K 507062E 7628349S	Pegmatite	Qtz+perthite+tml						

Sample No.	GPS coordinates	Rock Type	Description	Thin section	W-R geochemistry	Cassiterite data	CGM data	Tourmaline data	Apatite data
WCF Na-5	33K 507009E 7628434S	Pegmatite	Perthite+musc+CGM+cas						
WCF Na-6	33K 507062E 7628349S	Pegmatite	Alb+musc+CGM+cas						
Nein 1									
WCF en -1	33K 505166E 7627691S	Pegmatite	Qtz+alb+tml						
Nein 2									
WCF eb-1	33K 505048E 7627805S	Pegmatite	Alb+perthite+musc+apt						
WCF eb-2	33K 505081E 7627841S	Host-rock	Biotite schist						
WCF eb-3	33K 505033E 7627785S	Pegmatite	Qtz+musc+alb						
WCF eb-4	33K 505020E 7627753S	Pegmatite	Qtz+musc+alb						
Aubinhonis									
WCF eh-1	33K 513392E 7632584S	Pegmatite	Qtz+musc+tml						
WCF eh-2	33K 513392E 7632584S	Pegmatite	Lepidolite+Qtz+alb						
WCF eh-3	33K 513392E 7632584S	Quartz material	Qtz						
WCF eh-4	33K 513416E 7632554S	Host-rock	Biotite schist						
WCF eh-5	33K 513456E 7632618S	Pegmatite	Qtz+microcline+musc						

Appendix B: whole-rock data

The whole-rock geochemical data procedures and methods are given in Chapter 4

Granites

Sample #	SiO2	Al2O3	FeO	MnO	MgO	CaO	Na2O	K2O	TiO2	P2O5	Cr2O3	NiO	LOI	TOTAL	La	Ce	Pr	Nd	Sm	Eu	Gd	Tb	Dy	Ho	Er	Tm	Yb	Lu
WCF 8 - 1	73,49	14,56	1,18	0,03	0,46	1,27	3,37	4,79	0,25	0,09	0,00	0,00	0,84	100,34	40,88	85,48	8,38	28,50	5,46	0,78	3,88	0,53	2,93	0,53	1,41	0,21	1,32	0,20
WCF 8 - 2	72,58	14,69	1,19	0,03	0,47	1,83	3,50	4,50	0,27	0,07	0,01	0,00	1,14	100,28	32,49	68,00	7,01	23,24	4,42	0,73	3,49	0,44	2,13	0,44	1,04	0,16	1,00	0,16
WCF 8 - 3	73,33	14,67	1,14	0,07	0,42	1,39	3,67	4,28	0,24	0,08	0,00	0,00	0,74	100,03	33,29	70,75	6,74	22,38	4,24	0,70	3,23	0,45	2,41	0,46	1,27	0,17	1,34	0,20
WCF X - 1	74,18	14,62	1,37	0,05	0,36	1,32	5,57	1,80	0,22	0,16	0,01	0,00	0,51	100,16	40,19	79,70	7,62	25,56	4,53	0,82	4,21	0,62	3,79	0,78	2,07	0,31	2,40	0,34
WCF 8 - 6	74,83	14,84	0,57	0,11	0,14	0,84	3,32	5,14	0,07	0,04	0,00	0,00	0,95	100,86	7,89	17,91	1,89	6,50	2,02	0,22	2,16	0,44	3,04	0,59	1,78	0,32	2,23	0,34

Sample #	Rb	Sr	Ba	Sc	V	Cr	Co	Ni	Cu	Zn	Y	Zr	Nb	Mo	Sn	Cs	Hf	Ta	Pb	Th	**U**
WCF 8 - 1	202,90	218,85	572,53	15,08	30,82	15,39	5,30	11,44	31,35	66,85	14,30	194,09	17,91	2,14	n.a.	14,88	5,30	1,73	38,32	20,17	7,62
WCF 8 - 2	203,92	238,70	697,73	14,71	31,66	17,15	8,57	10,54	61,33	60,36	10,67	145,65	18,96	1,26	n.a.	13,93	4,18	1,89	37,95	16,03	3,33
WCF 8 - 3	226,77	228,51	680,27	14,99	32,08	14,28	5,10	13,64	31,32	68,29	13,29	136,54	20,84	1,21	n.a.	15,68	4,31	2,41	40,70	15,55	3,79
WCF X - 1	200,85	140,53	434,07	15,70	30,72	16,87	6,38	25,21	62,72	132,04	21,23	165,00	47,53	1,17	n.a.	18,70	4,72	7,29	20,47	15,93	6,35
WCF 8 - 6	270,72	43,60	67,29	14,54	20,48	13,76	3,37	9,65	56,04	15,43	18,78	67,82	27,83	3,14	n.a.	11,72	2,94	5,73	38,69	6,11	6,61

Metasediments

Sample #	SiO2	Al2O3	FeO	MnO	MgO	CaO	Na2O	K2O	TiO2	P2O5	Cr2O3	NiO	LOI	TOTAL	La	Ce	Pr	Nd	Sm	Eu	Gd	Tb	Dy	Ho	Er	Tm	Yb	Lu
WCF Ẍ - 2	59,90	18,00	4,38	0,08	3,03	2,29	1,05	0,80	0,78	1,53	0,01	0,01	2,09	93,93	42,31	85,96	10,39	40,21	8,90	1,04	7,48	1,08	6,73	1,32	3,83	0,49	3,61	0,53
WCF 2 - 1	61,95	17,35	5,06	0,11	3,69	0,94	1,69	4,21	0,79	0,15	0,02	0,00	2,54	98,48	47,54	97,35	10,95	42,04	8,75	1,65	7,84	1,14	6,76	1,40	3,99	0,58	3,81	0,56
WCF 3 - 1	60,88	17,09	5,18	0,14	3,59	0,85	3,04	4,10	0,83	0,25	0,02	0,01	1,84	97,81	40,67	80,12	9,21	34,18	6,57	1,45	6,48	0,93	5,64	1,14	3,30	0,52	3,43	0,51
WCF 3 - 2	56,61	21,39	4,41	0,09	2,92	1,53	1,23	1,13	0,64	1,12	0,02	0,00	2,27	93,37	37,43	74,60	8,99	33,61	6,89	1,39	5,51	0,91	5,27	1,04	3,19	0,46	3,17	0,47
WCF 3.1 - 6	60,87	16,61	4,40	0,10	3,16	2,19	0,47	4,67	0,80	0,24	0,01	0,00	3,13	96,66	41,49	83,19	10,16	37,98	7,50	1,27	6,41	0,98	6,25	1,24	3,84	0,51	3,55	0,53
WCF 3 - 8	62,79	16,56	5,01	0,11	3,45	0,77	1,45	4,25	0,82	0,13	0,01	0,00	3,82	99,18	44,73	87,37	10,42	39,68	7,43	1,09	6,69	1,06	6,84	1,36	4,12	0,57	4,32	0,66
WCF 3.2 - 2	59,76	17,23	5,64	0,22	3,83	1,16	3,22	3,90	0,79	0,15	0,01	0,01	1,87	97,78	43,61	90,33	10,24	40,11	8,05	1,45	6,92	1,08	6,53	1,33	3,51	0,50	3,42	0,51
WCF 3.3 -1	84,72	7,23	1,52	0,04	0,86	1,78	1,32	0,69	0,52	0,11	0,00	0,00	0,84	99,65	27,29	62,56	6,70	26,38	4,83	0,96	4,75	0,67	3,87	0,77	2,05	0,31	2,01	0,35
WCF 4 - 2	57,00	18,96	5,07	0,06	2,68	1,29	0,73	3,66	0,89	1,05	0,02	0,00	4,22	95,64	46,02	92,18	10,29	38,61	8,07	1,54	7,25	1,07	6,56	1,37	4,08	0,53	3,94	0,62
WCF 4 - 5	76,58	11,26	2,62	0,04	1,43	0,65	1,67	2,48	0,58	0,16	0,00	0,00	1,47	98,96	31,82	67,39	8,18	32,58	6,79	1,19	6,80	1,03	6,18	1,26	3,66	0,52	3,34	0,50
WCF 4 - 6	61,40	17,98	5,23	0,11	3,20	0,53	0,70	4,51	0,85	0,21	0,02	0,00	3,72	98,45	46,79	96,15	11,77	46,62	9,93	1,56	8,69	1,23	7,98	1,58	4,81	0,65	4,42	0,61
WCF 4 - 8	68,17	12,87	2,41	0,54	1,10	10,96	0,27	0,42	0,78	0,25	0,01	0,00	0,95	98,73	42,74	93,79	11,03	43,89	9,07	1,95	9,51	1,43	8,75	1,93	5,58	0,83	5,92	0,87
WCF 5.1 - 2	57,45	18,52	5,72	0,11	4,00	3,06	2,22	3,68	0,78	0,19	0,01	0,01	2,63	98,38	39,84	78,44	9,55	37,91	7,89	1,53	6,99	1,10	6,80	1,36	4,25	0,60	4,04	0,56
WCF 6 - 3	57,52	18,15	5,98	0,13	4,20	3,47	2,21	3,53	0,80	0,19	0,02	0,01	2,01	98,21	44,29	92,77	10,77	42,98	9,69	1,58	8,39	1,28	7,58	1,62	4,26	0,59	4,36	0,66
WCF 6 - 4	59,48	18,74	4,53	0,10	3,82	1,74	1,69	5,09	0,84	0,18	0,02	0,00	2,12	98,35	42,37	85,02	10,20	38,91	7,94	1,30	6,90	1,08	6,19	1,32	3,75	0,52	3,72	0,59
WCF 7 - 8	59,54	17,74	4,64	0,12	3,09	1,54	3,36	6,04	1,10	0,16	0,02	0,00	0,87	98,21	85,35	169,68	19,24	71,60	12,96	2,51	10,77	1,52	9,31	1,66	4,94	0,72	4,43	0,68
WCF 8 - 7	64,75	17,18	2,92	0,07	1,59	1,43	1,09	3,71	0,60	0,96	0,01	0,00	1,44	95,74	29,44	61,25	7,62	29,50	6,40	1,20	6,83	1,06	6,60	1,27	3,98	0,52	3,97	0,52
WCF 10 - 2	57,93	17,72	5,64	0,14	4,76	2,70	2,48	4,29	0,79	0,19	0,01	0,01	1,45	98,10	39,56	84,33	9,83	37,80	7,80	1,42	6,83	1,01	6,57	1,24	3,70	0,55	3,85	0,57
WCF 12 - 2	70,28	12,89	3,91	0,08	2,34	0,98	3,18	3,02	0,77	0,17	0,01	0,00	0,83	98,47	35,81	72,80	8,79	35,00	6,93	1,48	6,57	1,03	6,23	1,27	3,67	0,48	3,44	0,49
WCF C - 4	60,61	16,37	4,24	0,10	2,96	2,47	4,46	2,57	0,81	0,20	0,01	0,00	3,43	98,24	34,90	69,71	8,60	32,84	6,62	1,29	5,47	0,80	4,79	0,98	2,73	0,41	2,62	0,40
WCF D - 2	60,11	17,45	5,39	0,16	3,63	1,20	2,62	4,20	0,88	0,17	0,01	0,01	2,04	97,87	44,95	90,82	11,02	43,77	8,67	1,68	7,41	1,19	6,96	1,46	4,17	0,56	3,66	0,52
WCF F - 2	61,13	17,56	5,10	0,11	3,48	0,57	1,14	4,60	0,85	0,15	0,02	0,01	3,50	98,22	41,91	84,48	10,28	40,23	7,81	1,41	7,15	1,07	6,73	1,27	3,93	0,62	3,85	0,59
WCF G - 2	57,72	18,41	5,65	0,11	4,49	3,22	2,65	4,01	0,80	0,20	0,01	0,01	1,11	98,40	40,56	79,93	10,41	40,83	8,55	1,58	7,39	1,18	7,95	1,54	4,57	0,65	4,34	0,62
WCF J - 3	69,93	14,81	2,88	0,05	2,15	0,52	0,53	4,35	0,68	0,13	0,01	0,00	2,82	98,86	41,14	76,90	8,49	31,17	6,15	1,18	5,30	0,76	4,52	0,95	2,93	0,41	2,89	0,42
WCF K - 2	59,30	18,93	5,37	0,20	2,64	0,52	1,39	3,47	0,84	0,31	0,01	0,01	5,21	98,21	44,69	90,76	10,67	40,47	8,09	1,41	7,11	1,14	6,87	1,50	4,43	0,59	3,95	0,58
WCF L - 2	59,89	17,92	4,39	0,16	4,22	2,84	2,60	3,19	0,79	0,12	0,01	0,00	1,57	97,71	44,89	92,84	10,89	44,04	9,49	1,65	8,24	1,25	7,81	1,61	4,15	0,64	4,33	0,66
WCF M - 1	72,92	12,11	1,86	0,06	0,79	2,33	0,11	4,00	0,49	0,97	0,01	0,00	2,95	98,59	27,62	57,31	6,68	24,41	4,57	0,54	2,89	0,46	2,93	0,59	1,78	0,28	2,05	0,28
WCF M - 3	78,05	9,88	2,29	0,04	1,30	1,11	2,50	1,12	0,87	0,23	0,01	0,00	1,36	98,76	40,29	84,18	10,25	39,42	7,95	1,59	7,00	1,12	7,26	1,37	4,30	0,61	4,02	0,67
WCF Na - 2	60,55	18,81	5,18	0,14	3,53	1,19	1,55	3,93	0,83	0,19	0,01	0,00	2,43	98,34	44,33	91,51	10,92	43,07	8,97	1,79	8,00	1,20	7,35	1,50	4,16	0,61	4,38	0,63
WCF O - 3	56,24	19,17	5,25	0,06	4,25	1,33	2,99	6,82	0,74	0,17	0,01	0,00	1,66	98,69	52,38	108,36	13,28	53,08	10,38	1,54	7,79	1,16	6,51	1,36	3,80	0,52	3,76	0,57
WCF T - 1	77,37	9,83	2,57	0,04	1,27	1,29	2,51	1,34	0,81	0,25	0,01	0,00	1,23	98,51	39,29	82,61	9,83	39,07	7,86	1,43	7,48	1,08	6,62	1,39	4,01	0,56	3,92	0,56
WCF W - 2	78,13	9,78	2,36	0,03	1,27	0,68	2,50	1,53	0,66	0,17	0,00	0,00	1,40	98,52	38,48	80,32	9,76	38,14	7,62	1,49	7,15	1,09	6,74	1,34	4,02	0,57	4,27	0,58
WCF eb - 2	66,34	15,49	3,64	0,08	2,27	1,02	4,00	3,91	0,66	0,21	0,00	0,00	0,85	98,46	52,12	106,04	12,23	46,10	8,75	1,68	7,09	0,97	5,59	1,11	3,22	0,47	3,36	0,49
WCF eh - 4	64,39	16,67	4,36	0,08	2,87	0,92	3,01	3,55	0,78	0,15	0,01	0,01	1,49	98,27	47,52	95,02	11,11	43,71	8,77	1,54	6,94	1,03	6,52	1,23	3,93	0,51	3,77	0,56

Sample #	Rb	Sr	Ba	Sc	V	Cr	Co	Ni	Cu	Zn	Y	Zr	Nb	Mo	Sn	Cs	Hf	Ta	Pb	Th	**U**
WCF Ẍ - 2	89,63	220,03	304,02	21,33	168,60	101,84	11,61	36,87	49,07	300,86	35,74	173,02	31,09	5,64	180,06	11,31	5,01	4,44	17,26	17,26	5,75
WCF 2 - 1	176,28	139,30	567,25	23,66	143,23	108,01	25,15	54,83	65,76	150,83	36,61	155,51	15,59	0,71	4,94	24,15	4,62	1,17	16,14	16,14	4,08
WCF 3 - 1	1858,58	200,17	436,84	21,73	146,66	104,66	7,54	33,56	15,80	158,06	31,32	194,12	16,41	0,63	256,68	867,64	5,84	1,27	15,49	15,49	3,31
WCF 3 - 2	465,99	150,14	105,33	17,42	125,90	99,80	6,57	32,02	30,14	588,70	28,88	183,07	162,95	1,03	1084,23	61,32	8,47	251,99	12,94	12,94	6,37
WCF 3.1 - 6	177,02	100,02	613,58	20,97	170,49	101,48	19,14	45,37	36,33	151,06	33,89	186,79	14,92	1,48	5,17	19,96	5,47	1,09	14,88	14,88	5,69
WCF 3 - 8	1069,49	37,13	718,80	22,00	151,82	163,62	8,21	87,35	35,27	161,45	38,00	246,02	16,15	1,14	231,65	344,74	7,03	1,22	16,36	16,36	5,45
WCF 3.2 - 2	1268,05	164,52	456,71	21,92	147,70	102,49	19,89	55,31	33,42	179,66	33,35	153,41	15,32	0,65	252,06	829,99	4,48	1,17	14,81	14,81	3,66
WCF 3.3 -1	36,43	189,21	207,25	14,50	59,55	38,54	4,96	15,83	26,83	45,76	18,12	298,70	9,43	1,64	0,68	17,80	8,36	0,85	11,40	11,40	4,37
WCF 4 - 2	574,01	1280,50	445,17	21,92	187,19	132,65	6,27	28,72	32,29	366,14	35,83	225,45	79,12	4,38	833,17	80,75	6,75	19,66	17,58	17,58	10,78
WCF 4 - 5	110,36	86,09	460,21	16,02	90,37	54,65	8,45	27,01	26,69	77,29	34,12	247,03	10,49	0,88	17,87	52,28	6,95	0,87	10,30	10,30	2,83
WCF 4 - 6	187,27	55,79	720,11	23,25	184,26	111,46	20,20	50,19	45,76	175,32	41,96	183,85	15,14	2,42	16,35	32,43	5,41	1,20	15,58	15,58	3,68
WCF 4 - 8	24,15	391,01	29,84	17,02	106,56	65,83	9,04	25,65	36,27	60,57	52,57	403,61	14,07	2,54	139,48	7,28	11,13	1,07	16,34	16,34	5,15
WCF 5.1 - 2	189,86	186,00	623,95	22,85	211,65	112,61	21,65	60,93	9,23	185,66	37,07	147,25	15,26	1,64	5,75	62,08	4,40	1,23	15,80	15,80	4,64
WCF 6 - 3	189,98	155,13	867,47	22,94	160,18	110,93	21,84	61,46	25,12	184,40	41,57	156,44	15,38	1,77	7,72	78,71	4,77	1,21	17,41	17,41	3,57
WCF 6 - 4	194,23	99,11	964,59	24,05	204,73	111,20	10,84	37,67	34,82	163,70	34,96	165,40	16,39	1,05	6,62	71,57	5,17	1,28	18,35	18,35	4,50
WCF 7 - 8	248,09	461,02	2737,43	20,95	161,20	107,38	9,49	26,46	32,44	185,92	45,79	429,28	23,31	1,11	6,16	17,73	12,50	1,27	27,68	27,68	5,60
WCF 8 - 7	177,85	72,13	610,67	17,56	83,10	67,07	9,42	29,42	20,85	231,65	34,82	244,18	72,26	0,76	35,81	17,81	7,44	31,62	8,82	8,82	6,34
WCF 10 - 2	240,67	179,92	448,00	22,65	204,56	103,81	24,02	64,20	35,32	201,69	34,74	152,89	15,91	0,87	10,00	77,12	4,36	1,22	16,41	16,41	2,63
WCF 12 - 2	267,11	202,18	704,17	19,05	113,66	83,56	11,29	35,43	24,73	141,27	32,11	243,74	13,10	0,90	28,79	49,06	7,00	1,16	10,69	10,69	3,81
WCF C - 4	306,95	454,72	542,14	20,06	145,27	97,05	13,02	47,43	30,77	143,74	24,30	223,08	15,11	0,80	17,72	387,32	6,69	1,17	12,42	12,42	2,54
WCF D - 2	432,73	151,38	566,43	22,32	153,15	102,78	17,26	43,14	35,15	170,20	36,66	199,04	17,19	1,01	80,73	210,16	5,92	1,24	15,49	15,49	3,84
WCF F - 2	230,51	80,26	666,66	22,90	165,78	122,43	18,13	47,26	34,27	152,81	35,44	188,94	15,97	0,84	8,01	118,77	5,65	1,21	15,54	15,54	3,37
WCF G - 2	207,62	125,98	525,32	22,81	168,73	106,45	21,01	61,20	18,75	197,81	41,91	173,82	16,30	0,70	7,46	66,60	5,13	1,28	17,39	17,39	2,91
WCF J - 3	389,98	59,46	672,26	20,96	122,93	92,52	6,06	43,11	37,58	95,13	24,63	153,71	12,64	0,72	10,79	116,39	4,92	1,13	14,54	14,54	3,11
WCF K - 2	656,13	35,83	218,00	24,23	186,34	107,94	7,81	51,00	51,64	191,07	39,62	152,35	19,40	3,70	127,82	145,03	4,64	1,54	16,76	16,76	5,61
WCF L - 2	1366,21	271,59	835,22	22,54	155,51	105,16	4,90	21,66	21,32	155,19	40,60	158,64	15,59	0,83	103,17	557,52	4,65	1,16	16,94	16,94	4,82
WCF M - 1	1363,07	128,48	516,73	17,39	136,50	70,22	7,06	24,64	30,51	184,73	15,52	116,16	14,96	9,60	346,13	338,07	3,83	2,84	10,25	10,25	3,62
WCF M - 3	119,49	133,48	262,12	15,51	74,52	58,51	7,40	23,22	19,77	64,93	36,40	548,99	13,77	1,35	2,14	77,37	15,44	1,07	14,97	14,97	3,94
WCF Na - 2	186,44	172,37	651,32	23,11	173,64	113,78	13,99	45,46	21,36	160,18	38,24	184,22	14,94	1,06	6,48	43,07	5,41	1,22	15,85	15,85	3,99
WCF O - 3	220,33	132,62	968,44	24,05	193,63	117,61	16,64	53,31	37,40	207,89	34,55	146,71	13,07	0,65	6,96	18,88	4,68	1,02	17,70	17,70	4,69
WCF T - 1	81,12	158,49	265,54	15,55	83,19	58,32	6,38	21,34	30,53	59,28	35,86	435,87	13,36	0,94	1,77	12,01	12,71	1,08	13,04	13,04	3,81
WCF W - 2	190,09	105,47	471,67	15,12	87,41	52,15	6,57	22,43	13,79	68,30	35,30	394,73	12,05	0,76	6,22	67,56	11,17	1,01	14,11	14,11	3,66
WCF eb - 2	151,40	257,37	1060,71	17,26	95,91	66,08	11,89	29,37	16,38	103,01	28,99	283,70	15,59	1,10	3,06	11,86	8,30	1,17	17,51	17,51	4,32
WCF eh - 4	598,36	167,80	548,52	19,34	121,49	80,90	13,03	41,38	18,25	122,73	33,59	223,76	17,61	0,66	74,57	281,88	6,64	1,54	16,23	16,23	4,20

Nb-Ta-Sn type pegmatites

Sample #	SiO2	Al2O3	FeO	MnO	MgO	CaO	Na2O	K2O	TiO2	P2O5	Cr2O3	NiO	LOI	TOTAL	La	Ce	Pr	Nd	Sm	Eu	Gd	Tb	Dy	Ho	Er	Tm	Yb	Lu
WCF 12 - 1	70,30	15,95	0,22	0,02	0,08	0,15	2,86	9,25	0,01	0,50	d.l.	d.l.	1,44	100,77	0,33	0,63	0,07	0,26	0,12	0,09	0,18	0,03	0,23	0,03	0,12	0,02	0,12	0,02
WCF 12 - 4	76,30	13,29	0,53	0,06	0,14	0,46	4,68	2,65	0,02	0,22	d.l.	d.l.	1,45	99,80	0,82	1,67	0,16	0,50	0,21	0,08	0,23	0,06	0,34	0,05	0,15	0,03	0,22	0,04
WCF 2 - 2	66,51	19,45	0,60	0,06	0,43	0,82	8,46	1,06	0,07	0,71	0,00	0,00	1,84	100,02	7,82	16,21	1,88	7,02	1,39	0,28	1,26	0,18	0,94	0,19	0,53	0,08	0,49	0,09
WCF 2 - 4	72,16	14,34	0,93	0,18	0,16	0,75	3,78	4,58	0,02	0,80	0,00	0,00	2,27	99,97	0,34	0,49	0,04	d.l.	d.l.	d.l.	d.l.	d.l.	d.l.	d.l.	d.l.	d.l.	d.l.	d.l.
WCF 3 - 5	72,27	16,21	0,20	0,06	0,05	0,35	9,16	0,20	0,01	0,60	0,00	0,00	3,13	102,23	0,07	0,13	0,02	d.l.	d.l.	d.l.	d.l.	d.l.	d.l.	d.l.	d.l.	d.l.	d.l.	d.l.
WCF 3.1 - 1	70,68	15,85	0,42	0,16	0,09	1,30	6,93	1,06	0,01	1,37	0,00	0,00	3,82	101,68	0,11	0,14	d.l.	d.l.	d.l.	d.l.	d.l.	d.l.	d.l.	d.l.	d.l.	d.l.	d.l.	d.l.
WCF 4 - 9	73,10	15,76	0,18	0,03	0,03	0,19	8,75	0,63	0,01	0,27	d.l.	d.l.	1,47	100,41	0,36	0,53	0,04	0,13	0,05	d.l.	d.l.	0,02	0,08	d.l.	d.l.	d.l.	0,05	d.l.
WCF 4 - 13	69,23	17,59	0,21	0,03	0,06	0,99	9,23	0,58	0,01	0,86	d.l.	d.l.	3,72	102,51	1,05	0,72	0,23	1,03	0,22	0,35	0,41	0,07	0,41	0,07	0,18	0,03	0,13	0,02
WCF A - 1	73,60	14,68	0,42	0,11	0,05	0,30	3,94	5,01	0,01	0,43	d.l.	d.l.	0,83	99,38	0,19	0,26	0,02	0,06	0,09	d.l.	d.l.	d.l.	0,04	d.l.	d.l.	d.l.	d.l.	d.l.
WCF A - 2	73,16	15,46	0,52	0,18	0,05	0,66	6,79	1,21	0,01	0,59	d.l.	d.l.	3,43	102,06	0,39	0,59	0,04	0,12	d.l.	d.l.	d.l.	d.l.	0,03	d.l.	d.l.	d.l.	d.l.	d.l.
WCF C - 1	73,18	15,42	0,22	0,01	0,05	0,37	7,27	1,37	0,01	0,39	d.l.	d.l.	2,04	100,32	0,66	0,90	0,08	0,22	0,06	d.l.	d.l.	d.l.	0,09	d.l.	0,05	d.l.	0,05	d.l.
WCF C - 2	75,33	14,01	0,28	0,15	0,04	0,31	7,13	1,16	0,01	0,36	d.l.	d.l.	3,50	102,27	0,33	0,50	0,04	0,12	d.l.	d.l.	d.l.	0,02	0,08	d.l.	d.l.	d.l.	d.l.	d.l.
WCF D - 3	71,42	16,15	0,48	0,14	0,05	0,39	4,44	4,08	0,01	0,94	d.l.	d.l.	2,82	100,93	0,29	0,34	0,02	d.l.	d.l.	d.l.	d.l.	d.l.	d.l.	d.l.	d.l.	d.l.	d.l.	d.l.
WCF D - 4	71,74	16,30	0,52	0,18	0,05	0,32	8,33	0,72	0,01	0,45	d.l.	d.l.	5,21	103,81	0,39	0,53	0,03	d.l.	d.l.	d.l.	d.l.	d.l.	d.l.	d.l.	d.l.	d.l.	d.l.	d.l.
WCF eb - 3	69,70	16,17	0,22	0,02	0,08	1,46	7,99	1,22	0,01	1,60	d.l.	d.l.	2,95	101,42	0,12	0,15	d.l.	d.l.	d.l.	d.l.	d.l.	d.l.	d.l.	d.l.	d.l.	d.l.	d.l.	d.l.
WCF eb - 4	67,50	15,91	0,19	0,02	0,09	1,09	5,79	1,50	0,03	3,41	d.l.	d.l.	1,36	96,88	0,15	0,26	0,02	0,12	d.l.	d.l.	d.l.	d.l.	0,10	0,02	0,06	d.l.	0,07	d.l.
WCF F - 1	65,66	19,41	0,35	0,03	0,07	1,33	9,87	1,13	0,01	0,82	d.l.	d.l.	2,43	101,11	0,39	0,59	0,06	0,12	d.l.	d.l.	d.l.	d.l.	d.l.	d.l.	d.l.	d.l.	0,03	d.l.
WCF Na - 4	72,18	16,82	0,16	0,01	0,04	0,25	6,26	1,55	0,01	0,56	d.l.	d.l.	1,49	99,34	0,38	0,73	0,10	0,34	0,09	d.l.	0,17	0,04	0,15	0,03	0,07	d.l.	0,07	0,02
WCF T - 5	67,70	17,14	0,16	0,02	0,07	0,60	7,50	0,62	0,01	3,00	d.l.	d.l.	1,49	98,32	0,25	0,38	0,04	0,13	0,05	d.l.	d.l.	d.l.	d.l.	d.l.	d.l.	d.l.	d.l.	d.l.
WCF J - 5	68,32	17,37	0,21	0,02	0,04	0,65	7,45	0,94	0,01	2,18	d.l.	d.l.	1,23	98,41	0,21	0,33	0,03	d.l.	0,05	d.l.	d.l.	0,03	0,13	d.l.	d.l.	d.l.	d.l.	d.l.
WCF K - 3	72,29	15,88	0,98	0,44	0,10	0,49	4,02	2,56	0,01	0,43	d.l.	d.l.	1,40	98,61	0,42	0,49	0,05	0,18	0,06	d.l.	d.l.	d.l.	0,05	d.l.	d.l.	d.l.	d.l.	d.l.
WCF O - 2	73,84	14,45	0,44	0,01	0,11	0,47	4,65	3,82	0,04	0,56	d.l.	d.l.	1,49	99,87	1,00	1,79	0,20	0,61	0,22	d.l.	0,20	0,05	0,30	0,06	0,15	0,03	0,24	0,03

Sample #	Rb	Sr	Ba	Sc	V	Cr	Co	Ni	Cu	Zn	Y	Zr	Nb	Mo	Sn	Cs	Hf	Ta	Pb	Th	**U**
WCF 12 - 1	1008,19	57,91	246,73	5,80	11,15	7,46	9,99	9,13	217,86	841,39	1,41	3,86	26,37	0,73	466,84	47,52	0,20	2,85	51,43	0,16	1,09
WCF 12 - 4	360,62	24,15	53,37	7,08	12,74	7,35	1,47	11,97	50,21	96,55	2,08	16,33	67,12	0,71	28,49	39,67	1,05	13,81	25,13	0,67	2,10
WCF 2 - 2	209,49	40,15	18,17	6,68	25,16	26,18	42,94	20,81	503,22	3325,68	5,17	60,22	85,59	0,69	208,89	20,21	3,16	45,00	42,51	3,29	7,21
WCF 2 - 4	1153,39	269,42	37,90	6,40	18,78	9,30	29,47	14,51	825,94	2896,12	0,08	8,31	135,61	1,70	3131,53	146,85	0,78	92,89	30,70	0,67	2,92
WCF 3 - 5	32,13	513,29	23,15	6,28	13,05	8,23	1,35	8,29	40,21	51,25	0,13	20,53	88,20	0,66	1236,45	14,71	2,20	63,57	12,14	0,19	7,35
WCF 3.1 - 1	378,56	1482,76	100,54	5,45	16,91	6,94	2,56	12,65	94,12	103,59	0,11	2,49	29,90	1,85	558,82	31,36	0,24	15,65	27,01	0,16	6,67
WCF 4 - 9	229,30	84,36	13,38	5,84	12,00	10,93	17,67	20,57	249,96	1308,59	0,46	39,08	177,02	1,08	25,14	86,62	4,30	214,19	31,32	0,83	3,64
WCF 4 - 13	298,81	214,50	59,70	5,42	17,26	8,71	3,66	9,96	14,02	20,08	2,55	10,70	54,19	0,81	310,50	50,65	1,81	201,52	33,24	0,17	4,07
WCF A - 1	1307,43	132,46	42,72	5,97	14,47	14,22	2,72	54,28	322,03	134,69	0,18	18,38	55,04	1,05	68,01	110,76	1,58	10,99	34,08	0,19	3,64
WCF A - 2	384,16	115,66	48,62	5,68	15,50	7,87	9,82	11,86	239,10	906,47	0,25	18,32	93,85	1,67	80,87	24,54	1,41	30,98	14,11	0,39	8,30
WCF C - 1	494,67	39,43	13,04	6,38	10,62	8,09	1,29	10,65	114,20	34,15	0,46	10,33	190,17	0,52	3643,28	40,39	1,12	99,98	40,04	0,85	2,68
WCF C - 2	245,04	252,13	52,75	6,45	13,03	8,25	7,37	11,80	222,92	506,60	0,30	8,30	139,00	1,57	1607,84	20,98	1,46	169,24	44,04	0,41	7,81
WCF D - 3	984,80	275,22	16,81	5,77	11,49	6,59	1,17	11,44	86,25	171,68	0,05	18,36	64,71	2,75	140,38	134,42	1,07	22,98	33,21	0,18	17,34
WCF D - 4	185,44	63,52	18,13	5,86	14,00	8,25	3,18	22,80	27,13	288,61	0,09	36,99	87,53	4,03	44,98	11,62	2,98	76,31	11,64	0,38	7,81
WCF eb - 3	509,96	999,79	38,72	5,89	9,40	11,38	1,61	16,95	114,18	138,66	0,11	6,94	196,52	0,54	693,10	27,60	0,95	109,17	26,43	0,10	2,70
WCF eb - 4	301,41	561,70	53,57	6,00	10,65	8,75	1,57	9,49	32,55	72,86	0,72	21,09	71,91	0,57	10411,96	29,30	2,27	58,34	22,79	0,13	18,84
WCF F - 1	231,10	94,52	13,75	6,05	21,33	9,10	0,98	10,46	105,63	140,54	0,26	19,81	65,42	0,65	69,98	13,53	2,07	46,08	36,63	0,33	13,24
WCF Na - 4	863,75	44,96	15,42	6,09	10,01	6,88	2,68	9,99	157,35	55,13	0,87	13,63	164,03	0,63	4072,60	74,12	1,53	144,05	53,87	0,20	1,23
WCF T - 5	483,50	188,82	10,66	6,57	9,67	10,26	1,56	10,37	60,08	80,00	0,19	7,10	303,57	0,64	5357,65	33,38	0,86	81,72	14,44	0,45	8,93
WCF J - 5	1521,17	1388,02	49,41	6,02	9,63	7,70	11,31	9,40	219,59	1306,90	0,67	17,02	191,39	0,71	1387,71	107,67	2,33	153,22	8,39	0,57	6,36
WCF K - 3	888,67	75,35	61,57	6,92	31,48	7,06	19,61	20,65	721,93	1591,35	0,41	9,22	139,08	4,03	244,94	175,35	1,45	168,19	13,89	1,41	5,43
WCF O - 2	925,22	47,70	61,58	9,41	10,11	7,25	1,30	8,37	104,05	117,06	1,62	26,99	148,13	0,55	355,81	84,21	1,65	29,51	25,79	0,64	2,55

Gnt-Tml type pegmatites

Sample #	SiO2	Al2O3	FeO	MnO	MgO	CaO	Na2O	K2O	TiO2	P2O5	Cr2O3	NiO	LOI	TOTAL	La	Ce	Pr	Nd	Sm	Eu	Gd	Tb	Dy	Ho	Er	Tm	Yb	Lu
WCF 7 - 3	74,47	14,46	0,81	0,17	0,16	0,32	5,88	2,06	0,02	0,40	0,00	0,00	0,53	99,28	1,01	1,44	0,25	0,53	0,21	0,10	0,28	0,06	0,30	0,10	0,41	0,06	0,37	0,06
WCF 7 - 4	76,52	13,42	0,38	0,00	0,07	1,01	3,39	5,00	0,07	0,05	0,00	0,00	0,52	100,43	10,62	25,26	2,62	8,57	1,53	0,48	1,50	0,06	1,43	0,31	1,02	0,17	1,31	0,25
WCF X - 2	73,25	14,37	0,50	0,12	0,11	0,68	3,04	6,08	0,04	0,34	0,00	0,00	2,54	101,08	6,04	11,47	1,26	4,15	0,90	0,23	0,88	0,06	1,14	0,24	0,63	0,12	0,95	0,16
WCF 7 - 2	70,90	14,58	3,14	1,44	0,33	0,60	5,62	0,43	0,03	0,47	d.l.	d.l.	2,01	99,54	3,02	6,10	0,71	2,38	0,96	0,05	1,07	0,06	2,65	0,52	1,71	0,31	2,46	0,31
WCF 7 - 6	73,90	13,99	0,65	0,07	0,18	0,61	5,16	3,88	0,05	0,36	d.l.	d.l.	2,12	100,96	0,94	1,58	0,19	0,60	0,17	0,07	0,23	0,06	0,25	0,06	0,13	0,02	0,17	0,03
WCF 7 - 7	74,06	14,11	0,28	0,03	0,07	0,39	3,69	6,02	0,02	0,31	d.l.	d.l.	0,87	99,85	1,16	1,66	0,25	0,86	0,26	0,18	0,24	0,06	0,31	0,04	0,20	0,04	0,23	0,04

Sample #	Rb	Sr	Ba	Sc	V	Cr	Co	Ni	Cu	Zn	Y	Zr	Nb	Mo	Sn	Cs	Hf	Ta	Pb	Th	**U**
WCF 7 - 3	230,28	18,49	58,39	13,88	18,69	12,80	4,67	12,49	46,43	89,38	2,21	32,93	81,94	1,19	n.a.	19,63	1,45	15,34	12,20	0,73	2,27
WCF 7 - 4	145,90	229,20	262,60	15,44	26,32	12,15	3,93	8,65	6,85	11,32	9,39	114,10	14,91	1,48	n.a.	3,66	4,81	2,09	27,24	20,96	9,46
WCF X - 2	573,62	68,51	230,64	7,14	11,31	8,82	9,37	10,57	220,93	965,16	7,05	29,73	69,13	0,65	239,69	18,73	1,62	15,50	56,14	2,78	12,35
WCF 7 - 2	84,03	35,52	49,71	7,66	15,35	8,56	1,72	13,62	14,71	121,92	17,26	10,50	33,38	1,15	29,51	48,90	0,69	7,64	9,29	0,86	4,04
WCF 7 - 6	644,34	27,59	92,55	6,40	17,35	10,65	2,78	17,17	402,89	184,82	1,52	5,75	61,41	0,71	46,96	60,54	0,33	12,09	50,82	0,34	5,70
WCF 7 - 7	291,05	53,28	149,25	6,48	12,92	8,83	1,57	10,26	18,18	23,05	1,82	11,97	37,96	0,68	162,71	6,65	0,64	6,40	82,02	0,43	0,97

Li-bearing type pegmatites

Sample #	SiO2	Al2O3	FeO	MnO	MgO	CaO	Na2O	K2O	TiO2	P2O5	Cr2O3	NiO	LOI	TOTAL	La	Ce	Pr	Nd	Sm	Eu	Gd	Tb	Dy	Ho	Er	Tm	Yb	Lu
WCF 5.1 - 4	70,22	17,32	0,28	0,01	0,13	1,58	2,22	3,64	0,02	1,33	d.l.	d.l.	2,63	99,38	0,18	0,26	0,04	0,20	0,06	0,05	0,14	0,02	0,11	0,03	0,06	d.l.	0,06	d.l.

Sample #	Rb	Sr	Ba	Sc	V	Cr	Co	Ni	Cu	Zn	Y	Zr	Nb	Mo	Sn	Cs	Hf	Ta	Pb	Th	**U**
WCF 5.1 - 4	1756,99	113,39	34,93	5,80	12,67	8,67	1,64	12,61	178,84	97,61	0,89	14,86	215,81	0,74	1187,48	210,12	1,40	329,94	24,48	0,38	6,59

Alteration zones within pegmatites

Sample #	SiO2	Al2O3	FeO	MnO	MgO	CaO	Na2O	K2O	TiO2	P2O5	Cr2O3	NiO	LOI	TOTAL	La	Ce	Pr	Nd	Sm	Eu	Gd	Tb	Dy	Ho	Er	Tm	Yb	Lu
WCF Ä - 1	78,22	13,81	0,48	0,02	0,07	0,19	0,22	3,82	0,02	0,15	d.l.	d.l.	2,09	99,08	0,25	0,46	0,04	0,12	0,07	d.l.	d.l.	0,02	0,09	d.l.	d.l.	d.l.	d.l.	d.l.
WCF 3.1 - 2	42,83	35,90	0,22	0,01	0,11	1,97	0,52	9,86	0,06	0,06	d.l.	d.l.	1,87	93,41	0,04	0,11	d.l.	d.l.	d.l.	d.l.	d.l.	d.l.	d.l.	d.l.	d.l.	d.l.	d.l.	d.l.
WCF 5.1 - 1	52,64	31,72	0,59	0,02	0,13	0,18	2,01	7,95	0,02	0,10	d.l.	d.l.	0,95	96,32	0,05	0,10	d.l.	d.l.	d.l.	d.l.	d.l.	d.l.	d.l.	d.l.	d.l.	d.l.	d.l.	d.l.
WCF eb - 1	64,60	18,09	0,35	0,09	0,07	0,44	4,40	2,08	0,05	5,78	d.l.	d.l.	1,57	97,52	0,23	0,40	0,03	0,09	d.l.	d.l.	d.l.	0,02	0,10	0,02	d.l.	d.l.	d.l.	d.l.
WCF M - 2	51,05	32,18	0,38	0,03	0,40	0,31	1,81	8,20	0,14	0,23	d.l.	d.l.	0,85	95,57	0,09	0,13	0,02	d.l.	d.l.	d.l.	d.l.	d.l.	d.l.	d.l.	d.l.	d.l.	d.l.	d.l.
WCF G - 4	51,12	31,97	0,35	0,01	0,10	0,14	3,69	7,32	0,07	0,20	d.l.	d.l.	1,66	96,63	0,05	0,10	d.l.	d.l.	d.l.	d.l.	d.l.	0,03	0,33	0,11	0,50	0,13	1,30	0,26
WCF 3.3 - 2	70,52	17,90	0,20	0,01	0,06	0,26	9,25	0,67	0,01	0,63	d.l.	d.l.	0,84	100,33	0,25	0,42	0,04	0,14	0,10	d.l.	0,11	0,02	0,11	0,02	d.l.	d.l.	d.l.	d.l.
WCF 4 - 4	70,69	17,36	0,40	0,10	0,08	0,25	9,93	0,40	0,01	0,28	d.l.	d.l.	4,22	103,71	0,07	0,13	0,02	d.l.	d.l.	d.l.	d.l.	d.l.	d.l.	d.l.	d.l.	d.l.	d.l.	d.l.
WCF C - 3	71,22	16,90	0,28	0,03	0,05	0,40	7,99	1,07	0,01	0,42	d.l.	d.l.	1,11	99,47	0,50	0,69	0,06	0,19	0,05	d.l.	d.l.	0,02	0,09	0,02	d.l.	d.l.	0,10	d.l.
WCF W - 5	69,11	17,68	0,10	0,02	0,05	0,94	9,85	0,19	0,01	0,88	d.l.	d.l.	1,49	100,32	0,07	0,11	d.l.	d.l.	d.l.	d.l.	d.l.	d.l.	d.l.	d.l.	d.l.	d.l.	d.l.	d.l.

Sample #	Rb	Sr	Ba	Sc	V	Cr	Co	Ni	Cu	Zn	Y	Zr	Nb	Mo	Sn	Cs	Hf	Ta	Pb	Th	**U**
WCF Ä - 1	1289,44	8,15	32,37	7,25	11,05	10,97	9,55	14,78	189,28	930,49	0,44	8,45	63,38	0,81	3504,26	113,84	0,85	89,26	11,84	0,62	1,02
WCF 3.1 - 2	5151,21	31,43	6,60	3,58	12,84	8,36	0,95	11,88	13,85	156,97	0,03	0,63	70,23	0,43	955,12	1328,13	0,20	136,55	6,44	0,02	0,27
WCF 5.1 - 1	8889,69	159,03	26,48	4,47	15,35	8,38	30,99	10,99	623,56	4141,52	0,17	2,43	60,73	0,62	750,77	1317,41	0,47	102,27	26,74	6,82	7,00
WCF eb - 1	930,85	64,93	4,13	5,98	9,68	7,68	11,96	10,20	280,41	1164,61	0,62	4,20	123,37	0,63	5119,96	70,54	0,96	94,23	24,62	0,13	3,37
WCF M - 2	6597,75	21,88	100,56	5,52	19,64	6,73	2,10	12,24	51,96	293,02	0,13	13,26	106,37	0,50	852,23	1479,13	3,19	650,94	15,99	1,03	4,61
WCF G - 4	4980,50	5,02	2,31	5,63	12,82	6,61	36,20	10,46	535,16	3563,67	3,95	650,95	209,25	0,53	10016,49	180,94	57,67	185,61	23,07	7,63	10,45
WCF 3.3 - 2	411,07	55,11	15,36	6,39	12,76	6,79	1,05	7,60	33,22	31,34	0,70	16,82	80,62	0,57	61,90	55,40	1,60	55,92	30,32	0,51	5,71
WCF 4 - 4	88,86	45,35	43,83	5,75	18,55	7,89	1,00	8,76	21,60	85,23	0,08	17,80	311,83	1,27	31,21	15,79	2,40	255,63	17,67	0,27	2,01
WCF C - 3	369,17	78,76	24,46	6,06	12,93	7,60	1,17	11,57	27,68	63,59	0,59	13,06	175,40	0,71	1713,28	39,52	1,76	149,85	37,73	0,77	3,81
WCF W - 5	27,16	676,09	25,24	5,91	9,79	7,28	0,86	10,16	43,90	38,26	0,05	12,08	242,35	0,58	1287,91	4,03	2,49	463,48	16,90	2,02	3,25

Appendix C: mineral chemistry data

1. Columbite-group minerals and tapiolite mineral chemistry data

The procedures of methods of columbite-group minerals tapiolite and cassiterite data acquisition by microprobe is given in Chapter 5. The following are the detection limits of the microprobe given in ppm.

Sn: 168

U: 591

Ca: 78

W: 2243

Mg: 77

Ta: 198

Fe: 128

Mn: 125

Nb: 168

Ti: 83

Sc: 165

Point	SnO2	MgO	Ta2O5	FeO	MnO	Nb2O5	TiO2	Sc2O3	U2O	CaO	WO3	Total	Sn a.p.f.u	Mg	Ta	Fe	Mn	Nb	Ti	Sc	U	Ca	W	Total
Sample 12-1													6 anions											
1	0,00	0,40	6,44	15,65	4,32	67,85	2,16	0,07	0,00	0,00	3,93	100,81	0,00	0,03	0,10	0,75	0,21	1,76	0,09	0,00	0,00	0,00	0,06	3,00
2	0,10	0,30	9,51	15,31	4,65	65,54	1,86	0,06	0,00	0,01	3,55	100,88	0,00	0,03	0,15	0,74	0,23	1,72	0,08	0,00	0,00	0,00	0,05	3,01
3	0,09	0,38	9,87	15,59	4,12	65,19	1,81	0,03	0,00	0,01	3,96	101,03	0,00	0,03	0,16	0,76	0,20	1,71	0,08	0,00	0,00	0,00	0,06	3,00
4	0,02	0,39	5,18	15,59	4,22	70,46	2,11	0,00	0,00	0,00	1,90	99,86	0,00	0,03	0,08	0,74	0,20	1,82	0,09	0,00	0,00	0,00	0,03	3,00
5	0,00	0,53	3,89	15,99	3,75	71,84	2,16	0,20	0,00	0,00	3,01	101,36	0,00	0,04	0,06	0,75	0,18	1,82	0,09	0,01	0,00	0,00	0,04	3,00
6	0,06	0,43	12,73	15,55	3,97	64,12	1,60	0,05	0,00	0,00	2,50	101,02	0,00	0,04	0,20	0,76	0,20	1,70	0,07	0,00	0,00	0,00	0,04	3,00
7	0,02	0,47	4,80	15,62	4,29	71,44	1,64	0,05	0,00	0,04	2,55	100,91	0,00	0,04	0,07	0,74	0,21	1,83	0,07	0,00	0,00	0,00	0,04	3,00
8	0,02	0,43	5,57	15,57	4,55	70,53	1,55	0,06	0,00	0,01	1,87	100,17	0,00	0,04	0,09	0,74	0,22	1,82	0,07	0,00	0,00	0,00	0,03	3,01
9	0,04	0,46	5,57	15,52	4,56	70,91	1,56	0,02	0,00	0,01	1,48	100,13	0,00	0,04	0,09	0,74	0,22	1,83	0,07	0,00	0,00	0,00	0,02	3,01
10	0,05	0,44	5,03	15,56	4,45	69,77	2,39	0,02	0,00	0,00	1,93	99,64	0,00	0,04	0,08	0,74	0,22	1,80	0,10	0,00	0,00	0,00	0,03	3,01
11	0,04	0,53	5,50	15,70	4,15	71,40	1,61	0,03	0,00	0,00	1,10	100,05	0,00	0,05	0,09	0,75	0,20	1,84	0,07	0,00	0,00	0,00	0,02	3,01
12	0,02	0,47	5,73	15,50	4,58	70,79	1,55	0,04	0,00	0,01	1,21	99,90	0,00	0,04	0,09	0,74	0,22	1,83	0,07	0,00	0,00	0,00	0,02	3,01
13	0,00	0,47	4,40	15,54	4,41	71,99	1,61	0,07	0,00	0,00	2,16	100,64	0,00	0,04	0,07	0,74	0,21	1,84	0,07	0,00	0,00	0,00	0,03	3,00
14	0,00	0,31	4,71	12,30	8,39	70,56	2,39	0,15	0,00	0,01	2,08	100,91	0,00	0,03	0,07	0,58	0,40	1,80	0,10	0,01	0,00	0,00	0,03	3,02
15	0,14	0,00	31,29	10,17	8,74	50,25	0,22	0,00	0,00	0,00	0,07	100,87	0,00	0,00	0,54	0,54	0,47	1,44	0,01	0,00	0,00	0,00	0,00	3,01
16	0,09	0,00	28,68	10,53	8,50	52,71	0,27	0,01	0,00	0,00	0,54	101,33	0,00	0,00	0,49	0,55	0,45	1,49	0,01	0,00	0,00	0,00	0,01	3,00
17	0,04	0,45	5,38	15,87	4,07	70,08	2,04	0,09	0,00	0,00	1,98	99,99	0,00	0,04	0,08	0,76	0,20	1,81	0,09	0,00	0,00	0,00	0,03	3,01
18	0,26	0,00	34,62	9,40	8,87	46,23	0,32	0,01	0,00	0,02	0,68	100,40	0,01	0,00	0,61	0,51	0,49	1,36	0,02	0,00	0,00	0,00	0,01	3,00
19	0,09	0,47	5,24	15,57	4,37	70,64	1,98	0,06	0,00	0,01	2,01	100,44	0,00	0,04	0,08	0,74	0,21	1,82	0,08	0,00	0,00	0,00	0,03	3,01
20	0,03	0,46	5,66	15,52	4,33	70,30	2,27	0,05	0,00	0,00	1,77	100,38	0,00	0,04	0,09	0,74	0,21	1,81	0,10	0,00	0,00	0,00	0,03	3,01
21	0,11	0,16	5,89	14,29	6,19	70,94	1,15	0,04	0,00	0,00	1,80	100,56	0,00	0,01	0,09	0,68	0,30	1,83	0,05	0,00	0,00	0,00	0,03	3,00
22	0,00	0,41	4,93	16,00	4,10	70,32	1,70	0,03	0,00	0,00	1,74	99,22	0,00	0,04	0,08	0,77	0,20	1,83	0,07	0,00	0,00	0,00	0,03	3,01
23	0,05	0,45	4,75	15,63	4,34	71,43	1,57	0,02	0,00	0,00	1,50	99,74	0,00	0,04	0,07	0,75	0,21	1,85	0,07	0,00	0,00	0,00	0,02	3,01
24	0,00	0,47	4,57	15,67	4,14	71,44	1,95	0,07	0,00	0,00	1,97	100,26	0,00	0,04	0,07	0,74	0,20	1,83	0,08	0,00	0,00	0,00	0,03	3,00
25	0,06	0,46	4,69	15,68	4,53	71,96	1,54	0,04	0,00	0,02	1,37	100,33	0,00	0,04	0,07	0,74	0,22	1,85	0,07	0,00	0,00	0,00	0,02	3,01
26	0,00	0,53	4,40	15,92	4,14	71,24	2,17	0,09	0,00	0,02	2,41	100,92	0,00	0,04	0,07	0,75	0,20	1,82	0,09	0,00	0,00	0,00	0,04	3,01
27	0,04	0,53	5,13	15,84	4,42	70,91	1,78	0,07	0,00	0,00	2,40	101,12	0,00	0,04	0,08	0,75	0,21	1,81	0,08	0,00	0,00	0,00	0,04	3,01
28	0,04	0,55	5,73	15,64	4,35	70,44	2,05	0,05	0,00	0,01	1,61	100,47	0,00	0,05	0,09	0,74	0,21	1,81	0,09	0,00	0,00	0,00	0,02	3,01
29	0,09	0,56	4,47	15,58	4,12	70,79	2,04	0,17	0,00	0,00	1,79	99,61	0,00	0,05	0,07	0,74	0,20	1,83	0,09	0,01	0,00	0,00	0,03	3,01
30	0,03	0,45	4,68	15,67	4,29	70,79	2,00	0,07	0,00	0,00	1,52	99,50	0,00	0,04	0,07	0,75	0,21	1,83	0,09	0,00	0,00	0,00	0,02	3,01
31	0,02	0,34	4,62	15,95	4,37	71,64	1,45	0,08	0,00	0,01	2,30	100,78	0,00	0,03	0,07	0,76	0,21	1,84	0,06	0,00	0,00	0,00	0,03	3,00
32	0,00	0,42	4,59	16,02	4,24	72,87	1,48	0,04	0,00	0,00	1,23	100,90	0,00	0,04	0,07	0,76	0,20	1,86	0,06	0,00	0,00	0,00	0,02	3,01
33	0,06	0,51	6,15	15,92	4,08	70,79	1,81	0,06	0,00	0,00	0,89	100,29	0,00	0,04	0,10	0,76	0,20	1,82	0,08	0,00	0,00	0,00	0,01	3,01
34	0,05	0,46	4,57	15,73	4,42	71,93	1,64	0,04	0,00	0,01	1,59	100,44	0,00	0,04	0,07	0,75	0,21	1,84	0,07	0,00	0,00	0,00	0,02	3,01
35	0,25	0,00	43,92	7,41	10,46	38,51	0,20	0,00	0,00	0,02	0,62	101,38	0,01	0,00	0,80	0,42	0,59	1,17	0,01	0,00	0,00	0,00	0,01	3,01
36	0,00	0,50	4,94	15,56	4,32	71,81	1,68	0,06	0,00	0,00	1,95	100,82	0,00	0,04	0,08	0,74	0,21	1,84	0,07	0,00	0,00	0,00	0,03	3,00
37	0,42	0,00	37,31	9,41	8,80	44,19	0,50	0,00	0,00	0,01	0,39	101,01	0,01	0,00	0,66	0,51	0,49	1,30	0,02	0,00	0,00	0,00	0,01	3,01
38	0,09	0,41	13,14	15,69	3,80	62,34	1,79	0,07	0,00	0,00	3,14	100,47	0,00	0,04	0,21	0,77	0,19	1,66	0,08	0,00	0,00	0,00	0,05	3,01
39	0,03	0,38	6,59	15,73	4,40	67,13	2,10	0,08	0,00	0,00	3,88	100,32	0,00	0,03	0,10	0,76	0,21	1,75	0,09	0,00	0,00	0,00	0,06	3,01

Point	SnO2	MgO	Ta2O5	FeO	MnO	Nb2O5	TiO2	Sc2O3	U2O	CaO	WO3	Total	Sn a.p.f.u	Mg	Ta	Fe	Mn	Nb	Ti	Sc	U	Ca	W	Total
Sample 2-4													6 anions											
40	0,08	0,09	26,82	13,73	5,37	52,63	0,88	0,04	0,00	0,01	1,08	100,73	0,00	0,01	0,46	0,72	0,28	1,48	0,04	0,00	0,00	0,00	0,02	3,01
41	0,14	0,08	38,31	13,09	5,10	44,11	0,59	0,02	0,00	0,00	0,00	101,44	0,00	0,01	0,68	0,71	0,28	1,30	0,03	0,00	0,00	0,00	0,00	3,01
42	0,03	0,09	30,76	13,61	5,13	50,23	0,70	0,02	0,00	0,00	0,00	100,59	0,00	0,01	0,53	0,72	0,28	1,44	0,03	0,00	0,00	0,00	0,00	3,01
43	0,12	0,11	13,09	14,40	5,46	63,72	1,35	0,00	0,00	0,00	1,88	100,12	0,00	0,01	0,21	0,71	0,27	1,71	0,06	0,00	0,00	0,00	0,03	3,00
44	0,09	0,08	32,28	13,30	5,13	47,91	0,61	0,02	0,00	0,00	0,66	100,07	0,00	0,01	0,57	0,72	0,28	1,39	0,03	0,00	0,00	0,00	0,01	3,01
45	0,13	0,10	13,20	14,18	5,31	63,30	1,55	0,02	0,00	0,01	1,35	99,15	0,00	0,01	0,21	0,71	0,27	1,71	0,07	0,00	0,00	0,00	0,02	3,00
46	0,13	0,08	45,11	11,64	4,62	36,15	0,68	0,00	0,00	0,00	0,56	98,96	0,00	0,01	0,85	0,67	0,27	1,13	0,04	0,00	0,00	0,00	0,01	2,98
47	0,10	0,07	43,75	12,48	4,68	37,97	0,79	0,02	0,00	0,01	0,72	100,59	0,00	0,01	0,80	0,70	0,27	1,16	0,04	0,00	0,00	0,00	0,01	2,99
48	0,07	0,11	13,12	14,37	5,58	63,23	1,59	0,00	0,00	0,00	2,28	100,32	0,00	0,01	0,21	0,71	0,28	1,69	0,07	0,00	0,00	0,00	0,03	3,01
49	0,11	0,09	13,06	14,23	5,85	64,02	1,24	0,00	0,00	0,00	1,84	100,45	0,00	0,01	0,21	0,70	0,29	1,71	0,06	0,00	0,00	0,00	0,03	3,01
50	0,22	0,10	13,72	14,35	5,30	62,17	1,71	0,03	0,00	0,00	3,48	101,08	0,01	0,01	0,22	0,71	0,26	1,66	0,08	0,00	0,00	0,00	0,05	2,99
51	0,03	0,01	38,59	12,97	5,39	43,45	0,51	0,02	0,00	0,01	0,42	101,39	0,00	0,00	0,69	0,71	0,30	1,28	0,02	0,00	0,00	0,00	0,01	3,01
52	0,16	0,05	40,42	12,88	5,35	41,97	0,48	0,02	0,00	0,02	0,04	101,39	0,00	0,01	0,72	0,71	0,30	1,25	0,02	0,00	0,00	0,00	0,00	3,01
53	0,10	0,07	19,68	14,04	5,58	59,32	0,70	0,01	0,00	0,02	1,00	100,51	0,00	0,01	0,32	0,71	0,29	1,63	0,03	0,00	0,00	0,00	0,02	3,01
54	0,11	0,07	21,17	14,02	5,46	58,06	0,81	0,00	0,00	0,00	0,69	100,40	0,00	0,01	0,35	0,72	0,28	1,60	0,04	0,00	0,00	0,00	0,01	3,01
Sample Na-5																								
55	0,18	0,00	41,58	13,07	4,81	40,26	0,43	0,05	0,00	0,02	0,81	101,21	0,00	0,00	0,75	0,73	0,27	1,21	0,02	0,00	0,00	0,00	0,01	3,00
56	0,27	0,00	20,33	14,18	5,24	59,08	0,62	0,02	0,00	0,00	0,55	100,28	0,01	0,00	0,34	0,72	0,27	1,63	0,03	0,00	0,00	0,00	0,01	3,00
57	0,24	0,00	50,18	12,62	4,73	32,65	0,34	0,07	0,00	0,00	0,48	101,31	0,01	0,00	0,94	0,73	0,28	1,02	0,02	0,00	0,00	0,00	0,01	3,01
58	0,17	0,00	21,06	14,03	5,37	59,60	0,42	0,02	0,00	0,01	0,54	101,22	0,00	0,00	0,35	0,71	0,28	1,63	0,02	0,00	0,00	0,00	0,01	2,99
59	0,31	0,00	19,88	14,16	5,25	59,85	0,59	0,03	0,00	0,00	0,49	100,56	0,01	0,00	0,33	0,72	0,27	1,64	0,03	0,00	0,00	0,00	0,01	3,00
60	0,30	0,00	23,28	14,29	5,19	56,24	0,60	0,00	0,00	0,01	0,37	100,28	0,01	0,00	0,39	0,74	0,27	1,57	0,03	0,00	0,00	0,00	0,01	3,01
61	0,14	0,00	18,94	14,47	5,31	61,19	0,46	0,01	0,00	0,00	0,86	101,39	0,00	0,00	0,31	0,73	0,27	1,66	0,02	0,00	0,00	0,00	0,01	3,00
62	0,14	0,00	28,38	13,75	5,30	52,70	0,39	0,01	0,00	0,01	0,00	100,68	0,00	0,00	0,48	0,72	0,28	1,50	0,02	0,00	0,00	0,00	0,00	3,01
63	0,30	0,00	37,04	12,96	4,89	43,97	0,66	0,04	0,00	0,00	0,00	99,86	0,01	0,00	0,66	0,71	0,27	1,31	0,03	0,00	0,00	0,00	0,00	3,00
64	0,30	0,00	17,33	14,41	5,11	61,36	0,82	0,02	0,00	0,00	1,07	100,42	0,01	0,00	0,28	0,72	0,26	1,67	0,04	0,00	0,00	0,00	0,02	3,00
65	0,35	0,00	27,23	13,77	5,28	53,18	0,72	0,03	0,00	0,00	0,85	101,42	0,01	0,00	0,46	0,71	0,28	1,49	0,03	0,00	0,00	0,00	0,01	3,00
66	0,15	0,00	24,23	13,98	5,33	56,10	0,56	0,01	0,00	0,00	0,49	100,86	0,00	0,00	0,41	0,72	0,28	1,56	0,03	0,00	0,00	0,00	0,01	3,00
67	0,50	0,00	59,54	11,54	4,68	23,05	0,79	0,03	0,00	0,01	0,63	100,78	0,01	0,00	1,18	0,70	0,29	0,76	0,04	0,00	0,00	0,00	0,01	3,01
68	0,08	0,00	18,96	14,17	5,83	60,80	0,44	0,00	0,00	0,00	0,33	100,60	0,00	0,00	0,31	0,72	0,30	1,66	0,02	0,00	0,00	0,00	0,01	3,01
69	0,27	0,00	35,81	13,21	5,16	44,93	0,72	0,03	0,00	0,03	1,13	101,28	0,01	0,00	0,63	0,71	0,28	1,31	0,03	0,00	0,00	0,00	0,02	3,00
70	0,14	0,00	28,43	13,31	5,35	53,02	0,31	0,01	0,00	0,01	0,00	100,57	0,00	0,00	0,49	0,70	0,28	1,51	0,01	0,00	0,00	0,00	0,00	2,99
71	0,41	0,00	37,79	13,06	4,93	43,34	0,96	0,05	0,00	0,01	0,80	101,33	0,01	0,00	0,67	0,71	0,27	1,27	0,05	0,00	0,00	0,00	0,01	3,00
72	0,53	0,01	12,16	14,40	5,55	65,42	1,47	0,00	0,00	0,00	1,25	100,79	0,01	0,00	0,19	0,70	0,27	1,73	0,06	0,00	0,00	0,00	0,02	3,00
73	0,13	0,02	21,93	13,83	5,26	58,45	0,45	0,02	0,00	0,01	0,91	101,01	0,00	0,00	0,36	0,70	0,27	1,61	0,02	0,00	0,00	0,00	0,01	2,99
74	0,20	0,00	19,81	14,26	5,39	60,37	0,59	0,00	0,00	0,00	0,17	100,80	0,00	0,00	0,33	0,72	0,28	1,65	0,03	0,00	0,00	0,00	0,00	3,00
75	0,20	0,00	15,36	14,37	5,32	63,87	0,50	0,01	0,00	0,01	1,11	100,75	0,00	0,00	0,25	0,71	0,27	1,72	0,02	0,00	0,00	0,00	0,02	2,99
76	0,18	0,00	24,18	13,95	5,39	56,30	0,61	0,00	0,00	0,03	0,51	101,14	0,00	0,00	0,40	0,72	0,28	1,56	0,03	0,00	0,00	0,00	0,01	3,00

Point	SnO2	MgO	Ta2O5	FeO	MnO	Nb2O5	TiO2	Sc2O3	U2O	CaO	WO3	Total	Sn a.p.f.u	Mg	Ta	Fe	Mn	Nb	Ti	Sc	U	Ca	W	Total
Sample Na-6													6 anions											
77	0,24	0,00	21,84	13,70	5,98	58,16	0,49	0,02	0,00	0,00	0,95	101,39	0,01	0,00	0,36	0,70	0,31	1,60	0,02	0,00	0,00	0,00	0,01	3,01
78	0,23	0,00	17,82	13,92	5,79	61,84	0,67	0,01	0,00	0,00	0,98	101,26	0,01	0,00	0,29	0,69	0,29	1,67	0,03	0,00	0,00	0,00	0,02	3,00
79	0,82	0,00	41,48	12,18	5,42	38,55	1,03	0,03	0,00	0,00	0,45	99,96	0,02	0,00	0,76	0,69	0,31	1,17	0,05	0,00	0,00	0,00	0,01	3,01
80	0,68	0,00	41,08	12,18	5,19	39,47	0,90	0,05	0,00	0,01	0,83	100,38	0,02	0,00	0,75	0,68	0,29	1,19	0,05	0,00	0,00	0,00	0,01	3,00
81	0,58	0,00	37,64	12,54	5,37	42,13	0,85	0,03	0,00	0,00	0,72	99,85	0,02	0,00	0,68	0,69	0,30	1,26	0,04	0,00	0,00	0,00	0,01	3,01
82	0,74	0,00	36,68	12,44	5,47	43,99	0,88	0,03	0,00	0,01	0,66	100,91	0,02	0,00	0,65	0,68	0,30	1,29	0,04	0,00	0,00	0,00	0,01	3,00
83	0,47	0,00	35,65	12,83	5,58	45,60	0,75	0,00	0,00	0,01	0,00	100,88	0,01	0,00	0,63	0,69	0,31	1,33	0,04	0,00	0,00	0,00	0,00	3,01
84	0,52	0,00	35,83	12,75	5,35	44,54	0,82	0,03	0,00	0,01	0,61	100,47	0,01	0,00	0,64	0,69	0,30	1,31	0,04	0,00	0,00	0,00	0,01	3,00
85	0,24	0,00	20,50	13,77	5,57	58,49	0,64	0,01	0,00	0,00	1,14	100,36	0,01	0,00	0,34	0,70	0,29	1,61	0,03	0,00	0,00	0,00	0,02	3,00
86	0,75	0,00	36,23	12,71	5,02	43,49	0,88	0,01	0,00	0,00	1,00	100,08	0,02	0,00	0,65	0,70	0,28	1,29	0,04	0,00	0,00	0,00	0,02	3,00
87	0,19	0,00	29,42	13,03	5,82	50,79	0,31	0,04	0,00	0,00	1,45	101,06	0,00	0,00	0,51	0,69	0,31	1,45	0,01	0,00	0,00	0,00	0,02	3,00
88	0,17	0,00	52,61	11,44	5,48	30,77	0,32	0,03	0,00	0,00	0,42	101,24	0,00	0,00	1,00	0,67	0,33	0,97	0,02	0,00	0,00	0,00	0,01	3,00
89	0,22	0,00	55,26	11,55	5,49	28,14	0,29	0,07	0,00	0,00	0,19	101,22	0,01	0,00	1,07	0,69	0,33	0,90	0,02	0,00	0,00	0,00	0,00	3,01
90	0,30	0,00	32,19	13,33	5,30	48,45	0,66	0,05	0,00	0,00	0,52	100,79	0,01	0,00	0,56	0,71	0,29	1,40	0,03	0,00	0,00	0,00	0,01	3,01
91	0,32	0,00	26,19	13,26	5,73	53,24	0,72	0,01	0,00	0,00	0,77	100,25	0,01	0,00	0,45	0,69	0,30	1,51	0,03	0,00	0,00	0,00	0,01	3,00
92	0,40	0,00	25,96	13,25	5,81	53,66	0,74	0,02	0,00	0,01	0,98	100,83	0,01	0,00	0,44	0,69	0,31	1,51	0,03	0,00	0,00	0,00	0,02	3,00
93	0,39	0,00	32,78	12,73	5,90	47,45	0,70	0,00	0,00	0,01	0,94	100,90	0,01	0,00	0,57	0,68	0,32	1,37	0,03	0,00	0,00	0,00	0,02	3,01
94	0,26	0,00	27,67	13,16	5,86	52,39	0,48	0,03	0,00	0,00	1,11	100,95	0,01	0,00	0,47	0,69	0,31	1,48	0,02	0,00	0,00	0,00	0,02	3,00
95	0,30	0,00	34,74	12,97	5,35	45,44	0,61	0,00	0,00	0,02	0,55	99,98	0,01	0,00	0,62	0,71	0,30	1,34	0,03	0,00	0,00	0,00	0,01	3,01
96	0,23	0,00	25,16	13,12	5,91	52,94	0,44	0,01	0,00	0,02	1,33	99,17	0,01	0,00	0,43	0,69	0,32	1,51	0,02	0,00	0,00	0,00	0,02	3,01
97	0,14	0,00	33,80	12,68	5,99	47,59	0,47	0,02	0,00	0,01	0,57	101,27	0,00	0,00	0,59	0,68	0,32	1,38	0,02	0,00	0,00	0,00	0,01	3,01
98	0,68	0,00	62,13	10,58	5,21	20,88	0,32	0,06	0,00	0,00	0,00	99,86	0,02	0,00	1,26	0,66	0,33	0,71	0,02	0,00	0,00	0,00	0,00	3,00
99	0,16	0,00	26,12	13,36	6,04	54,39	0,43	0,00	0,00	0,00	0,57	101,07	0,00	0,00	0,44	0,69	0,32	1,53	0,02	0,00	0,00	0,00	0,01	3,01
100	0,23	0,00	25,19	13,47	6,01	54,31	0,61	0,01	0,00	0,00	0,81	100,63	0,01	0,00	0,43	0,70	0,32	1,53	0,03	0,00	0,00	0,00	0,01	3,01
101	0,42	0,00	37,37	12,81	5,32	42,82	0,73	0,01	0,00	0,00	1,52	100,99	0,01	0,00	0,67	0,70	0,29	1,27	0,04	0,00	0,00	0,00	0,03	3,00
102	0,21	0,00	57,85	11,43	5,26	25,23	0,33	0,05	0,00	0,01	0,41	100,78	0,01	0,00	1,14	0,69	0,32	0,83	0,02	0,00	0,00	0,00	0,01	3,01
103	0,28	0,00	20,16	13,79	5,63	58,67	0,65	0,02	0,00	0,00	0,61	99,81	0,01	0,00	0,34	0,71	0,29	1,62	0,03	0,00	0,00	0,00	0,01	3,00
104	0,37	0,00	36,88	12,98	5,28	44,37	0,65	0,02	0,00	0,00	0,65	101,19	0,01	0,00	0,65	0,71	0,29	1,30	0,03	0,00	0,00	0,00	0,01	3,00
Sample G-4																								
105	0,63	0,04	21,89	15,64	5,87	54,61	0,97	0,01	0,00	0,00	0,11	99,78	0,02	0,00	0,37	0,81	0,31	1,53	0,05	0,00	0,00	0,00	0,00	3,09
106	0,26	0,03	25,76	14,45	6,47	51,49	0,77	0,00	0,00	0,02	0,00	99,25	0,01	0,00	0,44	0,77	0,35	1,47	0,04	0,00	0,00	0,00	0,00	3,08
107	0,17	0,05	24,08	15,44	5,88	52,29	0,84	0,01	0,00	0,02	0,08	98,85	0,00	0,00	0,41	0,82	0,31	1,49	0,04	0,00	0,00	0,00	0,00	3,09
108	0,59	0,06	22,40	14,90	6,13	53,17	1,07	0,00	0,00	0,00	0,19	98,50	0,01	0,01	0,38	0,78	0,33	1,51	0,05	0,00	0,00	0,00	0,00	3,08
109	0,26	0,05	24,82	15,70	5,89	51,90	0,88	0,02	0,00	0,00	0,00	99,52	0,01	0,00	0,43	0,83	0,31	1,48	0,04	0,00	0,00	0,00	0,00	3,10
110	0,27	0,04	25,93	15,50	5,88	51,88	1,09	0,02	0,00	0,02	0,16	100,79	0,01	0,00	0,44	0,81	0,31	1,46	0,05	0,00	0,00	0,00	0,00	3,09
111	0,59	0,02	23,90	16,41	4,90	51,13	1,49	0,03	0,00	0,04	0,23	98,74	0,01	0,00	0,41	0,87	0,26	1,46	0,07	0,00	0,00	0,00	0,00	3,10
112	0,51	0,02	21,52	14,52	6,64	53,89	1,20	0,01	0,00	0,01	0,20	98,53	0,01	0,00	0,37	0,76	0,35	1,53	0,06	0,00	0,00	0,00	0,00	3,08
113	0,32	0,08	26,89	14,54	6,00	50,23	1,19	0,01	0,00	0,00	0,20	99,45	0,01	0,01	0,46	0,77	0,32	1,44	0,06	0,00	0,00	0,00	0,00	3,07
114	0,30	0,03	32,11	13,53	6,74	45,26	0,75	0,04	0,00	0,01	0,25	99,01	0,01	0,00	0,57	0,74	0,37	1,34	0,04	0,00	0,00	0,00	0,00	3,08

Point	SnO2	MgO	Ta2O5	FeO	MnO	Nb2O5	TiO2	Sc2O3	U2O	CaO	WO3	Total	Sn a.p.f.u	Mg	Ta	Fe	Mn	Nb	Ti	Sc	U	Ca	W	Total
115	0,17	0,01	21,80	13,82	7,51	55,55	0,47	0,03	0,00	0,02	0,11	99,49	0,00	0,00	0,37	0,72	0,40	1,56	0,02	0,00	0,00	0,00	0,00	3,08
116	0,33	0,00	20,28	15,86	5,45	56,55	0,99	0,00	0,00	0,03	0,35	99,85	0,01	0,00	0,34	0,82	0,28	1,57	0,05	0,00	0,00	0,00	0,01	3,07
117	0,28	0,03	28,24	13,87	6,89	48,44	0,91	0,02	0,00	0,00	0,27	98,94	0,01	0,00	0,49	0,75	0,38	1,41	0,04	0,00	0,00	0,00	0,00	3,08
118	0,22	0,03	24,82	14,98	6,21	51,83	0,82	0,00	0,00	0,00	0,11	99,02	0,01	0,00	0,43	0,79	0,33	1,48	0,04	0,00	0,00	0,00	0,00	3,09
Sample 4-4																								
119	0,39	0,03	26,38	12,29	7,58	53,28	0,56	0,00	0,00	0,00	0,03	100,55	0,01	0,00	0,45	0,64	0,40	1,50	0,03	0,00	0,00	0,00	0,00	3,03
120	0,09	0,02	50,08	11,43	6,58	30,83	0,39	0,01	0,00	0,00	0,07	99,52	0,00	0,00	0,96	0,68	0,39	0,99	0,02	0,00	0,00	0,00	0,00	3,05
121	0,25	0,03	27,57	12,22	7,74	52,80	0,55	0,02	0,00	0,01	0,20	101,37	0,01	0,00	0,47	0,64	0,41	1,48	0,03	0,00	0,00	0,00	0,00	3,03
122	0,18	0,03	28,42	11,66	8,17	51,70	0,54	0,00	0,00	0,03	0,36	101,08	0,00	0,00	0,48	0,61	0,43	1,46	0,03	0,00	0,00	0,00	0,01	3,03
123	0,24	0,01	28,01	11,63	8,22	52,04	0,53	0,00	0,00	0,00	0,05	100,73	0,01	0,00	0,48	0,61	0,44	1,48	0,03	0,00	0,00	0,00	0,00	3,04
124	0,18	0,02	29,63	11,10	8,45	49,88	0,44	0,00	0,00	0,02	0,15	99,87	0,00	0,00	0,51	0,59	0,46	1,44	0,02	0,00	0,00	0,00	0,00	3,04
125	0,16	0,01	32,71	9,74	9,27	48,10	0,40	0,00	0,00	0,01	0,22	100,62	0,00	0,00	0,57	0,52	0,50	1,40	0,02	0,00	0,00	0,00	0,00	3,02
126	0,15	0,03	42,72	11,88	6,78	38,32	0,32	0,01	0,00	0,00	0,18	100,38	0,00	0,00	0,78	0,67	0,39	1,17	0,02	0,00	0,00	0,00	0,00	3,04
127	0,16	0,02	33,04	12,75	6,69	46,62	0,34	0,01	0,00	0,02	0,17	99,80	0,00	0,00	0,58	0,69	0,37	1,37	0,02	0,00	0,00	0,00	0,00	3,04
128	0,18	0,04	23,14	14,13	6,07	57,20	0,54	0,02	0,00	0,02	0,00	101,33	0,00	0,00	0,38	0,72	0,31	1,58	0,02	0,00	0,00	0,00	0,00	3,03
129	0,26	0,01	33,03	10,03	9,07	47,11	0,40	0,02	0,00	0,03	0,00	99,96	0,01	0,00	0,58	0,54	0,50	1,38	0,02	0,00	0,00	0,00	0,00	3,03
130	0,19	0,05	26,84	13,47	6,63	52,88	0,42	0,01	0,00	0,01	0,00	100,49	0,00	0,00	0,46	0,71	0,35	1,50	0,02	0,00	0,00	0,00	0,00	3,04
Sample 4-12																								
131	0,17	0,00	31,62	11,37	7,04	49,26	0,33	0,01	0,00	0,02	0,00	99,82	0,00	0,00	0,55	0,61	0,38	1,43	0,02	0,00	0,00	0,00	0,00	3,00
132	0,25	0,00	47,70	11,00	6,18	35,68	0,44	0,03	0,00	0,02	0,00	101,29	0,01	0,00	0,88	0,63	0,36	1,10	0,02	0,00	0,00	0,00	0,00	3,00
133	0,08	0,00	31,05	12,00	6,46	50,70	0,33	0,02	0,00	0,00	0,00	100,65	0,00	0,00	0,54	0,64	0,35	1,46	0,02	0,00	0,00	0,00	0,00	3,00
134	0,36	0,00	15,66	12,29	7,43	62,74	0,77	0,01	0,00	0,03	0,13	99,41	0,01	0,00	0,26	0,62	0,38	1,71	0,03	0,00	0,00	0,00	0,00	3,01
135	0,46	0,00	16,08	12,47	7,50	62,12	0,76	0,00	0,00	0,01	0,17	99,55	0,01	0,00	0,26	0,63	0,38	1,69	0,03	0,00	0,00	0,00	0,00	3,02
136	0,18	0,00	44,70	11,57	6,22	36,80	0,53	0,02	0,00	0,00	0,14	100,16	0,00	0,00	0,83	0,66	0,36	1,13	0,03	0,00	0,00	0,00	0,00	3,02
137	0,27	0,00	13,81	12,15	7,97	64,55	0,65	0,00	0,00	0,01	0,00	99,41	0,01	0,00	0,22	0,61	0,40	1,74	0,03	0,00	0,00	0,00	0,00	3,01
138	0,27	0,00	14,61	11,98	7,86	64,01	0,61	0,00	0,00	0,01	0,11	99,46	0,01	0,00	0,24	0,60	0,40	1,73	0,03	0,00	0,00	0,00	0,00	3,01
139	0,39	0,00	14,30	12,93	7,39	64,14	0,74	0,01	0,00	0,02	0,32	100,24	0,01	0,00	0,23	0,64	0,37	1,72	0,03	0,00	0,00	0,00	0,00	3,02
140	0,64	0,00	15,28	12,31	7,17	62,16	1,30	0,00	0,06	0,00	0,77	99,68	0,02	0,00	0,25	0,62	0,36	1,68	0,06	0,00	0,00	0,00	0,01	3,00
141	0,13	0,00	12,63	12,94	7,50	66,49	0,37	0,00	0,00	0,01	0,28	100,35	0,00	0,00	0,20	0,64	0,37	1,77	0,02	0,00	0,00	0,00	0,00	3,01
142	0,13	0,02	12,12	12,93	7,23	66,06	0,34	0,01	0,00	0,02	0,00	98,85	0,00	0,00	0,20	0,65	0,37	1,78	0,02	0,00	0,00	0,00	0,00	3,01
143	0,28	0,00	11,86	12,83	7,33	66,71	0,96	0,01	0,00	0,02	0,00	100,00	0,01	0,00	0,19	0,63	0,36	1,77	0,04	0,00	0,00	0,00	0,00	3,01
144	0,22	0,00	12,60	12,78	7,41	65,11	0,64	0,01	0,00	0,00	0,00	98,76	0,01	0,00	0,21	0,64	0,38	1,76	0,03	0,00	0,00	0,00	0,00	3,02
145	0,33	0,00	13,61	12,48	7,33	64,32	0,81	0,00	0,00	0,00	0,61	99,48	0,01	0,00	0,22	0,62	0,37	1,74	0,04	0,00	0,00	0,00	0,01	3,00
146	0,39	0,01	14,32	12,58	7,29	63,69	0,85	0,00	0,00	0,01	0,48	99,62	0,01	0,00	0,23	0,63	0,37	1,72	0,04	0,00	0,00	0,00	0,01	3,01
147	0,27	0,00	14,46	11,88	7,92	63,12	0,70	0,01	0,00	0,02	0,86	99,24	0,01	0,00	0,24	0,60	0,40	1,72	0,03	0,00	0,00	0,00	0,01	3,01
148	0,24	0,00	18,08	12,37	7,46	60,78	0,63	0,01	0,00	0,01	0,40	99,97	0,01	0,00	0,30	0,63	0,38	1,66	0,03	0,00	0,00	0,00	0,01	3,01
149	0,35	0,00	16,74	12,22	7,10	61,42	0,82	0,00	0,00	0,02	0,53	99,20	0,01	0,00	0,28	0,62	0,36	1,68	0,04	0,00	0,00	0,00	0,01	3,00
150	0,36	0,00	16,43	12,50	7,14	61,89	0,81	0,00	0,00	0,02	0,11	99,25	0,01	0,00	0,27	0,63	0,37	1,69	0,04	0,00	0,00	0,00	0,00	3,01
151	0,25	0,00	32,79	10,60	7,74	47,41	0,39	0,00	0,00	0,01	0,00	99,19	0,01	0,00	0,58	0,58	0,43	1,40	0,02	0,00	0,00	0,00	0,00	3,01
152	0,37	0,01	32,23	11,68	6,77	48,54	0,51	0,04	0,00	0,01	0,50	100,66	0,01	0,00	0,56	0,62	0,37	1,40	0,02	0,00	0,00	0,00	0,01	3,00

Point	SnO2	MgO	Ta2O5	FeO	MnO	Nb2O5	TiO2	Sc2O3	U2O	CaO	WO3	Total	Sn a.p.f.u	Mg	Ta	Fe	Mn	Nb	Ti	Sc	U	Ca	W	Total
153	0,39	0,00	32,21	10,28	8,16	48,26	0,42	0,00	0,00	0,03	0,15	99,89	0,01	0,00	0,56	0,55	0,45	1,41	0,02	0,00	0,00	0,00	0,00	3,01
154	0,30	0,00	13,08	12,45	7,67	65,04	0,70	0,00	0,00	0,00	0,00	99,23	0,01	0,00	0,21	0,62	0,39	1,75	0,03	0,00	0,00	0,00	0,00	3,01
155	0,44	0,01	13,02	12,88	7,03	64,58	0,90	0,01	0,00	0,02	0,60	99,48	0,01	0,00	0,21	0,64	0,35	1,74	0,04	0,00	0,00	0,00	0,01	3,01
156	0,31	0,00	15,05	11,71	8,09	63,54	0,63	0,00	0,00	0,01	0,25	99,58	0,01	0,00	0,25	0,59	0,41	1,72	0,03	0,00	0,00	0,00	0,00	3,01
157	0,25	0,00	14,34	11,85	8,37	63,48	0,64	0,00	0,00	0,06	0,00	98,98	0,01	0,00	0,23	0,60	0,43	1,73	0,03	0,00	0,00	0,00	0,00	3,02
158	0,29	0,00	11,88	12,81	7,26	66,16	0,87	0,00	0,00	0,00	0,71	99,99	0,01	0,00	0,19	0,63	0,36	1,76	0,04	0,00	0,00	0,00	0,01	3,00
159	0,22	0,00	11,71	12,75	7,56	66,02	0,69	0,00	0,00	0,00	0,05	98,99	0,01	0,00	0,19	0,63	0,38	1,78	0,03	0,00	0,00	0,00	0,00	3,02
160	0,17	0,00	11,74	12,65	7,41	66,13	0,46	0,00	0,00	0,00	0,32	98,88	0,00	0,00	0,19	0,63	0,37	1,78	0,02	0,00	0,00	0,00	0,01	3,01
Sample 4-11																								
161	0,22	0,00	11,00	12,61	7,76	66,74	0,84	0,01	0,00	0,00	1,26	100,44	0,01	0,00	0,18	0,62	0,39	1,77	0,04	0,00	0,00	0,00	0,02	3,01
162	0,17	0,09	11,41	13,16	7,19	66,61	0,56	0,00	0,00	0,00	0,00	99,17	0,00	0,01	0,18	0,65	0,36	1,78	0,02	0,00	0,00	0,00	0,00	3,02
163	0,29	0,00	11,44	12,46	7,73	65,53	0,89	0,00	0,00	0,02	0,28	98,63	0,01	0,00	0,19	0,62	0,39	1,77	0,04	0,00	0,00	0,00	0,00	3,02
164	0,26	0,00	12,38	12,66	7,58	65,56	0,76	0,00	0,00	0,02	0,00	99,22	0,01	0,00	0,20	0,63	0,38	1,76	0,03	0,00	0,00	0,00	0,00	3,02
165	0,25	0,00	11,12	12,57	7,82	66,50	0,68	0,00	0,00	0,01	0,85	99,79	0,01	0,00	0,18	0,62	0,39	1,77	0,03	0,00	0,00	0,00	0,01	3,01
166	0,14	0,00	18,18	11,93	7,80	61,17	0,69	0,01	0,00	0,02	0,21	100,16	0,00	0,00	0,30	0,60	0,40	1,67	0,03	0,00	0,00	0,00	0,00	3,01
167	0,37	0,00	12,42	12,64	7,44	65,45	0,91	0,03	0,00	0,01	0,73	100,01	0,01	0,00	0,20	0,62	0,37	1,75	0,04	0,00	0,00	0,00	0,01	3,01
168	0,38	0,00	12,33	12,50	7,42	65,09	1,00	0,00	0,00	0,00	0,98	99,69	0,01	0,00	0,20	0,62	0,37	1,74	0,04	0,00	0,00	0,00	0,02	3,00
169	0,30	0,01	11,74	12,58	7,46	65,84	0,86	0,00	0,00	0,01	0,07	98,86	0,01	0,00	0,19	0,63	0,38	1,77	0,04	0,00	0,00	0,00	0,00	3,01
170	1,57	0,00	79,93	13,85	0,73	4,23	0,31	0,08	0,00	0,00	0,22	100,91	0,05	0,00	1,78	0,95	0,05	0,16	0,02	0,01	0,00	0,00	0,00	3,01
171	0,38	0,00	82,25	13,63	0,82	3,76	0,11	0,07	0,00	0,00	0,05	101,07	0,01	0,00	1,84	0,94	0,06	0,14	0,01	0,01	0,00	0,00	0,00	3,00
172	0,19	0,00	12,82	12,86	7,17	65,38	0,63	0,00	0,00	0,00	0,06	99,11	0,00	0,00	0,21	0,64	0,36	1,76	0,03	0,00	0,00	0,00	0,00	3,01
173	0,16	0,00	11,54	12,65	7,63	66,29	0,56	0,01	0,00	0,01	0,35	99,19	0,00	0,00	0,19	0,63	0,38	1,78	0,03	0,00	0,00	0,00	0,01	3,01
174	0,17	0,00	11,45	12,83	7,33	65,98	0,79	0,01	0,00	0,02	0,74	99,32	0,00	0,00	0,18	0,64	0,37	1,77	0,04	0,00	0,00	0,00	0,01	3,01
175	2,73	0,00	77,06	13,66	0,72	5,65	0,59	0,08	0,00	0,01	0,13	100,63	0,09	0,00	1,70	0,93	0,05	0,21	0,04	0,01	0,00	0,00	0,00	3,01
176	0,40	0,00	14,04	12,67	7,41	63,27	1,06	0,00	0,00	0,00	0,36	99,22	0,01	0,00	0,23	0,64	0,38	1,71	0,05	0,00	0,00	0,00	0,01	3,02
177	0,31	0,00	17,91	9,10	11,06	60,66	1,03	0,00	0,00	0,04	0,00	100,10	0,01	0,00	0,29	0,46	0,56	1,65	0,05	0,00	0,00	0,00	0,00	3,03
178	0,44	0,00	12,13	12,73	7,14	65,05	1,06	0,00	0,00	0,01	0,77	99,34	0,01	0,00	0,20	0,63	0,36	1,75	0,05	0,00	0,00	0,00	0,01	3,00
179	0,12	0,00	10,26	12,66	7,81	67,90	0,63	0,00	0,00	0,00	0,32	99,70	0,00	0,00	0,16	0,62	0,39	1,80	0,03	0,00	0,00	0,00	0,00	3,01
180	0,42	0,00	18,35	12,25	7,37	59,92	1,05	0,04	0,00	0,00	0,42	99,82	0,01	0,00	0,30	0,62	0,38	1,64	0,05	0,00	0,00	0,00	0,01	3,01
181	0,39	0,00	12,26	12,43	7,55	65,07	0,88	0,00	0,00	0,02	0,28	98,88	0,01	0,00	0,20	0,62	0,38	1,76	0,04	0,00	0,00	0,00	0,00	3,01
182	0,82	0,00	78,34	14,01	0,71	6,13	0,60	0,11	0,00	0,00	0,24	100,96	0,03	0,00	1,72	0,94	0,05	0,22	0,04	0,01	0,00	0,00	0,01	3,01
183	0,83	0,00	78,87	14,05	0,68	6,11	0,62	0,10	0,00	0,00	0,00	101,25	0,03	0,00	1,73	0,95	0,05	0,22	0,04	0,01	0,00	0,00	0,00	3,01
184	0,25	0,01	12,50	12,56	7,58	65,40	0,84	0,00	0,00	0,01	0,18	99,31	0,01	0,00	0,20	0,62	0,38	1,76	0,04	0,00	0,00	0,00	0,00	3,01
185	0,22	0,00	13,91	10,37	9,57	63,87	0,90	0,01	0,00	0,00	1,25	100,10	0,01	0,00	0,22	0,52	0,48	1,72	0,04	0,00	0,00	0,00	0,02	3,00
186	0,53	0,01	12,83	11,84	8,16	63,79	1,36	0,00	0,00	0,00	0,17	98,68	0,01	0,00	0,21	0,59	0,41	1,73	0,06	0,00	0,00	0,00	0,00	3,02
187	0,29	0,00	11,37	12,50	7,34	66,89	0,96	0,00	0,00	0,02	0,94	100,32	0,01	0,00	0,18	0,61	0,36	1,77	0,04	0,00	0,00	0,00	0,01	2,99
188	0,28	0,00	42,77	11,65	6,02	38,43	0,64	0,04	0,00	0,01	0,34	100,16	0,01	0,00	0,79	0,66	0,34	1,17	0,03	0,00	0,00	0,00	0,01	3,01
189	0,17	0,00	14,52	12,47	7,70	64,72	0,56	0,00	0,00	0,00	0,82	100,97	0,00	0,00	0,23	0,62	0,39	1,73	0,03	0,00	0,00	0,00	0,01	3,00
190	0,37	0,00	15,82	12,40	7,53	61,52	0,92	0,00	0,00	0,03	0,25	98,82	0,01	0,00	0,26	0,63	0,39	1,69	0,04	0,00	0,00	0,00	0,00	3,02
191	0,33	0,00	40,80	11,45	6,34	39,77	0,97	0,07	0,00	0,02	0,16	99,90	0,01	0,00	0,74	0,64	0,36	1,20	0,05	0,00	0,00	0,00	0,00	3,01

Point	SnO2	MgO	Ta2O5	FeO	MnO	Nb2O5	TiO2	Sc2O3	U2O	CaO	WO3	Total	Sn a.p.f.u	Mg	Ta	Fe	Mn	Nb	Ti	Sc	U	Ca	W	Total
192	0,30	0,01	11,52	12,89	7,17	66,15	0,94	0,03	0,00	0,00	0,27	99,27	0,01	0,00	0,19	0,64	0,36	1,77	0,04	0,00	0,00	0,00	0,00	3,01
193	0,37	0,01	12,79	12,50	7,48	65,49	0,83	0,00	0,00	0,01	0,21	99,69	0,01	0,00	0,21	0,62	0,38	1,75	0,04	0,00	0,00	0,00	0,00	3,01
194	0,21	0,01	11,03	12,70	7,62	66,11	0,78	0,00	0,00	0,00	0,25	98,70	0,01	0,00	0,18	0,63	0,38	1,78	0,03	0,00	0,00	0,00	0,00	3,02
Sample 4-9																								
195	0,25	0,04	54,55	11,06	4,96	28,22	0,29	0,05	0,00	0,02	0,00	99,44	0,01	0,00	1,07	0,67	0,30	0,92	0,02	0,00	0,00	0,00	0,00	2,99
196	0,21	0,00	35,76	8,70	9,04	44,91	0,26	0,02	0,00	0,01	0,39	99,30	0,01	0,00	0,64	0,48	0,51	1,34	0,01	0,00	0,00	0,00	0,01	2,99
197	0,57	0,00	60,43	9,93	5,44	21,42	1,22	0,02	0,00	0,01	0,00	99,03	0,02	0,00	1,22	0,62	0,34	0,72	0,07	0,00	0,00	0,00	0,00	3,00
198	0,11	0,00	38,99	7,45	9,74	41,78	0,22	0,04	0,00	0,00	0,60	98,92	0,00	0,00	0,71	0,42	0,56	1,27	0,01	0,00	0,00	0,00	0,01	2,99
199	0,21	0,00	29,57	9,86	8,54	50,38	0,39	0,00	0,00	0,00	0,14	99,09	0,01	0,00	0,52	0,53	0,46	1,46	0,02	0,00	0,00	0,00	0,00	3,00
200	0,52	0,00	60,51	9,43	6,38	22,00	0,99	0,00	0,00	0,00	0,20	100,03	0,02	0,00	1,21	0,58	0,40	0,73	0,05	0,00	0,00	0,00	0,00	3,00
201	0,04	0,03	45,34	11,62	5,23	36,76	0,22	0,03	0,00	0,01	0,00	99,28	0,00	0,00	0,85	0,67	0,31	1,15	0,01	0,00	0,00	0,00	0,00	2,99
202	0,15	0,00	37,53	10,66	6,65	44,15	0,19	0,03	0,00	0,00	0,06	99,43	0,00	0,00	0,68	0,59	0,37	1,32	0,01	0,00	0,00	0,00	0,00	2,98
203	0,18	0,00	39,19	7,67	9,65	42,79	0,14	0,04	0,00	0,02	0,56	100,23	0,00	0,00	0,71	0,43	0,54	1,28	0,01	0,00	0,00	0,00	0,01	2,98
204	0,23	0,00	32,06	9,38	8,18	48,31	0,30	0,03	0,00	0,00	0,47	98,94	0,01	0,00	0,57	0,51	0,45	1,42	0,01	0,00	0,00	0,00	0,01	2,98
205	0,25	0,00	32,07	9,42	8,28	48,61	0,37	0,04	0,00	0,01	0,00	99,05	0,01	0,00	0,57	0,51	0,46	1,43	0,02	0,00	0,00	0,00	0,00	2,99
206	0,52	0,00	55,69	9,48	6,27	25,94	1,10	0,03	0,00	0,00	0,18	99,21	0,02	0,00	1,10	0,58	0,39	0,85	0,06	0,00	0,00	0,00	0,00	2,99
207	0,63	0,07	53,52	10,73	4,68	28,67	1,00	0,03	0,00	0,00	0,00	99,33	0,02	0,01	1,04	0,64	0,28	0,93	0,05	0,00	0,00	0,00	0,00	2,98
208	0,50	0,00	44,27	10,83	5,85	37,30	0,76	0,03	0,00	0,00	0,00	99,55	0,01	0,00	0,82	0,62	0,34	1,15	0,04	0,00	0,00	0,00	0,00	2,99
Sample 4-3																								
209	0,20	0,00	57,28	9,35	6,41	25,29	0,63	0,00	0,00	0,00	0,00	99,16	0,01	0,00	1,14	0,57	0,40	0,84	0,03	0,00	0,00	0,00	0,00	2,99
210	0,24	0,00	52,67	9,81	6,10	27,90	0,85	0,00	0,00	0,00	1,28	98,86	0,01	0,00	1,03	0,59	0,37	0,91	0,05	0,00	0,00	0,00	0,02	2,98
211	0,46	0,00	58,53	10,49	5,14	23,81	0,94	0,06	0,00	0,01	0,00	99,43	0,01	0,00	1,17	0,64	0,32	0,79	0,05	0,00	0,00	0,00	0,00	2,99
212	0,71	0,00	37,03	11,04	6,12	43,69	0,20	0,00	0,00	0,01	0,00	98,79	0,02	0,00	0,67	0,62	0,35	1,32	0,01	0,00	0,00	0,00	0,00	2,98
Sample 10-4																								
213	0,74	0,37	20,15	14,35	4,37	56,50	1,93	0,04	0,00	0,00	0,94	99,38	0,02	0,03	0,34	0,73	0,23	1,56	0,09	0,00	0,00	0,00	0,01	3,02
214	0,66	0,37	20,77	14,46	4,51	56,45	1,87	0,06	0,00	0,00	1,32	100,47	0,02	0,03	0,34	0,73	0,23	1,55	0,09	0,00	0,00	0,00	0,02	3,02
215	0,60	0,34	20,70	14,18	4,48	56,14	1,74	0,03	0,00	0,00	1,34	99,56	0,01	0,03	0,35	0,73	0,23	1,56	0,08	0,00	0,00	0,00	0,02	3,01
216	0,60	0,33	20,19	14,34	4,80	56,55	1,87	0,03	0,00	0,00	0,96	99,69	0,01	0,03	0,34	0,73	0,25	1,56	0,09	0,00	0,00	0,00	0,02	3,02
217	0,66	0,40	20,12	14,29	4,38	57,37	1,91	0,04	0,00	0,00	1,44	100,63	0,02	0,04	0,33	0,72	0,22	1,57	0,09	0,00	0,00	0,00	0,02	3,01
218	0,75	0,36	25,00	14,10	4,28	52,20	2,32	0,03	0,00	0,00	1,46	100,49	0,02	0,03	0,42	0,73	0,22	1,46	0,11	0,00	0,00	0,00	0,02	3,01
219	0,70	0,17	24,39	13,11	5,42	51,92	2,17	0,07	0,00	0,02	0,57	98,55	0,02	0,02	0,42	0,69	0,29	1,48	0,10	0,00	0,00	0,00	0,01	3,02
220	0,75	0,32	22,69	14,15	4,33	53,85	2,29	0,05	0,00	0,00	1,16	99,57	0,02	0,03	0,38	0,73	0,23	1,50	0,11	0,00	0,00	0,00	0,02	3,01
221	1,10	0,39	45,49	12,63	4,02	34,56	2,22	0,06	0,00	0,00	0,26	100,72	0,03	0,04	0,83	0,71	0,23	1,05	0,11	0,00	0,00	0,00	0,00	3,02
222	0,88	0,44	28,93	13,99	4,45	48,18	2,05	0,03	0,00	0,02	0,99	99,95	0,02	0,04	0,50	0,74	0,24	1,38	0,10	0,00	0,00	0,00	0,02	3,03
223	0,26	0,48	55,27	12,19	3,35	27,25	0,46	0,01	0,00	0,27	0,00	99,53	0,01	0,05	1,08	0,73	0,20	0,89	0,02	0,00	0,00	0,02	0,00	3,01
224	0,75	0,27	19,49	15,13	4,24	56,99	1,99	0,05	0,00	0,03	0,98	99,92	0,02	0,02	0,32	0,77	0,22	1,57	0,09	0,00	0,00	0,00	0,02	3,03
225	0,81	0,28	18,96	15,24	4,10	56,70	2,10	0,05	0,00	0,00	1,10	99,33	0,02	0,03	0,31	0,78	0,21	1,56	0,10	0,00	0,00	0,00	0,02	3,03
226	0,75	0,31	20,39	15,29	4,08	56,20	2,05	0,06	0,00	0,02	0,81	99,97	0,02	0,03	0,34	0,78	0,21	1,55	0,09	0,00	0,00	0,00	0,01	3,03
227	0,90	0,12	18,36	14,50	5,01	56,79	2,38	0,05	0,00	0,00	1,13	99,24	0,02	0,01	0,30	0,74	0,26	1,56	0,11	0,00	0,00	0,00	0,02	3,03
228	0,96	0,26	22,84	14,78	4,20	52,95	2,34	0,05	0,00	0,00	0,89	99,27	0,02	0,02	0,39	0,77	0,22	1,48	0,11	0,00	0,00	0,00	0,01	3,03

Point	SnO2	MgO	Ta2O5	FeO	MnO	Nb2O5	TiO2	Sc2O3	U2O	CaO	WO3	Total	Sn a.p.f.u	Mg	Ta	Fe	Mn	Nb	Ti	Sc	U	Ca	W	Total
229	0,93	0,30	22,49	15,04	4,17	53,24	2,01	0,05	0,00	0,02	0,91	99,15	0,02	0,03	0,38	0,78	0,22	1,50	0,09	0,00	0,00	0,00	0,01	3,04
230	0,76	0,05	26,30	12,97	6,36	50,09	3,18	0,09	0,00	0,00	0,27	100,06	0,02	0,00	0,44	0,67	0,33	1,41	0,15	0,00	0,00	0,00	0,00	3,04
231	0,87	0,28	26,07	14,67	4,28	49,65	2,07	0,04	0,00	0,04	0,84	98,82	0,02	0,03	0,45	0,78	0,23	1,42	0,10	0,00	0,00	0,00	0,01	3,04
232	0,80	0,20	30,65	14,47	4,07	46,05	2,41	0,05	0,00	0,01	0,62	99,33	0,02	0,02	0,53	0,78	0,22	1,34	0,12	0,00	0,00	0,00	0,01	3,04
233	0,71	0,28	19,79	15,33	4,18	57,22	1,91	0,05	0,00	0,03	1,11	100,61	0,02	0,03	0,33	0,77	0,21	1,56	0,09	0,00	0,00	0,00	0,02	3,03
234	0,70	0,33	21,61	14,93	4,25	56,08	2,06	0,05	0,00	0,00	1,16	101,18	0,02	0,03	0,36	0,75	0,22	1,53	0,09	0,00	0,00	0,00	0,02	3,02
235	1,04	0,33	23,30	14,70	4,17	53,28	2,25	0,04	0,00	0,00	1,06	100,16	0,03	0,03	0,39	0,76	0,22	1,48	0,10	0,00	0,00	0,00	0,02	3,03
sample J-5																								
236	0,35	0,00	20,57	10,14	9,26	58,06	0,59	0,00	0,00	0,00	0,00	98,97	0,01	0,00	0,35	0,52	0,48	1,62	0,03	0,00	0,00	0,00	0,00	3,01
237	0,26	0,00	28,55	8,91	9,99	52,18	0,43	0,00	0,00	0,02	0,94	101,27	0,01	0,00	0,49	0,47	0,53	1,48	0,02	0,00	0,00	0,00	0,02	3,00
238	1,10	0,00	37,28	10,47	7,50	42,72	0,52	0,00	0,00	0,00	1,24	100,84	0,03	0,00	0,67	0,58	0,42	1,27	0,03	0,00	0,00	0,00	0,02	3,00
239	0,46	0,00	45,47	10,56	7,00	37,34	0,24	0,05	0,00	0,00	0,00	101,12	0,01	0,00	0,84	0,60	0,40	1,14	0,01	0,00	0,00	0,00	0,00	3,01
240	0,18	0,00	26,34	9,15	9,58	53,25	0,31	0,00	0,00	0,05	0,93	99,78	0,00	0,00	0,45	0,48	0,51	1,52	0,01	0,00	0,00	0,00	0,02	3,00
241	1,59	0,00	59,73	9,32	6,70	23,11	0,48	0,08	0,00	0,00	0,34	101,34	0,05	0,00	1,18	0,57	0,41	0,76	0,03	0,00	0,00	0,00	0,01	3,00
242	0,02	0,00	20,38	5,16	14,74	59,91	0,47	0,02	0,00	0,00	0,58	101,27	0,00	0,00	0,33	0,26	0,75	1,63	0,02	0,00	0,00	0,00	0,01	3,01
243	0,30	0,00	23,33	9,52	9,41	57,23	0,51	0,00	0,00	0,01	1,15	101,45	0,01	0,00	0,39	0,49	0,49	1,58	0,02	0,00	0,00	0,00	0,02	2,99
244	0,22	0,00	25,31	11,09	8,07	55,13	0,44	0,03	0,00	0,02	0,77	101,09	0,01	0,00	0,43	0,57	0,42	1,54	0,02	0,00	0,00	0,00	0,01	3,00
245	0,52	0,00	15,82	11,45	8,23	61,40	0,67	0,00	0,00	0,01	0,67	98,78	0,01	0,00	0,26	0,58	0,42	1,69	0,03	0,00	0,00	0,00	0,01	3,01
246	0,48	0,00	53,57	9,75	7,15	28,86	0,25	0,01	0,00	0,02	0,10	100,19	0,01	0,00	1,04	0,58	0,43	0,93	0,01	0,00	0,00	0,00	0,00	3,01
247	0,40	0,00	17,41	10,64	8,73	61,24	0,57	0,01	0,00	0,01	0,74	99,74	0,01	0,00	0,29	0,54	0,45	1,68	0,03	0,00	0,00	0,00	0,01	3,00
248	0,20	0,00	29,88	8,03	10,37	49,41	0,32	0,00	0,00	0,00	0,30	98,52	0,01	0,00	0,53	0,44	0,57	1,45	0,02	0,00	0,00	0,00	0,01	3,01
249	0,22	0,00	15,75	12,73	7,20	63,41	0,41	0,00	0,00	0,02	0,46	100,22	0,01	0,00	0,26	0,64	0,36	1,72	0,02	0,00	0,00	0,00	0,01	3,01
250	0,49	0,01	14,15	12,71	7,32	63,10	0,75	0,00	0,00	0,01	0,94	99,49	0,01	0,00	0,23	0,64	0,37	1,71	0,03	0,00	0,00	0,00	0,01	3,01
251	0,33	0,01	17,81	12,22	7,51	60,21	0,54	0,02	0,00	0,01	0,50	99,14	0,01	0,00	0,30	0,62	0,39	1,66	0,02	0,00	0,00	0,00	0,01	3,01
252	0,33	0,01	17,79	11,30	8,21	60,47	0,51	0,01	0,00	0,00	0,26	98,89	0,01	0,00	0,30	0,58	0,43	1,67	0,02	0,00	0,00	0,00	0,00	3,01
253	0,29	0,00	16,24	12,93	7,25	61,32	0,59	0,02	0,00	0,01	0,64	99,29	0,01	0,00	0,27	0,66	0,37	1,68	0,03	0,00	0,00	0,00	0,01	3,02
254	0,27	0,01	18,92	12,32	7,36	59,08	0,44	0,00	0,00	0,01	0,79	99,19	0,01	0,00	0,32	0,63	0,38	1,64	0,02	0,00	0,00	0,00	0,01	3,01
Sample B-2																								
255	0,31	0,07	24,49	14,52	4,60	53,92	1,04	0,00	0,00	0,00	0,51	99,45	0,01	0,01	0,42	0,76	0,24	1,52	0,05	0,00	0,00	0,00	0,01	3,02
256	0,20	0,00	55,40	10,70	6,17	27,46	0,33	0,09	0,00	0,01	0,21	100,55	0,01	0,00	1,08	0,64	0,37	0,89	0,02	0,01	0,00	0,00	0,00	3,02
257	96,56	0,11	1,78	0,96	3,81	1,89	0,33	0,00	0,00	0,53	0,22	106,19	2,69	0,01	0,03	0,06	0,23	0,06	0,02	0,00	0,00	0,04	0,00	3,14
258	14,09	0,05	67,88	9,00	3,55	5,17	0,19	0,04	0,00	0,07	0,28	100,30	0,45	0,01	1,49	0,61	0,24	0,19	0,01	0,00	0,00	0,01	0,01	3,01
259	0,09	0,03	61,30	11,41	5,12	24,01	0,32	0,08	0,00	0,00	0,18	102,53	0,00	0,00	1,20	0,69	0,31	0,78	0,02	0,00	0,00	0,00	0,00	3,01
260	0,23	0,07	25,54	12,73	6,40	55,51	0,70	0,01	0,00	0,00	0,18	101,36	0,01	0,01	0,43	0,65	0,33	1,54	0,03	0,00	0,00	0,00	0,00	3,00
261	0,45	0,00	24,79	11,60	7,27	55,29	1,16	0,01	0,00	0,00	0,00	100,57	0,01	0,00	0,42	0,60	0,38	1,54	0,05	0,00	0,00	0,00	0,00	3,00
262	0,24	0,01	27,36	10,86	9,58	49,99	0,35	0,00	0,00	0,00	0,17	98,55	0,01	0,00	0,48	0,58	0,52	1,46	0,02	0,00	0,00	0,00	0,00	3,07
263	0,57	0,04	23,75	16,18	5,50	52,38	1,16	0,01	0,00	0,00	0,29	99,88	0,01	0,00	0,40	0,85	0,29	1,48	0,05	0,00	0,00	0,00	0,00	3,10
264	0,29	0,00	24,89	10,82	9,75	52,78	0,30	0,02	0,00	0,01	0,28	99,14	0,01	0,00	0,43	0,57	0,52	1,51	0,01	0,00	0,00	0,00	0,00	3,06
265	0,24	0,04	22,02	15,12	6,25	54,42	0,62	0,00	0,00	0,02	0,30	99,03	0,01	0,00	0,37	0,79	0,33	1,54	0,03	0,00	0,00	0,00	0,00	3,08
266	0,89	0,06	24,98	15,93	5,18	50,82	1,89	0,02	0,00	0,00	0,43	100,21	0,02	0,01	0,42	0,83	0,27	1,43	0,09	0,00	0,00	0,00	0,01	3,09

Point	SnO2	MgO	Ta2O5	FeO	MnO	Nb2O5	TiO2	Sc2O3	U2O	CaO	WO3	Total	Sn a.p.f.u	Mg	Ta	Fe	Mn	Nb	Ti	Sc	U	Ca	W	Total
Sample W-3																								
267	0,05	0,00	62,49	5,55	10,42	20,19	0,10	0,07	0,00	0,02	0,62	99,50	0,00	0,00	1,28	0,35	0,67	0,69	0,01	0,00	0,00	0,00	0,01	3,01
268	0,29	0,00	59,26	1,46	14,87	23,89	0,13	0,02	0,00	0,01	0,56	100,49	0,01	0,00	1,18	0,09	0,92	0,79	0,01	0,00	0,00	0,00	0,01	3,01
269	0,24	0,00	51,36	1,30	15,82	31,62	0,08	0,06	0,00	0,01	0,74	101,22	0,01	0,00	0,97	0,08	0,93	1,00	0,00	0,00	0,00	0,00	0,01	3,01
270	0,48	0,00	57,74	1,71	14,98	25,92	0,11	0,05	0,00	0,06	0,18	101,24	0,01	0,00	1,13	0,10	0,91	0,84	0,01	0,00	0,00	0,00	0,00	3,02
271	0,50	0,00	64,04	1,60	13,81	18,72	0,18	0,07	0,00	0,14	0,22	99,29	0,02	0,00	1,33	0,10	0,89	0,64	0,01	0,00	0,00	0,01	0,00	3,01
272	0,36	0,00	61,18	1,18	15,15	22,76	0,09	0,06	0,00	0,02	0,16	100,96	0,01	0,00	1,22	0,07	0,94	0,75	0,00	0,00	0,00	0,00	0,00	3,01
273	0,44	0,00	63,28	1,16	14,97	20,52	0,13	0,07	0,00	0,02	0,00	100,59	0,01	0,00	1,28	0,07	0,94	0,69	0,01	0,00	0,00	0,00	0,00	3,02
274	0,64	0,00	58,62	1,06	15,09	23,97	0,15	0,06	0,00	0,03	0,00	99,61	0,02	0,00	1,17	0,07	0,94	0,80	0,01	0,00	0,00	0,00	0,00	3,01
275	0,32	0,00	62,71	4,92	11,05	21,40	0,07	0,06	0,00	0,00	0,00	100,53	0,01	0,00	1,27	0,31	0,70	0,72	0,00	0,00	0,00	0,00	0,00	3,01
276	0,03	0,00	58,65	5,76	10,82	25,54	0,09	0,02	0,00	0,02	0,44	101,35	0,00	0,00	1,15	0,35	0,66	0,83	0,00	0,00	0,00	0,00	0,01	3,01
277	0,22	0,00	60,61	1,19	15,07	22,21	0,14	0,07	0,00	0,04	0,47	100,02	0,01	0,00	1,22	0,07	0,95	0,74	0,01	0,00	0,00	0,00	0,01	3,02
278	0,26	0,00	53,17	1,10	15,80	29,99	0,08	0,03	0,00	0,03	0,47	100,93	0,01	0,00	1,02	0,06	0,94	0,96	0,00	0,00	0,00	0,00	0,01	3,01
279	0,07	0,00	62,33	2,22	12,96	20,90	0,17	0,06	0,00	0,15	0,94	99,79	0,00	0,00	1,27	0,14	0,82	0,71	0,01	0,00	0,00	0,01	0,02	2,98
280	0,48	0,00	58,29	1,14	15,56	25,40	0,09	0,08	0,00	0,05	0,29	101,37	0,01	0,00	1,14	0,07	0,95	0,83	0,01	0,00	0,00	0,00	0,01	3,02
281	0,15	0,00	56,60	1,13	15,71	26,23	0,06	0,08	0,00	0,01	0,00	99,96	0,00	0,00	1,12	0,07	0,97	0,86	0,00	0,00	0,00	0,00	0,00	3,02
282	0,18	0,00	56,10	1,05	15,64	26,80	0,12	0,05	0,00	0,04	0,42	100,38	0,01	0,00	1,10	0,06	0,95	0,87	0,01	0,00	0,00	0,00	0,01	3,01
283	0,05	0,00	59,41	7,82	8,64	24,25	0,17	0,07	0,00	0,00	0,24	100,65	0,00	0,00	1,18	0,48	0,53	0,80	0,01	0,00	0,00	0,00	0,00	3,01
284	0,29	0,00	52,08	1,15	15,87	30,74	0,09	0,07	0,00	0,02	0,68	100,98	0,01	0,00	0,99	0,07	0,94	0,97	0,00	0,00	0,00	0,00	0,01	3,01
285	0,03	0,00	57,78	3,47	13,17	26,07	0,15	0,01	0,00	0,03	0,20	100,91	0,00	0,00	1,13	0,21	0,80	0,85	0,01	0,00	0,00	0,00	0,00	3,01
286	0,27	0,00	61,66	1,16	14,94	21,65	0,16	0,02	0,00	0,03	0,84	100,73	0,01	0,00	1,24	0,07	0,94	0,72	0,01	0,00	0,00	0,00	0,02	3,01
287	0,54	0,00	57,73	1,12	15,31	25,88	0,09	0,07	0,00	0,02	0,00	100,76	0,02	0,00	1,13	0,07	0,94	0,84	0,01	0,00	0,00	0,00	0,00	3,01
288	0,15	0,00	58,32	1,12	15,26	24,07	0,09	0,05	0,00	0,02	0,78	99,87	0,00	0,00	1,17	0,07	0,95	0,80	0,01	0,00	0,00	0,00	0,01	3,01
289	0,02	0,00	54,28	1,15	15,99	28,83	0,19	0,06	0,00	0,04	0,45	100,99	0,00	0,00	1,05	0,07	0,96	0,92	0,01	0,00	0,00	0,00	0,01	3,02
290	0,01	0,00	62,53	4,99	10,91	22,08	0,10	0,05	0,00	0,00	0,63	101,29	0,00	0,00	1,25	0,31	0,68	0,73	0,01	0,00	0,00	0,00	0,01	2,99
291	0,06	0,00	63,08	4,77	11,48	21,46	0,15	0,03	0,00	0,02	0,00	101,05	0,00	0,00	1,27	0,29	0,72	0,72	0,01	0,00	0,00	0,00	0,00	3,01
292	0,06	0,00	63,09	7,51	8,70	20,83	0,21	0,06	0,00	0,00	0,19	100,64	0,00	0,00	1,28	0,47	0,55	0,70	0,01	0,00	0,00	0,00	0,00	3,01
293	0,00	0,00	61,57	5,22	11,21	22,51	0,09	0,08	0,00	0,02	0,00	100,70	0,00	0,00	1,23	0,32	0,70	0,75	0,01	0,01	0,00	0,00	0,00	3,02
294	0,13	0,00	58,68	1,63	15,07	24,51	0,17	0,06	0,00	0,03	0,74	101,01	0,00	0,00	1,16	0,10	0,93	0,80	0,01	0,00	0,00	0,00	0,01	3,02
295	0,41	0,00	56,05	0,99	15,62	27,39	0,11	0,04	0,00	0,00	0,72	101,33	0,01	0,00	1,09	0,06	0,94	0,88	0,01	0,00	0,00	0,00	0,01	3,00
296	0,19	0,00	58,33	1,26	15,26	25,12	0,15	0,08	0,00	0,03	0,41	100,83	0,01	0,00	1,15	0,08	0,94	0,82	0,01	0,01	0,00	0,00	0,01	3,01
297	0,11	0,00	58,94	1,12	15,42	24,92	0,11	0,06	0,00	0,02	0,00	100,70	0,00	0,00	1,16	0,07	0,95	0,82	0,01	0,00	0,00	0,00	0,00	3,01
298	0,10	0,00	51,84	1,09	15,78	30,07	0,09	0,05	0,00	0,00	0,35	99,38	0,00	0,00	1,01	0,07	0,95	0,97	0,00	0,00	0,00	0,00	0,01	3,01
299	0,09	0,00	53,55	1,15	15,95	28,79	0,11	0,05	0,00	0,03	0,00	99,73	0,00	0,00	1,04	0,07	0,97	0,93	0,01	0,00	0,00	0,00	0,00	3,03
300	1,78	0,00	75,54	15,04	0,70	5,25	0,32	0,02	0,00	0,00	0,00	98,66	0,06	0,00	1,70	1,04	0,05	0,20	0,02	0,00	0,00	0,00	0,00	3,07
301	0,64	0,00	76,93	15,09	0,78	5,25	0,23	0,02	0,00	0,00	0,00	98,94	0,02	0,00	1,73	1,05	0,05	0,20	0,01	0,00	0,00	0,00	0,00	3,07
302	0,44	0,00	77,89	15,09	0,68	4,83	0,11	0,03	0,00	0,00	0,08	99,17	0,01	0,00	1,76	1,05	0,05	0,18	0,01	0,00	0,00	0,00	0,00	3,06
303	0,73	0,01	78,76	14,87	0,67	3,75	0,19	0,00	0,00	0,00	0,00	98,99	0,02	0,00	1,79	1,04	0,05	0,14	0,01	0,00	0,00	0,00	0,00	3,06
304	0,63	0,00	76,63	15,04	0,72	5,96	0,35	0,02	0,00	0,00	0,00	99,35	0,02	0,00	1,71	1,03	0,05	0,22	0,02	0,00	0,00	0,00	0,00	3,06
305	0,79	0,00	78,00	15,11	0,67	4,19	0,13	0,01	0,00	0,00	0,00	98,90	0,03	0,00	1,77	1,06	0,05	0,16	0,01	0,00	0,00	0,00	0,00	3,07

Point	SnO2	MgO	Ta2O5	FeO	MnO	Nb2O5	TiO2	Sc2O3	U2O	CaO	WO3	Total	Sn a.p.f.u	Mg	Ta	Fe	Mn	Nb	Ti	Sc	U	Ca	W	Total
306	1,93	0,01	75,86	14,73	0,70	4,93	0,43	0,03	0,00	0,00	0,02	98,63	0,06	0,00	1,71	1,02	0,05	0,18	0,03	0,00	0,00	0,00	0,00	3,06
307	1,94	0,01	75,39	14,92	0,77	5,92	0,44	0,02	0,00	0,00	0,00	99,41	0,06	0,00	1,68	1,02	0,05	0,22	0,03	0,00	0,00	0,00	0,00	3,06
308	3,29	0,02	73,12	14,77	0,69	6,14	0,62	0,02	0,00	0,00	0,00	98,66	0,11	0,00	1,63	1,01	0,05	0,23	0,04	0,00	0,00	0,00	0,00	3,07
309	0,77	0,01	77,61	15,07	0,84	5,21	0,25	0,01	0,00	0,00	0,26	100,02	0,03	0,00	1,73	1,03	0,06	0,19	0,02	0,00	0,00	0,00	0,01	3,06
310	0,97	0,01	77,62	15,13	0,57	5,46	0,41	0,03	0,00	0,00	0,00	100,19	0,03	0,00	1,72	1,03	0,04	0,20	0,03	0,00	0,00	0,00	0,00	3,06
311	1,25	0,01	76,05	15,19	0,79	5,95	0,34	0,02	0,00	0,00	0,00	99,60	0,04	0,00	1,69	1,04	0,05	0,22	0,02	0,00	0,00	0,00	0,00	3,07
Sample A-2																								
312	0,15	0,00	31,22	12,51	6,18	48,64	0,44	0,01	0,00	0,01	0,06	99,23	0,00	0,00	0,55	0,68	0,34	1,42	0,02	0,00	0,00	0,00	0,00	3,01
313	0,23	0,00	27,28	12,76	6,17	53,24	0,58	0,00	0,00	0,00	0,52	100,78	0,01	0,00	0,46	0,67	0,33	1,50	0,03	0,00	0,00	0,00	0,01	3,00
314	0,12	0,00	25,79	12,57	6,62	55,14	0,30	0,00	0,00	0,00	0,02	100,56	0,00	0,00	0,44	0,65	0,35	1,55	0,01	0,00	0,00	0,00	0,00	3,00
315	0,18	0,01	13,49	13,24	6,92	66,63	0,45	0,03	0,00	0,00	0,02	100,95	0,00	0,00	0,22	0,65	0,34	1,77	0,02	0,00	0,00	0,00	0,00	3,00
316	0,12	0,02	12,80	14,98	6,70	65,10	0,53	0,00	0,00	0,05	1,17	101,45	0,00	0,00	0,20	0,73	0,33	1,73	0,02	0,00	0,00	0,00	0,02	3,04
317	0,16	0,00	22,06	13,44	6,44	58,60	0,48	0,00	0,00	0,01	0,01	101,19	0,00	0,00	0,36	0,68	0,33	1,61	0,02	0,00	0,00	0,00	0,00	3,01
318	0,27	0,00	21,35	13,40	6,34	58,22	0,55	0,01	0,00	0,00	0,00	100,13	0,01	0,00	0,36	0,69	0,33	1,61	0,03	0,00	0,00	0,00	0,00	3,02
319	0,25	0,02	14,79	13,73	6,52	64,67	1,00	0,00	0,00	0,01	0,00	100,99	0,01	0,00	0,24	0,68	0,33	1,72	0,04	0,00	0,00	0,00	0,00	3,01
320	0,31	0,03	14,53	13,81	6,52	64,81	0,90	0,01	0,00	0,01	0,43	101,35	0,01	0,00	0,23	0,68	0,32	1,72	0,04	0,00	0,00	0,00	0,01	3,01
321	0,17	0,02	13,67	13,45	6,86	65,22	0,65	0,00	0,00	0,00	0,00	100,05	0,00	0,00	0,22	0,67	0,34	1,75	0,03	0,00	0,00	0,00	0,00	3,01
322	0,15	0,01	13,52	13,32	6,71	64,24	0,84	0,02	0,00	0,00	0,96	99,77	0,00	0,00	0,22	0,66	0,34	1,73	0,04	0,00	0,00	0,00	0,01	3,01
323	0,47	0,00	46,31	11,80	5,60	35,35	0,81	0,06	0,00	0,01	0,00	100,42	0,01	0,00	0,86	0,67	0,32	1,09	0,04	0,00	0,00	0,00	0,00	3,01
324	0,30	0,01	17,95	13,07	6,47	61,39	0,78	0,02	0,00	0,00	0,23	100,21	0,01	0,00	0,29	0,66	0,33	1,67	0,04	0,00	0,00	0,00	0,00	3,00
325	0,23	0,00	13,53	13,43	6,78	65,29	0,85	0,00	0,00	0,00	0,11	100,22	0,01	0,00	0,22	0,66	0,34	1,74	0,04	0,00	0,00	0,00	0,00	3,01
326	0,28	0,00	53,73	11,69	5,55	29,16	0,82	0,04	0,00	0,00	0,00	101,28	0,01	0,00	1,03	0,69	0,33	0,93	0,04	0,00	0,00	0,00	0,00	3,02
327	0,19	0,00	14,26	13,08	6,97	64,57	0,63	0,00	0,00	0,00	0,63	100,33	0,00	0,00	0,23	0,65	0,35	1,73	0,03	0,00	0,00	0,00	0,01	3,00
328	0,12	0,03	14,19	12,95	7,23	65,16	0,61	0,00	0,00	0,01	0,60	100,89	0,00	0,00	0,23	0,64	0,36	1,74	0,03	0,00	0,00	0,00	0,01	3,01
329	0,12	0,00	14,27	12,74	7,10	65,01	0,58	0,00	0,00	0,01	0,67	100,48	0,00	0,00	0,23	0,63	0,36	1,74	0,03	0,00	0,00	0,00	0,01	3,00
330	0,12	0,01	14,15	13,00	7,16	66,14	0,55	0,01	0,00	0,06	0,30	101,50	0,00	0,00	0,23	0,64	0,36	1,75	0,02	0,00	0,00	0,00	0,00	3,00
331	0,36	0,00	58,23	11,58	5,69	23,08	0,82	0,08	0,00	0,02	0,32	100,17	0,01	0,00	1,16	0,71	0,35	0,76	0,05	0,01	0,00	0,00	0,01	3,05
332	0,13	0,04	28,69	13,06	6,03	52,06	0,45	0,02	0,00	0,06	0,00	100,55	0,00	0,00	0,49	0,69	0,32	1,48	0,02	0,00	0,00	0,00	0,00	3,02
333	0,19	0,00	25,76	13,18	6,27	54,98	0,60	0,03	0,00	0,00	0,34	101,34	0,00	0,00	0,43	0,68	0,33	1,53	0,03	0,00	0,00	0,00	0,01	3,01
334	0,32	0,00	14,01	13,59	6,85	63,99	0,98	0,00	0,00	0,02	0,79	100,55	0,01	0,00	0,23	0,67	0,34	1,71	0,04	0,00	0,00	0,00	0,01	3,02
335	0,26	0,00	14,32	13,59	6,34	63,78	0,99	0,02	0,00	0,01	0,42	99,73	0,01	0,00	0,23	0,68	0,32	1,72	0,04	0,00	0,00	0,00	0,01	3,01
336	0,28	0,00	14,95	12,86	6,93	64,20	1,01	0,01	0,00	0,00	0,75	100,97	0,01	0,00	0,24	0,63	0,35	1,71	0,04	0,00	0,00	0,00	0,01	3,00
Sample X-1																								
337	0,02	0,00	35,23	1,95	16,19	44,52	0,10	0,01	0,00	0,00	0,73	98,76	0,00	0,00	0,64	0,11	0,91	1,34	0,00	0,00	0,00	0,00	0,01	3,01
338	0,04	0,02	70,11	7,62	7,42	13,88	0,18	0,06	0,00	0,00	1,02	100,36	0,00	0,00	1,48	0,50	0,49	0,49	0,01	0,00	0,00	0,00	0,02	2,99
339	0,27	0,00	35,80	8,30	9,42	43,70	0,26	0,02	0,00	0,12	0,72	98,62	0,01	0,00	0,65	0,46	0,53	1,32	0,01	0,00	0,00	0,01	0,01	3,00
340	0,10	0,00	52,11	7,83	8,72	29,39	0,15	0,07	0,00	0,02	0,31	98,68	0,00	0,00	1,02	0,47	0,53	0,96	0,01	0,00	0,00	0,00	0,01	3,01
341	0,08	0,00	53,14	7,16	9,27	28,70	0,15	0,06	0,00	0,00	0,00	98,57	0,00	0,00	1,05	0,43	0,57	0,94	0,01	0,00	0,00	0,00	0,00	3,01
342	0,01	0,00	52,73	9,37	7,34	28,94	0,18	0,00	0,00	0,03	0,77	99,36	0,00	0,00	1,03	0,56	0,45	0,94	0,01	0,00	0,00	0,00	0,01	3,01
343	0,22	0,00	39,36	10,86	6,47	41,18	0,71	0,02	0,00	0,02	0,00	98,84	0,01	0,00	0,72	0,61	0,37	1,25	0,04	0,00	0,00	0,00	0,00	3,00

Point	SnO2	MgO	Ta2O5	FeO	MnO	Nb2O5	TiO2	Sc2O3	U2O	CaO	WO3	Total	Sn a.p.f.u	Mg	Ta	Fe	Mn	Nb	Ti	Sc	U	Ca	W	Total
344	0,25	0,00	48,92	11,04	5,74	32,27	0,78	0,03	0,00	0,03	0,32	99,38	0,01	0,00	0,93	0,65	0,34	1,02	0,04	0,00	0,00	0,00	0,01	3,00
345	0,67	0,00	76,15	13,32	1,10	7,52	0,49	0,08	0,00	0,00	0,00	99,33	0,02	0,00	1,69	0,91	0,08	0,28	0,03	0,01	0,00	0,00	0,00	3,00
346	0,08	0,27	57,55	10,65	5,16	23,98	0,19	0,05	0,00	0,01	0,72	98,66	0,00	0,03	1,16	0,66	0,32	0,80	0,01	0,00	0,00	0,00	0,01	3,01
347	0,06	0,20	66,04	9,67	5,30	17,68	0,16	0,05	0,00	0,01	0,58	99,76	0,00	0,02	1,37	0,62	0,34	0,61	0,01	0,00	0,00	0,00	0,01	2,99
348	0,14	0,25	51,50	7,76	8,21	29,32	0,41	0,03	0,00	0,03	1,86	99,49	0,00	0,03	1,00	0,46	0,50	0,94	0,02	0,00	0,00	0,00	0,03	2,99
Sample M-2																								
349	0,70	0,05	58,33	11,93	3,97	22,18	1,95	0,04	0,00	0,00	0,72	99,87	0,02	0,01	1,16	0,73	0,25	0,73	0,11	0,00	0,00	0,00	0,01	3,01
350	11,01	0,07	57,13	9,28	3,36	13,33	5,44	0,04	0,00	0,07	0,00	99,73	0,32	0,01	1,14	0,57	0,21	0,44	0,30	0,00	0,00	0,01	0,00	3,00
351	10,02	0,00	59,33	6,26	6,29	11,10	6,40	0,05	0,00	0,04	0,00	99,49	0,30	0,00	1,19	0,39	0,39	0,37	0,36	0,00	0,00	0,00	0,00	3,00
352	9,82	0,07	58,64	9,97	3,03	11,80	4,79	0,05	0,00	0,05	1,59	99,82	0,29	0,01	1,19	0,62	0,19	0,40	0,27	0,00	0,00	0,00	0,03	3,00
353	15,58	0,00	67,01	4,57	7,44	3,95	0,24	0,02	0,00	0,09	0,00	98,90	0,51	0,00	1,50	0,31	0,52	0,15	0,01	0,00	0,00	0,01	0,00	3,01
354	14,00	0,04	64,60	6,81	5,38	5,93	1,98	0,01	0,00	0,09	0,00	98,83	0,45	0,00	1,40	0,45	0,36	0,21	0,12	0,00	0,00	0,01	0,00	3,01
355	0,96	0,07	57,55	12,08	3,87	23,05	2,01	0,06	0,00	0,01	0,47	100,11	0,03	0,01	1,13	0,73	0,24	0,75	0,11	0,00	0,00	0,00	0,01	3,01
356	0,79	0,06	58,73	11,83	4,07	22,10	1,89	0,07	0,00	0,00	1,24	100,77	0,02	0,01	1,16	0,72	0,25	0,72	0,10	0,00	0,00	0,00	0,02	3,01
357	10,93	0,00	60,75	5,53	7,21	10,39	4,89	0,04	0,00	0,05	0,00	99,78	0,33	0,00	1,24	0,35	0,46	0,35	0,28	0,00	0,00	0,00	0,00	3,01
358	0,97	0,06	56,93	11,77	3,97	22,87	2,15	0,05	0,00	0,02	1,15	99,94	0,03	0,01	1,12	0,71	0,24	0,75	0,12	0,00	0,00	0,00	0,02	3,00
359	0,95	0,07	57,55	11,87	4,31	23,51	1,91	0,09	0,00	0,00	1,01	101,26	0,03	0,01	1,12	0,71	0,26	0,76	0,10	0,01	0,00	0,00	0,02	3,01
360	0,76	0,07	56,94	11,70	4,31	23,72	1,82	0,04	0,00	0,01	0,96	100,32	0,02	0,01	1,12	0,71	0,26	0,77	0,10	0,00	0,00	0,00	0,02	3,01
361	0,49	0,00	81,80	13,16	1,22	3,51	0,19	0,09	0,00	0,00	0,00	100,46	0,02	0,00	1,84	0,91	0,09	0,13	0,01	0,01	0,00	0,00	0,00	3,01
362	0,97	0,05	57,98	11,96	3,95	22,30	1,76	0,03	0,00	0,02	0,41	99,42	0,03	0,01	1,16	0,73	0,25	0,74	0,10	0,00	0,00	0,00	0,01	3,02
363	1,10	0,00	75,23	13,80	0,64	7,58	2,22	0,08	0,00	0,02	0,22	100,88	0,03	0,00	1,61	0,91	0,04	0,27	0,13	0,01	0,00	0,00	0,00	3,01
364	0,71	0,04	57,20	12,12	4,00	22,92	1,77	0,02	0,00	0,00	0,27	99,05	0,02	0,00	1,14	0,74	0,25	0,76	0,10	0,00	0,00	0,00	0,01	3,02
365	1,32	0,00	72,87	13,63	0,61	8,35	2,83	0,05	0,00	0,00	0,50	100,15	0,04	0,00	1,55	0,89	0,04	0,30	0,17	0,00	0,00	0,00	0,01	3,00
366	1,41	0,00	72,44	13,84	0,65	9,21	3,11	0,03	0,00	0,01	0,74	101,44	0,04	0,00	1,51	0,89	0,04	0,32	0,18	0,00	0,00	0,00	0,01	3,00
367	11,83	0,00	59,76	5,16	7,52	10,38	4,89	0,06	0,00	0,05	0,00	99,65	0,35	0,00	1,22	0,32	0,48	0,35	0,28	0,00	0,00	0,00	0,00	3,01
368	1,28	0,00	72,81	13,44	0,67	8,13	2,34	0,06	0,00	0,00	0,08	98,79	0,04	0,00	1,58	0,90	0,05	0,29	0,14	0,00	0,00	0,00	0,00	3,00
369	0,85	0,09	58,05	12,17	3,89	23,10	2,16	0,02	0,00	0,00	0,60	100,94	0,02	0,01	1,13	0,73	0,24	0,75	0,12	0,00	0,00	0,00	0,01	3,01
370	0,96	0,00	75,28	13,92	0,65	7,07	2,51	0,07	0,00	0,00	0,00	100,45	0,03	0,00	1,62	0,92	0,04	0,25	0,15	0,01	0,00	0,00	0,00	3,02
371	12,24	0,00	73,07	1,30	10,55	1,83	0,17	0,06	0,00	0,04	0,00	99,24	0,41	0,00	1,66	0,09	0,75	0,07	0,01	0,00	0,00	0,00	0,00	2,99
372	11,43	0,00	65,91	5,06	7,22	6,93	3,12	0,02	0,00	0,05	0,12	99,87	0,36	0,00	1,40	0,33	0,48	0,24	0,18	0,00	0,00	0,00	0,00	2,99
373	9,08	0,00	60,14	6,99	5,77	11,24	6,97	0,04	0,00	0,06	0,00	100,30	0,26	0,00	1,19	0,43	0,36	0,37	0,38	0,00	0,00	0,01	0,00	3,00
Sample T-4																								
374	0,03	0,00	24,43	11,59	7,37	56,06	0,10	0,02	0,00	0,01	0,88	100,48	0,00	0,00	0,41	0,60	0,39	1,57	0,00	0,00	0,00	0,00	0,01	2,99
375	0,37	0,01	11,96	13,85	6,39	64,70	1,04	0,01	0,00	0,07	1,50	99,90	0,01	0,00	0,19	0,69	0,32	1,73	0,05	0,00	0,00	0,00	0,02	3,01
376	0,06	0,00	28,68	11,30	7,33	52,49	0,16	0,02	0,00	0,02	0,27	100,32	0,00	0,00	0,49	0,60	0,39	1,50	0,01	0,00	0,00	0,00	0,00	3,00
377	0,50	0,00	14,55	13,22	6,38	63,08	0,81	0,00	0,00	0,00	0,41	98,96	0,01	0,00	0,24	0,67	0,33	1,72	0,04	0,00	0,00	0,00	0,01	3,00
378	0,15	0,00	13,92	13,40	6,40	65,68	0,47	0,00	0,00	0,00	0,73	100,74	0,00	0,00	0,22	0,66	0,32	1,75	0,02	0,00	0,00	0,00	0,01	2,99
379	0,21	0,00	60,86	10,09	6,03	21,82	0,42	0,05	0,00	0,00	0,07	99,55	0,01	0,00	1,23	0,63	0,38	0,74	0,02	0,00	0,00	0,00	0,00	3,01
380	0,06	0,00	32,55	11,54	6,78	48,28	0,28	0,01	0,00	0,01	0,39	99,90	0,00	0,00	0,57	0,62	0,37	1,41	0,01	0,00	0,00	0,00	0,01	3,00
381	0,13	0,00	39,88	11,19	6,71	42,33	0,15	0,00	0,00	0,00	0,16	100,56	0,00	0,00	0,72	0,62	0,38	1,27	0,01	0,00	0,00	0,00	0,00	3,00

Point	SnO2	MgO	Ta2O5	FeO	MnO	Nb2O5	TiO2	Sc2O3	U2O	CaO	WO3	Total	Sn a.p.f.u	Mg	Ta	Fe	Mn	Nb	Ti	Sc	U	Ca	W	Total
382	0,23	0,00	16,34	12,55	6,62	61,84	0,53	0,00	0,00	0,00	1,21	99,31	0,01	0,00	0,27	0,64	0,34	1,69	0,02	0,00	0,00	0,00	0,02	2,99
383	0,50	0,00	54,09	10,09	6,33	27,70	0,31	0,07	0,00	0,00	1,09	100,18	0,01	0,00	1,05	0,61	0,38	0,90	0,02	0,00	0,00	0,00	0,02	3,00
384	0,09	0,00	43,69	10,09	6,92	38,73	0,09	0,05	0,00	0,00	0,13	99,78	0,00	0,00	0,81	0,57	0,40	1,19	0,00	0,00	0,00	0,00	0,00	2,99
385	0,20	0,00	33,03	11,25	7,44	47,13	0,27	0,04	0,00	0,00	0,34	99,69	0,01	0,00	0,58	0,61	0,41	1,38	0,01	0,00	0,00	0,00	0,01	3,02
386	0,22	0,00	36,96	10,95	7,14	44,46	0,27	0,01	0,00	0,02	0,00	100,02	0,01	0,00	0,66	0,60	0,40	1,32	0,01	0,00	0,00	0,00	0,00	3,01
387	0,29	0,00	37,89	11,19	7,96	43,20	0,34	0,06	0,00	0,00	0,00	100,93	0,01	0,00	0,68	0,61	0,44	1,28	0,02	0,00	0,00	0,00	0,00	3,04
388	0,07	0,00	39,56	11,07	6,79	41,58	0,11	0,01	0,00	0,02	1,14	100,35	0,00	0,00	0,72	0,62	0,38	1,25	0,01	0,00	0,00	0,00	0,02	3,00
389	0,36	0,00	15,62	12,72	6,54	62,75	0,60	0,02	0,00	0,01	1,01	99,62	0,01	0,00	0,26	0,64	0,33	1,71	0,03	0,00	0,00	0,00	0,02	2,99
390	0,36	0,00	15,90	12,81	6,40	62,38	0,75	0,03	0,00	0,02	1,09	99,72	0,01	0,00	0,26	0,64	0,33	1,70	0,03	0,00	0,00	0,00	0,02	2,99
391	0,12	0,00	16,67	12,60	7,01	62,50	0,29	0,03	0,00	0,00	0,00	99,21	0,00	0,00	0,27	0,64	0,36	1,71	0,01	0,00	0,00	0,00	0,00	3,00
392	0,21	0,00	61,02	9,98	6,24	22,57	0,39	0,07	0,00	0,00	0,13	100,61	0,01	0,00	1,22	0,61	0,39	0,75	0,02	0,00	0,00	0,00	0,00	3,01
393	0,09	0,00	43,43	10,50	7,11	38,46	0,15	0,05	0,00	0,02	0,46	100,27	0,00	0,00	0,80	0,60	0,41	1,18	0,01	0,00	0,00	0,00	0,01	3,00
394	0,26	0,00	60,35	9,94	6,02	22,84	0,43	0,03	0,00	0,03	0,03	99,92	0,01	0,00	1,21	0,61	0,38	0,76	0,02	0,00	0,00	0,00	0,00	3,00
395	0,14	0,00	45,80	10,42	6,99	36,10	0,07	0,05	0,00	0,01	0,06	99,64	0,00	0,00	0,86	0,60	0,41	1,13	0,00	0,00	0,00	0,00	0,00	3,01
396	0,10	0,00	18,41	11,80	7,23	61,29	0,41	0,00	0,00	0,01	0,34	99,60	0,00	0,00	0,30	0,60	0,37	1,68	0,02	0,00	0,00	0,00	0,01	2,99
397	0,06	0,00	22,16	11,86	7,52	57,56	0,19	0,01	0,00	0,00	0,46	99,82	0,00	0,00	0,37	0,61	0,39	1,61	0,01	0,00	0,00	0,00	0,01	3,00
398	0,13	0,00	40,71	11,12	6,66	41,82	0,12	0,03	0,00	0,00	0,00	100,59	0,00	0,00	0,74	0,62	0,38	1,26	0,01	0,00	0,00	0,00	0,00	3,00
399	0,24	0,00	11,10	13,54	5,97	66,33	0,59	0,00	0,00	0,00	0,83	98,60	0,01	0,00	0,18	0,68	0,30	1,79	0,03	0,00	0,00	0,00	0,01	2,99
400	0,09	0,00	31,78	11,24	7,27	49,89	0,09	0,00	0,00	0,00	0,38	100,73	0,00	0,00	0,55	0,60	0,39	1,44	0,00	0,00	0,00	0,00	0,01	3,00
401	0,07	0,00	16,59	12,16	7,42	63,49	0,26	0,00	0,00	0,00	0,46	100,46	0,00	0,00	0,27	0,61	0,38	1,72	0,01	0,00	0,00	0,00	0,01	2,99
402	0,53	0,00	17,35	12,45	6,59	60,96	0,68	0,01	0,00	0,03	1,16	99,76	0,01	0,00	0,29	0,63	0,34	1,67	0,03	0,00	0,00	0,00	0,02	2,99
403	0,21	0,00	23,99	12,21	6,91	56,20	0,31	0,02	0,00	0,03	0,46	100,35	0,01	0,00	0,40	0,63	0,36	1,57	0,01	0,00	0,00	0,00	0,01	3,00
404	0,07	0,00	41,02	10,85	6,79	40,49	0,14	0,04	0,00	0,00	0,00	99,41	0,00	0,00	0,75	0,61	0,39	1,24	0,01	0,00	0,00	0,00	0,00	3,00
Sample 3-3																								
405	0,08	0,00	22,41	12,23	7,15	57,80	0,35	0,02	0,00	0,00	0,10	100,15	0,00	0,00	0,37	0,63	0,37	1,61	0,02	0,00	0,00	0,00	0,00	3,00
406	0,46	0,04	40,94	12,35	5,62	40,65	0,79	0,00	0,00	0,01	0,03	100,90	0,01	0,00	0,74	0,68	0,32	1,22	0,04	0,00	0,00	0,00	0,00	3,01
407	0,31	0,07	19,65	13,56	5,84	59,05	0,74	0,02	0,00	0,02	0,62	99,88	0,01	0,01	0,33	0,69	0,30	1,63	0,03	0,00	0,00	0,00	0,01	3,01
408	0,43	0,00	39,26	11,22	6,64	41,42	0,95	0,03	0,00	0,01	0,02	99,97	0,01	0,00	0,71	0,62	0,37	1,24	0,05	0,00	0,00	0,00	0,00	3,01
409	0,17	0,00	18,49	13,34	6,00	61,16	0,55	0,01	0,00	0,01	1,02	100,75	0,00	0,00	0,30	0,67	0,31	1,66	0,02	0,00	0,00	0,00	0,02	2,99
410	0,20	0,00	18,11	13,24	6,41	61,44	0,56	0,01	0,00	0,00	1,06	101,01	0,00	0,00	0,30	0,66	0,33	1,67	0,03	0,00	0,00	0,00	0,02	3,00
411	0,10	0,02	53,66	11,06	5,30	30,34	0,43	0,04	0,00	0,02	0,00	100,96	0,00	0,00	1,03	0,65	0,32	0,96	0,02	0,00	0,00	0,00	0,00	2,99
412	0,25	0,04	22,85	13,00	5,92	56,24	0,61	0,00	0,00	0,00	0,71	99,62	0,01	0,00	0,39	0,67	0,31	1,58	0,03	0,00	0,00	0,00	0,01	3,00
413	0,30	0,00	19,26	13,25	6,15	59,84	0,80	0,00	0,00	0,02	0,36	99,98	0,01	0,00	0,32	0,67	0,32	1,64	0,04	0,00	0,00	0,00	0,01	3,00
414	0,11	0,00	35,39	11,75	6,42	45,79	0,50	0,00	0,00	0,01	0,00	99,97	0,00	0,00	0,63	0,64	0,35	1,35	0,02	0,00	0,00	0,00	0,00	3,00
415	0,27	0,00	22,55	12,70	6,82	56,94	0,70	0,00	0,00	0,00	0,37	100,37	0,01	0,00	0,38	0,65	0,36	1,58	0,03	0,00	0,00	0,00	0,01	3,01
416	0,17	0,01	18,48	13,38	6,32	59,89	0,63	0,00	0,00	0,00	0,39	99,27	0,00	0,00	0,31	0,68	0,33	1,65	0,03	0,00	0,00	0,00	0,01	3,01
417	0,17	0,00	27,03	12,89	6,01	53,86	0,61	0,01	0,00	0,00	0,27	100,85	0,00	0,00	0,46	0,67	0,32	1,52	0,03	0,00	0,00	0,00	0,00	3,00
418	0,20	0,01	31,97	12,25	6,08	48,70	0,54	0,00	0,00	0,02	0,24	100,00	0,01	0,00	0,56	0,66	0,33	1,42	0,03	0,00	0,00	0,00	0,00	3,00
419	0,34	0,00	36,16	11,87	6,28	44,84	0,93	0,03	0,00	0,00	0,47	100,92	0,01	0,00	0,64	0,64	0,34	1,31	0,05	0,00	0,00	0,00	0,01	3,00
420	0,13	0,00	19,52	13,11	6,31	60,51	0,50	0,02	0,00	0,00	0,38	100,46	0,00	0,00	0,32	0,66	0,32	1,66	0,02	0,00	0,00	0,00	0,01	3,00

Point	SnO2	MgO	Ta2O5	FeO	MnO	Nb2O5	TiO2	Sc2O3	U2O	CaO	WO3	Total	Sn a.p.f.u	Mg	Ta	Fe	Mn	Nb	Ti	Sc	U	Ca	W	Total
421	0,42	0,01	60,95	11,01	4,99	21,98	0,93	0,06	0,00	0,01	0,35	100,70	0,01	0,00	1,22	0,68	0,31	0,73	0,05	0,00	0,00	0,00	0,01	3,00
422	0,26	0,03	30,85	12,98	5,68	50,15	0,64	0,03	0,00	0,02	0,45	101,08	0,01	0,00	0,53	0,69	0,30	1,43	0,03	0,00	0,00	0,00	0,01	3,00
423	0,26	0,00	28,19	12,26	6,44	52,50	0,75	0,01	0,00	0,01	0,70	101,12	0,01	0,00	0,48	0,64	0,34	1,48	0,04	0,00	0,00	0,00	0,01	3,00
424	0,16	0,01	19,24	13,44	6,18	60,24	0,66	0,00	0,00	0,00	0,18	100,10	0,00	0,00	0,32	0,68	0,32	1,65	0,03	0,00	0,00	0,00	0,00	3,01
425	0,19	0,00	34,98	11,80	6,70	46,11	0,54	0,04	0,00	0,00	0,44	100,81	0,01	0,00	0,62	0,64	0,37	1,35	0,03	0,00	0,00	0,00	0,01	3,01
426	0,10	0,03	19,13	13,29	6,56	60,22	0,42	0,02	0,00	0,00	0,00	99,76	0,00	0,00	0,32	0,68	0,34	1,66	0,02	0,00	0,00	0,00	0,00	3,02
427	0,19	0,00	22,50	12,77	6,32	56,35	0,55	0,02	0,00	0,01	0,19	98,90	0,00	0,00	0,38	0,67	0,33	1,59	0,03	0,00	0,00	0,00	0,00	3,01
428	0,25	0,00	36,40	11,46	6,43	44,41	0,71	0,04	0,00	0,00	1,18	100,88	0,01	0,00	0,64	0,62	0,35	1,31	0,03	0,00	0,00	0,00	0,02	2,99
429	0,33	0,06	20,80	13,41	5,73	57,95	0,95	0,04	0,00	0,00	0,00	99,27	0,01	0,01	0,35	0,69	0,30	1,61	0,04	0,00	0,00	0,00	0,00	3,01
430	0,33	0,00	36,06	11,73	6,44	43,62	0,76	0,01	0,00	0,02	0,05	99,02	0,01	0,00	0,65	0,65	0,36	1,31	0,04	0,00	0,00	0,00	0,00	3,02
431	0,20	0,00	19,44	13,29	6,32	59,78	0,64	0,01	0,00	0,02	0,55	100,24	0,00	0,00	0,32	0,67	0,33	1,64	0,03	0,00	0,00	0,00	0,01	3,01
432	0,15	0,01	30,52	12,69	5,99	49,51	0,50	0,02	0,00	0,00	0,18	99,56	0,00	0,00	0,53	0,68	0,33	1,44	0,02	0,00	0,00	0,00	0,00	3,01
433	0,19	0,00	19,40	13,31	6,34	60,56	0,68	0,02	0,00	0,00	0,72	101,21	0,00	0,00	0,32	0,67	0,32	1,64	0,03	0,00	0,00	0,00	0,01	3,00
434	0,27	0,00	23,33	12,55	6,63	56,33	0,70	0,00	0,00	0,00	0,00	99,82	0,01	0,00	0,39	0,65	0,35	1,58	0,03	0,00	0,00	0,00	0,00	3,01
435	0,18	0,00	19,98	13,19	6,39	60,31	0,67	0,02	0,00	0,01	0,57	101,32	0,00	0,00	0,33	0,66	0,33	1,64	0,03	0,00	0,00	0,00	0,01	3,00
436	0,11	0,00	21,26	13,28	6,28	58,78	0,56	0,02	0,00	0,00	0,19	100,48	0,00	0,00	0,35	0,68	0,32	1,62	0,03	0,00	0,00	0,00	0,00	3,01
437	0,14	0,01	18,44	13,41	6,41	61,82	0,51	0,01	0,00	0,00	0,00	100,76	0,00	0,00	0,30	0,67	0,33	1,68	0,02	0,00	0,00	0,00	0,00	3,01
Sample 3.2-1																								
438	0,39	0,26	27,71	13,38	5,16	51,81	1,24	0,02	0,00	0,00	0,62	100,59	0,01	0,02	0,47	0,70	0,27	1,46	0,06	0,00	0,00	0,00	0,01	3,01
439	0,58	0,22	27,02	13,02	5,29	50,55	2,01	0,02	0,00	0,00	1,13	99,85	0,01	0,02	0,46	0,68	0,28	1,43	0,10	0,00	0,00	0,00	0,02	3,01
440	0,73	0,55	20,44	13,63	4,69	56,63	2,31	0,06	0,00	0,02	1,00	100,05	0,02	0,05	0,34	0,69	0,24	1,55	0,11	0,00	0,00	0,00	0,02	3,01
441	0,41	0,22	28,17	13,29	5,40	50,95	1,53	0,01	0,00	0,02	0,58	100,57	0,01	0,02	0,48	0,70	0,29	1,44	0,07	0,00	0,00	0,00	0,01	3,02
442	0,40	0,15	32,86	12,64	5,50	47,32	1,09	0,02	0,00	0,00	0,45	100,43	0,01	0,01	0,57	0,68	0,30	1,37	0,05	0,00	0,00	0,00	0,01	3,01
443	0,52	0,10	44,38	12,09	5,35	36,33	1,32	0,07	0,00	0,01	0,73	100,89	0,01	0,01	0,81	0,68	0,31	1,11	0,07	0,00	0,00	0,00	0,01	3,01
444	0,36	0,19	29,87	12,97	5,39	50,18	1,25	0,00	0,00	0,01	0,74	100,96	0,01	0,02	0,51	0,68	0,29	1,43	0,06	0,00	0,00	0,00	0,01	3,00
445	0,30	0,38	30,97	13,21	4,93	49,28	1,23	0,01	0,00	0,00	0,40	100,70	0,01	0,04	0,53	0,70	0,26	1,41	0,06	0,00	0,00	0,00	0,01	3,01
446	0,45	0,15	42,63	12,11	5,19	37,60	1,15	0,02	0,00	0,01	0,53	99,83	0,01	0,02	0,78	0,68	0,30	1,15	0,06	0,00	0,00	0,00	0,01	3,01
447	0,38	0,25	28,05	13,34	5,12	51,38	1,48	0,06	0,00	0,00	0,75	100,79	0,01	0,02	0,48	0,70	0,27	1,45	0,07	0,00	0,00	0,00	0,01	3,01
448	0,34	0,15	32,24	12,91	5,41	47,84	0,99	0,05	0,00	0,04	0,55	100,53	0,01	0,01	0,56	0,69	0,29	1,38	0,05	0,00	0,00	0,00	0,01	3,01
449	0,48	0,10	43,19	11,97	5,32	37,62	1,37	0,07	0,00	0,01	0,00	100,15	0,01	0,01	0,79	0,67	0,30	1,15	0,07	0,00	0,00	0,00	0,00	3,01
450	0,36	0,19	31,07	12,94	5,25	48,33	1,23	0,04	0,00	0,00	1,13	100,53	0,01	0,02	0,54	0,69	0,28	1,39	0,06	0,00	0,00	0,00	0,02	3,00
451	0,88	0,53	21,88	13,74	4,57	55,07	2,73	0,06	0,00	0,01	1,43	100,89	0,02	0,05	0,36	0,69	0,23	1,50	0,12	0,00	0,00	0,00	0,02	3,01
452	0,88	0,54	21,68	13,61	4,46	54,48	2,73	0,07	0,00	0,00	1,43	99,87	0,02	0,05	0,36	0,69	0,23	1,50	0,13	0,00	0,00	0,00	0,02	3,01
453	0,81	0,52	20,37	13,89	4,59	57,03	2,51	0,02	0,00	0,00	0,39	100,12	0,02	0,05	0,33	0,70	0,23	1,56	0,11	0,00	0,00	0,00	0,01	3,02
454	0,49	0,19	27,45	13,33	5,17	51,64	1,51	0,03	0,00	0,00	0,65	100,45	0,01	0,02	0,47	0,70	0,27	1,46	0,07	0,00	0,00	0,00	0,01	3,01
455	0,38	0,22	27,74	13,29	5,26	52,34	1,30	0,01	0,00	0,00	0,25	100,79	0,01	0,02	0,47	0,69	0,28	1,47	0,06	0,00	0,00	0,00	0,00	3,01
456	0,31	0,28	27,67	13,29	5,34	51,02	1,23	0,01	0,00	0,01	0,00	99,17	0,01	0,03	0,48	0,70	0,29	1,46	0,06	0,00	0,00	0,00	0,00	3,02
457	0,23	0,21	29,54	13,11	5,07	50,12	1,16	0,05	0,00	0,00	0,26	99,75	0,01	0,02	0,51	0,70	0,27	1,44	0,06	0,00	0,00	0,00	0,00	3,01
458	0,93	0,52	27,26	13,29	4,53	49,70	2,59	0,08	0,00	0,00	0,83	99,71	0,02	0,05	0,46	0,70	0,24	1,41	0,12	0,00	0,00	0,00	0,01	3,02
459	0,57	0,26	25,83	13,36	5,15	51,45	1,88	0,00	0,00	0,08	0,77	99,35	0,01	0,02	0,44	0,70	0,27	1,46	0,09	0,00	0,00	0,01	0,01	3,02

Point	SnO2	MgO	Ta2O5	FeO	MnO	Nb2O5	TiO2	Sc2O3	U2O	CaO	WO3	Total	Sn a.p.f.u	Mg	Ta	Fe	Mn	Nb	Ti	Sc	U	Ca	W	Total
460	0,54	0,22	25,38	13,51	5,32	52,83	1,55	0,02	0,00	0,02	0,35	99,72	0,01	0,02	0,43	0,70	0,28	1,49	0,07	0,00	0,00	0,00	0,01	3,02
461	0,41	0,25	27,67	13,44	5,31	52,29	1,40	0,02	0,00	0,00	0,11	100,91	0,01	0,02	0,47	0,70	0,28	1,47	0,07	0,00	0,00	0,00	0,00	3,02
Sample 5-3																								
462	0,26	0,07	53,49	12,65	5,82	25,92	0,69	0,02	0,00	0,01	0,00	98,94	0,01	0,01	1,06	0,77	0,36	0,85	0,04	0,00	0,00	0,00	0,00	3,09
463	1,40	0,03	74,47	14,80	0,73	6,21	0,98	0,03	0,00	0,00	0,00	98,65	0,05	0,00	1,66	1,01	0,05	0,23	0,06	0,00	0,00	0,00	0,00	3,06
464	1,21	0,02	74,62	14,94	0,66	6,18	1,17	0,00	0,00	0,00	0,00	98,79	0,04	0,00	1,66	1,02	0,05	0,23	0,07	0,00	0,00	0,00	0,00	3,06
465	0,11	0,07	59,05	11,07	5,63	23,46	0,30	0,02	0,00	0,00	0,03	99,74	0,00	0,01	1,18	0,68	0,35	0,78	0,02	0,00	0,00	0,00	0,00	3,03
466	0,09	0,08	59,36	11,03	5,52	22,67	0,34	0,02	0,00	0,01	0,00	99,12	0,00	0,01	1,20	0,69	0,35	0,76	0,02	0,00	0,00	0,00	0,00	3,03
467	0,64	0,04	59,45	10,98	5,35	22,28	0,52	0,02	0,00	0,00	0,00	99,27	0,02	0,00	1,20	0,68	0,34	0,75	0,03	0,00	0,00	0,00	0,00	3,02
468	0,81	0,01	76,30	14,80	0,70	5,91	0,61	0,01	0,00	0,00	0,00	99,14	0,03	0,00	1,70	1,02	0,05	0,22	0,04	0,00	0,00	0,00	0,00	3,05
469	1,34	0,02	74,49	14,72	0,74	6,62	0,85	0,00	0,00	0,00	0,00	98,78	0,04	0,00	1,66	1,01	0,05	0,24	0,05	0,00	0,00	0,00	0,00	3,05
470	1,00	0,04	75,44	14,83	0,81	6,79	0,76	0,02	0,00	0,00	0,00	99,68	0,03	0,00	1,66	1,00	0,06	0,25	0,05	0,00	0,00	0,00	0,00	3,06
471	2,03	0,00	73,77	14,59	1,60	6,11	1,20	0,00	0,00	0,00	0,00	99,30	0,07	0,00	1,63	0,99	0,11	0,22	0,07	0,00	0,00	0,00	0,00	3,09
472	1,25	0,00	76,68	14,60	0,63	5,40	0,39	0,01	0,00	0,00	0,00	98,96	0,04	0,00	1,72	1,01	0,04	0,20	0,02	0,00	0,00	0,00	0,00	3,05
473	4,23	0,03	75,13	14,16	0,63	4,15	0,77	0,02	0,00	0,00	0,00	99,12	0,14	0,00	1,69	0,98	0,04	0,15	0,05	0,00	0,00	0,00	0,00	3,05
474	0,82	0,00	78,42	14,64	0,67	3,98	0,67	0,00	0,00	0,00	0,00	99,22	0,03	0,00	1,77	1,02	0,05	0,15	0,04	0,00	0,00	0,00	0,00	3,05
475	0,16	0,01	51,92	9,60	7,29	29,91	0,24	0,01	0,00	0,02	0,10	99,27	0,00	0,00	1,01	0,57	0,44	0,97	0,01	0,00	0,00	0,00	0,00	3,01
476	2,09	0,02	76,66	14,84	0,68	5,82	0,18	0,02	0,00	0,02	0,00	100,33	0,07	0,00	1,70	1,01	0,05	0,21	0,01	0,00	0,00	0,00	0,00	3,05
477	1,33	0,00	75,75	14,56	0,68	6,52	0,52	0,02	0,00	0,00	0,00	99,38	0,04	0,00	1,68	0,99	0,05	0,24	0,03	0,00	0,00	0,00	0,00	3,04
478	0,38	0,10	51,21	11,70	5,33	29,53	0,78	0,03	0,00	0,01	0,00	99,07	0,01	0,01	0,99	0,70	0,32	0,95	0,04	0,00	0,00	0,00	0,00	3,03
479	0,20	0,08	49,58	11,82	5,46	30,92	0,43	0,01	0,00	0,00	0,20	98,70	0,01	0,01	0,96	0,70	0,33	1,00	0,02	0,00	0,00	0,00	0,00	3,03
480	0,10	0,02	58,17	8,88	7,57	24,19	0,18	0,02	0,00	0,01	0,00	99,13	0,00	0,00	1,17	0,55	0,47	0,81	0,01	0,00	0,00	0,00	0,00	3,02
Sample 5.1-1																								
481	1,78	0,00	75,54	15,04	0,70	5,25	0,32	0,02	0,00	0,00	0,00	98,66	0,06	0,00	1,70	1,04	0,05	0,20	0,02	0,00	0,00	0,00	0,00	3,07
482	0,64	0,00	76,93	15,09	0,78	5,25	0,23	0,02	0,00	0,00	0,00	98,94	0,02	0,00	1,73	1,05	0,05	0,20	0,01	0,00	0,00	0,00	0,00	3,07
483	0,44	0,00	77,89	15,09	0,68	4,83	0,11	0,03	0,00	0,00	0,08	99,17	0,01	0,00	1,76	1,05	0,05	0,18	0,01	0,00	0,00	0,00	0,00	3,06
484	0,73	0,01	78,76	14,87	0,67	3,75	0,19	0,00	0,00	0,00	0,00	98,99	0,02	0,00	1,79	1,04	0,05	0,14	0,01	0,00	0,00	0,00	0,00	3,06
485	0,63	0,00	76,63	15,04	0,72	5,96	0,35	0,02	0,00	0,00	0,00	99,35	0,02	0,00	1,71	1,03	0,05	0,22	0,02	0,00	0,00	0,00	0,00	3,06
486	0,79	0,00	78,00	15,11	0,67	4,19	0,13	0,01	0,00	0,00	0,00	98,90	0,03	0,00	1,77	1,06	0,05	0,16	0,01	0,00	0,00	0,00	0,00	3,07
487	1,93	0,01	75,86	14,73	0,70	4,93	0,43	0,03	0,00	0,00	0,02	98,63	0,06	0,00	1,71	1,02	0,05	0,18	0,03	0,00	0,00	0,00	0,00	3,06
488	1,94	0,01	75,39	14,92	0,77	5,92	0,44	0,02	0,00	0,00	0,00	99,41	0,06	0,00	1,68	1,02	0,05	0,22	0,03	0,00	0,00	0,00	0,00	3,06
489	3,29	0,02	73,12	14,77	0,69	6,14	0,62	0,02	0,00	0,00	0,00	98,66	0,11	0,00	1,63	1,01	0,05	0,23	0,04	0,00	0,00	0,00	0,00	3,07
490	0,77	0,01	77,61	15,07	0,84	5,21	0,25	0,01	0,00	0,00	0,26	100,02	0,03	0,00	1,73	1,03	0,06	0,19	0,02	0,00	0,00	0,00	0,01	3,06
491	0,97	0,01	77,62	15,13	0,57	5,46	0,41	0,03	0,00	0,00	0,00	100,19	0,03	0,00	1,72	1,03	0,04	0,20	0,03	0,00	0,00	0,00	0,00	3,06
492	1,25	0,01	76,05	15,19	0,79	5,95	0,34	0,02	0,00	0,00	0,00	99,60	0,04	0,00	1,69	1,04	0,05	0,22	0,02	0,00	0,00	0,00	0,00	3,07
Sample 6-1																								
493	1,78	0,00	75,54	15,04	0,70	5,25	0,32	0,02	0,00	0,00	0,00	98,66	0,06	0,00	1,70	1,04	0,05	0,20	0,02	0,00	0,00	0,00	0,00	3,07
494	0,64	0,00	76,93	15,09	0,78	5,25	0,23	0,02	0,00	0,00	0,00	98,94	0,02	0,00	1,73	1,05	0,05	0,20	0,01	0,00	0,00	0,00	0,00	3,07
495	0,44	0,00	77,89	15,09	0,68	4,83	0,11	0,03	0,00	0,00	0,08	99,17	0,01	0,00	1,76	1,05	0,05	0,18	0,01	0,00	0,00	0,00	0,00	3,06
496	0,73	0,01	78,76	14,87	0,67	3,75	0,19	0,00	0,00	0,00	0,00	98,99	0,02	0,00	1,79	1,04	0,05	0,14	0,01	0,00	0,00	0,00	0,00	3,06

Point	SnO2	MgO	Ta2O5	FeO	MnO	Nb2O5	TiO2	Sc2O3	U2O	CaO	WO3	Total	Sn a.p.f.u	Mg	Ta	Fe	Mn	Nb	Ti	Sc	U	Ca	W	Total
497	0,63	0,00	76,63	15,04	0,72	5,96	0,35	0,02	0,00	0,00	0,00	99,35	0,02	0,00	1,71	1,03	0,05	0,22	0,02	0,00	0,00	0,00	0,00	3,06
498	0,79	0,00	78,00	15,11	0,67	4,19	0,13	0,01	0,00	0,00	0,00	98,90	0,03	0,00	1,77	1,06	0,05	0,16	0,01	0,00	0,00	0,00	0,00	3,07
499	1,93	0,01	75,86	14,73	0,70	4,93	0,43	0,03	0,00	0,00	0,02	98,63	0,06	0,00	1,71	1,02	0,05	0,18	0,03	0,00	0,00	0,00	0,00	3,06
500	1,94	0,01	75,39	14,92	0,77	5,92	0,44	0,02	0,00	0,00	0,00	99,41	0,06	0,00	1,68	1,02	0,05	0,22	0,03	0,00	0,00	0,00	0,00	3,06
501	3,29	0,02	73,12	14,77	0,69	6,14	0,62	0,02	0,00	0,00	0,00	98,66	0,11	0,00	1,63	1,01	0,05	0,23	0,04	0,00	0,00	0,00	0,00	3,07
502	0,77	0,01	77,61	15,07	0,84	5,21	0,25	0,01	0,00	0,00	0,26	100,02	0,03	0,00	1,73	1,03	0,06	0,19	0,02	0,00	0,00	0,00	0,01	3,06
503	0,97	0,01	77,62	15,13	0,57	5,46	0,41	0,03	0,00	0,00	0,00	100,19	0,03	0,00	1,72	1,03	0,04	0,20	0,03	0,00	0,00	0,00	0,00	3,06
504	1,25	0,01	76,05	15,19	0,79	5,95	0,34	0,02	0,00	0,00	0,00	99,60	0,04	0,00	1,69	1,04	0,05	0,22	0,02	0,00	0,00	0,00	0,00	3,07
SampleD-4																								
505	0,26	0,02	22,19	13,65	5,97	58,50	0,58	0,02	0,00	0,00	0,19	101,36	0,01	0,00	0,37	0,69	0,31	1,60	0,03	0,00	0,00	0,00	0,00	3,01
506	0,22	0,02	23,84	13,41	5,97	57,40	0,35	0,01	0,00	0,00	0,19	101,40	0,01	0,00	0,40	0,68	0,31	1,58	0,02	0,00	0,00	0,00	0,00	3,00
507	0,44	0,01	59,06	11,47	4,96	22,00	0,51	0,00	0,00	0,00	0,08	98,54	0,01	0,00	1,20	0,72	0,32	0,75	0,03	0,00	0,00	0,00	0,00	3,03
508	2,41	0,03	55,48	11,99	4,60	24,52	0,60	0,00	0,00	0,00	0,00	99,64	0,07	0,00	1,10	0,73	0,28	0,81	0,03	0,00	0,00	0,00	0,00	3,03
509	0,11	0,01	13,52	13,98	6,48	65,16	0,45	0,00	0,00	0,02	0,80	100,53	0,00	0,00	0,22	0,69	0,32	1,74	0,02	0,00	0,00	0,00	0,01	3,01
510	0,20	0,02	11,76	14,09	6,29	65,73	0,76	0,01	0,00	0,00	0,79	99,64	0,00	0,00	0,19	0,70	0,32	1,76	0,03	0,00	0,00	0,00	0,01	3,01
511	0,57	0,04	57,28	12,15	4,81	24,55	0,52	0,02	0,00	0,00	0,03	99,97	0,02	0,00	1,14	0,74	0,30	0,81	0,03	0,00	0,00	0,00	0,00	3,03
512	0,63	0,03	57,14	11,84	4,89	24,56	0,55	0,02	0,00	0,00	0,05	99,71	0,02	0,00	1,14	0,72	0,30	0,81	0,03	0,00	0,00	0,00	0,00	3,03
513	0,20	0,03	15,25	14,38	5,97	63,13	0,49	0,00	0,00	0,00	0,59	100,03	0,00	0,00	0,25	0,72	0,30	1,71	0,02	0,00	0,00	0,00	0,01	3,02
514	0,24	0,03	13,59	14,44	5,68	64,79	0,78	0,02	0,00	0,00	0,33	99,89	0,01	0,00	0,22	0,72	0,29	1,74	0,03	0,00	0,00	0,00	0,01	3,01
515	0,24	0,02	22,53	13,63	6,19	56,91	0,35	0,01	0,00	0,00	0,24	100,12	0,01	0,00	0,38	0,70	0,32	1,59	0,02	0,00	0,00	0,00	0,00	3,02
516	0,22	0,02	15,77	14,16	6,17	63,56	0,54	0,01	0,00	0,01	0,45	100,91	0,01	0,00	0,25	0,70	0,31	1,71	0,02	0,00	0,00	0,00	0,01	3,01
517	0,11	0,02	10,16	14,27	5,74	64,20	1,49	0,01	0,00	0,01	2,96	98,98	0,00	0,00	0,16	0,71	0,29	1,73	0,07	0,00	0,00	0,00	0,05	3,01
518	0,14	0,01	13,12	14,59	5,60	65,57	0,53	0,02	0,00	0,01	0,48	100,08	0,00	0,00	0,21	0,72	0,28	1,76	0,02	0,00	0,00	0,00	0,01	3,01
519	0,22	0,04	16,74	15,03	5,51	60,00	1,09	0,00	0,00	0,01	0,98	99,63	0,01	0,00	0,28	0,76	0,28	1,64	0,05	0,00	0,00	0,00	0,02	3,04
520	0,33	0,03	18,03	14,47	5,36	59,57	1,30	0,00	0,00	0,00	1,11	100,19	0,01	0,00	0,30	0,73	0,27	1,63	0,06	0,00	0,00	0,00	0,02	3,01
521	0,20	0,03	16,32	14,77	5,26	61,84	0,79	0,01	0,00	0,00	0,89	100,11	0,00	0,00	0,27	0,74	0,27	1,68	0,04	0,00	0,00	0,00	0,01	3,01
522	0,20	0,04	18,01	14,39	5,32	59,42	1,18	0,00	0,00	0,00	1,29	99,85	0,00	0,00	0,30	0,73	0,27	1,63	0,05	0,00	0,00	0,00	0,02	3,01
523	0,33	0,04	18,05	14,38	5,28	58,97	1,19	0,01	0,00	0,00	1,14	99,38	0,01	0,00	0,30	0,73	0,27	1,63	0,05	0,00	0,00	0,00	0,02	3,01
524	0,24	0,03	16,50	14,95	5,15	60,74	1,10	0,00	0,00	0,00	1,19	99,90	0,01	0,00	0,27	0,75	0,26	1,66	0,05	0,00	0,00	0,00	0,02	3,02
525	0,29	0,03	16,67	14,58	5,28	60,77	1,17	0,00	0,00	0,01	1,13	99,92	0,01	0,00	0,27	0,73	0,27	1,65	0,05	0,00	0,00	0,00	0,02	3,01
526	0,17	0,04	17,17	14,77	5,20	60,47	1,20	0,01	0,00	0,00	0,84	99,87	0,00	0,00	0,28	0,75	0,27	1,65	0,05	0,00	0,00	0,00	0,01	3,02
527	0,23	0,02	17,57	13,69	5,63	59,40	1,19	0,02	0,00	0,00	2,43	100,17	0,01	0,00	0,29	0,69	0,29	1,62	0,05	0,00	0,00	0,00	0,04	2,99
528	0,28	0,04	17,53	14,81	5,63	60,01	1,07	0,01	0,00	0,00	1,63	101,01	0,01	0,00	0,29	0,74	0,29	1,63	0,05	0,00	0,00	0,00	0,03	3,03
529	0,17	0,04	16,02	14,87	5,55	61,41	1,04	0,00	0,00	0,02	0,58	99,71	0,00	0,00	0,26	0,75	0,28	1,67	0,05	0,00	0,00	0,00	0,01	3,03
530	0,16	0,00	16,51	13,77	6,16	58,54	1,33	0,00	0,00	0,02	2,56	99,04	0,00	0,00	0,27	0,70	0,32	1,62	0,06	0,00	0,00	0,00	0,04	3,02
531	0,15	0,02	15,70	14,46	5,33	60,37	1,09	0,03	0,00	0,00	2,87	100,03	0,00	0,00	0,26	0,73	0,27	1,64	0,05	0,00	0,00	0,00	0,04	3,00
532	0,25	0,04	16,56	15,11	5,05	60,09	1,13	0,02	0,00	0,01	2,07	100,31	0,01	0,00	0,27	0,76	0,26	1,63	0,05	0,00	0,00	0,00	0,03	3,02
Sample 3.1-2																								
533	1,19	0,00	72,70	14,82	1,19	7,92	0,94	0,01	0,00	0,01	0,00	98,79	0,04	0,00	1,60	1,00	0,08	0,29	0,06	0,00	0,00	0,00	0,00	3,07
534	1,28	0,01	73,89	14,93	1,07	7,20	0,68	0,00	0,00	0,00	0,00	99,07	0,04	0,00	1,63	1,01	0,07	0,26	0,04	0,00	0,00	0,00	0,00	3,07

Point	SnO2	MgO	Ta2O5	FeO	MnO	Nb2O5	TiO2	Sc2O3	U2O	CaO	WO3	Total	Sn a.p.f.u	Mg	Ta	Fe	Mn	Nb	Ti	Sc	U	Ca	W	Total
535	1,20	0,00	73,43	14,98	0,97	7,18	0,81	0,01	0,00	0,00	0,12	98,71	0,04	0,00	1,63	1,02	0,07	0,26	0,05	0,00	0,00	0,00	0,00	3,07
536	1,35	0,02	74,52	14,94	1,04	6,88	1,20	0,01	0,00	0,00	0,00	99,95	0,04	0,00	1,63	1,00	0,07	0,25	0,07	0,00	0,00	0,00	0,00	3,07
537	1,27	0,00	72,71	15,35	1,03	7,56	0,85	0,01	0,00	0,02	0,00	98,81	0,04	0,00	1,60	1,04	0,07	0,28	0,05	0,00	0,00	0,00	0,00	3,09
538	1,14	0,00	73,65	15,05	1,10	7,52	0,83	0,01	0,00	0,00	0,00	99,31	0,04	0,00	1,62	1,02	0,08	0,27	0,05	0,00	0,00	0,00	0,00	3,07
539	1,23	0,01	73,80	15,26	0,79	7,20	0,83	0,01	0,00	0,00	0,00	99,12	0,04	0,00	1,63	1,03	0,05	0,26	0,05	0,00	0,00	0,00	0,00	3,07
540	1,45	0,01	72,42	14,97	1,14	7,66	1,46	0,01	0,00	0,01	0,00	99,12	0,05	0,00	1,58	1,00	0,08	0,28	0,09	0,00	0,00	0,00	0,00	3,08
541	1,63	0,01	71,86	14,84	1,12	8,18	1,61	0,00	0,00	0,00	0,00	99,26	0,05	0,00	1,56	0,99	0,08	0,30	0,10	0,00	0,00	0,00	0,00	3,07
542	1,03	0,01	74,65	15,17	0,91	6,75	0,67	0,01	0,00	0,00	0,00	99,18	0,03	0,00	1,65	1,03	0,06	0,25	0,04	0,00	0,00	0,00	0,00	3,07
543	1,11	0,01	73,50	14,96	1,15	7,60	0,86	0,01	0,00	0,00	0,00	99,21	0,04	0,00	1,62	1,01	0,08	0,28	0,05	0,00	0,00	0,00	0,00	3,07
544	0,92	0,01	74,06	15,10	0,91	6,84	0,90	0,02	0,00	0,04	0,00	98,78	0,03	0,00	1,64	1,03	0,06	0,25	0,06	0,00	0,00	0,00	0,00	3,08
545	1,31	0,00	75,65	14,95	1,05	5,43	0,62	0,02	0,00	0,00	0,04	99,07	0,04	0,00	1,69	1,03	0,07	0,20	0,04	0,00	0,00	0,00	0,00	3,08
546	1,43	0,01	75,38	14,80	1,14	5,60	0,66	0,01	0,00	0,00	0,00	99,04	0,05	0,00	1,68	1,02	0,08	0,21	0,04	0,00	0,00	0,00	0,00	3,08
547	0,93	0,01	74,17	15,18	1,05	6,78	0,81	0,01	0,00	0,00	0,00	98,93	0,03	0,00	1,64	1,03	0,07	0,25	0,05	0,00	0,00	0,00	0,00	3,08
548	1,17	0,01	74,46	15,11	1,02	6,91	1,09	0,00	0,00	0,00	0,00	99,77	0,04	0,00	1,63	1,02	0,07	0,25	0,07	0,00	0,00	0,00	0,00	3,07
549	1,06	0,00	74,89	15,34	1,03	6,63	0,58	0,00	0,00	0,00	0,00	99,53	0,03	0,00	1,66	1,04	0,07	0,24	0,04	0,00	0,00	0,00	0,00	3,08
550	0,25	0,01	78,52	14,80	1,28	5,02	0,27	0,01	0,00	0,02	0,00	100,17	0,01	0,00	1,75	1,01	0,09	0,19	0,02	0,00	0,00	0,00	0,00	3,07
551	1,38	0,00	72,31	14,87	1,21	7,73	1,41	0,01	0,00	0,00	0,00	98,93	0,04	0,00	1,58	1,00	0,08	0,28	0,09	0,00	0,00	0,00	0,00	3,08
552	1,54	0,00	72,62	15,03	1,13	7,96	1,23	0,00	0,00	0,00	0,00	99,51	0,05	0,00	1,58	1,01	0,08	0,29	0,07	0,00	0,00	0,00	0,00	3,07
553	1,31	0,01	72,71	15,34	0,93	7,68	0,95	0,03	0,00	0,00	0,00	98,96	0,04	0,00	1,60	1,04	0,06	0,28	0,06	0,00	0,00	0,00	0,00	3,08
554	1,12	0,00	74,01	14,82	1,29	7,44	0,89	0,00	0,00	0,00	0,00	99,57	0,04	0,00	1,62	1,00	0,09	0,27	0,05	0,00	0,00	0,00	0,00	3,07
555	1,15	0,00	73,77	14,86	1,13	7,19	0,97	0,00	0,00	0,02	0,00	99,08	0,04	0,00	1,63	1,01	0,08	0,26	0,06	0,00	0,00	0,00	0,00	3,07
556	1,48	0,00	72,75	14,85	1,11	7,18	1,34	0,02	0,00	0,00	0,00	98,72	0,05	0,00	1,60	1,00	0,08	0,26	0,08	0,00	0,00	0,00	0,00	3,07
557	1,17	0,01	73,86	15,04	1,15	7,54	0,73	0,03	0,00	0,00	0,00	99,51	0,04	0,00	1,62	1,01	0,08	0,27	0,04	0,00	0,00	0,00	0,00	3,07
558	1,34	0,01	73,51	15,25	1,06	7,32	0,76	0,01	0,00	0,00	0,00	99,27	0,04	0,00	1,62	1,03	0,07	0,27	0,05	0,00	0,00	0,00	0,00	3,08
559	1,16	0,00	74,44	15,02	1,14	7,32	1,18	0,01	0,00	0,00	0,00	100,27	0,04	0,00	1,62	1,00	0,08	0,26	0,07	0,00	0,00	0,00	0,00	3,07
560	0,98	0,00	74,92	15,10	1,11	6,72	0,84	0,02	0,00	0,00	0,00	99,70	0,03	0,00	1,65	1,02	0,08	0,25	0,05	0,00	0,00	0,00	0,00	3,08
561	1,52	0,02	72,89	15,05	0,94	7,61	1,44	0,03	0,00	0,00	0,00	99,50	0,05	0,00	1,59	1,01	0,06	0,28	0,09	0,00	0,00	0,00	0,00	3,07
562	1,39	0,00	73,37	15,16	1,06	7,63	1,47	0,01	0,00	0,00	0,00	100,10	0,04	0,00	1,59	1,01	0,07	0,27	0,09	0,00	0,00	0,00	0,00	3,07
563	3,04	0,00	73,40	14,79	0,99	6,30	0,93	0,01	0,00	0,00	0,00	99,47	0,10	0,00	1,62	1,00	0,07	0,23	0,06	0,00	0,00	0,00	0,00	3,07
564	1,31	0,01	74,09	15,03	1,18	7,53	0,74	0,00	0,00	0,00	0,00	99,89	0,04	0,00	1,62	1,01	0,08	0,27	0,04	0,00	0,00	0,00	0,00	3,07
565	1,29	0,00	73,54	14,76	1,05	8,01	1,00	0,01	0,00	0,02	0,00	99,67	0,04	0,00	1,60	0,99	0,07	0,29	0,06	0,00	0,00	0,00	0,00	3,06
566	1,41	0,01	73,26	14,56	1,25	7,57	1,01	0,00	0,00	0,00	0,06	99,15	0,05	0,00	1,61	0,98	0,09	0,28	0,06	0,00	0,00	0,00	0,00	3,06
567	0,90	0,01	75,38	14,99	1,16	6,18	0,69	0,00	0,00	0,01	0,00	99,31	0,03	0,00	1,67	1,02	0,08	0,23	0,04	0,00	0,00	0,00	0,00	3,08
568	0,92	0,00	75,32	14,93	1,00	6,90	0,72	0,01	0,00	0,00	0,00	99,80	0,03	0,00	1,66	1,01	0,07	0,25	0,04	0,00	0,00	0,00	0,00	3,06
569	1,24	0,01	74,72	15,15	0,88	6,89	0,61	0,01	0,00	0,00	0,00	99,51	0,04	0,00	1,65	1,03	0,06	0,25	0,04	0,00	0,00	0,00	0,00	3,07
570	0,99	0,01	74,49	14,95	1,23	6,89	0,84	0,01	0,00	0,00	0,00	99,41	0,03	0,00	1,64	1,01	0,08	0,25	0,05	0,00	0,00	0,00	0,00	3,08
571	1,15	0,00	76,62	13,16	1,13	7,10	1,18	0,00	0,00	0,00	0,00	100,33	0,04	0,00	1,67	0,88	0,08	0,26	0,07	0,00	0,00	0,00	0,00	3,00
572	1,56	0,00	75,22	13,18	1,05	7,52	1,37	0,00	0,00	0,00	0,00	99,90	0,05	0,00	1,64	0,88	0,07	0,27	0,08	0,00	0,00	0,00	0,00	3,00
573	1,52	0,00	76,04	13,15	1,02	7,44	1,35	0,00	0,00	0,00	0,00	100,53	0,05	0,00	1,65	0,88	0,07	0,27	0,08	0,00	0,00	0,00	0,00	2,99
574	1,42	0,00	75,66	13,23	1,03	7,70	1,35	0,00	0,00	0,00	0,00	100,49	0,05	0,00	1,64	0,88	0,07	0,28	0,08	0,00	0,00	0,00	0,00	3,01

Point	SnO2	MgO	Ta2O5	FeO	MnO	Nb2O5	TiO2	Sc2O3	U2O	CaO	WO3	Total	Sn a.p.f.u	Mg	Ta	Fe	Mn	Nb	Ti	Sc	U	Ca	W	Total
575	1,67	0,00	74,76	13,16	1,00	8,15	1,78	0,00	0,00	0,00	0,00	100,65	0,05	0,00	1,60	0,87	0,07	0,29	0,11	0,00	0,00	0,00	0,00	2,99
576	1,29	0,00	76,07	13,15	1,05	7,51	1,13	0,00	0,00	0,00	0,00	100,21	0,04	0,00	1,66	0,88	0,07	0,27	0,07	0,00	0,00	0,00	0,00	2,99
577	0,92	0,00	77,94	13,27	1,00	6,76	0,72	0,00	0,00	0,00	0,00	100,61	0,03	0,00	1,71	0,89	0,07	0,25	0,04	0,00	0,00	0,00	0,00	2,99
578	0,97	0,00	77,77	13,21	0,97	6,78	0,73	0,00	0,00	0,00	0,00	100,43	0,03	0,00	1,71	0,89	0,07	0,25	0,04	0,00	0,00	0,00	0,00	2,99
579	0,26	0,00	81,92	13,03	1,12	3,83	0,21	0,00	0,00	0,00	0,00	100,36	0,01	0,00	1,85	0,90	0,08	0,14	0,01	0,00	0,00	0,00	0,00	2,99
580	1,47	0,00	74,90	13,15	1,07	8,20	1,52	0,00	0,00	0,00	0,00	100,31	0,05	0,00	1,62	0,87	0,07	0,29	0,09	0,00	0,00	0,00	0,00	2,99
581	0,88	0,00	78,26	13,08	1,10	6,27	0,66	0,00	0,00	0,00	0,00	100,25	0,03	0,00	1,73	0,89	0,08	0,23	0,04	0,00	0,00	0,00	0,00	2,99
582	0,92	0,00	77,49	13,06	1,12	6,77	0,72	0,00	0,00	0,00	0,00	100,08	0,03	0,00	1,71	0,89	0,08	0,25	0,04	0,00	0,00	0,00	0,00	2,99
583	1,95	0,00	73,92	13,26	0,74	7,88	2,54	0,00	0,00	0,00	0,00	100,29	0,06	0,00	1,58	0,87	0,05	0,28	0,15	0,00	0,00	0,00	0,00	3,00
584	1,85	0,00	74,42	13,29	0,79	7,76	2,18	0,00	0,00	0,00	0,00	100,28	0,06	0,00	1,60	0,88	0,05	0,28	0,13	0,00	0,00	0,00	0,00	3,00
585	1,09	0,00	78,84	13,31	0,78	5,71	0,64	0,00	0,00	0,00	0,00	100,37	0,04	0,00	1,75	0,91	0,05	0,21	0,04	0,00	0,00	0,00	0,00	2,99
586	4,35	0,00	75,53	13,03	0,75	5,56	1,11	0,00	0,00	0,00	0,00	100,89	0,14	0,00	1,66	0,88	0,05	0,20	0,07	0,00	0,00	0,00	0,00	3,00
587	0,88	0,00	79,46	13,32	0,78	5,18	0,50	0,00	0,00	0,00	0,00	100,11	0,03	0,00	1,77	0,91	0,05	0,19	0,03	0,00	0,00	0,00	0,00	2,99
588	0,24	0,00	82,19	12,80	1,24	3,61	0,23	0,00	0,00	0,00	0,00	100,31	0,01	0,00	1,86	0,89	0,09	0,14	0,01	0,00	0,00	0,00	0,00	2,99
589	0,26	0,00	81,66	12,89	1,20	4,22	0,12	0,00	0,00	0,00	0,00	100,35	0,01	0,00	1,84	0,89	0,08	0,16	0,01	0,00	0,00	0,00	0,00	2,99
590	0,46	0,00	79,33	12,99	1,17	5,79	0,48	0,00	0,00	0,00	0,00	100,22	0,01	0,00	1,76	0,89	0,08	0,21	0,03	0,00	0,00	0,00	0,00	2,99
591	1,08	0,00	77,11	13,04	1,18	7,40	0,82	0,00	0,00	0,00	0,00	100,63	0,03	0,00	1,68	0,88	0,08	0,27	0,05	0,00	0,00	0,00	0,00	2,99
592	1,11	0,00	76,07	13,04	1,12	7,56	1,01	0,00	0,00	0,00	0,00	99,91	0,04	0,00	1,67	0,88	0,08	0,28	0,06	0,00	0,00	0,00	0,00	2,99
593	1,45	0,00	74,65	12,97	1,14	8,05	1,42	0,00	0,00	0,00	0,00	99,68	0,05	0,00	1,62	0,87	0,08	0,29	0,09	0,00	0,00	0,00	0,00	2,99
594	0,93	0,00	77,30	12,91	1,13	6,48	0,68	0,00	0,00	0,00	0,00	99,43	0,03	0,00	1,72	0,88	0,08	0,24	0,04	0,00	0,00	0,00	0,00	2,99
595	0,30	0,00	80,12	12,99	1,15	5,25	0,28	0,00	0,00	0,00	0,00	100,08	0,01	0,00	1,79	0,89	0,08	0,20	0,02	0,00	0,00	0,00	0,00	2,99
596	1,26	0,00	76,18	13,25	1,03	8,09	1,06	0,00	0,00	0,00	0,00	100,86	0,04	0,00	1,65	0,88	0,07	0,29	0,06	0,00	0,00	0,00	0,00	2,99
597	0,98	0,00	77,17	13,38	0,92	6,98	0,74	0,00	0,00	0,00	0,00	100,15	0,03	0,00	1,70	0,90	0,06	0,26	0,04	0,00	0,00	0,00	0,00	3,00
598	0,96	0,00	77,31	13,28	0,89	6,99	0,75	0,00	0,00	0,00	0,00	100,18	0,03	0,00	1,70	0,90	0,06	0,26	0,05	0,00	0,00	0,00	0,00	2,99
599	1,93	0,00	73,97	13,26	0,79	8,12	2,08	0,00	0,00	0,00	0,00	100,15	0,06	0,00	1,59	0,88	0,05	0,29	0,12	0,00	0,00	0,00	0,00	2,99
600	1,09	0,00	76,67	13,16	0,89	6,83	1,01	0,00	0,00	0,00	0,00	99,64	0,04	0,00	1,69	0,89	0,06	0,25	0,06	0,00	0,00	0,00	0,00	2,99
601	0,46	0,00	80,25	12,94	1,21	4,62	0,45	0,00	0,00	0,00	0,00	99,92	0,02	0,00	1,80	0,89	0,08	0,17	0,03	0,00	0,00	0,00	0,00	3,00
602	0,31	0,00	81,14	13,04	1,21	4,51	0,24	0,00	0,00	0,00	0,00	100,45	0,01	0,00	1,82	0,90	0,08	0,17	0,01	0,00	0,00	0,00	0,00	2,99
603	1,61	0,00	74,84	13,00	1,14	8,10	1,64	0,00	0,00	0,00	0,00	100,34	0,05	0,00	1,61	0,86	0,08	0,29	0,10	0,00	0,00	0,00	0,00	2,99
604	1,67	0,00	74,71	13,11	1,12	8,16	1,60	0,00	0,00	0,00	0,00	100,37	0,05	0,00	1,61	0,87	0,08	0,29	0,10	0,00	0,00	0,00	0,00	3,00
605	1,02	0,00	77,22	13,34	0,90	6,78	0,63	0,00	0,00	0,00	0,00	99,89	0,03	0,00	1,71	0,91	0,06	0,25	0,04	0,00	0,00	0,00	0,00	3,00
606	1,18	0,00	76,32	13,34	1,14	8,06	1,02	0,00	0,00	0,00	0,00	101,05	0,04	0,00	1,65	0,89	0,08	0,29	0,06	0,00	0,00	0,00	0,00	3,00
607	0,35	0,00	80,87	13,27	1,15	5,12	0,26	0,00	0,00	0,00	0,00	101,01	0,01	0,00	1,80	0,91	0,08	0,19	0,02	0,00	0,00	0,00	0,00	3,00
608	0,28	0,00	81,72	13,07	1,12	4,29	0,17	0,00	0,00	0,00	0,00	100,64	0,01	0,00	1,83	0,90	0,08	0,16	0,01	0,00	0,00	0,00	0,00	2,99
609	1,22	0,00	76,46	13,00	1,16	7,38	1,18	0,00	0,00	0,00	0,00	100,39	0,04	0,00	1,67	0,87	0,08	0,27	0,07	0,00	0,00	0,00	0,00	2,99
610	1,19	0,00	76,71	13,09	1,16	7,17	1,05	0,00	0,00	0,00	0,00	100,37	0,04	0,00	1,68	0,88	0,08	0,26	0,06	0,00	0,00	0,00	0,00	2,99
611	0,95	0,00	77,71	13,02	1,11	6,49	0,88	0,00	0,00	0,00	0,00	100,16	0,03	0,00	1,71	0,88	0,08	0,24	0,05	0,00	0,00	0,00	0,00	2,99
612	0,30	0,00	80,66	12,89	1,12	4,47	0,14	0,00	0,00	0,00	0,00	99,71	0,01	0,00	1,83	0,90	0,08	0,17	0,01	0,00	0,00	0,00	0,00	2,99
613	1,31	0,00	75,81	13,05	1,10	7,93	0,96	0,00	0,00	0,00	0,00	100,17	0,04	0,00	1,65	0,88	0,07	0,29	0,06	0,00	0,00	0,00	0,00	2,99
614	1,32	0,00	76,26	13,48	0,83	7,86	0,99	0,00	0,00	0,00	0,00	100,74	0,04	0,00	1,65	0,90	0,06	0,28	0,06	0,00	0,00	0,00	0,00	2,99

Point	SnO2	MgO	Ta2O5	FeO	MnO	Nb2O5	TiO2	Sc2O3	U2O	CaO	WO3	Total	Sn a.p.f.u	Mg	Ta	Fe	Mn	Nb	Ti	Sc	U	Ca	W	Total
615	1,02	0,00	77,55	13,45	0,77	6,97	0,63	0,00	0,00	0,00	0,00	100,39	0,03	0,00	1,70	0,91	0,05	0,25	0,04	0,00	0,00	0,00	0,00	2,99
616	1,29	0,00	75,69	13,42	0,78	7,61	1,01	0,00	0,00	0,00	0,00	99,80	0,04	0,00	1,66	0,90	0,05	0,28	0,06	0,00	0,00	0,00	0,00	2,99
617	0,98	0,00	77,78	13,37	0,84	6,60	0,48	0,00	0,00	0,00	0,00	100,04	0,03	0,00	1,72	0,91	0,06	0,24	0,03	0,00	0,00	0,00	0,00	2,99
618	1,29	0,00	75,97	13,23	0,87	7,18	1,06	0,00	0,00	0,00	0,00	99,60	0,04	0,00	1,67	0,89	0,06	0,26	0,06	0,00	0,00	0,00	0,00	2,99
619	1,23	0,00	75,98	13,11	1,00	7,37	0,94	0,00	0,00	0,00	0,00	99,63	0,04	0,00	1,67	0,89	0,07	0,27	0,06	0,00	0,00	0,00	0,00	2,99
620	0,93	0,00	78,06	13,21	0,93	6,12	0,62	0,00	0,00	0,00	0,00	99,87	0,03	0,00	1,73	0,90	0,06	0,23	0,04	0,00	0,00	0,00	0,00	2,99
621	1,14	0,00	77,68	13,15	0,97	6,32	0,72	0,00	0,00	0,00	0,00	99,98	0,04	0,00	1,72	0,89	0,07	0,23	0,04	0,00	0,00	0,00	0,00	2,99
622	1,30	0,00	75,91	13,23	0,89	7,62	1,08	0,00	0,00	0,00	0,00	100,03	0,04	0,00	1,66	0,89	0,06	0,28	0,07	0,00	0,00	0,00	0,00	2,99
623	0,92	0,00	77,78	13,14	1,07	6,38	0,56	0,00	0,00	0,00	0,00	99,83	0,03	0,00	1,73	0,90	0,07	0,24	0,03	0,00	0,00	0,00	0,00	2,99
624	1,36	0,00	75,50	13,01	1,10	7,30	1,53	0,00	0,00	0,00	0,00	99,80	0,04	0,00	1,65	0,87	0,07	0,26	0,09	0,00	0,00	0,00	0,00	3,00
625	1,43	0,00	75,67	13,29	0,96	7,52	1,44	0,00	0,00	0,00	0,00	100,31	0,05	0,00	1,64	0,89	0,06	0,27	0,09	0,00	0,00	0,00	0,00	3,00
626	0,86	0,00	77,99	13,18	1,11	6,52	0,55	0,00	0,00	0,00	0,00	100,21	0,03	0,00	1,72	0,90	0,08	0,24	0,03	0,00	0,00	0,00	0,00	3,00
627	1,54	0,00	74,82	12,95	1,25	8,19	1,47	0,00	0,00	0,00	0,00	100,22	0,05	0,00	1,62	0,86	0,08	0,29	0,09	0,00	0,00	0,00	0,00	2,99
628	1,26	0,00	76,80	13,15	1,12	7,25	0,77	0,00	0,00	0,00	0,00	100,35	0,04	0,00	1,68	0,89	0,08	0,26	0,05	0,00	0,00	0,00	0,00	2,99
629	1,00	0,00	77,33	13,00	1,15	6,92	0,61	0,00	0,00	0,00	0,00	100,02	0,03	0,00	1,71	0,88	0,08	0,25	0,04	0,00	0,00	0,00	0,00	2,99
630	0,24	0,00	81,71	12,96	1,25	4,24	0,16	0,00	0,00	0,00	0,00	100,56	0,01	0,00	1,83	0,89	0,09	0,16	0,01	0,00	0,00	0,00	0,00	2,99
631	2,06	0,00	74,11	12,94	1,15	7,69	2,02	0,00	0,00	0,00	0,00	100,09	0,07	0,00	1,60	0,86	0,08	0,28	0,12	0,00	0,00	0,00	0,00	3,00
632	0,85	0,00	77,38	13,09	1,19	7,01	0,56	0,00	0,00	0,00	0,00	100,09	0,03	0,00	1,71	0,89	0,08	0,26	0,03	0,00	0,00	0,00	0,00	2,99
633	3,49	0,00	74,73	12,73	1,10	6,87	1,73	0,00	0,00	0,00	0,00	100,77	0,11	0,00	1,61	0,85	0,07	0,25	0,10	0,00	0,00	0,00	0,00	2,99
634	1,30	0,00	77,14	13,02	1,16	6,91	0,89	0,00	0,00	0,00	0,00	100,42	0,04	0,00	1,69	0,88	0,08	0,25	0,05	0,00	0,00	0,00	0,00	2,99
635	0,41	0,00	79,06	13,13	1,07	5,61	0,46	0,00	0,00	0,00	0,00	99,72	0,01	0,00	1,77	0,90	0,07	0,21	0,03	0,00	0,00	0,00	0,00	2,99
636	2,03	0,00	74,07	13,42	0,73	8,08	2,00	0,00	0,00	0,00	0,00	100,34	0,06	0,00	1,59	0,89	0,05	0,29	0,12	0,00	0,00	0,00	0,00	3,00
637	1,91	0,00	74,17	13,40	0,72	7,87	2,02	0,00	0,00	0,00	0,00	100,09	0,06	0,00	1,60	0,89	0,05	0,28	0,12	0,00	0,00	0,00	0,00	3,00
638	0,96	0,00	77,40	13,42	0,81	6,77	0,60	0,00	0,00	0,00	0,00	99,96	0,03	0,00	1,71	0,91	0,06	0,25	0,04	0,00	0,00	0,00	0,00	2,99
639	0,87	0,00	77,58	13,43	0,79	6,76	0,66	0,00	0,00	0,00	0,00	100,10	0,03	0,00	1,71	0,91	0,05	0,25	0,04	0,00	0,00	0,00	0,00	2,99
640	1,30	0,00	75,80	13,50	0,77	7,41	1,02	0,00	0,00	0,00	0,00	99,80	0,04	0,00	1,66	0,91	0,05	0,27	0,06	0,00	0,00	0,00	0,00	3,00
641	0,38	0,00	80,14	13,18	1,05	5,26	0,30	0,00	0,00	0,00	0,00	100,30	0,01	0,00	1,79	0,90	0,07	0,20	0,02	0,00	0,00	0,00	0,00	2,99
642	0,94	0,00	78,09	13,26	1,04	6,63	0,52	0,00	0,00	0,00	0,00	100,49	0,03	0,00	1,72	0,90	0,07	0,24	0,03	0,00	0,00	0,00	0,00	2,99
643	1,39	0,00	75,89	13,23	1,00	7,61	1,37	0,00	0,00	0,00	0,00	100,48	0,04	0,00	1,65	0,88	0,07	0,27	0,08	0,00	0,00	0,00	0,00	2,99
644	0,26	0,00	81,98	12,99	1,09	4,00	0,18	0,00	0,00	0,00	0,00	100,49	0,01	0,00	1,84	0,90	0,08	0,15	0,01	0,00	0,00	0,00	0,00	2,99
645	1,22	0,00	77,00	13,10	1,07	7,14	0,94	0,00	0,00	0,00	0,00	100,65	0,04	0,00	1,68	0,88	0,07	0,26	0,06	0,00	0,00	0,00	0,00	2,99
646	0,50	0,00	78,73	13,09	1,13	5,91	0,68	0,00	0,00	0,00	0,00	100,03	0,02	0,00	1,75	0,89	0,08	0,22	0,04	0,00	0,00	0,00	0,00	2,99
647	1,73	0,00	74,58	13,04	1,11	7,68	1,79	0,00	0,00	0,00	0,00	99,94	0,06	0,00	1,62	0,87	0,08	0,28	0,11	0,00	0,00	0,00	0,00	3,00
648	1,06	0,00	76,57	12,98	1,15	7,21	1,18	0,00	0,00	0,00	0,00	100,15	0,03	0,00	1,67	0,87	0,08	0,26	0,07	0,00	0,00	0,00	0,00	2,99
649	1,30	0,00	75,59	12,98	1,13	7,54	1,16	0,00	0,00	0,00	0,00	99,70	0,04	0,00	1,66	0,87	0,08	0,27	0,07	0,00	0,00	0,00	0,00	2,99
650	0,26	0,00	81,66	12,90	1,20	3,94	0,19	0,00	0,00	0,00	0,00	100,15	0,01	0,00	1,84	0,90	0,08	0,15	0,01	0,00	0,00	0,00	0,00	2,99
651	1,45	0,00	76,56	12,96	1,17	7,24	0,88	0,00	0,00	0,00	0,00	100,25	0,05	0,00	1,68	0,87	0,08	0,26	0,05	0,00	0,00	0,00	0,00	2,99
652	1,20	0,00	75,81	12,88	1,20	7,15	1,29	0,00	0,00	0,00	0,00	99,52	0,04	0,00	1,66	0,87	0,08	0,26	0,08	0,00	0,00	0,00	0,00	2,99
653	1,22	0,00	78,90	13,40	0,75	4,99	0,64	0,00	0,00	0,00	0,00	100,07	0,04	0,00	1,76	0,92	0,05	0,19	0,04	0,00	0,00	0,00	0,00	3,00
654	0,30	0,00	82,00	13,19	0,92	3,58	0,36	0,00	0,00	0,00	0,00	100,34	0,01	0,00	1,85	0,91	0,06	0,13	0,02	0,00	0,00	0,00	0,00	2,99

Point	SnO2	MgO	Ta2O5	FeO	MnO	Nb2O5	TiO2	Sc2O3	U2O	CaO	WO3	Total	Sn a.p.f.u	Mg	Ta	Fe	Mn	Nb	Ti	Sc	U	Ca	W	Total
655	0,74	0,00	78,33	13,56	0,76	6,56	0,42	0,00	0,00	0,00	0,00	100,37	0,02	0,00	1,73	0,92	0,05	0,24	0,03	0,00	0,00	0,00	0,00	2,99
656	0,89	0,00	77,94	13,48	0,75	6,71	0,50	0,00	0,00	0,00	0,00	100,27	0,03	0,00	1,72	0,91	0,05	0,25	0,03	0,00	0,00	0,00	0,00	2,99
657	0,89	0,00	78,22	13,42	0,78	6,47	0,50	0,00	0,00	0,00	0,00	100,30	0,03	0,00	1,73	0,91	0,05	0,24	0,03	0,00	0,00	0,00	0,00	2,99

2. Cassiterite mineral chemistry data

Point	SnO2	MgO	Ta2O5	FeO	MnO	Nb2O5	TiO2	Sc2O3	U2O	CaO	WO3	Total	Sn a.p.f.u	Mg	Ta	Fe	Mn	Nb	Ti	Sc	U	Ca	W	Total
sample Na-5													6 anions											
1	99,30	0,10	0,91	0,27	0,04	0,62	0,05	0,00	0,00	0,54	0,00	101,82	2,91	0,01	0,02	0,02	0,00	0,02	0,00	0,00	0,00	0,04	0,00	3,03
2	97,58	0,10	1,71	0,36	0,05	0,59	0,18	0,00	0,00	0,52	0,00	101,08	2,88	0,01	0,03	0,02	0,00	0,02	0,01	0,00	0,00	0,04	0,00	3,03
3	99,42	0,14	0,81	0,17	0,03	0,27	0,06	0,00	0,00	0,51	0,00	101,41	2,93	0,01	0,02	0,01	0,00	0,01	0,00	0,00	0,00	0,04	0,00	3,03
4	100,30	0,11	0,04	0,02	0,00	0,20	0,04	0,00	0,00	0,54	0,00	101,25	2,96	0,01	0,00	0,00	0,00	0,01	0,00	0,00	0,00	0,04	0,00	3,03
5	100,66	0,12	0,06	0,03	0,00	0,03	0,01	0,00	0,00	0,53	0,42	101,85	2,96	0,01	0,00	0,00	0,00	0,00	0,00	0,00	0,00	0,04	0,01	3,02
6	97,75	0,11	0,39	0,42	0,01	1,39	0,16	0,00	0,00	0,52	0,11	100,85	2,88	0,01	0,01	0,03	0,00	0,05	0,01	0,00	0,00	0,04	0,00	3,03
7	94,57	0,11	4,18	0,91	0,00	1,20	0,08	0,00	0,00	0,50	0,37	101,91	2,78	0,01	0,08	0,06	0,00	0,04	0,00	0,00	0,00	0,04	0,01	3,02
8	94,03	0,10	3,33	0,97	0,01	2,04	0,17	0,00	0,00	0,52	0,26	101,42	2,76	0,01	0,07	0,06	0,00	0,07	0,01	0,00	0,00	0,04	0,00	3,02
9	100,25	0,09	0,78	0,12	0,01	0,16	0,07	0,00	0,00	0,55	0,00	102,01	2,94	0,01	0,02	0,01	0,00	0,01	0,00	0,00	0,00	0,04	0,00	3,03
10	101,56	0,09	0,19	0,05	0,00	0,24	0,04	0,00	0,00	0,55	0,00	102,71	2,96	0,01	0,00	0,00	0,00	0,01	0,00	0,00	0,00	0,04	0,00	3,02
Sample Na-6																								
11	99,61	0,11	1,46	0,19	0,01	0,07	0,09	0,00	0,00	0,54	0,00	102,08	2,92	0,01	0,03	0,01	0,00	0,00	0,01	0,00	0,00	0,04	0,00	3,03
12	98,88	0,13	0,36	0,23	0,00	1,18	0,21	0,00	0,00	0,52	0,86	102,36	2,87	0,01	0,01	0,01	0,00	0,04	0,01	0,00	0,00	0,04	0,02	3,01
13	101,23	0,13	0,15	0,01	0,01	0,14	0,03	0,00	0,00	0,51	0,01	102,22	2,96	0,01	0,00	0,00	0,00	0,00	0,00	0,00	0,00	0,04	0,00	3,03
14	100,40	0,11	0,25	0,17	0,01	0,44	0,14	0,00	0,00	0,51	0,00	102,03	2,94	0,01	0,01	0,01	0,00	0,01	0,01	0,00	0,00	0,04	0,00	3,03
Sample J-5																								
15	99,14	0,10	1,42	0,21	0,03	0,00	0,00	0,00	0,00	0,54	0,33	101,76	2,92	0,01	0,03	0,01	0,00	0,00	0,00	0,00	0,00	0,04	0,01	3,02
16	93,25	0,08	5,75	0,90	0,08	0,25	0,00	0,00	0,00	0,51	0,00	100,82	2,79	0,01	0,12	0,06	0,01	0,01	0,00	0,00	0,00	0,04	0,00	3,02
17	98,77	0,08	1,24	0,27	0,06	0,08	0,00	0,00	0,00	0,53	0,54	101,56	2,91	0,01	0,02	0,02	0,00	0,00	0,00	0,00	0,00	0,04	0,01	3,02
18	98,39	0,11	2,02	0,18	0,00	0,02	0,00	0,00	0,00	0,51	0,21	101,44	2,91	0,01	0,04	0,01	0,00	0,00	0,00	0,00	0,00	0,04	0,00	3,02
Sample B-2																								
19	98,99	0,11	0,61	0,48	0,00	1,50	0,30	0,00	0,00	0,54	0,04	102,57	2,86	0,01	0,01	0,03	0,00	0,05	0,02	0,00	0,00	0,04	0,00	3,03
20	100,12	0,10	0,40	0,30	0,00	0,78	0,01	0,00	0,00	0,54	0,01	102,26	2,92	0,01	0,01	0,02	0,00	0,03	0,00	0,00	0,00	0,04	0,00	3,03
21	97,91	0,09	1,12	0,47	0,00	1,42	0,11	0,00	0,00	0,53	0,00	101,65	2,87	0,01	0,02	0,03	0,00	0,05	0,01	0,00	0,00	0,04	0,00	3,02
22	100,33	0,19	0,53	0,12	0,00	0,08	0,42	0,00	0,00	0,54	0,09	102,28	2,92	0,02	0,01	0,01	0,00	0,00	0,02	0,00	0,00	0,04	0,00	3,03
23	100,96	0,12	0,34	0,05	0,00	0,07	0,00	0,00	0,00	0,56	0,00	102,11	2,96	0,01	0,01	0,00	0,00	0,00	0,00	0,00	0,00	0,04	0,00	3,03
24	99,27	0,09	0,26	0,17	0,00	0,70	0,16	0,00	0,00	0,53	0,00	101,18	2,92	0,01	0,01	0,01	0,00	0,02	0,01	0,00	0,00	0,04	0,00	3,02
25	100,89	0,13	0,04	0,11	0,01	0,30	0,05	0,00	0,00	0,57	0,00	102,10	2,95	0,01	0,00	0,01	0,00	0,01	0,00	0,00	0,00	0,04	0,00	3,03
26	100,12	0,11	0,26	0,20	0,00	1,05	0,15	0,00	0,00	0,53	0,00	102,42	2,91	0,01	0,01	0,01	0,00	0,03	0,01	0,00	0,00	0,04	0,00	3,02
Sample A-2																								
27	97,64	0,10	2,73	0,53	0,09	0,51	0,16	0,00	0,00	0,51	0,00	102,24	2,86	0,01	0,05	0,03	0,01	0,02	0,01	0,00	0,00	0,04	0,00	3,03
28	100,69	0,12	0,34	0,11	0,02	0,04	0,13	0,00	0,00	0,52	0,00	101,97	2,95	0,01	0,01	0,01	0,00	0,00	0,01	0,00	0,00	0,04	0,00	3,03
29	100,27	0,10	0,82	0,16	0,01	0,18	0,06	0,00	0,00	0,54	0,13	102,26	2,93	0,01	0,02	0,01	0,00	0,01	0,00	0,00	0,00	0,04	0,00	3,02
Sample X-1																								
30	98,74	0,12	0,31	0,15	0,00	0,25	0,02	0,00	0,00	0,53	0,00	100,13	2,95	0,01	0,01	0,01	0,00	0,01	0,00	0,00	0,00	0,04	0,00	3,03
31	97,93	0,11	0,90	0,14	0,01	0,09	0,05	0,00	0,00	0,53	0,00	99,76	2,94	0,01	0,02	0,01	0,00	0,00	0,00	0,00	0,00	0,04	0,00	3,03
32	94,08	0,09	2,66	0,82	0,05	2,00	0,09	0,00	0,00	0,50	0,02	100,31	2,79	0,01	0,05	0,05	0,00	0,07	0,01	0,00	0,00	0,04	0,00	3,02
33	98,55	0,10	0,27	0,17	0,00	0,84	0,06	0,00	0,00	0,50	0,42	100,90	2,91	0,01	0,01	0,01	0,00	0,03	0,00	0,00	0,00	0,04	0,01	3,02
34	98,07	0,10	1,00	0,15	0,02	0,05	0,07	0,00	0,00	0,54	0,00	100,00	2,94	0,01	0,02	0,01	0,00	0,00	0,00	0,00	0,00	0,04	0,00	3,03

Point	SnO2	MgO	Ta2O5	FeO	MnO	Nb2O5	TiO2	Sc2O3	U2O	CaO	WO3	Total	Sn a.p.f.u	Mg	Ta	Fe	Mn	Nb	Ti	Sc	U	Ca	W	Total
35	98,52	0,10	0,87	0,07	0,02	0,07	0,04	0,00	0,00	0,50	0,05	100,23	2,94	0,01	0,02	0,00	0,00	0,00	0,00	0,00	0,00	0,04	0,00	3,02
36	97,92	0,11	0,78	0,10	0,01	0,04	0,04	0,00	0,00	0,52	0,00	99,51	2,95	0,01	0,02	0,01	0,00	0,00	0,00	0,00	0,00	0,04	0,00	3,03
37	97,88	0,10	0,26	0,24	0,01	0,44	0,13	0,00	0,00	0,54	0,35	99,94	2,92	0,01	0,01	0,01	0,00	0,01	0,01	0,00	0,00	0,04	0,01	3,03
38	97,68	0,11	0,66	0,22	0,00	0,56	0,13	0,00	0,00	0,53	0,00	99,89	2,92	0,01	0,01	0,01	0,00	0,02	0,01	0,00	0,00	0,04	0,00	3,03
39	98,02	0,12	0,33	0,18	0,03	0,76	0,03	0,00	0,00	0,54	0,00	100,01	2,92	0,01	0,01	0,01	0,00	0,03	0,00	0,00	0,00	0,04	0,00	3,03
40	98,58	0,09	1,22	0,11	0,05	0,06	0,00	0,00	0,00	0,51	0,36	100,98	2,93	0,01	0,02	0,01	0,00	0,00	0,00	0,00	0,00	0,04	0,01	3,02
41	97,87	0,09	1,21	0,15	0,00	0,05	0,00	0,00	0,00	0,56	0,18	100,11	2,93	0,01	0,02	0,01	0,00	0,00	0,00	0,00	0,00	0,04	0,00	3,02
42	92,33	0,12	2,91	0,95	0,05	2,08	0,12	0,00	0,00	0,52	0,00	99,09	2,77	0,01	0,06	0,06	0,00	0,07	0,01	0,00	0,00	0,04	0,00	3,03
43	98,57	0,10	0,68	0,11	0,00	0,05	0,03	0,00	0,00	0,52	0,04	100,09	2,95	0,01	0,01	0,01	0,00	0,00	0,00	0,00	0,00	0,04	0,00	3,03
Sample M-2																								
44	98,52	0,10	1,33	0,20	0,01	0,05	0,16	0,00	0,00	0,52	0,71	101,60	2,90	0,01	0,03	0,01	0,00	0,00	0,01	0,00	0,00	0,04	0,01	3,02
45	97,89	0,10	1,15	0,19	0,01	0,10	0,25	0,00	0,00	0,52	0,00	100,20	2,92	0,01	0,02	0,01	0,00	0,00	0,01	0,00	0,00	0,04	0,00	3,03
46	95,20	0,11	3,61	0,56	0,00	0,29	0,32	0,00	0,00	0,53	0,00	100,64	2,83	0,01	0,07	0,04	0,00	0,01	0,02	0,00	0,00	0,04	0,00	3,02
47	87,66	0,06	10,33	1,44	0,25	0,47	0,20	0,00	0,00	0,43	0,00	100,83	2,63	0,01	0,21	0,09	0,02	0,02	0,01	0,00	0,00	0,03	0,00	3,02
Sample T-4																								
48	98,91	0,08	0,18	0,12	0,01	0,63	0,03	0,00	0,00	0,51	0,00	100,47	2,94	0,01	0,00	0,01	0,00	0,02	0,00	0,00	0,00	0,04	0,00	3,02
Sample 3-3																								
49	99,51	0,11	0,85	0,16	0,02	0,22	0,07	0,00	0,00	0,54	0,00	101,48	2,93	0,01	0,02	0,01	0,00	0,01	0,00	0,00	0,00	0,04	0,00	3,03
Sample 3.2-1																								
50	97,93	0,09	1,74	0,43	0,01	0,59	0,26	0,00	0,00	0,49	0,00	101,54	2,88	0,01	0,03	0,03	0,00	0,02	0,01	0,00	0,00	0,04	0,00	3,02
51	96,42	0,10	0,00	1,74	0,07	0,55	0,23	0,00	0,00	0,00	0,01	99,11	0,97	0,00	0,00	0,04	0,00	0,01	0,00	0,00	0,00	0,00	0,00	1,02
52	96,68	0,07	0,00	1,71	0,07	0,59	0,08	0,00	0,00	0,00	0,00	99,22	0,97	0,00	0,00	0,04	0,00	0,01	0,00	0,00	0,00	0,00	0,00	1,02
53	97,24	0,06	0,00	1,56	0,04	0,59	0,06	0,00	0,00	0,00	0,00	99,55	0,97	0,00	0,00	0,03	0,00	0,01	0,00	0,00	0,00	0,00	0,00	1,02
54	97,26	0,07	0,00	1,56	0,00	0,50	0,08	0,00	0,00	0,00	0,00	99,49	0,97	0,00	0,00	0,03	0,00	0,01	0,00	0,00	0,00	0,00	0,00	1,02
55	98,87	0,06	0,00	1,34	0,03	0,47	0,17	0,00	0,00	0,00	0,01	100,95	0,97	0,00	0,00	0,03	0,00	0,01	0,00	0,00	0,00	0,00	0,00	1,01
56	98,80	0,09	0,00	1,36	0,07	0,46	0,14	0,00	0,00	0,00	0,03	100,94	0,97	0,00	0,00	0,03	0,00	0,01	0,00	0,00	0,00	0,00	0,00	1,02
57	97,63	0,07	0,00	1,55	0,04	0,51	0,15	0,00	0,00	0,00	0,05	100,00	0,97	0,00	0,00	0,03	0,00	0,01	0,00	0,00	0,00	0,00	0,00	1,02
Sample 5-3																								
58	97,17	0,11	0,00	2,42	0,10	0,93	0,07	0,00	0,00	0,00	0,08	100,89	2,87	0,01	0,00	0,15	0,01	0,03	0,00	0,00	0,00	0,00	0,00	3,08
59	65,19	0,03	30,67	3,63	0,69	0,65	0,03	0,00	0,00	0,00	0,00	100,89	2,02	0,00	0,65	0,24	0,05	0,02	0,00	0,00	0,00	0,00	0,00	2,97
60	99,87	0,08	0,00	0,99	0,02	0,28	0,20	0,00	0,00	0,00	0,00	101,44	2,94	0,01	0,00	0,06	0,00	0,01	0,01	0,00	0,00	0,00	0,00	3,03
61	98,70	0,07	0,00	1,29	0,07	0,39	0,05	0,00	0,00	0,00	0,00	100,57	2,93	0,01	0,00	0,08	0,00	0,01	0,00	0,00	0,00	0,00	0,00	3,04
62	86,01	0,07	13,30	0,52	0,00	0,01	0,00	0,00	0,00	0,00	0,00	99,91	2,63	0,01	0,28	0,03	0,00	0,00	0,00	0,00	0,00	0,00	0,00	2,95
63	96,68	0,09	0,00	1,70	0,10	0,25	0,02	0,00	0,00	0,00	0,02	98,86	2,93	0,01	0,00	0,11	0,01	0,01	0,00	0,00	0,00	0,00	0,00	3,06
64	101,19	0,09	0,00	0,89	0,06	0,21	0,07	0,00	0,00	0,00	0,00	102,50	2,95	0,01	0,00	0,05	0,00	0,01	0,00	0,00	0,00	0,00	0,00	3,03
65	102,05	0,10	0,00	0,60	0,06	0,13	0,03	0,00	0,00	0,00	0,01	102,98	2,97	0,01	0,00	0,04	0,00	0,00	0,00	0,00	0,00	0,00	0,00	3,02
66	97,63	0,09	0,00	0,98	0,04	0,35	0,03	0,00	0,00	0,00	0,00	99,11	2,95	0,01	0,00	0,06	0,00	0,01	0,00	0,00	0,00	0,00	0,00	3,03
67	100,53	0,07	0,00	0,93	0,05	0,61	0,03	0,00	0,00	0,00	0,00	102,23	2,94	0,01	0,00	0,06	0,00	0,02	0,00	0,00	0,00	0,00	0,00	3,03
68	96,59	0,09	0,00	1,26	0,03	0,54	0,03	0,00	0,00	0,00	0,03	98,57	2,93	0,01	0,00	0,08	0,00	0,02	0,00	0,00	0,00	0,00	0,00	3,04

Point	SnO2	MgO	Ta2O5	FeO	MnO	Nb2O5	TiO2	Sc2O3	U2O	CaO	WO3	Total	Sn a.p.f.u	Mg	Ta	Fe	Mn	Nb	Ti	Sc	U	Ca	W	Total
69	96,86	0,07	0,00	1,14	0,03	0,46	0,09	0,00	0,00	0,00	0,09	98,74	2,93	0,01	0,00	0,07	0,00	0,02	0,01	0,00	0,00	0,00	0,00	3,04
70	97,74	0,09	0,00	1,07	0,03	0,29	0,04	0,00	0,00	0,00	0,00	99,26	2,95	0,01	0,00	0,07	0,00	0,01	0,00	0,00	0,00	0,00	0,00	3,04
71	98,21	0,07	0,00	1,05	0,04	0,28	0,01	0,00	0,00	0,00	0,00	99,66	2,95	0,01	0,00	0,07	0,00	0,01	0,00	0,00	0,00	0,00	0,00	3,04
72	100,10	0,08	0,00	0,75	0,01	0,18	0,09	0,00	0,00	0,00	0,00	101,21	2,96	0,01	0,00	0,05	0,00	0,01	0,01	0,00	0,00	0,00	0,00	3,03
sample 5.1-1																								
73	99,87	0,08	0,00	0,95	0,03	0,23	0,01	0,00	0,00	0,00	0,00	101,17	0,98	0,00	0,00	0,02	0,00	0,00	0,00	0,00	0,00	0,00	0,00	1,01
74	101,75	0,08	0,00	0,67	0,02	0,08	0,00	0,00	0,00	0,00	0,16	102,76	0,99	0,00	0,00	0,01	0,00	0,00	0,00	0,00	0,00	0,00	0,00	1,01
75	101,74	0,07	0,00	0,78	0,03	0,14	0,00	0,00	0,00	0,00	0,00	102,76	0,99	0,00	0,00	0,02	0,00	0,00	0,00	0,00	0,00	0,00	0,00	1,01
Sample G-4																								
76	99,53	0,08	0,00	0,76	0,02	1,97	0,20	0,00	0,00	0,00	0,00	102,61	2,88	0,01	0,00	0,05	0,00	0,06	0,01	0,00	0,00	0,00	0,00	3,01
77	100,34	0,07	0,00	0,41	0,07	1,36	0,05	0,00	0,00	0,00	0,00	102,39	2,92	0,01	0,00	0,02	0,00	0,04	0,00	0,00	0,00	0,00	0,00	3,00
78	95,18	0,08	0,00	1,93	0,06	2,68	0,44	0,00	0,00	0,00	0,00	100,39	2,80	0,01	0,00	0,12	0,00	0,09	0,02	0,00	0,00	0,00	0,00	3,04
79	95,26	0,08	0,00	1,83	0,04	2,40	0,30	0,00	0,00	0,00	0,00	99,90	2,82	0,01	0,00	0,11	0,00	0,08	0,02	0,00	0,00	0,00	0,00	3,04
Sample 6-1																								
80	98,50	0,09	0,00	1,18	0,00	2,06	0,35	0,00	0,00	0,00	0,00	102,38	0,95	0,00	0,00	0,02	0,00	0,02	0,01	0,00	0,00	0,00	0,00	1,00
81	99,15	0,00	0,11	0,11	0,00	0,23	0,06	0,00	0,00	0,00	0,00	99,67	2,98	0,00	0,00	0,01	0,00	0,01	0,00	0,00	0,00	0,00	0,00	3,00
82	98,55	0,00	0,21	0,19	0,00	0,74	0,07	0,00	0,00	0,00	0,00	99,77	2,95	0,00	0,00	0,01	0,00	0,03	0,00	0,00	0,00	0,00	0,00	3,00
83	98,70	0,00	0,13	0,22	0,00	0,96	0,08	0,00	0,00	0,00	0,00	100,09	2,94	0,00	0,00	0,01	0,00	0,03	0,00	0,00	0,00	0,00	0,00	3,00
84	97,68	0,00	0,49	0,36	0,00	1,26	0,09	0,00	0,00	0,00	0,00	99,88	2,92	0,00	0,01	0,02	0,00	0,04	0,01	0,00	0,00	0,00	0,00	3,00
85	96,09	0,00	1,64	0,60	0,00	1,55	0,21	0,00	0,00	0,00	0,00	100,09	2,86	0,00	0,03	0,04	0,00	0,05	0,01	0,00	0,00	0,00	0,00	3,00
86	99,00	0,00	0,11	0,15	0,00	0,51	0,00	0,00	0,00	0,00	0,00	99,77	2,97	0,00	0,00	0,01	0,00	0,02	0,00	0,00	0,00	0,00	0,00	3,00
87	99,56	0,00	0,00	0,15	0,00	0,32	0,00	0,00	0,00	0,00	0,00	100,03	2,98	0,00	0,00	0,01	0,00	0,01	0,00	0,00	0,00	0,00	0,00	3,00
88	99,29	0,00	0,00	0,15	0,00	0,52	0,00	0,00	0,00	0,00	0,00	99,96	2,97	0,00	0,00	0,01	0,00	0,02	0,00	0,00	0,00	0,00	0,00	3,00
89	94,24	0,00	3,07	0,88	0,00	1,76	0,07	0,00	0,00	0,00	0,00	100,02	2,82	0,00	0,06	0,05	0,00	0,06	0,00	0,00	0,00	0,00	0,00	3,00
90	99,52	0,00	0,11	0,12	0,00	0,31	0,00	0,00	0,00	0,00	0,00	100,06	2,98	0,00	0,00	0,01	0,00	0,01	0,00	0,00	0,00	0,00	0,00	3,00
91	99,76	0,00	0,00	0,11	0,00	0,26	0,00	0,00	0,00	0,00	0,00	100,13	2,99	0,00	0,00	0,01	0,00	0,01	0,00	0,00	0,00	0,00	0,00	3,00
92	99,53	0,00	0,00	0,14	0,00	0,34	0,07	0,00	0,00	0,00	0,00	100,08	2,98	0,00	0,00	0,01	0,00	0,01	0,00	0,00	0,00	0,00	0,00	3,00
93	95,86	0,00	0,90	0,61	0,00	2,12	0,25	0,00	0,00	0,00	0,00	99,74	2,85	0,00	0,02	0,04	0,00	0,07	0,01	0,00	0,00	0,00	0,00	3,00
94	94,90	0,00	1,67	0,77	0,00	2,30	0,29	0,00	0,00	0,00	0,00	100,23	2,80	0,00	0,03	0,05	0,00	0,08	0,02	0,00	0,00	0,00	0,00	3,00
95	95,81	0,00	1,30	0,71	0,00	2,28	0,25	0,00	0,00	0,00	0,00	100,35	2,84	0,00	0,03	0,04	0,00	0,08	0,01	0,00	0,00	0,00	0,00	3,00
96	98,66	0,00	1,05	0,21	0,00	0,22	0,12	0,00	0,00	0,00	0,00	100,24	2,95	0,00	0,02	0,01	0,00	0,01	0,01	0,00	0,00	0,00	0,00	3,00
97	99,28	0,00	0,94	0,16	0,00	0,21	0,15	0,00	0,00	0,00	0,00	100,74	2,95	0,00	0,02	0,01	0,00	0,01	0,01	0,00	0,00	0,00	0,00	3,00
98	99,04	0,00	0,37	0,20	0,00	0,77	0,00	0,00	0,00	0,00	0,00	100,38	2,95	0,00	0,01	0,01	0,00	0,03	0,00	0,00	0,00	0,00	0,00	3,00
99	99,00	0,00	0,21	0,17	0,00	0,69	0,00	0,00	0,00	0,00	0,00	100,06	2,96	0,00	0,00	0,01	0,00	0,02	0,00	0,00	0,00	0,00	0,00	3,00
100	98,29	0,00	0,40	0,27	0,00	0,97	0,00	0,00	0,00	0,00	0,00	99,93	2,94	0,00	0,01	0,02	0,00	0,03	0,00	0,00	0,00	0,00	0,00	3,00
101	94,16	0,00	2,89	0,95	0,00	2,03	0,16	0,00	0,00	0,00	0,00	100,19	2,80	0,00	0,06	0,06	0,00	0,07	0,01	0,00	0,00	0,00	0,00	3,00
102	94,26	0,00	3,00	0,88	0,00	1,85	0,20	0,00	0,00	0,00	0,00	100,19	2,81	0,00	0,06	0,06	0,00	0,06	0,01	0,00	0,00	0,00	0,00	3,00
103	94,40	0,00	2,65	0,89	0,00	2,10	0,18	0,00	0,00	0,00	0,00	100,22	2,81	0,00	0,05	0,06	0,00	0,07	0,01	0,00	0,00	0,00	0,00	3,00
104	94,26	0,00	2,87	0,91	0,00	2,06	0,21	0,00	0,00	0,00	0,00	100,31	2,80	0,00	0,06	0,06	0,00	0,07	0,01	0,00	0,00	0,00	0,00	3,00

3. Tourmaline mineral chemistry data

The procedures and methods of tourmaline and apatite data acquisition by microprobe are given in Chapter 6. The following are the detection limits of the microprobe given in ppm for this analysis.

Ca: 79

K: 95

Na: 99

Si: 139

Mg: 90

Fe: 199

Mn: 145

F: 133

Al: 115

Ti: 113

Point	SiO2	TiO2	Al2O3	FeO	MgO	CaO	MnO	Na2O	K2O	F	H2O*	B2O3*	Li2O*	Total	O=F	Total*	Mineral
sample D-3																	
1	35,11	0,16	33,49	12,94	0,59	0,02	0,29	1,70	0,05	0,28	3,39	10,22	0,39	98,63	0,12	98,51	Schorl
2	35,54	0,18	32,97	12,78	0,83	0,01	0,15	1,61	0,02	0,31	3,38	10,23	0,48	98,49	0,13	98,37	Schorl
3	35,23	0,19	33,12	12,64	0,85	0,03	0,18	1,75	0,07	0,32	3,37	10,21	0,43	98,38	0,14	98,24	Schorl
4	35,93	0,06	33,66	13,03	0,49	0,00	0,15	1,29	0,06	0,18	3,48	10,32	0,49	99,13	0,07	99,06	Foitite
5	36,03	0,11	33,69	12,45	0,46	0,01	0,12	1,25	0,04	0,14	3,49	10,32	0,61	98,70	0,06	98,64	Foitite
6	35,87	0,20	32,99	12,48	0,84	0,04	0,10	1,50	0,06	0,26	3,42	10,28	0,60	98,63	0,11	98,53	Schorl
7	35,43	0,15	33,40	12,68	0,78	0,04	0,11	1,74	0,09	0,26	3,42	10,26	0,45	98,80	0,11	98,70	Schorl
8	35,15	0,24	33,56	12,30	0,80	0,00	0,19	1,70	0,03	0,35	3,36	10,23	0,44	98,35	0,15	98,21	Schorl
9	35,12	0,28	33,63	12,45	0,80	0,03	0,14	1,70	0,06	0,21	3,43	10,24	0,43	98,52	0,09	98,43	Schorl
10	35,58	0,19	32,72	12,96	0,85	0,00	0,19	1,67	0,05	0,16	3,46	10,23	0,50	98,56	0,07	98,49	Schorl
11	35,03	0,19	33,59	12,74	0,80	0,02	0,15	1,74	0,03	0,42	3,33	10,23	0,39	98,65	0,18	98,47	Schorl
12	35,73	0,11	33,82	11,94	0,61	0,00	0,21	1,43	0,05	0,17	3,47	10,29	0,56	98,37	0,07	98,30	Foitite
13	35,46	0,18	33,66	12,63	0,87	0,03	0,11	1,69	0,06	0,35	3,39	10,30	0,42	99,14	0,15	98,99	Schorl
14	35,63	0,17	32,73	12,47	0,85	0,01	0,23	1,75	0,03	0,27	3,40	10,23	0,59	98,36	0,12	98,25	Schorl
15	35,34	0,19	33,95	12,26	0,85	0,04	0,12	1,64	0,03	0,05	3,53	10,29	0,43	98,71	0,02	98,69	Schorl
16	35,21	0,23	33,66	12,23	0,83	0,03	0,15	1,72	0,05	0,42	3,34	10,25	0,46	98,57	0,18	98,39	Schorl
17	35,54	0,22	33,88	12,38	0,88	0,03	0,15	1,65	0,05	0,38	3,38	10,33	0,43	99,32	0,16	99,16	Schorl
18	35,31	0,26	33,46	12,88	0,79	0,04	0,20	1,69	0,04	0,42	3,35	10,27	0,40	99,09	0,18	98,91	Schorl
19	35,07	0,23	33,33	12,32	0,87	0,02	0,15	1,63	0,05	0,32	3,36	10,19	0,42	97,95	0,13	97,82	Schorl
20	35,37	0,21	33,51	12,58	0,85	0,03	0,13	1,76	0,07	0,41	3,35	10,28	0,44	98,98	0,17	98,80	Schorl
Sample O-2																	
21	35,10	0,69	31,72	13,18	2,22	0,11	0,08	1,94	0,05	0,32	3,38	10,23	0,22	99,24	0,14	99,11	Schorl
22	34,91	0,88	31,58	13,33	1,79	0,17	0,11	1,91	0,11	0,36	3,35	10,19	0,30	98,98	0,15	98,83	Schorl
23	34,70	0,89	31,57	13,22	2,17	0,12	0,13	2,07	0,07	0,52	3,27	10,19	0,23	99,15	0,22	98,93	Schorl
24	34,40	0,79	31,91	12,78	2,16	0,12	0,10	2,00	0,04	0,33	3,34	10,14	0,23	98,34	0,14	98,20	Schorl
25	35,25	0,79	31,98	12,56	1,85	0,14	0,10	1,89	0,04	0,22	3,43	10,24	0,37	98,87	0,09	98,77	Schorl
26	34,88	0,80	31,60	12,86	2,39	0,10	0,09	1,94	0,06	0,38	3,34	10,19	0,21	98,85	0,16	98,69	Schorl
27	35,16	0,80	32,00	12,93	1,75	0,08	0,19	1,85	0,07	0,64	3,23	10,23	0,31	99,24	0,27	98,97	Schorl
28	34,64	0,79	31,81	12,51	2,02	0,12	0,14	1,93	0,05	0,41	3,30	10,14	0,30	98,15	0,17	97,98	Schorl
29	35,30	0,81	31,64	13,09	2,52	0,15	0,12	2,21	0,05	0,63	3,26	10,31	0,25	100,33	0,27	100,06	Schorl
30	36,21	0,96	32,01	12,04	2,61	0,15	0,10	2,01	0,05	0,51	3,37	10,46	0,42	100,90	0,21	100,69	Schorl
31	34,65	0,82	32,28	12,95	1,73	0,11	0,11	1,92	0,07	0,40	3,33	10,20	0,29	98,87	0,17	98,70	Schorl
32	35,01	0,79	32,23	12,86	1,67	0,12	0,13	1,81	0,09	0,51	3,29	10,22	0,32	99,05	0,21	98,84	Schorl
33	35,21	0,77	31,70	12,84	2,40	0,12	0,07	2,07	0,06	0,48	3,31	10,26	0,26	99,55	0,20	99,35	Schorl
34	34,79	0,68	31,85	13,21	2,04	0,12	0,09	1,93	0,05	0,39	3,33	10,18	0,22	98,88	0,16	98,72	Schorl
35	35,63	0,77	31,81	13,50	1,93	0,12	0,12	2,09	0,09	0,32	3,42	10,34	0,32	100,46	0,13	100,33	Schorl
36	34,91	0,77	31,33	13,10	1,92	0,11	0,18	1,98	0,08	0,58	3,23	10,15	0,29	98,62	0,24	98,37	Schorl
37	34,96	0,77	31,48	13,02	2,39	0,11	0,12	2,10	0,08	0,43	3,32	10,21	0,24	99,21	0,18	99,03	Schorl
38	34,89	0,79	31,51	13,10	2,12	0,13	0,11	1,90	0,08	0,60	3,23	10,17	0,24	98,87	0,25	98,62	Schorl

Point	SiO2	TiO2	Al2O3	FeO	MgO	CaO	MnO	Na2O	K2O	F	H2O*	B2O3*	Li2O*	Total	O=F	Total*	Mineral
39	35,30	0,83	31,32	13,27	1,96	0,12	0,15	1,79	0,09	0,40	3,33	10,21	0,29	99,06	0,17	98,89	Schorl
40	34,95	0,82	31,41	12,33	2,63	0,14	0,03	1,95	0,10	0,59	3,23	10,18	0,26	98,64	0,25	98,39	Schorl
41	35,03	0,70	31,64	12,93	2,14	0,09	0,17	1,93	0,06	0,44	3,31	10,19	0,24	98,88	0,18	98,70	Schorl
42	34,64	0,75	31,80	12,77	2,20	0,11	0,16	2,08	0,07	0,29	3,37	10,17	0,26	98,66	0,12	98,54	Schorl
Sample 3.2-1																	
43	35,85	0,38	31,77	10,22	3,50	0,09	0,09	1,84	0,06	0,27	3,42	10,29	0,43	98,20	0,11	98,09	Schorl
44	36,29	0,51	31,52	10,33	3,47	0,07	0,19	1,88	0,01	0,27	3,45	10,36	0,53	98,87	0,11	98,76	Schorl
45	35,56	0,50	31,74	10,37	3,26	0,08	0,12	1,83	0,03	0,10	3,48	10,24	0,39	97,71	0,04	97,66	Schorl
46	35,65	0,50	31,54	10,52	3,22	0,09	0,14	1,91	0,06	0,31	3,39	10,24	0,45	98,01	0,13	97,87	Schorl
47	35,65	0,47	31,80	10,78	3,29	0,03	0,14	1,93	0,04	0,43	3,34	10,28	0,33	98,52	0,18	98,33	Schorl
48	36,26	0,65	31,75	5,31	6,88	0,53	0,04	1,80	0,02	0,18	3,52	10,46	0,38	97,80	0,08	97,72	Dravite
49	35,78	0,69	30,77	8,94	4,97	0,14	0,11	2,03	0,07	0,40	3,36	10,28	0,36	97,89	0,17	97,72	Schorl
50	36,11	0,46	31,11	8,19	5,07	0,09	0,10	2,01	0,07	0,18	3,47	10,32	0,48	97,66	0,08	97,59	Dravite
51	36,11	0,58	31,24	8,20	5,29	0,12	0,07	2,06	0,04	0,26	3,45	10,36	0,40	98,19	0,11	98,08	Dravite
52	35,88	0,66	30,94	8,52	4,80	0,13	0,13	2,09	0,08	0,31	3,40	10,29	0,48	97,70	0,13	97,57	Dravite
53	35,93	0,66	30,93	8,89	4,94	0,12	0,07	2,03	0,08	0,23	3,45	10,31	0,39	98,03	0,09	97,94	Schorl
54	36,02	0,58	31,02	8,26	5,35	0,12	0,08	2,04	0,08	0,27	3,43	10,33	0,39	97,97	0,11	97,86	Dravite
55	36,06	0,37	31,46	8,89	4,52	0,09	0,10	2,00	0,04	0,51	3,32	10,32	0,46	98,14	0,22	97,92	Schorl
56	35,92	0,51	32,03	8,68	4,18	0,09	0,14	1,87	0,04	0,21	3,47	10,33	0,44	97,91	0,09	97,83	Schorl
57	35,78	0,55	31,26	8,57	4,90	0,13	0,07	1,97	0,04	0,25	3,43	10,29	0,37	97,61	0,11	97,50	Dravite
58	36,11	0,54	31,43	8,67	5,23	0,10	0,13	2,04	0,04	0,40	3,39	10,39	0,30	98,77	0,17	98,60	Dravite
59	36,43	0,57	31,44	8,36	5,29	0,11	0,10	2,12	0,05	0,48	3,38	10,45	0,42	99,19	0,20	98,99	Dravite
60	36,23	0,46	30,87	8,25	5,30	0,12	0,12	2,04	0,01	0,18	3,48	10,34	0,47	97,87	0,07	97,79	Dravite
sample PET-2																	
61	36,63	0,48	30,72	8,24	5,23	0,15	0,11	1,95	0,03	0,19	3,49	10,38	0,60	98,19	0,08	98,11	Dravite
62	35,83	0,49	31,25	8,18	5,33	0,12	0,09	2,04	0,06	0,42	3,36	10,31	0,33	97,79	0,18	97,61	Dravite
63	35,95	0,48	31,49	10,38	3,56	0,06	0,17	1,96	0,08	0,15	3,49	10,31	0,45	98,49	0,06	98,43	Schorl
64	35,99	0,53	31,48	9,69	4,27	0,11	0,17	1,90	0,07	0,39	3,38	10,34	0,35	98,66	0,16	98,49	Schorl
65	36,29	0,49	31,60	9,56	4,29	0,09	0,07	1,99	0,05	0,30	3,44	10,40	0,44	99,01	0,13	98,88	Schorl
66	36,15	0,51	31,55	9,43	4,40	0,09	0,06	2,00	0,05	0,20	3,48	10,37	0,41	98,71	0,09	98,62	Schorl
67	35,94	0,43	31,55	9,84	4,18	0,08	0,12	1,98	0,07	0,29	3,43	10,33	0,36	98,58	0,12	98,45	Schorl
68	35,72	0,55	31,89	9,01	4,52	0,13	0,05	1,91	0,04	0,20	3,47	10,33	0,28	98,10	0,08	98,02	Schorl
69	35,80	0,63	32,22	9,22	4,22	0,09	0,10	2,06	0,06	0,21	3,48	10,38	0,32	98,77	0,09	98,68	Schorl
70	35,70	0,54	31,92	9,90	3,91	0,09	0,10	2,14	0,07	0,27	3,44	10,34	0,32	98,74	0,11	98,62	Schorl
71	35,41	0,39	32,16	10,08	3,81	0,08	0,10	1,84	0,07	0,34	3,38	10,27	0,21	98,13	0,14	97,99	Schorl
72	35,48	0,37	31,74	10,24	3,55	0,11	0,14	1,91	0,08	0,16	3,46	10,24	0,34	97,82	0,07	97,75	Schorl
73	35,76	0,40	32,12	10,24	3,69	0,12	0,09	1,96	0,08	0,18	3,48	10,34	0,31	98,78	0,08	98,70	Schorl
74	36,10	0,61	32,02	8,69	4,71	0,14	0,07	1,97	0,06	0,20	3,50	10,42	0,35	98,82	0,08	98,74	Schorl
75	36,17	0,60	31,68	8,60	4,87	0,18	0,10	1,90	0,06	0,21	3,49	10,40	0,38	98,63	0,09	98,54	Dravite

Point	SiO2	TiO2	Al2O3	FeO	MgO	CaO	MnO	Na2O	K2O	F	H2O*	B2O3*	Li2O*	Total	O=F	Total*	Mineral
76	35,53	0,44	32,06	10,39	3,48	0,04	0,13	1,86	0,05	0,16	3,47	10,27	0,27	98,15	0,07	98,08	Schorl
77	35,42	0,33	32,01	10,15	3,55	0,10	0,06	1,98	0,02	0,27	3,41	10,24	0,31	97,85	0,11	97,73	Schorl
78	35,87	0,61	32,38	8,76	4,75	0,10	0,06	2,07	0,06	0,28	3,47	10,43	0,27	99,10	0,12	98,98	Schorl
79	36,18	0,59	32,55	8,57	4,60	0,13	0,10	1,80	0,07	0,16	3,53	10,46	0,31	99,04	0,07	98,97	Schorl
80	35,90	0,66	31,56	7,91	4,96	0,18	0,09	1,96	0,04	0,21	3,46	10,33	0,43	97,68	0,09	97,59	Dravite
81	35,73	0,53	31,95	10,03	3,65	0,07	0,10	1,93	0,06	0,17	3,48	10,31	0,36	98,35	0,07	98,27	Schorl
82	35,62	0,45	31,77	10,14	3,97	0,07	0,10	2,00	0,04	0,17	3,47	10,30	0,26	98,36	0,07	98,29	Schorl
83	35,92	0,56	32,35	9,33	4,26	0,09	0,06	1,90	0,08	0,34	3,43	10,40	0,28	98,98	0,14	98,84	Schorl
84	36,16	0,51	31,61	10,08	4,10	0,08	0,12	1,99	0,06	0,21	3,48	10,39	0,38	99,16	0,09	99,07	Schorl
sample 6-2																	
85	35,54	0,81	32,66	9,48	3,85	0,38	0,08	1,78	0,07	0,12	3,54	10,41	0,35	99,07	0,05	99,02	Schorl
86	35,34	0,69	32,19	11,06	2,74	0,10	0,15	1,62	0,06	0,18	3,45	10,24	0,28	98,11	0,08	98,03	Schorl
87	35,03	0,74	32,20	11,17	2,70	0,11	0,07	1,62	0,04	0,11	3,47	10,20	0,26	97,71	0,04	97,67	Schorl
88	35,16	0,72	32,30	11,31	2,67	0,09	0,17	1,75	0,05	0,05	3,51	10,25	0,27	98,32	0,02	98,30	Schorl
89	35,22	0,67	32,20	10,81	2,73	0,07	0,12	1,63	0,07	0,27	3,39	10,21	0,30	97,68	0,11	97,57	Schorl
90	35,41	0,83	32,32	10,91	3,35	0,13	0,11	1,86	0,09	0,16	3,50	10,35	0,25	99,27	0,07	99,21	Schorl
91	35,39	0,62	32,21	10,40	2,97	0,06	0,06	1,67	0,07	0,45	3,32	10,23	0,35	97,76	0,19	97,57	Schorl
92	34,93	0,59	32,27	10,79	2,99	0,09	0,10	1,74	0,06	0,02	3,51	10,19	0,25	97,53	0,01	97,52	Schorl
93	35,22	0,82	31,72	8,89	4,34	0,52	0,03	1,72	0,08	0,41	3,35	10,26	0,35	97,71	0,17	97,53	Schorl
94	34,72	0,94	32,51	9,05	4,12	0,45	0,01	1,73	0,05	0,36	3,37	10,28	0,31	97,89	0,15	97,74	Schorl
95	34,04	0,81	32,59	12,42	1,87	0,28	0,18	1,68	0,04	0,19	3,40	10,12	0,24	97,86	0,08	97,78	Schorl
96	35,09	0,61	32,42	11,16	2,86	0,10	0,13	1,77	0,06	0,02	3,53	10,25	0,25	98,24	0,01	98,23	Schorl
97	34,10	0,76	32,52	12,28	1,89	0,28	0,14	1,64	0,08	0,42	3,29	10,11	0,26	97,74	0,18	97,56	Schorl
98	34,34	1,07	32,17	10,53	3,20	0,39	0,06	1,74	0,07	0,25	3,40	10,18	0,29	97,70	0,10	97,60	Schorl
99	35,05	0,54	32,34	11,09	3,00	0,12	0,12	1,64	0,04	0,13	3,46	10,22	0,20	97,95	0,06	97,89	Schorl
100	35,24	0,64	31,60	11,98	2,63	0,07	0,13	1,74	0,06	0,33	3,36	10,19	0,25	98,20	0,14	98,06	Schorl
101	35,28	0,68	32,34	11,09	2,79	0,09	0,12	1,78	0,08	0,10	3,50	10,27	0,30	98,39	0,04	98,35	Schorl
102	35,44	0,87	32,48	9,66	3,85	0,36	0,03	1,77	0,07	0,23	3,47	10,37	0,33	98,92	0,10	98,82	Schorl
103	34,87	0,88	32,00	10,11	3,51	0,35	0,02	1,70	0,10	0,29	3,39	10,22	0,31	97,74	0,12	97,62	Schorl
104	34,97	0,86	32,35	9,71	3,82	0,29	0,08	1,86	0,05	0,20	3,46	10,29	0,29	98,24	0,08	98,15	Schorl
105	34,77	0,96	31,96	10,22	3,47	0,38	0,07	1,71	0,06	0,22	3,42	10,21	0,30	97,76	0,09	97,66	Schorl
Sample Na-2																	
106	35,06	0,02	33,96	12,61	0,25	0,01	0,20	1,38	0,04	0,47	3,29	10,18	0,41	97,88	0,20	97,68	Foitite
107	35,08	0,06	35,11	10,43	0,26	0,06	0,22	1,77	0,07	0,69	3,22	10,28	0,72	97,97	0,29	97,67	Schorl
108	34,97	0,08	34,67	11,03	0,31	0,04	0,13	1,82	0,05	0,49	3,30	10,24	0,67	97,78	0,21	97,57	Schorl
109	35,11	0,05	34,21	12,12	0,17	0,01	0,06	1,72	0,04	0,53	3,27	10,22	0,57	98,08	0,22	97,86	Schorl
sample eh-1																	
110	35,96	0,55	32,86	8,39	4,23	0,09	0,17	1,65	0,04	0,19	3,50	10,40	0,31	98,34	0,08	98,26	Schorl
111	35,89	0,57	32,60	8,61	4,19	0,07	0,08	1,75	0,05	0,16	3,51	10,38	0,34	98,19	0,07	98,13	Schorl
112	36,90	0,10	34,51	6,45	0,25	0,07	0,55	2,65	0,05	1,15	3,06	10,46	1,79	97,99	0,48	97,50	Elbaite

Point	SiO2	TiO2	Al2O3	FeO	MgO	CaO	MnO	Na2O	K2O	F	H2O*	B2O3*	Li2O*	Total	O=F	Total*	Mineral
113	35,38	0,64	32,50	8,55	4,18	0,13	0,05	1,86	0,07	0,12	3,50	10,31	0,33	97,63	0,05	97,58	Schorl
114	36,45	0,01	35,28	7,38	0,25	0,09	0,57	2,44	0,04	1,02	3,13	10,47	1,39	98,52	0,43	98,10	Elbaite
115	35,38	0,66	32,14	8,90	4,21	0,14	0,10	1,88	0,03	0,16	3,47	10,28	0,30	97,64	0,07	97,57	Schorl
116	36,90	0,00	35,46	4,94	0,19	0,23	1,36	2,40	0,06	1,20	3,06	10,51	1,76	98,09	0,51	97,58	Elbaite
sample5-2																	
117	36,61	0,39	32,09	9,15	4,40	0,08	0,12	1,60	0,04	0,33	3,45	10,45	0,43	99,13	0,14	98,99	Schorl
118	36,62	0,43	31,99	7,20	5,57	0,13	0,02	1,78	0,05	0,31	3,47	10,47	0,46	98,48	0,13	98,35	Dravite
119	36,47	0,29	32,22	8,50	4,55	0,08	0,06	1,64	0,03	0,30	3,45	10,42	0,45	98,46	0,13	98,34	Schorl
120	36,48	0,49	31,54	8,40	4,90	0,06	0,09	1,65	0,06	0,51	3,35	10,39	0,47	98,36	0,21	98,15	Dravite
121	36,49	0,71	31,62	7,88	5,15	0,14	0,02	1,75	0,06	0,34	3,44	10,43	0,48	98,53	0,14	98,38	Dravite
122	36,01	0,73	32,06	7,56	5,09	0,16	0,05	1,53	0,03	0,35	3,41	10,37	0,35	97,69	0,15	97,54	Dravite
123	36,48	0,63	31,86	7,33	5,26	0,07	0,00	1,69	0,05	0,27	3,47	10,42	0,50	98,03	0,11	97,91	Dravite
124	36,51	0,43	32,10	7,81	5,00	0,11	0,06	1,70	0,04	0,30	3,46	10,44	0,47	98,42	0,13	98,30	Dravite
125	36,36	0,53	32,17	8,29	4,96	0,10	0,06	1,74	0,04	0,36	3,44	10,45	0,35	98,82	0,15	98,67	Dravite
126	36,41	0,48	32,73	9,10	4,03	0,08	0,12	1,63	0,05	0,42	3,41	10,47	0,39	99,31	0,18	99,13	Schorl
127	36,57	0,62	31,95	7,43	5,36	0,11	0,00	1,74	0,04	0,19	3,52	10,47	0,47	98,46	0,08	98,38	Dravite
128	36,06	0,44	32,58	9,48	3,65	0,09	0,10	1,56	0,06	0,39	3,40	10,38	0,38	98,57	0,16	98,41	Schorl
129	36,35	0,33	31,97	7,94	5,39	0,08	0,13	1,79	0,01	0,50	3,36	10,43	0,32	98,60	0,21	98,39	Dravite
130	36,82	0,55	32,04	8,09	5,02	0,07	0,07	1,66	0,06	0,21	3,52	10,51	0,48	99,10	0,09	99,01	Dravite
131	36,56	0,30	32,40	7,90	4,63	0,08	0,07	1,35	0,03	0,17	3,51	10,41	0,48	97,90	0,07	97,83	Mg-Foitite
132	36,67	0,53	31,44	9,10	4,70	0,08	0,04	1,61	0,03	0,39	3,41	10,43	0,47	98,89	0,16	98,72	Schorl
133	37,25	0,15	31,50	7,99	4,99	0,08	0,07	1,66	0,58	0,41	3,43	10,51	0,75	99,36	0,17	99,19	Dravite
134	36,61	0,32	32,12	7,95	5,00	0,05	0,04	1,69	0,06	0,26	3,48	10,45	0,46	98,48	0,11	98,37	Dravite
samplex-1																	
135	36,13	0,54	31,90	10,49	3,59	0,05	0,17	1,87	0,06	0,45	3,37	10,38	0,37	99,36	0,19	99,17	Schorl
136	36,28	0,58	31,54	7,67	6,11	0,66	0,09	2,01	0,04	0,55	3,36	10,50	0,29	99,68	0,23	99,45	Dravite
137	36,25	0,39	31,78	7,85	5,78	0,56	0,14	1,85	0,04	0,57	3,34	10,47	0,29	99,31	0,24	99,07	Dravite
138	36,32	0,06	32,43	7,25	5,58	0,66	0,14	1,69	0,04	0,29	3,48	10,48	0,37	98,78	0,12	98,66	Dravite
139	36,23	0,55	31,57	10,45	3,89	0,04	0,20	1,87	0,04	0,52	3,34	10,39	0,36	99,44	0,22	99,22	Schorl
140	35,66	0,95	32,59	8,87	3,66	0,48	0,05	1,55	0,05	0,07	3,54	10,37	0,46	98,29	0,03	98,26	Schorl
141	36,18	0,42	31,32	11,04	4,01	0,07	0,18	2,12	0,02	0,52	3,34	10,39	0,30	99,90	0,22	99,68	Schorl
142	36,47	0,39	31,85	7,49	5,96	0,63	0,11	1,93	0,08	0,57	3,36	10,53	0,36	99,71	0,24	99,47	Dravite
143	36,50	0,07	32,59	8,27	4,91	0,57	0,12	1,62	0,04	0,28	3,49	10,50	0,40	99,34	0,12	99,22	Dravite
144	35,26	0,09	33,64	8,09	4,76	0,76	0,18	1,81	0,04	0,53	3,35	10,45	0,31	99,27	0,22	99,05	Dravite
145	35,94	0,47	31,78	7,85	5,67	0,53	0,14	1,96	0,07	0,68	3,27	10,43	0,28	99,06	0,29	98,78	Dravite
146	35,96	0,38	31,86	7,84	5,76	0,71	0,11	1,82	0,03	0,63	3,30	10,44	0,26	99,09	0,26	98,82	Dravite
147	36,19	0,41	31,14	9,96	4,18	0,09	0,19	1,98	0,05	0,56	3,30	10,34	0,45	98,83	0,24	98,59	Schorl
148	35,97	0,38	32,35	10,70	3,17	0,01	0,18	1,70	0,06	0,36	3,40	10,35	0,34	98,95	0,15	98,80	Schorl
149	36,58	0,10	32,69	7,81	5,09	0,66	0,15	1,73	0,05	0,36	3,47	10,54	0,44	99,66	0,15	99,51	Dravite
150	35,96	0,67	31,02	7,90	6,20	0,61	0,07	1,97	0,04	0,87	3,18	10,41	0,23	99,12	0,37	98,76	Dravite

Point	SiO2	TiO2	Al2O3	FeO	MgO	CaO	MnO	Na2O	K2O	F	H2O*	B2O3*	Li2O*	Total	O=F	Total*	Mineral
151	36,11	0,38	31,80	7,44	6,00	0,60	0,13	1,90	0,05	0,56	3,34	10,45	0,27	99,03	0,23	98,79	Dravite
152	36,68	0,18	32,32	5,88	6,68	0,76	0,11	1,73	0,06	0,38	3,47	10,57	0,39	99,20	0,16	99,04	Dravite
153	36,03	0,60	31,27	8,05	6,04	0,83	0,13	1,89	0,02	0,87	3,19	10,45	0,26	99,63	0,37	99,27	Dravite
154	36,50	0,38	31,50	7,79	5,78	0,42	0,10	1,99	0,06	0,56	3,35	10,48	0,41	99,31	0,23	99,07	Dravite
sample10-1																	
155	36,26	0,16	32,95	9,18	3,66	0,03	0,09	1,69	0,05	0,27	3,46	10,41	0,44	98,65	0,12	98,53	Schorl
156	36,49	0,21	32,52	9,63	3,84	0,04	0,13	1,99	0,05	0,41	3,42	10,47	0,46	99,66	0,17	99,49	Schorl
157	36,30	0,11	31,89	9,33	3,97	0,04	0,07	1,94	0,06	0,47	3,35	10,35	0,54	98,41	0,20	98,22	Schorl
158	36,27	0,24	31,99	9,44	4,27	0,08	0,10	2,00	0,06	0,51	3,35	10,40	0,41	99,11	0,22	98,89	Schorl
159	36,54	0,32	32,10	9,11	4,23	0,12	0,06	1,89	0,06	0,39	3,42	10,45	0,51	99,21	0,16	99,04	Schorl
160	36,03	0,34	32,00	8,93	4,42	0,12	0,13	1,97	0,09	0,26	3,46	10,37	0,39	98,49	0,11	98,39	Schorl
161	36,38	0,11	32,43	8,64	3,98	0,06	0,08	1,79	0,02	0,36	3,41	10,39	0,56	98,21	0,15	98,06	Schorl
162	36,12	0,30	31,40	9,07	4,75	0,11	0,08	2,10	0,03	0,54	3,32	10,35	0,41	98,56	0,23	98,33	Schorl
163	36,07	0,40	31,85	9,32	4,26	0,09	0,14	2,00	0,06	0,33	3,42	10,37	0,40	98,72	0,14	98,58	Schorl
164	36,35	0,53	31,48	9,24	4,73	0,09	0,08	2,15	0,04	0,38	3,42	10,43	0,42	99,33	0,16	99,17	Schorl
165	36,14	0,63	31,32	8,77	4,88	0,11	0,19	2,24	0,07	0,02	3,58	10,40	0,42	98,76	0,01	98,75	Schorl
166	36,16	0,20	32,42	9,29	4,19	0,04	0,15	1,98	0,05	0,50	3,36	10,41	0,35	99,09	0,21	98,88	Schorl
167	36,52	0,36	31,73	9,33	4,84	0,10	0,06	2,10	0,05	0,43	3,41	10,48	0,38	99,79	0,18	99,61	Schorl
168	36,16	0,60	31,51	9,34	4,69	0,11	0,10	1,95	0,04	0,41	3,39	10,39	0,34	99,03	0,17	98,86	Schorl
169	36,06	0,37	31,85	9,15	4,35	0,11	0,06	2,02	0,05	0,54	3,32	10,37	0,42	98,66	0,23	98,44	Schorl
170	36,56	0,10	32,38	9,21	4,11	0,05	0,08	1,86	0,05	0,46	3,39	10,45	0,49	99,19	0,19	99,00	Schorl
171	35,96	0,30	31,56	9,10	4,77	0,14	0,12	2,05	0,02	0,49	3,34	10,34	0,33	98,52	0,20	98,32	Schorl
172	36,01	0,48	31,14	8,89	4,86	0,11	0,09	2,01	0,05	0,36	3,39	10,32	0,40	98,11	0,15	97,96	Schorl
173	36,66	0,38	31,91	9,06	4,43	0,07	0,08	2,05	0,06	0,22	3,51	10,48	0,53	99,42	0,09	99,33	Schorl
174	36,09	0,42	31,06	9,03	4,79	0,11	0,11	2,09	0,07	0,55	3,30	10,33	0,44	98,38	0,23	98,15	Schorl
175	35,86	0,29	31,88	9,57	4,19	0,06	0,05	1,98	0,06	0,21	3,46	10,32	0,34	98,28	0,09	98,19	Schorl
176	37,02	0,51	32,48	8,06	3,54	0,07	0,11	2,00	0,06	0,48	3,40	10,51	0,92	99,14	0,20	98,94	Schorl
sampleT-3																	
177	35,70	0,23	32,03	15,06	0,75	0,05	0,13	1,46	0,06	0,14	3,47	10,24	0,32	99,64	0,06	99,58	Foitite
178	35,81	0,32	31,63	14,16	1,01	0,07	0,19	1,64	0,04	0,34	3,37	10,23	0,48	99,30	0,14	99,15	Schorl
179	35,35	0,29	31,64	14,40	0,94	0,06	0,20	1,72	0,07	0,32	3,35	10,16	0,37	98,87	0,14	98,74	Schorl
180	35,29	0,29	31,72	14,92	0,81	0,05	0,31	1,71	0,07	0,32	3,36	10,17	0,28	99,29	0,13	99,16	Schorl
181	35,47	0,22	31,76	14,14	0,56	0,02	0,24	1,52	0,03	0,16	3,42	10,13	0,50	98,14	0,07	98,07	Schorl
182	35,65	0,11	31,82	13,97	0,64	0,02	0,29	1,38	0,06	0,09	3,46	10,15	0,52	98,16	0,04	98,12	Foitite
183	35,06	0,22	32,25	14,04	1,29	0,06	0,15	1,75	0,05	0,33	3,36	10,18	0,20	98,93	0,14	98,79	Schorl
184	34,68	0,39	32,48	13,01	1,58	0,09	0,10	1,82	0,08	0,51	3,26	10,15	0,26	98,41	0,22	98,19	Schorl
185	35,50	0,32	31,96	13,98	0,99	0,05	0,15	1,68	0,06	0,30	3,38	10,20	0,40	98,96	0,13	98,84	Schorl
186	35,31	0,36	31,93	13,95	0,86	0,06	0,19	1,52	0,07	0,20	3,41	10,15	0,39	98,38	0,08	98,29	Schorl
187	35,23	0,37	31,42	14,64	0,70	0,08	0,22	1,63	0,05	0,15	3,42	10,11	0,39	98,41	0,06	98,34	Schorl
188	35,38	0,27	31,88	14,45	0,59	0,05	0,18	1,53	0,03	0,29	3,36	10,15	0,41	98,56	0,12	98,44	Schorl

Point	SiO2	TiO2	Al2O3	FeO	MgO	CaO	MnO	Na2O	K2O	F	H2O*	B2O3*	Li2O*	Total	O=F	Total*	Mineral
189	35,16	0,34	31,53	14,56	0,72	0,05	0,33	1,68	0,05	0,08	3,45	10,11	0,35	98,40	0,04	98,36	Schorl
190	35,52	0,32	31,65	14,36	1,08	0,06	0,18	1,69	0,06	0,39	3,33	10,19	0,37	99,20	0,17	99,03	Schorl
191	35,54	0,16	31,89	13,56	0,95	0,05	0,11	1,58	0,08	0,42	3,31	10,16	0,51	98,31	0,18	98,14	Schorl
192	35,35	0,32	31,41	14,89	0,78	0,05	0,15	1,51	0,06	0,30	3,35	10,13	0,35	98,66	0,13	98,53	Schorl
193	36,15	0,10	32,02	14,31	0,57	0,01	0,21	1,37	0,07	0,07	3,50	10,26	0,58	99,20	0,03	99,17	Foitite
194	35,61	0,15	32,09	14,12	0,67	0,04	0,16	1,39	0,04	0,28	3,38	10,17	0,45	98,55	0,12	98,43	Foitite
195	35,86	0,12	32,29	14,22	0,67	0,01	0,25	1,35	0,06	0,19	3,44	10,24	0,44	99,14	0,08	99,06	Foitite
196	35,29	0,38	31,81	13,55	1,03	0,09	0,20	1,62	0,10	0,15	3,43	10,15	0,43	98,22	0,06	98,15	Schorl
197	35,53	0,11	32,50	14,34	0,64	0,02	0,16	1,44	0,05	0,25	3,41	10,21	0,35	98,99	0,10	98,89	Foitite
198	36,03	0,09	32,42	14,19	0,78	0,00	0,21	1,34	0,06	0,13	3,49	10,28	0,44	99,46	0,05	99,40	Foitite
199	35,45	0,40	31,62	14,89	0,84	0,08	0,26	1,62	0,06	0,35	3,35	10,19	0,32	99,41	0,15	99,26	Schorl
200	35,72	0,10	32,32	13,99	1,06	0,01	0,12	1,37	0,05	0,21	3,43	10,23	0,36	98,96	0,09	98,87	Foitite
sample11-1																	
201	35,83	0,37	31,66	12,20	2,13	0,05	0,14	1,73	0,06	0,38	3,35	10,25	0,49	98,64	0,16	98,48	Schorl
202	35,62	0,40	31,88	12,43	2,07	0,07	0,16	1,87	0,05	0,14	3,47	10,25	0,40	98,81	0,06	98,75	Schorl
203	35,51	0,32	31,36	13,15	2,36	0,07	0,11	1,87	0,07	0,13	3,46	10,22	0,27	98,89	0,05	98,84	Schorl
204	35,63	0,42	31,87	12,29	1,89	0,05	0,15	1,78	0,06	0,14	3,46	10,23	0,46	98,42	0,06	98,36	Schorl
205	35,67	0,13	32,86	12,53	1,64	0,05	0,12	1,47	0,04	0,29	3,41	10,27	0,34	98,82	0,12	98,70	Foitite
206	35,42	0,15	32,76	12,45	1,69	0,02	0,15	1,57	0,04	0,06	3,50	10,23	0,29	98,32	0,03	98,29	Schorl
207	36,06	0,15	32,57	12,80	1,65	0,02	0,08	1,58	0,04	0,06	3,54	10,33	0,44	99,30	0,02	99,28	Schorl
208	35,91	0,29	31,10	12,69	2,18	0,05	0,12	1,80	0,03	0,19	3,43	10,22	0,52	98,52	0,08	98,44	Schorl
209	35,21	0,13	31,40	13,16	2,20	0,07	0,21	1,89	0,07	0,06	3,47	10,15	0,24	98,25	0,02	98,22	Schorl
210	35,60	0,35	31,97	12,12	1,91	0,03	0,18	1,61	0,05	0,18	3,44	10,21	0,44	98,07	0,08	98,00	Schorl
211	35,93	0,38	31,90	12,25	2,02	0,04	0,18	1,72	0,06	0,34	3,39	10,28	0,49	98,97	0,14	98,83	Schorl
212	35,92	0,38	31,87	12,45	2,05	0,05	0,15	1,74	0,05	0,04	3,53	10,29	0,45	98,98	0,02	98,96	Schorl
213	35,83	0,09	32,58	12,45	1,64	0,01	0,13	1,65	0,04	0,36	3,38	10,28	0,45	98,88	0,15	98,73	Schorl
214	35,77	0,21	31,94	12,12	1,88	0,03	0,13	1,53	0,05	0,00	3,52	10,21	0,50	97,90	0,00	97,90	Schorl
215	35,64	0,42	31,71	12,35	2,25	0,03	0,15	1,86	0,06	0,14	3,47	10,25	0,39	98,70	0,06	98,65	Schorl
216	35,59	0,39	31,79	12,73	2,08	0,01	0,16	1,62	0,07	0,27	3,40	10,23	0,32	98,67	0,11	98,56	Schorl
217	35,97	0,37	31,55	12,22	2,14	0,02	0,17	1,74	0,06	0,21	3,44	10,26	0,53	98,67	0,09	98,58	Schorl
sample1-1																	
218	37,63	0,01	36,24	2,82	0,05	0,34	1,81	2,42	0,05	1,10	3,16	10,66	2,12	98,42	0,46	97,96	Elbaite
219	37,75	0,03	36,83	2,64	0,04	0,14	1,55	2,30	0,06	1,26	3,10	10,70	2,09	98,48	0,53	97,95	Elbaite
220	37,21	0,04	35,43	4,78	0,18	0,16	1,29	2,63	0,04	1,27	3,05	10,57	1,89	98,54	0,53	98,01	Elbaite
221	37,21	0,02	36,74	2,98	0,09	0,21	1,63	2,46	0,04	1,12	3,14	10,64	1,93	98,20	0,47	97,73	Elbaite
sample1-2																	
222	35,61	0,30	32,04	13,12	1,52	0,06	0,13	1,87	0,06	0,53	3,28	10,24	0,43	99,18	0,22	98,96	Schorl
223	35,89	0,19	32,47	13,32	1,53	0,08	0,22	1,47	0,04	0,17	3,48	10,31	0,33	99,49	0,07	99,42	Foitite
224	35,85	0,20	32,42	13,46	1,59	0,08	0,14	1,52	0,02	0,24	3,44	10,30	0,31	99,58	0,10	99,48	Schorl
225	35,71	0,26	32,30	13,74	1,52	0,10	0,25	1,65	0,07	0,50	3,31	10,30	0,27	99,99	0,21	99,78	Schorl

Point	SiO2	TiO2	Al2O3	FeO	MgO	CaO	MnO	Na2O	K2O	F	H2O*	B2O3*	Li2O*	Total	O=F	Total*	Mineral
226	35,34	0,64	31,85	13,73	1,71	0,16	0,18	1,94	0,08	0,36	3,37	10,27	0,27	99,89	0,15	99,74	Schorl
227	35,29	0,69	31,75	13,64	1,73	0,16	0,22	1,82	0,06	0,38	3,36	10,24	0,25	99,60	0,16	99,44	Schorl
228	35,33	1,01	31,25	12,80	2,67	0,27	0,21	1,95	0,06	0,31	3,40	10,29	0,25	99,80	0,13	99,68	Schorl
229	35,77	0,19	32,82	13,25	1,50	0,08	0,13	1,61	0,06	0,17	3,48	10,33	0,30	99,69	0,07	99,62	Schorl
230	36,42	0,52	31,46	11,24	3,87	0,31	0,11	1,95	0,06	0,22	3,51	10,46	0,36	100,49	0,09	100,40	Schorl
231	36,26	0,22	32,74	13,35	1,54	0,07	0,18	1,49	0,05	0,23	3,48	10,40	0,38	100,38	0,10	100,29	Foitite
232	35,64	0,49	31,85	13,65	1,73	0,16	0,21	1,82	0,06	0,33	3,40	10,29	0,30	99,94	0,14	99,80	Schorl
233	35,13	0,94	31,04	14,51	1,75	0,17	0,19	2,11	0,09	0,34	3,37	10,23	0,24	100,11	0,14	99,96	Schorl
234	35,25	0,92	31,09	14,32	1,83	0,19	0,23	2,10	0,08	0,54	3,28	10,25	0,25	100,33	0,23	100,10	Schorl
235	35,36	1,05	31,66	13,40	2,46	0,26	0,13	1,96	0,07	0,54	3,32	10,35	0,22	100,77	0,23	100,55	Schorl
236	35,73	0,24	32,58	13,29	1,59	0,07	0,17	1,52	0,02	0,18	3,47	10,30	0,28	99,43	0,08	99,35	Schorl
237	36,31	0,63	31,66	11,32	3,75	0,28	0,14	1,86	0,06	0,33	3,45	10,46	0,30	100,54	0,14	100,40	Schorl
238	36,17	0,22	32,76	13,18	1,68	0,08	0,15	1,54	0,06	0,23	3,48	10,40	0,35	100,31	0,10	100,21	Schorl
239	36,06	0,24	32,33	13,67	1,52	0,08	0,20	1,55	0,05	0,15	3,50	10,34	0,35	100,04	0,06	99,97	Schorl
240	36,20	0,20	32,68	13,57	1,51	0,08	0,20	1,39	0,05	0,50	3,35	10,38	0,33	100,44	0,21	100,23	Foitite
241	35,91	0,20	32,54	13,26	1,52	0,07	0,17	1,60	0,06	0,30	3,42	10,32	0,36	99,73	0,13	99,60	Schorl
242	35,35	0,84	31,40	12,86	2,25	0,22	0,03	1,87	0,07	0,40	3,34	10,24	0,31	99,19	0,17	99,02	Schorl
243	35,98	0,19	32,67	13,51	1,53	0,05	0,23	1,51	0,03	0,47	3,35	10,35	0,29	100,15	0,20	99,96	Foitite
244	35,53	0,38	32,13	13,92	1,67	0,09	0,20	1,75	0,07	0,42	3,35	10,28	0,20	99,99	0,18	99,81	Schorl
245	35,80	0,16	32,81	13,09	1,47	0,06	0,16	1,53	0,02	0,36	3,38	10,31	0,33	99,47	0,15	99,32	Schorl
246	35,94	0,17	32,48	13,32	1,57	0,07	0,14	1,56	0,06	0,37	3,39	10,32	0,36	99,75	0,16	99,59	Schorl
247	35,77	0,68	31,77	12,03	3,07	0,26	0,13	1,92	0,04	0,32	3,43	10,37	0,25	100,03	0,13	99,90	Schorl
248	35,79	0,60	31,68	12,70	2,23	0,12	0,17	1,78	0,05	0,41	3,36	10,30	0,36	99,55	0,17	99,38	Schorl
249	35,74	0,70	31,44	13,37	2,30	0,12	0,15	1,87	0,07	0,25	3,44	10,31	0,27	100,02	0,11	99,91	Schorl
sample3-6																	
250	35,78	0,18	34,90	10,09	0,94	0,07	0,10	2,13	0,03	0,53	3,35	10,44	0,78	99,32	0,22	99,09	Schorl
251	35,74	0,18	34,59	9,76	1,01	0,06	0,15	2,02	0,06	0,59	3,30	10,38	0,78	98,62	0,25	98,37	Schorl
252	35,92	0,16	34,74	10,15	1,01	0,06	0,06	1,88	0,03	0,59	3,31	10,42	0,72	99,06	0,25	98,81	Schorl
253	35,93	0,14	34,67	9,57	1,06	0,05	0,14	1,96	0,04	0,46	3,37	10,40	0,80	98,57	0,19	98,38	Elbaite
254	35,67	0,15	34,46	9,94	1,02	0,03	0,12	2,14	0,06	0,65	3,27	10,36	0,78	98,64	0,27	98,36	Schorl
255	35,95	0,15	34,54	9,91	1,02	0,05	0,18	1,99	0,05	0,47	3,37	10,41	0,78	98,86	0,20	98,66	Schorl
256	35,50	0,18	34,68	10,22	1,00	0,08	0,12	2,03	0,03	0,65	3,27	10,37	0,72	98,85	0,27	98,58	Schorl
257	35,91	0,18	34,72	10,02	0,99	0,03	0,18	2,01	0,06	0,62	3,31	10,43	0,76	99,22	0,26	98,96	Schorl
258	35,58	0,11	34,59	9,62	0,92	0,09	0,16	2,08	0,05	0,50	3,33	10,34	0,82	98,18	0,21	97,97	Elbaite
259	35,45	0,20	34,65	10,05	0,95	0,04	0,13	2,04	0,03	0,55	3,31	10,35	0,74	98,48	0,23	98,25	Schorl
260	35,71	0,18	34,56	9,77	0,93	0,08	0,12	2,03	0,04	0,22	3,47	10,37	0,81	98,29	0,09	98,19	Schorl
261	35,67	0,19	34,70	9,86	1,08	0,05	0,09	1,91	0,02	0,53	3,33	10,38	0,73	98,54	0,22	98,31	Schorl
262	36,36	0,06	34,27	10,64	0,77	0,00	0,09	1,83	0,01	0,48	3,37	10,43	0,86	99,16	0,20	98,96	Schorl
263	36,65	0,07	34,13	11,34	0,74	0,02	0,16	1,79	0,03	0,45	3,41	10,49	0,83	100,10	0,19	99,91	Schorl
264	35,75	0,11	34,57	9,64	0,97	0,06	0,14	2,18	0,04	0,40	3,39	10,38	0,84	98,45	0,17	98,28	Elbaite

Point	SiO2	TiO2	Al2O3	FeO	MgO	CaO	MnO	Na2O	K2O	F	H2O*	B2O3*	Li2O*	Total	O=F	Total*	Mineral
265	36,00	0,15	34,63	10,19	0,95	0,06	0,14	1,96	0,04	0,49	3,37	10,43	0,75	99,16	0,20	98,95	Schorl
266	35,72	0,15	35,03	10,27	1,00	0,09	0,14	2,00	0,08	0,58	3,33	10,45	0,72	99,56	0,24	99,31	Schorl
267	35,89	0,20	34,47	9,88	0,92	0,07	0,13	1,98	0,02	0,61	3,29	10,38	0,81	98,65	0,26	98,39	Schorl
268	36,19	0,13	34,62	9,82	0,97	0,06	0,09	2,00	0,07	0,66	3,29	10,45	0,86	99,20	0,28	98,93	Schorl
269	35,73	0,13	34,84	10,04	0,98	0,04	0,13	2,00	0,02	0,62	3,29	10,40	0,73	98,94	0,26	98,68	Schorl
sample en-1																	
270	35,04	0,11	36,45	9,15	0,52	0,02	0,29	1,87	0,02	0,39	3,41	10,41	0,77	98,44	0,16	98,28	Elbaite
271	34,74	0,07	36,68	9,13	0,50	0,07	0,29	1,88	0,04	0,48	3,36	10,39	0,76	98,40	0,20	98,20	Elbaite
272	35,71	0,10	35,52	9,11	0,38	0,07	0,39	1,94	0,04	0,35	3,42	10,40	0,90	98,33	0,15	98,18	Elbaite
273	36,27	0,02	38,52	3,58	0,13	0,09	1,43	2,06	0,04	0,66	3,36	10,65	1,44	98,25	0,28	97,97	Elbaite
274	36,13	0,03	37,66	5,31	0,19	0,08	1,22	2,18	0,05	0,59	3,38	10,60	1,30	98,71	0,25	98,46	Elbaite
275	34,60	0,16	36,47	9,39	0,32	0,03	0,34	1,71	0,05	0,19	3,48	10,34	0,72	97,80	0,08	97,72	Elbaite
276	34,38	0,19	36,46	9,73	0,36	0,06	0,35	1,73	0,05	0,31	3,42	10,33	0,66	98,01	0,13	97,88	Elbaite
277	35,32	0,09	36,16	9,13	0,35	0,05	0,29	1,84	0,04	0,43	3,39	10,40	0,84	98,31	0,18	98,13	Elbaite
278	34,99	0,04	38,54	6,21	0,17	0,12	0,77	2,09	0,05	0,51	3,40	10,55	1,12	98,55	0,22	98,34	Elbaite
279	36,06	0,02	37,61	5,19	0,17	0,09	1,16	2,15	0,05	0,58	3,37	10,57	1,31	98,34	0,25	98,10	Elbaite
280	36,11	0,03	37,54	5,32	0,17	0,10	0,94	2,11	0,00	0,71	3,31	10,57	1,32	98,23	0,30	97,93	Elbaite
281	35,34	0,09	36,21	8,05	0,31	0,05	0,48	1,94	0,04	0,70	3,25	10,38	0,97	97,82	0,29	97,53	Elbaite
282	35,53	0,15	36,22	8,02	0,31	0,09	0,44	1,91	0,05	0,25	3,47	10,42	1,00	97,86	0,11	97,76	Elbaite
283	35,79	0,06	36,26	8,30	0,37	0,02	0,34	1,75	0,03	0,38	3,42	10,44	0,93	98,08	0,16	97,92	Elbaite
284	34,56	0,06	37,02	8,44	0,43	0,03	0,44	1,90	0,08	0,55	3,32	10,38	0,81	98,01	0,23	97,78	Elbaite
285	35,17	0,01	38,47	5,52	0,17	0,06	0,92	2,02	0,06	0,58	3,36	10,53	1,17	98,04	0,24	97,79	Elbaite
286	36,00	0,00	38,51	3,90	0,10	0,10	1,51	2,04	0,06	0,83	3,27	10,62	1,38	98,32	0,35	97,97	Elbaite
287	36,61	0,00	39,15	3,34	0,05	0,08	1,61	2,02	0,01	0,44	3,50	10,76	1,46	99,04	0,18	98,86	Elbaite
288	36,62	0,03	39,15	3,09	0,05	0,07	1,58	1,92	0,06	0,55	3,44	10,74	1,48	98,78	0,23	98,54	Elbaite
289	35,22	0,05	38,89	4,17	0,12	0,09	1,33	2,14	0,05	0,43	3,44	10,56	1,31	97,82	0,18	97,64	Elbaite
290	34,52	0,10	37,10	8,78	0,38	0,07	0,35	1,85	0,04	0,30	3,44	10,39	0,78	98,11	0,13	97,98	Elbaite
291	36,31	0,05	36,94	6,09	0,18	0,08	0,94	2,11	0,06	0,67	3,33	10,56	1,27	98,58	0,28	98,30	Elbaite
292	35,90	0,06	37,20	6,44	0,21	0,07	0,81	2,12	0,05	0,60	3,35	10,54	1,20	98,54	0,25	98,28	Elbaite
sample 2-2																	
293	36,30	0,50	31,15	8,17	5,25	0,14	0,10	2,06	0,08	0,36	3,41	10,38	0,48	98,38	0,15	98,24	Dravite
294	36,86	0,48	31,18	8,33	5,57	0,12	0,10	2,19	0,06	0,29	3,49	10,51	0,49	99,68	0,12	99,56	Dravite
295	36,58	0,48	31,32	8,59	5,34	0,15	0,15	2,06	0,04	0,35	3,45	10,46	0,41	99,37	0,15	99,22	Dravite
296	37,06	0,54	31,15	8,80	5,34	0,13	0,09	2,22	0,04	0,26	3,52	10,55	0,53	100,23	0,11	100,12	Dravite
297	36,42	0,62	31,63	5,88	7,02	1,49	0,10	1,33	0,09	0,36	3,48	10,56	0,37	99,35	0,15	99,20	Dravite
298	36,50	0,70	31,42	8,50	5,09	0,11	0,15	2,24	0,09	0,31	3,47	10,48	0,47	99,51	0,13	99,38	Dravite
299	36,35	0,55	31,43	8,68	4,95	0,12	0,12	2,15	0,05	0,22	3,49	10,42	0,44	98,97	0,09	98,88	Dravite
300	36,86	0,54	31,93	6,52	6,22	0,13	0,05	2,15	0,03	0,48	3,42	10,56	0,47	99,34	0,20	99,14	Dravite
301	36,75	0,56	31,70	8,34	5,09	0,08	0,10	2,15	0,03	0,31	3,48	10,52	0,51	99,60	0,13	99,47	Dravite
302	36,48	0,64	31,62	5,72	6,78	0,96	0,03	1,51	0,05	0,34	3,46	10,51	0,44	98,53	0,14	98,39	Dravite

Point	SiO2	TiO2	Al2O3	FeO	MgO	CaO	MnO	Na2O	K2O	F	H2O*	B2O3*	Li2O*	Total	O=F	Total*	Mineral
303	36,25	0,64	31,12	6,66	6,71	1,12	0,08	1,71	0,06	0,54	3,36	10,48	0,37	99,10	0,23	98,87	Dravite
304	36,16	0,71	30,75	8,81	4,67	0,11	0,10	2,02	0,09	0,06	3,53	10,32	0,55	97,88	0,03	97,86	Schorl
305	36,76	0,55	31,46	8,83	5,38	0,14	0,10	2,24	0,06	0,20	3,54	10,54	0,40	100,20	0,08	100,12	Dravite
306	36,60	0,52	31,24	8,65	5,32	0,11	0,13	2,12	0,06	0,48	3,38	10,47	0,43	99,52	0,20	99,32	Dravite
307	36,66	0,51	30,90	8,22	5,33	0,13	0,15	2,14	0,08	0,16	3,52	10,43	0,57	98,80	0,07	98,73	Dravite
308	37,15	0,47	31,86	8,22	5,55	0,11	0,11	2,09	0,05	0,36	3,49	10,62	0,46	100,51	0,15	100,36	Dravite
309	36,37	0,66	31,12	8,42	5,21	0,11	0,07	2,20	0,07	0,28	3,46	10,42	0,47	98,86	0,12	98,74	Dravite
310	36,65	0,55	30,62	8,36	5,62	0,14	0,10	2,16	0,06	0,27	3,47	10,43	0,51	98,94	0,11	98,83	Dravite
311	36,40	0,58	31,40	8,42	5,14	0,14	0,09	2,17	0,07	0,11	3,55	10,44	0,46	98,99	0,04	98,95	Dravite
312	37,16	0,34	32,64	6,03	6,43	0,39	0,12	1,74	0,03	0,23	3,57	10,66	0,43	99,77	0,09	99,67	Dravite
313	36,49	0,67	31,61	8,66	5,20	0,13	0,14	2,08	0,05	0,37	3,44	10,49	0,36	99,71	0,16	99,56	Dravite
314	36,64	0,60	31,27	7,95	5,32	0,08	0,11	2,12	0,05	0,39	3,42	10,46	0,54	98,94	0,17	98,78	Dravite
315	36,39	0,65	31,45	8,45	5,10	0,09	0,04	2,15	0,08	0,36	3,43	10,44	0,45	99,07	0,15	98,92	Dravite
316	36,20	0,66	31,53	7,80	4,93	0,14	0,11	2,14	0,06	0,08	3,55	10,39	0,54	98,12	0,03	98,09	Dravite
317	36,53	0,68	31,78	9,24	4,74	0,12	0,15	2,02	0,05	0,36	3,45	10,50	0,37	99,99	0,15	99,84	Schorl
318	36,57	0,44	31,41	6,45	6,41	0,19	0,13	2,22	0,06	0,48	3,39	10,48	0,46	98,69	0,20	98,49	Dravite
319	36,16	0,69	31,91	5,28	6,97	0,84	0,07	1,70	0,05	0,20	3,53	10,49	0,35	98,23	0,08	98,15	Dravite
320	36,53	0,50	31,16	8,48	5,19	0,11	0,10	2,06	0,06	0,30	3,46	10,42	0,49	98,85	0,13	98,72	Dravite
321	36,61	0,61	31,40	8,56	4,95	0,10	0,13	2,16	0,07	0,37	3,44	10,47	0,52	99,38	0,15	99,22	Dravite
322	36,84	0,65	31,10	8,95	4,81	0,07	0,13	1,99	0,05	0,31	3,46	10,47	0,58	99,40	0,13	99,27	Schorl
323	36,41	0,62	30,83	8,62	5,27	0,14	0,11	2,12	0,06	0,32	3,44	10,40	0,47	98,81	0,13	98,67	Dravite
324	37,02	0,42	31,27	8,74	5,32	0,10	0,06	2,05	0,03	0,20	3,54	10,53	0,51	99,78	0,09	99,70	Dravite
sample 7-1																	
325	35,82	0,30	30,43	12,16	3,32	0,11	0,12	2,20	0,04	0,56	3,26	10,23	0,42	98,97	0,24	98,74	Schorl
326	35,98	0,38	30,86	11,56	3,39	0,13	0,21	1,99	0,06	0,46	3,33	10,28	0,42	99,04	0,19	98,85	Schorl
327	35,05	0,19	31,48	14,38	0,76	0,02	0,24	2,01	0,05	0,55	3,22	10,09	0,41	98,43	0,23	98,20	Schorl
328	35,76	0,28	31,74	11,43	2,95	0,09	0,14	1,96	0,06	0,26	3,43	10,28	0,38	98,74	0,11	98,63	Schorl
329	35,60	0,29	30,23	12,48	2,90	0,07	0,15	2,00	0,07	0,37	3,32	10,14	0,44	98,06	0,16	97,90	Schorl
330	35,45	0,38	31,04	11,16	3,18	0,10	0,11	2,06	0,09	0,53	3,26	10,18	0,42	97,95	0,22	97,73	Schorl
331	36,00	0,34	31,16	10,98	3,46	0,15	0,10	2,01	0,08	0,36	3,38	10,30	0,47	98,80	0,15	98,65	Schorl
332	35,56	0,34	31,44	11,88	2,72	0,08	0,10	1,97	0,09	0,36	3,36	10,22	0,39	98,51	0,15	98,36	Schorl
333	35,83	0,32	31,29	10,61	3,77	0,12	0,07	1,98	0,07	0,33	3,39	10,28	0,38	98,43	0,14	98,29	Schorl
334	36,19	0,34	30,55	10,42	4,15	0,09	0,11	2,17	0,06	0,40	3,36	10,30	0,51	98,65	0,17	98,49	Schorl
335	35,98	0,27	31,75	11,32	2,71	0,07	0,15	1,78	0,08	0,20	3,45	10,29	0,50	98,56	0,08	98,47	Schorl
336	36,25	0,24	30,47	10,96	3,77	0,10	0,05	2,01	0,04	0,45	3,33	10,27	0,56	98,51	0,19	98,32	Schorl
337	35,78	0,15	31,50	11,05	3,18	0,07	0,16	1,94	0,05	0,34	3,37	10,25	0,42	98,26	0,14	98,12	Schorl
338	35,53	0,35	30,72	12,57	3,06	0,06	0,13	1,91	0,08	0,45	3,30	10,19	0,27	98,60	0,19	98,41	Schorl
339	35,45	0,41	30,86	11,45	3,27	0,07	0,13	2,01	0,05	0,32	3,36	10,17	0,36	97,92	0,14	97,78	Schorl
340	36,06	0,21	30,63	10,62	3,95	0,14	0,06	2,10	0,08	0,26	3,42	10,26	0,51	98,30	0,11	98,19	Schorl
341	35,76	0,26	30,26	11,28	3,73	0,14	0,07	2,13	0,10	0,60	3,23	10,19	0,47	98,23	0,25	97,98	Schorl

Point	SiO2	TiO2	Al2O3	FeO	MgO	CaO	MnO	Na2O	K2O	F	H2O*	B2O3*	Li2O*	Total	O=F	Total*	Mineral
342	36,06	0,36	31,39	10,80	3,56	0,13	0,20	1,94	0,08	0,26	3,44	10,33	0,42	98,98	0,11	98,87	Schorl
343	35,88	0,37	31,08	11,80	2,59	0,08	0,08	1,88	0,04	0,34	3,37	10,22	0,55	98,27	0,14	98,13	Schorl
344	35,79	0,39	30,71	11,63	3,19	0,08	0,11	1,94	0,08	0,37	3,35	10,21	0,45	98,29	0,16	98,13	Schorl
345	35,50	0,37	30,80	11,58	3,40	0,11	0,11	2,10	0,04	0,35	3,35	10,19	0,34	98,23	0,15	98,09	Schorl
346	35,85	0,31	30,64	12,05	3,07	0,09	0,12	2,12	0,08	0,55	3,27	10,23	0,47	98,85	0,23	98,61	Schorl
347	35,69	0,15	31,24	11,88	3,22	0,07	0,16	1,83	0,05	0,58	3,26	10,23	0,29	98,63	0,24	98,39	Schorl
348	35,32	0,35	31,03	13,90	1,82	0,04	0,22	2,01	0,06	0,34	3,34	10,16	0,31	98,89	0,14	98,75	Schorl
349	35,53	0,26	30,78	12,68	3,03	0,07	0,13	2,12	0,05	0,30	3,38	10,20	0,28	98,81	0,13	98,68	Schorl
350	35,89	0,32	30,42	12,24	3,03	0,05	0,15	1,96	0,05	0,60	3,24	10,20	0,47	98,61	0,25	98,36	Schorl
sample 7-2																	
351	35,90	0,27	30,52	12,44	3,08	0,06	0,14	2,08	0,06	0,36	3,36	10,23	0,42	98,91	0,15	98,76	Schorl
352	35,22	0,09	31,99	11,74	2,52	0,04	0,16	1,81	0,06	0,59	3,23	10,16	0,28	97,89	0,25	97,64	Schorl
353	34,43	0,23	31,79	12,64	2,38	0,05	0,13	2,09	0,02	0,41	3,28	10,08	0,17	97,71	0,17	97,54	Schorl
354	35,01	0,50	31,77	10,54	3,48	0,12	0,11	2,00	0,06	0,01	3,51	10,19	0,25	97,55	0,00	97,55	Schorl
355	34,83	0,34	31,73	12,48	2,51	0,08	0,11	2,00	0,08	0,69	3,17	10,14	0,20	98,35	0,29	98,06	Schorl
356	35,30	0,42	31,37	11,14	3,24	0,07	0,11	1,92	0,04	0,24	3,40	10,18	0,29	97,71	0,10	97,61	Schorl
357	35,50	0,51	31,04	10,76	3,81	0,15	0,04	1,96	0,10	0,36	3,36	10,22	0,31	98,13	0,15	97,97	Schorl
358	35,37	0,30	31,48	10,04	4,21	0,10	0,08	2,03	0,05	0,79	3,15	10,22	0,22	98,05	0,33	97,72	Schorl
359	35,47	0,28	31,72	10,84	3,38	0,08	0,12	1,96	0,07	0,38	3,35	10,23	0,30	98,17	0,16	98,01	Schorl
360	35,50	0,34	31,42	9,79	4,37	0,11	0,12	2,07	0,07	0,72	3,20	10,25	0,25	98,21	0,30	97,91	Schorl
361	35,13	0,23	31,92	12,02	2,51	0,11	0,15	1,78	0,06	0,65	3,20	10,17	0,23	98,16	0,27	97,88	Schorl
362	35,48	0,30	31,17	9,92	4,20	0,15	0,12	2,06	0,09	0,59	3,24	10,22	0,32	97,85	0,25	97,60	Schorl
363	35,33	0,41	31,25	11,83	3,10	0,10	0,22	1,98	0,09	0,34	3,36	10,20	0,24	98,44	0,14	98,29	Schorl
364	35,41	0,34	31,26	11,18	3,31	0,11	0,17	2,03	0,05	0,53	3,27	10,20	0,32	98,18	0,22	97,96	Schorl
365	35,38	0,42	30,88	10,95	3,92	0,16	0,14	2,04	0,05	0,35	3,35	10,20	0,24	98,09	0,15	97,94	Schorl
366	34,88	0,49	31,53	11,60	3,63	0,16	0,08	1,93	0,06	0,32	3,36	10,19	0,10	98,33	0,14	98,20	Schorl
367	35,62	0,44	31,66	10,98	3,34	0,06	0,02	2,03	0,06	0,64	3,24	10,27	0,34	98,71	0,27	98,44	Schorl
368	35,53	0,41	31,66	10,79	3,67	0,12	0,16	1,98	0,06	0,30	3,40	10,27	0,24	98,58	0,12	98,45	Schorl
369	35,15	0,44	31,46	11,75	3,31	0,12	0,11	1,92	0,07	0,38	3,34	10,20	0,15	98,40	0,16	98,24	Schorl
370	35,22	0,42	31,83	9,72	4,10	0,15	0,07	2,00	0,07	0,39	3,34	10,23	0,25	97,79	0,17	97,62	Schorl
371	35,02	0,38	31,20	10,73	3,93	0,13	0,12	2,10	0,03	0,56	3,24	10,16	0,17	97,76	0,24	97,53	Schorl
372	35,04	0,42	32,04	11,18	3,55	0,07	0,13	1,87	0,09	0,50	3,29	10,23	0,12	98,51	0,21	98,30	Schorl
373	35,25	0,40	31,05	10,91	3,95	0,15	0,06	1,96	0,07	0,30	3,37	10,18	0,19	97,83	0,13	97,71	Schorl
374	34,81	0,32	31,33	12,54	2,58	0,08	0,15	1,93	0,07	0,58	3,21	10,09	0,17	97,86	0,25	97,61	Schorl
sample K-4																	
375	34,76	0,26	32,57	13,61	1,13	0,08	0,16	1,74	0,04	0,33	3,34	10,14	0,25	98,39	0,14	98,25	Schorl
376	34,54	0,08	32,80	13,99	0,74	0,03	0,16	1,44	0,05	0,17	3,40	10,07	0,18	97,63	0,07	97,56	Foitite
377	34,97	0,25	32,21	14,08	0,95	0,07	0,21	1,72	0,02	0,47	3,27	10,13	0,25	98,60	0,20	98,40	Schorl
378	34,79	0,08	33,28	14,15	0,63	0,01	0,16	1,39	0,04	0,29	3,37	10,16	0,17	98,51	0,12	98,39	Foitite
379	35,50	0,25	32,35	14,33	1,07	0,07	0,19	1,83	0,03	0,25	3,42	10,27	0,28	99,83	0,11	99,73	Schorl

Point	SiO2	TiO2	Al2O3	FeO	MgO	CaO	MnO	Na2O	K2O	F	H2O*	B2O3*	Li2O*	Total	O=F	Total*	Mineral
380	35,03	0,07	33,18	13,89	0,73	0,02	0,16	1,48	0,03	0,31	3,37	10,18	0,22	98,65	0,13	98,52	Foitite
381	34,81	0,23	31,87	14,07	1,01	0,03	0,23	1,61	0,08	0,31	3,32	10,06	0,23	97,87	0,13	97,74	Schorl
382	35,21	0,26	32,27	14,15	0,95	0,04	0,20	1,55	0,05	0,39	3,33	10,17	0,25	98,80	0,16	98,64	Schorl
383	34,90	0,04	32,90	13,51	0,74	0,04	0,19	1,38	0,05	0,55	3,23	10,11	0,24	97,88	0,23	97,65	Foitite
384	34,73	0,04	33,05	13,59	0,72	0,03	0,13	1,44	0,05	0,33	3,33	10,10	0,23	97,78	0,14	97,64	Foitite
385	34,38	0,07	33,28	14,20	0,67	0,04	0,12	1,39	0,04	0,17	3,40	10,10	0,13	97,99	0,07	97,92	Foitite
386	34,72	0,09	33,08	13,74	0,65	0,03	0,20	1,42	0,05	0,20	3,39	10,11	0,22	97,92	0,08	97,83	Foitite
387	34,49	0,08	33,40	13,88	0,71	0,01	0,15	1,44	0,08	0,35	3,33	10,13	0,17	98,22	0,15	98,08	Foitite
388	34,78	0,10	33,44	14,00	0,76	0,03	0,16	1,32	0,04	0,42	3,31	10,17	0,14	98,66	0,18	98,49	Foitite
389	34,25	0,10	32,83	14,28	0,85	0,00	0,20	1,53	0,05	0,26	3,35	10,06	0,10	97,84	0,11	97,73	Schorl
390	34,44	0,26	32,33	14,11	0,99	0,06	0,20	1,66	0,02	0,45	3,26	10,07	0,17	98,04	0,19	97,85	Schorl
391	34,95	0,08	33,03	13,45	0,69	0,01	0,19	1,39	0,04	0,23	3,39	10,13	0,25	97,83	0,10	97,73	Foitite
392	34,52	0,08	33,05	13,60	0,79	0,03	0,16	1,45	0,04	0,42	3,28	10,08	0,20	97,70	0,18	97,52	Foitite
393	34,70	0,27	32,42	14,28	1,16	0,03	0,18	1,66	0,03	0,44	3,29	10,13	0,13	98,72	0,19	98,54	Schorl
394	34,76	0,21	32,07	13,66	1,10	0,05	0,17	1,82	0,08	0,46	3,26	10,09	0,28	98,00	0,19	97,81	Schorl
sample K-4																	
395	36,68	0,09	35,21	6,53	0,29	0,09	0,68	2,43	0,04	1,22	3,04	10,49	1,56	98,34	0,51	97,83	Elbaite
396	36,48	0,04	35,05	6,69	0,30	0,12	0,71	2,64	0,06	1,42	2,94	10,46	1,53	98,45	0,60	97,85	Elbaite
397	36,67	0,11	35,20	7,91	0,49	0,08	0,23	2,31	0,02	1,03	3,14	10,52	1,33	99,03	0,43	98,60	Elbaite
398	35,67	0,10	35,02	8,72	0,51	0,09	0,15	2,34	0,04	0,90	3,15	10,36	1,06	98,12	0,38	97,74	Elbaite
399	36,65	0,02	35,39	6,85	0,21	0,12	0,69	2,45	0,04	1,13	3,09	10,50	1,50	98,64	0,47	98,17	Elbaite
400	36,45	0,12	35,52	6,59	0,27	0,11	0,69	2,40	0,03	1,24	3,03	10,48	1,45	98,36	0,52	97,83	Elbaite
401	37,11	0,00	35,06	7,03	0,21	0,11	0,65	2,62	0,03	1,04	3,15	10,57	1,65	99,23	0,44	98,79	Elbaite
402	35,75	0,17	32,51	13,01	0,85	0,03	0,19	1,70	0,05	0,41	3,34	10,24	0,57	98,81	0,17	98,64	Schorl
403	36,35	0,09	34,04	9,26	0,55	0,07	0,14	2,24	0,05	0,76	3,22	10,39	1,22	98,39	0,32	98,07	Elbaite
404	36,84	0,06	35,24	6,58	0,31	0,12	0,70	2,34	0,03	1,17	3,07	10,51	1,57	98,54	0,49	98,05	Elbaite
405	36,79	0,11	35,13	6,53	0,28	0,10	0,60	2,48	0,07	0,97	3,17	10,50	1,62	98,35	0,41	97,94	Elbaite
406	36,79	0,01	35,28	6,57	0,17	0,07	0,73	2,46	0,04	1,07	3,12	10,50	1,60	98,41	0,45	97,95	Elbaite
407	36,67	0,01	35,04	6,44	0,19	0,10	0,63	2,57	0,03	0,99	3,14	10,46	1,66	97,93	0,42	97,51	Elbaite
408	36,78	0,02	35,63	6,95	0,20	0,03	0,59	1,99	0,04	0,85	3,22	10,50	1,44	98,23	0,36	97,87	Elbaite
409	36,98	0,01	35,90	6,49	0,20	0,05	0,70	2,08	0,03	0,72	3,30	10,56	1,50	98,53	0,30	98,22	Elbaite
410	36,46	0,00	35,62	6,51	0,21	0,12	0,73	2,46	0,06	0,92	3,18	10,48	1,47	98,23	0,39	97,84	Elbaite
411	36,63	0,04	35,15	6,49	0,22	0,14	0,66	2,48	0,06	1,03	3,12	10,47	1,60	98,10	0,43	97,66	Elbaite
412	36,58	0,00	35,24	6,47	0,20	0,12	0,74	2,46	0,02	0,88	3,19	10,46	1,57	97,93	0,37	97,56	Elbaite
413	36,21	0,00	34,98	8,76	0,17	0,01	0,76	1,95	0,06	0,84	3,19	10,40	1,10	98,42	0,35	98,06	Elbaite
414	36,38	0,00	34,93	8,86	0,20	0,02	0,88	1,82	0,05	0,53	3,35	10,42	1,09	98,51	0,22	98,29	Elbaite
sample J-1																	
415	36,24	0,03	33,27	11,17	0,01	0,09	0,23	2,28	0,03	0,61	3,28	10,33	1,16	98,71	0,26	98,45	Schorl
416	36,49	0,01	33,37	10,42	0,00	0,00	0,23	2,09	0,05	0,73	3,22	10,33	1,30	98,24	0,31	97,93	Elbaite
417	36,22	0,00	33,62	10,63	0,01	0,05	0,35	2,13	0,02	0,71	3,22	10,32	1,15	98,44	0,30	98,14	Schorl

Point	SiO2	TiO2	Al2O3	FeO	MgO	CaO	MnO	Na2O	K2O	F	H2O*	B2O3*	Li2O*	Total	O=F	Total*	Mineral
418	36,27	0,00	33,75	9,78	0,02	0,03	0,21	2,27	0,02	0,81	3,18	10,32	1,31	97,97	0,34	97,63	Elbaite
419	36,15	0,07	33,45	10,55	0,02	0,01	0,24	2,20	0,04	0,90	3,13	10,30	1,19	98,23	0,38	97,85	Schorl
420	35,65	0,01	34,82	9,75	0,00	0,04	0,33	2,15	0,04	0,76	3,20	10,32	0,98	98,04	0,32	97,72	Elbaite
421	36,45	0,01	34,14	8,56	0,00	0,04	0,39	2,41	0,02	0,82	3,19	10,37	1,48	97,87	0,34	97,52	Elbaite
422	36,16	0,01	33,64	9,68	0,03	0,02	0,24	2,49	0,04	0,98	3,09	10,31	1,34	98,01	0,41	97,60	Elbaite
423	36,22	0,00	33,24	11,27	0,02	0,02	0,10	1,95	0,02	0,52	3,30	10,28	1,13	98,07	0,22	97,85	Schorl
424	36,53	0,01	34,59	9,63	0,00	0,02	0,39	2,01	0,02	0,74	3,25	10,43	1,20	98,82	0,31	98,51	Elbaite
425	35,71	0,00	33,45	11,25	0,00	0,04	0,22	2,30	0,02	0,87	3,12	10,25	1,01	98,23	0,37	97,87	Schorl
426	35,69	0,05	32,96	11,73	0,01	0,03	0,20	2,26	0,01	0,72	3,18	10,21	1,00	98,04	0,30	97,74	Schorl
427	36,40	0,03	34,03	8,39	0,00	0,07	0,38	2,58	0,04	1,41	2,91	10,36	1,53	98,13	0,59	97,54	Elbaite
428	35,77	0,00	33,29	11,51	0,01	0,03	0,17	2,17	0,07	1,09	3,02	10,24	1,00	98,37	0,46	97,91	Schorl
429	35,40	0,04	33,09	12,13	0,00	0,01	0,19	2,41	0,02	0,87	3,11	10,20	0,86	98,34	0,37	97,97	Schorl
430	36,66	0,01	33,93	8,90	0,00	0,00	0,40	2,45	0,01	0,82	3,20	10,39	1,50	98,27	0,34	97,92	Elbaite
431	35,97	0,04	33,55	11,29	0,00	0,02	0,14	2,09	0,03	0,52	3,30	10,29	1,03	98,27	0,22	98,06	Schorl

4. Tourmaline Structural chemical data (based on 31 anions: O, OH and F)

Point	T: Si	Al	B	Z:Al	Mg	Y:Al	Ti	Mg	Mn	Fe2+	Li*	∑Y	X:Ca	Na	K	r	OH	F
sample D-3																		
1	5,97	0,03	3,00	6,00	0,00	0,68	0,02	0,15	0,04	1,84	0,27	3,00	0,00	0,56	0,01	0,43	3,85	0,15
2	6,04	0,00	3,00	6,00	0,00	0,60	0,02	0,21	0,02	1,82	0,33	3,00	0,00	0,53	0,00	0,46	3,84	0,16
3	6,00	0,00	3,00	6,00	0,00	0,64	0,02	0,22	0,03	1,80	0,29	3,00	0,01	0,58	0,01	0,40	3,83	0,17
4	6,05	0,00	3,00	6,00	0,00	0,68	0,01	0,12	0,02	1,83	0,33	3,00	0,00	0,42	0,01	0,57	3,91	0,09
5	6,07	0,00	3,00	6,00	0,00	0,69	0,01	0,11	0,02	1,75	0,41	3,00	0,00	0,41	0,01	0,58	3,93	0,07
6	6,07	0,00	3,00	6,00	0,00	0,58	0,03	0,21	0,01	1,76	0,41	3,00	0,01	0,49	0,01	0,49	3,86	0,14
7	6,00	0,00	3,00	6,00	0,00	0,67	0,02	0,20	0,02	1,80	0,31	3,00	0,01	0,57	0,02	0,40	3,86	0,14
8	5,97	0,03	3,00	6,00	0,00	0,69	0,03	0,20	0,03	1,75	0,30	3,00	0,00	0,56	0,01	0,43	3,81	0,19
9	5,96	0,04	3,00	6,00	0,00	0,68	0,04	0,20	0,02	1,77	0,29	3,00	0,00	0,56	0,01	0,42	3,89	0,11
10	6,04	0,00	3,00	6,00	0,00	0,55	0,02	0,22	0,03	1,84	0,34	3,00	0,00	0,55	0,01	0,44	3,92	0,08
11	5,95	0,05	3,00	6,00	0,00	0,68	0,02	0,20	0,02	1,81	0,27	3,00	0,00	0,57	0,01	0,41	3,77	0,23
12	6,04	0,00	3,00	6,00	0,00	0,73	0,01	0,15	0,03	1,69	0,38	3,00	0,00	0,47	0,01	0,52	3,91	0,09
13	5,98	0,02	3,00	6,00	0,00	0,68	0,02	0,22	0,02	1,78	0,28	3,00	0,01	0,55	0,01	0,43	3,81	0,19
14	6,05	0,00	3,00	6,00	0,00	0,55	0,02	0,22	0,03	1,77	0,40	3,00	0,00	0,58	0,01	0,41	3,85	0,15
15	5,97	0,03	3,00	6,00	0,00	0,72	0,02	0,21	0,02	1,73	0,29	3,00	0,01	0,54	0,01	0,45	3,97	0,03
16	5,97	0,03	3,00	6,00	0,00	0,70	0,03	0,21	0,02	1,73	0,31	3,00	0,00	0,57	0,01	0,42	3,78	0,22
17	5,98	0,02	3,00	6,00	0,00	0,70	0,03	0,22	0,02	1,74	0,29	3,00	0,01	0,54	0,01	0,45	3,80	0,20
18	5,98	0,02	3,00	6,00	0,00	0,65	0,03	0,20	0,03	1,82	0,27	3,00	0,01	0,55	0,01	0,43	3,78	0,22
19	5,98	0,02	3,00	6,00	0,00	0,68	0,03	0,22	0,02	1,76	0,29	3,00	0,00	0,54	0,01	0,45	3,83	0,17
20	5,98	0,02	3,00	6,00	0,00	0,66	0,03	0,21	0,02	1,78	0,30	3,00	0,00	0,58	0,01	0,40	3,78	0,22
Sample O-2																		
21	5,96	0,04	3,00	6,00	0,00	0,32	0,09	0,56	0,01	1,87	0,15	3,00	0,02	0,64	0,01	0,33	3,83	0,17
22	5,96	0,04	3,00	6,00	0,00	0,31	0,11	0,45	0,02	1,90	0,21	3,00	0,03	0,63	0,02	0,31	3,81	0,19
23	5,92	0,08	3,00	6,00	0,00	0,27	0,11	0,55	0,02	1,89	0,16	3,00	0,02	0,68	0,02	0,28	3,72	0,28
24	5,90	0,10	3,00	6,00	0,00	0,34	0,10	0,55	0,01	1,83	0,16	3,00	0,02	0,66	0,01	0,31	3,82	0,18
25	5,98	0,02	3,00	6,00	0,00	0,38	0,10	0,47	0,01	1,78	0,25	3,00	0,03	0,62	0,01	0,34	3,88	0,12
26	5,95	0,05	3,00	6,00	0,00	0,30	0,10	0,61	0,01	1,83	0,15	3,00	0,02	0,64	0,01	0,33	3,79	0,21
27	5,97	0,03	3,00	6,00	0,00	0,38	0,10	0,44	0,03	1,84	0,21	3,00	0,01	0,61	0,01	0,36	3,66	0,34
28	5,94	0,06	3,00	6,00	0,00	0,36	0,10	0,52	0,02	1,79	0,20	3,00	0,02	0,64	0,01	0,32	3,78	0,22
29	5,95	0,05	3,00	6,00	0,00	0,23	0,10	0,63	0,02	1,84	0,17	3,00	0,03	0,72	0,01	0,24	3,66	0,34
30	6,02	0,00	3,00	6,00	0,00	0,27	0,12	0,65	0,01	1,67	0,28	3,00	0,03	0,65	0,01	0,32	3,73	0,27
31	5,91	0,09	3,00	6,00	0,00	0,39	0,11	0,44	0,02	1,85	0,20	3,00	0,02	0,63	0,01	0,33	3,78	0,22
32	5,95	0,05	3,00	6,00	0,00	0,41	0,10	0,42	0,02	1,83	0,22	3,00	0,02	0,59	0,02	0,36	3,73	0,27
33	5,96	0,04	3,00	6,00	0,00	0,29	0,10	0,61	0,01	1,82	0,18	3,00	0,02	0,68	0,01	0,29	3,74	0,26
34	5,94	0,06	3,00	6,00	0,00	0,34	0,09	0,52	0,01	1,88	0,15	3,00	0,02	0,64	0,01	0,33	3,79	0,21
35	5,99	0,01	3,00	6,00	0,00	0,29	0,10	0,48	0,02	1,90	0,22	3,00	0,02	0,68	0,02	0,28	3,83	0,17
36	5,98	0,02	3,00	6,00	0,00	0,31	0,10	0,49	0,03	1,88	0,20	3,00	0,02	0,66	0,02	0,30	3,69	0,31
37	5,95	0,05	3,00	6,00	0,00	0,26	0,10	0,61	0,02	1,85	0,16	3,00	0,02	0,69	0,02	0,27	3,77	0,23
38	5,96	0,04	3,00	6,00	0,00	0,31	0,10	0,54	0,02	1,87	0,17	3,00	0,02	0,63	0,02	0,33	3,68	0,32

Point	T: Si	Al	B	Z:Al	Mg	Y:Al	Ti	Mg	Mn	Fe2+	Li*	∑Y	X:Ca	Na	K	r	OH	F
39	6,01	0,00	3,00	6,00	0,00	0,29	0,11	0,50	0,02	1,89	0,20	3,00	0,02	0,59	0,02	0,37	3,78	0,22
40	5,97	0,03	3,00	6,00	0,00	0,28	0,10	0,67	0,00	1,76	0,18	3,00	0,03	0,65	0,02	0,31	3,68	0,32
41	5,97	0,03	3,00	6,00	0,00	0,33	0,09	0,54	0,02	1,84	0,17	3,00	0,02	0,64	0,01	0,33	3,76	0,24
42	5,92	0,08	3,00	6,00	0,00	0,32	0,10	0,56	0,02	1,82	0,18	3,00	0,02	0,69	0,01	0,28	3,84	0,16
Sample 3.2-1																		
43	6,05	0,00	3,00	6,00	0,00	0,32	0,05	0,88	0,01	1,44	0,29	3,00	0,02	0,60	0,01	0,37	3,86	0,14
44	6,09	0,00	3,00	6,00	0,00	0,23	0,06	0,87	0,03	1,45	0,36	3,00	0,01	0,61	0,00	0,37	3,86	0,14
45	6,04	0,00	3,00	6,00	0,00	0,35	0,06	0,83	0,02	1,47	0,27	3,00	0,01	0,60	0,01	0,38	3,95	0,05
46	6,05	0,00	3,00	6,00	0,00	0,31	0,06	0,81	0,02	1,49	0,30	3,00	0,02	0,63	0,01	0,34	3,83	0,17
47	6,03	0,00	3,00	6,00	0,00	0,34	0,06	0,83	0,02	1,52	0,23	3,00	0,01	0,63	0,01	0,35	3,77	0,23
48	6,02	0,00	3,00	6,00	0,00	0,22	0,08	1,71	0,01	0,74	0,25	3,00	0,10	0,58	0,00	0,32	3,90	0,10
49	6,05	0,00	3,00	6,00	0,00	0,13	0,09	1,25	0,02	1,26	0,24	3,00	0,03	0,67	0,01	0,29	3,79	0,21
50	6,08	0,00	3,00	6,00	0,00	0,18	0,06	1,27	0,01	1,15	0,32	3,00	0,02	0,66	0,01	0,31	3,90	0,10
51	6,06	0,00	3,00	6,00	0,00	0,18	0,07	1,32	0,01	1,15	0,27	3,00	0,02	0,67	0,01	0,30	3,86	0,14
52	6,06	0,00	3,00	6,00	0,00	0,16	0,08	1,21	0,02	1,20	0,32	3,00	0,02	0,69	0,02	0,27	3,83	0,17
53	6,06	0,00	3,00	6,00	0,00	0,15	0,08	1,24	0,01	1,25	0,27	3,00	0,02	0,66	0,02	0,30	3,88	0,12
54	6,06	0,00	3,00	6,00	0,00	0,15	0,07	1,34	0,01	1,16	0,26	3,00	0,02	0,67	0,02	0,29	3,85	0,15
55	6,07	0,00	3,00	6,00	0,00	0,24	0,05	1,13	0,01	1,25	0,31	3,00	0,02	0,65	0,01	0,32	3,73	0,27
56	6,04	0,00	3,00	6,00	0,00	0,35	0,07	1,05	0,02	1,22	0,30	3,00	0,02	0,61	0,01	0,37	3,89	0,11
57	6,05	0,00	3,00	6,00	0,00	0,23	0,07	1,23	0,01	1,21	0,25	3,00	0,02	0,65	0,01	0,32	3,87	0,13
58	6,04	0,00	3,00	6,00	0,00	0,20	0,07	1,30	0,02	1,21	0,20	3,00	0,02	0,66	0,01	0,31	3,79	0,21
59	6,06	0,00	3,00	6,00	0,00	0,16	0,07	1,31	0,01	1,16	0,28	3,00	0,02	0,68	0,01	0,29	3,75	0,25
60	6,09	0,00	3,00	6,00	0,00	0,12	0,06	1,33	0,02	1,16	0,32	3,00	0,02	0,66	0,00	0,31	3,91	0,09
sample PET-2																		
61	6,13	0,00	3,00	6,00	0,00	0,06	0,06	1,30	0,02	1,15	0,41	3,00	0,03	0,63	0,01	0,33	3,90	0,10
62	6,04	0,00	3,00	6,00	0,00	0,21	0,06	1,34	0,01	1,15	0,22	3,00	0,02	0,67	0,01	0,30	3,78	0,22
63	6,06	0,00	3,00	6,00	0,00	0,26	0,06	0,89	0,02	1,46	0,30	3,00	0,01	0,64	0,02	0,33	3,92	0,08
64	6,05	0,00	3,00	6,00	0,00	0,24	0,07	1,07	0,02	1,36	0,24	3,00	0,02	0,62	0,01	0,35	3,79	0,21
65	6,07	0,00	3,00	6,00	0,00	0,23	0,06	1,07	0,01	1,34	0,30	3,00	0,02	0,64	0,01	0,33	3,84	0,16
66	6,06	0,00	3,00	6,00	0,00	0,23	0,06	1,10	0,01	1,32	0,28	3,00	0,02	0,65	0,01	0,32	3,89	0,11
67	6,05	0,00	3,00	6,00	0,00	0,26	0,05	1,05	0,02	1,38	0,24	3,00	0,01	0,64	0,01	0,33	3,85	0,15
68	6,01	0,00	3,00	6,00	0,00	0,33	0,07	1,14	0,01	1,27	0,19	3,00	0,02	0,62	0,01	0,34	3,90	0,10
69	5,99	0,01	3,00	6,00	0,00	0,35	0,08	1,05	0,01	1,29	0,21	3,00	0,02	0,67	0,01	0,30	3,89	0,11
70	6,00	0,00	3,00	6,00	0,00	0,33	0,07	0,98	0,01	1,39	0,22	3,00	0,02	0,70	0,02	0,27	3,85	0,15
71	5,99	0,01	3,00	6,00	0,00	0,41	0,05	0,96	0,01	1,43	0,14	3,00	0,01	0,60	0,02	0,37	3,82	0,18
72	6,02	0,00	3,00	6,00	0,00	0,35	0,05	0,90	0,02	1,45	0,23	3,00	0,02	0,63	0,02	0,33	3,92	0,08
73	6,01	0,00	3,00	6,00	0,00	0,36	0,05	0,92	0,01	1,44	0,21	3,00	0,02	0,64	0,02	0,32	3,90	0,10
74	6,02	0,00	3,00	6,00	0,00	0,30	0,08	1,17	0,01	1,21	0,23	3,00	0,03	0,64	0,01	0,33	3,90	0,10
75	6,04	0,00	3,00	6,00	0,00	0,24	0,08	1,21	0,01	1,20	0,26	3,00	0,03	0,61	0,01	0,34	3,89	0,11

Point	T: Si	Al	B	Z:Al	Mg	Y:Al	Ti	Mg	Mn	Fe2+	Li*	∑Y	X:Ca	Na	K	r	OH	F
76	6,01	0,00	3,00	6,00	0,00	0,39	0,06	0,88	0,02	1,47	0,18	3,00	0,01	0,61	0,01	0,37	3,91	0,09
77	6,01	0,00	3,00	6,00	0,00	0,40	0,04	0,90	0,01	1,44	0,21	3,00	0,02	0,65	0,00	0,33	3,85	0,15
78	5,98	0,02	3,00	6,00	0,00	0,34	0,08	1,18	0,01	1,22	0,18	3,00	0,02	0,67	0,01	0,30	3,85	0,15
79	6,01	0,00	3,00	6,00	0,00	0,37	0,07	1,14	0,01	1,19	0,21	3,00	0,02	0,58	0,01	0,38	3,92	0,08
80	6,04	0,00	3,00	6,00	0,00	0,26	0,08	1,24	0,01	1,11	0,29	3,00	0,03	0,64	0,01	0,32	3,89	0,11
81	6,02	0,00	3,00	6,00	0,00	0,35	0,07	0,92	0,01	1,41	0,24	3,00	0,01	0,63	0,01	0,35	3,91	0,09
82	6,01	0,00	3,00	6,00	0,00	0,32	0,06	1,00	0,01	1,43	0,18	3,00	0,01	0,65	0,01	0,32	3,91	0,09
83	6,00	0,00	3,00	6,00	0,00	0,37	0,07	1,06	0,01	1,30	0,19	3,00	0,02	0,61	0,02	0,35	3,82	0,18
84	6,05	0,00	3,00	6,00	0,00	0,23	0,06	1,02	0,02	1,41	0,25	3,00	0,01	0,65	0,01	0,33	3,89	0,11
sample 6-2																		
85	5,94	0,06	3,00	6,00	0,00	0,37	0,10	0,96	0,01	1,32	0,24	3,00	0,07	0,58	0,02	0,34	3,94	0,06
86	6,00	0,00	3,00	6,00	0,00	0,44	0,09	0,69	0,02	1,57	0,19	3,00	0,02	0,53	0,01	0,44	3,90	0,10
87	5,97	0,03	3,00	6,00	0,00	0,44	0,09	0,69	0,01	1,59	0,18	3,00	0,02	0,54	0,01	0,44	3,94	0,06
88	5,96	0,04	3,00	6,00	0,00	0,42	0,09	0,68	0,02	1,60	0,19	3,00	0,02	0,58	0,01	0,40	3,98	0,02
89	6,00	0,00	3,00	6,00	0,00	0,46	0,09	0,69	0,02	1,54	0,20	3,00	0,01	0,54	0,01	0,44	3,85	0,15
90	5,95	0,05	3,00	6,00	0,00	0,34	0,11	0,84	0,02	1,53	0,17	3,00	0,02	0,61	0,02	0,35	3,92	0,08
91	6,01	0,00	3,00	6,00	0,00	0,45	0,08	0,75	0,01	1,48	0,24	3,00	0,01	0,55	0,01	0,43	3,76	0,24
92	5,96	0,04	3,00	6,00	0,00	0,44	0,08	0,76	0,01	1,54	0,17	3,00	0,02	0,58	0,01	0,39	3,99	0,01
93	5,97	0,03	3,00	6,00	0,00	0,30	0,10	1,10	0,00	1,26	0,24	3,00	0,09	0,56	0,02	0,33	3,78	0,22
94	5,87	0,13	3,00	6,00	0,00	0,35	0,12	1,04	0,00	1,28	0,21	3,00	0,08	0,57	0,01	0,34	3,81	0,19
95	5,85	0,15	3,00	6,00	0,00	0,44	0,10	0,48	0,03	1,78	0,17	3,00	0,05	0,56	0,01	0,38	3,90	0,10
96	5,95	0,05	3,00	6,00	0,00	0,43	0,08	0,72	0,02	1,58	0,17	3,00	0,02	0,58	0,01	0,39	3,99	0,01
97	5,86	0,14	3,00	6,00	0,00	0,45	0,10	0,49	0,02	1,77	0,18	3,00	0,05	0,55	0,02	0,39	3,77	0,23
98	5,86	0,14	3,00	6,00	0,00	0,33	0,14	0,82	0,01	1,50	0,20	3,00	0,07	0,58	0,02	0,34	3,87	0,13
99	5,96	0,04	3,00	6,00	0,00	0,44	0,07	0,76	0,02	1,58	0,13	3,00	0,02	0,54	0,01	0,43	3,93	0,07
100	6,01	0,00	3,00	6,00	0,00	0,35	0,08	0,67	0,02	1,71	0,17	3,00	0,01	0,58	0,01	0,40	3,82	0,18
101	5,97	0,03	3,00	6,00	0,00	0,42	0,09	0,70	0,02	1,57	0,20	3,00	0,02	0,58	0,02	0,38	3,95	0,05
102	5,94	0,06	3,00	6,00	0,00	0,35	0,11	0,96	0,00	1,35	0,22	3,00	0,06	0,57	0,01	0,35	3,88	0,12
103	5,93	0,07	3,00	6,00	0,00	0,35	0,11	0,89	0,00	1,44	0,21	3,00	0,06	0,56	0,02	0,36	3,84	0,16
104	5,91	0,09	3,00	6,00	0,00	0,35	0,11	0,96	0,01	1,37	0,20	3,00	0,05	0,61	0,01	0,33	3,89	0,11
105	5,92	0,08	3,00	6,00	0,00	0,33	0,12	0,88	0,01	1,45	0,21	3,00	0,07	0,57	0,01	0,35	3,88	0,12
Sample Na-2																		
106	5,99	0,01	3,00	6,00	0,00	0,82	0,00	0,06	0,03	1,80	0,28	3,00	0,00	0,46	0,01	0,53	3,74	0,26
107	5,93	0,07	3,00	6,00	0,00	0,93	0,01	0,07	0,03	1,47	0,49	3,00	0,01	0,58	0,02	0,39	3,63	0,37
108	5,94	0,06	3,00	6,00	0,00	0,87	0,01	0,08	0,02	1,57	0,45	3,00	0,01	0,60	0,01	0,38	3,74	0,26
109	5,97	0,03	3,00	6,00	0,00	0,83	0,01	0,04	0,01	1,72	0,39	3,00	0,00	0,57	0,01	0,42	3,71	0,29
sample eh-1																		
110	6,01	0,00	3,00	6,00	0,00	0,47	0,07	1,05	0,02	1,17	0,21	3,00	0,02	0,53	0,01	0,44	3,90	0,10
111	6,01	0,00	3,00	6,00	0,00	0,44	0,07	1,05	0,01	1,21	0,23	3,00	0,01	0,57	0,01	0,41	3,92	0,08
112	6,13	0,00	3,00	6,00	0,00	0,76	0,01	0,06	0,08	0,90	1,19	3,00	0,01	0,85	0,01	0,12	3,40	0,60

Point	T: Si	Al	B	Z:Al	Mg	Y:Al	Ti	Mg	Mn	Fe2+	Li*	∑Y	X:Ca	Na	K	r	OH	F
76	6,01	0,00	3,00	6,00	0,00	0,39	0,06	0,88	0,02	1,47	0,18	3,00	0,01	0,61	0,01	0,37	3,91	0,09
77	6,01	0,00	3,00	6,00	0,00	0,40	0,04	0,90	0,01	1,44	0,21	3,00	0,02	0,65	0,00	0,33	3,85	0,15
78	5,98	0,02	3,00	6,00	0,00	0,34	0,08	1,18	0,01	1,22	0,18	3,00	0,02	0,67	0,01	0,30	3,85	0,15
79	6,01	0,00	3,00	6,00	0,00	0,37	0,07	1,14	0,01	1,19	0,21	3,00	0,02	0,58	0,01	0,38	3,92	0,08
80	6,04	0,00	3,00	6,00	0,00	0,26	0,08	1,24	0,01	1,11	0,29	3,00	0,03	0,64	0,01	0,32	3,89	0,11
81	6,02	0,00	3,00	6,00	0,00	0,35	0,07	0,92	0,01	1,41	0,24	3,00	0,01	0,63	0,01	0,35	3,91	0,09
82	6,01	0,00	3,00	6,00	0,00	0,32	0,06	1,00	0,01	1,43	0,18	3,00	0,01	0,65	0,01	0,32	3,91	0,09
83	6,00	0,00	3,00	6,00	0,00	0,37	0,07	1,06	0,01	1,30	0,19	3,00	0,02	0,61	0,02	0,35	3,82	0,18
84	6,05	0,00	3,00	6,00	0,00	0,23	0,06	1,02	0,02	1,41	0,25	3,00	0,01	0,65	0,01	0,33	3,89	0,11
sample 6-2																		
85	5,94	0,06	3,00	6,00	0,00	0,37	0,10	0,96	0,01	1,32	0,24	3,00	0,07	0,58	0,02	0,34	3,94	0,06
86	6,00	0,00	3,00	6,00	0,00	0,44	0,09	0,69	0,02	1,57	0,19	3,00	0,02	0,53	0,01	0,44	3,90	0,10
87	5,97	0,03	3,00	6,00	0,00	0,44	0,09	0,69	0,01	1,59	0,18	3,00	0,02	0,54	0,01	0,44	3,94	0,06
88	5,96	0,04	3,00	6,00	0,00	0,42	0,09	0,68	0,02	1,60	0,19	3,00	0,02	0,58	0,01	0,40	3,98	0,02
89	6,00	0,00	3,00	6,00	0,00	0,46	0,09	0,69	0,02	1,54	0,20	3,00	0,01	0,54	0,01	0,44	3,85	0,15
90	5,95	0,05	3,00	6,00	0,00	0,34	0,11	0,84	0,02	1,53	0,17	3,00	0,02	0,61	0,02	0,35	3,92	0,08
91	6,01	0,00	3,00	6,00	0,00	0,45	0,08	0,75	0,01	1,48	0,24	3,00	0,01	0,55	0,01	0,43	3,76	0,24
92	5,96	0,04	3,00	6,00	0,00	0,44	0,08	0,76	0,01	1,54	0,17	3,00	0,02	0,58	0,01	0,39	3,99	0,01
93	5,97	0,03	3,00	6,00	0,00	0,30	0,10	1,10	0,00	1,26	0,24	3,00	0,09	0,56	0,02	0,33	3,78	0,22
94	5,87	0,13	3,00	6,00	0,00	0,35	0,12	1,04	0,00	1,28	0,21	3,00	0,08	0,57	0,01	0,34	3,81	0,19
95	5,85	0,15	3,00	6,00	0,00	0,44	0,10	0,48	0,03	1,78	0,17	3,00	0,05	0,56	0,01	0,38	3,90	0,10
96	5,95	0,05	3,00	6,00	0,00	0,43	0,08	0,72	0,02	1,58	0,17	3,00	0,02	0,58	0,01	0,39	3,99	0,01
97	5,86	0,14	3,00	6,00	0,00	0,45	0,10	0,49	0,02	1,77	0,18	3,00	0,05	0,55	0,02	0,39	3,77	0,23
98	5,86	0,14	3,00	6,00	0,00	0,33	0,14	0,82	0,01	1,50	0,20	3,00	0,07	0,58	0,02	0,34	3,87	0,13
99	5,96	0,04	3,00	6,00	0,00	0,44	0,07	0,76	0,02	1,58	0,13	3,00	0,02	0,54	0,01	0,43	3,93	0,07
100	6,01	0,00	3,00	6,00	0,00	0,35	0,08	0,67	0,02	1,71	0,17	3,00	0,01	0,58	0,01	0,40	3,82	0,18
101	5,97	0,03	3,00	6,00	0,00	0,42	0,09	0,70	0,02	1,57	0,20	3,00	0,02	0,58	0,02	0,38	3,95	0,05
102	5,94	0,06	3,00	6,00	0,00	0,35	0,11	0,96	0,00	1,35	0,22	3,00	0,06	0,57	0,01	0,35	3,88	0,12
103	5,93	0,07	3,00	6,00	0,00	0,35	0,11	0,89	0,00	1,44	0,21	3,00	0,06	0,56	0,02	0,36	3,84	0,16
104	5,91	0,09	3,00	6,00	0,00	0,35	0,11	0,96	0,01	1,37	0,20	3,00	0,05	0,61	0,01	0,33	3,89	0,11
105	5,92	0,08	3,00	6,00	0,00	0,33	0,12	0,88	0,01	1,45	0,21	3,00	0,07	0,57	0,01	0,35	3,88	0,12
Sample Na-2																		
106	5,99	0,01	3,00	6,00	0,00	0,82	0,00	0,06	0,03	1,80	0,28	3,00	0,00	0,46	0,01	0,53	3,74	0,26
107	5,93	0,07	3,00	6,00	0,00	0,93	0,01	0,07	0,03	1,47	0,49	3,00	0,01	0,58	0,02	0,39	3,63	0,37
108	5,94	0,06	3,00	6,00	0,00	0,87	0,01	0,08	0,02	1,57	0,45	3,00	0,01	0,60	0,01	0,38	3,74	0,26
109	5,97	0,03	3,00	6,00	0,00	0,83	0,01	0,04	0,01	1,72	0,39	3,00	0,00	0,57	0,01	0,42	3,71	0,29
sample eh-1																		
110	6,01	0,00	3,00	6,00	0,00	0,47	0,07	1,05	0,02	1,17	0,21	3,00	0,02	0,53	0,01	0,44	3,90	0,10
111	6,01	0,00	3,00	6,00	0,00	0,44	0,07	1,05	0,01	1,21	0,23	3,00	0,01	0,57	0,01	0,41	3,92	0,08
112	6,13	0,00	3,00	6,00	0,00	0,76	0,01	0,06	0,08	0,90	1,19	3,00	0,01	0,85	0,01	0,12	3,40	0,60

Point	T: Si	Al	B	Z:Al	Mg	Y:Al	Ti	Mg	Mn	Fe2+	Li*	∑Y	X:Ca	Na	K	r	OH	F
113	5,97	0,03	3,00	6,00	0,00	0,43	0,08	1,05	0,01	1,21	0,23	3,00	0,02	0,61	0,02	0,35	3,94	0,06
114	6,05	0,00	3,00	6,00	0,00	0,90	0,00	0,06	0,08	1,03	0,93	3,00	0,02	0,79	0,01	0,19	3,47	0,53
115	5,98	0,02	3,00	6,00	0,00	0,38	0,08	1,06	0,01	1,26	0,20	3,00	0,03	0,62	0,01	0,35	3,92	0,08
116	6,10	0,00	3,00	6,00	0,00	0,91	0,00	0,05	0,19	0,68	1,17	3,00	0,04	0,77	0,01	0,18	3,37	0,63
sample5-2																		
117	6,09	0,00	3,00	6,00	0,00	0,29	0,05	1,09	0,02	1,27	0,29	3,00	0,01	0,52	0,01	0,46	3,83	0,17
118	6,08	0,00	3,00	6,00	0,00	0,26	0,05	1,38	0,00	1,00	0,31	3,00	0,02	0,57	0,01	0,40	3,84	0,16
119	6,08	0,00	3,00	6,00	0,00	0,33	0,04	1,13	0,01	1,19	0,30	3,00	0,01	0,53	0,01	0,45	3,84	0,16
120	6,10	0,00	3,00	6,00	0,00	0,22	0,06	1,22	0,01	1,17	0,31	3,00	0,01	0,53	0,01	0,44	3,73	0,27
121	6,08	0,00	3,00	6,00	0,00	0,21	0,09	1,28	0,00	1,10	0,32	3,00	0,02	0,56	0,01	0,40	3,82	0,18
122	6,04	0,00	3,00	6,00	0,00	0,34	0,09	1,27	0,01	1,06	0,23	3,00	0,03	0,50	0,01	0,47	3,82	0,18
123	6,08	0,00	3,00	6,00	0,00	0,26	0,08	1,31	0,00	1,02	0,33	3,00	0,01	0,55	0,01	0,43	3,86	0,14
124	6,08	0,00	3,00	6,00	0,00	0,30	0,05	1,24	0,01	1,09	0,31	3,00	0,02	0,55	0,01	0,42	3,84	0,16
125	6,05	0,00	3,00	6,00	0,00	0,31	0,07	1,23	0,01	1,15	0,24	3,00	0,02	0,56	0,01	0,41	3,81	0,19
126	6,04	0,00	3,00	6,00	0,00	0,40	0,06	1,00	0,02	1,26	0,26	3,00	0,01	0,52	0,01	0,45	3,78	0,22
127	6,07	0,00	3,00	6,00	0,00	0,25	0,08	1,33	0,00	1,03	0,31	3,00	0,02	0,56	0,01	0,41	3,90	0,10
128	6,04	0,00	3,00	6,00	0,00	0,43	0,06	0,91	0,01	1,33	0,26	3,00	0,02	0,51	0,01	0,46	3,79	0,21
129	6,06	0,00	3,00	6,00	0,00	0,28	0,04	1,34	0,02	1,11	0,21	3,00	0,01	0,58	0,00	0,40	3,73	0,27
130	6,09	0,00	3,00	6,00	0,00	0,25	0,07	1,24	0,01	1,12	0,32	3,00	0,01	0,53	0,01	0,44	3,89	0,11
131	6,10	0,00	3,00	6,00	0,00	0,37	0,04	1,15	0,01	1,10	0,32	3,00	0,01	0,44	0,01	0,54	3,91	0,09
132	6,11	0,00	3,00	6,00	0,00	0,18	0,07	1,17	0,01	1,27	0,32	3,00	0,01	0,52	0,01	0,46	3,79	0,21
133	6,16	0,00	3,00	6,00	0,00	0,14	0,02	1,23	0,01	1,10	0,50	3,00	0,01	0,53	0,12	0,33	3,79	0,21
134	6,09	0,00	3,00	6,00	0,00	0,30	0,04	1,24	0,01	1,11	0,31	3,00	0,01	0,54	0,01	0,44	3,86	0,14
samplex-1																		
135	6,05	0,00	3,00	6,00	0,00	0,29	0,07	0,89	0,02	1,47	0,25	3,00	0,01	0,61	0,01	0,37	3,76	0,24
136	6,00	0,00	3,00	6,00	0,00	0,15	0,07	1,51	0,01	1,06	0,20	3,00	0,12	0,65	0,01	0,23	3,71	0,29
137	6,02	0,00	3,00	6,00	0,00	0,22	0,05	1,43	0,02	1,09	0,19	3,00	0,10	0,60	0,01	0,30	3,70	0,30
138	6,03	0,00	3,00	6,00	0,00	0,34	0,01	1,38	0,02	1,01	0,25	3,00	0,12	0,54	0,01	0,33	3,85	0,15
139	6,06	0,00	3,00	6,00	0,00	0,23	0,07	0,97	0,03	1,46	0,24	3,00	0,01	0,61	0,01	0,38	3,72	0,28
140	5,97	0,03	3,00	6,00	0,00	0,41	0,12	0,92	0,01	1,24	0,31	3,00	0,09	0,50	0,01	0,40	3,96	0,04
141	6,05	0,00	3,00	6,00	0,00	0,18	0,05	1,00	0,03	1,54	0,20	3,00	0,01	0,69	0,00	0,30	3,72	0,28
142	6,02	0,00	3,00	6,00	0,00	0,20	0,05	1,47	0,01	1,03	0,24	3,00	0,11	0,62	0,02	0,26	3,70	0,30
143	6,04	0,00	3,00	6,00	0,00	0,36	0,01	1,21	0,02	1,14	0,26	3,00	0,10	0,52	0,01	0,37	3,85	0,15
144	5,86	0,14	3,00	6,00	0,00	0,45	0,01	1,18	0,03	1,12	0,20	3,00	0,14	0,58	0,01	0,27	3,72	0,28
145	5,99	0,01	3,00	6,00	0,00	0,23	0,06	1,41	0,02	1,09	0,18	3,00	0,10	0,63	0,02	0,25	3,64	0,36
146	5,99	0,01	3,00	6,00	0,00	0,24	0,05	1,43	0,01	1,09	0,17	3,00	0,13	0,59	0,01	0,28	3,67	0,33
147	6,08	0,00	3,00	6,00	0,00	0,17	0,05	1,05	0,03	1,40	0,30	3,00	0,02	0,65	0,01	0,33	3,70	0,30
148	6,04	0,00	3,00	6,00	0,00	0,40	0,05	0,79	0,03	1,50	0,23	3,00	0,00	0,55	0,01	0,43	3,81	0,19
149	6,03	0,00	3,00	6,00	0,00	0,35	0,01	1,25	0,02	1,08	0,29	3,00	0,12	0,55	0,01	0,32	3,81	0,19
150	6,00	0,00	3,00	6,00	0,00	0,10	0,08	1,54	0,01	1,10	0,16	3,00	0,11	0,64	0,01	0,24	3,54	0,46

Point	T: Si	Al	B	Z:Al	Mg	Y:Al	Ti	Mg	Mn	Fe2+	Li*	∑Y	X:Ca	Na	K	r	OH	F
151	6,00	0,00	3,00	6,00	0,00	0,23	0,05	1,49	0,02	1,03	0,18	3,00	0,11	0,61	0,01	0,27	3,71	0,29
152	6,03	0,00	3,00	6,00	0,00	0,26	0,02	1,64	0,02	0,81	0,25	3,00	0,13	0,55	0,01	0,30	3,80	0,20
153	5,99	0,01	3,00	6,00	0,00	0,12	0,07	1,50	0,02	1,12	0,17	3,00	0,15	0,61	0,00	0,24	3,54	0,46
154	6,05	0,00	3,00	6,00	0,00	0,16	0,05	1,43	0,01	1,08	0,27	3,00	0,07	0,64	0,01	0,27	3,71	0,29
sample10-1																		
155	6,05	0,00	3,00	6,00	0,00	0,48	0,02	0,91	0,01	1,28	0,29	3,00	0,00	0,55	0,01	0,44	3,86	0,14
156	6,06	0,00	3,00	6,00	0,00	0,36	0,03	0,95	0,02	1,34	0,31	3,00	0,01	0,64	0,01	0,34	3,79	0,21
157	6,09	0,00	3,00	6,00	0,00	0,31	0,01	0,99	0,01	1,31	0,36	3,00	0,01	0,63	0,01	0,35	3,75	0,25
158	6,06	0,00	3,00	6,00	0,00	0,30	0,03	1,06	0,01	1,32	0,28	3,00	0,01	0,65	0,01	0,33	3,73	0,27
159	6,08	0,00	3,00	6,00	0,00	0,29	0,04	1,05	0,01	1,27	0,34	3,00	0,02	0,61	0,01	0,36	3,79	0,21
160	6,04	0,00	3,00	6,00	0,00	0,32	0,04	1,10	0,02	1,25	0,26	3,00	0,02	0,64	0,02	0,32	3,86	0,14
161	6,09	0,00	3,00	6,00	0,00	0,39	0,01	0,99	0,01	1,21	0,38	3,00	0,01	0,58	0,00	0,40	3,81	0,19
162	6,06	0,00	3,00	6,00	0,00	0,21	0,04	1,19	0,01	1,27	0,28	3,00	0,02	0,68	0,01	0,29	3,71	0,29
163	6,04	0,00	3,00	6,00	0,00	0,29	0,05	1,06	0,02	1,31	0,27	3,00	0,02	0,65	0,01	0,32	3,83	0,17
164	6,06	0,00	3,00	6,00	0,00	0,18	0,07	1,17	0,01	1,29	0,28	3,00	0,02	0,69	0,01	0,28	3,80	0,20
165	6,04	0,00	3,00	6,00	0,00	0,17	0,08	1,22	0,03	1,23	0,28	3,00	0,02	0,73	0,02	0,24	3,99	0,01
166	6,04	0,00	3,00	6,00	0,00	0,38	0,02	1,04	0,02	1,30	0,24	3,00	0,01	0,64	0,01	0,34	3,74	0,26
167	6,06	0,00	3,00	6,00	0,00	0,20	0,04	1,20	0,01	1,29	0,25	3,00	0,02	0,68	0,01	0,30	3,77	0,23
168	6,05	0,00	3,00	6,00	0,00	0,21	0,08	1,17	0,01	1,31	0,23	3,00	0,02	0,63	0,01	0,34	3,78	0,22
169	6,05	0,00	3,00	6,00	0,00	0,29	0,05	1,09	0,01	1,28	0,28	3,00	0,02	0,66	0,01	0,31	3,71	0,29
170	6,08	0,00	3,00	6,00	0,00	0,35	0,01	1,02	0,01	1,28	0,33	3,00	0,01	0,60	0,01	0,38	3,76	0,24
171	6,04	0,00	3,00	6,00	0,00	0,25	0,04	1,20	0,02	1,28	0,22	3,00	0,02	0,67	0,01	0,30	3,74	0,26
172	6,07	0,00	3,00	6,00	0,00	0,18	0,06	1,22	0,01	1,25	0,27	3,00	0,02	0,66	0,01	0,31	3,81	0,19
173	6,08	0,00	3,00	6,00	0,00	0,24	0,05	1,09	0,01	1,26	0,35	3,00	0,01	0,66	0,01	0,32	3,89	0,11
174	6,07	0,00	3,00	6,00	0,00	0,16	0,05	1,20	0,02	1,27	0,30	3,00	0,02	0,68	0,02	0,28	3,71	0,29
175	6,04	0,00	3,00	6,00	0,00	0,33	0,04	1,05	0,01	1,35	0,23	3,00	0,01	0,64	0,01	0,33	3,89	0,11
176	6,12	0,00	3,00	6,00	0,00	0,33	0,06	0,87	0,01	1,11	0,61	3,00	0,01	0,64	0,01	0,34	3,75	0,25
sampleT-3																		
177	6,06	0,00	3,00	6,00	0,00	0,41	0,03	0,19	0,02	2,14	0,22	3,00	0,01	0,48	0,01	0,50	3,93	0,07
178	6,08	0,00	3,00	6,00	0,00	0,33	0,04	0,26	0,03	2,01	0,33	3,00	0,01	0,54	0,01	0,44	3,82	0,18
179	6,05	0,00	3,00	6,00	0,00	0,38	0,04	0,24	0,03	2,06	0,25	3,00	0,01	0,57	0,01	0,40	3,83	0,17
180	6,03	0,00	3,00	6,00	0,00	0,39	0,04	0,21	0,04	2,13	0,19	3,00	0,01	0,57	0,01	0,41	3,83	0,17
181	6,09	0,00	3,00	6,00	0,00	0,42	0,03	0,14	0,03	2,03	0,34	3,00	0,00	0,50	0,01	0,48	3,92	0,08
182	6,11	0,00	3,00	6,00	0,00	0,42	0,01	0,16	0,04	2,00	0,36	3,00	0,00	0,46	0,01	0,52	3,95	0,05
183	5,99	0,01	3,00	6,00	0,00	0,48	0,03	0,33	0,02	2,01	0,14	3,00	0,01	0,58	0,01	0,40	3,82	0,18
184	5,94	0,06	3,00	6,00	0,00	0,49	0,05	0,40	0,02	1,86	0,18	3,00	0,02	0,60	0,02	0,36	3,72	0,28
185	6,05	0,00	3,00	6,00	0,00	0,42	0,04	0,25	0,02	1,99	0,28	3,00	0,01	0,55	0,01	0,42	3,84	0,16
186	6,05	0,00	3,00	6,00	0,00	0,44	0,05	0,22	0,03	2,00	0,27	3,00	0,01	0,50	0,01	0,47	3,89	0,11
187	6,06	0,00	3,00	6,00	0,00	0,37	0,05	0,18	0,03	2,10	0,27	3,00	0,01	0,54	0,01	0,43	3,92	0,08
188	6,06	0,00	3,00	6,00	0,00	0,44	0,03	0,15	0,03	2,07	0,28	3,00	0,01	0,51	0,01	0,48	3,85	0,15

Point	T: Si	Al	B	Z:Al	Mg	Y:Al	Ti	Mg	Mn	Fe2+	Li*	∑Y	X:Ca	Na	K	r	OH	F
189	6,04	0,00	3,00	6,00	0,00	0,39	0,04	0,18	0,05	2,09	0,24	3,00	0,01	0,56	0,01	0,42	3,95	0,05
190	6,05	0,00	3,00	6,00	0,00	0,36	0,04	0,27	0,03	2,05	0,25	3,00	0,01	0,56	0,01	0,42	3,79	0,21
191	6,08	0,00	3,00	6,00	0,00	0,43	0,02	0,24	0,02	1,94	0,35	3,00	0,01	0,52	0,02	0,45	3,77	0,23
192	6,07	0,00	3,00	6,00	0,00	0,36	0,04	0,20	0,02	2,14	0,24	3,00	0,01	0,50	0,01	0,47	3,84	0,16
193	6,13	0,00	3,00	6,00	0,00	0,40	0,01	0,14	0,03	2,03	0,39	3,00	0,00	0,45	0,02	0,53	3,96	0,04
194	6,08	0,00	3,00	6,00	0,00	0,46	0,02	0,17	0,02	2,02	0,31	3,00	0,01	0,46	0,01	0,52	3,85	0,15
195	6,09	0,00	3,00	6,00	0,00	0,46	0,01	0,17	0,04	2,02	0,30	3,00	0,00	0,44	0,01	0,54	3,90	0,10
196	6,05	0,00	3,00	6,00	0,00	0,42	0,05	0,26	0,03	1,94	0,30	3,00	0,02	0,54	0,02	0,42	3,92	0,08
197	6,05	0,00	3,00	6,00	0,00	0,52	0,01	0,16	0,02	2,04	0,24	3,00	0,00	0,48	0,01	0,51	3,87	0,13
198	6,09	0,00	3,00	6,00	0,00	0,46	0,01	0,20	0,03	2,01	0,30	3,00	0,00	0,44	0,01	0,55	3,93	0,07
199	6,05	0,00	3,00	6,00	0,00	0,36	0,05	0,21	0,04	2,12	0,22	3,00	0,01	0,53	0,01	0,44	3,81	0,19
200	6,07	0,00	3,00	6,00	0,00	0,47	0,01	0,27	0,02	1,99	0,24	3,00	0,00	0,45	0,01	0,54	3,89	0,11
sample11-1																		
201	6,08	0,00	3,00	6,00	0,00	0,33	0,05	0,54	0,02	1,73	0,33	3,00	0,01	0,57	0,01	0,41	3,79	0,21
202	6,04	0,00	3,00	6,00	0,00	0,37	0,05	0,52	0,02	1,76	0,27	3,00	0,01	0,61	0,01	0,36	3,92	0,08
203	6,04	0,00	3,00	6,00	0,00	0,29	0,04	0,60	0,02	1,87	0,19	3,00	0,01	0,62	0,02	0,36	3,93	0,07
204	6,05	0,00	3,00	6,00	0,00	0,38	0,05	0,48	0,02	1,75	0,32	3,00	0,01	0,59	0,01	0,39	3,93	0,07
205	6,03	0,00	3,00	6,00	0,00	0,55	0,02	0,41	0,02	1,77	0,23	3,00	0,01	0,48	0,01	0,50	3,85	0,15
206	6,02	0,00	3,00	6,00	0,00	0,56	0,02	0,43	0,02	1,77	0,20	3,00	0,00	0,52	0,01	0,47	3,97	0,03
207	6,07	0,00	3,00	6,00	0,00	0,46	0,02	0,41	0,01	1,80	0,30	3,00	0,00	0,52	0,01	0,47	3,97	0,03
208	6,11	0,00	3,00	6,00	0,00	0,23	0,04	0,55	0,02	1,80	0,36	3,00	0,01	0,59	0,01	0,39	3,90	0,10
209	6,03	0,00	3,00	6,00	0,00	0,34	0,02	0,56	0,03	1,88	0,17	3,00	0,01	0,63	0,01	0,35	3,97	0,03
210	6,06	0,00	3,00	6,00	0,00	0,42	0,04	0,48	0,03	1,73	0,30	3,00	0,00	0,53	0,01	0,45	3,90	0,10
211	6,07	0,00	3,00	6,00	0,00	0,35	0,05	0,51	0,03	1,73	0,33	3,00	0,01	0,56	0,01	0,42	3,82	0,18
212	6,07	0,00	3,00	6,00	0,00	0,35	0,05	0,52	0,02	1,76	0,31	3,00	0,01	0,57	0,01	0,41	3,98	0,02
213	6,06	0,00	3,00	6,00	0,00	0,49	0,01	0,41	0,02	1,76	0,30	3,00	0,00	0,54	0,01	0,45	3,81	0,19
214	6,09	0,00	3,00	6,00	0,00	0,41	0,03	0,48	0,02	1,73	0,34	3,00	0,00	0,50	0,01	0,48	4,00	0,00
215	6,05	0,00	3,00	6,00	0,00	0,34	0,05	0,57	0,02	1,75	0,27	3,00	0,01	0,61	0,01	0,37	3,93	0,07
216	6,05	0,00	3,00	6,00	0,00	0,37	0,05	0,53	0,02	1,81	0,22	3,00	0,00	0,53	0,02	0,45	3,85	0,15
217	6,09	0,00	3,00	6,00	0,00	0,30	0,05	0,54	0,02	1,73	0,36	3,00	0,00	0,57	0,01	0,41	3,89	0,11
sample1-1																		
218	6,13	0,00	3,00	6,00	0,00	0,96	0,00	0,01	0,25	0,38	1,39	3,00	0,06	0,77	0,01	0,16	3,44	0,56
219	6,13	0,00	3,00	6,00	0,00	1,05	0,00	0,01	0,21	0,36	1,37	3,00	0,02	0,72	0,01	0,24	3,35	0,65
220	6,12	0,00	3,00	6,00	0,00	0,86	0,01	0,04	0,18	0,66	1,25	3,00	0,03	0,84	0,01	0,12	3,34	0,66
221	6,08	0,00	3,00	6,00	0,00	1,08	0,00	0,02	0,23	0,41	1,27	3,00	0,04	0,78	0,01	0,18	3,42	0,58
sample1-2																		
222	6,04	0,00	3,00	6,00	0,00	0,41	0,04	0,38	0,02	1,86	0,29	3,00	0,01	0,61	0,01	0,36	3,72	0,28
223	6,05	0,00	3,00	6,00	0,00	0,45	0,02	0,39	0,03	1,88	0,23	3,00	0,01	0,48	0,01	0,50	3,91	0,09
224	6,05	0,00	3,00	6,00	0,00	0,44	0,03	0,40	0,02	1,90	0,21	3,00	0,01	0,50	0,00	0,49	3,87	0,13
225	6,03	0,00	3,00	6,00	0,00	0,42	0,03	0,38	0,04	1,94	0,19	3,00	0,02	0,54	0,02	0,43	3,73	0,27

Point	T: Si	Al	B	Z:Al	Mg	Y:Al	Ti	Mg	Mn	Fe2+	Li*	∑Y	X:Ca	Na	K	r	OH	F
226	5,98	0,02	3,00	6,00	0,00	0,33	0,08	0,43	0,03	1,94	0,19	3,00	0,03	0,64	0,02	0,32	3,81	0,19
227	5,99	0,01	3,00	6,00	0,00	0,34	0,09	0,44	0,03	1,94	0,17	3,00	0,03	0,60	0,01	0,36	3,80	0,20
228	5,97	0,03	3,00	6,00	0,00	0,19	0,13	0,67	0,03	1,81	0,17	3,00	0,05	0,64	0,01	0,30	3,84	0,16
229	6,02	0,00	3,00	6,00	0,00	0,51	0,02	0,38	0,02	1,87	0,21	3,00	0,01	0,52	0,01	0,45	3,91	0,09
230	6,05	0,00	3,00	6,00	0,00	0,16	0,07	0,96	0,02	1,56	0,24	3,00	0,06	0,63	0,01	0,31	3,89	0,11
231	6,06	0,00	3,00	6,00	0,00	0,45	0,03	0,38	0,03	1,87	0,25	3,00	0,01	0,48	0,01	0,49	3,88	0,12
232	6,02	0,00	3,00	6,00	0,00	0,34	0,06	0,44	0,03	1,93	0,20	3,00	0,03	0,60	0,01	0,36	3,82	0,18
233	5,97	0,03	3,00	6,00	0,00	0,18	0,12	0,44	0,03	2,06	0,17	3,00	0,03	0,69	0,02	0,26	3,82	0,18
234	5,97	0,03	3,00	6,00	0,00	0,19	0,12	0,46	0,03	2,03	0,17	3,00	0,03	0,69	0,02	0,26	3,71	0,29
235	5,94	0,06	3,00	6,00	0,00	0,20	0,13	0,61	0,02	1,88	0,15	3,00	0,05	0,64	0,02	0,30	3,71	0,29
236	6,03	0,00	3,00	6,00	0,00	0,48	0,03	0,40	0,02	1,88	0,19	3,00	0,01	0,50	0,00	0,49	3,90	0,10
237	6,03	0,00	3,00	6,00	0,00	0,20	0,08	0,93	0,02	1,57	0,20	3,00	0,05	0,60	0,01	0,34	3,83	0,17
238	6,05	0,00	3,00	6,00	0,00	0,45	0,03	0,42	0,02	1,84	0,24	3,00	0,02	0,50	0,01	0,47	3,88	0,12
239	6,06	0,00	3,00	6,00	0,00	0,40	0,03	0,38	0,03	1,92	0,24	3,00	0,01	0,50	0,01	0,47	3,92	0,08
240	6,06	0,00	3,00	6,00	0,00	0,45	0,02	0,38	0,03	1,90	0,22	3,00	0,01	0,45	0,01	0,52	3,74	0,26
241	6,04	0,00	3,00	6,00	0,00	0,46	0,03	0,38	0,02	1,87	0,25	3,00	0,01	0,52	0,01	0,45	3,84	0,16
242	6,00	0,00	3,00	6,00	0,00	0,28	0,11	0,57	0,00	1,83	0,21	3,00	0,04	0,62	0,02	0,33	3,78	0,22
243	6,04	0,00	3,00	6,00	0,00	0,47	0,02	0,38	0,03	1,90	0,20	3,00	0,01	0,49	0,01	0,49	3,75	0,25
244	6,00	0,00	3,00	6,00	0,00	0,40	0,05	0,42	0,03	1,97	0,14	3,00	0,02	0,57	0,02	0,39	3,77	0,23
245	6,04	0,00	3,00	6,00	0,00	0,52	0,02	0,37	0,02	1,85	0,22	3,00	0,01	0,50	0,01	0,48	3,81	0,19
246	6,05	0,00	3,00	6,00	0,00	0,45	0,02	0,39	0,02	1,88	0,24	3,00	0,01	0,51	0,01	0,47	3,80	0,20
247	6,00	0,00	3,00	6,00	0,00	0,27	0,09	0,77	0,02	1,69	0,17	3,00	0,05	0,62	0,01	0,32	3,83	0,17
248	6,04	0,00	3,00	6,00	0,00	0,30	0,08	0,56	0,02	1,79	0,25	3,00	0,02	0,58	0,01	0,39	3,78	0,22
249	6,02	0,00	3,00	6,00	0,00	0,24	0,09	0,58	0,02	1,88	0,18	3,00	0,02	0,61	0,02	0,35	3,87	0,13
sample3-6																		
250	5,96	0,04	3,00	6,00	0,00	0,80	0,02	0,23	0,01	1,40	0,52	3,00	0,01	0,69	0,01	0,29	3,72	0,28
251	5,98	0,02	3,00	6,00	0,00	0,81	0,02	0,25	0,02	1,37	0,53	3,00	0,01	0,65	0,01	0,32	3,69	0,31
252	5,99	0,01	3,00	6,00	0,00	0,82	0,02	0,25	0,01	1,42	0,49	3,00	0,01	0,61	0,01	0,38	3,69	0,31
253	6,00	0,00	3,00	6,00	0,00	0,83	0,02	0,26	0,02	1,34	0,54	3,00	0,01	0,64	0,01	0,35	3,76	0,24
254	5,98	0,02	3,00	6,00	0,00	0,79	0,02	0,25	0,02	1,39	0,53	3,00	0,01	0,69	0,01	0,29	3,65	0,35
255	6,00	0,00	3,00	6,00	0,00	0,80	0,02	0,25	0,03	1,38	0,52	3,00	0,01	0,65	0,01	0,34	3,75	0,25
256	5,95	0,05	3,00	6,00	0,00	0,80	0,02	0,25	0,02	1,43	0,48	3,00	0,02	0,66	0,01	0,32	3,65	0,35
257	5,98	0,02	3,00	6,00	0,00	0,80	0,02	0,25	0,03	1,40	0,51	3,00	0,01	0,65	0,01	0,33	3,67	0,33
258	5,98	0,02	3,00	6,00	0,00	0,83	0,01	0,23	0,02	1,35	0,55	3,00	0,02	0,68	0,01	0,30	3,73	0,27
259	5,95	0,05	3,00	6,00	0,00	0,81	0,03	0,24	0,02	1,41	0,50	3,00	0,01	0,66	0,01	0,32	3,71	0,29
260	5,99	0,01	3,00	6,00	0,00	0,81	0,02	0,23	0,02	1,37	0,54	3,00	0,01	0,66	0,01	0,32	3,88	0,12
261	5,97	0,03	3,00	6,00	0,00	0,82	0,02	0,27	0,01	1,38	0,49	3,00	0,01	0,62	0,00	0,37	3,72	0,28
262	6,06	0,00	3,00	6,00	0,00	0,73	0,01	0,19	0,01	1,48	0,57	3,00	0,00	0,59	0,00	0,41	3,75	0,25
263	6,07	0,00	3,00	6,00	0,00	0,66	0,01	0,18	0,02	1,57	0,55	3,00	0,00	0,58	0,01	0,41	3,77	0,23
264	5,99	0,01	3,00	6,00	0,00	0,81	0,01	0,24	0,02	1,35	0,56	3,00	0,01	0,71	0,01	0,27	3,79	0,21

Point	T: Si	Al	B	Z:Al	Mg	Y:Al	Ti	Mg	Mn	Fe2+	Li*	∑Y	X:Ca	Na	K	r	OH	F
265	6,00	0,00	3,00	6,00	0,00	0,80	0,02	0,24	0,02	1,42	0,50	3,00	0,01	0,63	0,01	0,35	3,74	0,26
266	5,94	0,06	3,00	6,00	0,00	0,81	0,02	0,25	0,02	1,43	0,48	3,00	0,02	0,65	0,02	0,32	3,70	0,30
267	6,01	0,00	3,00	6,00	0,00	0,80	0,02	0,23	0,02	1,38	0,55	3,00	0,01	0,64	0,00	0,34	3,68	0,32
268	6,02	0,00	3,00	6,00	0,00	0,79	0,02	0,24	0,01	1,37	0,58	3,00	0,01	0,64	0,01	0,33	3,65	0,35
269	5,97	0,03	3,00	6,00	0,00	0,83	0,02	0,24	0,02	1,40	0,49	3,00	0,01	0,65	0,00	0,34	3,67	0,33
sample en-1																		
270	5,85	0,15	3,00	6,00	0,00	1,02	0,01	0,13	0,04	1,28	0,52	3,00	0,00	0,60	0,01	0,39	3,80	0,20
271	5,81	0,19	3,00	6,00	0,00	1,04	0,01	0,12	0,04	1,28	0,51	3,00	0,01	0,61	0,01	0,37	3,75	0,25
272	5,97	0,03	3,00	6,00	0,00	0,96	0,01	0,09	0,06	1,27	0,61	3,00	0,01	0,63	0,01	0,35	3,82	0,18
273	5,92	0,08	3,00	6,00	0,00	1,33	0,00	0,03	0,20	0,49	0,95	3,00	0,02	0,65	0,01	0,32	3,66	0,34
274	5,92	0,08	3,00	6,00	0,00	1,20	0,00	0,05	0,17	0,73	0,85	3,00	0,01	0,69	0,01	0,28	3,69	0,31
275	5,82	0,18	3,00	6,00	0,00	1,05	0,02	0,08	0,05	1,32	0,48	3,00	0,01	0,56	0,01	0,43	3,90	0,10
276	5,79	0,21	3,00	6,00	0,00	1,02	0,02	0,09	0,05	1,37	0,45	3,00	0,01	0,56	0,01	0,42	3,84	0,16
277	5,90	0,10	3,00	6,00	0,00	1,02	0,01	0,09	0,04	1,28	0,57	3,00	0,01	0,60	0,01	0,39	3,77	0,23
278	5,76	0,24	3,00	6,00	0,00	1,25	0,00	0,04	0,11	0,86	0,74	3,00	0,02	0,67	0,01	0,30	3,73	0,27
279	5,93	0,07	3,00	6,00	0,00	1,21	0,00	0,04	0,16	0,71	0,87	3,00	0,02	0,68	0,01	0,29	3,70	0,30
280	5,94	0,06	3,00	6,00	0,00	1,22	0,00	0,04	0,13	0,73	0,87	3,00	0,02	0,67	0,00	0,31	3,63	0,37
281	5,92	0,08	3,00	6,00	0,00	1,06	0,01	0,08	0,07	1,13	0,66	3,00	0,01	0,63	0,01	0,35	3,63	0,37
282	5,93	0,07	3,00	6,00	0,00	1,05	0,02	0,08	0,06	1,12	0,67	3,00	0,02	0,62	0,01	0,36	3,87	0,13
283	5,96	0,04	3,00	6,00	0,00	1,07	0,01	0,09	0,05	1,16	0,62	3,00	0,00	0,56	0,01	0,43	3,80	0,20
284	5,79	0,21	3,00	6,00	0,00	1,10	0,01	0,11	0,06	1,18	0,54	3,00	0,01	0,62	0,02	0,36	3,71	0,29
285	5,81	0,19	3,00	6,00	0,00	1,29	0,00	0,04	0,13	0,76	0,78	3,00	0,01	0,65	0,01	0,33	3,70	0,30
286	5,89	0,11	3,00	6,00	0,00	1,32	0,00	0,02	0,21	0,53	0,91	3,00	0,02	0,65	0,01	0,32	3,57	0,43
287	5,91	0,09	3,00	6,00	0,00	1,37	0,00	0,01	0,22	0,45	0,95	3,00	0,01	0,63	0,00	0,35	3,78	0,22
288	5,93	0,07	3,00	6,00	0,00	1,39	0,00	0,01	0,22	0,42	0,96	3,00	0,01	0,60	0,01	0,37	3,72	0,28
289	5,79	0,21	3,00	6,00	0,00	1,34	0,01	0,03	0,19	0,57	0,87	3,00	0,02	0,68	0,01	0,29	3,77	0,23
290	5,77	0,23	3,00	6,00	0,00	1,09	0,01	0,10	0,05	1,23	0,52	3,00	0,01	0,60	0,01	0,38	3,84	0,16
291	5,98	0,02	3,00	6,00	0,00	1,14	0,01	0,04	0,13	0,84	0,84	3,00	0,01	0,67	0,01	0,30	3,65	0,35
292	5,92	0,08	3,00	6,00	0,00	1,15	0,01	0,05	0,11	0,89	0,79	3,00	0,01	0,68	0,01	0,30	3,69	0,31
sample 2-2																		
293	6,08	0,00	3,00	6,00	0,00	0,15	0,06	1,31	0,01	1,14	0,32	3,00	0,02	0,67	0,02	0,29	3,81	0,19
294	6,09	0,00	3,00	6,00	0,00	0,07	0,06	1,37	0,01	1,15	0,33	3,00	0,02	0,70	0,01	0,26	3,85	0,15
295	6,08	0,00	3,00	6,00	0,00	0,13	0,06	1,32	0,02	1,19	0,27	3,00	0,03	0,66	0,01	0,30	3,82	0,18
296	6,10	0,00	3,00	6,00	0,00	0,05	0,07	1,31	0,01	1,21	0,35	3,00	0,02	0,71	0,01	0,26	3,86	0,14
297	5,99	0,01	3,00	6,00	0,00	0,13	0,08	1,72	0,01	0,81	0,25	3,00	0,26	0,42	0,02	0,29	3,82	0,18
298	6,05	0,00	3,00	6,00	0,00	0,14	0,09	1,26	0,02	1,18	0,31	3,00	0,02	0,72	0,02	0,24	3,84	0,16
299	6,06	0,00	3,00	6,00	0,00	0,18	0,07	1,23	0,02	1,21	0,30	3,00	0,02	0,69	0,01	0,27	3,88	0,12
300	6,06	0,00	3,00	6,00	0,00	0,19	0,07	1,52	0,01	0,90	0,31	3,00	0,02	0,69	0,01	0,29	3,75	0,25
301	6,07	0,00	3,00	6,00	0,00	0,17	0,07	1,25	0,01	1,15	0,34	3,00	0,01	0,69	0,01	0,29	3,84	0,16
302	6,03	0,00	3,00	6,00	0,00	0,16	0,08	1,67	0,00	0,79	0,29	3,00	0,17	0,48	0,01	0,34	3,82	0,18

Point	T: Si	Al	B	Z:Al	Mg	Y:Al	Ti	Mg	Mn	Fe2+	Li*	∑Y	X:Ca	Na	K	r	OH	F
303	6,01	0,00	3,00	6,00	0,00	0,08	0,08	1,66	0,01	0,92	0,25	3,00	0,20	0,55	0,01	0,24	3,72	0,28
304	6,09	0,00	3,00	6,00	0,00	0,11	0,09	1,17	0,01	1,24	0,37	3,00	0,02	0,66	0,02	0,30	3,97	0,03
305	6,06	0,00	3,00	6,00	0,00	0,11	0,07	1,32	0,01	1,22	0,27	3,00	0,02	0,72	0,01	0,25	3,90	0,10
306	6,08	0,00	3,00	6,00	0,00	0,11	0,07	1,32	0,02	1,20	0,29	3,00	0,02	0,68	0,01	0,28	3,75	0,25
307	6,11	0,00	3,00	6,00	0,00	0,07	0,06	1,32	0,02	1,14	0,38	3,00	0,02	0,69	0,02	0,27	3,92	0,08
308	6,08	0,00	3,00	6,00	0,00	0,15	0,06	1,35	0,01	1,13	0,30	3,00	0,02	0,66	0,01	0,31	3,81	0,19
309	6,07	0,00	3,00	6,00	0,00	0,12	0,08	1,30	0,01	1,18	0,32	3,00	0,02	0,71	0,02	0,25	3,85	0,15
310	6,11	0,00	3,00	6,00	0,00	0,01	0,07	1,40	0,01	1,16	0,34	3,00	0,02	0,70	0,01	0,26	3,86	0,14
311	6,06	0,00	3,00	6,00	0,00	0,16	0,07	1,28	0,01	1,17	0,31	3,00	0,03	0,70	0,02	0,26	3,94	0,06
312	6,06	0,00	3,00	6,00	0,00	0,27	0,04	1,56	0,02	0,82	0,28	3,00	0,07	0,55	0,01	0,38	3,88	0,12
313	6,04	0,00	3,00	6,00	0,00	0,17	0,08	1,28	0,02	1,20	0,24	3,00	0,02	0,67	0,01	0,30	3,81	0,19
314	6,09	0,00	3,00	6,00	0,00	0,13	0,07	1,32	0,02	1,11	0,36	3,00	0,01	0,68	0,01	0,29	3,79	0,21
315	6,06	0,00	3,00	6,00	0,00	0,17	0,08	1,27	0,01	1,18	0,30	3,00	0,02	0,69	0,02	0,27	3,81	0,19
316	6,06	0,00	3,00	6,00	0,00	0,22	0,08	1,23	0,02	1,09	0,36	3,00	0,03	0,69	0,01	0,27	3,96	0,04
317	6,04	0,00	3,00	6,00	0,00	0,20	0,08	1,17	0,02	1,28	0,25	3,00	0,02	0,65	0,01	0,32	3,81	0,19
318	6,07	0,00	3,00	6,00	0,00	0,14	0,05	1,59	0,02	0,90	0,31	3,00	0,03	0,71	0,01	0,24	3,75	0,25
319	5,99	0,01	3,00	6,00	0,00	0,22	0,09	1,72	0,01	0,73	0,23	3,00	0,15	0,55	0,01	0,29	3,90	0,10
320	6,09	0,00	3,00	6,00	0,00	0,12	0,06	1,29	0,01	1,18	0,33	3,00	0,02	0,67	0,01	0,30	3,84	0,16
321	6,08	0,00	3,00	6,00	0,00	0,14	0,08	1,22	0,02	1,19	0,35	3,00	0,02	0,69	0,02	0,27	3,81	0,19
322	6,12	0,00	3,00	6,00	0,00	0,08	0,08	1,19	0,02	1,24	0,38	3,00	0,01	0,64	0,01	0,34	3,84	0,16
323	6,09	0,00	3,00	6,00	0,00	0,07	0,08	1,31	0,02	1,20	0,32	3,00	0,03	0,69	0,01	0,28	3,83	0,17
324	6,11	0,00	3,00	6,00	0,00	0,09	0,05	1,31	0,01	1,21	0,34	3,00	0,02	0,66	0,01	0,32	3,89	0,11
sample 7-1																		
325	6,09	0,00	3,00	6,00	0,00	0,09	0,04	0,84	0,02	1,73	0,29	3,00	0,02	0,73	0,01	0,24	3,70	0,30
326	6,08	0,00	3,00	6,00	0,00	0,15	0,05	0,85	0,03	1,63	0,29	3,00	0,02	0,65	0,01	0,31	3,75	0,25
327	6,04	0,00	3,00	6,00	0,00	0,39	0,02	0,19	0,04	2,07	0,28	3,00	0,00	0,67	0,01	0,31	3,70	0,30
328	6,05	0,00	3,00	6,00	0,00	0,32	0,04	0,74	0,02	1,62	0,26	3,00	0,02	0,64	0,01	0,33	3,86	0,14
329	6,10	0,00	3,00	6,00	0,00	0,11	0,04	0,74	0,02	1,79	0,30	3,00	0,01	0,67	0,01	0,31	3,80	0,20
330	6,05	0,00	3,00	6,00	0,00	0,25	0,05	0,81	0,02	1,59	0,29	3,00	0,02	0,68	0,02	0,28	3,71	0,29
331	6,08	0,00	3,00	6,00	0,00	0,20	0,04	0,87	0,01	1,55	0,32	3,00	0,03	0,66	0,02	0,30	3,81	0,19
332	6,05	0,00	3,00	6,00	0,00	0,30	0,04	0,69	0,01	1,69	0,27	3,00	0,01	0,65	0,02	0,32	3,81	0,19
333	6,06	0,00	3,00	6,00	0,00	0,24	0,04	0,95	0,01	1,50	0,26	3,00	0,02	0,65	0,02	0,32	3,83	0,17
334	6,11	0,00	3,00	6,00	0,00	0,08	0,04	1,04	0,02	1,47	0,35	3,00	0,02	0,71	0,01	0,26	3,79	0,21
335	6,08	0,00	3,00	6,00	0,00	0,32	0,03	0,68	0,02	1,60	0,34	3,00	0,01	0,58	0,02	0,39	3,89	0,11
336	6,13	0,00	3,00	6,00	0,00	0,08	0,03	0,95	0,01	1,55	0,38	3,00	0,02	0,66	0,01	0,31	3,76	0,24
337	6,07	0,00	3,00	6,00	0,00	0,30	0,02	0,81	0,02	1,57	0,29	3,00	0,01	0,64	0,01	0,34	3,82	0,18
338	6,06	0,00	3,00	6,00	0,00	0,18	0,04	0,78	0,02	1,79	0,19	3,00	0,01	0,63	0,02	0,34	3,76	0,24
339	6,06	0,00	3,00	6,00	0,00	0,21	0,05	0,83	0,02	1,64	0,25	3,00	0,01	0,67	0,01	0,31	3,83	0,17
340	6,11	0,00	3,00	6,00	0,00	0,11	0,03	1,00	0,01	1,50	0,35	3,00	0,03	0,69	0,02	0,27	3,86	0,14
341	6,10	0,00	3,00	6,00	0,00	0,08	0,03	0,95	0,01	1,61	0,32	3,00	0,03	0,71	0,02	0,25	3,67	0,33

Point	T: Si	Al	B	Z:Al	Mg	Y:Al	Ti	Mg	Mn	Fe2+	Li*	∑Y	X:Ca	Na	K	r	OH	F
342	6,07	0,00	3,00	6,00	0,00	0,22	0,05	0,89	0,03	1,52	0,29	3,00	0,02	0,63	0,02	0,33	3,86	0,14
343	6,10	0,00	3,00	6,00	0,00	0,23	0,05	0,66	0,01	1,68	0,38	3,00	0,01	0,62	0,01	0,36	3,82	0,18
344	6,09	0,00	3,00	6,00	0,00	0,16	0,05	0,81	0,02	1,66	0,31	3,00	0,01	0,64	0,02	0,33	3,80	0,20
345	6,05	0,00	3,00	6,00	0,00	0,19	0,05	0,86	0,02	1,65	0,24	3,00	0,02	0,69	0,01	0,28	3,81	0,19
346	6,09	0,00	3,00	6,00	0,00	0,13	0,04	0,78	0,02	1,71	0,32	3,00	0,02	0,70	0,02	0,27	3,70	0,30
347	6,07	0,00	3,00	6,00	0,00	0,26	0,02	0,82	0,02	1,69	0,19	3,00	0,01	0,60	0,01	0,37	3,69	0,31
348	6,04	0,00	3,00	6,00	0,00	0,26	0,05	0,46	0,03	1,99	0,21	3,00	0,01	0,67	0,01	0,31	3,82	0,18
349	6,05	0,00	3,00	6,00	0,00	0,18	0,03	0,77	0,02	1,81	0,19	3,00	0,01	0,70	0,01	0,28	3,84	0,16
350	6,11	0,00	3,00	6,00	0,00	0,11	0,04	0,77	0,02	1,74	0,32	3,00	0,01	0,65	0,01	0,33	3,68	0,32
sample 7-2																		
351	6,10	0,00	3,00	6,00	0,00	0,11	0,03	0,78	0,02	1,77	0,29	3,00	0,01	0,69	0,01	0,29	3,80	0,20
352	6,02	0,00	3,00	6,00	0,00	0,45	0,01	0,64	0,02	1,68	0,19	3,00	0,01	0,60	0,01	0,38	3,68	0,32
353	5,94	0,06	3,00	6,00	0,00	0,40	0,03	0,61	0,02	1,82	0,12	3,00	0,01	0,70	0,00	0,29	3,78	0,22
354	5,97	0,03	3,00	6,00	0,00	0,36	0,06	0,89	0,02	1,50	0,17	3,00	0,02	0,66	0,01	0,30	3,99	0,01
355	5,97	0,03	3,00	6,00	0,00	0,37	0,04	0,64	0,02	1,79	0,14	3,00	0,01	0,66	0,02	0,31	3,62	0,38
356	6,03	0,00	3,00	6,00	0,00	0,31	0,05	0,83	0,02	1,59	0,20	3,00	0,01	0,64	0,01	0,34	3,87	0,13
357	6,04	0,00	3,00	6,00	0,00	0,22	0,07	0,97	0,01	1,53	0,21	3,00	0,03	0,65	0,02	0,31	3,81	0,19
358	6,01	0,00	3,00	6,00	0,00	0,31	0,04	1,07	0,01	1,43	0,15	3,00	0,02	0,67	0,01	0,30	3,58	0,42
359	6,02	0,00	3,00	6,00	0,00	0,35	0,04	0,85	0,02	1,54	0,21	3,00	0,01	0,64	0,02	0,33	3,80	0,20
360	6,02	0,00	3,00	6,00	0,00	0,28	0,04	1,10	0,02	1,39	0,17	3,00	0,02	0,68	0,02	0,28	3,61	0,39
361	6,01	0,00	3,00	6,00	0,00	0,43	0,03	0,64	0,02	1,72	0,16	3,00	0,02	0,59	0,01	0,38	3,65	0,35
362	6,04	0,00	3,00	6,00	0,00	0,25	0,04	1,06	0,02	1,41	0,22	3,00	0,03	0,68	0,02	0,27	3,68	0,32
363	6,02	0,00	3,00	6,00	0,00	0,28	0,05	0,79	0,03	1,69	0,17	3,00	0,02	0,65	0,02	0,31	3,82	0,18
364	6,03	0,00	3,00	6,00	0,00	0,28	0,04	0,84	0,02	1,59	0,22	3,00	0,02	0,67	0,01	0,30	3,72	0,28
365	6,03	0,00	3,00	6,00	0,00	0,20	0,05	1,00	0,02	1,56	0,17	3,00	0,03	0,67	0,01	0,29	3,81	0,19
366	5,95	0,05	3,00	6,00	0,00	0,28	0,06	0,92	0,01	1,65	0,07	3,00	0,03	0,64	0,01	0,32	3,83	0,17
367	6,03	0,00	3,00	6,00	0,00	0,31	0,06	0,84	0,00	1,55	0,23	3,00	0,01	0,67	0,01	0,31	3,66	0,34
368	6,01	0,00	3,00	6,00	0,00	0,31	0,05	0,93	0,02	1,53	0,16	3,00	0,02	0,65	0,01	0,32	3,84	0,16
369	5,99	0,01	3,00	6,00	0,00	0,31	0,06	0,84	0,02	1,68	0,10	3,00	0,02	0,64	0,02	0,33	3,80	0,20
370	5,98	0,02	3,00	6,00	0,00	0,35	0,05	1,04	0,01	1,38	0,17	3,00	0,03	0,66	0,02	0,30	3,79	0,21
371	5,99	0,01	3,00	6,00	0,00	0,28	0,05	1,00	0,02	1,54	0,12	3,00	0,02	0,70	0,01	0,27	3,70	0,30
372	5,95	0,05	3,00	6,00	0,00	0,36	0,05	0,90	0,02	1,59	0,08	3,00	0,01	0,61	0,02	0,35	3,73	0,27
373	6,02	0,00	3,00	6,00	0,00	0,25	0,05	1,01	0,01	1,56	0,13	3,00	0,03	0,65	0,01	0,31	3,84	0,16
374	5,99	0,01	3,00	6,00	0,00	0,35	0,04	0,66	0,02	1,81	0,12	3,00	0,01	0,64	0,02	0,33	3,68	0,32
sample K-4																		
375	5,96	0,04	3,00	6,00	0,00	0,54	0,03	0,29	0,02	1,95	0,17	3,00	0,01	0,58	0,01	0,40	3,82	0,18
376	5,96	0,04	3,00	6,00	0,00	0,64	0,01	0,19	0,02	2,02	0,12	3,00	0,01	0,48	0,01	0,50	3,91	0,09
377	6,00	0,00	3,00	6,00	0,00	0,51	0,03	0,24	0,03	2,02	0,17	3,00	0,01	0,57	0,00	0,41	3,74	0,26
378	5,95	0,05	3,00	6,00	0,00	0,67	0,01	0,16	0,02	2,02	0,11	3,00	0,00	0,46	0,01	0,53	3,84	0,16
379	6,01	0,00	3,00	6,00	0,00	0,45	0,03	0,27	0,03	2,03	0,19	3,00	0,01	0,60	0,01	0,38	3,87	0,13

Point	T: Si	Al	B	Z:Al	Mg	Y:Al	Ti	Mg	Mn	Fe2+	Li*	∑Y	X:Ca	Na	K	r	OH	F
380	5,98	0,02	3,00	6,00	0,00	0,65	0,01	0,19	0,02	1,98	0,15	3,00	0,00	0,49	0,01	0,50	3,83	0,17
381	6,01	0,00	3,00	6,00	0,00	0,49	0,03	0,26	0,03	2,03	0,16	3,00	0,01	0,54	0,02	0,44	3,83	0,17
382	6,02	0,00	3,00	6,00	0,00	0,50	0,03	0,24	0,03	2,02	0,17	3,00	0,01	0,51	0,01	0,47	3,79	0,21
383	6,00	0,00	3,00	6,00	0,00	0,67	0,00	0,19	0,03	1,94	0,17	3,00	0,01	0,46	0,01	0,52	3,70	0,30
384	5,97	0,03	3,00	6,00	0,00	0,67	0,01	0,18	0,02	1,95	0,16	3,00	0,01	0,48	0,01	0,50	3,82	0,18
385	5,92	0,08	3,00	6,00	0,00	0,67	0,01	0,17	0,02	2,04	0,09	3,00	0,01	0,46	0,01	0,52	3,91	0,09
386	5,97	0,03	3,00	6,00	0,00	0,67	0,01	0,17	0,03	1,97	0,15	3,00	0,01	0,47	0,01	0,51	3,89	0,11
387	5,92	0,08	3,00	6,00	0,00	0,68	0,01	0,18	0,02	1,99	0,12	3,00	0,00	0,48	0,02	0,50	3,81	0,19
388	5,94	0,06	3,00	6,00	0,00	0,68	0,01	0,19	0,02	2,00	0,10	3,00	0,01	0,44	0,01	0,55	3,78	0,22
389	5,92	0,08	3,00	6,00	0,00	0,61	0,01	0,22	0,03	2,06	0,07	3,00	0,00	0,51	0,01	0,48	3,86	0,14
390	5,95	0,05	3,00	6,00	0,00	0,52	0,03	0,26	0,03	2,04	0,12	3,00	0,01	0,55	0,01	0,43	3,75	0,25
391	6,00	0,00	3,00	6,00	0,00	0,68	0,01	0,18	0,03	1,93	0,17	3,00	0,00	0,46	0,01	0,52	3,88	0,12
392	5,95	0,05	3,00	6,00	0,00	0,66	0,01	0,20	0,02	1,96	0,14	3,00	0,01	0,48	0,01	0,50	3,77	0,23
393	5,95	0,05	3,00	6,00	0,00	0,50	0,03	0,30	0,03	2,05	0,09	3,00	0,00	0,55	0,01	0,44	3,76	0,24
394	5,99	0,01	3,00	6,00	0,00	0,50	0,03	0,28	0,02	1,97	0,19	3,00	0,01	0,61	0,02	0,37	3,75	0,25
sample K-4																		
395	6,08	0,00	3,00	6,00	0,00	0,88	0,01	0,07	0,09	0,90	1,04	3,00	0,02	0,78	0,01	0,19	3,36	0,64
396	6,06	0,00	3,00	6,00	0,00	0,86	0,00	0,08	0,10	0,93	1,03	3,00	0,02	0,85	0,01	0,12	3,26	0,74
397	6,06	0,00	3,00	6,00	0,00	0,86	0,01	0,12	0,03	1,09	0,89	3,00	0,01	0,74	0,00	0,24	3,46	0,54
398	5,98	0,02	3,00	6,00	0,00	0,90	0,01	0,13	0,02	1,22	0,71	3,00	0,02	0,76	0,01	0,21	3,52	0,48
399	6,06	0,00	3,00	6,00	0,00	0,90	0,00	0,05	0,10	0,95	1,00	3,00	0,02	0,79	0,01	0,18	3,41	0,59
400	6,04	0,00	3,00	6,00	0,00	0,94	0,02	0,07	0,10	0,91	0,97	3,00	0,02	0,77	0,01	0,20	3,35	0,65
401	6,10	0,00	3,00	6,00	0,00	0,80	0,00	0,05	0,09	0,97	1,09	3,00	0,02	0,83	0,01	0,14	3,46	0,54
402	6,07	0,00	3,00	6,00	0,00	0,50	0,02	0,22	0,03	1,85	0,39	3,00	0,01	0,56	0,01	0,42	3,78	0,22
403	6,08	0,00	3,00	6,00	0,00	0,71	0,01	0,14	0,02	1,30	0,82	3,00	0,01	0,73	0,01	0,25	3,60	0,40
404	6,09	0,00	3,00	6,00	0,00	0,87	0,01	0,08	0,10	0,91	1,04	3,00	0,02	0,75	0,01	0,22	3,39	0,61
405	6,09	0,00	3,00	6,00	0,00	0,85	0,01	0,07	0,08	0,90	1,08	3,00	0,02	0,80	0,01	0,17	3,49	0,51
406	6,09	0,00	3,00	6,00	0,00	0,88	0,00	0,04	0,10	0,91	1,06	3,00	0,01	0,79	0,01	0,19	3,44	0,56
407	6,09	0,00	3,00	6,00	0,00	0,86	0,00	0,05	0,09	0,89	1,11	3,00	0,02	0,83	0,01	0,15	3,48	0,52
408	6,09	0,00	3,00	6,00	0,00	0,95	0,00	0,05	0,08	0,96	0,96	3,00	0,00	0,64	0,01	0,35	3,56	0,44
409	6,09	0,00	3,00	6,00	0,00	0,96	0,00	0,05	0,10	0,89	0,99	3,00	0,01	0,66	0,01	0,32	3,63	0,37
410	6,04	0,00	3,00	6,00	0,00	0,96	0,00	0,05	0,10	0,90	0,98	3,00	0,02	0,79	0,01	0,17	3,52	0,48
411	6,08	0,00	3,00	6,00	0,00	0,88	0,01	0,06	0,09	0,90	1,07	3,00	0,03	0,80	0,01	0,16	3,46	0,54
412	6,08	0,00	3,00	6,00	0,00	0,90	0,00	0,05	0,10	0,90	1,05	3,00	0,02	0,79	0,00	0,18	3,54	0,46
413	6,05	0,00	3,00	6,00	0,00	0,89	0,00	0,04	0,11	1,22	0,74	3,00	0,00	0,63	0,01	0,35	3,56	0,44
414	6,06	0,00	3,00	6,00	0,00	0,86	0,00	0,05	0,12	1,24	0,73	3,00	0,00	0,59	0,01	0,40	3,72	0,28
sample J-1																		
415	6,10	0,00	3,00	6,00	0,00	0,60	0,00	0,00	0,03	1,57	0,79	3,00	0,02	0,74	0,01	0,24	3,68	0,32
416	6,14	0,00	3,00	6,00	0,00	0,62	0,00	0,00	0,03	1,47	0,88	3,00	0,00	0,68	0,01	0,31	3,61	0,39
417	6,10	0,00	3,00	6,00	0,00	0,67	0,00	0,00	0,05	1,50	0,78	3,00	0,01	0,70	0,00	0,29	3,62	0,38

Point	T: Si	Al	B	Z:Al	Mg	Y:Al	Ti	Mg	Mn	Fe2+	Li*	∑Y	X:Ca	Na	K	r	OH	F
418	6,11	0,00	3,00	6,00	0,00	0,70	0,00	0,01	0,03	1,38	0,89	3,00	0,01	0,74	0,00	0,25	3,57	0,43
419	6,10	0,00	3,00	6,00	0,00	0,65	0,01	0,00	0,03	1,49	0,81	3,00	0,00	0,72	0,01	0,27	3,52	0,48
420	6,01	0,00	3,00	6,00	0,00	0,91	0,00	0,00	0,05	1,37	0,67	3,00	0,01	0,70	0,01	0,28	3,59	0,41
421	6,11	0,00	3,00	6,00	0,00	0,75	0,00	0,00	0,06	1,20	1,00	3,00	0,01	0,78	0,00	0,20	3,57	0,43
422	6,10	0,00	3,00	6,00	0,00	0,69	0,00	0,01	0,03	1,36	0,91	3,00	0,00	0,81	0,01	0,17	3,48	0,52
423	6,12	0,00	3,00	6,00	0,00	0,62	0,00	0,00	0,01	1,59	0,77	3,00	0,00	0,64	0,00	0,35	3,72	0,28
424	6,09	0,00	3,00	6,00	0,00	0,79	0,00	0,00	0,06	1,34	0,81	3,00	0,00	0,65	0,00	0,34	3,61	0,39
425	6,06	0,00	3,00	6,00	0,00	0,69	0,00	0,00	0,03	1,60	0,69	3,00	0,01	0,76	0,00	0,23	3,53	0,47
426	6,08	0,00	3,00	6,00	0,00	0,61	0,01	0,00	0,03	1,67	0,68	3,00	0,00	0,75	0,00	0,25	3,61	0,39
427	6,11	0,00	3,00	6,00	0,00	0,73	0,00	0,00	0,05	1,18	1,04	3,00	0,01	0,84	0,01	0,14	3,25	0,75
428	6,07	0,00	3,00	6,00	0,00	0,66	0,00	0,00	0,02	1,63	0,68	3,00	0,00	0,71	0,01	0,27	3,42	0,58
429	6,03	0,00	3,00	6,00	0,00	0,65	0,00	0,00	0,03	1,73	0,59	3,00	0,00	0,80	0,00	0,20	3,53	0,47
430	6,13	0,00	3,00	6,00	0,00	0,69	0,00	0,00	0,06	1,25	1,01	3,00	0,00	0,80	0,00	0,20	3,57	0,43
431	6,08	0,00	3,00	6,00	0,00	0,68	0,00	0,00	0,02	1,60	0,70	3,00	0,00	0,68	0,01	0,30	3,72	0,28

5. Apatite mineral chemistry data

Phosphates are one of the most studied minerals in pegmatites since such a variety of species occur with a significant amount being restricted to pegmatites. Keller (1991) did a regional study of phosphate phases within Damaran pegmatites and found species, not mentioning abundant apatite, such as Ferrisicklerite, heterosite and triplite within the Karlowa and Strathmore swarms, noting specifically that the Uis swarm showed little phosphate assemblages. Keller (1991) observed that dendritic phosphates were more common in the Cape Cross-Uis pegmatite belt and used the Fe/Fe+Mn ratios of the phosphates to infer Ta-Nb-Sn- and Li-mineralisation in pegmatites and quote an undercooling model for their crystallisation.

Apatite mineral chemistry data are generally used as igneous petrogenetic and mineralisation indicators (e.g. Sha and Chappell, 1999). However, more so than not, the trace element signatures and REE contents of apatite are primarily used; major element makeup being of little importance (e.g. Belousa et al., 2001, 2002). This is a particular reason why the apatite data below is of no use since 95% of the trace element and REE data are below the detection of the microprobe (e.g. Pyle et al., 2002). Although this is unfortunate for this study, it is an interesting observation since Belousa et al. (2002) also used only microprobe analytical techniques which yielded sufficient data and detectable REE and trace-element values. A possible explanation as to why apatite from the Cape Cross-Uis pegmatite belt has below detection limit values is that the pegmatites on a whole-rock geochemical scale also show below detection limit values for these elements. This confirms that the whole-rock data from Fuchsloch et al. (2018*a*) is reliable and that the pegmatites of the Cape Cross-Uis pegmatite belt are truly depleted in rare earth elements, subsequently confirming other observations by Fuchsloch et al. (2018*a,c*; Chapter 4).

Furthermore, the data is limited because it covers few points on few grains from less than half of the pegmatite samples. A more comprehensive dataset might yield greater results, however, ICPMS should be the analytical technique used in future. In summary, the data that was obtained which are above detection limits, showed no correlations, even when compared across mineralogical boundaries with CGM minerals. The only information obtained was to classify the apatite as fluorapatite which consequently aids Fuchsloch et al. (2018*b*) observations that there was a high fluorine activity during crystallisation of Ta-Nb- and Sn-oxides, since apatite co-occurs with CGM, tapiolite and cassiterite in most cases.

Point	SrO	SiO2	P2O5	La2O3	Ce2O3	SO3	Cl	Na2O	CaO	F	MnO	FeO	BaO	Total
Sample 3-9														
1	b.d.l.	b.d.l.	42,25	b.d.l.	b.d.l.	b.d.l.	b.d.l.	b.d.l.	51,39	4,03	2,63	0,28	b.d.l.	100,58
2	0,12	b.d.l.	42,99	b.d.l.	b.d.l.	b.d.l.	0,01	b.d.l.	52,66	3,84	1,63	b.d.l.	b.d.l.	101,25
3	0,05	b.d.l.	42,66	b.d.l.	0,08	b.d.l.	0,01	b.d.l.	51,22	3,64	2,8	0,45	b.d.l.	100,91
4	0,05	b.d.l.	42,72	b.d.l.	b.d.l.	b.d.l.	0,01	b.d.l.	52,57	3,97	1,61	0,09	b.d.l.	101,02
5	0,03	b.d.l.	42,99	b.d.l.	0,06	b.d.l.	0,01	b.d.l.	51,89	3,89	2,67	0,39	0,02	101,95
6	b.d.l.	b.d.l.	43,08	b.d.l.	b.d.l.	b.d.l.	0,01	b.d.l.	51,63	3,75	2,46	0,37	b.d.l.	101,3
7	b.d.l.	b.d.l.	42,89	b.d.l.	0,05	b.d.l.	0,01	b.d.l.	52,83	3,68	1,64	0,11	b.d.l.	101,21
8	b.d.l.	b.d.l.	42,63	b.d.l.	0,09	b.d.l.	0,01	b.d.l.	51,64	3,7	2,65	0,33	0,03	101,08
9	b.d.l.	b.d.l.	42,29	b.d.l.	b.d.l.	b.d.l.	b.d.l.	b.d.l.	51,36	3,6	2,5	0,32	b.d.l.	100,07
10	b.d.l.	b.d.l.	42,8	b.d.l.	b.d.l.	b.d.l.	b.d.l.	b.d.l.	51,22	3,8	2,81	0,16	0,03	100,82
Sample 4-1														
11	b.d.l.	b.d.l.	42,51	b.d.l.	b.d.l.	0,02	b.d.l.	b.d.l.	51,32	3,83	2,99	0,3	b.d.l.	100,97
12	0,02	b.d.l.	42,77	b.d.l.	b.d.l.	b.d.l.	b.d.l.	b.d.l.	52,79	3,92	1,31	0,11	b.d.l.	100,92
13	0,03	b.d.l.	42,71	b.d.l.	b.d.l.	b.d.l.	b.d.l.	b.d.l.	52,01	3,94	2,55	0,17	b.d.l.	101,41
14	b.d.l.	b.d.l.	42,75	b.d.l.	b.d.l.	b.d.l.	0,01	b.d.l.	51,29	3,69	3,01	0,48	b.d.l.	101,23
15	b.d.l.	b.d.l.	42,36	b.d.l.	b.d.l.	b.d.l.	0,01	b.d.l.	51,6	3,73	2,55	0,23	b.d.l.	100,48
16	0,06	b.d.l.	42,26	b.d.l.	0,06	b.d.l.	0,01	b.d.l.	51,33	3,77	2,61	0,33	0,06	100,49
17	b.d.l.	b.d.l.	42,47	b.d.l.	b.d.l.	0,03	0,01	b.d.l.	53,94	3,67	0,22	0,09	b.d.l.	100,43
18	0,03	b.d.l.	42,61	b.d.l.	b.d.l.	0,03	b.d.l.	b.d.l.	51,47	3,82	2,32	0,15	0,01	100,44
19	b.d.l.	b.d.l.	42,56	b.d.l.	b.d.l.	0,02	0,01	b.d.l.	51,79	3,72	2,09	0,19	b.d.l.	100,38
20	0,04	b.d.l.	41,94	b.d.l.	b.d.l.	b.d.l.	b.d.l.	b.d.l.	51,23	3,92	2,9	0,24	b.d.l.	100,27
Sample 4-4														
21	b.d.l.	b.d.l.	42,86	b.d.l.	b.d.l.	0,03	0,01	b.d.l.	51,88	3,9	2,19	0,34	b.d.l.	101,21
22	0,34	b.d.l.	42,18	b.d.l.	b.d.l.	b.d.l.	0,01	b.d.l.	52,66	3,99	0,91	0,08	0,01	100,18
23	b.d.l.	b.d.l.	42,8	b.d.l.	0,05	0,02	0,01	b.d.l.	51,8	3,46	2,1	0,32	0,03	100,59
24	0,05	b.d.l.	42,66	b.d.l.	0,06	b.d.l.	0,01	b.d.l.	51,71	3,86	2,11	0,16	b.d.l.	100,62
25	b.d.l.	b.d.l.	42,78	b.d.l.	b.d.l.	0,02	0,01	0,03	51,45	3,54	2,07	0,3	b.d.l.	100,2
26	b.d.l.	b.d.l.	42,46	b.d.l.	b.d.l.	b.d.l.	b.d.l.	b.d.l.	52,42	3,71	1,89	0,15	0,06	100,69
27	b.d.l.	b.d.l.	42,61	b.d.l.	b.d.l.	0,02	b.d.l.	b.d.l.	51,81	3,82	2,54	0,41	b.d.l.	101,21
28	b.d.l.	b.d.l.	42,49	b.d.l.	0,05	b.d.l.	b.d.l.	b.d.l.	51,72	3,72	2,43	0,41	b.d.l.	100,82
29	b.d.l.	b.d.l.	42,93	b.d.l.	b.d.l.	b.d.l.	b.d.l.	b.d.l.	51,43	3,73	1,64	0,22	0,03	99,98
30	0,03	b.d.l.	43,17	b.d.l.	0,06	b.d.l.	b.d.l.	0,02	52,01	3,6	2,38	0,16	b.d.l.	101,43
Sample 4-12														
31	b.d.l.	b.d.l.	42,14	b.d.l.	b.d.l.	b.d.l.	0,01	b.d.l.	51,36	3,74	2,69	0,23	b.d.l.	100,17
32	b.d.l.	b.d.l.	41,85	b.d.l.	b.d.l.	0,04	0,02	0,03	51,94	3,96	1,5	0,35	b.d.l.	99,69
33	b.d.l.	b.d.l.	42,43	b.d.l.	b.d.l.	b.d.l.	0,02	0,03	51,39	3,84	2,31	0,22	b.d.l.	100,24
34	b.d.l.	b.d.l.	42,07	b.d.l.	b.d.l.	0,05	0,01	b.d.l.	50,85	3,77	3,05	0,28	b.d.l.	100,08
35	0,04	b.d.l.	42,76	b.d.l.	b.d.l.	b.d.l.	0,01	b.d.l.	53,05	3,71	0,9	b.d.l.	b.d.l.	100,47
36	b.d.l.	b.d.l.	42,47	b.d.l.	0,1	0,04	0,01	0,03	51,61	3,95	2,52	0,07	b.d.l.	100,8

Point	SrO	SiO2	P2O5	La2O3	Ce2O3	SO3	Cl	Na2O	CaO	F	MnO	FeO	BaO	Total
37	0,03	b.d.l.	42,78	b.d.l.	0,05	b.d.l.	b.d.l.	b.d.l.	51,32	3,64	2,55	0,44	b.d.l.	100,81
38	0,03	b.d.l.	42,2	b.d.l.	b.d.l.	0,03	0,02	b.d.l.	50,72	3,92	2,31	0,36	b.d.l.	99,59
39	0,04	b.d.l.	42,07	b.d.l.	b.d.l.	0,02	b.d.l.	b.d.l.	51,47	3,71	2,43	0,28	b.d.l.	100,02
40	b.d.l.	b.d.l.	42,01	b.d.l.	b.d.l.	b.d.l.	b.d.l.	0,05	52,1	3,64	1,15	0,08	b.d.l.	99,03
Sample D-4														
41	0,05	b.d.l.	42,26	b.d.l.	b.d.l.	0,03	0,01	b.d.l.	50,08	3,69	4,44	0,79	b.d.l.	101,35
42	b.d.l.	b.d.l.	42,59	b.d.l.	0,07	b.d.l.	0,01	b.d.l.	50,29	3,71	4,05	0,52	b.d.l.	101,24
43	b.d.l.	b.d.l.	42,25	b.d.l.	0,1	b.d.l.	b.d.l.	b.d.l.	49,98	3,86	4,15	0,44	0,03	100,81
44	b.d.l.	b.d.l.	42,48	b.d.l.	0,11	b.d.l.	b.d.l.	b.d.l.	50,16	3,88	4,23	0,55	b.d.l.	101,41
45	b.d.l.	b.d.l.	42,17	b.d.l.	0,14	b.d.l.	b.d.l.	b.d.l.	49,77	3,86	4,42	0,69	b.d.l.	101,05
46	b.d.l.	b.d.l.	42,24	b.d.l.	0,08	b.d.l.	b.d.l.	b.d.l.	49,79	3,64	3,8	0,72	b.d.l.	100,27
47	0,07	b.d.l.	42,57	b.d.l.	0,12	0,02	0,01	0,02	49,84	3,85	4,5	0,75	b.d.l.	101,75
48	0,04	b.d.l.	42,89	b.d.l.	0,06	0,04	b.d.l.	b.d.l.	49,26	3,77	4,45	0,5	b.d.l.	101,01
49	b.d.l.	b.d.l.	42,96	b.d.l.	0,05	b.d.l.	b.d.l.	b.d.l.	51,47	3,71	2,48	0,48	b.d.l.	101,15
50	b.d.l.	b.d.l.	42,56	b.d.l.	b.d.l.	b.d.l.	b.d.l.	b.d.l.	49,97	3,68	4,77	0,09	b.d.l.	101,07
Sample 10-1														
51	b.d.l.	b.d.l.	42,13	b.d.l.	0,09	0,03	b.d.l.	0,04	51,71	3,72	2,18	0,29	b.d.l.	100,19
52	0,02	b.d.l.	41,48	b.d.l.	0,08	b.d.l.	b.d.l.	b.d.l.	51,15	3,79	2,23	0,24	b.d.l.	98,99
53	0,03	b.d.l.	42,54	b.d.l.	0,13	b.d.l.	b.d.l.	b.d.l.	50,24	3,7	3,18	0,34	b.d.l.	100,16
54	0,03	b.d.l.	42,67	b.d.l.	b.d.l.	0,03	b.d.l.	0,04	51,77	3,73	1,67	0,11	b.d.l.	100,05
55	b.d.l.	b.d.l.	42,49	b.d.l.	b.d.l.	b.d.l.	b.d.l.	b.d.l.	51,42	3,73	2,1	0,35	b.d.l.	100,09
56	0,08	b.d.l.	41,61	b.d.l.	0,05	0,03	b.d.l.	0,02	51,17	3,59	2,25	0,07	0,02	98,89
57	0,04	b.d.l.	41,98	b.d.l.	0,14	b.d.l.	b.d.l.	0,03	51,26	3,84	2,05	0,28	b.d.l.	99,62
58	0,06	b.d.l.	41,81	b.d.l.	0,07	b.d.l.	0,01	0,03	50,02	3,73	2,83	0,37	b.d.l.	98,93
59	0,03	b.d.l.	42,15	b.d.l.	0,11	0,02	b.d.l.	b.d.l.	50,56	3,81	2,82	0,41	b.d.l.	99,91
60	0,09	b.d.l.	42,15	b.d.l.	0,09	b.d.l.	0,01	b.d.l.	51,06	3,78	1,99	0,28	b.d.l.	99,45
Sample 10-4														
61	0,07	b.d.l.	41,47	b.d.l.	b.d.l.	b.d.l.	0,01	0,02	51,27	3,94	2,39	0,21	0,06	99,44
62	0,04	b.d.l.	41,06	b.d.l.	0,1	0,02	b.d.l.	0,04	50,96	3,46	2,19	0,46	b.d.l.	98,33
63	0,03	b.d.l.	41,63	b.d.l.	0,09	b.d.l.	b.d.l.	b.d.l.	50,4	3,48	3,14	0,35	b.d.l.	99,12
64	0,04	b.d.l.	42,06	b.d.l.	0,11	0,02	b.d.l.	b.d.l.	51,84	3,7	2,38	0,31	b.d.l.	100,46
65	0,05	b.d.l.	42,7	b.d.l.	b.d.l.	b.d.l.	b.d.l.	0,04	53,07	3,74	1,33	0,1	b.d.l.	101,03
66	0,05	b.d.l.	41,53	b.d.l.	0,08	b.d.l.	0,02	0,03	51,66	3,82	2,51	0,43	b.d.l.	100,13
67	b.d.l.	b.d.l.	41,71	b.d.l.	0,06	b.d.l.	0,01	0,02	51,91	3,72	2,38	0,3	b.d.l.	100,11
68	0,03	b.d.l.	41,37	b.d.l.	b.d.l.	b.d.l.	b.d.l.	b.d.l.	51,24	3,83	2,26	0,34	b.d.l.	99,07
69	0,08	b.d.l.	42,23	b.d.l.	0,12	0,02	b.d.l.	b.d.l.	49,99	3,73	3,33	0,32	b.d.l.	99,82
70	0,05	b.d.l.	41,97	b.d.l.	b.d.l.	b.d.l.	b.d.l.	b.d.l.	51,49	3,75	2,67	0,19	b.d.l.	100,12
Sample 5.1-1														
71	b.d.l.	b.d.l.	42,48	b.d.l.	b.d.l.	0,03	0,01	b.d.l.	51,83	3,88	2,02	0,27	b.d.l.	100,52

Point	SrO	SiO2	P2O5	La2O3	Ce2O3	SO3	Cl	Na2O	CaO	F	MnO	FeO	BaO	Total
72	0,02	b.d.l.	42,69	b.d.l.	0,07	b.d.l.	b.d.l.	b.d.l.	51,4	3,69	2	0,32	b.d.l.	100,19
73	0,05	b.d.l.	42,08	b.d.l.	b.d.l.	b.d.l.	b.d.l.	b.d.l.	51,66	3,76	1,96	0,21	b.d.l.	99,72
74	0,03	b.d.l.	42,65	b.d.l.	b.d.l.	b.d.l.	b.d.l.	b.d.l.	51,68	3,86	2,11	0,32	b.d.l.	100,65
75	0,05	b.d.l.	41,57	b.d.l.	b.d.l.	b.d.l.	b.d.l.	b.d.l.	51,55	3,78	1,93	0,3	b.d.l.	99,18
76	0,05	b.d.l.	42,42	b.d.l.	b.d.l.	b.d.l.	b.d.l.	b.d.l.	52,1	3,64	1,74	0,16	b.d.l.	100,11
77	0,03	b.d.l.	42,35	b.d.l.	b.d.l.	b.d.l.	b.d.l.	b.d.l.	51,91	3,82	2,15	b.d.l.	b.d.l.	100,26
78	0,09	b.d.l.	42,26	b.d.l.	b.d.l.	b.d.l.	b.d.l.	b.d.l.	51,47	3,91	1,96	0,22	b.d.l.	99,91
79	0,05	b.d.l.	43,28	b.d.l.	b.d.l.	b.d.l.	b.d.l.	b.d.l.	52,02	3,87	2,14	0,35	b.d.l.	101,71
80	0,02	b.d.l.	42,42	b.d.l.	b.d.l.	b.d.l.	b.d.l.	b.d.l.	51,87	3,78	2,35	0,28	b.d.l.	100,72
Sample Na-5														
81	0,05	b.d.l.	42,29	b.d.l.	b.d.l.	0,02	b.d.l.	b.d.l.	51,92	3,86	2,07	0,42	b.d.l.	100,63
82	b.d.l.	b.d.l.	42,85	b.d.l.	0,07	b.d.l.	b.d.l.	b.d.l.	52,2	3,74	1,77	0,27	b.d.l.	100,9
83	0,05	b.d.l.	41,88	b.d.l.	b.d.l.	b.d.l.	0,01	b.d.l.	52,08	3,52	1,8	0,44	b.d.l.	99,78
84	b.d.l.	b.d.l.	42,61	b.d.l.	b.d.l.	b.d.l.	0,01	b.d.l.	52,16	3,76	1,69	0,38	b.d.l.	100,61
85	b.d.l.	b.d.l.	42,47	b.d.l.	0,07	b.d.l.	0,01	b.d.l.	51,72	4,05	1,99	0,28	b.d.l.	100,59
86	b.d.l.	b.d.l.	42,17	b.d.l.	b.d.l.	b.d.l.	0,01	b.d.l.	52,17	3,68	1,86	0,34	b.d.l.	100,23
87	0,04	b.d.l.	42,16	b.d.l.	b.d.l.	b.d.l.	b.d.l.	b.d.l.	51,62	3,85	1,84	0,28	b.d.l.	99,79
88	b.d.l.	b.d.l.	42,09	b.d.l.	b.d.l.	b.d.l.	b.d.l.	b.d.l.	52,18	3,68	1,57	0,25	b.d.l.	99,77
89	0,04	b.d.l.	42,3	b.d.l.	b.d.l.	0,02	b.d.l.	b.d.l.	51,87	3,72	1,78	0,27	b.d.l.	100
90	b.d.l.	b.d.l.	42,49	b.d.l.	b.d.l.	b.d.l.	b.d.l.	b.d.l.	51,77	3,9	2,08	0,18	0,03	100,45
Sample Na-6														
91	b.d.l.	b.d.l.	42,36	b.d.l.	b.d.l.	b.d.l.	0,01	b.d.l.	50,99	3,85	2,21	0,4	b.d.l.	99,82
92	b.d.l.	b.d.l.	41,61	b.d.l.	b.d.l.	b.d.l.	0,01	b.d.l.	51,71	3,53	2,48	0,24	b.d.l.	99,58
93	0,07	b.d.l.	42,11	b.d.l.	b.d.l.	0,04	0,01	b.d.l.	51,7	3,64	2,28	0,29	b.d.l.	100,14
94	b.d.l.	b.d.l.	41,91	b.d.l.	0,05	b.d.l.	b.d.l.	0,03	51,89	3,87	2,4	0,32	b.d.l.	100,47
95	b.d.l.	b.d.l.	41,73	b.d.l.	0,05	b.d.l.	0,01	b.d.l.	51,69	3,67	1,95	0,39	b.d.l.	99,49
96	b.d.l.	b.d.l.	42,43	b.d.l.	0,07	b.d.l.	0,01	0,06	51,2	3,82	2,32	0,17	b.d.l.	100,08
97	b.d.l.	b.d.l.	42,35	b.d.l.	b.d.l.	b.d.l.	0,01	0,05	51,74	3,87	2,07	0,31	0,05	100,45
98	b.d.l.	b.d.l.	42,64	b.d.l.	b.d.l.	b.d.l.	0,01	b.d.l.	51,76	3,75	2,04	0,3	b.d.l.	100,5
99	b.d.l.	b.d.l.	41,87	b.d.l.	b.d.l.	b.d.l.	0,01	b.d.l.	51,31	3,82	2,08	0,25	b.d.l.	99,34
100	b.d.l.	b.d.l.	41,83	b.d.l.	b.d.l.	b.d.l.	0,01	0,02	51,24	3,8	2,2	0,27	0,05	99,42
Sample 3.1-7														
101	b.d.l.	b.d.l.	38,46	b.d.l.	b.d.l.	0,05	0,15	0,06	46,97	3,48	2,85	0,3	b.d.l.	92,32
102	b.d.l.	b.d.l.	42,04	b.d.l.	b.d.l.	b.d.l.	0,01	0,03	51,22	3,72	2,03	0,31	b.d.l.	99,36
103	0,04	b.d.l.	42,49	b.d.l.	b.d.l.	b.d.l.	b.d.l.	b.d.l.	50,96	3,79	2,8	0,49	b.d.l.	100,57
104	b.d.l.	b.d.l.	41,95	b.d.l.	b.d.l.	b.d.l.	0,01	b.d.l.	51,35	3,86	2,83	0,41	b.d.l.	100,41
105	b.d.l.	b.d.l.	42,74	b.d.l.	0,06	b.d.l.	b.d.l.	b.d.l.	51,46	3,79	2,21	0,11	b.d.l.	100,37
106	0,04	b.d.l.	42,13	b.d.l.	b.d.l.	b.d.l.	0,01	b.d.l.	50,43	3,52	2,84	0,43	0,01	99,41
107	0,07	b.d.l.	41,67	b.d.l.	b.d.l.	0,03	0,01	0,24	50,68	3,81	1,57	0,58	b.d.l.	98,66
108	b.d.l.	b.d.l.	41,9	b.d.l.	0,08	b.d.l.	b.d.l.	b.d.l.	50,92	3,86	2,59	0,14	b.d.l.	99,49

Point	SrO	SiO2	P2O5	La2O3	Ce2O3	SO3	Cl	Na2O	CaO	F	MnO	FeO	BaO	Total
109	0,07	b.d.l.	42,21	b.d.l.	0,08	0,03	0,01	b.d.l.	51,19	3,77	2,66	0,28	b.d.l.	100,3
110	b.d.l.	b.d.l.	42,22	b.d.l.	b.d.l.	0,03	0,01	b.d.l.	52	3,62	1,88	0,05	b.d.l.	99,81
Sample B-1														
111	0,31	b.d.l.	41,15	b.d.l.	0,08	0,05	0,01	0,2	49,98	3,68	2,09	0,54	b.d.l.	98,09
112	0,04	b.d.l.	42,69	b.d.l.	0,13	b.d.l.	b.d.l.	b.d.l.	49,52	3,64	4,25	0,57	b.d.l.	100,84
113	0,07	b.d.l.	41,59	b.d.l.	b.d.l.	b.d.l.	0,01	b.d.l.	49,48	3,85	4,52	0,74	b.d.l.	100,26
114	0,04	b.d.l.	41,12	b.d.l.	0,09	b.d.l.	0,01	b.d.l.	49,21	3,72	5,02	0,77	b.d.l.	99,98
115	0,07	b.d.l.	42,14	b.d.l.	b.d.l.	b.d.l.	b.d.l.	0,03	49,35	3,84	5,25	0,42	0,02	101,12
116	0,11	b.d.l.	41,55	b.d.l.	b.d.l.	b.d.l.	0,01	b.d.l.	48,78	3,8	5,04	0,59	0,05	99,93
117	0,15	b.d.l.	41,65	b.d.l.	b.d.l.	b.d.l.	0,01	b.d.l.	50,06	3,78	5,02	0,32	0,08	101,07
118	0,15	b.d.l.	42,26	b.d.l.	b.d.l.	b.d.l.	0,01	b.d.l.	48,51	3,85	5,43	0,85	b.d.l.	101,06
119	0,04	b.d.l.	41,71	b.d.l.	b.d.l.	b.d.l.	0,01	b.d.l.	49,55	3,78	4,55	0,38	0,04	100,06
120	0,09	b.d.l.	42,43	b.d.l.	0,09	b.d.l.	b.d.l.	b.d.l.	49,92	3,85	4,7	0,38	0,04	101,5
Sample B-2														
121	0,07	b.d.l.	41,63	b.d.l.	b.d.l.	0,02	b.d.l.	0,03	47,75	3,77	5,79	0,78	b.d.l.	99,84
122	0,06	b.d.l.	42,24	b.d.l.	b.d.l.	0,02	b.d.l.	b.d.l.	47,57	3,93	5,88	0,86	b.d.l.	100,56
123	0,04	b.d.l.	41,84	b.d.l.	b.d.l.	b.d.l.	0,01	b.d.l.	47,58	3,71	5,79	0,74	b.d.l.	99,71
124	0,08	b.d.l.	42,48	b.d.l.	b.d.l.	b.d.l.	0,02	b.d.l.	47	3,91	6,06	0,93	b.d.l.	100,48
125	0,05	b.d.l.	41,03	b.d.l.	0,05	b.d.l.	0,01	b.d.l.	47,2	3,6	6,19	0,87	b.d.l.	99
126	0,05	b.d.l.	41,93	b.d.l.	0,1	0,03	b.d.l.	b.d.l.	47,41	3,8	5,86	0,76	b.d.l.	99,94
127	0,04	b.d.l.	41,88	b.d.l.	b.d.l.	0,06	0,03	b.d.l.	48,88	3,77	4,35	0,19	b.d.l.	99,2
128	0,05	b.d.l.	41,88	b.d.l.	b.d.l.	b.d.l.	0,02	b.d.l.	48,3	3,77	5,36	0,55	b.d.l.	99,93
129	b.d.l.	1,07	41,42	b.d.l.	b.d.l.	b.d.l.	0,02	b.d.l.	47,33	3,82	5,26	0,58	0,04	99,54
Sample W-3														
130	b.d.l.	b.d.l.	41,77	b.d.l.	b.d.l.	0,02	0,01	0,04	49,81	3,73	4,52	b.d.l.	b.d.l.	99,9
131	b.d.l.	b.d.l.	41,74	b.d.l.	b.d.l.	0,02	b.d.l.	b.d.l.	49,62	3,79	3,93	b.d.l.	b.d.l.	99,1
132	b.d.l.	b.d.l.	41,93	b.d.l.	b.d.l.	b.d.l.	0,01	b.d.l.	49,98	3,63	3,39	0,19	0,04	99,17
133	b.d.l.	b.d.l.	41,99	b.d.l.	0,11	b.d.l.	0,01	b.d.l.	50,55	3,77	3,95	b.d.l.	b.d.l.	100,38
134	0,02	b.d.l.	42,17	b.d.l.	b.d.l.	b.d.l.	b.d.l.	b.d.l.	49,8	3,91	4,16	0,21	b.d.l.	100,27
135	b.d.l.	b.d.l.	42,09	b.d.l.	b.d.l.	b.d.l.	b.d.l.	b.d.l.	49,54	3,76	3,82	b.d.l.	b.d.l.	99,21
136	b.d.l.	b.d.l.	42,27	b.d.l.	0,06	b.d.l.	b.d.l.	b.d.l.	50,21	3,86	3,66	b.d.l.	b.d.l.	100,06
137	b.d.l.	b.d.l.	42,51	b.d.l.	b.d.l.	0,04	0,01	b.d.l.	50,19	3,76	4,24	b.d.l.	b.d.l.	100,75
138	b.d.l.	b.d.l.	41,89	b.d.l.	b.d.l.	b.d.l.	0,01	b.d.l.	50,33	3,56	4,39	b.d.l.	b.d.l.	100,18
139	0,05	b.d.l.	41,75	b.d.l.	b.d.l.	b.d.l.	0,01	b.d.l.	50,37	3,81	4,03	0,06	b.d.l.	100,08
Sample eb-1														
140	0,04	b.d.l.	42,06	b.d.l.	b.d.l.	b.d.l.	b.d.l.	0,02	51,35	3,83	2,31	0,54	0,02	100,17
141	b.d.l.	b.d.l.	42,36	b.d.l.	b.d.l.	0,03	b.d.l.	b.d.l.	51,48	3,85	2,25	0,58	b.d.l.	100,55
142	0,04	b.d.l.	42,76	b.d.l.	0,11	b.d.l.	b.d.l.	0,08	50,96	3,79	2,04	0,64	b.d.l.	100,42
143	b.d.l.	b.d.l.	42,13	b.d.l.	b.d.l.	b.d.l.	b.d.l.	b.d.l.	51,34	3,98	2,09	0,34	b.d.l.	99,88
144	b.d.l.	b.d.l.	42,14	b.d.l.	b.d.l.	0,04	0,01	0,06	50,93	3,8	2,1	0,34	b.d.l.	99,42

Point	SrO	SiO2	P2O5	La2O3	Ce2O3	SO3	Cl	Na2O	CaO	F	MnO	FeO	BaO	Total
145	0,07	b.d.l.	42,53	b.d.l.	b.d.l.	b.d.l.	0,01	b.d.l.	51,77	3,97	2,04	0,45	b.d.l.	100,84
146	0,05	b.d.l.	42,37	b.d.l.	b.d.l.	b.d.l.	b.d.l.	b.d.l.	51,44	3,54	2,08	0,58	0,03	100,09
147	b.d.l.	b.d.l.	42,77	b.d.l.	0,07	b.d.l.	b.d.l.	0,07	51,24	3,96	2,5	0,37	b.d.l.	100,98
148	b.d.l.	b.d.l.	42,65	b.d.l.	b.d.l.	b.d.l.	b.d.l.	b.d.l.	51,78	3,74	1,82	0,47	b.d.l.	100,46
149	b.d.l.	b.d.l.	42,4	b.d.l.	0,16	b.d.l.	b.d.l.	0,12	50,99	3,74	2,13	0,4	b.d.l.	99,94
Sample J-1														
150	0,48	b.d.l.	42,34	b.d.l.	b.d.l.	b.d.l.	0,02	b.d.l.	50,16	3,6	4,12	0,08	0,03	100,83
151	0,53	b.d.l.	42,32	b.d.l.	b.d.l.	0,03	0,02	b.d.l.	50,97	3,76	3,19	0,09	b.d.l.	100,91
152	0,03	b.d.l.	42,46	b.d.l.	b.d.l.	0,02	0,08	b.d.l.	50,84	3,74	3,29	0,18	b.d.l.	100,64
153	0,63	b.d.l.	41,55	b.d.l.	0,06	b.d.l.	0,01	b.d.l.	48,91	3,86	5,29	0,29	b.d.l.	100,6
154	0,75	b.d.l.	41,94	b.d.l.	b.d.l.	b.d.l.	b.d.l.	b.d.l.	49,19	3,82	4,3	0,08	0,01	100,09
155	0,4	b.d.l.	43,02	b.d.l.	b.d.l.	0,03	0,01	b.d.l.	51,51	3,85	2,86	0,06	0,01	101,75
156	0,7	b.d.l.	41,76	b.d.l.	b.d.l.	0,03	0,03	b.d.l.	49,07	3,8	4,84	0,05	b.d.l.	100,28
157	0,57	b.d.l.	41,99	b.d.l.	b.d.l.	b.d.l.	0,01	b.d.l.	49,38	3,58	4,81	b.d.l.	b.d.l.	100,34
158	0,48	b.d.l.	42,2	b.d.l.	b.d.l.	b.d.l.	0,01	b.d.l.	50	3,92	4,24	0,21	b.d.l.	101,06
159	0,49	b.d.l.	42,39	b.d.l.	0,09	0,04	0,01	b.d.l.	50,53	3,9	3,21	0,21	b.d.l.	100,87
Sample Sm-3														
160	0,03	b.d.l.	42,44	b.d.l.	0,09	b.d.l.	0,01	b.d.l.	51,51	3,98	2,88	0,33	0,01	101,28
161	0,05	b.d.l.	43,05	b.d.l.	0,08	0,02	b.d.l.	b.d.l.	54,03	3,8	0,59	b.d.l.	b.d.l.	101,62
162	b.d.l.	b.d.l.	42,64	b.d.l.	0,07	b.d.l.	0,01	0,04	49,97	3,85	3,41	0,69	b.d.l.	100,68
163	b.d.l.	b.d.l.	41,82	b.d.l.	0,08	b.d.l.	b.d.l.	0,08	51,58	3,76	0,91	0,1	b.d.l.	98,33
164	0,07	b.d.l.	41,38	b.d.l.	0,15	0,06	0,04	0,04	48,89	3,75	3,43	0,39	b.d.l.	98,2
165	0,08	b.d.l.	42,32	b.d.l.	0,13	b.d.l.	b.d.l.	0,02	51,6	3,69	1,89	0,09	b.d.l.	99,82
166	0,03	b.d.l.	42,34	b.d.l.	0,12	b.d.l.	0,01	b.d.l.	50,57	3,96	3,37	0,56	0,02	100,98
167	0,03	0,24	42,28	b.d.l.	b.d.l.	b.d.l.	b.d.l.	0,03	51,3	3,66	2,62	0,08	0,03	100,27
168	0,04	b.d.l.	42,72	b.d.l.	0,12	0,02	b.d.l.	0,06	50,96	3,91	3,36	0,1	b.d.l.	101,29
169	b.d.l.	b.d.l.	42,67	b.d.l.	0,1	b.d.l.	b.d.l.	0,03	51,13	3,95	2,29	0,38	b.d.l.	100,55
Sample T-4														
170	b.d.l.	b.d.l.	42,31	b.d.l.	0,21	b.d.l.	b.d.l.	0,08	50,92	3,85	2,63	0,23	b.d.l.	100,23
171	b.d.l.	b.d.l.	41,86	0,05	0,14	b.d.l.	b.d.l.	0,04	51,24	3,81	2,26	0,24	b.d.l.	99,64
172	b.d.l.	b.d.l.	42,21	b.d.l.	0,14	0,03	b.d.l.	0,03	50,61	3,83	2,56	0,49	b.d.l.	99,9
173	0,02	b.d.l.	42,57	b.d.l.	b.d.l.	b.d.l.	0,01	0,05	51,5	3,75	1,78	0,22	0,02	99,92
174	b.d.l.	b.d.l.	42,72	b.d.l.	0,08	0,03	0,01	b.d.l.	51,56	3,92	2,72	0,38	b.d.l.	101,42
175	0,03	b.d.l.	42,02	b.d.l.	0,11	0,02	0,01	0,05	51,11	3,65	2,71	0,36	b.d.l.	100,07
176	b.d.l.	b.d.l.	41,95	b.d.l.	0,11	0,03	0,01	b.d.l.	51,14	3,68	2,73	0,4	b.d.l.	100,05
177	0,03	b.d.l.	42,97	b.d.l.	0,11	b.d.l.	b.d.l.	0,02	51,97	3,63	2,19	0,2	b.d.l.	101,12
178	b.d.l.	b.d.l.	42,83	b.d.l.	0,09	b.d.l.	b.d.l.	0,02	51,28	3,68	2,76	0,18	b.d.l.	100,84
179	b.d.l.	b.d.l.	42,36	b.d.l.	b.d.l.	b.d.l.	b.d.l.	0,03	50,47	3,56	3,12	0,06	b.d.l.	99,6
Sample 5-3														
180	b.d.l.	b.d.l.	42,07	b.d.l.	b.d.l.	b.d.l.	b.d.l.	b.d.l.	51,2	3,82	2,66	0,41	b.d.l.	100,16

Point	SrO	SiO2	P2O5	La2O3	Ce2O3	SO3	Cl	Na2O	CaO	F	MnO	FeO	BaO	Total
181	b.d.l.	b.d.l.	42,57	b.d.l.	b.d.l.	b.d.l.	0,01	b.d.l.	52,43	3,98	1,38	0,23	b.d.l.	100,6
182	b.d.l.	b.d.l.	41,75	b.d.l.	0,08	b.d.l.	0,01	0,03	52,12	3,96	1,76	0,3	0,04	100,05
183	0,06	b.d.l.	42,07	b.d.l.	b.d.l.	b.d.l.	b.d.l.	b.d.l.	51,77	3,74	2,42	0,27	b.d.l.	100,33
184	b.d.l.	b.d.l.	42,01	b.d.l.	b.d.l.	b.d.l.	0,01	0,04	51,75	3,82	1,74	b.d.l.	0,03	99,4
185	0,03	b.d.l.	42,06	b.d.l.	b.d.l.	b.d.l.	b.d.l.	b.d.l.	52,04	3,74	2,48	0,24	b.d.l.	100,59
186	0,05	1,13	36,14	b.d.l.	b.d.l.	0,67	0,02	0,34	52,24	3,22	b.d.l.	b.d.l.	b.d.l.	93,81
187	0,04	b.d.l.	42,49	b.d.l.	0,09	b.d.l.	b.d.l.	b.d.l.	51,39	3,94	2,44	0,34	b.d.l.	100,73
188	b.d.l.	b.d.l.	42,09	b.d.l.	0,1	b.d.l.	b.d.l.	b.d.l.	51,44	3,73	2,69	0,39	b.d.l.	100,44
189	b.d.l.	b.d.l.	42,11	b.d.l.	0,06	0,03	0,01	b.d.l.	51,6	3,85	2,37	0,23	0,02	100,28
Sample G-1														
190	b.d.l.	b.d.l.	42,07	b.d.l.	0,06	b.d.l.	b.d.l.	0,03	51,55	3,54	1,47	0,33	0,03	99,08
191	0,05	b.d.l.	40,89	b.d.l.	b.d.l.	0,09	0,01	0,11	51,38	3,59	1,35	0,43	b.d.l.	97,9
192	b.d.l.	b.d.l.	42,67	b.d.l.	0,05	b.d.l.	b.d.l.	b.d.l.	51,89	3,79	1,77	0,45	b.d.l.	100,62
193	0,03	b.d.l.	41,82	b.d.l.	0,06	0,03	b.d.l.	b.d.l.	51,44	3,61	1,54	0,33	b.d.l.	98,86
194	b.d.l.	b.d.l.	41,71	b.d.l.	0,1	b.d.l.	b.d.l.	b.d.l.	51,47	3,73	1,78	0,71	b.d.l.	99,5
195	b.d.l.	b.d.l.	42,08	b.d.l.	0,07	0,03	b.d.l.	b.d.l.	51,25	3,66	2,09	0,45	b.d.l.	99,63
196	b.d.l.	b.d.l.	41,82	b.d.l.	0,09	b.d.l.	b.d.l.	b.d.l.	51,72	3,84	1,6	0,36	b.d.l.	99,43
197	0,04	b.d.l.	41,44	b.d.l.	0,13	b.d.l.	b.d.l.	b.d.l.	51,76	3,63	1,6	0,47	b.d.l.	99,07
198	b.d.l.	b.d.l.	42,04	b.d.l.	0,06	b.d.l.	0,01	b.d.l.	52,04	3,71	1,97	0,37	0,03	100,23
199	0,02	b.d.l.	42	b.d.l.	b.d.l.	b.d.l.	b.d.l.	0,03	51,86	3,68	1,61	0,47	b.d.l.	99,67
Sample C-2														
200	0,04	b.d.l.	42,38	b.d.l.	b.d.l.	b.d.l.	0,01	b.d.l.	53,08	3,92	0,86	0,08	0,03	100,4
201	0,02	b.d.l.	41,65	b.d.l.	b.d.l.	b.d.l.	b.d.l.	b.d.l.	50,57	3,97	3,35	0,39	b.d.l.	99,95
202	b.d.l.	b.d.l.	41,72	b.d.l.	b.d.l.	0,03	0,01	b.d.l.	50,31	3,79	3,98	0,38	b.d.l.	100,22
203	0,04	b.d.l.	42,01	b.d.l.	b.d.l.	b.d.l.	b.d.l.	b.d.l.	50,13	3,91	3,35	0,42	b.d.l.	99,86
204	b.d.l.	b.d.l.	42,76	b.d.l.	b.d.l.	b.d.l.	b.d.l.	0,02	50,66	3,62	3,42	0,51	0,05	101,04
205	0,03	b.d.l.	42,41	b.d.l.	0,06	b.d.l.	b.d.l.	b.d.l.	50,69	3,55	3,22	0,35	0,02	100,33
206	0,03	b.d.l.	42,11	b.d.l.	0,06	b.d.l.	b.d.l.	b.d.l.	52,23	3,6	1,73	0,23	0,03	100,02
207	b.d.l.	b.d.l.	41,72	b.d.l.	b.d.l.	b.d.l.	b.d.l.	b.d.l.	50,39	3,7	3,53	0,43	b.d.l.	99,77
208	0,02	b.d.l.	41,96	b.d.l.	b.d.l.	b.d.l.	0,01	b.d.l.	50,96	3,76	2,95	0,53	b.d.l.	100,19
Sample M-2														
209	0,06	b.d.l.	42,09	b.d.l.	b.d.l.	b.d.l.	0,01	b.d.l.	50,35	3,9	2,77	0,36	b.d.l.	99,54
210	0,11	b.d.l.	41,62	b.d.l.	0,07	b.d.l.	0,01	b.d.l.	51,2	3,82	2,71	0,37	b.d.l.	99,91
211	0,06	b.d.l.	42,38	b.d.l.	b.d.l.	b.d.l.	0,01	b.d.l.	50,5	3,78	2,82	0,49	b.d.l.	100,04
212	0,08	b.d.l.	41,87	b.d.l.	b.d.l.	0,02	0,01	b.d.l.	51,11	3,87	2,31	0,37	b.d.l.	99,64
213	0,03	b.d.l.	42,58	b.d.l.	b.d.l.	b.d.l.	0,01	b.d.l.	51,21	3,73	2,73	0,37	b.d.l.	100,66
214	0,1	b.d.l.	42,41	b.d.l.	b.d.l.	0,03	0,01	b.d.l.	51,02	3,8	2,27	0,34	0,01	99,99
215	0,11	b.d.l.	41,93	b.d.l.	0,1	0,02	0,01	b.d.l.	51,35	4,08	2,33	b.d.l.	0,01	99,94
216	0,07	b.d.l.	42	b.d.l.	0,07	b.d.l.	0,01	b.d.l.	50,02	3,91	3,38	0,48	b.d.l.	99,94
217	b.d.l.	b.d.l.	42,7	b.d.l.	b.d.l.	b.d.l.	b.d.l.	b.d.l.	51,74	3,62	1,58	0,23	b.d.l.	99,87

Point	SrO	SiO2	P2O5	La2O3	Ce2O3	SO3	Cl	Na2O	CaO	F	MnO	FeO	BaO	Total
218	b.d.l.	b.d.l.	41,81	b.d.l.	b.d.l.	0,03	0,01	b.d.l.	49,47	3,69	5,04	0,39	b.d.l.	100,44
Sample 3.2-1														
219	b.d.l.	b.d.l.	42,35	b.d.l.	0,1	b.d.l.	0,01	b.d.l.	51,71	3,61	2,07	b.d.l.	b.d.l.	99,85
220	0,02	b.d.l.	42,08	b.d.l.	0,18	0,02	b.d.l.	0,07	50,12	4,03	3,72	0,49	b.d.l.	100,73
221	0,04	b.d.l.	42,45	b.d.l.	0,13	b.d.l.	0,01	0,03	50,98	3,89	3,11	0,32	b.d.l.	100,96
222	0,04	b.d.l.	41,77	b.d.l.	0,13	b.d.l.	0,01	0,04	50,46	3,75	2,84	0,53	b.d.l.	99,57
223	b.d.l.	b.d.l.	41,57	b.d.l.	0,1	0,03	b.d.l.	0,05	50,36	3,79	3,3	0,25	b.d.l.	99,45
224	0,04	b.d.l.	42,12	b.d.l.	0,06	0,02	b.d.l.	0,04	50,99	3,59	3,5	0,37	b.d.l.	100,73
225	0,08	b.d.l.	42,39	b.d.l.	0,12	b.d.l.	b.d.l.	0,05	51,1	3,75	2,93	0,32	b.d.l.	100,74
226	0,03	b.d.l.	42,29	b.d.l.	0,1	b.d.l.	b.d.l.	0,03	51,49	3,67	3,27	0,21	0,02	101,11
227	b.d.l.	b.d.l.	41,86	b.d.l.	b.d.l.	b.d.l.	b.d.l.	0,06	51,25	3,65	2,5	0,15	b.d.l.	99,47
228	0,02	b.d.l.	42,27	b.d.l.	0,05	0,03	b.d.l.	0,04	50,79	3,69	2,82	0,23	b.d.l.	99,94
Sample X-1														
229	0,08	b.d.l.	42,08	b.d.l.	b.d.l.	b.d.l.	0,02	b.d.l.	50,36	3,78	4,05	0,36	0,01	100,74
230	0,06	b.d.l.	41,48	b.d.l.	b.d.l.	b.d.l.	0,03	b.d.l.	50,53	3,86	3,55	0,44	b.d.l.	99,95
231	0,06	b.d.l.	42,25	b.d.l.	b.d.l.	b.d.l.	0,01	b.d.l.	50,55	3,93	3,09	0,28	b.d.l.	100,17
232	0,22	b.d.l.	41,48	b.d.l.	0,06	0,04	0,02	b.d.l.	49,84	3,61	3,94	0,47	b.d.l.	99,68
233	0,1	b.d.l.	42,19	b.d.l.	b.d.l.	b.d.l.	0,02	0,02	50,58	3,72	3,43	0,23	b.d.l.	100,29
234	0,07	b.d.l.	41,27	b.d.l.	b.d.l.	0,04	0,03	b.d.l.	50,35	3,9	3,05	0,31	b.d.l.	99,02
235	0,2	b.d.l.	42,3	b.d.l.	b.d.l.	b.d.l.	0,01	b.d.l.	52,69	3,75	1,76	0,16	b.d.l.	100,87
236	0,08	b.d.l.	41,34	b.d.l.	b.d.l.	b.d.l.	0,06	b.d.l.	49,17	3,84	4,49	0,54	b.d.l.	99,52
237	0,19	b.d.l.	41,73	b.d.l.	b.d.l.	0,02	b.d.l.	b.d.l.	50,18	3,78	4,58	0,45	b.d.l.	100,93
238	0,09	b.d.l.	42,12	b.d.l.	0,05	0,03	0,03	0,03	50,36	3,82	3,15	0,26	b.d.l.	99,94
Sample A-2														
239	0,02	b.d.l.	41,15	b.d.l.	0,08	b.d.l.	b.d.l.	b.d.l.	48,41	3,77	5,86	0,47	0,02	99,78
240	b.d.l.	b.d.l.	41,36	b.d.l.	0,05	b.d.l.	0,01	b.d.l.	48,51	3,57	5,68	0,47	b.d.l.	99,65
241	b.d.l.	b.d.l.	41,49	b.d.l.	0,09	b.d.l.	b.d.l.	b.d.l.	48,48	3,65	5,08	1,52	b.d.l.	100,31
242	b.d.l.	b.d.l.	41,97	b.d.l.	b.d.l.	b.d.l.	0,01	b.d.l.	47,93	3,81	5,86	0,64	b.d.l.	100,22
243	0,02	b.d.l.	41,97	b.d.l.	b.d.l.	b.d.l.	b.d.l.	b.d.l.	48,44	3,65	5,58	0,48	b.d.l.	100,14
244	b.d.l.	b.d.l.	41,18	b.d.l.	0,06	b.d.l.	0,01	b.d.l.	48,62	3,77	5,4	0,47	b.d.l.	99,51
245	b.d.l.	b.d.l.	41,99	b.d.l.	0,06	0,04	0,02	b.d.l.	48,17	3,59	5,44	0,41	b.d.l.	99,72
246	0,04	b.d.l.	42,17	b.d.l.	0,11	b.d.l.	b.d.l.	0,03	48,21	3,56	6,28	0,64	b.d.l.	101,04
247	0,05	b.d.l.	41,76	b.d.l.	b.d.l.	0,02	b.d.l.	b.d.l.	48,48	3,38	5,72	0,41	b.d.l.	99,82
248	b.d.l.	b.d.l.	42,02	b.d.l.	b.d.l.	b.d.l.	b.d.l.	b.d.l.	47,61	3,7	5,9	1,1	0,01	100,34

Appendix D: Glossary of important terms

Introduction:

This section of the thesis is designed to described specific terms that are pertinent to this thesis. These terms are often misinterpreted in literature or have multiple meanings. Similarly, in some cases, there is a historical precedent for specific terms being used to describe certain features. The terms are given here in alphabetical order.

Albitised zone: This term refers to an area within the pegmatite that has undergone alteration in which all the primary minerals have been altered into fine-grained, equigranular albite. These zones often exhibit a saccharoidal texture in hand specimen and may contain considerable cassiterite or Ta-Nb-oxide phases. The alteration process is termed albitisation.

Alteration: In this case the term alteration refers to internal pegmatitic alteration, caused by fluids that are derived from the pegmatite. The nature of the fluid is irrelevant (aqueous or metasomatic magmatic), it is only important that it is pegmatite derived. Examples of such are greisenisation.

CGM: an abbreviation for the columbite-group minerals series

CUPB: an abbreviation for the Cape Cross-Uis pegmatite belt.

Exsolved hydrothermal fluid: This term refers to an event that occurs in the late stages of pegmatite petrogenesis. During the late-stages of pegmatite petrogenesis, a residual, highly fractionated (see below) magma should be present. This magma will be highly enriched in water and fluxes and will subsequently exsolve an aqueous fluid. Therefore, the fluid is derived from the pegmatite and not from external source.

Fractionation: The term fractionation is used in this thesis in its simplest form. The term refers to the enrichment of elements within a homogeneous and near-equilibrium magmatic system due to incompatibility. Similarly, mineral chemistry fractionation implies that the compositional makeup of a given mineral will change during crystallisation due to differences in the incompatibility of the elements that make up the particular mineral. For example, the Ta/Nb ratio in columbite-group

minerals should increase during fractionation since Ta is more soluble (therefore incompatible) than Nb in a pegmatitic magma

Greisen: A greisen is the term given to the alteration product of greisenisation. Greisenisation is a type of alteration caused by pegmatite-derived fluids, similar to albitisation, either being an exsolved aqueous fluid or metasomatic late-stage magmatic fluid. The primary rocks mineralogy is partially or completely changed to quartz and mica and is associated with abundant cassiterite and CGM.

Intragranitic: A term used to describe a pegmatite magma which has intruded into a granitic host-rock. Therefore, the pegmatite and granitic are not necessarily genetically related. The opposite term would be metasediment-hosted pegmatite, i.e. the pegmatites have intruded into the metasedimentary lithologies of the pegmatite belt.

Knotenschiefer: The local term given to schist metasediment host rocks which show porphyroblasts or "knots" within the schists. Often these porphyroblasts are composed of biotite and quartz and show alignment with the regional structural fabric of the belt. It is therefore hypothesised that these represent cordierite crystals which have retrogressed following peak metamorphic conditions.

LCT: Abbreviated for Lithium, Cesium and Tantalum. See section 3.3.

Mineralogical zonation: This term often implies a specific consolidation model for pegmatites, however, since most of the pegmatites within the Cape Cross-Uis pegmatite belt are homogenous masses, this term is used in its basic descriptive sense throughout the thesis. The term describes, in a broad sense, different zones within a pegmatite which show specific mineral assemblages, such as in the Petalite pegmatite (Section 2.3.3.1). Textural anisotropy and features as such are not implied (London and Morgan, 2012). Often the word "zone" is also used with the thesis and it describes in simplicity a specific area within the pegmatite and does not imply that the pegmatite has zones with different mineral assemblages.

Metasomatism: This term refers to the alteration of pegmatite host rocks by fluids. The alternating fluid in this case is derived from the pegmatite, being an exsolved aqueous fluid which pegmatites commonly produce at the late-stages of crystallisation (see London, 2008). The fluids are known to be rich in boron and subsequently crystallise large amounts of tourmaline in the rock that is metasomatised by the fluid. Often the biotite in the host rock schists is converted to tourmaline and the result metasomatic rock is composed solely of quartz and tourmaline in extreme cases. Furthermore, alteration halos may surround pegmatite bodies in terms of tourmaline abundances moving away from the contact. Other elements which may occur in these fluids are Sn, Ta and Nb, and thus subsequently also enrich the effected host rocks in these elements, however, the mobility of Ta and Nb is highly debated in these fluids (Chapter 5).

NYF: Abbreviated for Niobium, Yttrium and Fluorine. See Section 3.3

Pegmatite belt: A grouping of pegmatite intrusions. See Section 3.2 for a full description

Pegmatite swarm: A subgrouping of pegmatite intrusions. See Section 3.2 for a full description

UST: The term UST refers to a texture seen in pegmatites, often near the contact with host rocks. The abbreviation refers to a unidirectional solidification texture where minerals show perpendicular growth directions to wall rock contacts. Another example is comb-structured tourmaline. This is analogous to line rock (e.g. Snook, 2014 and described in London and Morgan, 2012).